DTIC
ELECTE
DEC 0 5 1995
S D
F

ARMY RESEARCH LABORATORY

Real Surface (Non-Ideal) Effects on Nuclear Explosion Airblast From PRISCILLA-Type Events, Part I: Comparison and Evaluation of Ideal and Non-Ideal Airblast From PRISCILLA Computations; and Part II: SHARC Hydrocode Calculations of the PRISCILLA Event (Phase I)

Noel H. Ethridge
John H. Keefer
APPLIED RESEARCH ASSOCIATES, INC.
30 Centennial Lane, P.O. Box 548
Aberdeen, MD 21001

Joseph E. Crepeau
Robert G. Ekler
Lynn W. Kennedy
Charles E. Needham
Shelley H. Rogers
S-CUBED, A DIVISION OF MAXWELL LABORATORIES
2501 Yale Boulevard, SE, Suite 300
Albuquerque, NM 87106

ARL-CR-277 October 1995

prepared under contract

DAAL01-94-P-2125
and
DAAL03-91-C-0034

19951130 060

DTIC QUALITY INSPECTED 5

APPROVED FOR PUBLIC RELEASE; DISTRIBUTION IS UNLIMITED.

NOTICES

Destroy this report when it is no longer needed. DO NOT return it to the originator.

Additional copies of this report may be obtained from the National Technical Information Service, U.S. Department of Commerce, 5285 Port Royal Road, Springfield, VA 22161.

The findings of this report are not to be construed as an official Department of the Army position, unless so designated by other authorized documents.

The use of trade names or manufacturers' names in this report does not constitute indorsement of any commercial product.

REPORT DOCUMENTATION PAGE

Form Approved
OMB No. 0704-0188

Public reporting burden for this collection of information is estimated to average 1 hour per response, including the time for reviewing instructions, searching existing data sources, gathering and maintaining the data needed, and completing and reviewing the collection of information. Send comments regarding this burden estimate or any other aspect of this collection of information, including suggestions for reducing this burden, to Washington Headquarters Services, Directorate for Information Operations and Reports, 1215 Jefferson Davis Highway, Suite 1204, Arlington, VA 22202-4302, and to the Office of Management and Budget, Paperwork Reduction Project (0704-0188), Washington, DC 20503.

1. AGENCY USE ONLY *(Leave blank)*

2. REPORT DATE
October 1995

3. REPORT TYPE AND DATES COVERED
Final, 12 March 1992 - 30 May 1995

4. TITLE AND SUBTITLE Real (Non-Ideal) Surface Effects on Nuclear Explosion Airblast From PRISCILLA-Type Events, Part I: Comparison and Evaluation of Ideal and Non-Ideal Airblast From PRISCILLA Computations; and Part II: SHARC Hydrocode Calculations of the PRISCILLA Event (Phase I)

5. FUNDING NUMBERS
C: DAAL01-94-P-2125
C: DAAL03-91-C-0034

6. AUTHOR(S)
Noel H. Ethridge and John H. Keefer (ARA, Inc.), and Robert G. Ekler, Lynn W. Kennedy, and Charles E. Needham (S-Cubed)

7. PERFORMING ORGANIZATION NAME(S) AND ADDRESS(ES)
Applied Research Associates, Inc.
30 Centennial Lane
P.O. Box 548
Aberdeen, MD 21001

S-Cubed
Albuquerque Office
A Division of Maxwell Laboratories
2501 Yale Blvd, SE, Suite 300
Albuquerque, NM 87106

8. PERFORMING ORGANIZATION REPORT NUMBER

9. SPONSORING/MONITORING AGENCY NAME(S) AND ADDRESS(ES)
U.S. Army Research Laboratory
ATTN: AMSRL-WT-NC
Aberdeen Proving Ground, MD 21005-5066

10. SPONSORING/MONITORING AGENCY REPORT NUMBER
ARL-CR-277

11. SUPPLEMENTARY NOTES
The point of contact for this report is Richard E. Lottero, U.S. Army Research Laboratory, ATTN: AMSRL-WT-NC, Aberdeen Proving Ground, MD 21005-5066.

12a. DISTRIBUTION/AVAILABILITY STATEMENT
Approved for public release; distribution is unlimited.

12b. DISTRIBUTION CODE

13. ABSTRACT *(Maximum 200 words)*
An extensive analysis of the 24 June 1957 PRISCILLA 36.6 KT nuclear event at a 700 ft height of burst over a desert surface at the Nevada Test Site is presented, along with early time results from three hydrocode computations simulating that event. The computations included simulations of ideal, actual desert, and grassland surfaces. The desert computation produced reasonable agreement with most of the data from PRISCILLA. However, the precursor was not as advanced as that observed. The grassland computation produced a strong and persistent precursor. There was a mismatch between arrival times used for developing the thermal layers and those actually computed, indicating the need for coupling of the SHARC hydrocode and the THRML thermal layer codes. Both desert and grassland cases produced enhanced dynamic pressure impulses that attained a maximum of a factor of 8 above ideal in the range of concern to Army equipment. Overturning computations for combat vehicles showed ranges for overturning were extended by factors as large as 1.8 over ideal ground ranges. These effects have implications for Army tactics and doctrine and show the need for continuing non-ideal computations for other surfaces, yields, and heights of burst. Recommendations for further studies are included.

14. SUBJECT TERMS
airblast, non-ideal airblast, ideal airblast, SHARC code, THRML code, precursor, vehicle overturning, dynamic pressure impulse, thermal layer, blast simulation, blast effects, PRISCILLA, perturbed airblast, turbulence

15. NUMBER OF PAGES
350

16. PRICE CODE

17. SECURITY CLASSIFICATION OF REPORT	18. SECURITY CLASSIFICATION OF THIS PAGE	19. SECURITY CLASSIFICATION OF ABSTRACT	20. LIMITATION OF ABSTRACT
UNCLASSIFIED	UNCLASSIFIED	UNCLASSIFIED	UL

INTENTIONALLY LEFT BLANK.

REAL SURFACE (NON-IDEAL) EFFECTS ON NUCLEAR EXPLOSION AIRBLAST FROM PRISCILLA-TYPE EVENTS

PART I: Comparison and Evaluation of Ideal and Non-Ideal Airblast from PRISCILLA Computations

Noel H. Ethridge
John H. Keefer

Accesion For	
NTIS CRA&I	☑
DTIC TAB	☐
Unannounced	☐
Justification	
By	
Distribution /	
Availability Codes	
Dist	Avail and / or Special
A-1	

30 June 1995

Applied Research Associates, Inc.
30 Centennial Lane, P. O. Box 548
Aberdeen, MD 21001

Contract Number DAAL01-P-2125 with
Army Research Laboratory
Aberdeen Proving Ground, MD 21005

Scientific Services Agreement with Battelle Corporation,
Task Control No. 91603, Delivery Order No. 0069, under
Contract No. DAAL03-91-C-0034, sponsored by the
Army Research Laboratory, Aberdeen Proving Ground, MD 21005

INTENTIONALLY LEFT BLANK.

PREFACE

This report presents work performed by the Aberdeen Research Center office of Applied Research Associates, Inc. (ARA), Aberdeen, Maryland, under Purchase Order DAAL01-94-P-2125 for Engineering Services for the Army Research Laboratory (ARL), Aberdeen Proving Ground, Maryland. The services to be provided were to support, compare, and evaluate three state-of-the-art hydrocode computations of blast from the nuclear explosion PRISCILLA over three surfaces: ideal; desert, simulating the PRISCILLA event; and grassland, which was expected to produce a very non-ideal blast wave. These services and the three hydrocode computations were part of the ARL non-ideal blast program.

The hydrocode computations were performed by the Albuquerque, New Mexico, office of S-Cubed, a Division of Maxwell Laboratories, with support from the La Jolla, California, office of S-Cubed. The computations were performed in two phases. In the first phase, the computations were carried to two seconds for all three cases. The second phase was performed when additional funding became available, and the three cases were run to completion at four seconds.

In the first phase, the S-Cubed ideal and desert computations were supported by a subcontract from ARA, who had a Scientific Services Agreement with the Battelle Corporation, Task Control No. 91603, Delivery Order No. 0069, authorized under Contract DAAL03-91-C-0034. Battelle is the contracting agency for the Army Research Office. The first phase of the grassland computation was partially supported by the Defense Nuclear Agency under contract DNA001-92-C-0165. These phase one computations are presented in the report as Part II:

Crepeau, J. E., R. G. Ekler, L. W. Kennedy, C. E. Needham, and S. H. Rogers. "SHARC Hydrocode Calculations of the PRISCILLA Event." S-Cubed Report No. SSS-DTR-93-14269.

This Phase I report is included because it presents information not contained in the Phase II reports listed below that present the completed computations. The reader is cautioned that the Phase I report in Part II is numbered independently from Part I, including page and figure numbering and appendix information.

In Phase II, the ideal and desert computations were run to completion at four seconds by S-Cubed under Contract DAAL01-94-P-1217 with the ARL. The results are presented in the following report:

Needham, C. E., R. G. Ekler, and L. W. Kennedy. "Extended Desert Calculation Results with Comparisons to PRISCILLA Experimental Data and a Near-Ideal Calculation." S-Cubed Report No. SSS-DTR-94-14802. This report was published as an ARL contractor report, ARL-CR-235, in July 1995.

The grassland computation was completed under Contract DAAL01-94-P-2257 with the ARL. The work is contained in the following report:

Ekler, R. G., C. E. Needham, and L. W. Kennedy. "Extended Grassland Calculation Results With Comparisons to PRISCILLA Experimental Data and a Near-Ideal Calculation." S-Cubed Report No. SSS-DFR-94-14920. This report was published as an ARL contractor report, ARL-CR-236, in July 1995.

The Defense Nuclear Agency provided time on their computer for these computations.

Additional data from the computations were provided by Mr. Ken Schneider of the Albuquerque office of S-Cubed, and are contained in Appendix A.

Part I of this report was prepared utilizing the material presented in the three S-Cubed reports and in supplementary communications.

ACKNOWLEDGEMENTS

Mr. Rich Lottero, the director of the non-ideal blast program at the Army Research Laboratory (ARL), provided many valuable technical discussions, guidance and assistance. We thank Mr. Bud Raley of ARL for his forceful support of a non-ideal blast program and for his vision of what its output should be, and Mr. Klaus Opalka and Mr. Steve Schraml of ARL for valuable technical discussions.

Dr. John Polk of the Army Research Laboratory was the contract technical monitor on the contract through Battelle, and we thank him very much for valuable technical discussions, guidance, and assistance. Dr. Layman Franklin of Battelle provided excellent assistance in his role as contract administrator for Battelle.

The authors greatly appreciate the enthusiastic cooperation and assistance of the S-Cubed personnel in this examination of their computational study of non-ideal blast. The many technical discussions and explanations of features of the codes and the results of the computations provided by Mr. Charles Needham and Dr. Lynn Kennedy of the Albuquerque office were invaluable. The supplementary tabulations and explanations of unusual features in the computational results provided by Mr. Ken Schneider of the S-Cubed Albuquerque office were essential for this report and are very much appreciated.

We thank Dr. Shelley Rogers and Dr. Jim Barthel of the La Jolla office of S-Cubed for information on the THRML code and many useful discussions of its characteristics and capabilities. We thank Dr. Barthel for his description of a proposed program to improve the THRML code, which is contained in Appendix B.

Mr. Jerry Carpenter, Carpenter Research Corporation, and Mr. Tom Mazzola of RDA provided many useful discussions and data concerning thermal layers, information on boundary layers, and aspects of hydrocode computations. Mr. Carpenter supplied the sound speed versus ground range data derived from experimental arrival time measurements that were used to construct the desert thermal layer.

We have utilized much material from the people listed above. The responsibility for any misinterpretations and errors is our own.

The prompt response of Mr. Ed Martin of DASIAC for weapons tests reports and other related reports is greatly appreciated.

We express our appreciation to Ms. Sheila Fischer and Ms. Jennifer Heninger of the Rocky Mountain Division of ARA for their preparation of viewgraphs, figures, and tables and for providing other support for this project.

TABLE OF CONTENTS

		Page
	PREFACE	v
	ACKNOWLEDGMENTS	vii
	LIST OF FIGURES	xi
	LIST OF TABLES	xv
1.	INTRODUCTION	1
2.	OBJECTIVES	3
3.	THE PRISCILLA EVENT	3
4.	THE THRML CODE	18
5.	THE DESERT THERMAL LAYER	20
6.	THE GRASSLAND THERMAL LAYER	21
7.	THE HYDROCODE	28
8.	THE SHARC COMPUTATIONS	28
8.1	Ideal Surface Computation	29
8.2	The Desert Surface Computation	30
8.3	The Grassland Surface Computations	34
9.	RESULTS AND DISCUSSION	35
9.1	Arrival Times	38
9.2	Waveforms	41
9.3	Estimation of Peak Overpressures from the Ideal Surface Computation	54
9.4	Comparison of Ideal Peak Overpressures and Dynamic Pressure Impulses With Predictions by REFLECT-4	56
9.5	Comparison of Computed Overpressures with PRISCILLA Experimental Data	60
9.6	Comparison of Dynamic Pressure Impulse Over Desert With Experimental Data	60

Page

9.7 Comparison of Dynamic Pressure Impulse for the Three Computations 64
9.8 Enhancement of dynamic Pressure Impulse versus Ground Range 64
9.9 Non-Ideal Blast Extensions of Vehicle Overturning Limits 68
9.10 System Design Implications 73
9.11 Implications for Simulation Tests 75

10. CONCLUSIONS 76

11. REFERENCES 78

APPENDIX A: TABULATIONS FOR DESERT, GRASSLAND, AND IDEAL COMPUTATIONS A-1

APPENDIX B: SUGGESTED PROGRAM FOR IMPROVEMENT OF THERMAL LAYER PREDICTIVE CAPABILITY B-1

APPENDIX C: PRISCILLA BLAST DATA C-1

APPENDIX D: CONVERSION TABLE D-1

DISTRIBUTION LIST DIST-1

LIST OF FIGURES

Figure		Page
1	Main blast line gage layout for Project 1.1, BRL, WT-1401	5
2	Main blast line gage layout for Project 1.3, SRI, WT-1403	6
3	View of the PRISCILLA event showing the great variation in raised dust clouds with azimuth. The view is perpendicular to the main blast line which is to the left of the explosion column	8
4	Station locations used for all three calculations	19
5	Thermal layer sound speed for PRISCILLA main blast line as derived by J. Carpenter	22
6	PRISCILLA sound speed versus range as used for desert surface computations (Part II of this report),(2)	23
7	Grassland sound speeds versus height and ground range predicted by THRML (assuming shock arrival times from the PRISCILLA test)	26
8	PRISCILLA grassland maximum sound speed versus ground range compared with desert sound speeds	27
9	Mesh configuration at initiation of first phase, ideal surface computation	31
10	Mesh configuration at initiation of second phase, ideal surface computation	32
11	Initial configuration for grassland and desert surface calculations	33
12	Comparison of blast wave pressure contours at 200 ms after detonation when overpressure at the base of the ideal Mach stem is 155 psi	36
13	Comparison of blast wave pressure contours at 500 ms after detonation when overpressure at the base of the ideal Mach stem is 44 psi	37
14	Comparison of arrival times from the ideal, desert, and grassland SHARC computations	39
15	Differences in arrival times at surface level between the ideal computation and desert and grassland cases, and measured desert values from the Stanford Research Institute (SRI) surface gage measurements. The larger the difference, the earlier the arrival	40

LIST OF FIGURES (continued)

Figure		Page
16	Comparison of overpressure waveforms at 1650 ft (503 m) for grassland, desert, and PRISCILLA data with ideal waveforms	43
17	Comparison of overpressure waveforms at 2000 ft (610 m) for grassland, desert, and PRISCILLA data with ideal waveforms	44
18	Comparison of overpressure waveforms at 2250 ft (686 m) for grassland, desert, and PRISCILLA data with ideal waveforms	45
19	Comparison of overpressure waveforms at 2500 ft (762 m) for grassland, desert, and PRISCILLA data with ideal waveforms	46
20	Comparison of overpressure waveforms at 3000 ft (914 m) for grassland, desert, and PRISCILLA data with ideal waveforms	48
21	Comparison of overpressure waveforms at 3500 ft (1067 m) for grassland, desert, and PRISCILLA data with ideal waveforms. The computed dynamic pressure waveforms for desert and ideal computations are shown in the right-hand panel	49
22	Comparison of overpressure and dynamic pressure waveforms at 4000 ft (1219 m) for grassland, desert, and PRISCILLA data with ideal waveforms	50
23	Comparison of computed dynamic pressure waveforms at 4500 ft (1372 m) from the grassland, desert, and ideal computations	52
24	Comparison of overpressure and dynamic pressure waveforms at 5000 ft (1524 m) for grassland, desert, and PRISCILLA data with ideal waveforms	53
25	The initial part of the ideal overpressure waveform at 1371.6 meters, showing the damped oscillations at the front	55
26	Comparison of overpressures from the ideal PRISCILLA computation to a curve of REFLECT-4 values scaled to PRISCILLA conditions	57
27	Comparison of dynamic pressure impulse from a 200-foot scaled height of burst REFLECT-4 computation with the horizontal dynamic pressure impulse at an elevation of 0.914 meters (3 ft) from the the ideal computation	59
28	Comparison of maximum overpressure from the ideal and desert computations with experimental data from SRI and BRL gages on the surface	61

LIST OF FIGURES (concluded)

Figure		Page
29	Comparison of horizontal dynamic pressure impulse versus range at the 3 ft (0.914 m) elevation from the desert computation with experimental data and the impulse from the ideal computation. Ranges for ideal overpressures are indicated by the arrows	62
30	Comparison of horizontal dynamic pressure impulse versus range at the 10 ft (3.048 m) elevation from the desert computation with experimental data and the impulse from the ideal computation	63
31	Dynamic pressure impulse at the 3-ft (0.914 m) elevation versus ground range for the ideal, desert, and grassland computations	65
32	Horizontal dynamic pressure impulse versus ground range at the 10-ft (3.048 m) elevation for the three computations. The peak at 1370 meters for the grassland was computed and appears to correspond to passage of a vortex	66
33	Enhancement in horizontal dynamic pressure impulse above ideal at the 3-ft (0.914 m) elevation versus ground range for the desert and grassland cases. The arrows at the top of the figure show the ranges for ideal shock overpressures	67
34	Ratio of ground ranges for equal dynamic pressure impulse versus ideal shock overpressure	69
35	Increase in non-ideal ground range over ideal ground range versus horizontal dynamic pressure impulse. The arrows show the predicted levels of DPI for overturning (side-on orientation) of the vehicles computed using the BRL overturning code with ideal waveforms and reduced diffraction loading	70
36	Displacement versus dynamic pressure impulse for Jeeps exposed side-on to long-duration blast waves. Computed overturning levels for vehicles are shown by arrows at the top of the figure	72
37	Comparison of the DPI levels for overturning of vehicles with the DPI versus ground range curves for the three computations. The arrows show the increase in range for overturning of the tank, the heavy armored vehicle (HAV), the light armored vehicle (LAV), and loaded truck produced by the enhancement of dynamic pressure impulses above the ideal values	74

INTENTIONALLY LEFT BLANK.

LIST OF TABLES

Table		Page
1	The PRISCILLA event	4
2	PRISCILLA overpressure data - as-read values from original records	9
3	Mach number and dynamic pressures from SRI gages on PRISCILLA	11
4	BRL Q-gage results, main blast line, maximum values	12
5	BRL Q-gage results, Project 3.4, maximum values	13
6	BRL Q-gage results, Project 4.3/33.2, maximum values	13
7	Stations for the PRISCILLA computations	15
8	Vegetation and soil parameters used in THRML for PRISCILLA grassland thermal layer	25
9	Estimated peak values of surface-level overpressure derived from the computed ideal waveforms	58

INTENTIONALLY LEFT BLANK.

COMPARISON AND EVALUATION OF COMPUTATIONS OF IDEAL AND NON-IDEAL AIRBLAST FOR PRISCILLA CONDITIONS

1. INTRODUCTION

The Army is interested in the effects and consequences of non-ideal air blast environments produced by nuclear weapon detonations over the ground surface. The lethality to enemy ground targets and the survivability of Army tactical equipment can be significantly affected. The results from tests of nuclear devices at the Nevada Test Site and at the Pacific Proving Grounds show that explosions in the tactical yield range over desert or coral sand can produce non-ideal airblast that extends the damage radii of tactical Army equipment.

Future conflicts may occur in terrain with different soil compositions and different ground covers. To estimate to what extent non-ideal blast occurs and its effects, techniques must be developed to derive the blast environment in the range of interest for Army tactical equipment - approximately 30 to 5 psi for an undisturbed or ideal blast wave.

To evaluate current prediction techniques and develop recommendations for their improvement, the Army Research Laboratory at the Aberdeen Proving Ground, Maryland, sponsored three state-of-the-art computations of the PRISCILLA event, a nuclear explosion in the 1957 PLUMBBOB series at the Nevada Test Site. Why was PRISCILLA selected?

(1) PRISCILLA was of a yield appropriate for tactical nuclear weapons, 36.6 kilotons.

(2) PRISCILLA was detonated at a height of burst above the surface that is normally used for tactical nuclear weapons.

(3) PRISCILLA was suspended by a balloon, and therefore did not have any heavy shielding around the device. Hence its output was representative of a weapon.

(4) The ground surface was a flat smooth desert lake bed.

(5) Weather conditions were excellent.

(6) PRISCILLA was heavily instrumented, providing data for comparison with

computations. The instrumentation was much improved over that used in earlier tests.

(7) The armed services had many military projects on PRISCILLA, including minefields, foxholes, bunkers, vehicles, etc. (1).

(8) There were previous computations of the PRISCILLA event.

The first of the sponsored computations was that for the explosion of the PRISCILLA device under conditions that would produce an ideal blast wave, undisturbed by the development of a thermal layer or the raising and ingestion of dust. This computation was intended to provide the reference computation for comparison with changes produced by non-ideal blast.

The second computation was intended to duplicate the PRISCILLA event and produce computed waveforms for direct comparison with measured waveforms. This computation required predictions of the thermal layer and dust raising and ingestion.

The third computation was for the PRISCILLA event with the ground surface covered by vegetation, a layer of dry grass. This condition was expected to produce a thermal layer with different characteristics and greater extent than that produced over the desert surface, and provide an indication of the maximum non-ideal effects for a PRISCILLA event.

These computations were performed by S-Cubed. Their THRML code was used to predict thermal layers, and the SHARC code was used to compute the blast field. The original plan for the three computations was that they would all be run with the same fine zone size on the same machine so that the only changes in output from the ideal computations would be that produced by the thermal layers and dust. However, it was necessary to use larger zones for the desert and grassland computations because of the very long computing times required for these non-ideal computations.

The S-Cubed computations are described in three reports. The first (Part II of this report) describes the ideal, desert and grassland computations that were run to two seconds and were incomplete. The resources available did not provide for the

computations to be carried to the times necessary to describe the full positive phase of the five psi waveform. Eventually additional support was provided by ARL, and extended computations of the ideal, desert and grassland surfaces were run to four seconds and completed (2, 3).

2. OBJECTIVES.

The objectives for ARA in this work were to support, compare, and evaluate computations performed by S-Cubed of the blast fields from three variations on the PRISCILLA event, to describe the military significance of the non-ideal effects, and to make recommendations for further work.

3. THE PRISCILLA EVENT.

Event PRISCILLA was the fifth nuclear detonation of Operation PLUMBBOB. The purpose of the PLUMBBOB series was to test nuclear devices for possible inclusion in the United States arsenal. In all, 24 test events were included in the PLUMBBOB operation in 1957 at the Nevada Test Site.

The PRISCILLA device was suspended from a tethered balloon at a height of 700 feet (213.4 meters) above the dry lake bed of Frenchman Flat in Area 5 of the Nevada Test Site. The device was detonated at 0630 on June 24, 1957. At the time of the detonation the sky was clear and sunny. Winds were calm at surface level and blowing moderately out of the southwest above 2000 feet from the surface. Table 1 lists further details.

The main blast line was covered with a layer of loose powder composed of extremely fine dust particles. On other blast lines and at other gage locations where traffic had not been as extensive there was not as much free dust.

Three agencies made blast measurements. The Ballistic Research Laboratories (BRL) (WT 1401 and WT 1426)(4,5), the Stanford Research Institute (SRI) (WT 1403)(6),

Table 1. The PRISCILLA event.

Operation:	PLUMBBOB, Shot 5
Date and time:	24 June 1957 at 0630 Pacific Daylight Time
Location:	Frenchman Flat, Nevada Test Site
Shot yield:	36.6 KT
Height of burst:	700 feet (213.4 meters)
Support:	Tethered balloon
Surface elevation:	3076 feet (937.6 meters)
Ambient air pressure:	
Burst height:	12.86 psi (886.7 millibars)
Surface:	13.19 psi (909.4 millibars)
Ambient air temperature:	
Burst height:	24 +- 2 degrees Celsius
Surface:	17.5 +- 1 degrees Celsius
Relative humidity:	
Burst height:	20 +- 2
Surface:	29
Surface wind:	Calm

Modlfied Sachs' scaling factors to one kiloton at sea level at 15 degrees Celsius:

Pressure	Distance	Time	Impulse
Sp = 1.1145	Sd = 0.2905	St = 0.2918	Si = 0.3252

Scaled height of burst: 203.4 feet (62.0 meters)

Frenchman Flat is a dry lake bed that is flat and has a soil composed of very fine particles. Loose dust up to several inches thick was created by traffic, the large amount of excavation, and heavy construction. There were several blast lines. The main blast line and several auxilliary blast lines were heavily instrumented. The main blast line was very dusty. A strong precursor was formed on PRISCILLA near 500 feet (152.4 meters) ground range and was dissipated by 4500 feet (1372 meters). A shot was fired in the same area in 1955.

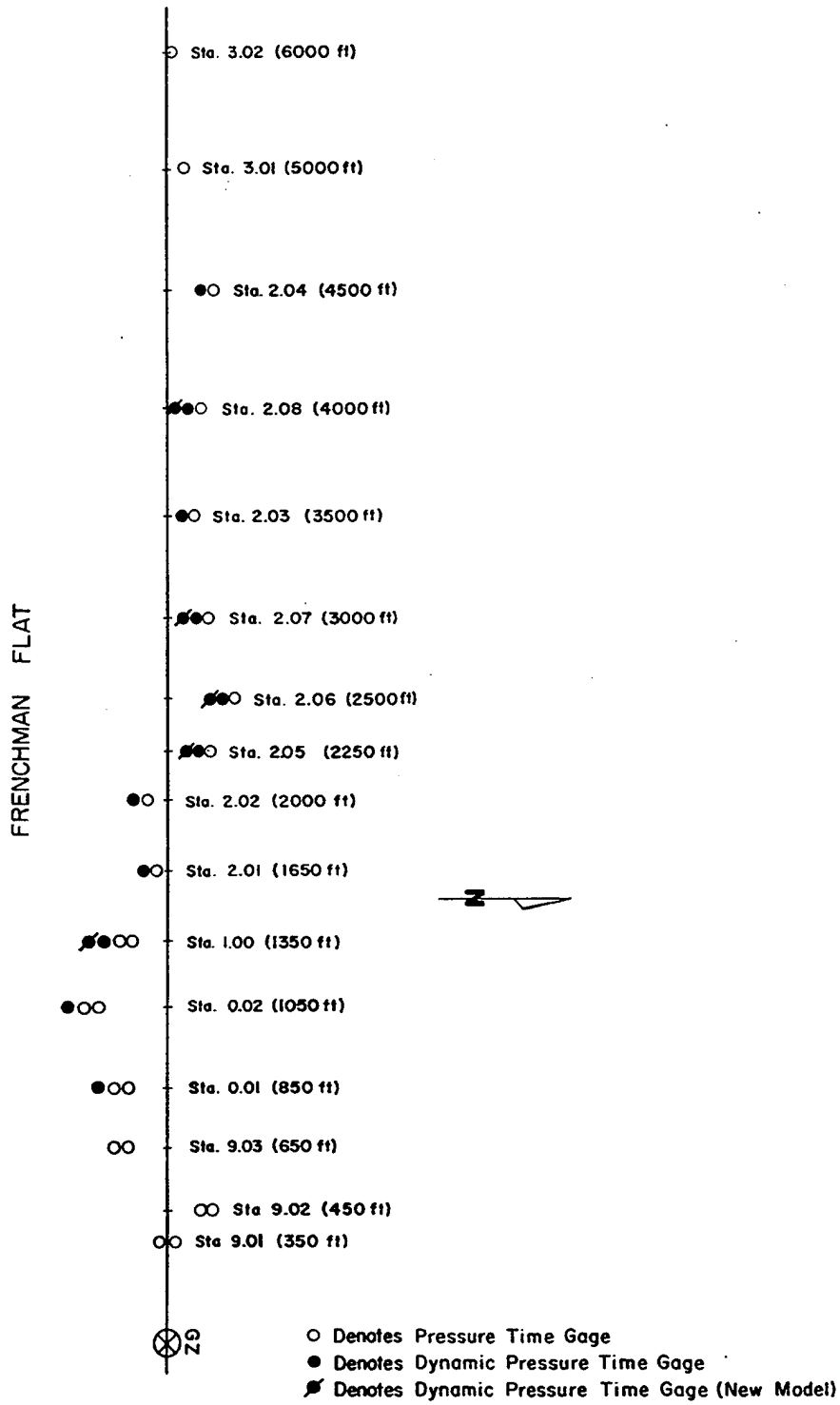

Figure 1. Main blast line gage layout for Project 1.1, BRL, WT-1401.

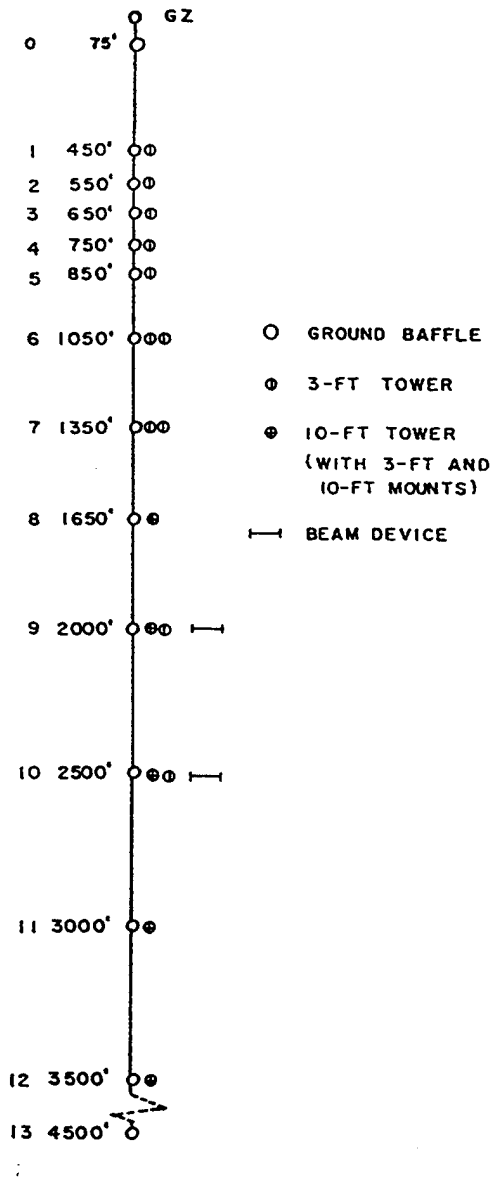

Pressure gage layout.

PROJECT 1.3 GAGE LAYOUT

Station Number	Ground Range ft	Gage Code*	Predicted Peak psi	Galvanometer Frequency cps
0		OB	1,500	300
1	450	1B	750	300
		1Z3	1,320	300, 300
2	550	2B	600	300
		2Z3	1,150	300, 200
3	650	3B	450	300
		3Z3	1,450	300
4	750	4B	320	300
		4Z3	1,240	300, 200
5	850	5B	200	300
		5Z3	1,000	300, 200
6	1,050	6B	100	300
		6Z3	730	300, 300
		6Q3	630	300
7	1,350	7B	50	300
		7Z3	465	300, 300
		7Q3	415	300
8	1,650	8B	33	300
		8P3	33	300
		8Q3	270	300
		8P10	33	300
		8Q10	270	300, 300
9	2,000	9B	21	300
		9Z3	175	300
		9P3	21	300
		9Q3	155	300
		9P10	21	300
		9Q10	155	300, 300
		9F3	—	300
10	2,500	10B	12.5	300
		10Z3	71	300
		10P3	12.5	300
		10Q3	56	300
		10P10	12.5	300
		10Q10	56	300, 300
		10F3	—	300
11	3,000	11B	8.4	300
		11P3	8.4	300
		11Q3	21	300
		11P10	8.4	300
		11Q10	21	300, 300
12	3,500	12B	8.3	300
		12P3	8.3	300
		12Q3	7	300
		12P10	8.3	300
		12Q10	7	300, 300
13	4,500	13B	6.5	300

* Station number, gage type, and gage height. B = surface-level, baffle-mounted pressure gage; P = side-on (overpressure) component, pitot-tube; Q = subsonic pitot-tube, dynamic pressure; and Z = supersonic total-pressure gage.

Figure 2. Main blast line gage layout for Project 1.3, SRI, WT-1403.

and Sandia Corporation (SC) (WT 1405, ITR 1472, and WT 1472)(7,8,9). Figure 1 shows the BRL gage layout on the main blast line. Figure 2 shows the layout of SRI stations and gages. From a range of 2250 feet out the gages of the two agencies were on opposite sides of the blast line.

The BRL used mechanical self-recording gages triggered by a photocell with a low melting point thermal link as backup, or by a hard-wire signal. A pressure capsule drove a stylus that scratched a very fine line on an aluminized disk mounted on a turntable. The turntable was driven by a very well regulated motor supplied with battery power. One version of the gage was designed to be placed in the ground for a surface measurement. Another version was in the form of a cylindrical probe for measuring stagnation pressure and side-on overpressure at elevation for deriving dynamic pressure. The self-recording gages were used on many shots on Operation PLUMBBOB because they were complete self-initiating systems that were immune to nuclear radiation effects and electromagnetic pulse effects, and were easy to transport and install.

The motor speeds were calibrated. However, there was no timing device in each gage to periodically mark the rotating disk. (A modification to provide such independent timing appeared on later models.) Thus the timing on the PRISCILLA records is not as reliable as that provided by electronic recording. Normally the timing error would be a few percent, but a few records differ from SRI records by a factor of 1.5, which suggests that an error occurred in processing the data. The cause is not known at this time.

The SRI and SC used electronic gages. The SRI had two types of gages to measure dynamic pressure. One was a SC-designed cylindrical probe with a hemispherical nose like the BRL probe. It was designed for subsonic use, and measured differential pressure and the side-on overpressure. A total head probe for use in supersonic flow was designed by SRI. It had a bleed port to reduce the possibility of dust clogging.

The SC designed and used two other probe gages. One was designed to measure the air stagnation pressure only, with a minimum of influence of the dust (SNOB gage).

Figure 3. View of the PRISCILLA event showing the great variation in raised dust clouds with azimuth. The view is perpendicular to the main blast line which is to the left of the explosion column.

Table 2. PRISCILLA overpressure data - as-read values from original records.

Station Number	Horizontal Distance	Maximum Overpressure	Arrival Time	Positive Duration	Positive Impulse	Wave Type	Agency and Source	Record Quality
	feet	psi	msec	msec	psi-msec			
9039.01	350	1,030	-	-	-	-	BRL WT 1401	Poor
9039.02	450	760	-	-	-	-	BRL WT 1401	Peak
	450	750	-	175	-	I	BRL WT 1401	Good
9039.03	650	480	364	95	10,563	II	BRL WT 1401	Poor
	650	400	676	162	8,896	II	BRL WT 1401	Good
9040.01	850	225	-	236	11,957	II	BRL WT 1401	Good
	850	206	-	-	-	II	BRL WT 1401	Peak
9040.02	1,050	125	-	233	6,156	II	BRL WT 1401	Good
	1,050	138	-	195	5,613	II	BRL WT 1401	Good
9041.00	1,350	60	-	343	4,503	II	BRL WT 1401	Good
	1,350	62	512	280	4,501	II	BRL WT 1401	Good
9042.01	1,650	31	-	467	3,973	II	BRL WT 1401	Good
9042.02	2,000	16.3	-	-	-	-	BRL WT 1401	Peak
9042.05	2,250	12.4	570	687	4,039	III	BRL WT 1401	Good
9042.06	2,500	9.2	523	852	4,179	III	BRL WT 1401	Good
9042.07	3,000	9.1	912	727	2,849	IV	BRL WT 1401	Good
9042.03	3,500	9.9	-	-	-	-	BRL WT 1401	Peak
9042.08	4,000	8.8	1,729	818	2,595	IV	BRL WT 1401	Good
9042.04	4,500	7.4	-	-	-	-	BRL WT 1401	Peak
9043.01	5,000	5.9	2,485	916	-	V	BRL WT 1401	Good
9014.01A	860	175	148	260	11,516	II	BRL WT 1426	Good
9014.02A	1,040	118	1,155	254	5,513	II	BRL WT 1426	Good
9014.03A	1,360	56	-	-	-	-	BRL WT 1426	Peak
9016.01A	970	145	603	234	6,797	II	BRL WT 1426	Good
9016.04C	1,040	122	116	206	4,883	II	BRL WT 1426	Good
9016.05	1,150	98	128	336	6,919	II	BRL WT 1426	Good
9019.01A	1,150	101	-	-	-	-	BRL WT 1426	Peak
9019.03B	1,360	56	-	361	5,703	II	BRL WT 1426	Good
8002.00	1,650	37	222	476	5,607	II	BRL WT 1426	Good
8003.01	1,250	97	-	-	-	-	BRL WT 1426	Peak
8003.02	1,450	49	-	-	-	-	BRL WT 1426	Peak
8003.03	1,750	33	304	529	5,118	II	BRL WT 1426	Good
8015.01	2,030	13.0	317	610	4,227	III	BRL WT 1426	Good
8015.02	2,280	13.8	433	661	3,830	III	BRL WT 1426	Good
8015.03	2,730	9.0	826	737	3,329	III	BRL WT 1426	Good
8015.04	3,930	8.8	1,764	823	2,574	V	BRL WT 1426	Good
8015.05	4,770	6.3	2,297	920	2,202	V	BRL WT 1426	Good
8015.06	5,320	4.9	-	-	-	-	BRL WT 1426	Peak

Table 2. PRISCILLA overpressure data - as-read values from original records (continued).

Station Number	Horizontal Distance	Maximum Overpressure	Arrival Time	Positive Duration	Positive Impulse	Wave Type	Agency and Source	Record Quality
	feet	psi	msec	msec	psi-msec			
1B	450	554	103	-	-	I	SRI WT 1403	Poor
2B	550	366	116	-	-	II	SRI WT 1403	Peak
3B	650	342	131	149	12,200	II	SRI WT 1403	Good
4B	750	229	146	164	10,100	II	SRI WT 1403	Good
5B	850	221	163	197	11,200	II	SRI WT 1403	Good
6B	1,050	101	201	314	9,150	II	SRI WT 1403	Good
7B	1,350	59.1	268	357	6,620	II	SRI WT 1403	Good
8B	1,650	37.2	350	395	5,020	II	SRI WT 1403	Good
9B	2,000	31.9	475	510	5,820	II	SR WT 1403	Good
10B	2,500	11.3	716	774	4,540	III	SRI WT 1403	Good
11B	3,000	10.9	1,049	789	3,660	IV	SRI WT 1403	Good
12B	3,500	7.7	1,445	490	1,670	IV	SRI WT 1403	Poor
F-1.5-9012.01	650	270	130	211	14,200	II	SC WT 1405	Good
F-1.5-9012.02	850	187	164	235	9,700	II	SC WT 1405	Good
F-1.5-9012.03	1,050	120	203	307	7,800	II	SC WT 1405	Good
F-1.5-9012.04	1,350	59.1	270	442	6,500	II	SC WT 1405	Good
PGB	1,150	85.0	223	406	8,140	II	SC WT 1472	Good
PGB	1,700	32.0	370	445	5,680	II	SC WT 1472	Good
PGBU	1,700	35.0	369	710	6,920	II	SC WT 1472	Good
PGBU	1,800	22.0	403	720	5,640	II	SC WT 1472	Good
PGBU	1,800	21.5	402	558	5,180	II	SC WT 1472	Good
PGB	1,900	27.5	439	573	4,200	II	SC WT 1472	Good
PGBa	2,000	25.5	483	549	4,960	II	SC WT 1472	Good
PGBb	2,000	24.5	484	595	4,240	II	SC WT 1472	Good
PGB	2,100	15.1	524	575	3,810	III	SC WT 1472	Good
9031.01A	760	235	81	-	-	II	BRL WT 1426	Poor
B	760	225	101	178	7,048	II	BRL WT 1426	Good
C	760	210	54	-	-	II	BRL WT 1426	Poor
9031.02A	1,040	115	136	253	5,358	II	BRL WT 1426	Good
B	1,040	105	131	285	6,219	II	BRL WT 1426	Good
C	1,040	112	147	307	7,367	II	BRL WT 1426	Good
D	1,040	110	189	256	6,523	II	BRL WT 1426	Good
9031.03A	1,360	60	200	404	6,414	II	BRL WT 1426	Good
B	1,360	40	255	-	-	-	BRL WT 1426	Poor
1A	1,430	40	927	403	4,766	II	BRL WT 1426	Good
2A	1,720	28	1,901	401	3,326	II	BRL WT 1426	Good
3A	2,280	11	300	600	3,719	III	BRL WT 1426	Good
5B	3,900	9.2	-	842	3,286	V	BRL WT 1426	Good

Table 3. Mach number and dynamic pressure from SRI gages on PRISCILLA.

Station	Ground Range (ft.)	Gage Height (ft.)	Mach No. Calculation Method	Maximum Mach No.	Time of Maximum Mach No. (sec.)	Maximum Dynamic Pressure (psi)	Time of Maximum Dynamic Pressure (sec)	Maximum Differential Pressure (pitot) (psi)	Time of Maximum Differential Pressure (pitot) (sec)	Maximum Total-Head Minus Static Pressure (psi)	Time of Maximum Total-Head Minus Static Pressure (sec)	Dynamic Pressure Impulse (psi-sec)	Remarks
As-read from original records													
1	450	3	Z	0.93*	0.124	258	0.109	--	--	310	0.112	--	Partial record
2	550	3	Z	1.89*	0.119	287	0.126	--	--	373	0.126	--	Partial record
3	650	3	Z	1.73*	0.139	211	0.150	--	--	270	0.150	--	Partial record
4	750	3	Z	1.63*	0.163	211	0.169	--	--	308	0.169	--	Partial record
5	850	3	Z	1.88	0.192	309	0.201	--	--	498	0.200	9.3	Good record
6	1,050	3	Z	2.17	0.257	225	0.271	--	--	519	0.266	8.3	Good record
7	1,350	3	Z	2.33	0.382	143	0.390	--	--	412	0.386	6.8	Good record
8	1,650	3	$\Delta p + Q$	1.81	0.480	44.1	0.475	98.1	0.480	--	--	9.2	Record did not return to the base line
8	1,650	10	$\Delta p + Q$	2.27	0.525	72.6	0.545	193	0.525	--	--	11.6	Good record
9	2,000	3	$\Delta p + Q$	1.42	0.740	29.0	0.530	42.3	0.530	--	--	8.9	Good record
10	2,500	3	Z	1.26	1.230	23.1	0.758	19.9	0.746	32.51	0.758	8.1	Good record
10	2,500	3	$\Delta p + Q$	1.09	1.260	18.0	0.750	19.9	0.746	--	--	8.1	Good record
10	2,500	10	$\Delta p + Q$	1.36	1.110	27.7	0.825	28.2	0.865	--	--	11.0	Good record
11	3,000	10	$\Delta p + Q$	1.15	1.370	17.5	0.370	20.6	1.370	--	--	5.2	Good record
12	3,500	3	$\Delta p + Q$	0.74	1.890	5.31	1.890	2.81	1.890	--	--	2.9	Good small record

Table 4. BRL Q-gage results, main blast line, maximum values.

Station	Ground Range (ft.)	Gage Height (ft.)	Total Pressure (psi)	Static Overpressure (psi)	Pressure Difference $(P_p - P_o)^{*'}$ (psi)	Dynamic Pressure q* (psi)	Mach No. (u/a)	Dynamic Pressure Impulse DPI (psi)	Remarks
F1.1-9040.01	850	3	--	--	--	--	--	--	Record destroyed by acceleration effects.
F1.1-9040.02	1050	3	470.0	125.0	445.0	240.0	3.3	--	Total head is a partial record. May not be maximum.
F1.1-9041.00	1350	3	275.0	60.0	255.0	150.0	3.6	--	Partial record.
F1.1-9041.00N[x]	1350	3	--	--	--	--	--	--	New prototype gage was effected by acceleration.
F1.1-9042.01	1650	3	143.5	31.0	150.0	80.0	2.3	--	Total head had only a partial record.
F1.1-9042.02	2000	3	58.5	23.0x	44.0	32.0	1.3	--	Gage failed at 240 msec.
F1.1-9042.05N	2250	3	48.0	12.4	36.0	27.0	1.4	--	Acceleration effected prototype gage.
F1.1-9042.06	2500	3	47.0	9.2	38.0	25.0	1.3	5.45	Good record.
F1.1-9042.06Nx	2500	3	35.0	9.2	28.0	19.0	1.2	--	Total head plug by dust.
F1.1-9042.07	3000	3	29.0	9.1	20.0	15.1	1.0	3.18	Good record.
F1.1-9042.07Nx	3000	3	26.5	9.1	20.5	17.0	1.04	3.37	Gage plugs on arrival of main shock.
F1.1-9042.03	3500	3	11.2	8.6x	3.4	2.8	0.45	0.79	Good record.
F1.1-9042.08	4000	3	10.0	9.0	1.3	1.3	0.29	--	Ratio of two small numbers. Good records.
F1.1-9042.08N	4000	3	--	--	--	--	--	--	
F1.1-9042.04	4500	3	7.8	6.5x	1.7	1.2	0.29	0.33	Ratio of two small numbers. Good records.

N, refers to new q-gage. x, values from q-gage.

Table 5. BRL Q-gage results, Project 3.4, maximum values.

Station	Ground Range (ft.)	Gage Height (ft.)	Total Pressure (psi)	Static Overpressure (psi)	Pressure Difference $(P_p - P_o)^{*'}$ (psi)	Dynamic Pressure q* (psi)	Mach No. (u/a)	Dynamic Pressure Impulse DPI (psi)	Remarks
F3.4-9021	900	3	--	--	--	--	--	--	No record.
F3.4-9024.01	4200	3	8.2	6.7x	1.3	1.2	0.28	0.20	Good record but ratio of two small numbers.
F3.4-9022.01	3600	10	13.0	10.2x	3.8	3.7	0.47	0.68	Good record.
F3.4-9022.02	5000	10	6.7	6.0x	1.9	1.8	0.38	0.18	Good record but ratio of two small numbers.

x Obtained from q-gage as opposed to ground baffle gages.

Table 6. BRL Q-gage results, Project 4.3/33.2, maximum values.

Station	Ground Range (ft.)	Gage Height (ft.)	Total Pressure (psi)	Static Overpressure (psi)	Pressure Difference $(P_p - P_o)^{*'}$ (psi)	Dynamic Pressure q* (psi)	Mach No. (u/a)	Dynamic Pressure Impulse DPI (psi)	Remarks
F33.2-8015.01	2030	3	61.0	13.0	51.0	37.0	1.6	--	Partial record.
F33.2-8015.02	2280	3	50.0	13.8	41.0	28.0	1.3	3.5	Good record. Max. corresponds to main shock.
F33.2-8015.03	2730	3	23.7	9.0	14.5	11.5	0.89	2.6	Good record.
F33.2-8015.04	3930	3	11.0	8.8	2.4	2.3	0.39	0.26	Good record. End of precursor.
F33.2-8015.05	4770	3	6.8	6.3	0.9	0.9	0.23	0.26	Good record.
F33.2-8015.06	5320	3	6.4	5.1x	1.2	1.2	0.31	0.28	Good record.
F33.2-8015.07	6120	3	4.9	4.7x	0.3	0.35	0.18	--	Ratio of two small numbers.

x, obtained from q-gage as opposed to ground baffle gage.

Another was designed to record both air stagnation pressure and the pressure generated by dust impacts (GREG gage). The contribution of the dust to pressure measured by the other probe gages was not very well established.

The flow in the precursor region is very turbulent and will vary in magnitude and direction at a fixed station. Because of this off-angle flow the side-on overpressure records from the probes will have errors. The agencies agreed that using the surface-level overpressure record with the elevated total head or differential pressure record should produce a better estimate of the dynamic pressure waveform (10). However, using records from such separated gages would produce differences also.

Comparison of gages located only tens of feet apart on an arc is complicated by the large variations in the character of the precursor, both in waveshape, dust loading, magnitude, and flow direction that can occur. Figure 3 shows the large variation with azimuth of the dust clouds raised by the blast wave on PRISCILLA.

Interpretation of the data is made difficult by the uncertainty in dust registry coefficients, the questions of if and when dust clogging occurred, acceleration effects, thermal effects, off-angle flow, baseline shifts, separation of gages vertically and on an arc, and accuracy of timing on the BRL gages.

Tables 2 through 6 list the results derived from the gage measurements. The data from the main blast line are used in the comparisons with the desert computation. They are listed in Table 2, stations 9039.01 - 9043.01 for BRL and stations 1B - 12B for SRI, Table 3 for SRI and Table 4 for BRL. These data and waveforms were reviewed and a number of corrections were made. Waveforms and additional information are presented in Appendix C.

A minimum list of the ground ranges and elevations (stations) at which waveforms were to be computed in the three computations was constructed, with emphasis on stations where measurements were made. These stations are listed in Table 7. In performing the computations, S-Cubed added many more for a total of 1010 (Part II of this report). These

Table 7. Stations for the PRISCILLA computations.

Ground Range (ft)	Elevation 0 ft	3 ft	6 ft	10 ft	20 ft	40 ft
0	x	x	x	x	x	x
50	x	x	x	x	x	x
100	x	x	x	x	x	x
150	x	x	x	x	x	x
200	x	x	x	x	x	x
250	x	x	x	x	x	x
350	G*	x	x	x	x	x
450	G*	G*	x	x	x	x
550	G*	G*	x	x	x	x
650	G*	G*	x	x	x	x
750	G*	G*	x	x	x	x
760	G*	x	x	x	x	x
850	G*	G*	x	x	x	x
860	G*	x	x	x	x	x
970	G*	x	x	x	x	x
1000	x	x	x	x	x	x
1040	G*	x	x	x	x	x
1050	G*	G*	x	x	x	x
1150	G*	x	x	x	x	x
1250	G*	x	x	x	x	x
1350	G*	G*	x	x	x	x
1360	G*	x	x	x	x	x
1430	G*	x	x	x	x	x
1450	G*	x	x	x	x	x
1650	G*	G*	x	G*	x	x
1700	G*	x	x	x	x	x
1720	G*	x	x	x	x	x
1750	G*	x	x	x	x	x
1800	G*	x	x	x	x	x
1900	G*	x	x	x	x	x
2000	G*	G*	x	G*	x	x
2030	G*	G*	x	x	x	x
2100	G*	x	x	x	x	x
2250	G*	G*	x	x	x	x
2280	G*	G*	x	x	x	x
2300	x	x	x	x	x	x
2350	x	x	x	x	x	x
2400	x	x	x	x	x	x
2450	x	x	x	x	x	x
2475	x	x	x	x	x	x
2500* 20 psi	G*	G*	x	G*	x	x
2525	x	x	x	x	x	x
2550	x	x	x	x	x	x
2600	x	x	x	x	x	x
2650	x	x	x	x	x	x
2730	G*	G*	x	x	x	x
2800	x	x	x	x	x	x
2850	x	x	x	x	x	x

Table 7. Stations for the PRISCILLA computations (continued).

Ground Range (ft)	Elevation 0 ft	3 ft	6 ft	10 ft	20 ft	40 ft
2900* 15 psi	x	x	x	x	x	x
2925	x	x	x	x	x	x
2950	x	x	x	x	x	x
3000	G*	G*	x	G*	x	x
3250	x	x	x	x	x	x
3350	x	x	x	x	x	x
3500	G*	G*	x	G*	x	x
3525	x	x	x	x	x	x
3550	x	x	x	x	x	x
3575	x	x	x	x	x	x
3600* 10 psi	x	x	x	G*	x	x
3625	x	x	x	x	x	x
3650	x	x	x	x	x	x
3675	x	x	x	x	x	x
3700	x	x	x	x	x	x
3800	x	x	x	x	x	x
3900	G*	x	x	x	x	x
3930	G*	G*	x	x	x	x
4000	G*	G*	x	x	x	x
4050	x	x	x	x	x	x
4100	x	x	x	x	x	x
4150	x	x	x	x	x	x
4175	x	x	x	x	x	x
4200*7.3 psi	x	G*	x	x	x	x
4225	x	x	x	x	x	x
4250	x	x	x	x	x	x
4300	x	x	x	x	x	x
4400	x	x	x	x	x	x
4500	G*	G*	x	x	x	x
4600	x	x	x	x	x	x
4770	G*	G*	x	x	x	x
4900	x	x	x	x	x	x
5000	G*	G*	x	G*	x	x
5100	x	x	x	x	x	x
5200	x	x	x	x	x	x
5250	x	x	x	x	x	x
5300	x	x	x	x	x	x
5320* 5 psi	G*	G*	x	x	x	x
5350	x	x	x	x	x	x
5400	x	x	x	x	x	x
5500	x	x	x	x	x	x
5600	x	x	x	x	x	x
5700	x	x	x	x	x	x
6000	x	x	x	x	x	x
6120	G*	G*	x	x	x	x
7000	x	x	x	x	x	x
7500	x	x	x	x	x	x

Table 7. Stations for the PRISCILLA computations (concluded).

x = station for saving data.

G* = a gage or gages were located at this station. Save data.

For all stations having G* at three feet, save data for all zones from zero to four feet. Do this also for stations at 2900, 3250, 3350, and 3600 feet.

For direct comparison with records, need to compute stagnation pressure and differential pressure for elevated stations where records exist.

Need to compute dynamic pressure versus time for all stations.

Add other stations so load computations can be made for pressure levels shown.

are shown by dots in Figure 4.

4. THE THRML CODE.

The THRML code was developed to predict the thermal layers developed by various terrain and vegetative ground covers in response to irradiation by a nuclear weapon explosion (11). The main application prior to this current work treated grasslands and crop lands. The interest was in the low-to-medium airblast overpressure regions of concern to mobile strategic systems.

THRML is a one-dimensional code which provides the response of a surface and surface cover to time-dependent incident thermal radiation. For a given weapon yield and height of burst, soil characteristics such as bound water content and particle-size distribution, and characteristics of the vegetative cover, such as mass distribution, water content and heat of combustion and vaporization, THRML can compute the time evolution of the thermal layer at a given range.

THRML determines the heating of the vegetation and soil, the onset of pyrolysis, the rate of combustion as limited by available oxygen (which is brought to the combustion from above by turbulent diffusion), the production of soot, and the lofting of soil. Some of its capabilities include treating multiple particle size groups; radiation transport including multiple frequency groups and multiple angular groups; multiphase motion allowing separate interactive motion of air, steam, and particulates; and turbulent diffusion of species, particle size groups, and internal energy. See Appendix B.

The code is not coupled to the hydrocode computing the progress of the blast wave. To construct a thermal layer it is necessary to estimate the shock arrival time versus range. At the expected time of arrival of the blast wave at a given range, the THRML output describing the state of the thermal layer at that range and time is saved and combined with the values computed for other ranges and times to define the values to place in the hydrocode grid.

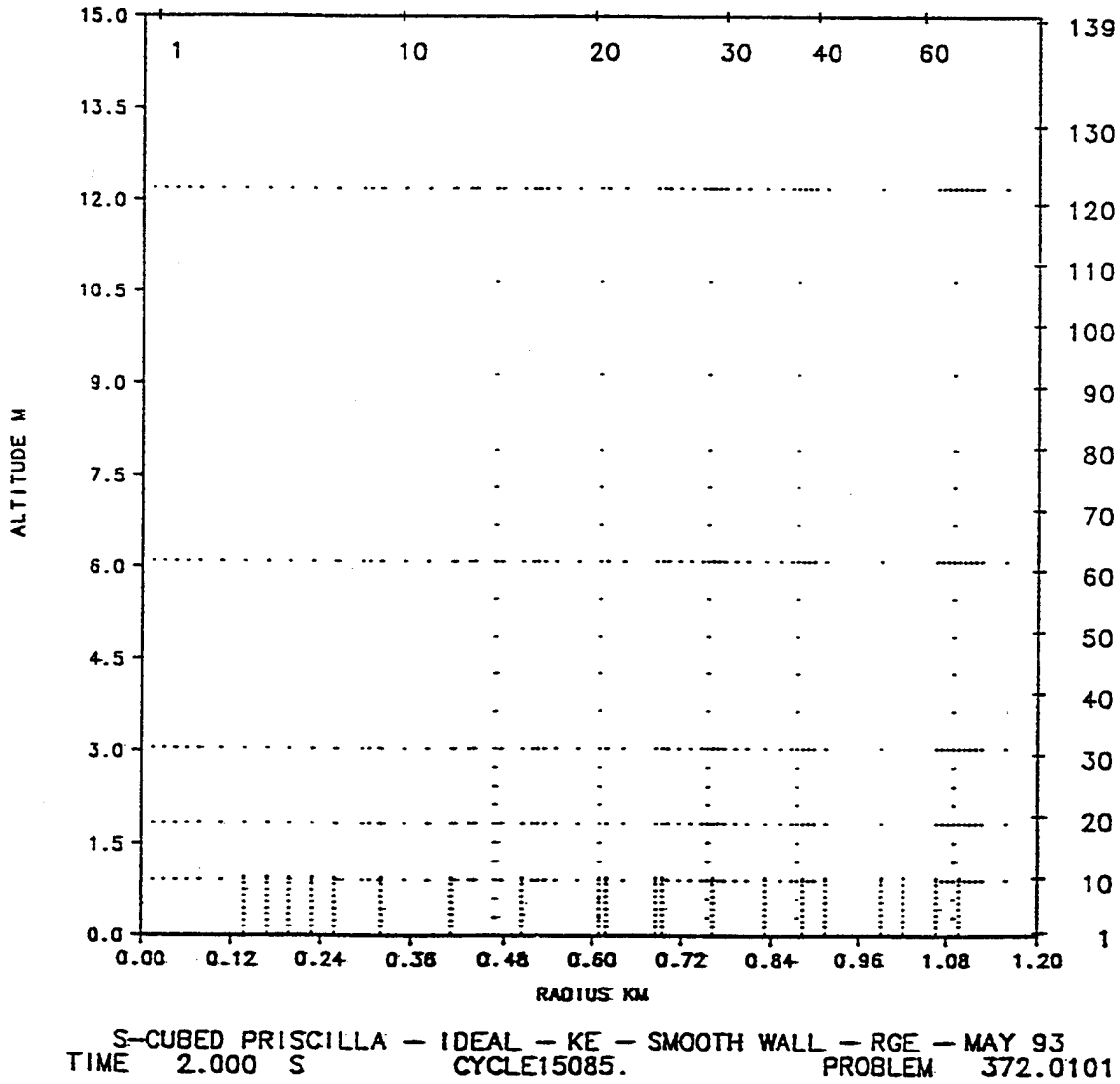

Figure 4. Station locations used for all three calculations.

5. THE DESERT THERMAL LAYER.

The desert computation was intended to duplicate the PRISCILLA blast wave for direct comparison with experimental data. The original plan for this study was to use the THRML code to predict the thermal layer. The code was designed for predicting layers for surfaces with vegetation, and is not as well developed for bare soil. There is much greater uncertainty in input parameters and a lack of suitable experiments for validation.

Despite considerable effort by Barthel and Rogers of S-Cubed and variation of input parameters within physically reasonable bounds, the THRML predictions did not agree well with the available experimental data from PRISCILLA. The experimental data show that hottest region was near the surface and decreased with elevation. The THRML code predictions showed temperature increasing with height to the top of the layer. In addition, the sound velocities seemed too high. Use of the THRML code predictions was judged to guarantee that the hydrocode predictions of blast would disagree with the observed PRISCILLA results. See Appendix B for a program to improve the THRML code.

Another method of developing a thermal layer can be employed if measured blast waveforms are available (12,13,14,15). The times of wavefront arrival at surface overpressure gages are fitted as a function of ground range, the slopes are determined from the fits for each station, and the wavefront speed derived. If the wavefront is a shock, the shock overpressure is measured and the shock Mach number M is computed from the following relation:

$$M = \left[1 + \frac{(\gamma+1)}{2\gamma}\frac{OP}{AP}\right]^{1/2}$$

where OP = shock overpressure,

AP = ambient pressure,

γ = ratio of specific heats, assumed to be 1.4.

The effective sound speed is computed from the shock Mach number definition:

$$M = U/a, \text{ and } a = U/M,$$

where U = wavefront speed determined from fitting the experimental arrival time data,

a = effective sound speed to be assigned to the thermal layer,

M = Mach number derived from the measured shock front overpressure. If the wave has a slowly rising front with no indication of a shock, it is assumed to be an acoustic wave, so M = 1 and a = U.

The latest version of the effective sound speed derived from the PRISCILLA data was provided by Carpenter (16), and is shown in Figure 5 by the solid curve. The dashed curve is an estimate for an acoustic wave in the region indicated. Mazzola (17) performed an independent analysis over the range of available data and arrived at a similar curve only slightly lower than the solid curve in Figure 5.

Figure 6 shows the curve as transcribed for use in the computation by S-Cubed personnel. The original computation used the solid non-acoustic curve in the figure. The results from that computation are described in Appendix A. This thermal layer did not produce a precursor of the extent observed on PRISCILLA. In a follow-on effort (2), the computation was restarted when the shock front was at about 1450 feet and used the first revision shown in the figure. The final run and the one from which results are discussed in this report included the second revision. Thus the final effective sound speed curve used was based on Carpenter's curve but did not precisely duplicate it.

The layer was constructed having the first two zones above the surface at the same sound speed and an exponential decay vertically above them. The cell values were adjusted to achieve pressure equilibrium to prevent material movement before wavefront arrival.

6. THE GRASSLAND THERMAL LAYER.

The characteristics of the grassland surface were chosen to produce the most damaging precursor for mobile equipment. They were based on earlier work for a strategic system (18). The vegetation was dry grass of 30 centimeters height, corresponding to what might grow in a semi-arid region.

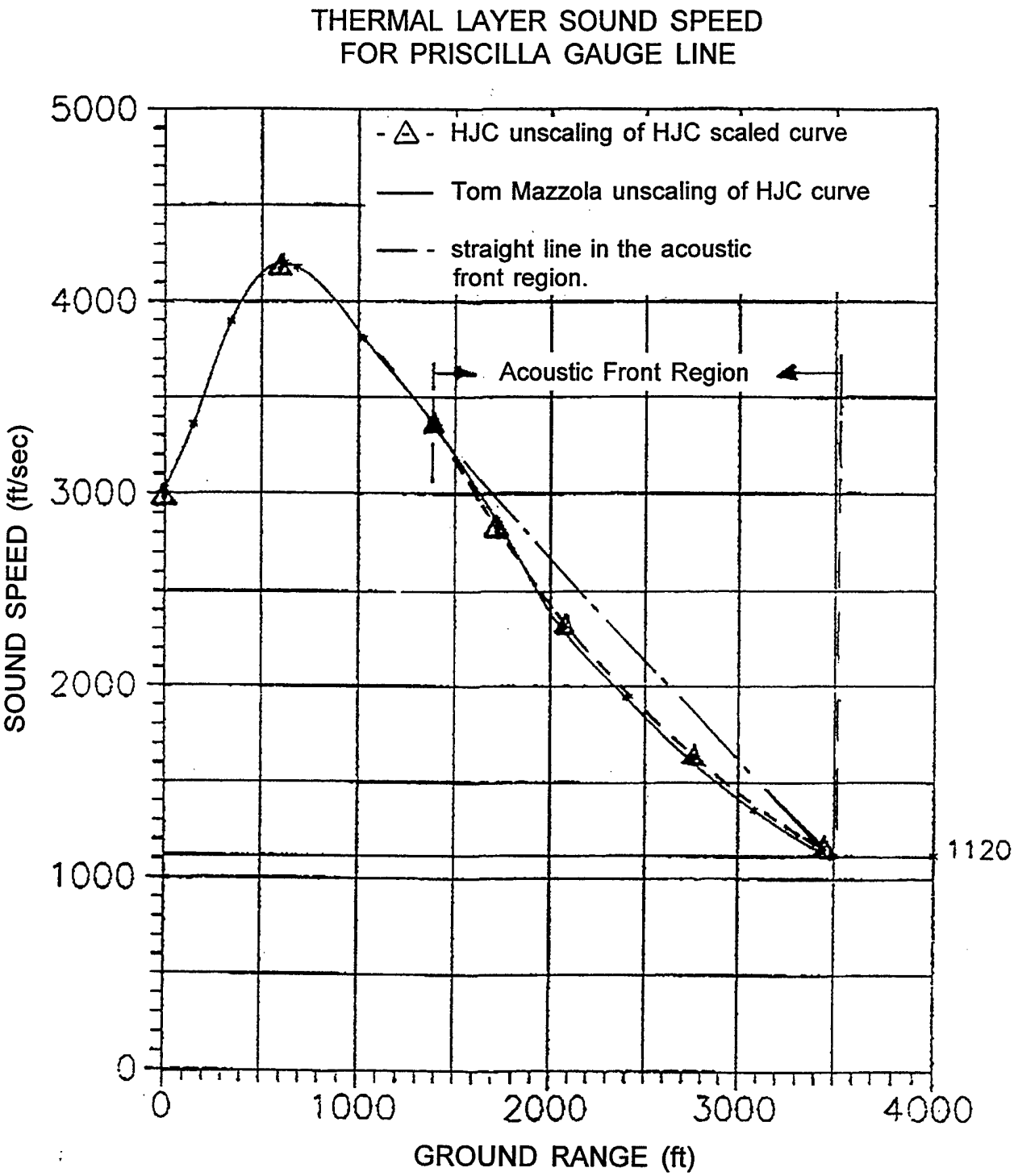

Figure 5. Thermal layer sound speed for PRISCILLA main blast line as derived by H. J. Carpenter, Carpenter Research Corporation.

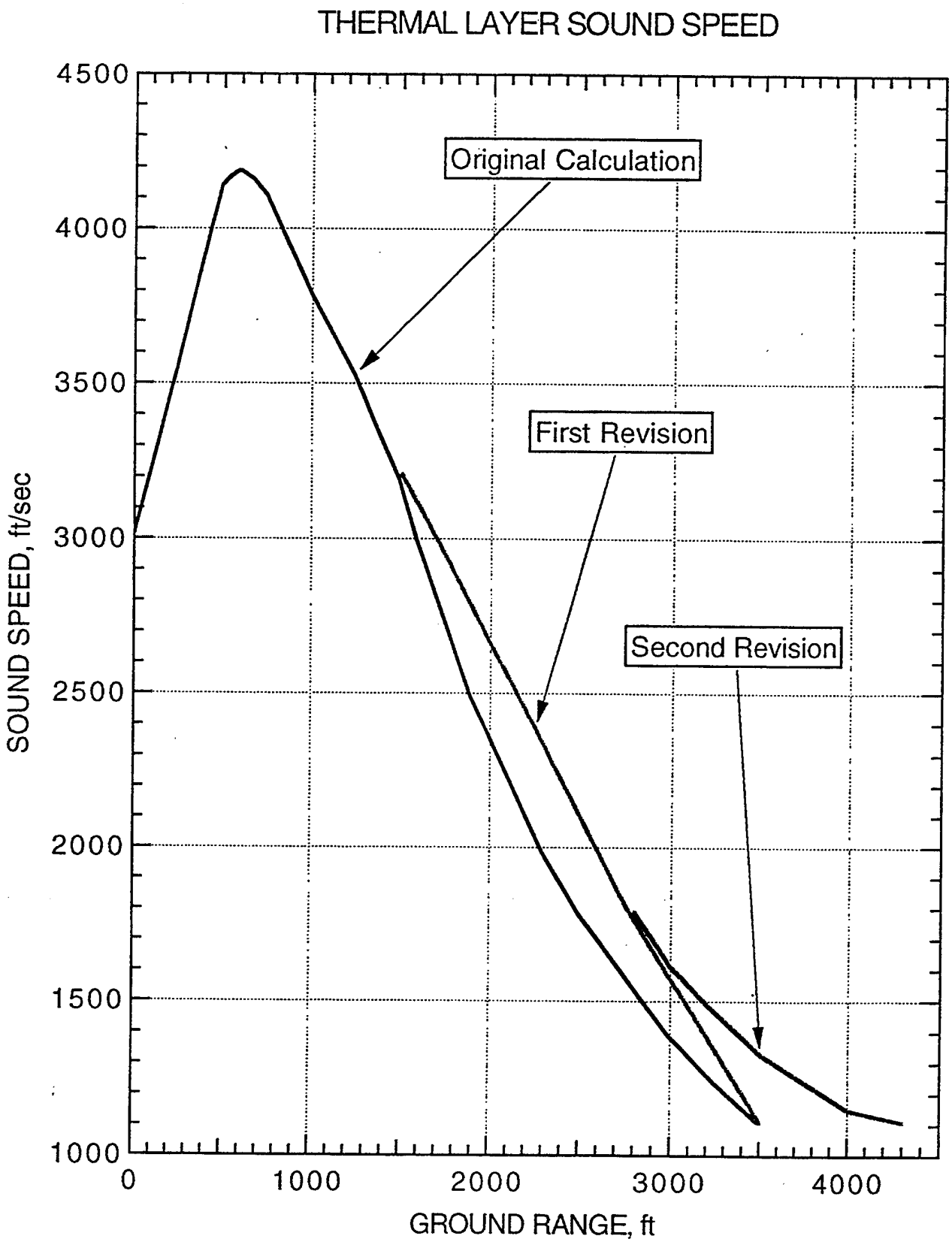

Figure 6. PRISCILLA sound speed versus range as used for desert surface computations (Part II of this report),(2).

Table 8 lists the input soil and vegetation parameters used (Appendix A). Atmospheric conditions for an elevation of 3100 feet were used to correspond to PRISCILLA conditions.

For lack of other data, the arrival times measured on the PRISCILLA event were used to develop the thermal layer. As will be seen later when results of the computation are presented, the precursor on the grassland surface arrived as much as 300 milliseconds earlier than the measured desert arrival time. So the thermal layer used for the grassland computation was higher and of a different effective temperature than one appropriate for the grassland arrival times. If a new thermal layer were computed for the grassland using the computed arrival times, the hydrocode would produce still different arrival times. The THRML code needs to be coupled to the hydrocode so that when the shock is near a given range, the THRML code predictions for that range are inserted into the grid just ahead of the wavefront.

Figure 7 shows the grassland thermal layer versus range and height derived from the THRML runs for the measured desert arrival times (Part II of this report).

The vertical thermal layer profile at a given range and time is finely resolved by the THRML code. For insertion into the hydrocode, the results are averaged over the height of each cell at the given range, and average values assigned to the center of the cell. The THRML code runs were made at ground range intervals of about 52 meters. Values for the cells in between were determined by linear interpolation (Part II of this report).

The values for all cells were processed to establish pressure equilibrium between the cells so that no hydrodynamic action would occur prior to shock arrival. This represents another change in the THRML values that would be unnecessary if the codes were coupled (Part II of this report).

Figure 8 shows the maximum value of sound speed for the grassland thermal layer versus ground range as used in the computation (19). The values are much larger and extend to a greater range than those for the desert thermal layer. The sharp drop that

Table 8. Vegetation and soil parameters used in THRML for PRISCILLA grassland thermal layer (Appendix A).

Vegetation Characteristics:

Vegetation height (top and bottom)	30 cm, 0 cm (ground surface)
Mass Distribution	Uniform
Dry Mass Load	0.022 gm/cm^2
Bound Water Content	0.003 gm/cm^2 (14% of dry mass load)
Free Water Content	none
Bound Water Release Temperature	375° K
Heat of Combustion	3600 cal/cm^2
Onset and Completion of Pyrolysis	475° K, 800° K
Plant Residue in Ash and Soot	2.97% and 0.03%, respectively, of burned mass
Leaf Index	3.56
Density of Dry, Compacted Plant	0.35 gm/cm^3

Soil:

Particle Categories	2, loftable and immobile
Amount in Loftable Particles	1% by mass
Particle Diameters	10 microns, 400 microns
Bound Water Content	13.8% of dry mass
Bound Water Release Temperature	600° K
Void Space	30%
Density of Dry, Compacted Soil	2.2 gm/cm^3
Melt Temperature	2000° K

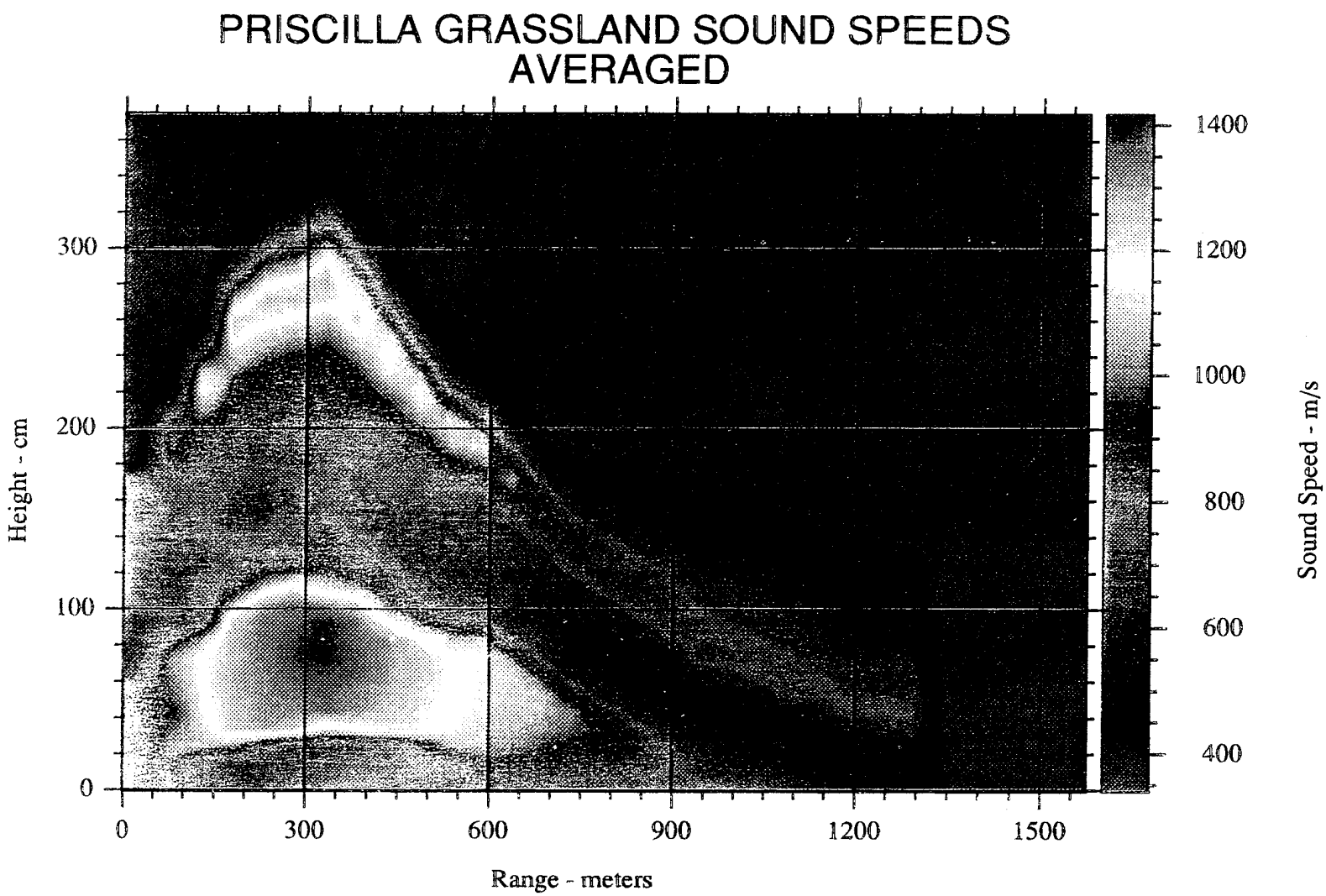

Figure 7. Grassland sound speeds versus height and ground range predicted by THRML (assuming shock arrival times from the PRISCILLA test).

PRISCILLA DESERT CALCULATION
THERMAL LAYER REVISITED

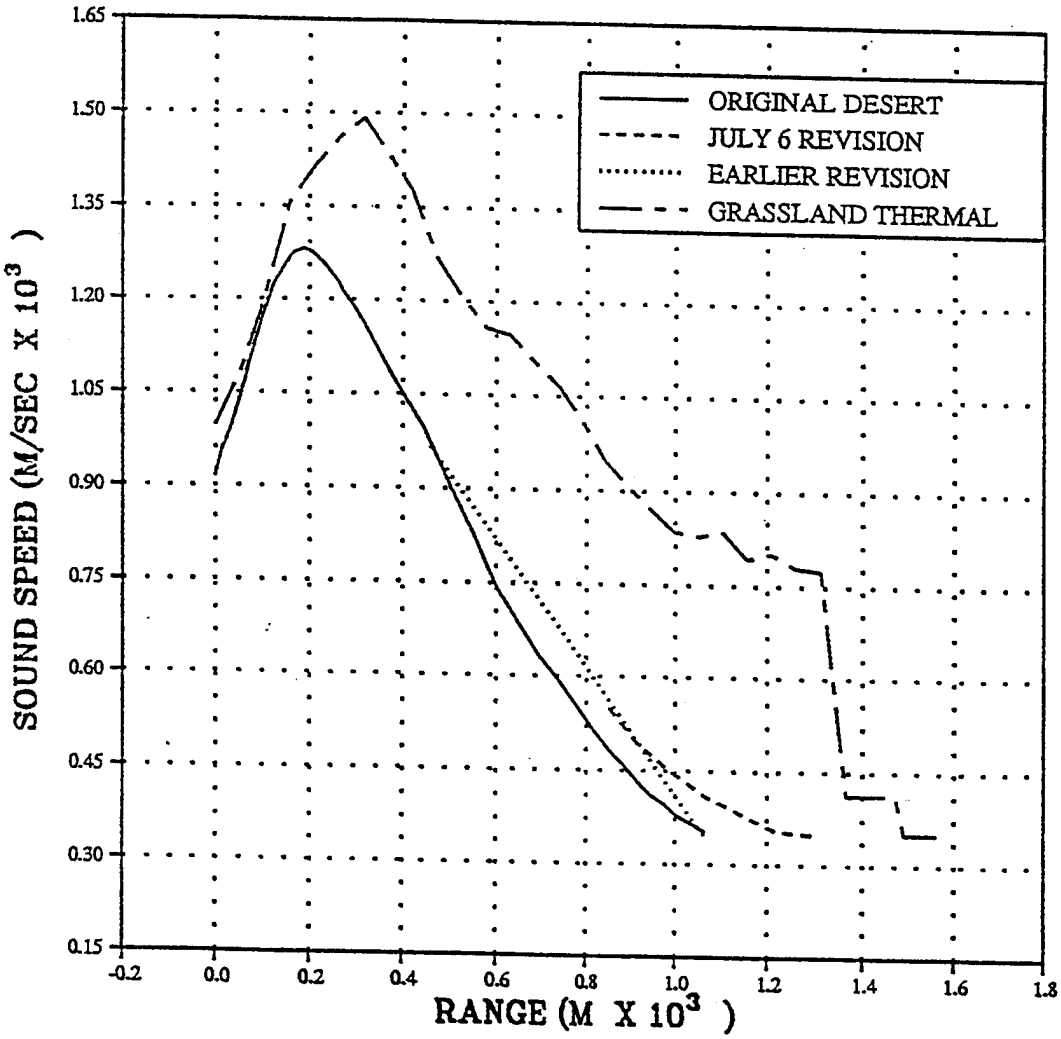

This plot shows the maximum sound speed of the grassland thermal layer versus ground range. The calculation was remapped when the precursor toe was just short of 1.5 kilometers in order to expedite resolution of a problem with pressure instability. For this reason the sound speed drops abruptly to ambient. The first sharp drop at about 1320 meters marks the limit of combustion.

Figure 8. PRISCILLA grassland maximum sound speed versus ground range compared with desert sound speeds.

occurs at about 1300 meters marks the end of the range for combustion of the grass. Because of a pressure instability that developed in the thermal layer, a remapping was done at about 1480 meters and the sound speed dropped to ambient.

7. THE HYDROCODE.

The hydrocode computations were performed by S-Cubed (Part II of this report),(2,3). The code used was the latest version of S-CUBED Hydrodynamic Advanced Research Code (SHARC). The code has fully second-order differencing, and is optimized for use on the DNA Cray computer at the Los Alamos National Laboratory (20,21). It includes a version of a k-ε turbulence model modified for non-steady compressible flow (22). For the precursor calculations an extension permitting modeling of the non-equilibrium conditions in the turbulent field was utilized. The turbulence model has a rough law of the wall boundary layer model (23) and a dust sweep-up model (24). SHARC has alternative boundary layer models, and many other options and capabilities.

The experimental data for guiding the development and providing a validation of SHARC modeling of precursor phenomena were obtained by Reisler, et al.(25), in the DNA-sponsored DIAMOND ARC 87 test series conducted at the Defense Research Establishment-Suffield, Alberta, Canada. This test series modeled the HOOD nuclear test using high-quality HMX-based 1000-lb HE charges, and segmented helium bags to produce high-speed sound velocity layers on the surface. The use of data from Shot 2 to test turbulence and boundary layer models in SHARC and determine those that worked and those that did not are described by Barthel (23). The version of SHARC developed through this work produced excellent agreement with the DIAMOND ARC 87 data, and it is the version used for the three PRISCILLA computations.

8. THE SHARC COMPUTATIONS.

The descriptions of the computations that follow were taken directly from the S-Cubed reports with only a few alterations. They are included to promote better understanding of the results presented.

The SHARC computations were run using a two-dimensional, cylindrically-symmetric coordinate system, with the axis normal to the surface and through the center of the explosion. The initial conditions for the computations were scaled from the one-dimensional spherically symmetric calculations of a 30 kiloton nuclear explosion using the SPUTTER radiation-hydrodynamic code (26). The radius of the SPUTTER input region was 210 meters, so that the shock front was about three meters above the surface when the SHARC computations were initiated, and hence had not entered the thermal layer region. An atmosphere constant with elevation was used.

For finer resolution of the region involving the wavefront, a constant subgrid of limited dimensions was placed in the SHARC mesh at the surface. When the wavefront expanded to the subgrid boundary, a rezone occurred in which cells from the opposite boundary were moved to that boundary approached by the wave and added to provide room for additional expansion. The outer SHARC mesh was adjusted to accomodate the change. This procedure maintained the cells in the subgrid the same size and did not disturb the wave in the subgrid.

There were 1010 stations at which all parameters were stored for later analyses. These were placed from the axis of symmetry to a range of 2286 meters, and from the surface to a height of 12.2 meters. See Table 7 and Figure 4.

The performance of the computations for the three surfaces was divided between two efforts at different times. The first effort by S-Cubed produced computations for all three surfaces out to two seconds after detonation, when available funding was expended. These are described in Part II of this report. Follow-on contracts enabled S-Cubed to extend the three computations to about four seconds and completion of the positive phase at five psi for the ideal surface (2, 3).

8.1 Ideal Surface Computation.

The ideal SHARC computation used the S-Cubed extension of the k-ε turbulence model that had the variable coefficient for formation and dissipation of turbulence, based

on local conditions and history of the flow. A smooth-wall Clauser law-of-the-wall was used (22,23).

The ideal surface SHARC computation was run in two phases. The first phase ran from initiation at 55 milliseconds to 250 milliseconds. In the second phase the main grid was expanded and the computation ran from 250 milliseconds to completion under the first effort at 2 seconds.

The zone size in the subgrid was 20 cm (horizontal) and 10 cm (vertical). In the first phase the subgrid was 5 meters high and 30 meters long. Initially it was placed to span the range from 220 to 250 meters. Figure 9 shows the subgrid and full mesh configuration of the first phase. For the second phase the subgrid was 12 meters high and 90 meters long, and was initially placed to span the range from 240 to 330 meters. Figure 10 shows the subgrid and full mesh. The computation was carried to two seconds (Part II of this report).

The follow-on computation was carried from two seconds to four seconds. The shock front decayed to an overpressure slightly less than four psi at a range somewhat beyond 6000 feet (2). The zone height in the subgrid was maintained at 10 cm to a range beyond 1.2 kilometers. The zone height was then gradually increased to a maximum of 30 cm as the shock approached a range of two kilometers.

8.2 The Desert Surface Computation.

The desert computation used the extended k-ε turbulence model, a dust sweep-up model, and a smooth-wall Rubesin law-of-the-wall to represent the surface interaction (22,23,24).

The desert computation was run with one basic subgrid and mesh configuration, as shown in Figure 11. The outer vertical boundary was expanded as required to contain the moving shock. The subgrid zones were 30 cm square, in contrast to the ideal surface grid zones of 10 cm vertical and 20 cm horizontal. The grid change was required because the

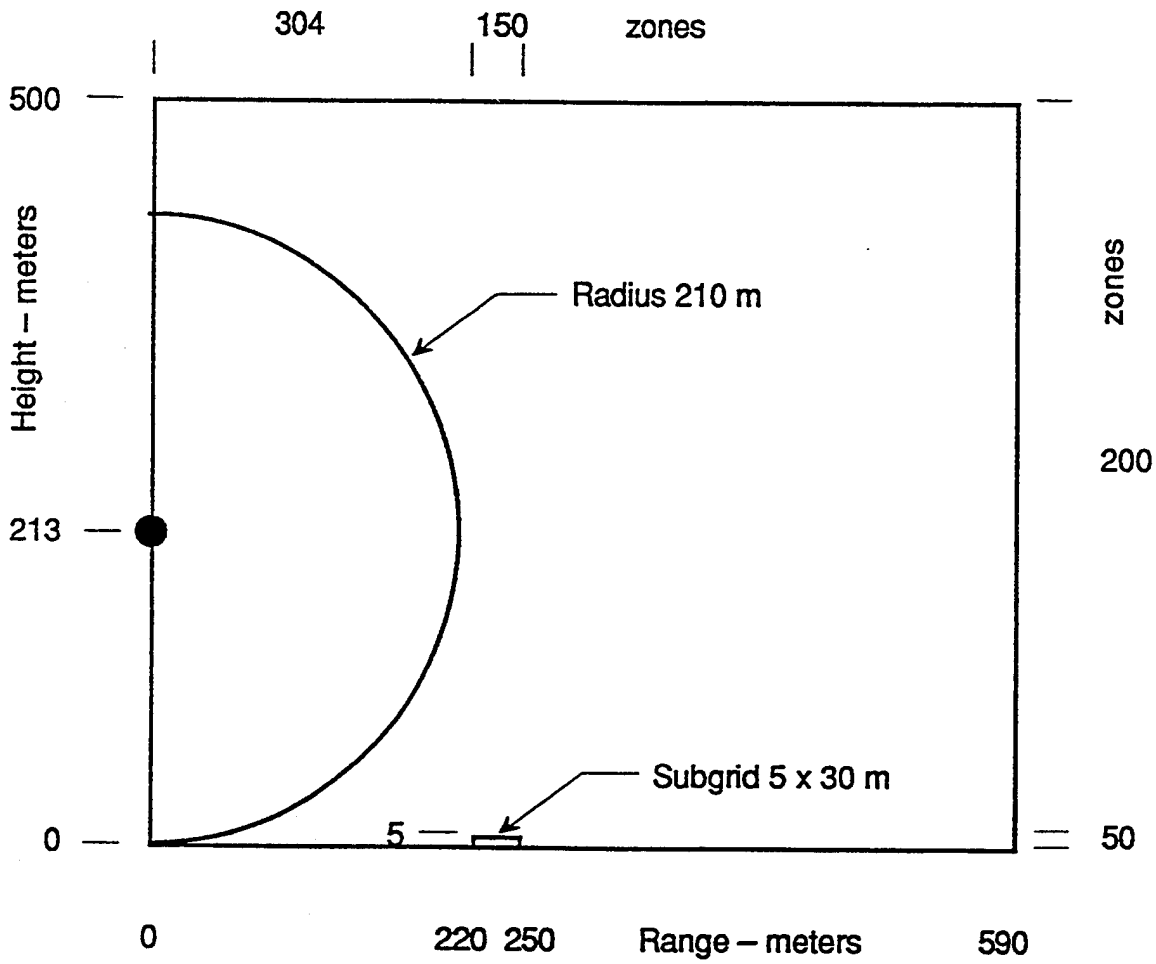

Figure 9. Mesh configuration at initiation of first phase, ideal surface computation.

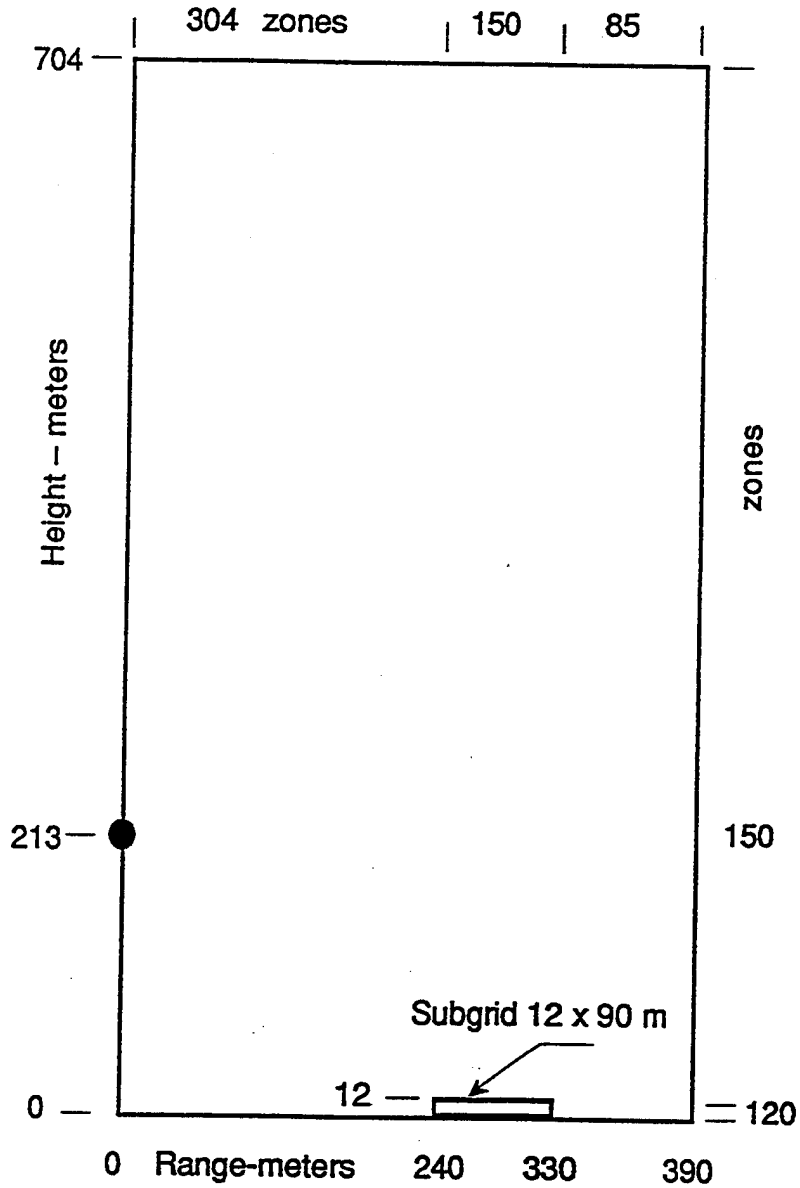

Figure 10. Mesh configuration at initiation of second phase, ideal surface computation.

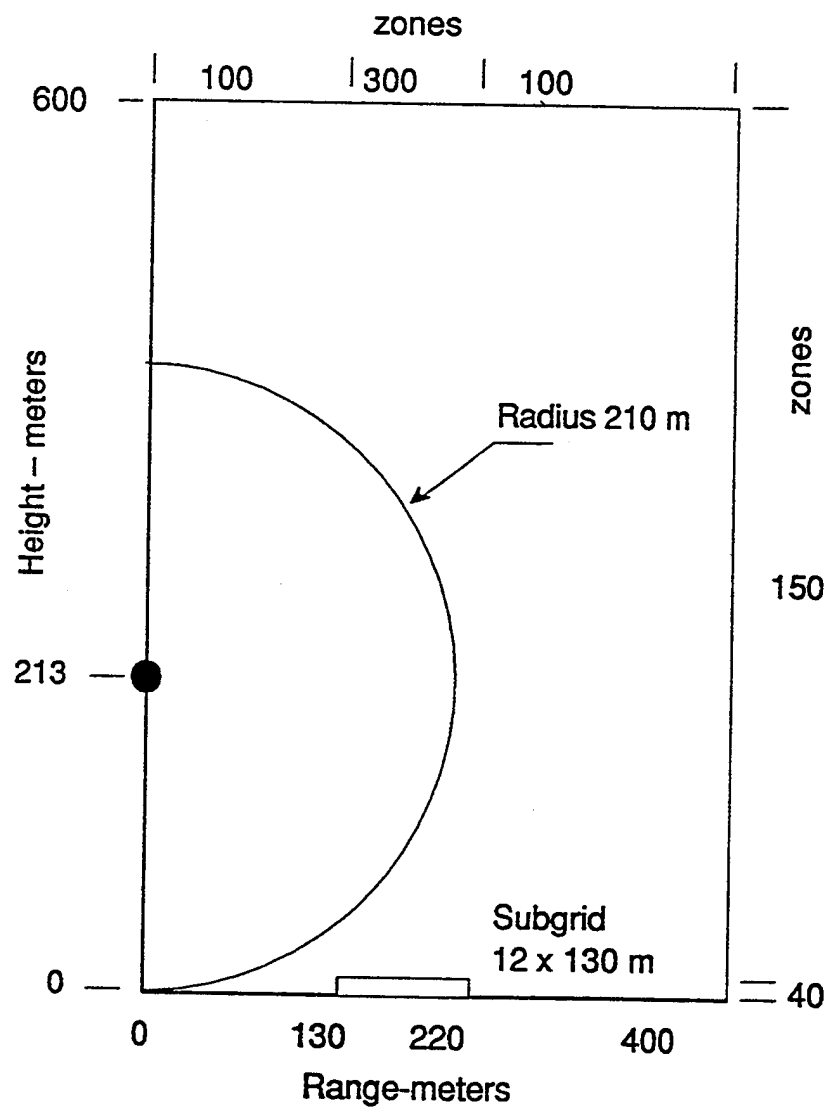

Figure 11. Initial configuration for grassland and desert surface calculations.

addition of the dust sweep-up model and extended turbulence model increased computation times beyond practical limits for the finer zoning used for the ideal surface.

The first effort carried the computation to two seconds (Part II of this report). For this first effort the original curve in Figure 6 was used. In the follow-on program the desert computation was restarted when the shock front was at about 1450 feet to follow the revision in the sound speed curve, because the precursor was not as advanced as observed on PRISCILLA. Revision 2 was added to extend the thermal layer to 4300 feet. The computation was restarted a second time when the shock front was at 2500 feet and continued to four seconds at a range of 6000 feet. The results from these runs provide a computation for the original curve to 1450 feet, the first revision to 2500 feet, and the second revision to completion. They are reported in reference (2).

8.3 The Grassland Surface Computation.

The extended k-ε turbulence model was used for this computation. A rough wall model was used to represent the soil surface under the grass. The parameters chosen were an average height of roughness elements of 2 centimeters, having a 35 percent coverage of the surface. (22,23,24).

The plant and soil material from the THRML-generated layer was treated by the two-material, or multiphase, dust equation of state included in the SHARC code. Both vaporized and solid dust were allowed in the calculation, and mass could be transformed from one phase to another as it was heated or cooled by its surroundings. Dust scouring by the shock structure beyond that lofted pre-shock by THRML and existing in the thermal layer was not included. The judgment was made that the roots of the grass would remain intact and prevent the ingestion of large amounts of dust. The additional thermal radiation from the fireball after shock arrival was not considered.

In the first computational effort, this computation used the same zoning as for the ideal computation and was carried to 200 milliseconds. Continuing with this zoning would have consumed several hundred hours on the DNA Cray computer, so for the follow-on

effort the coarser zoning shown in Figure 11 was used, the same as for the desert computation. This follow-on computation is reported in reference (3).

9. RESULTS AND DISCUSSION.

Results for all three computations carried to a time of two seconds are contained in Part II of this report. The ideal and desert surface computations were carried to four seconds and completed under a new Army contract, and are contained in reference (2). Another Army contract supported computation of the grassland to four seconds and completion. The results are presented in reference (3).

Summary tabulations of the blast parameters for all three cases were supplied by S-Cubed (27). They are presented in Appendix A.

The funding for S-Cubed supported very little analysis. The results presented here were taken from the three reports and developed using the summary tabulations.

The high sound-speed layers produced strong precursor action on the desert and grassland surfaces. Figure 12 shows the pressure contours of the blast bubble for the three cases at 200 milliseconds after detonation. The ideal surface overpressure at the base of the Mach shock is 155 psi (1070 kPa). The precursor on the grassland is already well ahead of that on the desert. The height and structure of the thermal layer is indicated by the height and irregularity of the precursor toe wavefront.

Figure 13 shows the pressure contours at 500 milliseconds, when the ideal surface overpressure at the base of the Mach shock is 44 psi (300 kPa). Here the desert precursor is 80 meters in advance of the ground level ideal Mach shock front, and the grassland precursor is 65 meters in front of the desert precursor. The pressure decay behind the ideal Mach shock front looks relatively clean, while the pressure contours for the precursed cases are very complex.

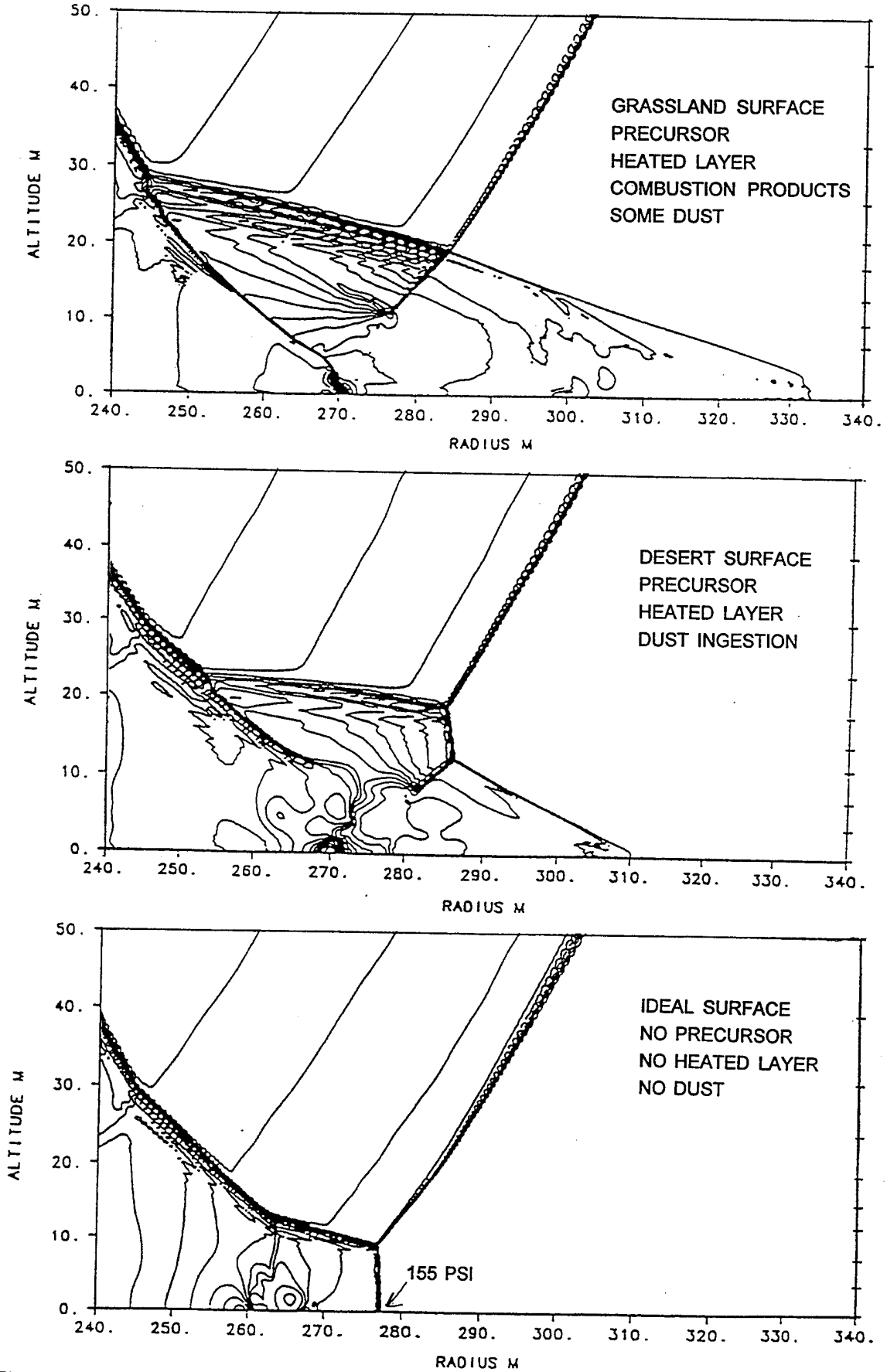

Figure 12. Comparison of blast wave pressure contours at 200 ms after detonation when overpressure at the base of the ideal Mach stem is 155 psi.

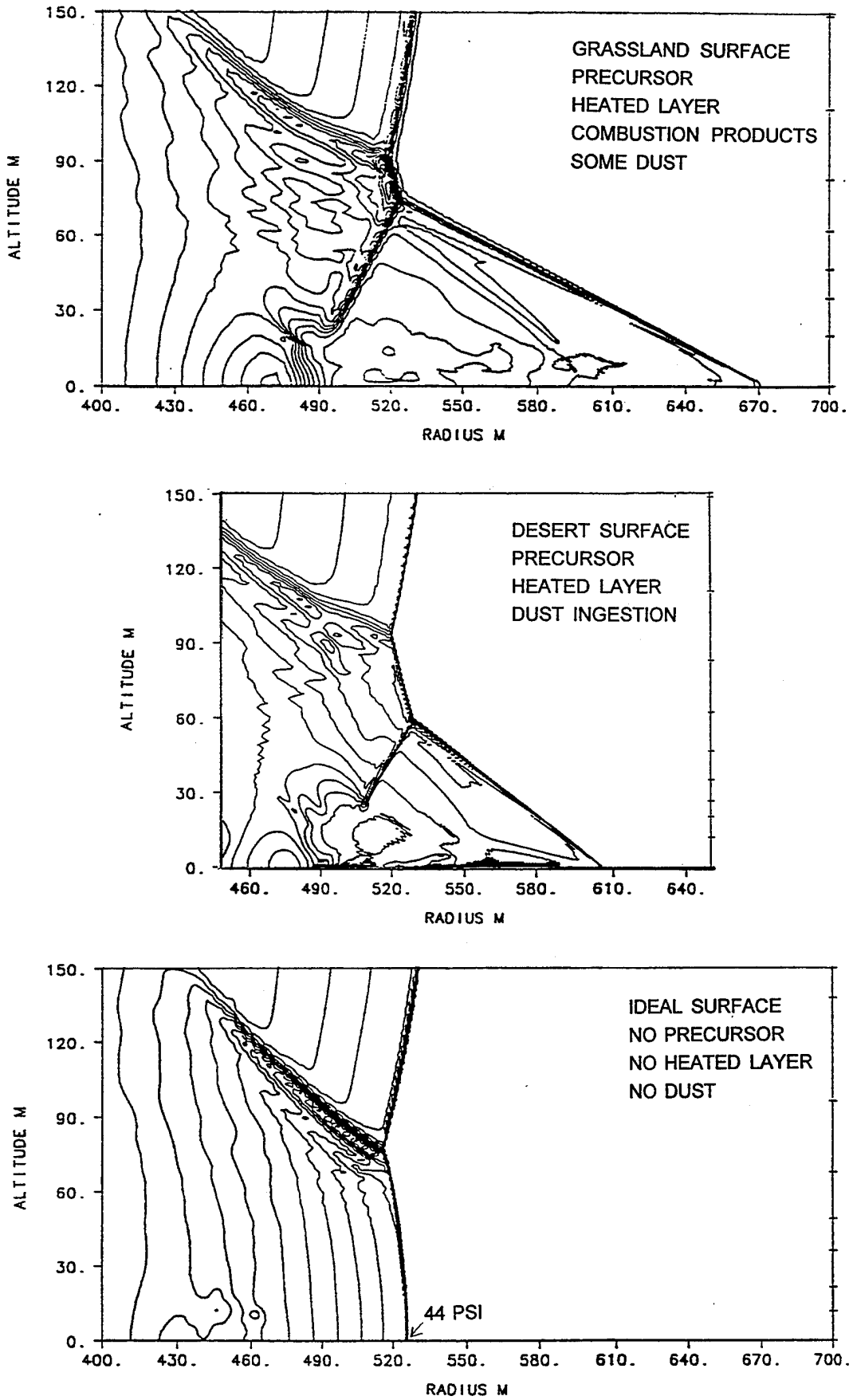

Figure 13. Comparison of blast wave pressure contours at 500 ms after detonation when overpressure at the base of the ideal Mach stem is 44 psi.

9.1 Arrival Times.

A comparison of the arrival times versus ground range for the three computations is shown in Figure 14. The curve for the desert approaches that for the ideal at about 1200 meters, while that for the grassland remains well separated.

Figure 15 show the differences in arrival times between the ideal arrival times and those for the desert and grassland computations, and the arrival times actually measured on PRISCILLA by the SRI gages. The SRI measurements are used for the comparison because they sensed and were recorded electronically. The larger the amplitude of the curves the earlier the arrival time compared to the ideal case. The computed arrival time differences for the desert are less than the SRI curve beyond 250 meters. The computed precursor did not extend as far in front of the main blast wave as actually occurred on the PRISCILLA event. The overpressure waveforms show this shorter precursor also when compared to the SRI records.

The thermal layer used for the desert computation was based on sound speeds derived from the SRI arrival time data, and this difference should not occur if other aspects of the computational modeling are correct. It was discovered too late to correct that the dust diffusion routine was not turned on for the first 700 feet of travel of the shock front along the surface. A partial rerun of the computation was made later by S-Cubed for Jerry Carpenter of Carpenter Research Corporation with no change except for turned-on diffusion. Carpenter reports that quick-look results show improved agreement in arrival times (28).

Other factors that can affect precursor development and progress include the amount of dust that is swept up, the turbulence model, and the configuration of the thermal layer with height. In the SHARC computation, the dust mass is injected into the surface-level zones of the grid depending on the shear layer strength as determined by the wall/boundary layer model (Part II of this report).

The differences in arrival times for the grassland computation are very large. The

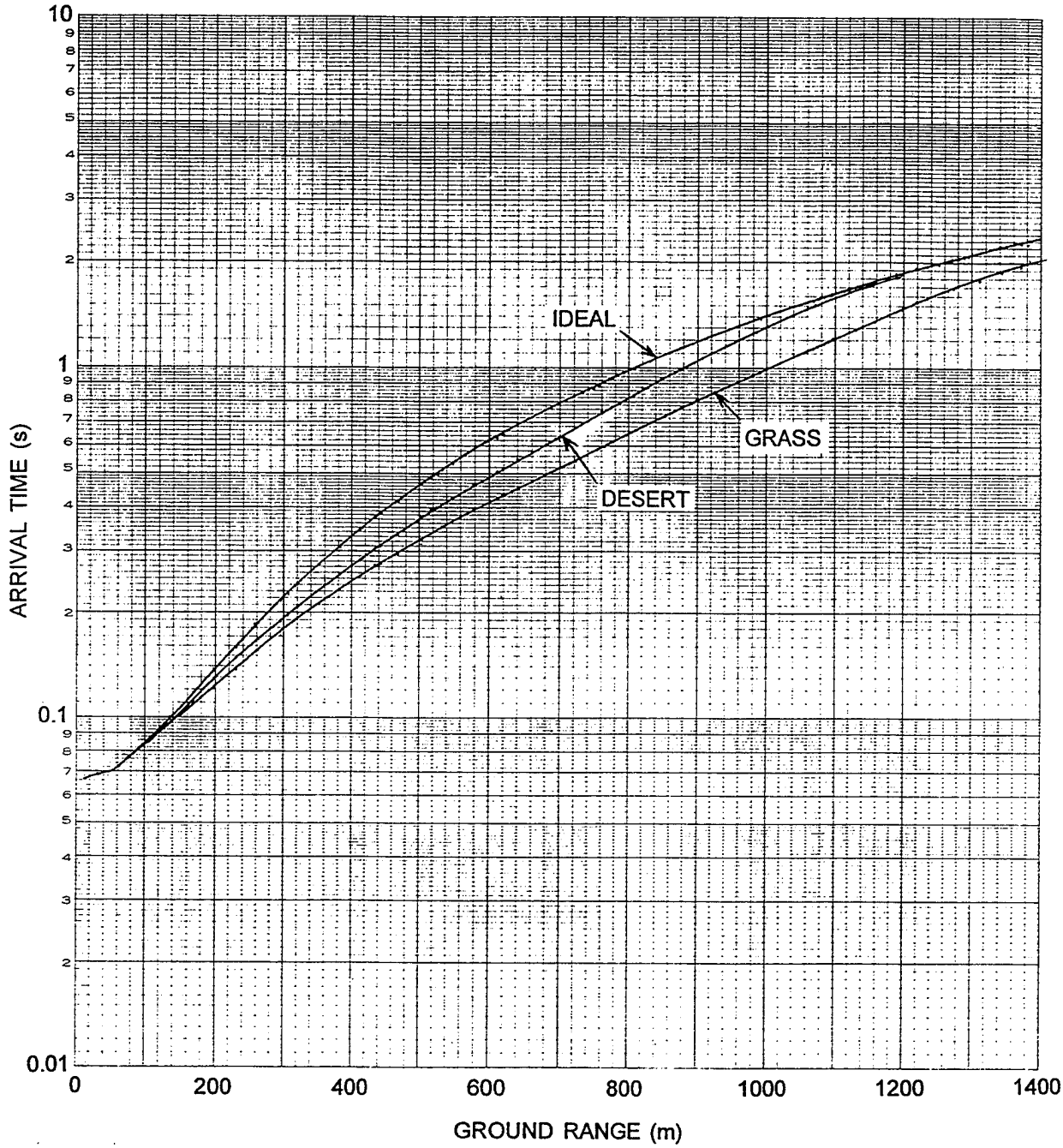

Figure 14. Comparison of surface-level arrival times from the ideal, desert, and grassland SHARC computations.

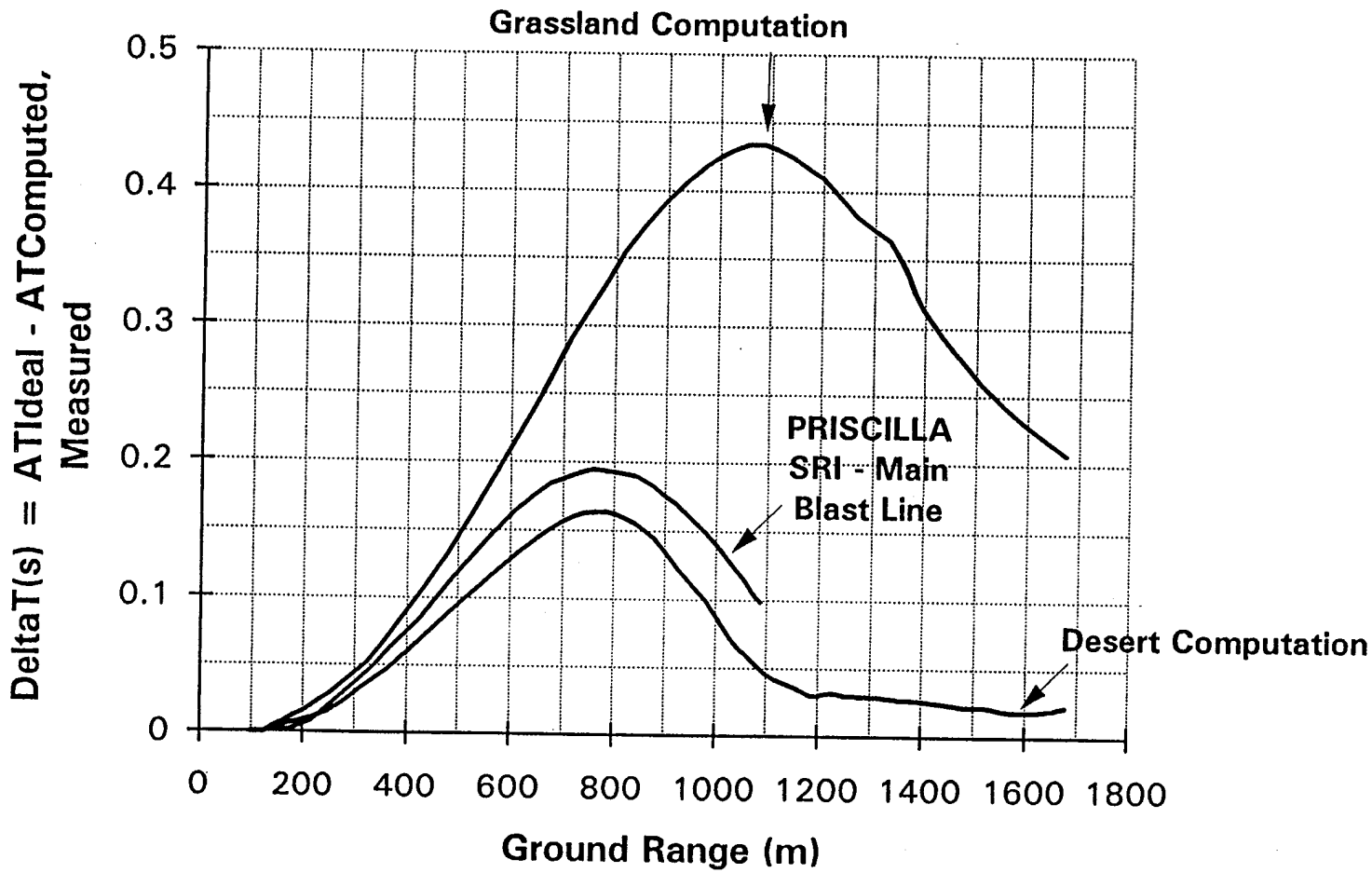

Figure 15. Differences in arrival times at surface level between the ideal computation and desert and grassland cases, and measured desert values from the Stanford Research Institute (SRI) surface gage records. The larger the difference, the earlier the arrival.

precursor developed rapidly and extended far in front of the ideal blast wave. At maximum, it was about 198 meters ahead and 430 milliseconds early at 1080 meters ground range.

The thermal layer for the grassland was computed assuming that the arrival times were those from the SRI measurements. The figure shows a very large mismatch between the assumed arrival times and those generated by the grassland computations. At the range of 1080 meters the difference in arrival times between the grassland computation and the SRI measurements is 330 milliseconds. Since the THRML code computed the thermal layer for later shock arrival times than occurred in the computation, the thermal layer predicted was higher (thicker) than it would have been if computed for the earlier arrival times from the grassland computation. It is not possible to state off-hand that it also would have been hotter, because of competing processes that take place over the grassland when it is irradiated (29).

Nevertheless, the computation provides an indication of the extreme precursor development that can take place over dry grass. The computation should be repeated with the SHARC and THRML codes coupled, if necessary by an iterative process, so that the arrival times in the SHARC computations will correspond to those for which the thermal layer was predicted by THRML.

9.2 Waveforms.

Figure 16 through 24 show comparisons of overpressure waveforms for the three computations. The desert waveforms are shown compared with measured waveforms also. The overpressure range begins at about 50 psi, and ends with the farthest stations at about 5 psi. Some dynamic pressure waveforms are shown also. All figures were taken from (2) and (3). Many were modified to contain only computed waveforms.

The upper figure is for the grassland surface, the middle is for desert, and the lower figure is desert waveforms compared to measured waveforms from PRISCILLA. The ideal waveform is shown in all three figures.

Figure 16 shows the waveforms at a range of 1650 feet (503 meters) for an ideal overpressure of about 50 psi (345 kPa). The grassland and desert waveforms are similar, with the precursor more advanced for the grassland waveform. The lower figure shows that the precursor in the desert computation was not as advanced as that of the SRI record, which has accurate timing. The BRL shows very good agreement in magnitude and shape. However, the timing on the BRL record is apparently in error, possibly due to use of an incorrect conversion factor during the data reduction. What actually happened is not known. The gages were on opposite sides of the blast line, and some differences in the extent of the precursor can be expected. However, the amount shown seems too large to attribute to the variations known to occur in the precursor. The basic shape of the computed waveform agrees well with both the BRL and SRI records, and the agreement in magnitudes is good.

Figure 17 shows waveshapes at the range of 2000 feet (610 meters) for an ideal overpressure of 32 psi (220 kPa). The grassland waveforms show a region of negative pressure (below ambient) in between the precursor and the main peak. The precursor is advanced beyond that for the desert surface shown in the middle figure. In the lower figure the precursor pressure is not much less than that of the experimental records, but the computed main peak is much less than the sharp spikes on the two experimental records.

Figure 18 shows the waveforms at the range of 2250 feet (686 meters) for an ideal overpressure of 25 psi (172 kPa). The magnitude of the precursor fronts is about the same for the grassland and desert, but the grassland waveform has variations and a negative pressure section in the precursor part. In the lower figure the computed desert curve does not have the many oscillations present on the measured waveform but has a similar basic shape. The measured waveform has a slower rise at the precursor front.

Figure 19 shows the waveforms for 2500 feet (762 meters) at an ideal overpressure of 20 psi (138 kPa). Note the change in the time scale for the upper figure. At this range the desert precursor has about reached its maximum extent, while the grassland precursor is still growing. The grassland waveform is quite different from the desert waveform. In

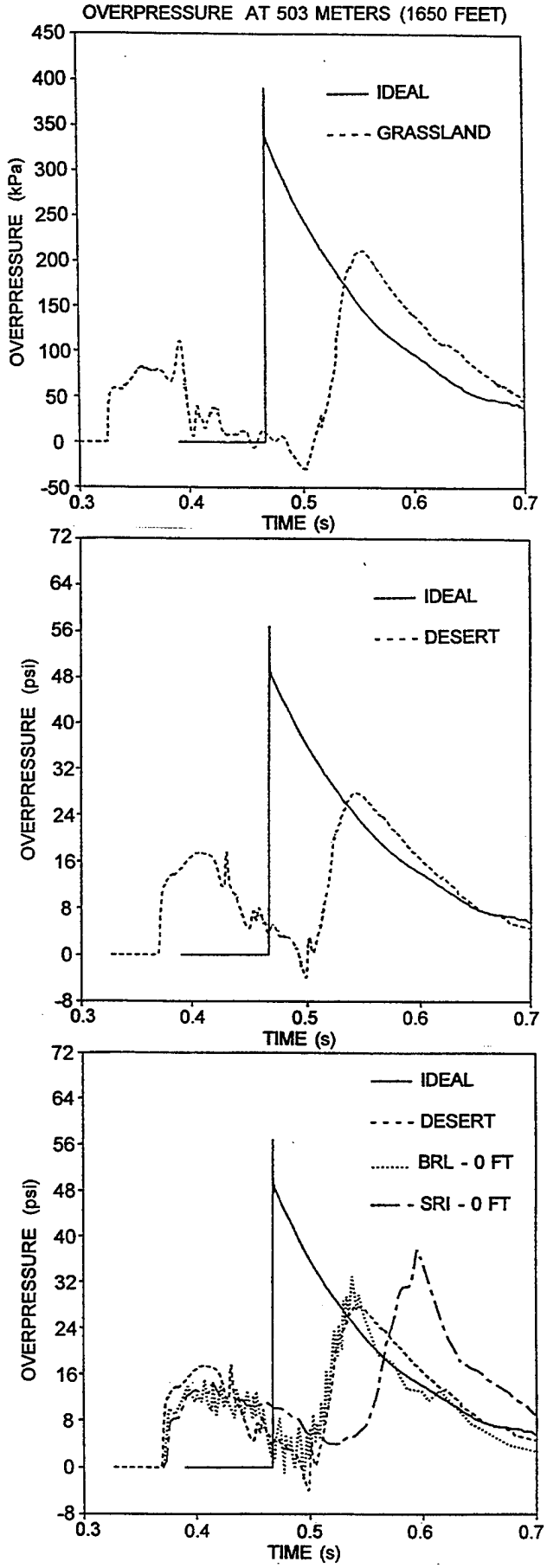

Figure 16. Comparison of overpressure waveforms at 1650 ft (503 m) for grassland, desert, and PRISCILLA data with ideal waveforms.

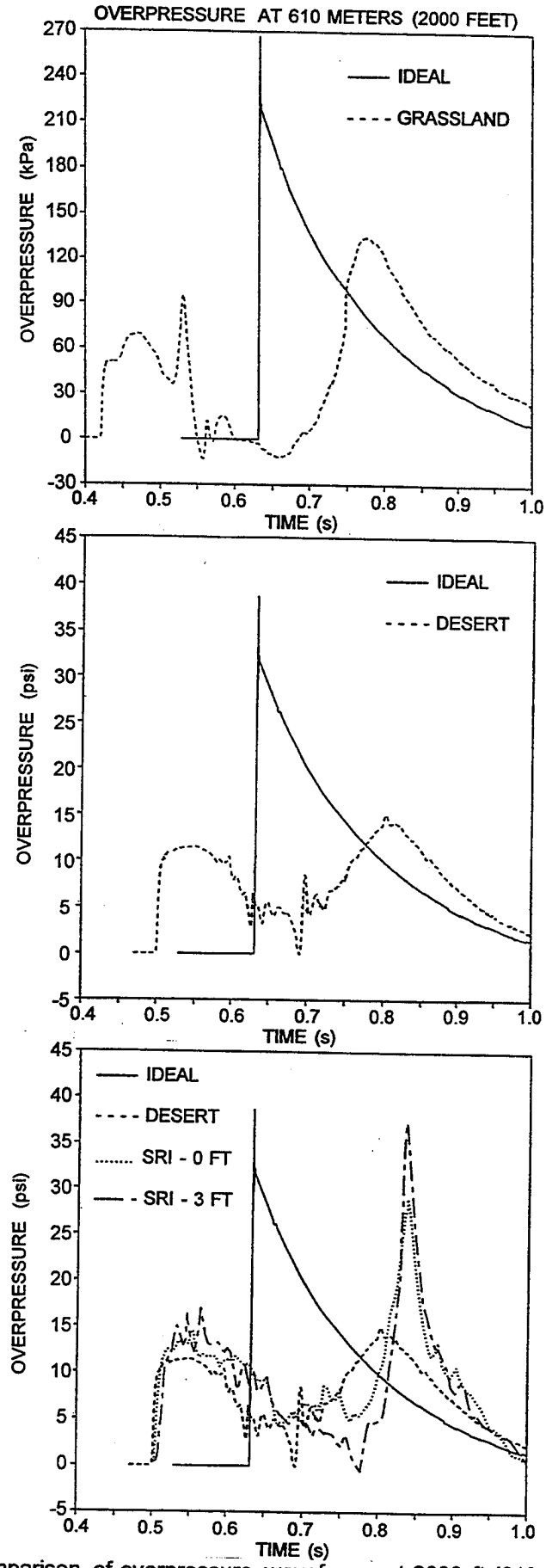

Figure 17. Comparison of overpressure waveforms at 2000 ft (610 m) for grassland, desert, and PRISCILLA data with ideal waveforms.

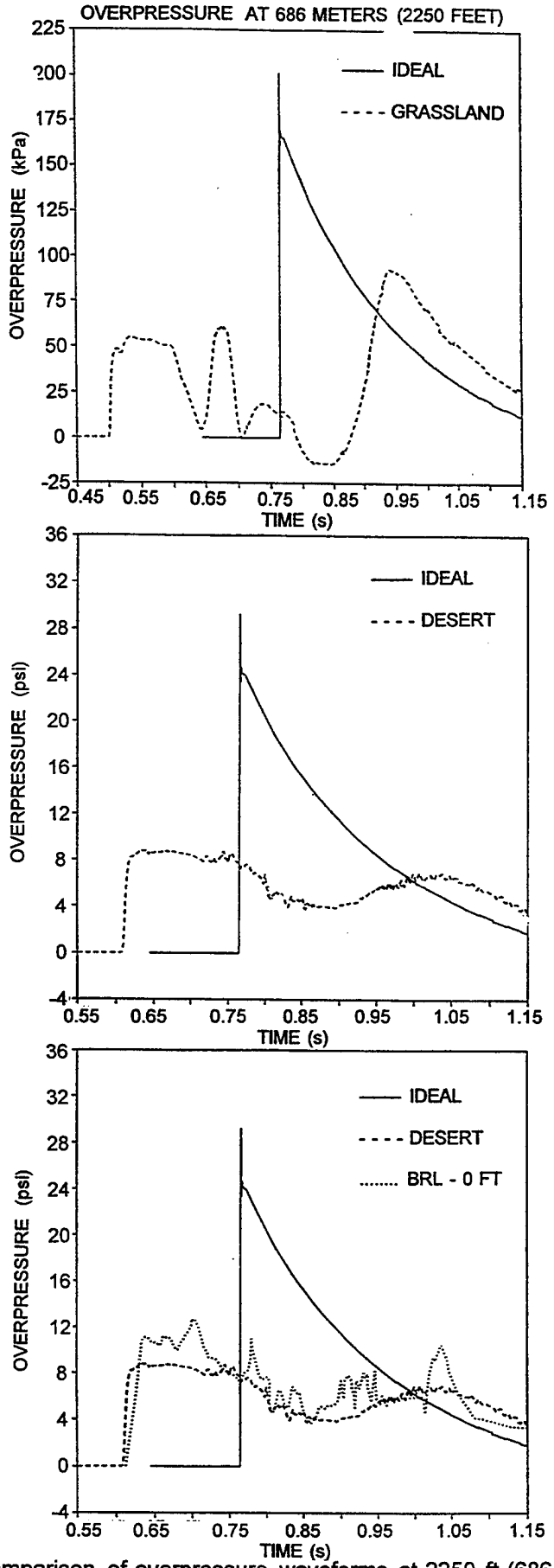

Figure 18. Comparison of overpressure waveforms at 2250 ft (686 m) for grassland, desert, and PRISCILLA data with ideal waveforms.

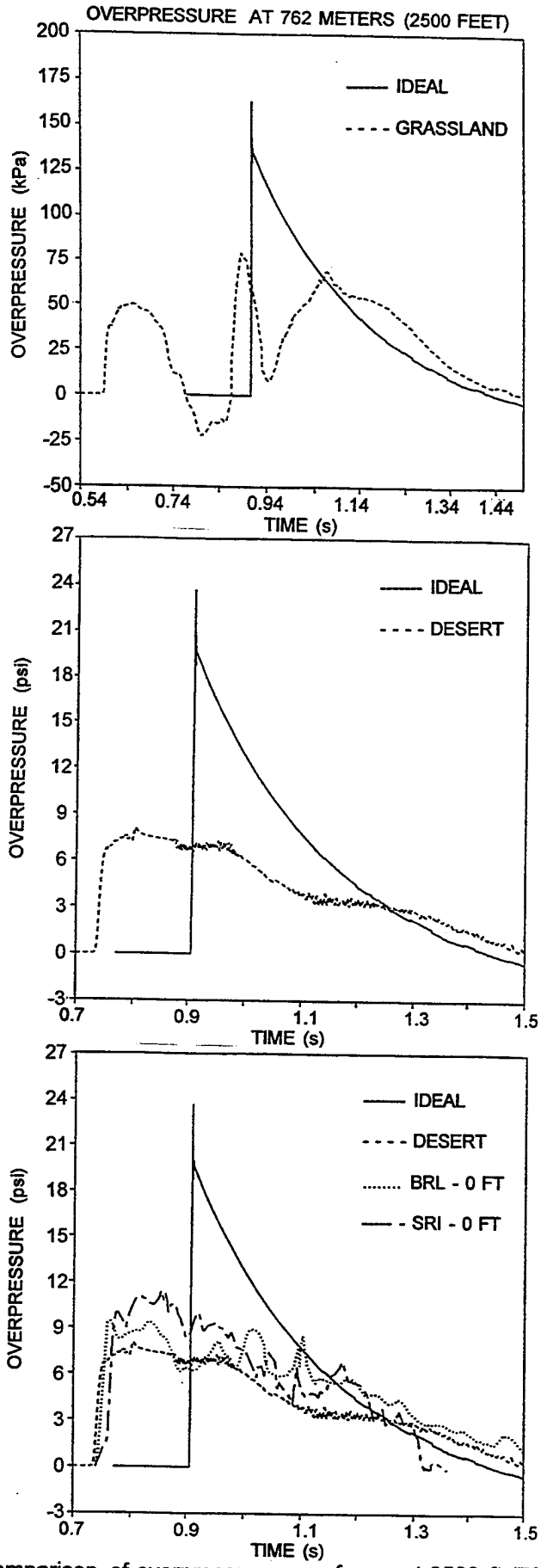

Figure 19. Comparison of overpressure waveforms at 2500 ft (762 m) for grassland, desert, and PRISCILLA data with ideal waveforms.

the lower figure the computed waveform is lower and does not have the many oscillations of the experimental records, but has the general shape.

In Figure 20 the waveforms for 3000 feet (914 meters) for an ideal overpressure of 14 psi (97 kPa) are shown. The time scale is different for the upper figure. The desert waveform is beginning the recovery phase, while the grassland precursor is still growing. It has a negative pressure section in the precursor. The peak magnitude in the precursor is about the same as that of the desert waveform. The lower figure shows the comparison with measured data. Here the computed waveform generally matches those measured except for the high narrow peak that occurs at both elevations.

Figure 21 shows the waveforms for 3500 feet (1067 meters) for an ideal overpressure of 10 psi (70 kPa). The grassland precursor in the upper figure is just about at its maximum length, while that computed for the desert is approaching cleanup, when the precursor front merges with the shock front of the main blast wave. The large variations in magnitude in the grassland precursor present in earlier waveforms are absent.

Also shown in the figure are the dynamic pressure waveforms computed for the ideal and desert surfaces. Even though the desert wave is near cleanup, the desert dynamic pressure waveform has oscillations and increased magnitudes behind the main wave. This waveform is unusual because the decaying portion does not approach the baseline at late times, and hence the impulse keeps increasing. The waveform and other parameters at this station should be examined further to explain this behavior.

Figure 22 shows the waveforms for 4000 feet (1219 meters) at an ideal overpressure of 8 psi (55 kPa). The grassland precursor has decreased in length, and oscillations in the precursor region are gone. The dynamic pressure waveform for the grassland is presented in the upper right of the page. It has multiple peaks and a larger impulse than the ideal waveform. Here also the tail of the grassland waveform does not approach the baseline.

The desert waveform in the middle left frame is clear of a precursor, but it does

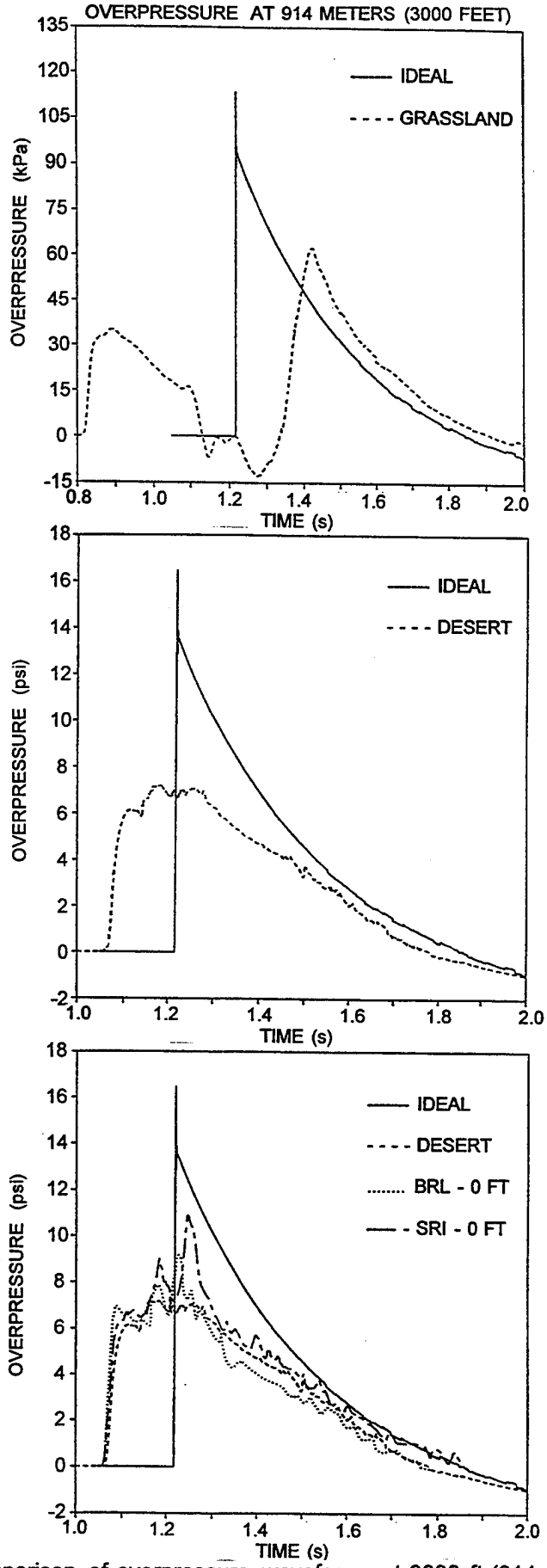

Figure 20. Comparison of overpressure waveforms at 3000 ft (914 m) for grassland, desert, and PRISCILLA data with ideal waveforms.

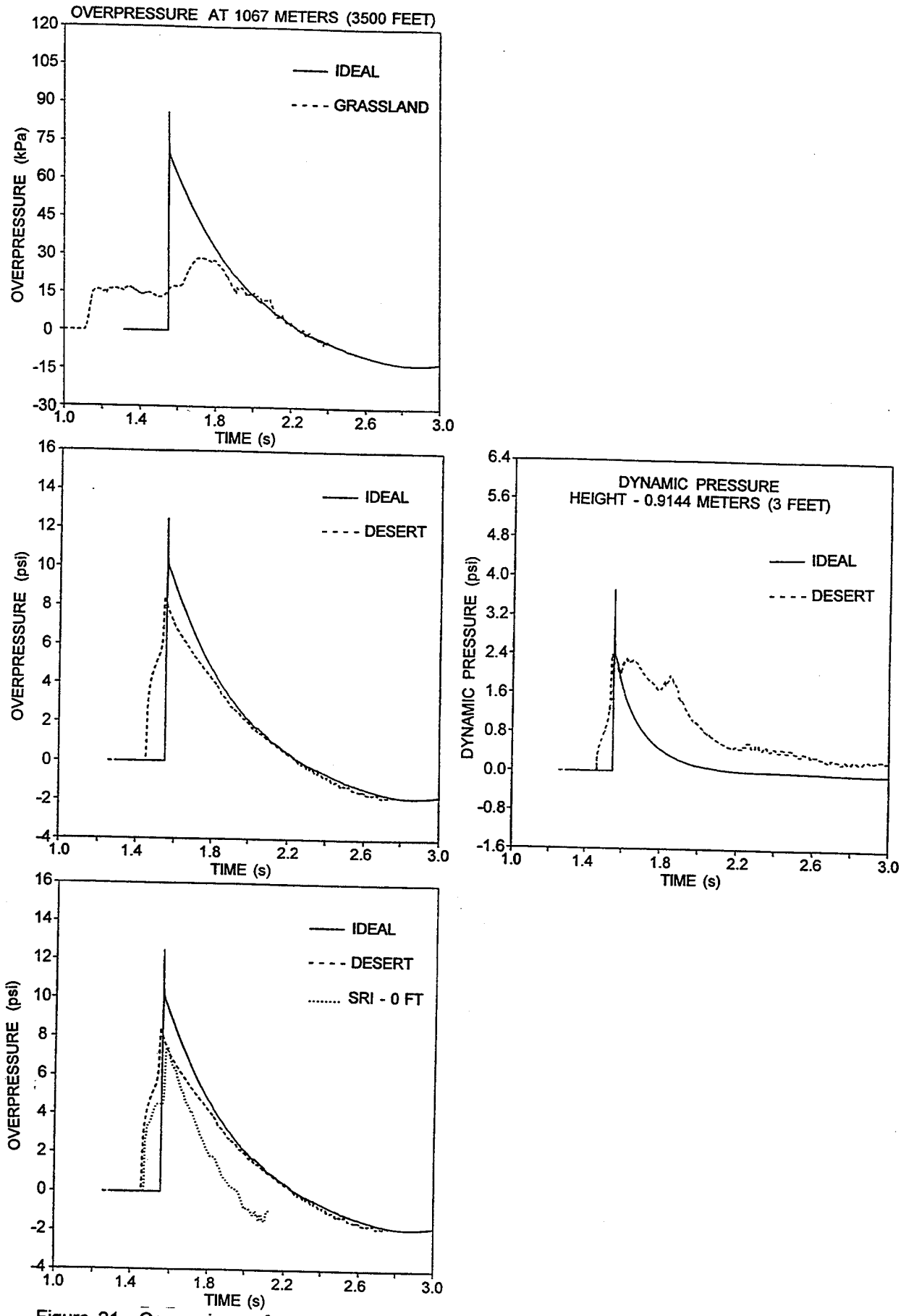

Figure 21. Comparison of overpressure and dynamic pressure waveforms at 3500 ft (1067 m) for grassland, desert, and PRISCILLA data with ideal waveforms.

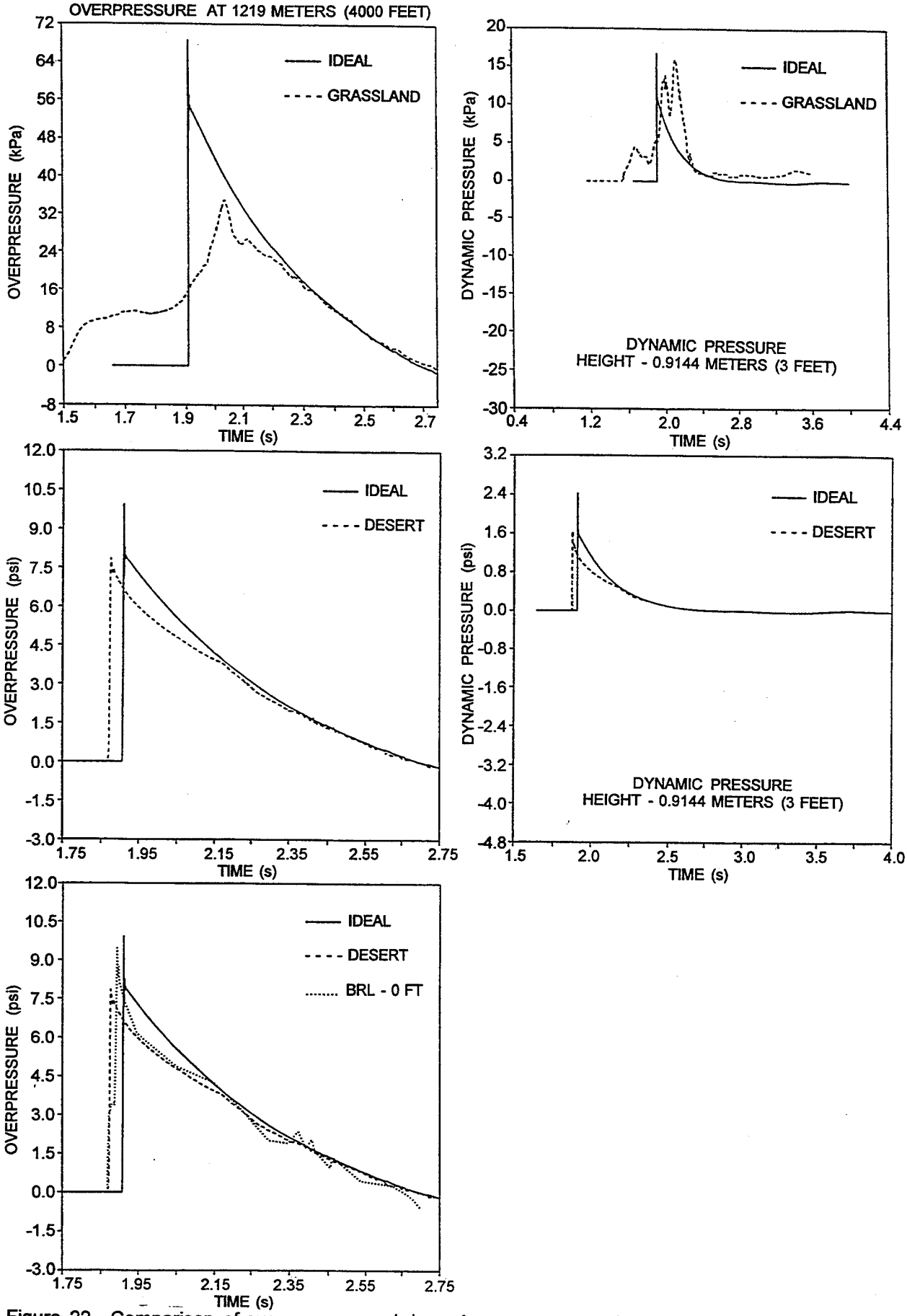

Figure 22. Comparison of overpressure and dynamic pressure waveforms at 4000 ft (1219 m) for grassland, desert, and PRISCILLA data with ideal waveforms.

have a small variation in shape in its decay. The dynamic pressure waveform in the right frame appears to have the same variation in its decay also. The measured record compared with the computed desert waveform in the lower frame still shows a precursor of limited extent. The precursor on the main blast line of PRISCILLA cleaned up about 4300 feet. Otherwise the magnitude and decay rate seem to agree well. On another blast line on PRISCILLA the precursor was not as strong as on the main blast line, and had cleaned up before the 4000 foot ground range. See Part II of this report.

Figure 23 shows the dynamic pressure waveforms at 4500 feet (1372 meters). The overpressure waveforms were not published in the reports describing the computations. The bottom figure shows there is still a slight distortion in the decay of the desert waveform compared to the ideal waveform. The grassland waveform in the upper figure has a precursor and shows large oscillations in the main part of the wave.

Figure 24 shows the waveforms at 5000 feet (1524 meters) at an ideal overpressure of about 5 psi (34 kPa). The grassland waveform has a precursor that extends about 300 milliseconds in front of the main wave, and has large oscillations in the main part of the waveform. The oscillations of the dynamic pressure waveform seem to follow those of the overpressure waveform. The desert dynamic pressure waveform in Figure 21 also shows oscillations in the main wave near precursor cleanup, and a higher impulse than the ideal waveform. In Figure 24 the dynamic pressure impulse for the grassland is less than for the ideal waveform. These waveforms should be examined further to seek the explanation for these differences. The presence of an extended precursor at such a low overpressure having a dynamic pressure impulse significantly less than that of the ideal wave is unexpected.

The computed desert waveform in the middle figure still does not have the smooth decay of the ideal waveform, but the shape seems to match the measured record shown in the bottom figure. The agreement with the experimental record is very good.

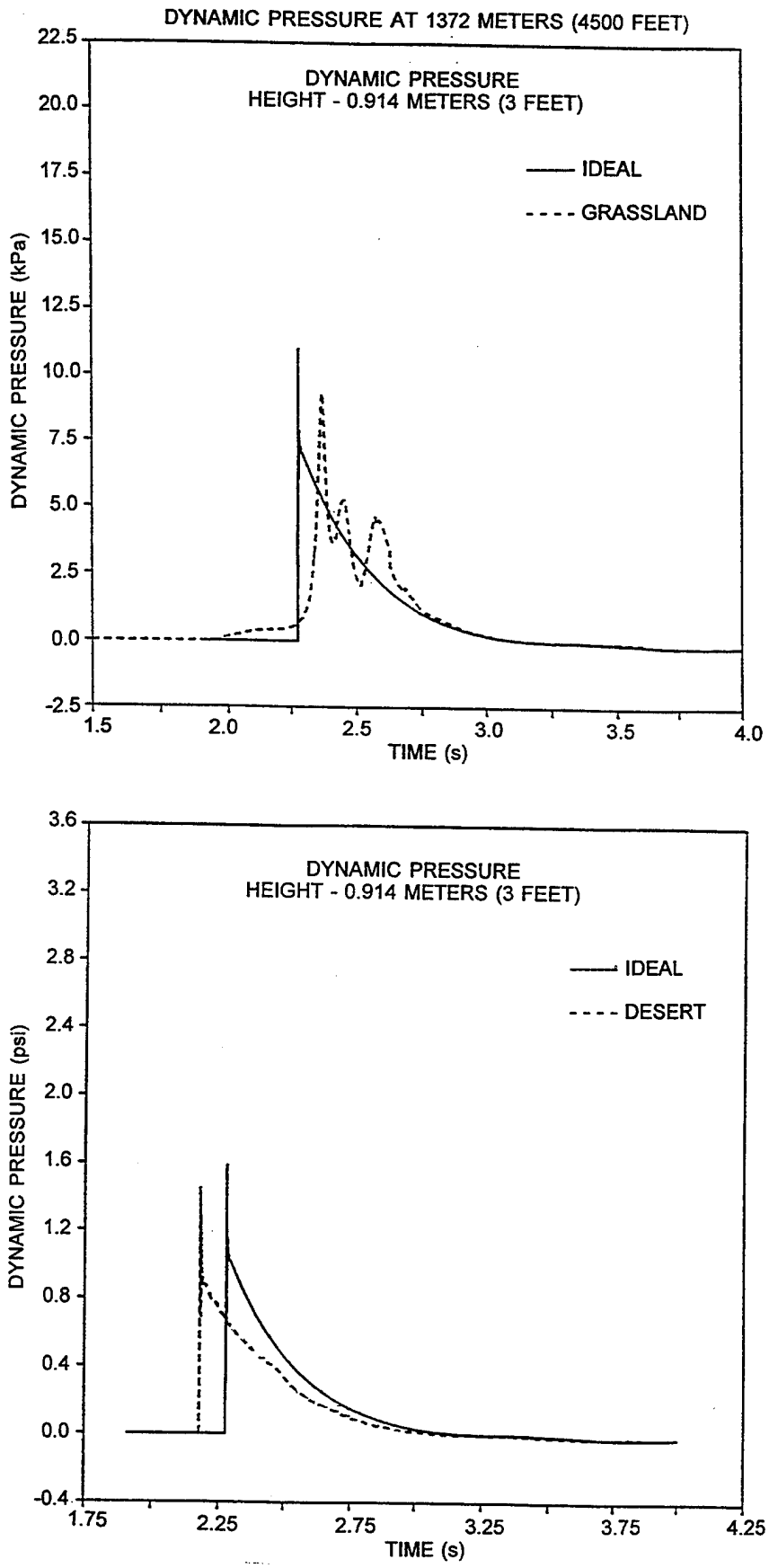

Figure 23. Comparison of computed dynamic pressure waveforms at 1372 meters (4500 feet) from the grassland, desert, and ideal computations.

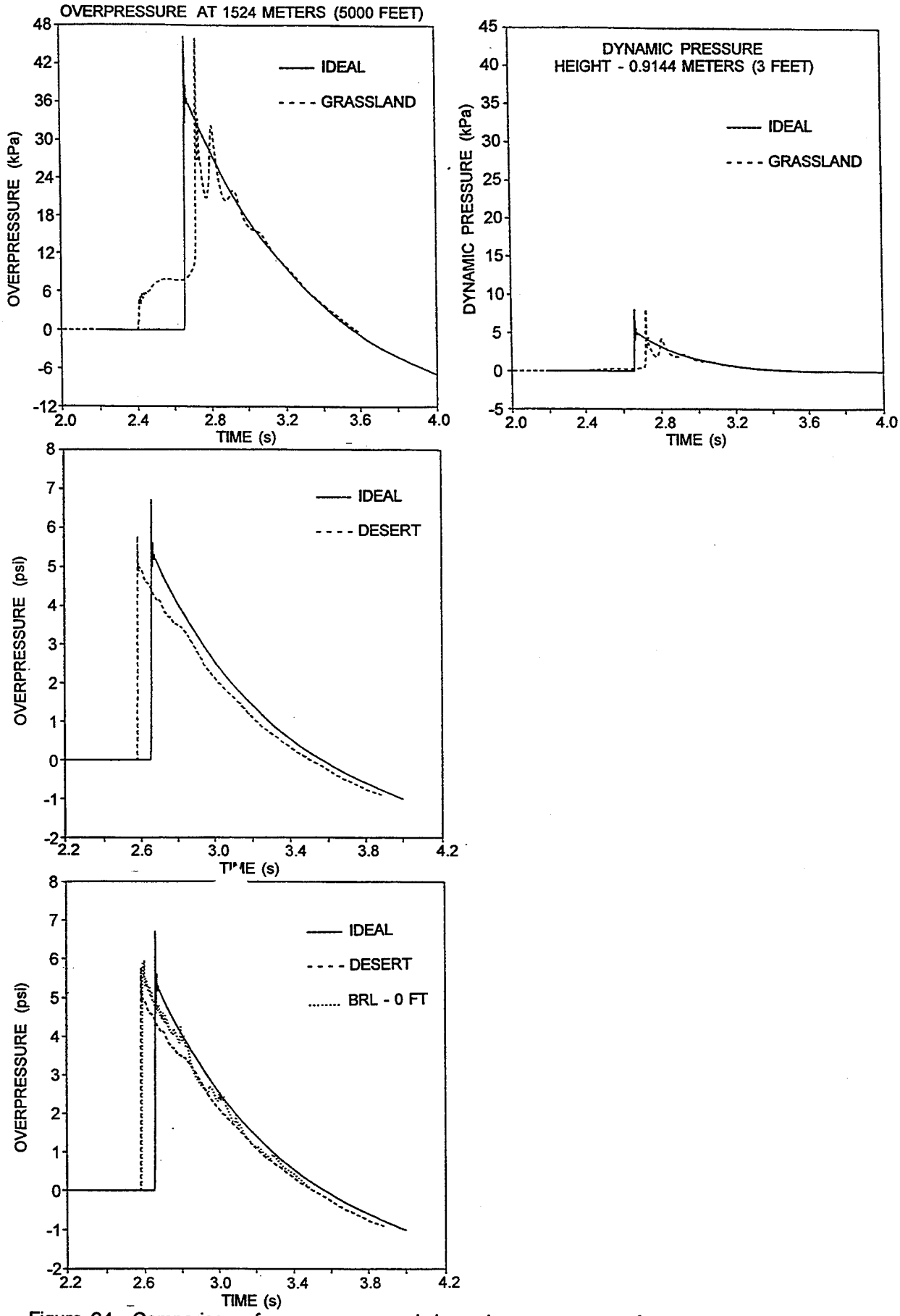

Figure 24. Comparison of overpressure and dynamic pressure waveforms at 5000 ft (1524 m) for grassland, desert, and PRISCILLA data with ideal waveforms.

9.3 Estimation of Peak Overpressures from the Ideal Surface Computation.

The SHARC ideal computation is a fine-zoned state-of-the-art computation. However, there are oscillations that occur at the shock front for overpressure (and dynamic pressure). An additional exercise was necessary to estimate the "true" peak overpressure for a waveform and its corresponding ground range.

Figure 25 shows the first part of the waveform at 1371.6 meters ground range. The oscillations are large. The numerical process used by S-Cubed to estimate the peak pressure was to take the geometric mean of the first maximum and first minimum. However, for establishing ground ranges for particular ideal overpressures of interest to the Army, improved estimates were sought.

S-Cubed provided plots like that of Figure 25 and corresponding tabulations of the first part of the surface overpressure waveforms for the overpressure range from 50 psi to 4 psi, or 503 meters to 1829 meters. To obtain an improved estimate, the following procedure was used: Beginning at a time when the oscillations had completely decayed on the waveform, five points were read from the tabulation for the waveform, spaced about one half-cycle of the oscillations apart. A linear least squares fit was made through these five points. The fitted line was extrapolated to the time of half-rise to the first peak, and the overpressure computed. The values obtained for the waveforms are listed in Table 9 beginning at 502.9 meters. Peak values for ranges less than 502.9 meters were read from the waveform plots, since the wave shape was not appropriate for the extrapolation technique.

In the range where the extrapolation technique was used, the geometric mean technique use by S-Cubed produced values that were from two to seven percent high compared to the values obtained by extrapolation.

Table 9 also lists the ideal horizontal dynamic pressure impulses at a height of 3 feet for the ground ranges shown. These values were derived from the tabulations in Appendix A.

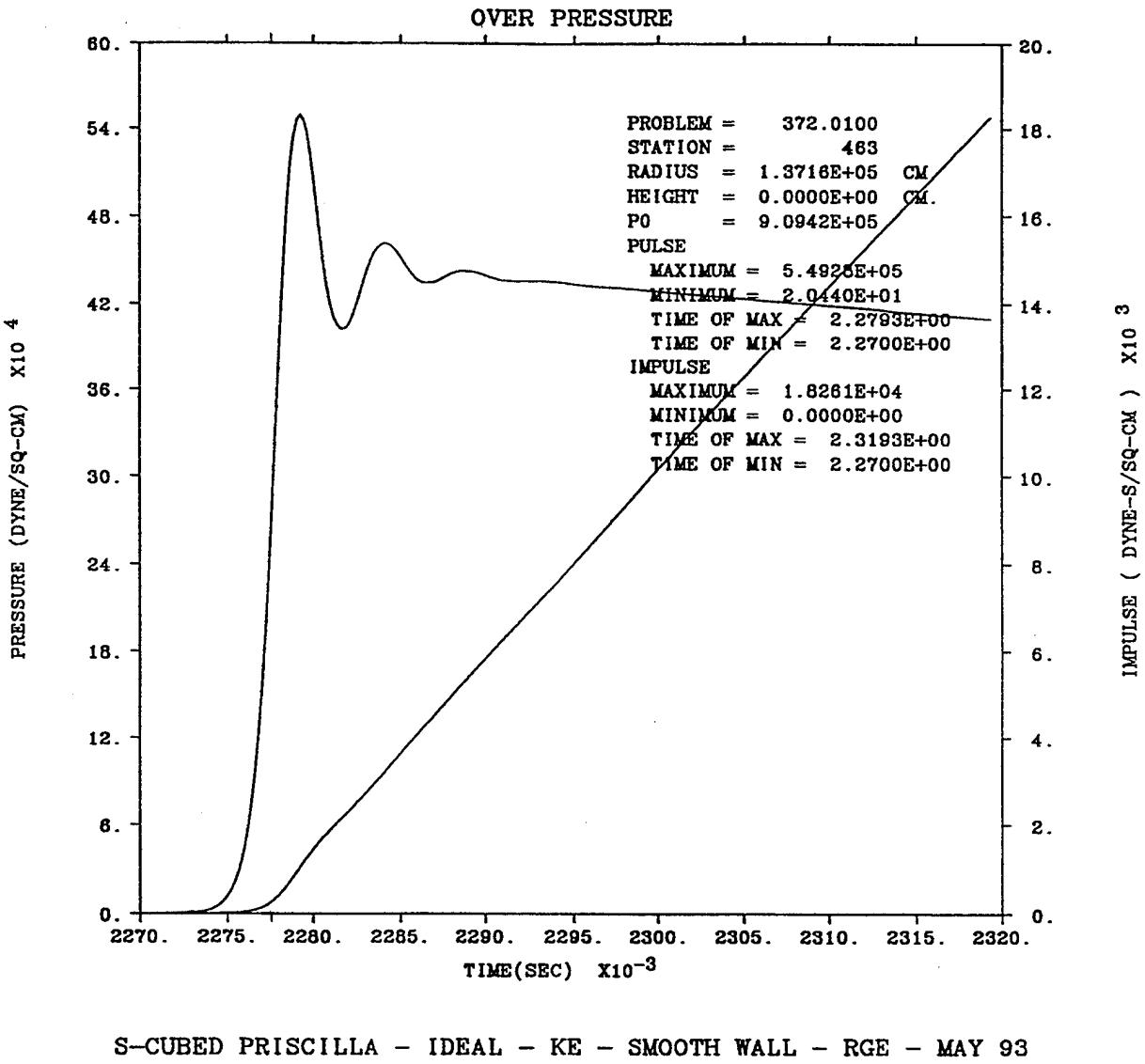

Figure 25. The initial part of the ideal overpressure waveform at 1371.6 meters, showing the damped oscillations at the front.

9.4 Comparison of Ideal Peak Overpressure and Dynamic Pressure Impulse with Predictions by REFLECT-4.

REFLECT-4 is a sharp-shock hydrodynamics code developed by the Avidyne Division of Kaman Sciences Corporation (30) for predicting the blast field from nuclear explosions above the surface. One of the computations was for a 40 kiloton explosion at a scaled height of burst of 200 feet, which is very close to the PRISCILLA scaled height of burst of 204 feet.

Overpressure versus ground range values from this computation were scaled to PRISCILLA conditions using modified Sachs scaling. They were plotted and a smooth curve drawn through them as shown in Figure 26. The circled data points are the ideal values taken from Table 9. The agreement is very good, especially in the range of Army interest from 50 psi to 4 psi.

Figure 27 shows a comparison of the ideal horizontal dynamic pressure impulse with that computed by REFLECT-4. Here the curve is from the SHARC computation and the circled data points are from REFLECT-4. Again the agreement is good.

The SHARC computation was performed for a constant atmosphere, while the REFLECT-4 considered the variation in atmospheric properties with altitude. Some differences in computed values may be due to this difference in treatment of the atmosphere and the small difference in scaled height of burst, as well as the different computing technique.

The REFLECT-4 code is an older code that uses a quite different computational technique. It has been used for many different applications, including generating the ideal dynamic pressure impulse chart in EM-1 (31). Perhaps SHARC is validating REFLECT-4 in the present circumstances. Nevetheless, it is reassuring to observe the good agreement between the two.

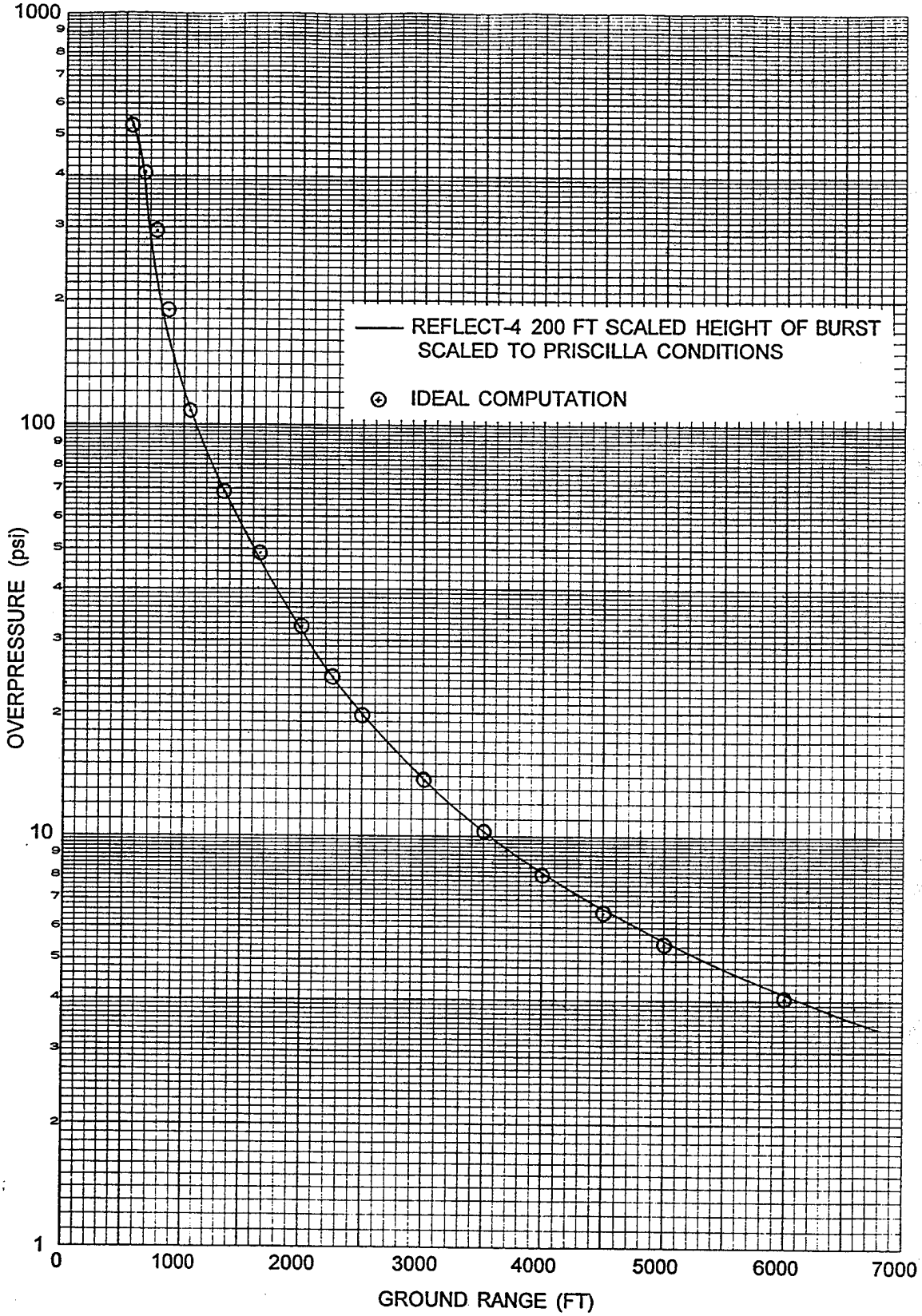

Figure 26. Comparison of overpressures from the ideal PRISCILLA computations to a curve of REFLECT-4 values scaled to PRISCILLA conditions.

Table 9. Estimated peak values of surface-level overpressure from the ideal computation.

Ground Range (m)	Ground Range (ft)	Overpressure (kPa)	Overpressure (psi)	DPIH (3 ft)** (kPa-s)
167.6	550	3711*	538*	41.6
198.1	650	2803*	407*	44.9
228.6	750	2034*	295*	52.0
259.1	850	1303*	189*	60.5
320.0	1050	752*	109*	69.8
411.5	1350	476*	69*	48.6
502.9	1650	341	49.5	26.1
609.6	2000	223	32.3	14.8
685.8	2250	168	24.4	10.9
762.0	2500	137	19.9	8.32
914.4	3000	95.0	13.8	5.18
1066.8	3500	70.5	10.2	3.46
1219.2	4000	55.4	8.03	3.04
1371.6	4500	45.0	6.52	1.79
1524.0	5000	37.6	5.46	1.36
1828.8	6000	27.9	4.05	0.77

* Read from plots. All other values in column from extrapolation to time to rise to one-half of first peak.

** Horizontal dynamic pressure impulse from tabluations in Appendix A.

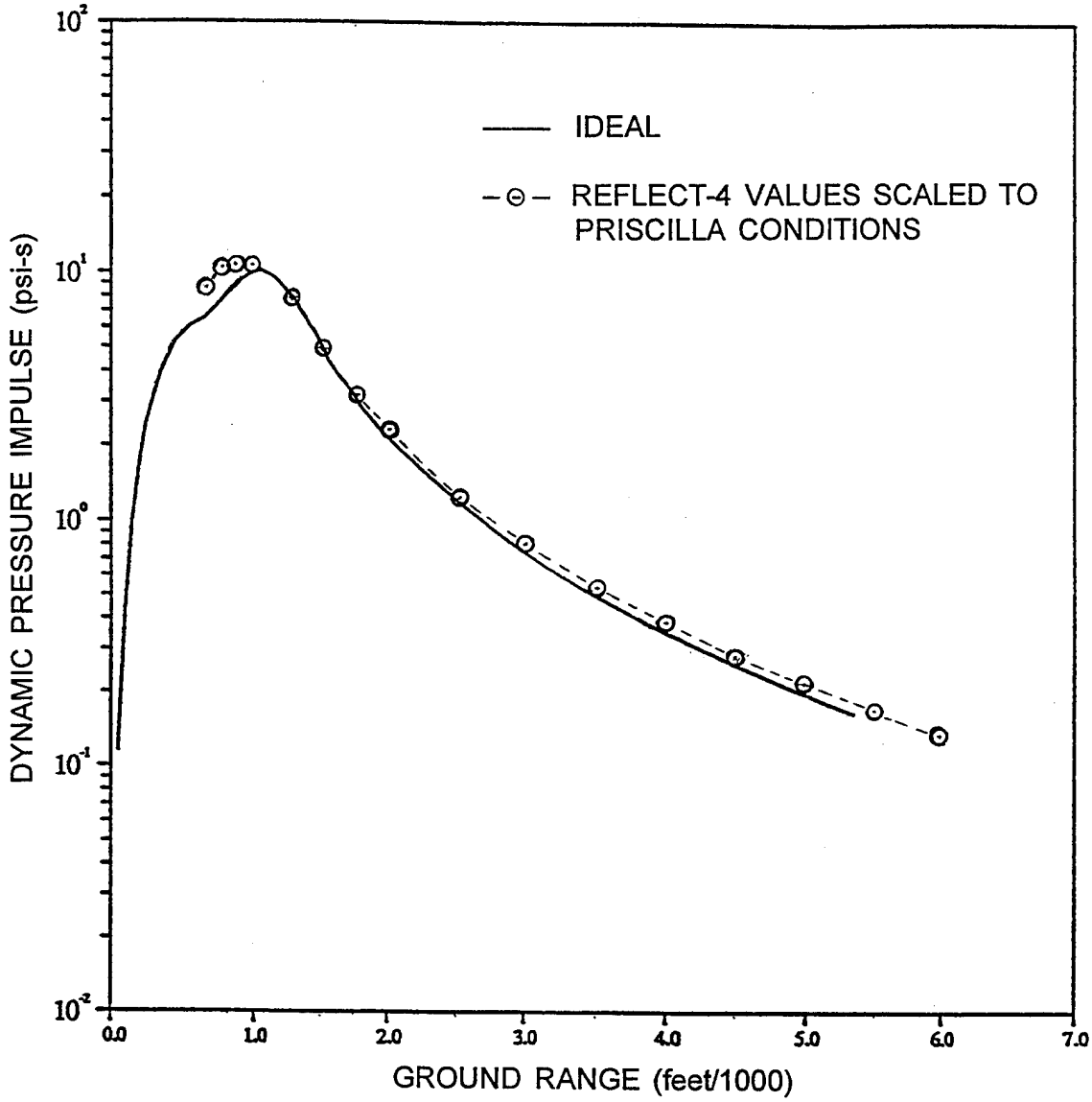

Figure 27. Comparison of dynamic pressure impulse from a 200-foot scaled height of burst REFLECT-4 computation with the horizontal dynamic pressure impulse at an elevation of 0.914 meters (3 ft) from the ideal computation.

9.5 Comparison of Computed Overpressures with Experimental Data.

Figure 28 shows the ideal peak overpressure curve plotted using the extrapolated values from Table 9, the peak overpressure from the desert computation taken from the S-Cubed tabulations in Appendix A, and experimental data from Table 2.

There is scatter in the data points, such as the two at 610 meters. But scatter is to be expected for reasons noted before in Section 3 above. The data seem to agree with the ideal curve close in and beginning at 1070 meters. The failure of the desert curve to return to the ideal pressure curve far out is unexplained. The experimental data from a number of nuclear tests, including PRISCILLA, show that usually the overpressure recovers from the precursor effects somewhat above the ideal and then approaches the ideal curve, as shown by the BRL data in Figure 28.

9.6 Comparison of Dynamic Pressure Impulse over Desert with Experimental Data.

The dynamic pressure impulse is the parameter of particular concern for overturning and displacing combat and transport vehicles, towed generators, and other mobile systems. Figure 29 shows the comparison of the experimental data with the horizontal dynamic pressure impulse versus range at the 3 foot (0.914 meters) elevation from the desert computation. The vertical component is negligible beyond a range of 76 meters. The agreement is generally good. The disagreement of the point at about 1620 meters is not surprising, since the differences between a stagnation pressure record and a side-on overpressure record at such low overpressures can have large errors.

The SRI and BRL values at about 760 meters differ from each other, but the difference is easily within the range that can be expected in the precursor region. In any case both the experimental data and the desert computation show large increases in impulse above the ideal curve.

Figure 30 shows the comparison for an elevation of 10 feet (3.048 meters). Here there are fewer data points, but the agreement is very good. Only the SRI electronic

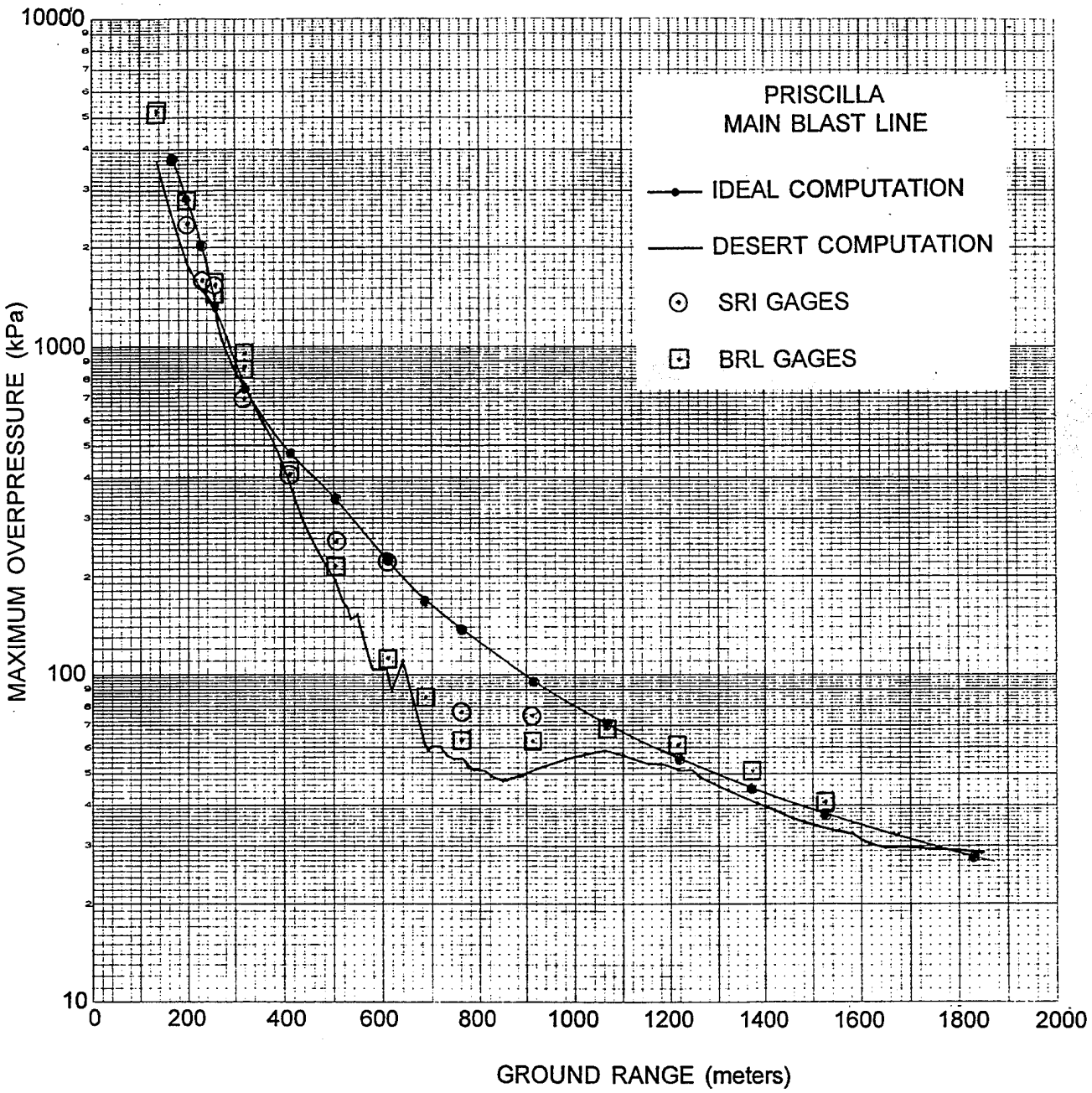

Figure 28. Comparison of maximum overpressure from the ideal and desert computations with experimental data from SRI and BRL gages on the surface.

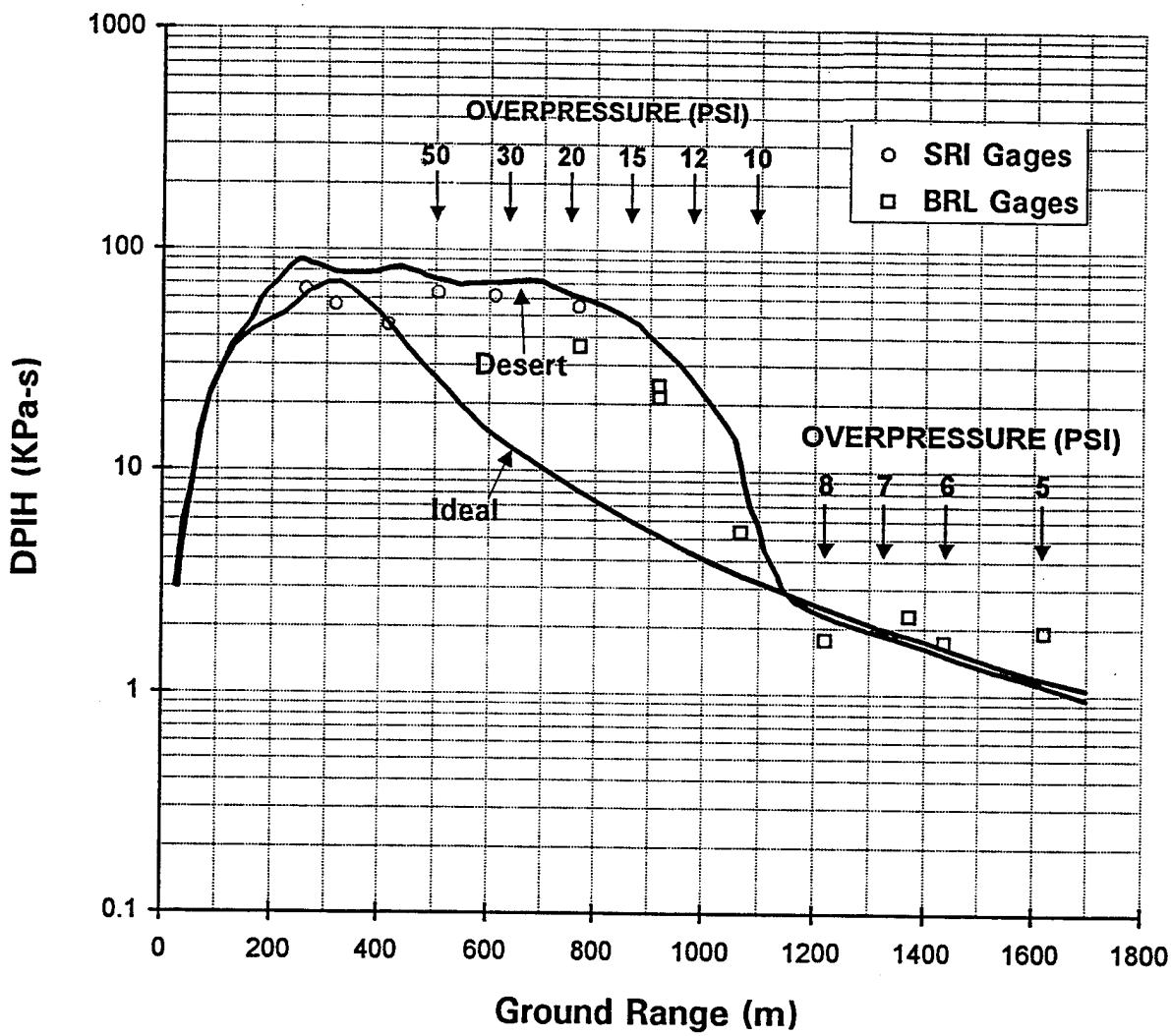

Figure 29. Comparison of horizontal dynamic pressure impulse versus range at the 3 ft (0.914 m) elevation from the desert computation with experimental data and the impulse from the ideal computation. Ranges for ideal overpressures are indicated by the arrows.

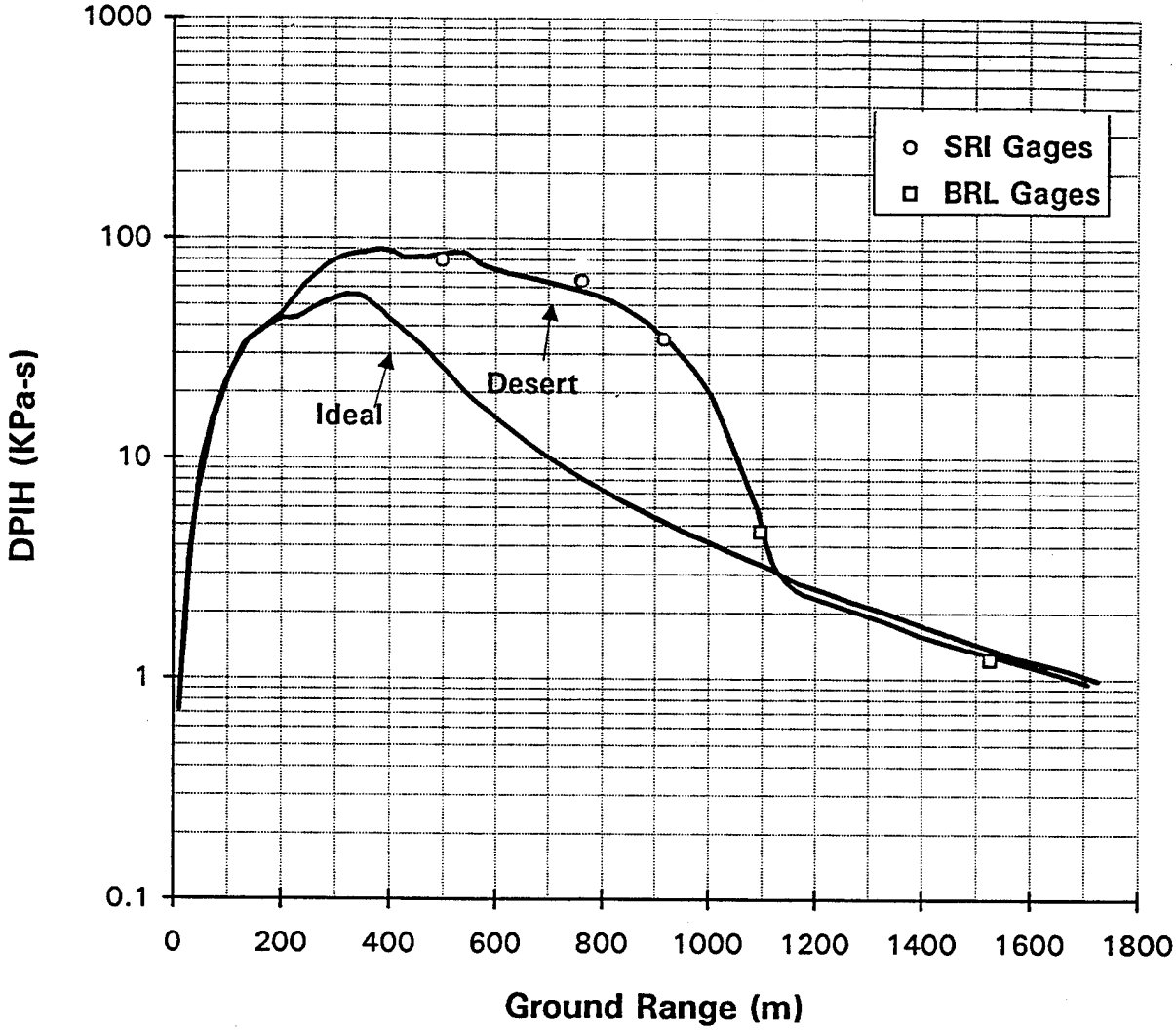

Figure 30. Comparison of horizontal dynamic pressure impulse versus range at the 10 ft (3.048 m) elevation from the desert computation with experimental data and the impulse from the ideal computation.

gages were placed where the increase is very large, but the values derived from them appear on or near the computed curve.

9.7 Comparison of Dynamic Pressure Impulse for the Three Computations.

Figure 31 shows a comparison of dynamic pressure impulse versus ground range for all three cases for an elevation of 3 feet (0.914 meters). The curve for the grassland shows an increase over the ideal curve greater than that produced over desert. It extends to over 1380 meters. The increase over desert begins at a lesser ground range but it increases faster with decreasing ground range than the grassland curve. The reason for the desert and grassland curves falling below the ideal curve at late times is not known. As noted earlier, the desert overpressures are less than ideal in this region, but the wave shape is essentially ideal. The grassland case still has an extended precursor in this region, but it is well into the cleanup phase. Further analysis is needed to explain this lowering of pressure and impulse.

Figure 32 shows the results for an elevation of 10 feet (3.048 meters). Here the grassland impulses are higher in the range from 300 to 800 meters than those for the 3 foot (0.914 meters) elevation. The peak at 1370 meters in the grassland curve is as computed, caused by dust raised to the elevation of that station (32).

9.8 Enhancement of Dynamic Pressure Impulse versus Ground Range.

Figure 33 shows the ratio of the horizontal dynamic pressure impulse at the 3 foot (0.914 meters) elevation from the desert and grassland computation to that of the ideal surface versus ground range. The enhancement is very large in the range of primary interest to the Army (up to 30 psi). The peak ratio is 7.8 at about 17 psi for the desert, and 8 for the grassland at about 17.5 psi. At the beginning of the increase at the farthest ranges a decrease in range of about 75 meters provides values double that of the ideal values. For the desert, reducing the ground range from 1150 meters by 150 meters (13 percent) yields an increase above the ideal value of a factor of five. The change for the grassland curve is not as great. A decrease of 350 meters from 1375 meters(25 percent)

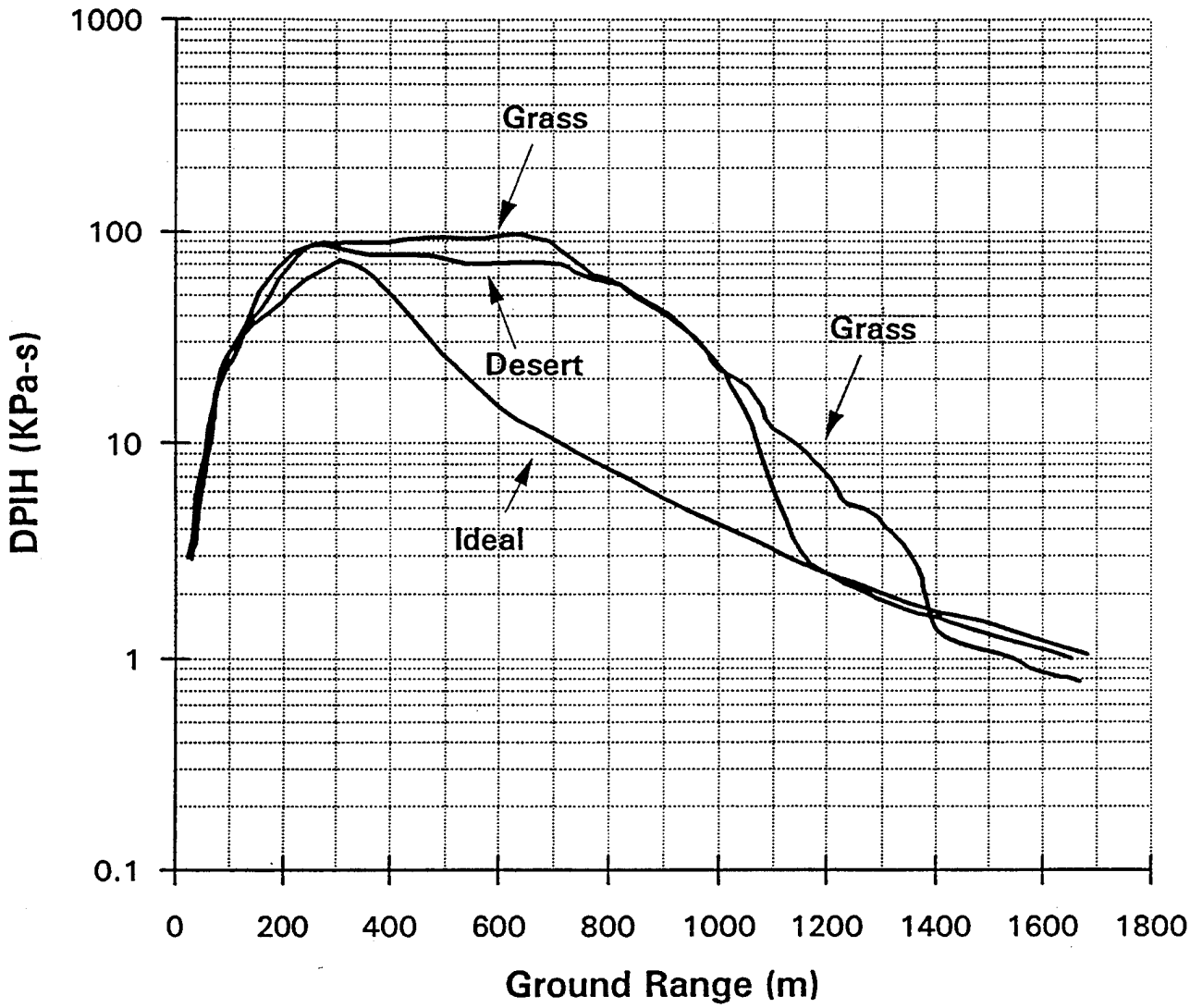

Figure 31. Dynamic pressure impulse at the 3-ft (0.914 m) elevation versus ground range for the ideal, desert, and grassland computations.

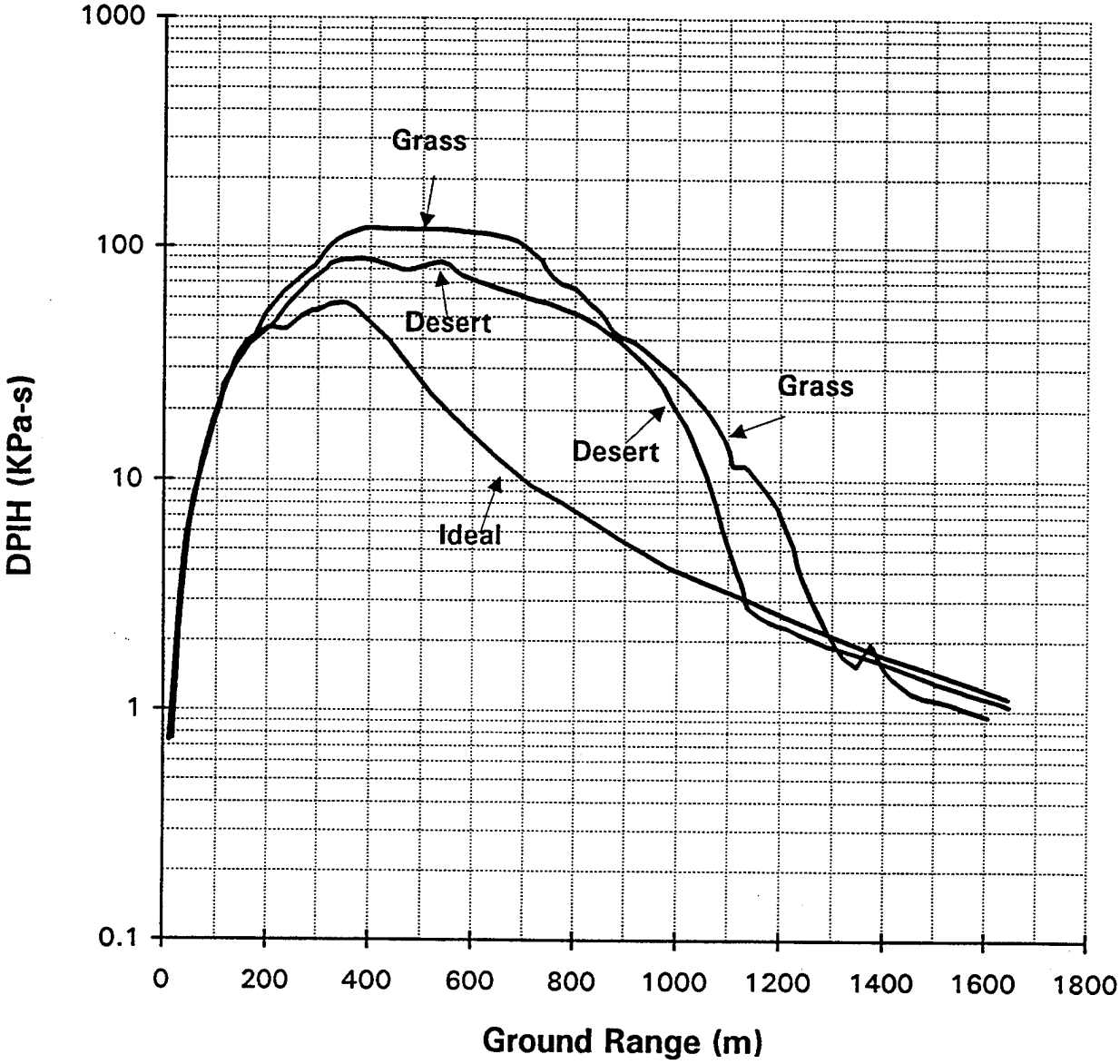

Figure 32. Horizontal dynamic pressure impulse versus ground range at the 10-ft (3.048 m) elevation for the three computations. The peak at 1370 meters for the grassland was computed and appears to correspond to passage of a vortex.

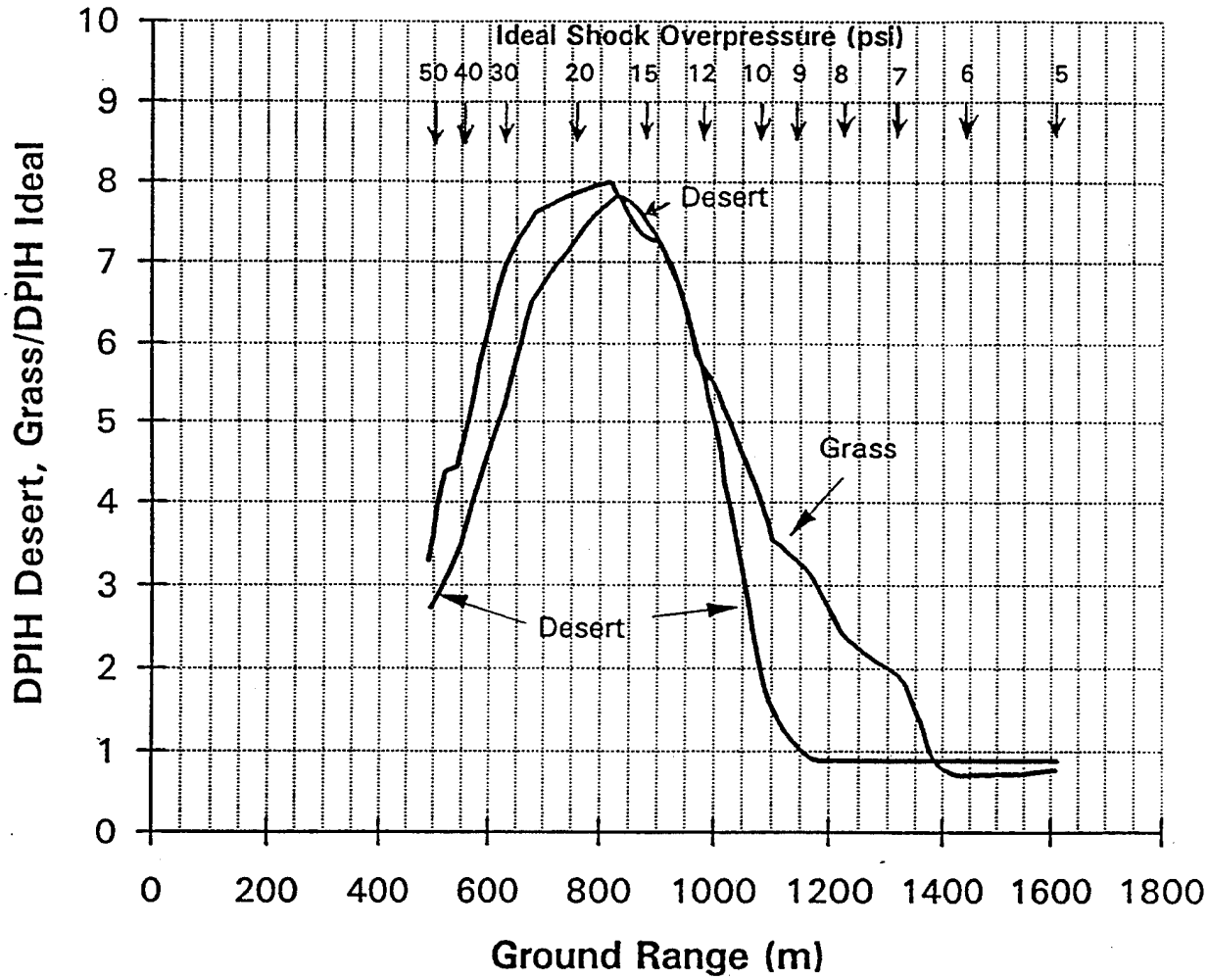

Figure 33. Enhancement in horizontal dynamic pressure impulse above ideal at the 3-ft (0.914 m) elevation versus ground range for the desert and grassland cases. The arrows at the top of the figure show the ranges for ideal shock overpressures.

is required to produce an increase of a factor of five. These enhanced values of dynamic pressure impulse can produce displacement and damage of military equipment at ranges significantly greater than for an ideal surface.

The increase in ground range for a given value of dynamic pressure impulse to be produced by non-ideal blast compared to ideal blast is shown in Figure 34 for the desert and grassland surfaces. For 10 psi ideal overpressure, the increase is 24 percent for grassland and 6 percent for the desert case. The desert radii probably would be extended farther if the computation had produced a precursor that matched the arrival times and separation between the precursor front and main wave that actually occurred.

At 15 psi ideal, the increase is 39 percent for the grassland and 26 percent for the desert. At 20 psi the increase is 55 percent for the grassland and 41 percent for the desert case. This corresponds to an increase in area for producing the 20 psi ideal dynamic pressure impulse by a factor of 2.4 for grassland and 2 for the desert.

Figure 35 shows the same ground range ratios, except they are plotted against dynamic pressure impulse. The arrows at the top mark the dynamic pressure impulses that correspond to the ideal overpressures listed.

9.9 Non-Ideal Blast Extensions of Vehicle Overturning Limits.

A tank, a heavy armored vehicle (HAV), a light armored vehicle (LAV), a 2-1/2 ton truck with canvas over the bed and carrying a 5000 pound load, and the 1/4 ton truck (Jeep) had previously been modeled in the BRL overturning code (33). They were selected to provide a range of vehicle targets from soft to hard. The code was run for PRISCILLA conditions using the ideal waveforms in the code for a scaled height of burst of 60 meters (197 feet). The code has an option for running using only drag loading. Since the slow rise of the precursor waveforms in the region involved would reduce or eliminate diffraction loading, that option was used for these overturning calculations. All vehicles were assumed to be side-on to the blast. No sliding was allowed. The code

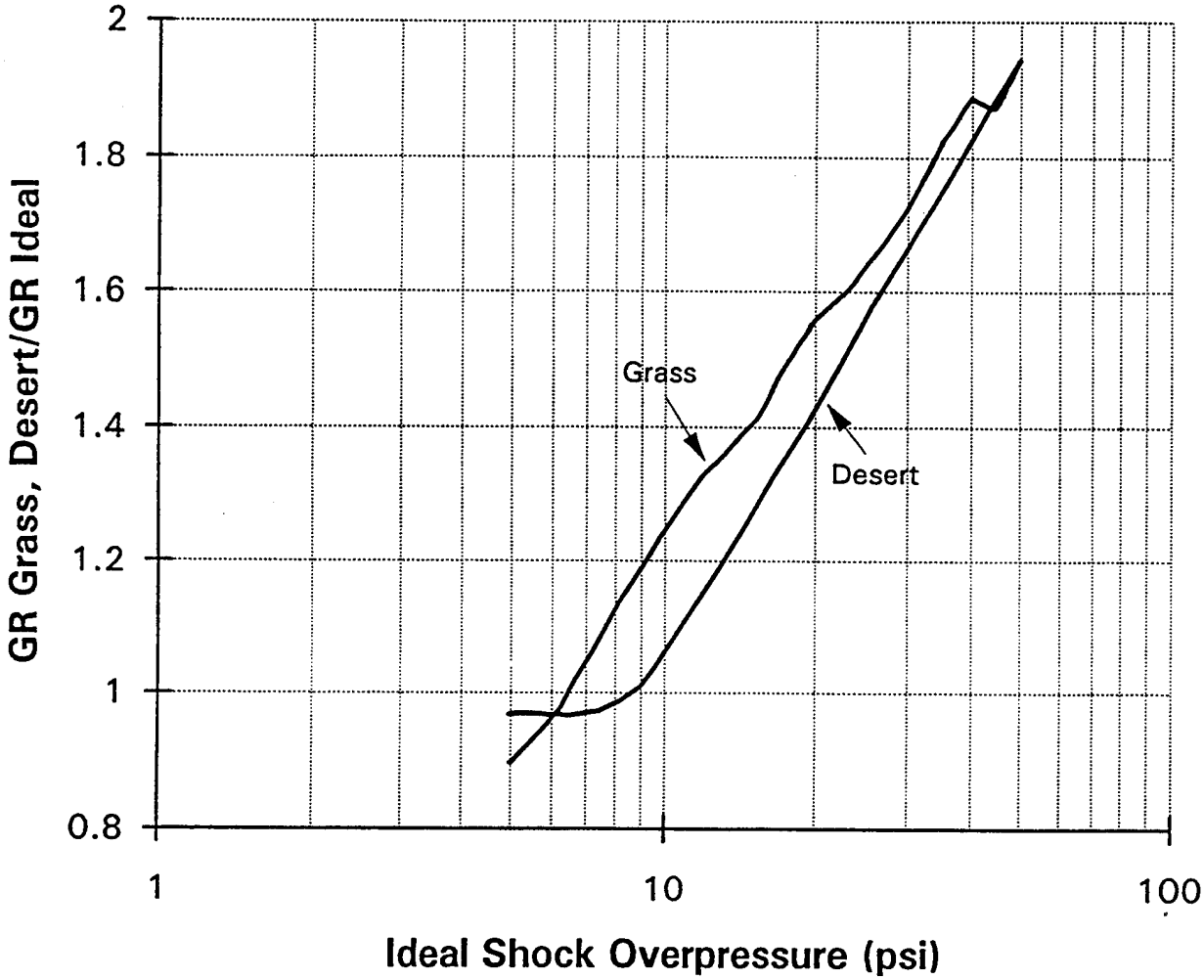

Figure 34. Ratio of ground ranges for equal dynamic pressure impulse versus ideal shock overpressure.

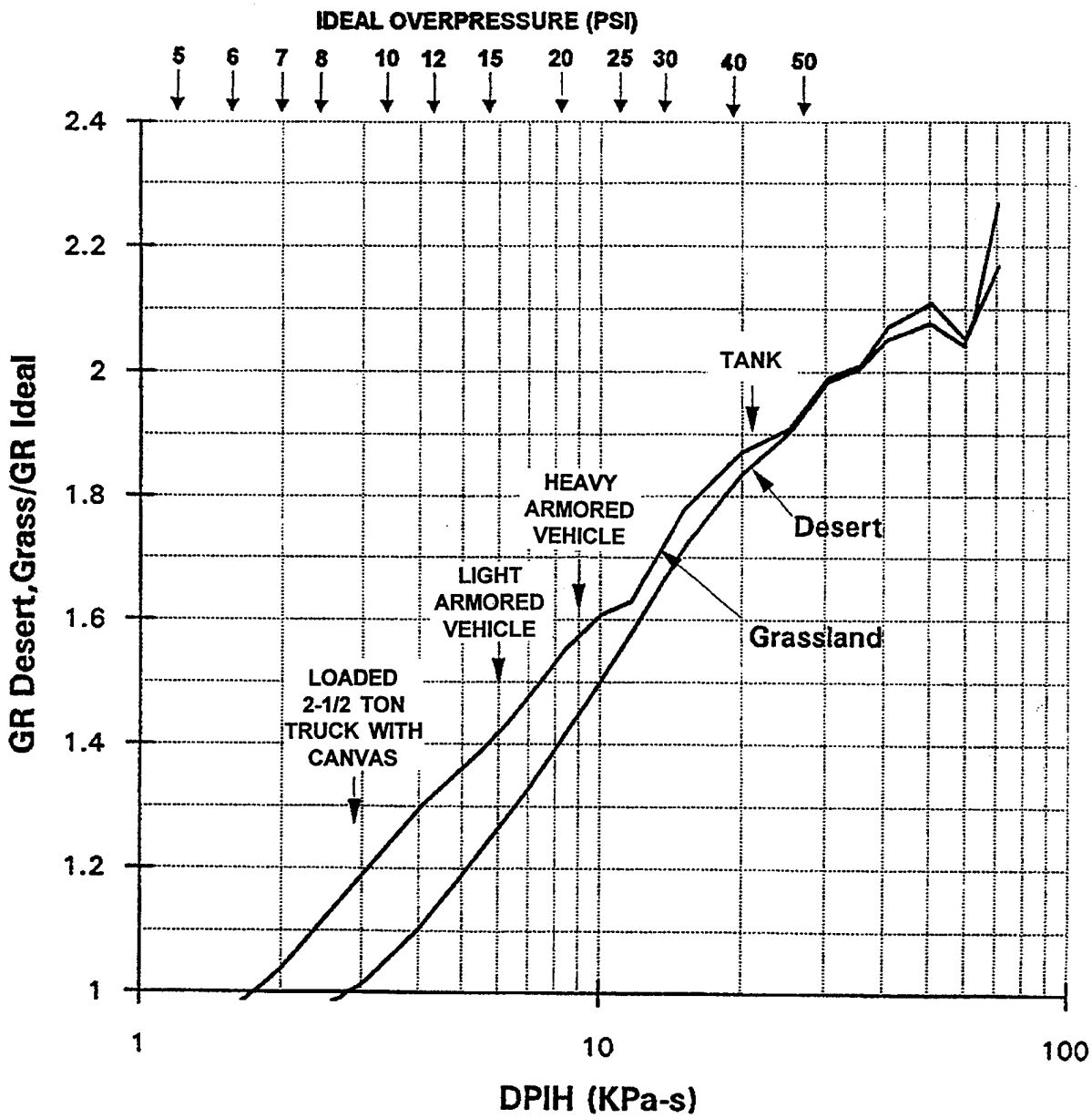

Figure 35. Increase in non-ideal ground range over ideal ground range versus horizontal dynamic pressure impulse. The arrows show the predicted levels of DPI for overturning (side-on orientation) of the vehicles computed using the BRL overturning code with ideal waveforms and reduced diffraction loading.

computed the overturning threshold, and one of the outputs is the dynamic pressure impulse of the waveform that just produced overturning. The arrows in Figure 35 under the vehicle names show the resulting impulses. It is assumed that non-ideal dynamic pressure impulses of the same magnitudes would also produce overturning. The non-ideal waveform may be more effective because of the higher values maintained for longer times in the waveform than occur for the ideal exponentially-decaying waveform.

The curves in the figure show the ratio of the non-ideal ground range to the ideal ground range for a given dynamic pressure impulse, i. e., the factor by which the ideal ground range is increased by the non-ideal blast for a given dynamic pressure impulse on the abscissa. For the tank the increase in range is 1.83 for the desert and 1.87 for the grassland, for an area increase of about 3.5. For the heavy armored vehicle the increase in range is 1.45 for desert to 1.58 for grassland, for area increases of 2.1 and 2.5. For the light armored vehicle, the increase in range is 1.27 for the desert and 1.42 for grassland, for area increases of 1.6 for desert and 2.0 for grassland.

The truck overturning occurs at a dynamic pressure impulse level where the ground range is increased only for the grassland, and the factor is 1.17 for an area increase of 1.37. As noted earlier, the desert precursor in the computation was not as extensive as that on the actual PRISCILLA event, and cleaned up earlier. A new computation for the desert surface that produced a precursor that matched the experimental data in extent might well show an increase in ground range for the DPI for truck overturning on the desert surface.

Figure 36 shows the total displacements of 1/4 ton trucks (Jeeps) exposed side-on to blast versus dynamic pressure impulse. The data are from a variety of nuclear explosion yields and heights of burst (34). The Jeeps were not loaded and had no canvas tops. The computed impulse levels for overturning for the tank, heavy armored vehicle, light armored vehicle, and 2-1/2 ton truck are presented across the top of the figure with arrows showing the levels for overturning for PRISCILLA. An examination of Jeep displacements at the levels of overturning for the heavier vehicles provides some indication

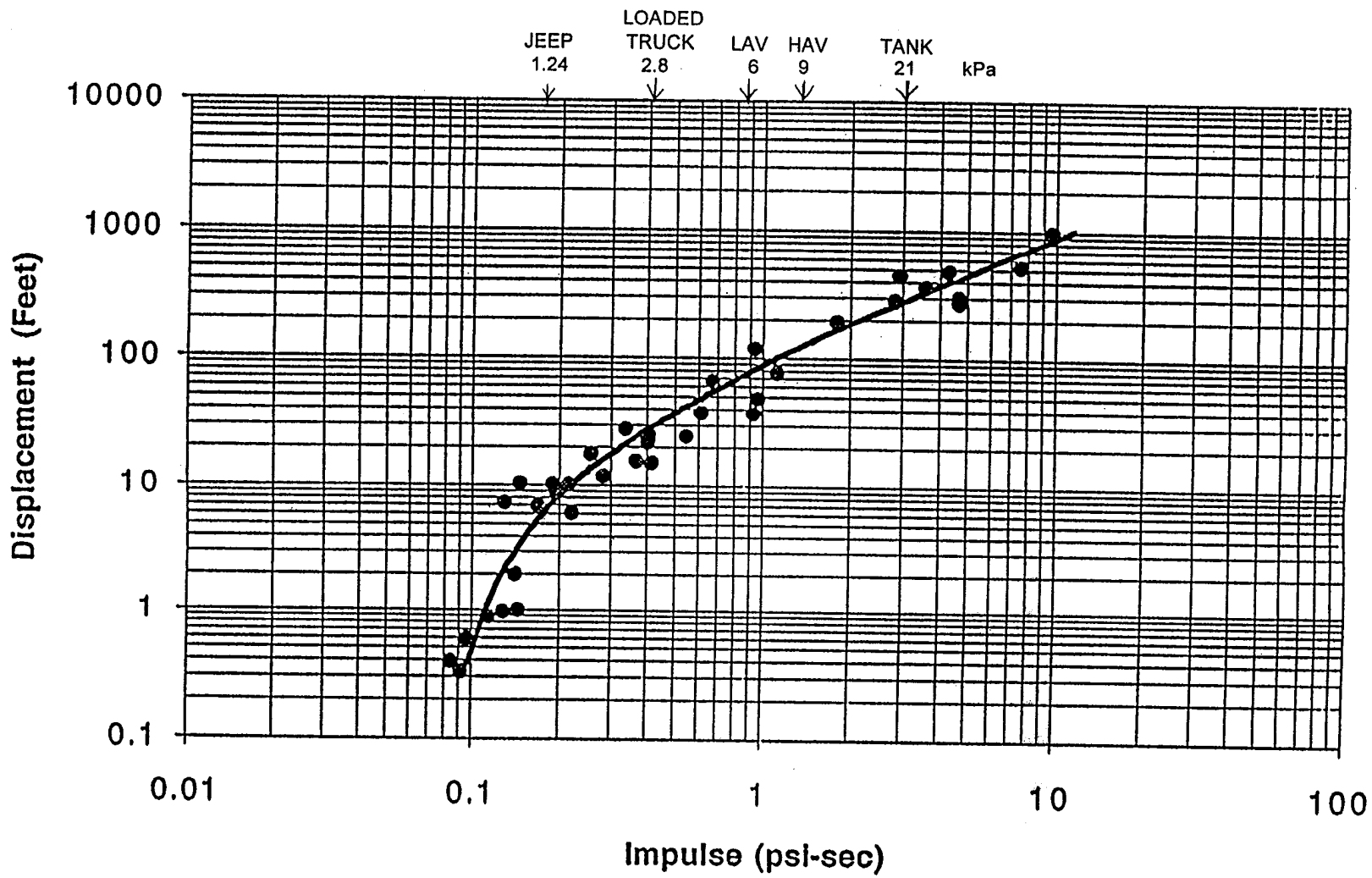

Figure 36. Displacement versus dynamic pressure impulse for Jeeps exposed side-on to long-duration blast waves. Computed overturning levels for vehicles are shown by arrows at the top of the figure.

of the forces involved. The data and curve in Figure 36 show that a Jeep would be displaced 200-450 feet if exposed alongside a tank that barely overturned. For the heavy armored vehicle, the Jeep displacement would be about 120 feet. The light armored vehicle overturning threshold corresponds to Jeep displacements of 40 to 120 feet. At the truck overturning threshold the displacements range from 15 to 30 feet.

Also shown is the computed overturning threshold for a Jeep. Diffraction loading was included for the Jeep because the overturning overpressure was 5 psi, at which level the precursor had cleaned up on the nuclear tests. The curve shows a displacement of six feet. Simple overturning of the Jeep onto its side would move the center of gravity 4.5 feet, while overturning on its back would move it about 8 feet. So the threshold overturning code prediction for a Jeep seems reasonable.

9.10 System Design Implications.

Figure 37 shows the ground range shift for the overturning threshold of dynamic pressure impulse for the tank, the heavy armored vehicle, the light armored vehicle, and the loaded 2-1/2 ton truck. The changes in ground range produced by non-ideal blast have been shown before in Figure 35. The intersections of the horizontal lines, which are the threshold overturning levels, with the desert and grassland curves mark the overturning thresholds on those curves. The increase in dynamic pressure impulse as the ground range is decreased from the intersection points in the desert and grassland curves is rapid. The dynamic pressure impulse loading is doubled for all vehicles for a decrease in ground range of 10 percent or less. A change in effects radii of ten percent or less is usually considered not significant.

Overturning will have detrimental effects on vehicle systems and crew personnel. However, modifying a vehicle so that it will not overturn under double the loading normally required may be difficult. An appropriate design goal may be to have the vehicle system remain combat-effective after exposure to the non-ideal, high-drag environment as long as it remains upright or until it translates a distance equal to its own length.

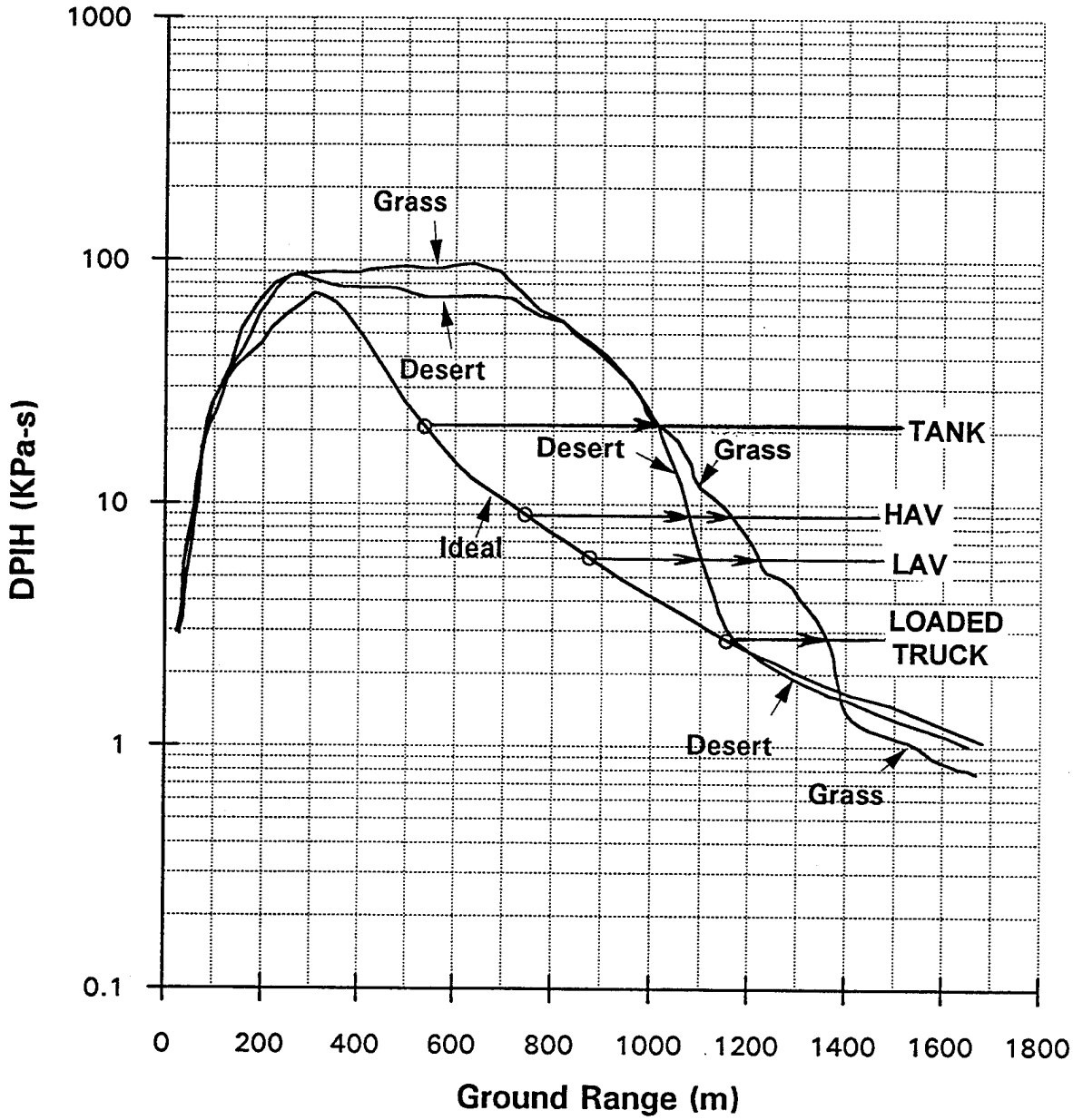

Figure 37. Comparison of the DPI levels for overturning of vehicles with the DPI versus ground range curves for the three computations. The arrows show the increase in range for overturning of the tank, the heavy armored vehicle (HAV), the light armored vehicle (LAV), and loaded truck produced by the enhancement of dynamic pressure impulses above the ideal values.

9.11. Implications for Simulation Tests.

The above proposed design goal for vehicle system reponse suggests that a system that can produce a short-duration high-speed flow with dynamic pressure impulses somewhat above the overturning thresholds of these vehicles (to allow for other than side-on orientation) would be a candidate for testing Army systems. The records from nuclear tests show that the precursor waveforms usually have a slow rise that will reduce or eliminate diffraction loading. Thus it is not very important to provide a shock front for testing in the region of enhanced dynamic pressure impulse.

The waveform of the exit jet from the 5.5 foot diameter shock tube at ARL, Aberdeen Proving Ground, Maryland, looks similar to one phase of the precursor cycle when the dynamic pressure impulse is enhanced. It produces turbulent, high-speed flow. The jet has adequate energy for testing, not only for the design goal proposed, but also for serious damage to equipment. This was demonstrated by a test in which an armored personnel carrier was displaced more than 100 feet.

The unmodified jet is narrow, but a device to spread the jet has been designed by ARL, and is currently under development. It will be possible to add sand or other material in the shock tube expansion section to produce a material-laden jet that can sandblast a system as would occur in the non-ideal blast from a nuclear explosion.

Another prime candidate for a non-ideal blast simulator is the Large Blast/Thermal Simulator (LB/TS) constructed near the Stallion Range Center, White Sands Missile Range, New Mexico. This facility was designed to test military equipment to ideal blast waves up to 35 psi and a yield of 600 kilotons. The exit jet from the LB/TS may provide a suitable high-speed, short-duration flow for simulation of non-ideal blast.

The grassland computation produced a precursor that apparently does not clean up until around 3 psi. THe LB/TS may be able to produce such a waveform by dividing the drivers into two sets and firing them at different times to produce the far-out precursor

waveform. The Defense Nuclear Agency is sponsoring a program to explore ways to utilize the LB/TS to simulate non-ideal blast.

10. CONCLUSIONS.

The three PRISCILLA computations performed by S-Cubed using SHARC are the finest-zoned computations to date that were run to a time of four seconds and for the complete positive phase of the five psi overpressure waveform for an ideal surface.

The desert computation produced reasonable agreement with most of the PRISCILLA data, particularly the dynamic pressure impulse. The experimental data are limited and subject to variations due to the complex conditions in the precursed region and the severe environment of a nuclear explosion. The enhancement of dynamic pressure impulse over that for the ideal surface began at 1160 meters and attained a maximum of of a factor of 7.8 increase over ideal at the range of 850 meters and 16 psi ideal overpressure. However, the arrival times were later than actually occurred, the extension of the precursor was less, and it cleaned up earlier than actually occurred on the main blast line. These differences may be caused partially by the omission of the use of the dust diffusion routine for the first 700 feet of travel of the shock front along the surface. The omission was discovered too late to rerun the computation.

The grassland computation produced a strong and persistent precursor. The enhancement of dynamic pressure impulse began at 1380 meters, 18 percent farther out than for the desert, and reached a maximum enhancement of eight above the ideal impulse at a range of 825 meters and 17 psi ideal overpressure. At the 5 psi ideal overpressure level at the end of the computation, the grassland waveform had a precursor extending 300 milliseconds in front of the main wave. Extrapolation of the arrival time curve in Figure 15 suggests that cleanup would occur at about 3 psi. The range for which Army equipment will be subject to non-ideal blast is greatly extended for this computation. However, the dynamic pressure impulse from the computation at these far-out ranges is less than ideal rather than more. This region needs to be explored further.

The non-ideal enhanced dynamic pressure impulses extend the limiting ranges for survivability of military equipment by factors as large as 1.8. Because of the rapid increase in impulse with decreasing range, the change from little damage to severe damage will occur for a relatively small decrease in ground range compared to that for the ideal blast wave.

These three computations have shown that non-ideal blast can extend effects radii by large factors. This is confirmed by the nuclear test data for military equipment exposed on desert surfaces. The grassland computation shows that the effects radii can be extended still farther. Such enhancements can influence targeting and damage assessment doctrine. A program to explore non-ideal blast versus surface conditions, yields, and heights of burst needs to be pursued.

The original plan for the computations, that of using the same zone size and same machine for the runs was found to be impractical because of the very long running times required for the desert and grassland cases. The zone sizes used are still too large to provide a good representation of the complex conditions in the precursor. Very fast codes and machines must be developed so that non-ideal blast simulations can be run with finer zones, ideally in three dimensions, in reasonable times per run.

The original intent was to use the THRML code to predict the thermal layer for both the desert and grassland surfaces. THRML produced unrealistic predictions for the desert surface compared to known experimental data. The thermal layer used for the desert surface was based on sound speed versus ground range derived from the experimental arrival times. The THRML code has been most thoroughly developed for vegetated surfaces. The code needs to be improved and validated where practical by experiments so that it can make reasonable predictions for bare soil. A program to improve THRML is described in Appendix B.

The thermal layer for the grassland case was computed using the experimental arrival times over the desert. There is a very large mismatch between these arrival times

and those produced by the grassland hydrocode computation. The effect of using a thermal layer computed for much later times than occurred in the hydrocode computation is not known.

The hydrocode and THRML need to be coupled so that the predictions by THRML are made for the arrival times produced by the hydrocode. The codes currently can be coupled by a labor-intensive process of extrapolating arrival times from the hydrocode a short distance, using THRML to predict conditions at those times, inserting them into the hydrocode, running the hydrocode, and repeating the process to maintain reasonable agreement. The hydrocode should be modified so that the THRML values are inserted into the hydrocode as the wavefront progresses, so that there is no need to modify the thermal layer to produce pressure equilibrium.

The grassland and desert computations need to be repeated in such a way that optimum use is made of both SHARC and THRML. This is particularly important to develop an understanding of the precursor in the far-out cleanup region .

The extreme conditions that can occur in the precursor with relatively small changes in ground range have implications for systems design. High drag flows for testing equipment can be produced at the ARL 5.5 foot diameter shock tube, and ultimately in the LB/TS.

11. RECOMMENDATIONS.

Determine if the far out behavior of the desert and grassland blast waves (low dynamic pressure impulses, persistent precursor) is maintained for reruns of the cases using SHARC and THRML to best advantage.

Analyze the current three computations for information that explains some of their peculiarities and can be used to improve the follow-on computations. For example: Why do the dynamic impulses for the desert and grassland computations stabilize below the

ideal curve, far out? The grassland values are well below the ideal. What is the reason for the region of enhanced dynamic pressure impulse for the grassland to end while the waveform still has an extended precursor? Why are there large oscillations in the overpressure and dynamic pressure waveforms in the low-pressure region of the grassland computation beyond the enhanced dynamic pressure impulse region? How much dust was scoured from the desert and grassland surfaces, and is it a reasonable amount?

Rerun the three PRISCILLA computations for a stratified rather than a constant atmosphere, and with finer zoning, if practical. Make the subgrid long enough to include the precursor and the front of the main peak.

Recompute the grassland computation with the THRML code coupled so that shock arrival times match the times for which the THMRL code made predictions for the thermal layer. This can be done manually until faster codes and machines permit direct coupling.

For the desert thermal layer derived from experimental arrival time measurements, run computational experiments to determine how many cells thick the region of constant temperature with height should be to adequately register the presence of the thermal layer in the computation.

Repeat the desert computation using a thermal layer constructed from Carpenter's experimentally derived sound speed values assuming an acoustic wavefront. Choose the number of cells versus height based on the results of the study recommended above. Monitor the computation from blast wave contact with the surface and make periodic adjustments, if necessary, to insure that the wavefront arrival times match those measured on PRISCILLA.

Run SHARC so that the thermal layer values are inserted at the time of shock arrival, so that altering the predicted thermal layer densities to produce pressure equilibrium is unnecessary.

Improve the THRML code so that it can make good predictions for desert surfaces in particular and for other soil types if possible, using additional experiments to check the modeling where possible. Support the program for improving the THRML code that was prepared by Barthel and is described in Appendix B.

Initiate a program to develop faster codes for faster machines to enable using the fine zones required for full development of the complex flow field of non-ideal blast, and direct coupling of a hydrocode and the code predicting the thermal layer. A major step in meeting this need would be to modify SHARC to run on a massively parallel multiprocessor machine (35,36).

To evaluate improvements made in the codes, perform computations for ideal, desert, and grassland surfaces for other nuclear tests on which measurements were made and thermal layer predictions made from arrival time measurements, and where device shielding was minimal. These include MET (22 KT), HOOD (74.1 KT), WILSON (10.3 KT). Compare and evaluate the computations for each shot and make any indicated improvements in the codes before proceeding to the next shot.

Design and perform a matrix of computations of non-ideal blast to cover the range of interests of the Army, considering variation in yield, scaled height of burst, surface conditions, and typography. Analyze the results and their significance for the Army.

Consider the implications of non-ideal blast effects for systems design.

Continue development of the ARL 5.5 foot diameter shock tube exit jet as a non-ideal blast simulator, and investigate methods of using the LB/TS for simulating non-ideal blast waves.

12. LIST OF REFERENCES.

1. DESERT ROCK Exercise VII and VIII, Final Report, Annex L, 1957, Las Vegas, NV. AD-A078 561.

2. Needham, C. E., Ekler, R. G., and Kennedy, L. W., "Extended Desert Calculation Results with Comparisons to PRISCILLA Experimental Data and a Near-Ideal Calculation". S-Cubed Report No. SSS-DTR-94-14802. This report will be published as ARL Contract Report No. 235, July 1995.

3. Ekler, R. G., Needham, C. E., and Kennedy, L. W., "Extended Grassland Calculation Results with Comparisons to PRISCILLA Experimental Data and a Near-Ideal Calculation", S-Cubed Report No. SSS-DFR-94-14920. This report will be published as ARL Contract Report No. 236, July 1995.

4. Bryant, E. J., and Keefer, J. H., "Basic Air Blast Phenomena", Operation PLUMBBOB - Project 1.1, WT-1401, Ballistic Research Laboratories, Aberdeen Proving Ground, MD, June 1962.

5. Meszaros, J. J., Hoover, C. J., Day, J. D., Schwartz, E. G., and Burden, J. G., "Instrumentation of Structures for Airblast and Ground Shock Effects", Project 3.7, Operation PLUMBBOB, WT-1426, Ballistic Research Laboratories, Aberdeen Proving Ground, MD, 1959.

6. Swift, L. M., Sachs, D. C., and Kriebel, A. R., "Air-Blast Phenomena in the High-Pressure Region", Project 1.3, Operation PLUMBBOB, WT-1403, Stanford Research Institute, Menlo Park, California, December, 1960.

7. Wistor, J. W., and Perret, W. R., "Ground Motion Studies at High Incident Overpressure", Project 1.5, Operation PLUMBBOB, WT-1405, Sandia Corporation, Albuquerque, New Mexico.

8. Vortman, L. J., "Effects of a Non-Ideal Shock Wave on Blast Loading of a Structure", Project 34.1, Operation PLUMBBOB, ITR-1472, Sandia Corporation, Albuquerque, New Mexico, August 1957.

9. Banister, J. R., and Vortman, L. J., "Effects of a Precursor Shock Wave on Blast Loading of a Structure", Project 34.1, Operation PLUMBBOB, WT-1472, Sandia Corporation, Albuquerque, New Mexico, October 1960.

10. Kelso, J. R., Editor, "Data Reduction Procedures for Nuclear Blast Instrumentation", AFSWP-1084, Defense Nuclear Agency, Alexandria, Virginia, August 1959.

11. Rogers, S. H., "Stressing Thermal Layer Sensitivity to Parameters in the THRML Code Model", DNA-TR-90-10, Defense Nuclear Agency, Alexandria, VA, June 1990.

12. Kuhl, A. L., "NTS Precursor Data Interpretation", presented at DNA-sponsored Thermal Effects Meeting at R&D Associates, Marina Del Rey, CA, April 1984.

13. Barthel, J. R., "On the Relationship Between Thermal Layer Sound Speed and Precursor Observables", DNA-TR-88-241, Defense Nuclear Agency, Alexandria, VA, January 1992.

14. Mazzola, T. A., "Small ICBM Nuclear Hardness and Survivability Technology Development, A Summary of Thermal Layers for HML Non-Ideal Airblast Calculations", DNA-TR-89-118-SUP, Defense Nuclear Agency, Alexandria, VA, February 1991.

15. Carpenter, H. J., Engler, M. J., McCaffree, L. A., "Pre-Shock Thermal Layer Sound-Speeds Developed from Nuclear Test Data", DNA-TR-89-190, Defense Nuclear Agency, Alexandria, VA, August 1991.

16. Carpenter, H. J., Private Communication.

17. Mazzola, T. A., Private Communication.

18. Kennedy, L. W., and Rogers, S. H., "Thermal Layer Computations for Non-Ideal Airblast Scenario Assessment", S-Cubed Report SSS-DFR-92-13512, September 1992.

19. Kennedy, L. W., Private Communication.

20. Hikida, S., Bell, R., and Needham, C., "The SHARC Codes: Documentation and Sample Problems", S-Cubed Report SSS-R-89-9878, September 1988.

21. Needham, C. E., and Kennedy, L. W., "SHARC - S-CUBED Hydrodynamic Advanced Research Code", S-Cubed Report SSS-VQ-89-10617/R2, July 1989.

22. Pierce, T. H., "Numerical Boundary Layer Analysis with k-e Turbulence Model and Wall Functions", DNA-TR-87-15, Defense Nuclear Agency, Alexandria, VA, September 1986.

23. Barthel, J. R., Needham, C. E., Pierce, T. H., and Schneyer, G. P., "A Computational Model for Precursed Airblasts over Rough Surfaces", S-Cubed Report SSS-R-89-10003, August 1989.

24. Pierce, T. H., "Turbulence and Real-Surface Sub-Models in S-Cubed Hydrocodes", S-Cubed Draft Report DTR-91-12671, 1991.

25. Reisler, R. E., et al., "DIAMOND ARC 87 - Blast Phenomenology Results from HOB, HE Tests with a Helium Layer, Volume 1, DNA-TR-88-99-V1, Defense Nuclear Agency, Alexandria, VA, March 1988.

26. Sharp, A. L., "A Thermal Source Model from SPUTTER Calculations", AFWL-TR-72-49, Phillips Laboratory, Kirtland AFB, Albuquerque, NM, March 1973.

27. Schneider, K. D., Private Communication, 1995.

28. Carpenter, H. J., Private Communication, 1995.

29. Barthel, J. R., Private Communication, 1995.

30. Smiley, R. F., Ruetenik, J. R., and Tomayko, M. A., "REFLECT-4 Code Computations of 40 KT Nuclear Blast Waves REflected From the Ground", KA TR-201, DNA-TR-81-203, November 1982.

31. EM-1, Capabilities of Nuclear Weapons, Chapter 2, Section 2II, DNA-EM-CH-2-SEC-2II, Defense Nuclear Agency, Alexandria, VA, February 1992.

32. Schneider, K. D., Private Communication, 1995.

33. Ethridge, N. H., "Blast Overturning Model for Ground Targets", BRL Report No. 1889, Ballistic Research Laboratory, Aberdeen Proving Ground, MD, June 1976. The diffraction loading algorithms have been updated since the report was written.

34. Bryant, E. J., and Allen, F. J., "Dynamic Pressure Impulse for Near-Ideal and Non-Ideal Blast Waves - Height-of-Burst Charts", Contract No. DNA001-80-C-0156, Defense Nuclear Agency, Alexandria, VA.

35. Schraml, S. J., "A Data Parallel Implementation of the BRL-Q1D Code, Technical Report BRL-TR-3389, Ballistic Research Laboratory, Aberdeen Proving Ground, MD, September 1992.

36. Schraml, S. J., "Evaluation of a Multiple Instruction/Multiple Data (MIMD) Parallel Computer for CFD Applications, ARL-TR-589, US Army Research Laboratory, Aberdeen Proving Ground, MD, October 1994.

INTENTIONALLY LEFT BLANK.

APPENDIX A

TABULATIONS OF BLAST PARAMETERS FOR DESERT, GRASSLAND, AND IDEAL CALCULATIONS

Kennneth D. Schneider

23 March 1995

S-Cubed, a Division of Maxwell Laboratories
2501 Yale Boulevard, SE, Suite 300
Albuquerque, New Mexico 87106

LIST OF TABLES

Table		Page
A-1	PRISCILLA desert thermal layer (July 6 revision) - station locations at 0 ft (0 m) height	A-4
A-2	PRISCILLA desert thermal layer (July 6 revision) - station locations at 3 ft (0.9144 m) height	A-8
A-3	PRISCILLA desert thermal layer (July 6 revision) - station locations at 10 ft (3.048 m) height	A-12
A-4	PRISCILLA for grassland surface and THRML thermal layer - station locations at 0 ft (0 m) height. Arrival time corrected to 0.15 of distance to peak	A-16
A-5	PRISCILLA for grassland surface and THRML thermal layer - station locations at 3 ft (0.9144 m) height	A-20
A-6	PRISCILLA for grassland surface and THRML thermal layer - station locations at 10 ft (3.048 m) height	A-24
A-7	PRISCILLA for ideal surface - station locations at height of 0 ft (0 m)	A-28
A-8	PRISCILLA for ideal surface - station locations at height of 3 ft (0.914 m)	A-32
A-9	PRISCILLA for ideal surface - station locations at height of 10 ft (3.048 m)	A-36

Blast parameters are presented in the tabluations for the desert, grassland, and ideal surfaces for heights of 0 ft (0 m), 3 ft (0.9144 m), and 10 ft (3.048) above the surface.

The column headings are described below:

sta = assigned station number.

xcord = ground range (m).

at = arrival time of wave front (s), time to rise to magnitude of one-half of first peak for ideal waveform, variable choice for precursed waveforms.

fop = overpressure of first peak of waveform (kPa).

ops = second peak - maximum overpressure (kPa).

opm = maximum overpressure (kPa)

opi = overpressure positive phase impulse (kPa-s).

hdpp = peak pressure of horizontal dynamic pressure component (kPa).

vdpp = peak pressure of vertical dynamic pressure component (kPa).

ppd = duration of positive phase of overpressure (s).

dpih = positive phase impulse of horizontal dynamic pressure component (kPa-s).

dpiv = positive phase impulse of vertical dynamic pressure component (kPa-s).

Note: Beyond a range of about 1600 meters the positive phase durations are incomplete and the impulses are therefore low.

Table A-1. PRISCILLA desert thermal layer (July 6 revision) - station locations at 0 ft (0 m) height.

sta	xcord (m)	at (s)	fop (kpa)	ops (kpa)	opi (kpa-s)
1	0.000E+00	6.727E-02	1.400E+04	1.400E+04	1.414E+02
9	1.524E+01	6.746E-02	1.016E+04	1.352E+04	1.407E+02
17	3.048E+01	6.862E-02	1.218E+04	1.218E+04	1.387E+02
25	4.572E+01	7.044E-02	1.054E+04	1.054E+04	1.353E+02
33	6.096E+01	7.303E-02	9.199E+03	9.199E+03	1.308E+02
41	7.620E+01	7.666E-02	8.045E+03	8.045E+03	1.251E+02
49	1.067E+02	8.577E-02	5.853E+03	5.853E+03	1.133E+02
57	1.372E+02	9.838E-02	3.681E+03	3.681E+03	1.008E+02
65	1.676E+02	1.106E-01	2.455E+02	2.408E+03	8.812E+01
73	1.981E+02	1.280E-01	3.914E+02	1.773E+03	7.710E+01
81	2.286E+02	1.484E-01	4.860E+02	1.468E+03	6.822E+01
89	2.590E+02	1.655E-01	1.462E+02	1.326E+03	6.063E+01
97	2.621E+02	1.674E-01	1.823E+02	1.303E+03	5.996E+01
105	2.956E+02	1.898E-01	1.322E+02	9.580E+02	5.317E+01
113	3.048E+02	1.963E-01	1.316E+02	8.712E+02	5.110E+01
121	3.170E+02	2.048E-01	1.296E+02	7.885E+02	4.941E+01
129	3.200E+02	2.072E-01	1.288E+02	7.631E+02	4.909E+01
137	3.504E+02	2.303E-01	1.152E+02	6.109E+02	4.520E+01
145	3.810E+02	2.557E-01	1.010E+02	5.067E+02	4.104E+01
153	4.114E+02	2.824E-01	9.512E+01	3.852E+02	3.931E+01
161	4.144E+02	2.850E-01	9.466E+01	3.785E+02	3.930E+01
169	4.358E+02	3.055E-01	1.065E+02	2.960E+02	3.679E+01
177	4.419E+02	3.103E-01	1.283E+02	2.787E+02	3.635E+01
185	4.678E+02	3.347E-01	1.016E+02	2.345E+02	3.422E+01
193	4.754E+02	3.420E-01	8.575E+01	2.253E+02	3.348E+01
201	5.029E+02	3.743E-01	8.447E+01	1.948E+02	3.202E+01
209	5.182E+02	3.918E-01	8.032E+01	1.668E+02	2.992E+01
217	5.242E+02	3.988E-01	7.950E+01	1.582E+02	2.956E+01
225	5.333E+02	4.093E-01	7.955E+01	1.482E+02	2.922E+01
233	5.488E+02	4.278E-01	8.104E+01	1.532E+02	2.945E+01
241	5.794E+02	4.651E-01	9.051E+01	1.039E+02	2.854E+01
249	6.090E+02	5.027E-01	7.751E+01	1.043E+02	2.725E+01
257	6.194E+02	5.167E-01	7.382E+01	8.826E+01	2.723E+01
265	6.402E+02	5.456E-01	6.501E+01	1.108E+02	2.686E+01
273	6.848E+02	6.122E-01	5.759E+01	6.071E+01	2.481E+01
281	6.934E+02	6.259E-01	5.477E+01	5.851E+01	2.416E+01
289	6.979E+02	6.332E-01	5.513E+01	6.020E+01	2.391E+01
297	7.130E+02	6.579E-01	5.262E+01	6.035E+01	2.425E+01
305	7.286E+02	6.852E-01	4.950E+01	5.662E+01	2.328E+01
313	7.437E+02	7.124E-01	5.083E+01	5.564E+01	2.250E+01
321	7.533E+02	7.304E-01	5.196E+01	5.534E+01	2.257E+01
329	7.600E+02	7.423E-01	4.730E+01	5.559E+01	2.259E+01
337	7.654E+02	7.534E-01	4.919E+01	5.498E+01	2.248E+01
345	7.744E+02	7.713E-01	5.068E+01	5.211E+01	2.187E+01
353	7.875E+02	7.967E-01	4.878E+01	5.160E+01	2.153E+01
361	8.051E+02	8.329E-01	4.612E+01	5.109E+01	2.109E+01
369	8.266E+02	8.789E-01	4.510E+01	4.817E+01	2.073E+01
377	8.461E+02	9.225E-01	4.545E+01	4.755E+01	2.068E+01
385	8.643E+02	9.647E-01	4.484E+01	4.827E+01	2.017E+01
393	8.730E+02	9.856E-01	4.586E+01	4.837E+01	2.021E+01

Table A-1. PRISCILLA desert thermal layer (July 6 revision) - station locations at 0 ft (0 m) height (continued).

sta	xcord (m)	at (s)	fop (kpa)	ops (kpa)	opi (kpa-s)
401	8.806E+02	1.004E+00	4.561E+01	4.935E+01	2.001E+01
409	8.893E+02	1.025E+00	4.330E+01	4.889E+01	1.997E+01
417	8.925E+02	1.032E+00	4.320E+01	4.919E+01	1.996E+01
425	9.107E+02	1.078E+00	4.551E+01	5.083E+01	1.995E+01
433	9.824E+02	1.268E+00	5.503E+01	5.503E+01	1.959E+01
441	1.060E+03	1.480E+00	5.820E+01	5.820E+01	1.923E+01
449	1.070E+03	1.506E+00	5.805E+01	5.805E+01	1.895E+01
457	1.079E+03	1.527E+00	5.754E+01	5.754E+01	1.884E+01
465	1.086E+03	1.547E+00	5.733E+01	5.733E+01	1.863E+01
473	1.095E+03	1.567E+00	5.672E+01	5.672E+01	1.847E+01
481	1.101E+03	1.583E+00	5.626E+01	5.626E+01	1.840E+01
489	1.103E+03	1.589E+00	5.605E+01	5.605E+01	1.836E+01
497	1.113E+03	1.613E+00	5.544E+01	5.544E+01	1.816E+01
505	1.123E+03	1.639E+00	5.503E+01	5.503E+01	1.798E+01
513	1.156E+03	1.722E+00	5.370E+01	5.370E+01	1.740E+01
521	1.189E+03	1.806E+00	5.273E+01	5.273E+01	1.688E+01
529	1.192E+03	1.813E+00	5.267E+01	5.267E+01	1.684E+01
537	1.218E+03	1.873E+00	5.411E+01	5.114E+01	1.647E+01
545	1.224E+03	1.888E+00	6.005E+01	5.068E+01	1.637E+01
553	1.244E+03	1.936E+00	5.877E+01	5.109E+01	1.616E+01
561	1.258E+03	1.971E+00	5.759E+01	4.919E+01	1.598E+01
569	1.267E+03	1.993E+00	5.682E+01	4.848E+01	1.589E+01
577	1.277E+03	2.016E+00	5.575E+01	4.771E+01	1.580E+01
585	1.287E+03	2.040E+00	5.513E+01	4.679E+01	1.567E+01
593	1.292E+03	2.052E+00	5.488E+01	4.643E+01	1.563E+01
601	1.305E+03	2.085E+00	5.257E+01	4.535E+01	1.550E+01
609	1.320E+03	2.122E+00	5.273E+01	4.443E+01	1.526E+01
617	1.343E+03	2.179E+00	5.119E+01	4.249E+01	1.504E+01
625	1.384E+03	2.281E+00	4.612E+01	4.033E+01	1.463E+01
633	1.433E+03	2.403E+00	4.320E+01	3.798E+01	1.416E+01
641	1.467E+03	2.490E+00	4.095E+01	3.598E+01	1.382E+01
649	1.503E+03	2.580E+00	3.977E+01	3.440E+01	1.353E+01
657	1.530E+03	2.650E+00	3.890E+01	3.390E+01	1.330E+01
665	1.557E+03	2.719E+00	3.706E+01	3.327E+01	1.306E+01
673	1.581E+03	2.779E+00	3.593E+01	3.293E+01	1.287E+01
681	1.596E+03	2.817E+00	3.552E+01	3.190E+01	1.275E+01
689	1.599E+03	2.826E+00	3.537E+01	3.107E+01	1.273E+01
697	1.608E+03	2.850E+00	3.527E+01	3.076E+01	1.266E+01
705	1.615E+03	2.869E+00	3.455E+01	3.056E+01	1.259E+01
713	1.651E+03	2.961E+00	3.368E+01	2.979E+01	1.233E+01
721	1.678E+03	3.028E+00	3.012E+01	3.276E+01	1.206E+01
729	1.717E+03	3.129E+00	2.950E+01	3.219E+01	1.144E+01
737	1.794E+03	3.330E+00	2.749E+01	2.984E+01	9.622E+00
745	1.853E+03	3.483E+00	2.606E+01	2.835E+01	7.656E+00

Table A-1. PRISCILLA desert thermal layer (July 6 revision) - station locations at 0 ft (0 m) height (continued).

sta	xcord (m)	hdpp (kpa)	vdpp (kpa)	ppd (s)	dpih (kpa-s)	dpiv (kpa-s)
1	0.000E+00	1.190E+00	-4.719E+03	1.327E-01	1.066E-01	-4.316E+00
9	1.524E+01	1.423E+02	-4.470E+03	1.329E-01	1.042E+00	-4.062E+00
17	3.048E+01	4.865E+02	-3.980E+03	1.348E-01	3.720E+00	-3.543E+00
25	4.572E+01	9.487E+02	-3.497E+03	1.382E-01	8.274E+00	-3.040E+00
33	6.096E+01	1.444E+03	-2.849E+03	1.413E-01	1.368E+01	-2.327E+00
41	7.620E+01	2.070E+03	-2.069E+03	1.434E-01	2.058E+01	-1.517E+00
49	1.067E+02	3.375E+03	-7.744E+02	1.543E-01	3.637E+01	-4.829E-01
57	1.372E+02	5.165E+03	5.474E+01	1.517E-01	5.892E+01	3.790E-02
65	1.676E+02	5.607E+03	-3.569E+01	1.571E-01	8.216E+01	-2.619E-02
73	1.981E+02	5.275E+03	4.933E+00	1.653E-01	1.008E+02	4.050E-03
81	2.286E+02	4.555E+03	5.004E+00	1.805E-01	9.623E+01	6.451E-03
89	2.590E+02	3.541E+03	-3.937E+00	2.005E-01	9.051E+01	-4.204E-03
97	2.621E+02	3.433E+03	-3.103E+00	2.025E-01	9.035E+01	-3.104E-03
105	2.956E+02	2.986E+03	3.920E+00	2.334E-01	8.668E+01	3.880E-03
113	3.048E+02	2.666E+03	2.611E+00	2.463E-01	8.471E+01	-2.782E-03
121	3.170E+02	2.367E+03	2.389E+00	2.640E-01	8.323E+01	-3.184E-03
129	3.200E+02	2.301E+03	2.228E+00	2.621E-01	8.314E+01	-3.239E-03
137	3.504E+02	1.675E+03	8.968E-01	2.960E-01	8.185E+01	-3.112E-03
145	3.810E+02	1.500E+03	-3.927E+01	3.264E-01	8.733E+01	-1.277E-01
153	4.114E+02	1.942E+03	-1.249E+01	3.613E-01	9.525E+01	-2.736E-02
161	4.144E+02	1.867E+03	-3.487E+00	3.718E-01	9.738E+01	-1.003E-02
169	4.358E+02	1.951E+03	-4.865E+00	3.941E-01	1.088E+02	-2.797E-02
177	4.419E+02	1.876E+03	-4.575E+00	4.087E-01	1.145E+02	-4.765E-02
185	4.678E+02	1.794E+03	-1.819E+02	4.331E-01	1.314E+02	-8.562E-01
193	4.754E+02	1.872E+03	-1.643E+02	4.442E-01	1.358E+02	-9.582E-01
201	5.029E+02	2.027E+03	-5.802E+02	1.274E-01	1.499E+02	-6.410E+00
209	5.182E+02	1.858E+03	-2.840E+01	4.894E-01	1.536E+02	-4.285E-01
217	5.242E+02	1.759E+03	-8.757E+00	4.894E-01	1.544E+02	-1.122E-01
225	5.333E+02	1.538E+03	-1.042E+01	4.912E-01	1.615E+02	-1.735E-01
233	5.488E+02	1.378E+03	-2.567E+02	5.079E-01	1.785E+02	-3.854E+00
241	5.794E+02	1.011E+03	-4.940E+00	5.571E-01	1.617E+02	-5.063E-02
249	6.090E+02	9.655E+02	-9.165E+01	1.897E-01	1.866E+02	-7.280E-01
257	6.194E+02	9.801E+02	-3.316E+01	6.238E-01	1.785E+02	-4.659E-01
265	6.402E+02	8.146E+02	-1.596E+02	6.429E-01	1.536E+02	-1.046E+00
273	6.848E+02	4.254E+02	-4.710E-01	7.098E-01	9.839E+01	-5.112E-03
281	6.934E+02	3.997E+02	-5.230E-01	7.225E-01	9.066E+01	-7.555E-03
289	6.979E+02	3.810E+02	-5.771E-01	7.271E-01	8.735E+01	-5.453E-03
297	7.130E+02	2.356E+02	1.416E-01	7.349E-01	7.591E+01	3.513E-03
305	7.286E+02	1.671E+02	6.236E-02	7.696E-01	6.455E+01	1.802E-03
313	7.437E+02	1.462E+02	3.955E-02	7.737E-01	5.966E+01	1.301E-03
321	7.533E+02	1.494E+02	-3.760E-02	7.948E-01	5.857E+01	1.185E-03
329	7.600E+02	1.500E+02	5.257E-02	7.905E-01	5.748E+01	1.373E-03
337	7.654E+02	1.494E+02	5.622E-02	7.928E-01	5.618E+01	1.650E-03
345	7.744E+02	1.387E+02	-2.823E-02	8.023E-01	5.385E+01	1.185E-03
353	7.875E+02	1.178E+02	-2.572E-02	7.917E-01	5.060E+01	1.343E-03
361	8.051E+02	1.024E+02	3.556E-02	7.892E-01	5.024E+01	7.408E-04
369	8.266E+02	9.549E+01	2.376E-02	8.023E-01	4.588E+01	7.743E-04
377	8.461E+02	8.868E+01	2.553E-02	7.959E-01	4.496E+01	6.972E-04
385	8.643E+02	7.739E+01	4.813E-02	7.834E-01	4.255E+01	6.432E-04
393	8.730E+02	7.766E+01	-2.639E-02	7.734E-01	4.040E+01	6.818E-04

Table A-1. PRISCILLA desert thermal layer (July 6 revision) - station locations at 0 ft (0 m) height (concluded).

sta	xcord (m)	hdpp (kpa)	vdpp (kpa)	ppd (s)	dpih (kpa-s)	dpiv (kpa-s)
401	8.806E+02	7.588E+01	2.571E-02	7.618E-01	3.938E+01	4.680E-04
409	8.893E+02	7.559E+01	1.864E-02	7.490E-01	3.855E+01	4.242E-04
417	8.925E+02	7.259E+01	2.112E-02	7.411E-01	3.826E+01	3.975E-04
425	9.107E+02	8.419E+01	1.713E-01	7.130E-01	3.670E+01	-8.198E-04
433	9.824E+02	4.150E+01	1.211E-02	7.582E-01	2.340E+01	2.544E-04
441	1.060E+03	1.805E+01	6.526E-04	7.981E-01	1.024E+01	6.710E-05
449	1.070E+03	1.877E+01	3.392E-04	8.101E-01	8.839E+00	4.206E-05
457	1.079E+03	1.943E+01	5.488E-04	8.141E-01	7.840E+00	3.556E-05
465	1.086E+03	1.982E+01	5.626E-04	8.126E-01	7.114E+00	3.802E-05
473	1.095E+03	1.900E+01	6.399E-04	8.150E-01	6.317E+00	3.879E-05
481	1.101E+03	1.837E+01	6.407E-04	8.139E-01	5.763E+00	3.799E-05
489	1.103E+03	1.810E+01	6.152E-04	8.075E-01	5.567E+00	4.109E-05
497	1.113E+03	1.710E+01	6.205E-04	8.065E-01	4.852E+00	4.198E-05
505	1.123E+03	1.611E+01	5.334E-04	8.276E-01	4.225E+00	4.069E-05
513	1.156E+03	1.393E+01	3.886E-04	8.082E-01	2.980E+00	2.800E-05
521	1.189E+03	1.196E+01	2.861E-04	8.292E-01	2.448E+00	2.854E-06
529	1.192E+03	1.194E+01	2.322E-04	8.212E-01	2.418E+00	2.273E-06
537	1.218E+03	1.067E+01	2.485E-04	8.280E-01	2.134E+00	1.461E-06
545	1.224E+03	1.109E+01	2.168E-04	8.269E-01	2.070E+00	1.211E-06
553	1.244E+03	1.006E+01	1.549E-04	8.294E-01	1.905E+00	7.170E-07
561	1.258E+03	9.507E+00	1.231E-04	8.311E-01	1.827E+00	4.016E-07
569	1.267E+03	9.265E+00	6.240E-05	8.417E-01	1.789E+00	2.372E-07
577	1.277E+03	9.034E+00	7.358E-05	8.612E-01	1.757E+00	2.090E-07
585	1.287E+03	8.373E+00	5.629E-05	8.547E-01	1.723E+00	2.462E-07
593	1.292E+03	8.270E+00	3.912E-05	8.489E-01	1.705E+00	2.465E-07
601	1.305E+03	7.824E+00	3.895E-05	8.589E-01	1.651E+00	3.059E-07
609	1.320E+03	7.458E+00	1.559E-04	8.728E-01	1.593E+00	9.754E-07
617	1.343E+03	6.933E+00	-8.768E-05	8.788E-01	1.505E+00	6.748E-07
625	1.384E+03	6.344E+00	-4.311E-05	9.003E-01	1.383E+00	-1.583E-07
633	1.433E+03	5.742E+00	8.137E-05	9.011E-01	1.283E+00	3.200E-07
641	1.467E+03	5.140E+00	-1.787E-05	9.105E-01	1.216E+00	-1.496E-07
649	1.503E+03	4.991E+00	3.493E-05	9.227E-01	1.165E+00	2.812E-07
657	1.530E+03	4.740E+00	-1.457E-04	9.368E-01	1.118E+00	-3.005E-07
665	1.557E+03	4.412E+00	9.499E-06	9.366E-01	1.092E+00	-7.603E-08
673	1.581E+03	4.252E+00	1.129E-03	9.502E-01	1.057E+00	1.442E-06
681	1.596E+03	3.969E+00	8.056E-06	9.476E-01	1.040E+00	9.667E-08
689	1.599E+03	3.957E+00	6.104E-06	9.548E-01	1.038E+00	4.677E-08
697	1.608E+03	3.889E+00	-8.978E-06	9.548E-01	1.028E+00	1.390E-07
705	1.615E+03	3.791E+00	-1.802E-03	9.556E-01	1.015E+00	-3.050E-06
713	1.651E+03	3.533E+00	1.634E-05	9.318E-01	9.649E-01	2.084E-07
721	1.678E+03	3.431E+00	-6.645E-06	8.625E-01	9.342E-01	9.822E-08
729	1.717E+03	3.300E+00	6.853E-05	7.613E-01	8.769E-01	3.557E-07
737	1.794E+03	2.869E+00	2.719E-06	5.629E-01	7.418E-01	4.552E-08
745	1.853E+03	2.590E+00	1.856E-06	4.092E-01	6.042E-01	4.685E-08
753	2.116E+03	0.000E+00	9.215E-11	0.000E+00	0.000E+00	1.356E-12

Table A-2. PRISCILLA desert thermal layer (July 6 revision) - station locations at 3 ft (0.9144 m) height.

sta	xcord (m)	at (s)	fop (kpa)	ops (kpa)	opi (kpa-s)
2	0.000E+00	6.586E-02	1.463E+03	1.197E+04	1.194E+02
10	1.524E+01	6.622E-02	1.397E+03	1.179E+04	1.188E+02
18	3.048E+01	6.726E-02	1.262E+03	1.137E+04	1.178E+02
26	4.572E+01	6.914E-02	1.246E+03	1.084E+04	1.175E+02
34	6.096E+01	7.179E-02	1.170E+03	1.013E+04	1.176E+02
42	7.620E+01	7.549E-02	1.092E+03	8.796E+03	1.152E+02
50	1.067E+02	8.482E-02	9.387E+02	6.395E+03	1.070E+02
58	1.372E+02	9.741E-02	1.030E+03	4.800E+03	9.791E+01
66	1.676E+02	1.109E-01	2.304E+02	2.725E+03	8.683E+01
74	1.981E+02	1.269E-01	2.159E+02	1.769E+03	7.690E+01
82	2.286E+02	1.460E-01	1.376E+02	1.402E+03	6.754E+01
90	2.590E+02	1.657E-01	1.507E+02	1.151E+03	5.968E+01
98	2.621E+02	1.676E-01	1.465E+02	1.139E+03	5.914E+01
106	2.956E+02	1.899E-01	1.281E+02	9.032E+02	5.216E+01
114	3.048E+02	1.964E-01	1.281E+02	8.413E+02	5.019E+01
122	3.170E+02	2.050E-01	1.249E+02	7.672E+02	4.851E+01
130	3.200E+02	2.074E-01	1.239E+02	7.473E+02	4.823E+01
138	3.504E+02	2.304E-01	1.103E+02	6.056E+02	4.432E+01
170	4.358E+02	3.052E-01	8.500E+01	2.983E+02	3.561E+01
186	4.678E+02	3.344E-01	7.953E+01	2.366E+02	3.274E+01
194	4.754E+02	3.418E-01	7.776E+01	2.274E+02	3.182E+01
218	5.242E+02	3.982E-01	7.522E+01	1.600E+02	2.736E+01
226	5.333E+02	4.087E-01	7.474E+01	1.485E+02	2.727E+01
234	5.488E+02	4.271E-01	6.327E+01	1.420E+02	2.641E+01
274	6.848E+02	6.103E-01	5.938E+01	6.005E+01	2.248E+01
282	6.934E+02	6.240E-01	5.645E+01	5.795E+01	2.199E+01
290	6.979E+02	6.312E-01	5.687E+01	5.728E+01	2.164E+01
298	7.130E+02	6.556E-01	5.518E+01	5.631E+01	2.264E+01
306	7.286E+02	6.825E-01	5.347E+01	5.375E+01	2.188E+01
314	7.437E+02	7.089E-01	5.204E+01	5.247E+01	2.116E+01
322	7.533E+02	7.263E-01	4.776E+01	5.247E+01	2.120E+01
330	7.600E+02	7.386E-01	4.842E+01	4.848E+01	2.127E+01
338	7.654E+02	7.494E-01	5.068E+01	5.216E+01	2.120E+01
346	7.744E+02	7.667E-01	4.952E+01	5.068E+01	2.068E+01
354	7.875E+02	7.920E-01	4.862E+01	4.991E+01	2.048E+01
362	8.051E+02	8.278E-01	4.742E+01	4.853E+01	2.000E+01
370	8.266E+02	8.731E-01	4.297E+01	4.336E+01	1.986E+01
378	8.461E+02	9.161E-01	4.515E+01	4.520E+01	1.984E+01
386	8.643E+02	9.579E-01	4.528E+01	4.633E+01	1.942E+01
394	8.730E+02	9.782E-01	4.563E+01	4.704E+01	1.956E+01
402	8.806E+02	9.967E-01	4.576E+01	4.622E+01	1.939E+01
410	8.893E+02	1.017E+00	4.709E+01	4.709E+01	1.940E+01
418	8.925E+02	1.025E+00	4.758E+01	4.766E+01	1.942E+01
426	9.107E+02	1.070E+00	4.924E+01	4.924E+01	1.946E+01
434	9.824E+02	1.252E+00	5.393E+01	5.426E+01	1.934E+01
442	1.060E+03	1.455E+00	5.861E+01	5.861E+01	1.920E+01
450	1.070E+03	1.482E+00	5.866E+01	5.866E+01	1.893E+01
458	1.079E+03	1.505E+00	5.841E+01	5.841E+01	1.884E+01
466	1.086E+03	1.525E+00	5.815E+01	5.815E+01	1.863E+01
474	1.095E+03	1.547E+00	5.754E+01	5.754E+01	1.848E+01

Table A-2. PRISCILLA desert thermal layer (July 6 revision) - station locations at 3 ft (0.9144 m) (continued).

sta	xcord (m)	at (s)	fop (kpa)	ops (kpa)	opi (kpa-s)
482	1.101E+03	1.563E+00	5.692E+01	5.692E+01	1.841E+01
490	1.103E+03	1.570E+00	5.672E+01	5.672E+01	1.837E+01
498	1.113E+03	1.594E+00	2.267E+01	5.595E+01	1.817E+01
506	1.123E+03	1.622E+00	5.539E+01	5.539E+01	1.799E+01
514	1.156E+03	1.708E+00	5.390E+01	5.390E+01	1.741E+01
522	1.189E+03	1.796E+00	5.334E+01	5.334E+01	1.689E+01
530	1.192E+03	1.803E+00	2.469E+01	5.354E+01	1.684E+01
538	1.218E+03	1.871E+00	5.300E+01	5.605E+01	1.648E+01
546	1.224E+03	1.887E+00	5.451E+01	6.322E+01	1.638E+01
554	1.244E+03	1.934E+00	5.144E+01	5.196E+01	1.617E+01
562	1.258E+03	1.970E+00	5.053E+01	6.010E+01	1.599E+01
570	1.267E+03	1.991E+00	4.933E+01	5.877E+01	1.590E+01
578	1.277E+03	2.015E+00	4.856E+01	5.759E+01	1.581E+01
586	1.287E+03	2.039E+00	4.754E+01	5.697E+01	1.567E+01
594	1.292E+03	2.051E+00	4.715E+01	5.662E+01	1.564E+01
602	1.305E+03	2.084E+00	4.553E+01	4.571E+01	1.550E+01
610	1.320E+03	2.120E+00	4.419E+01	4.494E+01	1.526E+01
618	1.343E+03	2.178E+00	4.268E+01	5.114E+01	1.505E+01
626	1.384E+03	2.279E+00	4.136E+01	4.592E+01	1.464E+01
634	1.433E+03	2.402E+00	3.926E+01	4.320E+01	1.416E+01
642	1.467E+03	2.488E+00	3.725E+01	4.090E+01	1.383E+01
650	1.503E+03	2.578E+00	3.650E+01	3.957E+01	1.354E+01
658	1.530E+03	2.648E+00	3.579E+01	3.916E+01	1.330E+01
666	1.557E+03	2.717E+00	3.423E+01	3.711E+01	1.306E+01
674	1.581E+03	2.777E+00	3.320E+01	3.614E+01	1.288E+01
682	1.596E+03	2.815E+00	3.262E+01	3.547E+01	1.275E+01
690	1.599E+03	2.824E+00	3.246E+01	3.537E+01	1.273E+01
698	1.608E+03	2.848E+00	3.219E+01	3.521E+01	1.266E+01
706	1.615E+03	2.867E+00	3.200E+01	3.491E+01	1.260E+01
714	1.651E+03	2.959E+00	3.057E+01	3.363E+01	1.233E+01
722	1.678E+03	3.028E+00	3.014E+01	3.281E+01	1.206E+01
730	1.717E+03	3.129E+00	2.947E+01	3.214E+01	1.144E+01
738	1.794E+03	3.330E+00	2.749E+01	2.984E+01	9.625E+00
746	1.853E+03	3.483E+00	2.606E+01	2.841E+01	7.659E+00

Table A-2. PRISCILLA desert thermal layer (July 6 revision) - station locations at 3 ft (0.9144 m) height (continued).

sta	xcord (m)	hdpp (kpa)	vdpp (kpa)	ppd (s)	dpih (kpa-s)	dpiv (kpa-s)
2	0.000E+00	1.370E+00	-3.590E+03	1.340E-01	1.569E-01	-1.003E+01
10	1.524E+01	1.189E+02	-3.451E+03	1.336E-01	8.475E-01	-9.997E+00
18	3.048E+01	4.417E+02	-3.067E+03	1.351E-01	2.966E+00	-9.513E+00
26	4.572E+01	9.263E+02	-2.721E+03	1.379E-01	6.699E+00	-8.042E+00
34	6.096E+01	1.460E+03	-2.437E+03	1.413E-01	1.121E+01	-6.177E+00
42	7.620E+01	1.981E+03	-2.138E+03	1.437E-01	1.699E+01	-4.617E+00
50	1.067E+02	2.715E+03	-1.556E+03	1.550E-01	2.802E+01	-3.079E+00
58	1.372E+02	3.185E+03	-7.957E+02	1.516E-01	3.724E+01	-1.539E+00
66	1.676E+02	2.791E+03	-5.747E+02	1.575E-01	4.737E+01	-7.237E-01
74	1.981E+02	2.472E+03	1.471E+02	1.647E-01	6.454E+01	1.326E-01
82	2.286E+02	2.802E+03	-1.378E+02	1.789E-01	7.809E+01	1.496E-01
90	2.590E+02	2.931E+03	-1.804E+02	2.012E-01	8.778E+01	-2.470E-01
98	2.621E+02	3.012E+03	-1.476E+02	2.022E-01	8.689E+01	-2.117E-01
106	2.956E+02	2.752E+03	7.719E+01	2.327E-01	8.171E+01	1.760E-01
114	3.048E+02	2.647E+03	4.743E+01	2.440E-01	8.095E+01	1.483E-01
122	3.170E+02	2.437E+03	3.914E+01	2.634E-01	7.851E+01	1.293E-01
130	3.200E+02	2.383E+03	3.708E+01	2.613E-01	7.798E+01	1.257E-01
138	3.504E+02	1.791E+03	1.943E+01	2.957E-01	7.520E+01	7.813E-02
146	3.810E+02	1.568E+03	1.602E+01	5.056E-02	7.712E+01	5.956E-02
154	4.114E+02	1.253E+03	1.289E+01	6.373E-02	7.616E+01	5.027E-02
162	4.144E+02	1.211E+03	1.266E+01	6.437E-02	7.652E+01	4.529E-02
170	4.358E+02	9.889E+02	1.172E+01	3.935E-01	7.922E+01	3.935E-02
178	4.419E+02	9.358E+02	1.151E+01	7.351E-02	8.015E+01	4.094E-02
186	4.678E+02	1.248E+03	1.047E+01	4.342E-01	7.682E+01	5.960E-02
194	4.754E+02	1.080E+03	1.002E+01	4.436E-01	7.480E+01	6.663E-02
202	5.029E+02	8.758E+02	7.765E+00	9.180E-02	7.165E+01	6.272E-02
210	5.182E+02	9.191E+02	6.847E+00	9.845E-02	7.061E+01	4.965E-02
218	5.242E+02	6.474E+02	6.503E+00	4.887E-01	7.152E+01	3.156E-02
226	5.333E+02	8.192E+02	6.080E+00	4.922E-01	7.120E+01	2.685E-02
234	5.488E+02	6.977E+02	6.248E+00	5.080E-01	6.625E+01	6.727E-02
242	5.794E+02	5.203E+02	5.756E+00	1.209E-01	7.037E+01	2.192E-02
250	6.090E+02	5.463E+02	4.472E+00	1.828E-01	6.870E+01	2.683E-02
258	6.194E+02	5.369E+02	3.974E+00	1.258E-01	6.864E+01	3.439E-02
266	6.402E+02	4.701E+02	3.264E+00	1.371E-01	7.028E+01	3.707E-02
274	6.848E+02	2.532E+02	2.190E+00	7.095E-01	7.096E+01	2.855E-02
282	6.934E+02	2.160E+02	2.033E+00	7.158E-01	6.938E+01	2.680E-02
290	6.979E+02	2.075E+02	1.956E+00	7.209E-01	6.871E+01	2.618E-02
298	7.130E+02	1.946E+02	1.672E+00	7.384E-01	6.694E+01	2.414E-02
306	7.286E+02	1.781E+02	1.404E+00	7.653E-01	6.434E+01	1.851E-02
314	7.437E+02	1.647E+02	1.174E+00	7.720E-01	6.217E+01	1.283E-02
322	7.533E+02	1.556E+02	1.070E+00	7.830E-01	6.089E+01	1.072E-02
330	7.600E+02	1.496E+02	1.010E+00	7.877E-01	6.031E+01	1.131E-02
338	7.654E+02	1.468E+02	9.457E-01	7.872E-01	5.979E+01	1.196E-02
346	7.744E+02	1.412E+02	8.746E-01	7.997E-01	5.902E+01	1.115E-02
354	7.875E+02	1.327E+02	7.692E-01	7.886E-01	5.743E+01	1.087E-02
362	8.051E+02	1.122E+02	6.426E-01	7.826E-01	5.502E+01	8.477E-03
370	8.266E+02	1.000E+02	5.370E-01	7.856E-01	5.230E+01	9.962E-03
378	8.461E+02	9.443E+01	4.222E-01	7.855E-01	4.910E+01	7.660E-03
386	8.643E+02	8.585E+01	3.296E-01	7.706E-01	4.640E+01	8.272E-03
394	8.730E+02	8.335E+01	2.900E-01	7.601E-01	4.475E+01	8.145E-03

Table A-2. PRISCILLA desert thermal layer (July 6 revision) - station locations at 3 ft (0.9144 m) height (concluded).

sta	xcord (m)	hdpp (kpa)	vdpp (kpa)	ppd (s)	dpih (kpa-s)	dpiv (kpa-s)
402	8.806E+02	8.060E+01	2.585E-01	7.474E-01	4.360E+01	7.197E-03
410	8.893E+02	7.727E+01	2.241E-01	7.329E-01	4.197E+01	6.354E-03
418	8.925E+02	7.544E+01	2.146E-01	7.277E-01	4.136E+01	6.022E-03
426	9.107E+02	6.742E+01	-2.148E-01	7.087E-01	3.786E+01	5.209E-03
434	9.824E+02	4.527E+01	2.502E-01	7.539E-01	2.456E+01	4.390E-03
442	1.060E+03	1.654E+01	2.395E-02	7.978E-01	1.027E+01	1.743E-03
450	1.070E+03	1.554E+01	2.832E-02	8.089E-01	8.787E+00	1.206E-03
458	1.079E+03	1.491E+01	3.345E-02	8.137E-01	7.659E+00	1.009E-03
466	1.086E+03	1.395E+01	3.903E-02	8.084E-01	6.831E+00	9.336E-04
474	1.095E+03	1.352E+01	3.849E-02	8.147E-01	5.985E+00	8.225E-04
482	1.101E+03	1.313E+01	3.470E-02	8.136E-01	5.423E+00	7.891E-04
490	1.103E+03	1.300E+01	3.452E-02	8.072E-01	5.230E+00	7.776E-04
498	1.113E+03	1.263E+01	3.033E-02	8.069E-01	4.522E+00	6.989E-04
506	1.123E+03	1.210E+01	2.585E-02	8.254E-01	3.919E+00	5.990E-04
514	1.156E+03	1.099E+01	1.598E-02	8.099E-01	2.900E+00	3.286E-04
522	1.189E+03	1.032E+01	1.027E-02	8.290E-01	2.485E+00	8.995E-05
530	1.192E+03	1.034E+01	1.062E-02	8.223E-01	2.465E+00	8.606E-05
538	1.218E+03	1.019E+01	1.302E-02	8.269E-01	2.280E+00	5.314E-05
546	1.224E+03	1.057E+01	1.245E-02	8.267E-01	2.241E+00	4.127E-05
554	1.244E+03	9.736E+00	9.207E-03	8.312E-01	2.121E+00	2.662E-05
562	1.258E+03	9.154E+00	7.423E-03	8.310E-01	2.057E+00	1.726E-05
570	1.267E+03	8.933E+00	6.057E-03	8.416E-01	2.019E+00	1.299E-05
578	1.277E+03	8.800E+00	4.673E-03	8.631E-01	1.989E+00	1.048E-05
586	1.287E+03	8.182E+00	3.835E-03	8.556E-01	1.955E+00	8.163E-06
594	1.292E+03	8.054E+00	3.454E-03	8.478E-01	1.940E+00	8.104E-06
602	1.305E+03	7.704E+00	2.456E-03	8.588E-01	1.886E+00	6.969E-06
610	1.320E+03	7.488E+00	-4.373E-04	8.747E-01	1.818E+00	6.774E-06
618	1.343E+03	6.878E+00	1.727E-03	8.778E-01	1.741E+00	1.296E-05
626	1.384E+03	6.371E+00	8.203E-05	8.983E-01	1.634E+00	2.186E-06
634	1.433E+03	5.774E+00	-1.189E-04	9.011E-01	1.481E+00	1.769E-06
642	1.467E+03	5.162E+00	-5.145E-05	9.105E-01	1.397E+00	1.194E-06
650	1.503E+03	5.002E+00	4.444E-04	9.257E-01	1.310E+00	3.276E-06
658	1.530E+03	4.638E+00	5.498E-04	9.368E-01	1.258E+00	1.787E-06
666	1.557E+03	4.414E+00	6.540E-05	9.366E-01	1.213E+00	2.062E-06
674	1.581E+03	4.170E+00	1.379E-03	9.511E-01	1.164E+00	3.073E-06
682	1.596E+03	3.961E+00	7.977E-05	9.476E-01	1.138E+00	8.336E-07
690	1.599E+03	3.961E+00	4.646E-05	9.548E-01	1.133E+00	8.015E-07
698	1.608E+03	3.906E+00	6.697E-05	9.548E-01	1.113E+00	5.446E-07
706	1.615E+03	4.007E+00	2.262E-04	9.557E-01	1.101E+00	6.554E-07
714	1.651E+03	3.546E+00	-7.540E-04	9.318E-01	1.040E+00	-2.378E-06
722	1.678E+03	3.442E+00	1.622E-05	8.625E-01	9.927E-01	5.037E-07
730	1.717E+03	3.264E+00	-6.178E-05	7.613E-01	9.241E-01	5.640E-07
738	1.794E+03	2.874E+00	1.026E-05	5.629E-01	7.689E-01	3.535E-07
746	1.853E+03	2.594E+00	1.364E-05	4.092E-01	6.191E-01	3.197E-07
754	2.116E+03	0.000E+00	9.215E-11	0.000E+00	0.000E+00	1.356E-12

Table A-3. PRISCILLA desert thermal layer (July 6 revision) - station locations at 10 ft (3.048 m) height.

sta	xcord (m)	at (s)	fop (kpa)	ops (kpa)	opi (kpa-s)
6	0.000E+00	6.438E-02	1.863E+03	8.950E+03	1.031E+02
14	1.524E+01	6.473E-02	1.829E+03	8.819E+03	1.026E+02
22	3.048E+01	6.583E-02	1.476E+03	8.553E+03	1.014E+02
30	4.572E+01	6.771E-02	1.501E+03	8.019E+03	9.912E+01
38	6.096E+01	7.038E-02	1.434E+03	7.269E+03	9.696E+01
46	7.620E+01	7.406E-02	1.221E+03	6.405E+03	9.461E+01
54	1.067E+02	8.342E-02	1.063E+03	5.994E+03	9.387E+01
62	1.372E+02	9.625E-02	9.054E+02	4.713E+03	8.906E+01
70	1.676E+02	1.127E-01	8.535E+02	2.845E+03	8.454E+01
78	1.981E+02	1.296E-01	3.796E+02	2.058E+03	7.321E+01
86	2.286E+02	1.488E-01	3.136E+02	1.291E+03	6.596E+01
94	2.590E+02	1.686E-01	2.025E+02	8.679E+02	5.712E+01
102	2.621E+02	1.705E-01	1.980E+02	8.569E+02	5.645E+01
110	2.956E+02	1.931E-01	1.692E+02	6.293E+02	4.886E+01
118	3.048E+02	1.996E-01	1.633E+02	6.607E+02	4.753E+01
126	3.170E+02	2.081E-01	1.578E+02	5.626E+02	4.564E+01
134	3.200E+02	2.105E-01	1.560E+02	5.630E+02	4.551E+01
142	3.504E+02	2.334E-01	6.030E+01	5.370E+02	4.237E+01
150	3.810E+02	2.592E-01	1.172E+02	4.610E+02	3.909E+01
158	4.114E+02	2.859E-01	1.039E+02	3.742E+02	3.755E+01
166	4.144E+02	2.884E-01	1.032E+02	3.570E+02	3.750E+01
174	4.358E+02	3.088E-01	9.937E+01	2.906E+02	3.573E+01
182	4.419E+02	3.132E-01	9.814E+01	2.771E+02	3.547E+01
190	4.678E+02	3.381E-01	9.384E+01	2.333E+02	3.400E+01
198	4.754E+02	3.456E-01	9.207E+01	2.236E+02	3.342E+01
206	5.029E+02	3.778E-01	8.357E+01	1.873E+02	3.094E+01
214	5.182E+02	3.953E-01	7.943E+01	1.666E+02	2.977E+01
222	5.242E+02	4.022E-01	7.763E+01	1.603E+02	2.980E+01
230	5.333E+02	4.126E-01	7.685E+01	1.498E+02	2.997E+01
238	5.488E+02	4.312E-01	8.853E+01	1.423E+02	3.135E+01
246	5.794E+02	4.680E-01	7.516E+01	1.050E+02	2.643E+01
254	6.090E+02	5.057E-01	6.822E+01	9.957E+01	2.853E+01
262	6.194E+02	5.196E-01	6.567E+01	8.626E+01	2.738E+01
270	6.402E+02	5.484E-01	6.061E+01	7.121E+01	2.517E+01
278	6.848E+02	6.144E-01	5.641E+01	6.322E+01	2.342E+01
286	6.934E+02	6.282E-01	5.454E+01	6.071E+01	2.274E+01
294	6.979E+02	6.352E-01	5.349E+01	6.005E+01	2.246E+01
302	7.130E+02	6.597E-01	5.188E+01	5.754E+01	2.241E+01
310	7.286E+02	6.865E-01	5.341E+01	5.539E+01	2.151E+01
318	7.437E+02	7.130E-01	4.999E+01	5.267E+01	2.072E+01
326	7.533E+02	7.304E-01	5.137E+01	5.262E+01	2.067E+01
334	7.600E+02	7.426E-01	4.689E+01	5.206E+01	2.067E+01
342	7.654E+02	7.534E-01	5.034E+01	5.093E+01	2.063E+01
350	7.744E+02	7.705E-01	4.904E+01	4.981E+01	2.018E+01
358	7.875E+02	7.957E-01	4.843E+01	4.914E+01	2.003E+01
366	8.051E+02	8.311E-01	4.589E+01	4.633E+01	1.966E+01
374	8.266E+02	8.766E-01	4.674E+01	4.807E+01	1.958E+01
382	8.461E+02	9.191E-01	4.430E+01	4.576E+01	1.948E+01
390	8.643E+02	9.608E-01	4.752E+01	4.822E+01	1.913E+01
398	8.730E+02	9.810E-01	4.520E+01	4.796E+01	1.931E+01

Table A-3. PRISCILLA desert thermal layer (July 6 revision) station locations at 10 ft (3.048 m) (continued).

sta	xcord (m)	at (s)	fop (kpa)	ops (kpa)	opi (kpa-s)
406	8.806E+02	9.992E-01	4.556E+01	4.607E+01	1.922E+01
414	8.893E+02	1.020E+00	4.684E+01	4.709E+01	1.921E+01
422	8.925E+02	1.028E+00	4.598E+01	4.740E+01	1.925E+01
430	9.107E+02	1.072E+00	4.858E+01	5.006E+01	1.945E+01
438	9.824E+02	1.253E+00	4.446E+01	4.617E+01	1.919E+01
446	1.060E+03	1.454E+00	2.298E+01	6.169E+01	1.917E+01
454	1.070E+03	1.482E+00	2.339E+01	6.266E+01	1.891E+01
462	1.079E+03	1.504E+00	2.330E+01	6.307E+01	1.882E+01
470	1.086E+03	1.526E+00	5.931E+01	6.363E+01	1.862E+01
478	1.095E+03	1.546E+00	2.341E+01	6.199E+01	1.847E+01
486	1.101E+03	1.564E+00	5.795E+01	6.092E+01	1.839E+01
494	1.103E+03	1.569E+00	2.383E+01	6.041E+01	1.836E+01
502	1.113E+03	1.595E+00	2.428E+01	5.913E+01	1.816E+01
510	1.123E+03	1.621E+00	2.392E+01	5.800E+01	1.798E+01
518	1.156E+03	1.708E+00	5.580E+01	5.580E+01	1.741E+01
526	1.189E+03	1.795E+00	2.541E+01	5.590E+01	1.689E+01
534	1.192E+03	1.803E+00	2.564E+01	5.626E+01	1.684E+01
542	1.218E+03	1.872E+00	5.462E+01	5.984E+01	1.648E+01
550	1.224E+03	1.887E+00	5.533E+01	6.675E+01	1.637E+01
558	1.244E+03	1.935E+00	5.243E+01	5.273E+01	1.617E+01
566	1.258E+03	1.970E+00	5.108E+01	6.240E+01	1.599E+01
574	1.267E+03	1.992E+00	4.998E+01	6.076E+01	1.589E+01
582	1.277E+03	2.015E+00	4.840E+01	4.894E+01	1.581E+01
590	1.287E+03	2.039E+00	4.823E+01	5.872E+01	1.567E+01
598	1.292E+03	2.051E+00	4.776E+01	5.825E+01	1.564E+01
606	1.305E+03	2.084E+00	4.614E+01	4.638E+01	1.550E+01
614	1.320E+03	2.120E+00	4.458E+01	4.458E+01	1.526E+01
622	1.343E+03	2.178E+00	4.229E+01	4.412E+01	1.505E+01
630	1.384E+03	2.279E+00	4.124E+01	4.597E+01	1.464E+01
638	1.433E+03	2.402E+00	3.944E+01	4.366E+01	1.416E+01
646	1.467E+03	2.488E+00	3.764E+01	4.131E+01	1.383E+01
654	1.503E+03	2.578E+00	3.631E+01	3.957E+01	1.353E+01
662	1.530E+03	2.648E+00	3.574E+01	3.900E+01	1.330E+01
670	1.557E+03	2.717E+00	3.429E+01	3.747E+01	1.307E+01
678	1.581E+03	2.777E+00	3.284E+01	3.542E+01	1.287E+01
686	1.596E+03	2.815E+00	3.268E+01	3.598E+01	1.275E+01
694	1.599E+03	2.824E+00	3.234E+01	3.542E+01	1.273E+01
702	1.608E+03	2.848E+00	3.208E+01	3.486E+01	1.266E+01
710	1.615E+03	2.867E+00	3.198E+01	3.506E+01	1.260E+01
718	1.651E+03	2.959E+00	3.068E+01	3.368E+01	1.233E+01
726	1.678E+03	3.028E+00	3.012E+01	3.271E+01	1.206E+01
734	1.717E+03	3.129E+00	2.949E+01	3.225E+01	1.144E+01
742	1.794E+03	3.330E+00	2.747E+01	2.984E+01	9.624E+00
750	1.853E+03	3.483E+00	2.603E+01	2.835E+01	7.646E+00

Table A-3. PRISCILLA desert thermal layer (July 6 revision) - station locations at 10 ft (3.048 m) height (continued).

sta	xcord (m)	hdpp (kpa)	vdpp (kpa)	ppd (s)	dpih (kpa-s)	dpiv (kpa-s)
6	0.000E+00	1.106E+00	-4.298E+03	1.354E-01	1.885E-01	-1.760E+01
14	1.524E+01	9.943E+01	-4.130E+03	1.351E-01	7.485E-01	-1.752E+01
22	3.048E+01	3.499E+02	-3.634E+03	1.384E-01	2.451E+00	-1.724E+01
30	4.572E+01	7.253E+02	-3.061E+03	1.388E-01	5.739E+00	-1.674E+01
38	6.096E+01	1.159E+03	-2.672E+03	1.473E-01	9.540E+00	-1.569E+01
46	7.620E+01	1.470E+03	-2.303E+03	1.458E-01	1.343E+01	-1.411E+01
54	1.067E+02	2.305E+03	-1.674E+03	1.557E-01	2.204E+01	-9.226E+00
62	1.372E+02	3.288E+03	-1.090E+03	1.537E-01	3.250E+01	-5.657E+00
70	1.676E+02	1.706E+03	-6.944E+02	1.537E-01	3.871E+01	-1.926E+00
78	1.981E+02	1.755E+03	-4.238E+02	1.608E-01	4.105E+01	-1.480E+00
86	2.286E+02	1.809E+03	-3.083E+02	1.763E-01	5.299E+01	-5.333E-01
94	2.590E+02	1.787E+03	-3.823E+02	1.987E-01	6.290E+01	-5.024E-01
102	2.621E+02	1.823E+03	-3.868E+02	1.987E-01	6.435E+01	-6.045E-01
110	2.956E+02	1.692E+03	-3.462E+02	2.295E-01	7.607E+01	-9.594E-01
118	3.048E+02	2.054E+03	-2.212E+02	2.408E-01	7.819E+01	-6.216E-01
126	3.170E+02	1.860E+03	-2.053E+02	2.605E-01	7.989E+01	-7.438E-01
134	3.200E+02	1.812E+03	-1.815E+02	2.581E-01	8.032E+01	-7.198E-01
142	3.504E+02	1.449E+03	-9.201E+01	2.927E-01	8.153E+01	-4.841E-01
150	3.810E+02	1.360E+03	-5.290E+01	3.209E-01	8.683E+01	-3.461E-01
158	4.114E+02	1.123E+03	3.220E+01	3.586E-01	8.551E+01	2.921E-01
166	4.144E+02	1.120E+03	3.164E+01	3.673E-01	8.552E+01	2.857E-01
174	4.358E+02	1.011E+03	2.918E+01	3.894E-01	8.349E+01	2.465E-01
182	4.419E+02	1.021E+03	2.868E+01	4.046E-01	8.415E+01	2.270E-01
190	4.678E+02	8.792E+02	2.604E+01	4.300E-01	8.436E+01	2.210E-01
198	4.754E+02	8.189E+02	2.497E+01	4.398E-01	8.455E+01	2.777E-01
206	5.029E+02	7.632E+02	2.009E+01	4.703E-01	8.432E+01	1.909E-01
214	5.182E+02	6.053E+02	1.786E+01	4.870E-01	8.263E+01	1.518E-01
222	5.242E+02	6.304E+02	1.758E+01	4.848E-01	8.247E+01	1.503E-01
230	5.333E+02	6.173E+02	1.786E+01	4.865E-01	8.333E+01	1.507E-01
238	5.488E+02	5.745E+02	1.752E+01	5.063E-01	8.424E+01	1.650E-01
246	5.794E+02	4.343E+02	1.494E+01	5.534E-01	7.722E+01	1.493E-01
254	6.090E+02	3.255E+02	1.187E+01	6.100E-01	7.326E+01	1.430E-01
262	6.194E+02	3.088E+02	1.092E+01	6.215E-01	7.154E+01	1.464E-01
270	6.402E+02	2.872E+02	9.125E+00	6.381E-01	6.760E+01	1.333E-01
278	6.848E+02	2.029E+02	6.380E+00	7.049E-01	6.362E+01	1.318E-01
286	6.934E+02	1.887E+02	5.792E+00	7.136E-01	6.284E+01	1.252E-01
294	6.979E+02	1.883E+02	5.454E+00	7.188E-01	6.273E+01	1.206E-01
302	7.130E+02	1.748E+02	4.633E+00	7.333E-01	6.120E+01	1.076E-01
310	7.286E+02	1.672E+02	3.971E+00	7.573E-01	6.030E+01	1.011E-01
318	7.437E+02	1.593E+02	3.412E+00	7.680E-01	5.947E+01	8.702E-02
326	7.533E+02	1.516E+02	3.137E+00	7.740E-01	5.839E+01	8.085E-02
334	7.600E+02	1.466E+02	3.062E+00	7.799E-01	5.774E+01	7.972E-02
342	7.654E+02	1.433E+02	2.881E+00	7.754E-01	5.713E+01	7.958E-02
350	7.744E+02	1.358E+02	2.617E+00	7.871E-01	5.646E+01	7.571E-02
358	7.875E+02	1.274E+02	2.355E+00	7.780E-01	5.493E+01	7.249E-02
366	8.051E+02	1.110E+02	2.026E+00	7.670E-01	5.269E+01	6.476E-02
374	8.266E+02	1.005E+02	1.633E+00	7.733E-01	4.971E+01	6.576E-02
382	8.461E+02	9.231E+01	1.280E+00	7.650E-01	4.649E+01	5.445E-02
390	8.643E+02	8.589E+01	1.097E+00	7.540E-01	4.365E+01	4.879E-02
398	8.730E+02	8.345E+01	9.087E-01	7.363E-01	4.203E+01	4.818E-02

Table A-3. PRISCILLA desert thermal layer (July 6 revision) - station locations at 10 ft (3.048 m) height (concluded).

sta	xcord (m)	hdpp (kpa)	vdpp (kpa)	ppd (s)	dpih (kpa-s)	dpiv (kpa-s)
406	8.806E+02	8.009E+01	8.656E-01	7.200E-01	4.087E+01	4.512E-02
414	8.893E+02	7.697E+01	7.865E-01	7.043E-01	3.932E+01	4.288E-02
422	8.925E+02	7.548E+01	8.385E-01	6.901E-01	3.879E+01	4.074E-02
430	9.107E+02	6.725E+01	4.648E-01	7.064E-01	3.556E+01	3.608E-02
438	9.824E+02	3.626E+01	-6.871E-01	7.468E-01	2.159E+01	1.853E-02
446	1.060E+03	1.526E+01	9.647E-02	7.986E-01	8.558E+00	1.185E-02
454	1.070E+03	1.529E+01	4.097E-02	8.073E-01	7.272E+00	8.832E-03
462	1.079E+03	1.379E+01	2.859E-02	8.172E-01	6.294E+00	7.256E-03
470	1.086E+03	1.350E+01	3.110E-02	8.072E-01	5.628E+00	6.650E-03
478	1.095E+03	1.308E+01	3.122E-02	8.154E-01	4.929E+00	6.033E-03
486	1.101E+03	1.281E+01	2.848E-02	8.115E-01	4.469E+00	5.655E-03
494	1.103E+03	1.272E+01	2.782E-02	8.085E-01	4.301E+00	5.652E-03
502	1.113E+03	1.232E+01	2.516E-02	8.064E-01	3.709E+00	5.039E-03
510	1.123E+03	1.257E+01	2.074E-02	8.268E-01	3.237E+00	4.393E-03
518	1.156E+03	1.149E+01	1.238E-02	8.101E-01	2.606E+00	1.566E-03
526	1.189E+03	1.070E+01	6.669E-03	8.297E-01	2.389E+00	2.207E-04
534	1.192E+03	1.076E+01	7.134E-03	8.216E-01	2.377E+00	1.918E-04
542	1.218E+03	1.077E+01	5.277E-03	8.256E-01	2.246E+00	8.950E-05
550	1.224E+03	1.107E+01	1.851E-03	8.265E-01	2.212E+00	7.053E-05
558	1.244E+03	1.012E+01	2.214E-03	8.291E-01	2.120E+00	3.485E-05
566	1.258E+03	9.529E+00	2.054E-03	8.338E-01	2.067E+00	2.190E-05
574	1.267E+03	9.101E+00	2.020E-03	8.394E-01	2.031E+00	1.623E-05
582	1.277E+03	8.849E+00	1.818E-03	8.610E-01	2.001E+00	1.492E-05
590	1.287E+03	8.479E+00	1.495E-03	8.554E-01	1.966E+00	1.496E-05
598	1.292E+03	8.318E+00	1.273E-03	8.506E-01	1.951E+00	1.572E-05
606	1.305E+03	7.892E+00	1.128E-03	8.607E-01	1.896E+00	1.500E-05
614	1.320E+03	7.461E+00	3.458E-04	8.737E-01	1.838E+00	1.952E-05
622	1.343E+03	7.222E+00	9.404E-04	8.788E-01	1.763E+00	1.983E-05
630	1.384E+03	6.366E+00	2.061E-04	8.983E-01	1.638E+00	1.510E-05
638	1.433E+03	5.766E+00	-4.225E-04	9.010E-01	1.481E+00	1.175E-05
646	1.467E+03	5.197E+00	2.955E-04	9.095E-01	1.394E+00	9.663E-06
654	1.503E+03	4.977E+00	-4.129E-04	9.257E-01	1.324E+00	1.209E-05
662	1.530E+03	4.823E+00	-2.012E-04	9.368E-01	1.277E+00	6.386E-06
670	1.557E+03	4.428E+00	9.835E-05	9.356E-01	1.222E+00	8.414E-06
678	1.581E+03	4.161E+00	5.804E-04	9.511E-01	1.171E+00	9.723E-06
686	1.596E+03	3.992E+00	1.680E-04	9.475E-01	1.142E+00	5.635E-06
694	1.599E+03	3.949E+00	1.196E-04	9.557E-01	1.138E+00	5.265E-06
702	1.608E+03	3.892E+00	7.537E-05	9.529E-01	1.121E+00	5.746E-06
710	1.615E+03	3.843E+00	-2.474E-04	9.555E-01	1.107E+00	5.390E-06
718	1.651E+03	3.585E+00	6.222E-05	9.318E-01	1.044E+00	5.160E-06
726	1.678E+03	3.446E+00	7.143E-05	8.625E-01	9.992E-01	3.910E-06
734	1.717E+03	3.259E+00	6.527E-05	7.613E-01	9.281E-01	3.712E-06
742	1.794E+03	2.873E+00	4.289E-05	5.629E-01	7.710E-01	2.620E-06
750	1.853E+03	2.580E+00	1.294E-04	4.082E-01	6.224E-01	2.066E-06

Table A-4. PRISCILLA for grassland surface and THRML thermal layer - station locations at 0 ft (0 m) height. Arrival time corrected to 0.15 of distance to peak.

sta	xcord (m)	at (s)	fop (kpa)	opmax (kpa)	opi (kpa-s)
9	1.524E+01	6.703E-02	1.036E+04	1.057E+04	1.425E+02
17	3.048E+01	6.828E-02	8.948E+03	9.704E+03	1.404E+02
25	4.572E+01	7.015E-02	7.281E+03	8.598E+03	1.371E+02
33	6.096E+01	7.283E-02	5.577E+03	7.324E+03	1.326E+02
41	7.620E+01	7.669E-02	4.647E+03	6.529E+03	1.265E+02
49	1.067E+02	8.638E-02	4.817E+03	4.824E+03	1.139E+02
57	1.372E+02	9.659E-02	7.029E+02	3.805E+03	1.005E+02
65	1.676E+02	1.089E-01	6.175E+02	2.892E+03	8.807E+01
73	1.981E+02	1.219E-01	4.569E+02	3.023E+03	7.726E+01
81	2.286E+02	1.371E-01	3.212E+02	2.093E+03	6.798E+01
89	2.591E+02	1.541E-01	2.159E+02	1.200E+03	6.051E+01
97	2.621E+02	1.559E-01	2.101E+02	1.133E+03	5.965E+01
105	2.957E+02	1.765E-01	1.685E+02	7.136E+02	5.298E+01
113	3.048E+02	1.823E-01	1.651E+02	7.000E+02	5.265E+01
121	3.170E+02	1.898E-01	1.614E+02	6.511E+02	5.056E+01
129	3.200E+02	1.918E-01	1.604E+02	6.581E+02	5.051E+01
137	3.505E+02	2.114E-01	1.204E+02	5.339E+02	4.576E+01
145	3.810E+02	2.318E-01	1.136E+02	4.108E+02	4.300E+01
153	4.115E+02	2.529E-01	7.023E+01	3.342E+02	4.009E+01
161	4.145E+02	2.550E-01	6.903E+01	3.265E+02	3.991E+01
169	4.359E+02	2.706E-01	6.084E+01	2.830E+02	3.748E+01
177	4.420E+02	2.752E-01	5.809E+01	2.917E+02	3.704E+01
185	4.679E+02	2.954E-01	4.955E+01	2.474E+02	3.485E+01
193	4.755E+02	3.014E-01	4.832E+01	2.332E+02	3.402E+01
201	5.029E+02	3.243E-01	5.931E+01	2.119E+02	3.239E+01
209	5.182E+02	3.371E-01	5.747E+01	1.958E+02	3.200E+01
217	5.243E+02	3.425E-01	5.652E+01	1.865E+02	3.173E+01
225	5.334E+02	3.503E-01	5.572E+01	1.804E+02	3.119E+01
233	5.486E+02	3.639E-01	5.485E+01	1.707E+02	2.984E+01
241	5.791E+02	3.922E-01	5.280E+01	1.433E+02	2.975E+01
249	6.096E+02	4.217E-01	5.237E+01	1.348E+02	2.840E+01
257	6.187E+02	4.310E-01	5.105E+01	1.243E+02	2.786E+01
265	6.401E+02	4.527E-01	5.005E+01	1.116E+02	2.545E+01
273	6.858E+02	5.018E-01	4.817E+01	9.330E+01	2.462E+01
281	6.949E+02	5.120E-01	4.783E+01	8.718E+01	2.467E+01
289	7.010E+02	5.188E-01	4.519E+01	9.308E+01	2.438E+01
297	7.163E+02	5.363E-01	4.362E+01	8.191E+01	2.367E+01
305	7.315E+02	5.542E-01	4.052E+01	8.901E+01	2.518E+01
313	7.468E+02	5.726E-01	3.985E+01	8.899E+01	2.774E+01
321	7.544E+02	5.825E-01	3.906E+01	9.058E+01	2.759E+01
329	7.620E+02	5.924E-01	4.382E+01	7.927E+01	2.729E+01
337	7.696E+02	6.027E-01	4.519E+01	7.778E+01	2.651E+01
345	7.772E+02	6.128E-01	4.556E+01	7.303E+01	2.589E+01
353	7.925E+02	6.338E-01	4.606E+01	6.653E+01	2.372E+01
361	8.077E+02	6.559E-01	4.684E+01	6.168E+01	2.243E+01
369	8.321E+02	6.916E-01	4.331E+01	5.568E+01	2.234E+01
377	8.534E+02	7.237E-01	3.945E+01	6.179E+01	2.168E+01
385	8.687E+02	7.473E-01	3.432E+01	6.483E+01	2.124E+01
393	8.763E+02	7.600E-01	3.937E+01	6.829E+01	2.122E+01

Table A-4. PRISCILLA for grassland surface and THRML thermal layer - station locations at 0 ft (0 m) height. Arrival time corrected to 0.15 of distance to peak (continued).

sta	xcord (m)	at (s)	fop (kpa)	opmax (kpa)	opi (kpa-s)
401	8.839E+02	7.728E-01	3.878E+01	6.939E+01	2.091E+01
409	8.915E+02	7.850E-01	3.635E+01	6.718E+01	2.068E+01
417	8.992E+02	7.974E-01	3.457E+01	6.267E+01	2.028E+01
425	9.144E+02	8.242E-01	3.499E+01	6.240E+01	2.006E+01
433	9.906E+02	9.665E-01	2.433E+01	3.098E+01	1.966E+01
441	1.067E+03	1.124E+00	1.617E+01	2.871E+01	1.809E+01
449	1.074E+03	1.141E+00	1.533E+01	2.841E+01	1.832E+01
457	1.082E+03	1.158E+00	1.463E+01	2.700E+01	1.876E+01
465	1.090E+03	1.175E+00	1.422E+01	2.568E+01	1.870E+01
473	1.097E+03	1.193E+00	1.395E+01	2.620E+01	1.844E+01
481	1.105E+03	1.211E+00	1.359E+01	2.852E+01	1.831E+01
489	1.113E+03	1.230E+00	1.316E+01	2.971E+01	1.799E+01
497	1.120E+03	1.248E+00	1.297E+01	3.038E+01	1.815E+01
505	1.128E+03	1.266E+00	1.264E+01	3.066E+01	1.813E+01
513	1.158E+03	1.343E+00	1.150E+01	2.923E+01	1.708E+01
521	1.189E+03	1.427E+00	1.046E+01	3.236E+01	1.700E+01
529	1.198E+03	1.450E+00	1.019E+01	3.184E+01	1.684E+01
537	1.219E+03	1.505E+00	9.734E+00	3.495E+01	1.660E+01
545	1.234E+03	1.548E+00	1.040E+01	3.307E+01	1.664E+01
553	1.250E+03	1.598E+00	9.689E+00	3.341E+01	1.634E+01
561	1.265E+03	1.633E+00	9.824E+00	3.366E+01	1.606E+01
569	1.273E+03	1.654E+00	9.702E+00	3.302E+01	1.608E+01
577	1.280E+03	1.675E+00	9.841E+00	3.253E+01	1.584E+01
585	1.288E+03	1.697E+00	9.704E+00	3.256E+01	1.568E+01
593	1.295E+03	1.718E+00	9.811E+00	3.221E+01	1.563E+01
601	1.311E+03	1.757E+00	7.978E+00	3.172E+01	1.547E+01
609	1.341E+03	1.842E+00	9.601E+00	3.036E+01	1.545E+01
617	1.372E+03	1.942E+00	3.778E+00	3.342E+01	1.500E+01
625	1.402E+03	2.040E+00	4.294E+00	3.870E+01	1.444E+01
633	1.454E+03	2.198E+00	5.625E+00	5.244E+01	1.390E+01
641	1.494E+03	2.317E+00	5.934E+00	5.758E+01	1.358E+01
649	1.524E+03	2.403E+00	5.126E+00	4.596E+01	1.330E+01
657	1.554E+03	2.490E+00	5.166E+00	4.037E+01	1.301E+01
673	1.600E+03	2.622E+00	5.194E+00	3.525E+01	1.178E+01
681	1.615E+03	2.666E+00	5.178E+00	3.404E+01	1.185E+01
689	1.622E+03	2.683E+00	5.156E+00	3.372E+01	1.200E+01
697	1.631E+03	2.710E+00	5.140E+00	3.318E+01	1.178E+01
705	1.646E+03	2.756E+00	5.094E+00	3.290E+01	1.126E+01
713	1.676E+03	2.839E+00	4.993E+00	3.231E+01	1.042E+01
721	1.707E+03	2.928E+00	4.898E+00	3.154E+01	9.370E+00
729	1.737E+03	3.015E+00	4.812E+00	3.071E+01	8.160E+00
737	1.829E+03	3.277E+00	4.666E+00	2.793E+01	3.690E+00
745	1.865E+03	3.382E+00	4.619E+00	2.670E+01	1.431E+00

Table A-4. PRISCILLA for grassland surface and THRML thermal layer - station locations at 0 ft (0 m) height. Arrival time corrected to 0.15 of distance to peak (continued).

sta	xcord (m)	hdpp (kpa)	vdpp (kpa)	ppd (s)	dpih (kpa-s)	dpiv (kpa-s)
1	0.000E+00	1.735E+00	-1.962E+03	1.429E-01	1.261E-02	-5.625E-01
9	1.524E+01	1.090E+02	-1.860E+03	1.410E-01	6.979E-01	-5.213E-01
17	3.048E+01	4.399E+02	-1.663E+03	1.413E-01	2.798E+00	-4.199E-01
25	4.572E+01	8.790E+02	-1.297E+03	1.438E-01	5.497E+00	-2.795E-01
33	6.096E+01	1.472E+03	-6.741E+02	1.469E-01	8.725E+00	-1.439E-01
41	7.620E+01	2.303E+03	-1.536E+02	1.491E-01	1.254E+01	-4.589E-02
49	1.067E+02	4.270E+03	-8.221E+00	1.545E-01	1.976E+01	-4.827E-03
57	1.372E+02	4.898E+03	-8.113E+01	1.518E-01	2.455E+01	-1.104E-02
65	1.676E+02	4.052E+03	-7.147E+01	1.567E-01	2.499E+01	-1.107E-02
73	1.981E+02	6.640E+03	-4.144E+01	1.681E-01	2.839E+01	-8.238E-03
81	2.286E+02	5.573E+03	-1.656E+01	1.881E-01	2.983E+01	-3.801E-03
89	2.591E+02	3.084E+03	-4.357E+00	2.138E-01	2.839E+01	-1.296E-03
97	2.621E+02	2.928E+03	-3.831E+00	2.170E-01	2.826E+01	-9.556E-04
105	2.957E+02	1.231E+03	1.373E+00	4.069E-02	2.748E+01	-2.417E-04
113	3.048E+02	1.337E+03	1.306E+00	4.294E-02	2.851E+01	-2.068E-04
121	3.170E+02	1.267E+03	1.221E+00	4.554E-02	2.993E+01	-2.255E-04
129	3.200E+02	1.179E+03	1.209E+00	4.864E-02	2.975E+01	-1.674E-04
137	3.505E+02	7.859E+02	-4.274E-01	5.775E-02	2.915E+01	-2.218E-04
145	3.810E+02	7.449E+02	4.983E-02	6.870E-02	2.883E+01	-1.137E-04
153	4.115E+02	4.696E+02	-1.657E-01	8.679E-02	2.863E+01	-1.460E-04
161	4.145E+02	4.596E+02	-1.532E-01	8.765E-02	2.891E+01	-1.423E-04
169	4.359E+02	3.971E+02	-7.879E-02	9.893E-02	2.824E+01	-9.632E-05
177	4.420E+02	3.981E+02	-5.961E-02	9.995E-02	2.816E+01	-1.061E-04
185	4.679E+02	3.334E+02	-2.115E-02	1.034E-01	2.819E+01	-9.841E-05
193	4.755E+02	3.113E+02	-1.587E-02	1.248E-01	2.848E+01	-8.197E-05
201	5.029E+02	2.614E+02	-8.476E-03	1.283E-01	2.805E+01	-6.262E-05
209	5.182E+02	2.650E+02	-1.515E-02	1.307E-01	2.845E+01	-1.013E-04
217	5.243E+02	2.703E+02	-1.612E-02	8.682E-02	2.893E+01	-9.354E-05
225	5.334E+02	2.685E+02	-8.528E-03	8.911E-02	2.869E+01	-5.526E-05
233	5.486E+02	2.292E+02	-5.441E-03	1.347E-01	2.799E+01	-5.943E-05
241	5.791E+02	2.733E+02	-1.370E-02	1.084E-01	2.944E+01	-1.107E-04
249	6.096E+02	2.501E+02	-1.224E-02	1.273E-01	3.056E+01	-8.381E-05
257	6.187E+02	2.589E+02	-1.007E-02	1.318E-01	3.117E+01	-7.719E-05
265	6.401E+02	2.176E+02	-8.044E-03	1.457E-01	3.079E+01	-5.564E-05
273	6.858E+02	1.710E+02	-5.098E-03	2.016E-01	2.922E+01	-6.990E-05
281	6.949E+02	1.592E+02	-7.746E-03	2.083E-01	2.958E+01	-7.545E-05
289	7.010E+02	1.684E+02	-8.964E-03	1.552E-01	2.948E+01	-1.022E-04
297	7.163E+02	1.707E+02	-6.773E-03	1.456E-01	2.817E+01	-6.719E-05
305	7.315E+02	1.541E+02	-1.069E-02	1.712E-01	2.433E+01	-1.089E-04
313	7.468E+02	1.321E+02	-4.922E-03	1.702E-01	2.252E+01	-1.113E-04
321	7.544E+02	1.197E+02	-4.381E-03	1.719E-01	2.139E+01	-7.741E-05
329	7.620E+02	1.199E+02	5.795E-03	1.718E-01	2.109E+01	-6.344E-05
337	7.696E+02	1.217E+02	3.514E-03	1.728E-01	2.060E+01	-4.795E-05
345	7.772E+02	1.168E+02	-2.169E-03	1.876E-01	1.996E+01	-5.291E-05
353	7.925E+02	9.583E+01	-2.224E-03	1.868E-01	2.021E+01	-4.749E-05
361	8.077E+02	8.097E+01	-2.254E-03	1.910E-01	2.003E+01	-3.923E-05
369	8.321E+02	7.795E+01	-1.412E-03	2.025E-01	1.838E+01	-3.340E-05
377	8.534E+02	6.454E+01	6.068E-04	2.188E-01	1.596E+01	-2.404E-05
385	8.687E+02	5.536E+01	3.642E-03	2.350E-01	1.487E+01	2.408E-05

Table A-4. PRISCILLA for grassland surface and THRML thermal layer - station locations at 0 ft (0 m) height. Arrival time corrected to 0.15 of distance to peak (concluded).

sta	xcord (m)	hdpp (kpa)	vdpp (kpa)	ppd (s)	dpih (kpa-s)	dpiv (kpa-s)
393	8.763E+02	5.267E+01	1.095E-03	2.419E-01	1.480E+01	-1.977E-05
401	8.839E+02	4.959E+01	-1.697E-03	2.523E-01	1.489E+01	-2.648E-05
409	8.915E+02	4.942E+01	5.738E-04	2.592E-01	1.454E+01	-1.700E-05
417	8.992E+02	5.523E+01	8.483E-04	2.748E-01	1.442E+01	-1.508E-05
425	9.144E+02	6.294E+01	-1.066E-03	2.986E-01	1.388E+01	-2.383E-05
433	9.906E+02	3.098E+01	1.540E-03	1.201E+00	8.976E+00	9.322E-06
441	1.067E+03	1.657E+01	1.229E-03	1.122E+00	6.743E+00	1.825E-05
449	1.074E+03	1.605E+01	1.338E-03	1.123E+00	6.153E+00	3.128E-05
457	1.082E+03	1.506E+01	-3.451E-03	1.194E+00	5.449E+00	4.676E-05
465	1.090E+03	1.429E+01	4.036E-03	1.236E+00	4.725E+00	4.215E-05
473	1.097E+03	1.342E+01	-3.931E-03	1.207E+00	4.475E+00	4.225E-05
481	1.105E+03	1.281E+01	8.626E-04	1.232E+00	4.502E+00	-7.326E-06
489	1.113E+03	1.172E+01	-1.479E-03	1.206E+00	4.394E+00	-1.702E-05
497	1.120E+03	1.069E+01	-2.468E-03	1.211E+00	4.242E+00	-1.810E-05
505	1.128E+03	9.742E+00	3.863E-03	1.215E+00	4.132E+00	4.733E-05
513	1.158E+03	7.290E+00	2.794E-03	1.230E+00	3.789E+00	3.468E-05
521	1.189E+03	8.092E+00	2.846E-03	1.163E+00	3.579E+00	4.108E-05
529	1.198E+03	8.221E+00	1.382E-03	1.185E+00	3.365E+00	2.737E-05
537	1.219E+03	8.265E+00	6.885E-04	1.206E+00	2.708E+00	2.427E-05
545	1.234E+03	8.623E+00	-1.092E-03	1.193E+00	2.029E+00	2.157E-05
553	1.250E+03	5.988E+00	-5.769E-04	1.192E+00	1.930E+00	8.545E-06
561	1.265E+03	7.622E+00	-3.103E-04	1.182E+00	1.943E+00	-2.984E-06
569	1.273E+03	7.697E+00	-2.917E-04	1.182E+00	1.941E+00	3.816E-06
577	1.280E+03	7.535E+00	2.530E-04	1.188E+00	1.897E+00	4.304E-06
585	1.288E+03	6.326E+00	1.887E-04	1.186E+00	1.975E+00	-4.139E-06
593	1.295E+03	7.714E+00	1.821E-04	1.182E+00	1.991E+00	-3.697E-06
601	1.311E+03	7.111E+00	-5.235E-04	1.199E+00	1.929E+00	-4.552E-06
609	1.341E+03	7.451E+00	2.003E-04	1.186E+00	1.646E+00	1.233E-05
617	1.372E+03	3.983E+00	-5.416E-04	1.210E+00	1.064E+00	1.670E-05
625	1.402E+03	4.748E+00	7.969E-04	1.195E+00	7.615E-01	1.104E-05
633	1.454E+03	9.268E+00	-5.925E-03	1.187E+00	6.567E-01	-1.714E-05
641	1.494E+03	1.208E+01	-1.939E-02	1.175E+00	6.580E-01	-4.925E-05
649	1.524E+03	7.155E+00	-3.313E-04	1.176E+00	5.302E-01	-1.122E-06
657	1.554E+03	5.628E+00	-5.742E-05	1.105E+00	5.262E-01	-4.562E-07
665	1.585E+03	4.720E+00	-3.385E-05	1.402E+00	5.222E-01	-4.588E-07
673	1.600E+03	4.395E+00	-2.715E-05	9.723E-01	5.190E-01	-3.860E-07
681	1.615E+03	4.140E+00	-4.263E-05	9.288E-01	5.136E-01	-3.834E-07
689	1.622E+03	4.067E+00	-1.880E-05	9.116E-01	5.156E-01	-3.263E-07
697	1.631E+03	3.943E+00	-1.781E-05	8.848E-01	5.099E-01	-3.218E-07
705	1.646E+03	3.722E+00	-1.725E-05	8.407E-01	5.050E-01	-3.098E-07
713	1.676E+03	3.415E+00	-1.481E-05	7.537E-01	4.907E-01	-2.962E-07
721	1.707E+03	3.222E+00	-1.240E-05	6.644E-01	4.633E-01	-2.514E-07
729	1.737E+03	3.125E+00	-9.363E-06	5.766E-01	4.249E-01	-2.445E-07
737	1.829E+03	2.736E+00	-8.381E-06	3.132E-01	2.202E-01	-1.615E-07
745	1.865E+03	2.628E+00	-7.152E-06	2.078E-01	5.400E-02	-5.846E-08

Table A-5. PRISCILLA for grassland surface and THRML thermal layer - station locations at 3 ft (0.9144 m) height.

sta	xcord (m)	at (s)	fop (kpa)	opmax (kpa)	opi (kpa-s)
2	0.000E+00	6.598E-02	1.333E+03	1.183E+04	1.217E+02
10	1.524E+01	6.627E-02	1.299E+03	1.170E+04	1.215E+02
18	3.048E+01	7.091E-02	1.123E+04	1.123E+04	1.210E+02
26	4.572E+01	7.263E-02	1.098E+04	1.098E+04	1.216E+02
34	6.096E+01	7.518E-02	9.628E+03	9.628E+03	1.203E+02
42	7.620E+01	7.895E-02	8.209E+03	8.209E+03	1.165E+02
50	1.067E+02	8.832E-02	5.982E+03	5.982E+03	1.074E+02
58	1.372E+02	9.866E-02	1.229E+03	4.894E+03	9.693E+01
66	1.676E+02	1.087E-01	3.043E+02	3.000E+03	8.576E+01
74	1.981E+02	1.384E-01	2.508E+03	2.508E+03	7.677E+01
82	2.286E+02	1.626E-01	1.721E+03	1.721E+03	6.734E+01
90	2.591E+02	1.539E-01	1.599E+02	1.145E+03	6.061E+01
98	2.621E+02	1.557E-01	1.622E+02	1.100E+03	5.986E+01
106	2.957E+02	1.762E-01	8.648E+01	7.373E+02	5.338E+01
114	3.048E+02	1.820E-01	8.480E+01	7.143E+02	5.314E+01
122	3.170E+02	1.895E-01	8.255E+01	6.619E+02	5.087E+01
130	3.200E+02	1.916E-01	8.225E+01	6.702E+02	5.093E+01
138	3.505E+02	2.112E-01	7.899E+01	5.522E+02	4.610E+01
146	3.810E+02	2.316E-01	7.384E+01	4.236E+02	4.327E+01
154	4.115E+02	2.532E-01	6.920E+01	3.450E+02	4.036E+01
162	4.145E+02	2.553E-01	6.872E+01	3.353E+02	4.016E+01
170	4.359E+02	2.710E-01	6.532E+01	2.921E+02	3.785E+01
178	4.420E+02	2.756E-01	6.427E+01	2.984E+02	3.747E+01
186	4.679E+02	2.959E-01	6.169E+01	2.542E+02	3.524E+01
194	4.755E+02	3.019E-01	6.148E+01	2.397E+02	3.442E+01
202	5.029E+02	3.249E-01	5.960E+01	2.172E+02	3.269E+01
210	5.182E+02	3.377E-01	5.764E+01	2.006E+02	3.230E+01
218	5.243E+02	3.431E-01	5.680E+01	1.911E+02	3.206E+01
226	5.334E+02	3.509E-01	5.593E+01	1.853E+02	3.150E+01
234	5.486E+02	3.647E-01	5.522E+01	1.749E+02	3.019E+01
242	5.791E+02	3.931E-01	5.283E+01	1.461E+02	3.008E+01
250	6.096E+02	4.228E-01	5.242E+01	1.361E+02	2.871E+01
258	6.187E+02	4.318E-01	3.720E+01	1.259E+02	2.815E+01
266	6.401E+02	4.539E-01	4.744E+01	1.125E+02	2.561E+01
274	6.858E+02	5.031E-01	4.406E+01	9.317E+01	2.430E+01
282	6.949E+02	5.135E-01	4.512E+01	8.402E+01	2.428E+01
290	7.010E+02	5.204E-01	4.531E+01	8.103E+01	2.403E+01
298	7.163E+02	5.379E-01	4.267E+01	7.225E+01	2.329E+01
306	7.315E+02	5.560E-01	4.058E+01	8.129E+01	2.475E+01
314	7.468E+02	5.747E-01	3.908E+01	8.164E+01	2.735E+01
322	7.544E+02	5.850E-01	3.894E+01	8.516E+01	2.733E+01
330	7.620E+02	5.950E-01	3.799E+01	7.766E+01	2.721E+01
338	7.696E+02	6.055E-01	3.738E+01	7.869E+01	2.660E+01
346	7.772E+02	6.157E-01	3.697E+01	7.335E+01	2.602E+01
354	7.925E+02	6.374E-01	3.715E+01	6.626E+01	2.395E+01
362	8.077E+02	6.597E-01	3.818E+01	6.181E+01	2.265E+01
370	8.321E+02	6.961E-01	3.815E+01	5.609E+01	2.251E+01
378	8.534E+02	7.288E-01	3.743E+01	6.197E+01	2.189E+01
386	8.687E+02	7.531E-01	3.479E+01	6.522E+01	2.143E+01
394	8.763E+02	7.658E-01	3.645E+01	6.812E+01	2.142E+01

Table A-5. PRISCILLA for grassland surface and THRML thermal layer - station locations at 3 ft (0.9144 m) height (continued).

sta	xcord (m)	at (s)	fop (kpa)	opmax (kpa)	opi (kpa-s)
402	8.839E+02	7.786E-01	3.549E+01	6.991E+01	2.110E+01
410	8.915E+02	7.915E-01	3.523E+01	6.838E+01	2.086E+01
418	8.992E+02	8.046E-01	3.512E+01	6.345E+01	2.044E+01
426	9.144E+02	8.310E-01	3.163E+01	6.283E+01	2.016E+01
434	9.906E+02	9.754E-01	2.454E+01	3.118E+01	1.953E+01
442	1.067E+03	1.136E+00	1.537E+01	2.869E+01	1.782E+01
450	1.074E+03	1.155E+00	1.562E+01	2.832E+01	1.807E+01
458	1.082E+03	1.172E+00	1.505E+01	2.681E+01	1.854E+01
466	1.090E+03	1.191E+00	1.466E+01	2.552E+01	1.851E+01
474	1.097E+03	1.209E+00	1.406E+01	2.609E+01	1.832E+01
482	1.105E+03	1.228E+00	1.371E+01	2.843E+01	1.831E+01
490	1.113E+03	1.247E+00	1.324E+01	2.956E+01	1.805E+01
498	1.120E+03	1.266E+00	1.299E+01	3.043E+01	1.788E+01
506	1.128E+03	1.285E+00	1.265E+01	3.080E+01	1.771E+01
514	1.158E+03	1.366E+00	1.147E+01	2.901E+01	1.707E+01
522	1.189E+03	1.449E+00	1.059E+01	3.254E+01	1.676E+01
530	1.198E+03	1.476E+00	1.102E+01	3.204E+01	1.683E+01
538	1.219E+03	1.535E+00	1.038E+01	3.510E+01	1.662E+01
546	1.234E+03	1.579E+00	1.035E+01	3.323E+01	1.646E+01
554	1.250E+03	1.624E+00	1.032E+01	3.363E+01	1.625E+01
562	1.265E+03	1.666E+00	9.864E+00	3.382E+01	1.601E+01
570	1.273E+03	1.690E+00	1.026E+01	3.329E+01	1.601E+01
578	1.280E+03	1.712E+00	1.020E+01	3.274E+01	1.583E+01
586	1.288E+03	1.727E+00	8.672E+00	3.282E+01	1.577E+01
594	1.295E+03	1.756E+00	1.011E+01	3.239E+01	1.571E+01
602	1.311E+03	1.793E+00	8.710E+00	3.192E+01	1.556E+01
610	1.341E+03	1.887E+00	9.611E+00	3.048E+01	1.517E+01
618	1.372E+03	1.976E+00	9.263E+00	3.351E+01	1.486E+01
626	1.402E+03	2.041E+00	3.972E+00	3.861E+01	1.443E+01
634	1.454E+03	2.199E+00	5.379E+00	4.985E+01	1.392E+01
642	1.494E+03	2.319E+00	5.716E+00	5.339E+01	1.358E+01
650	1.524E+03	2.407E+00	5.130E+00	4.587E+01	1.331E+01
658	1.554E+03	2.495E+00	5.167E+00	4.033E+01	1.300E+01
666	1.585E+03	2.583E+00	5.202E+00	3.665E+01	1.257E+01
674	1.600E+03	2.627E+00	5.198E+00	3.523E+01	1.230E+01
682	1.615E+03	2.671E+00	5.175E+00	3.403E+01	1.198E+01
690	1.622E+03	2.688E+00	5.156E+00	3.371E+01	1.187E+01
698	1.631E+03	2.715E+00	5.142E+00	3.317E+01	1.164E+01
706	1.646E+03	2.759E+00	5.092E+00	3.289E+01	1.127E+01
714	1.676E+03	2.846E+00	4.995E+00	3.236E+01	1.043E+01
722	1.707E+03	2.935E+00	4.894E+00	3.157E+01	9.380E+00
730	1.737E+03	3.023E+00	4.823E+00	3.073E+01	8.169E+00
738	1.829E+03	3.287E+00	4.667E+00	2.791E+01	3.694E+00
746	1.865E+03	3.392E+00	4.625E+00	2.670E+01	1.433E+00

Table A-5. PRISCILLA for grassland surface and THRML thermal layer - station locations at 3 ft (0.9144 m) height (continued).

sta	xcord (m)	hdpp (kpa)	vdpp (kpa)	ppd (s)	dpih (kpa-s)	dpiv (kpa-s)
2	0.000E+00	2.118E+00	-3.557E+03	1.436E-01	1.211E-02	-9.968E+00
10	1.524E+01	8.996E+01	-3.502E+03	1.401E-01	5.987E-01	-9.921E+00
18	3.048E+01	4.321E+02	-3.210E+03	1.387E-01	3.000E+00	-9.211E+00
26	4.572E+01	8.658E+02	-2.730E+03	1.413E-01	6.278E+00	-7.509E+00
34	6.096E+01	1.138E+03	-2.404E+03	1.415E-01	1.063E+01	-6.064E+00
42	7.620E+01	1.491E+03	-2.166E+03	1.439E-01	1.647E+01	-5.105E+00
50	1.067E+02	2.255E+03	-1.652E+03	1.526E-01	2.831E+01	-3.610E+00
58	1.372E+02	4.133E+03	-1.134E+03	1.498E-01	4.137E+01	-2.230E+00
66	1.676E+02	4.560E+03	-8.482E+02	1.568E-01	6.144E+01	-1.527E+00
74	1.981E+02	4.134E+03	-3.997E+02	1.521E-01	7.377E+01	-4.955E-01
82	2.286E+02	3.744E+03	-5.927E+02	1.616E-01	7.841E+01	-4.182E-01
90	2.591E+02	4.142E+03	-1.659E+02	2.132E-01	9.418E+01	-1.364E-01
98	2.621E+02	4.074E+03	-1.192E+02	2.187E-01	9.552E+01	-9.067E-02
106	2.957E+02	2.822E+03	-2.096E+01	4.171E-02	9.064E+01	3.062E-02
114	3.048E+02	2.559E+03	5.006E+00	4.413E-02	8.941E+01	3.914E-02
122	3.170E+02	2.262E+03	-1.037E+01	2.911E-01	8.909E+01	2.720E-02
130	3.200E+02	2.324E+03	4.524E+00	4.908E-02	8.878E+01	2.826E-02
138	3.505E+02	1.684E+03	-3.444E+00	5.715E-02	8.827E+01	1.431E-02
146	3.810E+02	1.653E+03	-2.725E+00	6.819E-02	8.946E+01	1.208E-02
154	4.115E+02	1.154E+03	-3.306E+00	8.589E-02	8.904E+01	-1.025E-02
162	4.145E+02	1.136E+03	-2.853E+00	8.673E-02	8.954E+01	1.281E-02
170	4.359E+02	9.952E+02	-1.676E+00	9.836E-02	8.837E+01	-8.726E-03
178	4.420E+02	9.848E+02	-1.874E+00	9.945E-02	8.774E+01	7.940E-03
186	4.679E+02	8.579E+02	-3.109E+00	1.029E-01	8.855E+01	-1.258E-02
194	4.755E+02	8.075E+02	-2.550E+00	1.241E-01	8.786E+01	-1.143E-02
202	5.029E+02	6.684E+02	-2.760E+00	1.279E-01	8.761E+01	-1.181E-02
210	5.182E+02	6.495E+02	-3.434E+00	1.306E-01	8.972E+01	-2.026E-02
218	5.243E+02	6.276E+02	-2.680E+00	8.677E-02	9.062E+01	-2.026E-02
226	5.334E+02	5.813E+02	-1.595E+00	8.840E-02	9.113E+01	-9.309E-03
234	5.486E+02	5.539E+02	-2.051E+00	1.332E-01	8.753E+01	-1.293E-02
242	5.791E+02	4.862E+02	-3.343E+00	1.078E-01	9.124E+01	-2.608E-02
250	6.096E+02	4.597E+02	-3.678E+00	1.268E-01	9.397E+01	-2.499E-02
258	6.187E+02	4.415E+02	-2.634E+00	1.312E-01	9.541E+01	-1.742E-02
266	6.401E+02	4.172E+02	-2.302E+00	1.443E-01	9.128E+01	-1.622E-02
274	6.858E+02	3.769E+02	-1.259E+00	1.992E-01	8.298E+01	-1.499E-02
282	6.949E+02	3.389E+02	-1.797E+00	2.068E-01	8.235E+01	-2.434E-02
290	7.010E+02	3.167E+02	-1.969E+00	1.562E-01	8.113E+01	-2.989E-02
298	7.163E+02	2.690E+02	-1.494E+00	1.450E-01	7.582E+01	-2.231E-02
306	7.315E+02	2.659E+02	-1.493E+00	1.722E-01	6.804E+01	-3.202E-02
314	7.468E+02	2.429E+02	-1.137E+00	1.692E-01	6.289E+01	-3.178E-02
322	7.544E+02	2.305E+02	-1.181E+00	1.718E-01	5.955E+01	-2.579E-02
330	7.620E+02	2.128E+02	-1.019E+00	1.713E-01	5.946E+01	-2.423E-02
338	7.696E+02	2.047E+02	-9.495E-01	1.726E-01	5.720E+01	-2.303E-02
346	7.772E+02	2.308E+02	-7.517E-01	1.859E-01	5.713E+01	-1.644E-02
354	7.925E+02	2.304E+02	5.897E-01	1.850E-01	5.804E+01	-1.251E-02
362	8.077E+02	2.271E+02	5.050E-01	1.900E-01	5.815E+01	-8.060E-03
370	8.321E+02	2.018E+02	5.019E-01	2.013E-01	5.354E+01	6.900E-03
378	8.534E+02	1.935E+02	4.821E-01	2.173E-01	4.733E+01	7.567E-03
386	8.687E+02	1.780E+02	4.132E-01	2.318E-01	4.315E+01	7.658E-03
394	8.763E+02	1.714E+02	3.345E-01	2.396E-01	4.248E+01	6.314E-03

Table A-5. PRISCILLA for grassland surface and THRML thermal layer - station locations at 3 ft (0.9144 m) height (concluded).

sta	xcord (m)	hdpp (kpa)	vdpp (kpa)	ppd (s)	dpih (kpa-s)	dpiv (kpa-s)
402	8.839E+02	1.678E+02	2.554E-01	2.502E-01	4.297E+01	5.464E-03
410	8.915E+02	1.616E+02	3.040E-01	2.571E-01	4.143E+01	8.010E-03
418	8.992E+02	1.545E+02	3.386E-01	2.718E-01	4.112E+01	7.826E-03
426	9.144E+02	1.642E+02	5.405E-01	2.951E-01	4.001E+01	7.974E-03
434	9.906E+02	9.627E+01	3.348E-01	1.201E+00	2.379E+01	7.351E-03
442	1.067E+03	4.012E+01	1.091E-01	1.125E+00	1.644E+01	3.431E-03
450	1.074E+03	4.234E+01	8.874E-02	1.122E+00	1.516E+01	4.716E-03
458	1.082E+03	4.260E+01	-1.821E-01	1.193E+00	1.364E+01	4.026E-03
466	1.090E+03	4.217E+01	-3.624E-01	1.250E+00	1.182E+01	-4.903E-03
474	1.097E+03	3.889E+01	3.524E-01	1.206E+00	1.144E+01	4.900E-03
482	1.105E+03	3.448E+01	3.034E-01	1.230E+00	1.116E+01	3.704E-03
490	1.113E+03	3.201E+01	2.321E-01	1.203E+00	1.101E+01	5.276E-03
498	1.120E+03	2.803E+01	-1.454E-01	1.210E+00	1.076E+01	3.530E-03
506	1.128E+03	2.484E+01	3.684E-01	1.215E+00	1.062E+01	6.466E-03
514	1.158E+03	1.889E+01	-3.301E-01	1.227E+00	9.355E+00	-5.837E-03
522	1.189E+03	1.967E+01	3.026E-01	1.162E+00	8.022E+00	-4.104E-03
530	1.198E+03	2.368E+01	-1.095E-01	1.183E+00	7.554E+00	-2.229E-03
538	1.219E+03	1.615E+01	-5.860E-02	1.206E+00	6.226E+00	-1.607E-03
546	1.234E+03	2.259E+01	-9.472E-02	1.190E+00	5.325E+00	-1.830E-03
554	1.250E+03	1.621E+01	-3.385E-02	1.180E+00	5.092E+00	-1.200E-03
562	1.265E+03	1.739E+01	1.518E-02	1.180E+00	5.044E+00	-5.681E-04
570	1.273E+03	1.905E+01	-2.734E-02	1.180E+00	4.936E+00	-6.402E-04
578	1.280E+03	1.960E+01	9.771E-03	1.186E+00	4.731E+00	-4.217E-04
586	1.288E+03	1.776E+01	-9.749E-03	1.189E+00	4.665E+00	-2.793E-04
594	1.295E+03	1.781E+01	-1.277E-02	1.178E+00	4.530E+00	2.793E-04
602	1.311E+03	1.690E+01	-7.581E-03	1.194E+00	4.039E+00	2.162E-04
610	1.341E+03	1.803E+01	5.938E-02	1.185E+00	3.320E+00	2.851E-03
618	1.372E+03	9.315E+00	1.905E-02	1.179E+00	2.041E+00	1.190E-03
626	1.402E+03	6.351E+00	2.437E-03	1.197E+00	1.360E+00	2.583E-04
634	1.454E+03	9.779E+00	-1.220E-02	1.186E+00	1.182E+00	-4.037E-05
642	1.494E+03	1.113E+01	-1.924E-02	1.172E+00	1.129E+00	-6.281E-05
650	1.524E+03	8.144E+00	-1.461E-04	1.175E+00	1.055E+00	-1.688E-06
658	1.554E+03	6.339E+00	-1.125E-04	1.105E+00	1.004E+00	-1.577E-06
666	1.585E+03	5.261E+00	-1.334E-04	1.017E+00	9.557E-01	-1.871E-06
674	1.600E+03	4.866E+00	-1.321E-04	9.723E-01	9.299E-01	-1.547E-06
682	1.615E+03	4.540E+00	-2.307E-04	9.288E-01	9.006E-01	-1.822E-06
690	1.622E+03	4.460E+00	-1.280E-04	9.116E-01	8.924E-01	-1.596E-06
698	1.631E+03	4.316E+00	-1.222E-04	8.848E-01	8.735E-01	-1.422E-06
706	1.646E+03	4.253E+00	-1.225E-04	8.407E-01	8.446E-01	-1.377E-06
714	1.676E+03	4.095E+00	-7.383E-05	7.537E-01	7.837E-01	-9.623E-07
722	1.707E+03	3.877E+00	-6.113E-05	6.644E-01	7.054E-01	-8.004E-07
730	1.737E+03	3.668E+00	-4.909E-05	5.765E-01	6.147E-01	-7.384E-07
738	1.829E+03	3.012E+00	-2.866E-05	3.132E-01	2.615E-01	-3.487E-07
746	1.865E+03	2.765E+00	-1.815E-05	2.077E-01	5.730E-02	-1.654E-07

Table A-6. PRISCILLA for grassland surface and THRML thermal layer - station locations at 10 ft (3.048 m) height.

sta	xcord (m)	at (s)	fop (kpa)	opmax (kpa)	opi (kpa-s)
6	0.000E+00	6.461E-02	1.880E+03	8.766E+03	1.047E+02
14	1.524E+01	6.492E-02	1.872E+03	8.688E+03	1.044E+02
22	3.048E+01	6.625E-02	1.814E+03	8.310E+03	1.031E+02
30	4.572E+01	6.822E-02	1.737E+03	7.643E+03	1.014E+02
38	6.096E+01	7.102E-02	1.667E+03	6.801E+03	9.947E+01
46	7.620E+01	7.496E-02	1.584E+03	6.104E+03	9.695E+01
54	1.067E+02	8.468E-02	1.392E+03	5.479E+03	9.469E+01
62	1.372E+02	9.741E-02	1.278E+03	4.243E+03	8.985E+01
70	1.676E+02	1.096E-01	5.157E+02	3.137E+03	7.862E+01
78	1.981E+02	1.227E-01	3.042E+02	2.215E+03	7.177E+01
86	2.286E+02	1.377E-01	2.036E+02	1.581E+03	6.520E+01
94	2.591E+02	1.547E-01	1.348E+02	1.106E+03	5.934E+01
102	2.621E+02	1.564E-01	1.325E+02	1.070E+03	5.881E+01
110	2.957E+02	1.771E-01	1.064E+02	7.431E+02	5.258E+01
118	3.048E+02	1.828E-01	1.023E+02	6.842E+02	5.158E+01
126	3.170E+02	1.904E-01	9.925E+01	6.357E+02	4.956E+01
134	3.200E+02	1.924E-01	1.008E+02	6.501E+02	4.957E+01
142	3.505E+02	2.122E-01	1.097E+02	5.541E+02	4.554E+01
150	3.810E+02	2.328E-01	1.213E+02	4.241E+02	4.253E+01
158	4.115E+02	2.545E-01	1.014E+02	3.454E+02	4.021E+01
166	4.145E+02	2.567E-01	9.972E+01	3.360E+02	4.008E+01
174	4.359E+02	2.726E-01	9.641E+01	2.967E+02	3.758E+01
182	4.420E+02	2.772E-01	9.464E+01	2.912E+02	3.695E+01
190	4.679E+02	2.976E-01	8.076E+01	2.518E+02	3.446E+01
198	4.755E+02	3.037E-01	7.791E+01	2.370E+02	3.427E+01
206	5.029E+02	3.269E-01	7.299E+01	2.149E+02	3.239E+01
214	5.182E+02	3.398E-01	6.843E+01	2.000E+02	3.172E+01
222	5.243E+02	3.452E-01	6.598E+01	1.904E+02	3.162E+01
230	5.334E+02	3.531E-01	6.247E+01	1.848E+02	3.096E+01
238	5.486E+02	3.668E-01	5.673E+01	1.719E+02	3.001E+01
246	5.791E+02	3.953E-01	4.979E+01	1.433E+02	2.962E+01
254	6.096E+02	4.251E-01	4.504E+01	1.340E+02	2.805E+01
262	6.187E+02	4.346E-01	4.397E+01	1.239E+02	2.729E+01
270	6.401E+02	4.564E-01	4.303E+01	1.104E+02	2.476E+01
278	6.858E+02	5.059E-01	3.880E+01	9.230E+01	2.340E+01
286	6.949E+02	5.165E-01	4.843E+01	8.351E+01	2.329E+01
294	7.010E+02	5.233E-01	4.779E+01	8.029E+01	2.286E+01
302	7.163E+02	5.409E-01	4.397E+01	7.159E+01	2.201E+01
310	7.315E+02	5.591E-01	4.105E+01	7.426E+01	2.342E+01
318	7.468E+02	5.780E-01	4.446E+01	7.561E+01	2.609E+01
326	7.544E+02	5.882E-01	4.403E+01	8.014E+01	2.627E+01
334	7.620E+02	5.984E-01	4.473E+01	7.344E+01	2.619E+01
342	7.696E+02	6.090E-01	4.537E+01	7.259E+01	2.605E+01
350	7.772E+02	6.192E-01	4.354E+01	6.934E+01	2.530E+01
358	7.925E+02	6.407E-01	4.256E+01	6.558E+01	2.346E+01
366	8.077E+02	6.629E-01	4.261E+01	5.990E+01	2.221E+01
374	8.321E+02	6.989E-01	4.005E+01	5.428E+01	2.206E+01
382	8.534E+02	7.315E-01	3.931E+01	6.135E+01	2.145E+01
390	8.687E+02	7.556E-01	3.509E+01	6.430E+01	2.100E+01
398	8.763E+02	7.687E-01	3.891E+01	6.710E+01	2.095E+01

Table A-6. PRISCILLA for grassland surface and THRML thermal layer - station locations at 10 ft (3.048 m) height (continued).

sta	xcord (m)	at (s)	fop (kpa)	opmax (kpa)	opi (kpa-s)
406	8.839E+02	7.816E-01	3.858E+01	6.857E+01	2.055E+01
414	8.915E+02	7.940E-01	3.580E+01	6.734E+01	2.032E+01
422	8.992E+02	8.070E-01	3.569E+01	6.276E+01	1.989E+01
430	9.144E+02	8.334E-01	3.140E+01	6.210E+01	1.953E+01
438	9.906E+02	9.779E-01	2.459E+01	3.076E+01	1.898E+01
446	1.067E+03	1.139E+00	1.643E+01	2.860E+01	1.741E+01
454	1.074E+03	1.157E+00	1.577E+01	2.808E+01	1.775E+01
462	1.082E+03	1.175E+00	1.519E+01	2.657E+01	1.825E+01
470	1.090E+03	1.193E+00	1.467E+01	2.540E+01	1.825E+01
478	1.097E+03	1.211E+00	1.420E+01	2.632E+01	1.809E+01
486	1.105E+03	1.230E+00	1.379E+01	2.875E+01	1.810E+01
494	1.113E+03	1.249E+00	1.332E+01	3.008E+01	1.786E+01
502	1.120E+03	1.268E+00	1.298E+01	3.058E+01	1.769E+01
510	1.128E+03	1.287E+00	1.276E+01	3.075E+01	1.751E+01
518	1.158E+03	1.367E+00	1.150E+01	2.979E+01	1.689E+01
526	1.189E+03	1.454E+00	1.207E+01	3.304E+01	1.672E+01
534	1.198E+03	1.480E+00	1.200E+01	3.187E+01	1.680E+01
542	1.219E+03	1.539E+00	1.142E+01	3.509E+01	1.659E+01
550	1.234E+03	1.582E+00	1.105E+01	3.316E+01	1.646E+01
558	1.250E+03	1.626E+00	1.075E+01	3.392E+01	1.626E+01
566	1.265E+03	1.669E+00	1.050E+01	3.449E+01	1.601E+01
574	1.273E+03	1.691E+00	1.037E+01	3.386E+01	1.601E+01
582	1.280E+03	1.712E+00	1.020E+01	3.334E+01	1.584E+01
590	1.288E+03	1.735E+00	1.019E+01	3.348E+01	1.578E+01
598	1.295E+03	1.756E+00	1.008E+01	3.316E+01	1.572E+01
606	1.311E+03	1.799E+00	9.862E+00	3.283E+01	1.558E+01
614	1.341E+03	1.887E+00	9.554E+00	3.151E+01	1.516E+01
622	1.372E+03	1.976E+00	9.265E+00	3.418E+01	1.486E+01
630	1.402E+03	2.065E+00	8.948E+00	3.821E+01	1.444E+01
638	1.454E+03	2.199E+00	4.631E+00	4.627E+01	1.392E+01
646	1.494E+03	2.319E+00	5.379E+00	4.962E+01	1.358E+01
654	1.524E+03	2.407E+00	5.128E+00	4.555E+01	1.331E+01
662	1.554E+03	2.495E+00	5.162E+00	4.017E+01	1.300E+01
670	1.585E+03	2.583E+00	5.201E+00	3.655E+01	1.257E+01
678	1.600E+03	2.627E+00	5.205E+00	3.513E+01	1.230E+01
686	1.615E+03	2.671E+00	5.173E+00	3.395E+01	1.198E+01
694	1.622E+03	2.688E+00	5.158E+00	3.364E+01	1.187E+01
702	1.631E+03	2.715E+00	5.135E+00	3.311E+01	1.164E+01
710	1.646E+03	2.759E+00	5.091E+00	3.265E+01	1.127E+01
718	1.676E+03	2.846E+00	4.994E+00	3.215E+01	1.043E+01
726	1.707E+03	2.935E+00	4.905E+00	3.136E+01	9.380E+00
734	1.737E+03	3.023E+00	4.824E+00	3.060E+01	8.169E+00
742	1.829E+03	3.287E+00	4.668E+00	2.783E+01	3.694E+00
750	1.865E+03	3.392E+00	4.626E+00	2.672E+01	1.433E+00

Table A-6. PRISCILLA for grassland surface and THRML thermal layer - station locations at 10 ft (3.048 m) height (continued).

sta	xcord (m)	hdpp (kpa)	vdpp (kpa)	ppd (s)	dpih (kpa-s)	dpiv (kpa-s)
6	0.000E+00	1.454E+00	-4.044E+03	1.450E-01	1.228E-02	-1.748E+01
14	1.524E+01	6.821E+01	-3.994E+03	1.418E-01	4.957E-01	-1.746E+01
22	3.048E+01	2.702E+02	-3.743E+03	1.433E-01	2.531E+00	-1.707E+01
30	4.572E+01	5.100E+02	-3.464E+03	1.455E-01	5.316E+00	-1.638E+01
38	6.096E+01	7.530E+02	-3.212E+03	1.450E-01	8.866E+00	-1.527E+01
46	7.620E+01	1.030E+03	-2.926E+03	1.474E-01	1.288E+01	-1.374E+01
54	1.067E+02	1.843E+03	-2.269E+03	1.561E-01	2.154E+01	-9.418E+00
62	1.372E+02	2.173E+03	-1.038E+03	1.510E-01	3.184E+01	-5.564E+00
70	1.676E+02	2.456E+03	-8.864E+02	1.564E-01	3.794E+01	-5.004E+00
78	1.981E+02	2.675E+03	-6.677E+02	1.680E-01	4.962E+01	-3.099E+00
86	2.286E+02	2.890E+03	-5.056E+02	1.866E-01	6.039E+01	-1.642E+00
94	2.591E+02	2.335E+03	-3.872E+02	2.125E-01	6.853E+01	-6.711E-01
102	2.621E+02	2.283E+03	-3.620E+02	2.179E-01	6.904E+01	-5.788E-01
110	2.957E+02	2.069E+03	-2.233E+02	2.578E-01	8.011E+01	-3.384E-01
118	3.048E+02	1.936E+03	-1.927E+02	2.714E-01	8.736E+01	-3.348E-01
126	3.170E+02	1.977E+03	-1.092E+02	2.881E-01	9.790E+01	-2.675E-01
134	3.200E+02	1.941E+03	-8.102E+01	2.968E-01	9.979E+01	-1.947E-01
142	3.505E+02	1.731E+03	-3.113E+01	3.900E-02	1.078E+02	-1.346E-01
150	3.810E+02	1.551E+03	-1.886E+01	7.149E-02	1.127E+02	-1.206E-01
158	4.115E+02	1.255E+03	-2.207E+01	9.456E-02	1.158E+02	7.596E-02
166	4.145E+02	1.209E+03	1.993E+01	9.550E-02	1.168E+02	8.163E-02
174	4.359E+02	1.141E+03	2.004E+01	1.052E-01	1.157E+02	9.229E-02
182	4.420E+02	1.207E+03	1.968E+01	9.884E-02	1.156E+02	7.401E-02
190	4.679E+02	1.064E+03	-2.381E+01	1.064E-01	1.158E+02	-9.387E-02
198	4.755E+02	1.032E+03	-2.106E+01	1.312E-01	1.183E+02	-7.565E-02
206	5.029E+02	8.346E+02	-2.701E+01	1.273E-01	1.162E+02	-1.178E-01
214	5.182E+02	8.084E+02	-2.407E+01	1.319E-01	1.160E+02	-1.075E-01
222	5.243E+02	7.635E+02	-2.147E+01	8.328E-02	1.160E+02	-8.608E-02
230	5.334E+02	7.483E+02	-1.792E+01	8.547E-02	1.147E+02	5.623E-02
238	5.486E+02	6.338E+02	-1.861E+01	9.800E-02	1.117E+02	-1.018E-01
246	5.791E+02	6.259E+02	-2.484E+01	1.044E-01	1.122E+02	-1.856E-01
254	6.096E+02	5.669E+02	-2.786E+01	1.221E-01	1.133E+02	-1.769E-01
262	6.187E+02	5.449E+02	-2.335E+01	1.269E-01	1.134E+02	-1.133E-01
270	6.401E+02	4.828E+02	-3.004E+01	1.401E-01	1.104E+02	-2.070E-01
278	6.858E+02	4.250E+02	-1.734E+01	1.935E-01	1.027E+02	-2.113E-01
286	6.949E+02	3.811E+02	-1.899E+01	2.010E-01	1.020E+02	-2.159E-01
294	7.010E+02	3.435E+02	-1.838E+01	1.526E-01	9.815E+01	-2.168E-01
302	7.163E+02	3.183E+02	-1.457E+01	1.404E-01	9.222E+01	-2.069E-01
310	7.315E+02	2.849E+02	-1.366E+01	1.694E-01	8.398E+01	-2.643E-01
318	7.468E+02	2.632E+02	-1.256E+01	1.648E-01	7.693E+01	-2.893E-01
326	7.544E+02	2.555E+02	-1.112E+01	1.718E-01	7.315E+01	-2.056E-01
334	7.620E+02	2.382E+02	-8.831E+00	1.672E-01	7.057E+01	-1.865E-01
342	7.696E+02	2.271E+02	-7.193E+00	1.719E-01	6.758E+01	-1.975E-01
350	7.772E+02	2.250E+02	-5.489E+00	1.885E-01	6.700E+01	-1.492E-01
358	7.925E+02	2.015E+02	-4.247E+00	1.869E-01	6.562E+01	-1.096E-01
366	8.077E+02	1.986E+02	-3.875E+00	1.861E-01	6.384E+01	8.150E-02
374	8.321E+02	1.948E+02	3.387E+00	1.975E-01	5.799E+01	9.759E-02
382	8.534E+02	1.919E+02	3.030E+00	2.130E-01	4.971E+01	1.081E-01
390	8.687E+02	1.743E+02	3.381E+00	2.271E-01	4.305E+01	1.137E-01
398	8.763E+02	1.709E+02	3.576E+00	2.339E-01	4.199E+01	1.232E-01

Table A-6. PRISCILLA for grassland surface and THRML thermal layer - station locations at 10 ft (3.048 m) height (concluded).

sta	xcord (m)	hdpp (kpa)	vdpp (kpa)	ppd (s)	dpih (kpa-s)	dpiv (kpa-s)
406	8.839E+02	1.572E+02	3.397E+00	2.441E-01	4.176E+01	1.095E-01
414	8.915E+02	1.719E+02	3.822E+00	2.524E-01	4.126E+01	1.429E-01
422	8.992E+02	1.589E+02	3.635E+00	2.669E-01	4.051E+01	1.357E-01
430	9.144E+02	1.427E+02	4.312E+00	2.896E-01	3.860E+01	1.184E-01
438	9.906E+02	1.040E+02	2.408E+00	1.201E+00	2.768E+01	1.016E-01
446	1.067E+03	4.180E+01	-8.176E-01	1.117E+00	1.863E+01	4.038E-02
454	1.074E+03	4.407E+01	-6.510E-01	1.113E+00	1.750E+01	5.643E-02
462	1.082E+03	4.460E+01	-1.416E+00	1.192E+00	1.554E+01	4.907E-02
470	1.090E+03	4.448E+01	-8.228E-01	1.239E+00	1.305E+01	3.240E-02
478	1.097E+03	4.284E+01	-5.128E-01	1.203E+00	1.211E+01	1.813E-02
486	1.105E+03	3.970E+01	-4.179E-01	1.227E+00	1.127E+01	1.446E-02
494	1.113E+03	3.525E+01	5.114E-01	1.199E+00	1.138E+01	2.472E-02
502	1.120E+03	3.193E+01	-9.750E-01	1.206E+00	1.134E+01	2.177E-02
510	1.128E+03	2.765E+01	-9.793E-01	1.210E+00	1.137E+01	3.435E-02
518	1.158E+03	2.534E+01	1.401E+00	1.218E+00	9.957E+00	2.429E-02
526	1.189E+03	1.693E+01	6.337E-01	1.156E+00	7.891E+00	2.226E-02
534	1.198E+03	1.855E+01	3.863E-01	1.180E+00	7.204E+00	1.727E-02
542	1.219E+03	1.564E+01	1.681E-01	1.197E+00	5.200E+00	1.013E-02
550	1.234E+03	1.133E+01	1.330E-01	1.186E+00	4.184E+00	9.680E-03
558	1.250E+03	9.650E+00	8.765E-02	1.175E+00	3.500E+00	4.489E-03
566	1.265E+03	7.136E+00	2.911E-02	1.177E+00	2.947E+00	2.240E-03
574	1.273E+03	6.109E+00	-5.867E-02	1.179E+00	2.650E+00	1.941E-03
582	1.280E+03	5.561E+00	-7.180E-02	1.186E+00	2.408E+00	2.684E-03
590	1.288E+03	5.760E+00	9.388E-02	1.181E+00	2.234E+00	2.727E-03
598	1.295E+03	5.076E+00	-6.290E-02	1.180E+00	2.098E+00	2.482E-03
606	1.311E+03	4.738E+00	6.272E-02	1.185E+00	1.810E+00	2.750E-03
614	1.341E+03	4.441E+00	-1.576E-01	1.185E+00	1.549E+00	3.482E-03
622	1.372E+03	7.170E+00	1.385E-01	1.180E+00	1.977E+00	8.779E-03
630	1.402E+03	6.224E+00	8.603E-03	1.172E+00	1.439E+00	2.345E-03
638	1.454E+03	8.428E+00	-1.594E-02	1.187E+00	1.178E+00	-5.315E-05
646	1.494E+03	9.578E+00	-7.554E-03	1.172E+00	1.119E+00	-3.352E-05
654	1.524E+03	8.026E+00	-4.496E-04	1.176E+00	1.070E+00	-3.417E-06
662	1.554E+03	6.290E+00	-5.000E-04	1.105E+00	1.022E+00	-4.425E-06
670	1.585E+03	5.231E+00	-5.874E-04	1.017E+00	9.706E-01	-4.580E-06
678	1.600E+03	4.838E+00	-5.757E-04	9.723E-01	9.436E-01	-4.533E-06
686	1.615E+03	4.518E+00	-6.112E-04	9.288E-01	9.123E-01	-4.458E-06
694	1.622E+03	4.438E+00	-5.768E-04	9.116E-01	9.040E-01	-4.922E-06
702	1.631E+03	4.299E+00	-5.582E-04	8.848E-01	8.836E-01	-4.632E-06
710	1.646E+03	4.196E+00	-5.454E-04	8.406E-01	8.534E-01	-4.535E-06
718	1.676E+03	4.045E+00	-4.684E-04	7.537E-01	7.894E-01	-4.188E-06
726	1.707E+03	3.830E+00	-4.145E-04	6.643E-01	7.090E-01	-3.841E-06
734	1.737E+03	3.639E+00	-2.663E-04	5.765E-01	6.169E-01	-2.789E-06
742	1.829E+03	2.993E+00	-1.238E-04	3.131E-01	2.617E-01	-1.076E-06

Table A-7. PRISCILLA for ideal surface - station locations at height of 0 ft (0 m).

sta	xcord (m)	at (s)	fop (kpa)	ops (kpa)	opi (kpa-s)
7	1.524E+01	6.731E-02	1.174E+04	1.038E+04	1.417E+02
13	3.048E+01	6.859E-02	1.107E+04	9.809E+03	1.397E+02
19	4.572E+01	7.059E-02	1.038E+04	9.185E+03	1.366E+02
25	6.096E+01	7.346E-02	9.647E+03	8.536E+03	1.322E+02
31	7.620E+01	7.720E-02	8.906E+03	7.873E+03	1.269E+02
37	1.067E+02	8.704E-02	7.495E+03	6.544E+03	1.151E+02
43	1.372E+02	1.002E-01	6.329E+03	5.136E+03	1.028E+02
49	1.676E+02	1.171E-01	4.681E+03	4.026E+03	9.068E+01
55	1.981E+02	1.368E-01	2.049E+03	2.337E+03	7.995E+01
61	2.286E+02	1.591E-01	1.584E+03	1.222E+03	7.024E+01
67	2.591E+02	1.839E-01	1.283E+03	9.095E+02	6.232E+01
73	2.621E+02	1.865E-01	1.233E+03	8.809E+02	6.174E+01
79	2.957E+02	2.172E-01	9.990E+02	9.310E+02	5.493E+01
85	3.048E+02	2.261E-01	9.403E+02	8.756E+02	5.340E+01
91	3.170E+02	2.381E-01	8.770E+02	8.128E+02	5.158E+01
97	3.200E+02	2.414E-01	8.616E+02	7.977E+02	5.108E+01
103	3.505E+02	2.738E-01	7.307E+02	6.766E+02	4.714E+01
109	3.810E+02	3.087E-01	6.331E+02	5.856E+02	4.391E+01
115	4.115E+02	3.456E-01	5.515E+02	5.088E+02	4.126E+01
121	4.145E+02	3.493E-01	5.436E+02	5.016E+02	4.107E+01
127	4.359E+02	3.765E-01	5.156E+02	4.780E+02	3.900E+01
133	4.420E+02	3.842E-01	5.050E+02	4.670E+02	3.841E+01
139	4.679E+02	4.182E-01	4.597E+02	4.239E+02	3.661E+01
145	4.755E+02	4.285E-01	4.463E+02	4.101E+02	3.614E+01
151	5.029E+02	4.666E-01	3.920E+02	3.601E+02	3.427E+01
157	5.182E+02	4.886E-01	3.680E+02	3.372E+02	3.315E+01
163	5.243E+02	4.977E-01	3.594E+02	3.290E+02	3.278E+01
169	5.334E+02	5.114E-01	3.455E+02	3.167E+02	3.229E+01
175	5.486E+02	5.345E-01	3.259E+02	2.981E+02	3.158E+01
181	5.791E+02	5.821E-01	2.945E+02	2.657E+02	3.032E+01
187	6.096E+02	6.322E-01	2.670E+02	2.381E+02	2.913E+01
193	6.187E+02	6.472E-01	2.586E+02	2.304E+02	2.883E+01
199	6.401E+02	6.837E-01	2.410E+02	2.141E+02	2.806E+01
205	6.858E+02	7.647E-01	2.016E+02	1.813E+02	2.663E+01
211	6.949E+02	7.811E-01	1.954E+02	1.761E+02	2.641E+01
217	7.010E+02	7.925E-01	1.929E+02	1.739E+02	2.616E+01
223	7.163E+02	8.206E-01	1.857E+02	1.669E+02	2.578E+01
229	7.315E+02	8.491E-01	1.782E+02	1.599E+02	2.536E+01
235	7.468E+02	8.780E-01	1.705E+02	1.529E+02	2.493E+01
241	7.544E+02	8.925E-01	1.670E+02	1.495E+02	2.478E+01
247	7.620E+02	9.076E-01	1.634E+02	1.463E+02	2.454E+01
253	7.696E+02	9.224E-01	1.601E+02	1.434E+02	2.433E+01
259	7.772E+02	9.372E-01	1.573E+02	1.406E+02	2.418E+01
265	7.925E+02	9.671E-01	1.510E+02	1.350E+02	2.386E+01
271	8.077E+02	9.973E-01	1.452E+02	1.296E+02	2.352E+01
277	8.321E+02	1.047E+00	1.369E+02	1.220E+02	2.294E+01
283	8.534E+02	1.090E+00	1.301E+02	1.160E+02	2.244E+01
289	8.687E+02	1.122E+00	1.260E+02	1.120E+02	2.215E+01
295	8.763E+02	1.138E+00	1.235E+02	1.100E+02	2.199E+01
301	8.839E+02	1.154E+00	1.217E+02	1.082E+02	2.187E+01

Table A-7. PRISCILLA for ideal surface - station locations at height of 0 ft (0 m) (continued).

sta	xcord (m)	at (s)	fop (kpa)	ops (kpa)	opi (kpa·s)
307	8.915E+02	1.169E+00	1.195E+02	1.063E+02	2.168E+01
313	8.992E+02	1.185E+00	1.174E+02	1.046E+02	2.154E+01
319	9.144E+02	1.218E+00	1.136E+02	1.011E+02	2.125E+01
325	9.906E+02	1.383E+00	9.834E+01	8.662E+01	1.986E+01
331	1.067E+03	1.554E+00	8.615E+01	7.525E+01	1.863E+01
337	1.074E+03	1.571E+00	8.502E+01	7.424E+01	1.851E+01
343	1.082E+03	1.589E+00	8.400E+01	7.330E+01	1.839E+01
349	1.090E+03	1.606E+00	8.301E+01	7.236E+01	1.832E+01
355	1.097E+03	1.624E+00	8.192E+01	7.141E+01	1.818E+01
361	1.105E+03	1.641E+00	8.096E+01	7.051E+01	1.809E+01
367	1.113E+03	1.658E+00	8.007E+01	6.967E+01	1.798E+01
373	1.120E+03	1.676E+00	7.914E+01	6.879E+01	1.787E+01
379	1.128E+03	1.694E+00	7.821E+01	6.794E+01	1.779E+01
385	1.158E+03	1.765E+00	7.458E+01	6.466E+01	1.735E+01
391	1.189E+03	1.836E+00	7.154E+01	6.173E+01	1.695E+01
397	1.198E+03	1.858E+00	7.071E+01	6.091E+01	1.684E+01
403	1.219E+03	1.909E+00	6.858E+01	5.900E+01	1.655E+01
409	1.234E+03	1.945E+00	6.710E+01	5.770E+01	1.639E+01
415	1.250E+03	1.981E+00	6.571E+01	5.642E+01	1.619E+01
421	1.265E+03	2.018E+00	6.198E+01	5.455E+01	1.600E+01
427	1.273E+03	2.036E+00	6.290E+01	5.465E+01	1.594E+01
433	1.280E+03	2.054E+00	6.188E+01	5.392E+01	1.584E+01
439	1.288E+03	2.073E+00	6.040E+01	5.299E+01	1.578E+01
445	1.295E+03	2.091E+00	6.105E+01	5.294E+01	1.568E+01
451	1.311E+03	2.128E+00	5.988E+01	5.180E+01	1.553E+01
457	1.341E+03	2.203E+00	5.722E+01	4.956E+01	1.519E+01
463	1.372E+03	2.278E+00	5.493E+01	4.757E+01	1.486E+01
469	1.402E+03	2.352E+00	5.390E+01	4.606E+01	1.458E+01
475	1.454E+03	2.481E+00	5.057E+01	4.310E+01	1.409E+01
481	1.494E+03	2.581E+00	4.831E+01	4.109E+01	1.372E+01
487	1.524E+03	2.657E+00	4.600E+01	3.947E+01	1.347E+01
493	1.555E+03	2.734E+00	4.482E+01	3.817E+01	1.320E+01
499	1.585E+03	2.812E+00	4.357E+01	3.697E+01	1.295E+01
505	1.600E+03	2.850E+00	4.252E+01	3.618E+01	1.285E+01
511	1.615E+03	2.889E+00	4.226E+01	3.580E+01	1.274E+01
517	1.622E+03	2.905E+00	4.216E+01	3.561E+01	1.268E+01
523	1.631E+03	2.928E+00	4.136E+01	3.511E+01	1.264E+01
529	1.646E+03	2.968E+00	4.093E+01	3.465E+01	1.248E+01
535	1.676E+03	3.045E+00	3.974E+01	3.361E+01	1.231E+01

Table A-7. PRISCILLA for ideal surface - station locations at height of 0 ft (0 m) (continued).

sta	xcord (m)	hdpp (kpa)	vdpp (kpa)	ppd (s)	dpih (kpa-s)	dpiv (kpa-s)
1	0.000E+00	2.798E-01	-3.325E+03	1.428E-01	8.978E-02	-6.612E-01
7	1.524E+01	9.580E+01	-3.190E+03	1.447E-01	8.605E-01	-6.416E-01
13	3.048E+01	3.557E+02	-3.374E+03	1.350E-01	3.132E+00	-5.993E-01
19	4.572E+01	6.257E+02	-2.907E+03	1.374E-01	6.377E+00	-5.116E-01
25	6.096E+01	9.932E+02	-2.047E+03	1.405E-01	9.968E+00	-3.741E-01
31	7.620E+01	1.379E+03	-1.312E+03	1.433E-01	1.406E+01	-2.360E-01
37	1.067E+02	2.637E+03	-3.992E+02	1.526E-01	2.320E+01	-7.449E-02
43	1.372E+02	2.922E+03	-1.246E+03	1.499E-01	3.161E+01	-2.497E-01
49	1.676E+02	3.468E+03	-3.551E+02	1.499E-01	3.680E+01	-5.868E-02
55	1.981E+02	7.092E+03	1.943E+00	1.549E-01	5.177E+01	1.195E-03
61	2.286E+02	6.181E+03	1.940E+00	1.631E-01	6.254E+01	1.227E-03
67	2.591E+02	4.028E+03	9.261E-01	1.797E-01	6.736E+01	8.744E-04
73	2.621E+02	3.867E+03	7.638E-01	1.808E-01	6.753E+01	7.963E-04
79	2.957E+02	2.765E+03	2.976E-01	2.020E-01	6.459E+01	4.894E-04
85	3.048E+02	2.321E+03	3.534E-01	2.061E-01	6.307E+01	5.383E-04
91	3.170E+02	2.159E+03	2.518E-01	2.184E-01	6.065E+01	4.517E-04
97	3.200E+02	2.045E+03	2.458E-01	2.217E-01	5.993E+01	4.770E-04
103	3.505E+02	1.532E+03	1.460E-01	2.424E-01	5.184E+01	2.955E-04
109	3.810E+02	8.487E+02	5.146E-02	2.635E-01	4.233E+01	1.550E-04
115	4.115E+02	5.686E+02	1.609E-02	2.945E-01	3.430E+01	6.886E-05
121	4.145E+02	5.567E+02	1.172E-02	2.956E-01	3.365E+01	6.821E-05
127	4.359E+02	5.156E+02	1.997E-02	3.145E-01	2.924E+01	7.057E-05
133	4.420E+02	4.974E+02	1.077E-02	3.132E-01	2.813E+01	4.807E-05
139	4.679E+02	4.257E+02	5.547E-03	3.443E-01	2.359E+01	4.810E-05
145	4.755E+02	4.031E+02	3.701E-03	3.504E-01	2.230E+01	4.024E-05
151	5.029E+02	3.253E+02	1.697E-03	3.736E-01	1.887E+01	1.234E-05
157	5.182E+02	2.914E+02	-1.097E-03	3.777E-01	1.729E+01	1.168E-05
163	5.243E+02	2.798E+02	-9.543E-04	3.855E-01	1.654E+01	7.073E-06
169	5.334E+02	2.622E+02	-9.139E-04	3.827E-01	1.556E+01	6.766E-06
175	5.486E+02	2.371E+02	-7.541E-04	3.981E-01	1.366E+01	4.034E-06
181	5.791E+02	1.943E+02	-6.626E-04	4.216E-01	1.150E+01	-1.016E-06
187	6.096E+02	1.601E+02	-5.828E-04	4.396E-01	9.917E+00	-9.056E-07
193	6.187E+02	1.516E+02	-4.841E-04	4.517E-01	9.549E+00	-8.109E-07
199	6.401E+02	1.330E+02	-4.061E-04	4.538E-01	8.742E+00	-7.692E-07
205	6.858E+02	9.961E+01	-1.841E-04	4.906E-01	7.319E+00	-4.273E-07
211	6.949E+02	9.446E+01	-2.227E-04	5.031E-01	7.084E+00	-4.541E-07
217	7.010E+02	9.244E+01	-2.227E-04	5.059E-01	6.922E+00	-3.948E-07
223	7.163E+02	8.578E+01	-1.397E-04	5.051E-01	6.559E+00	-3.493E-07
229	7.315E+02	7.921E+01	-1.169E-04	5.264E-01	6.218E+00	5.079E-07
235	7.468E+02	7.313E+01	-1.028E-04	5.429E-01	5.897E+00	3.694E-07
241	7.544E+02	7.025E+01	-1.092E-04	5.426E-01	5.750E+00	-2.808E-07
247	7.620E+02	6.754E+01	-1.059E-04	5.426E-01	5.593E+00	-2.695E-07
253	7.696E+02	6.511E+01	-8.748E-05	5.452E-01	5.453E+00	-4.053E-07
259	7.772E+02	6.278E+01	-9.300E-05	5.490E-01	5.319E+00	-2.463E-07
265	7.925E+02	5.837E+01	-6.928E-05	5.654E-01	5.068E+00	6.086E-07
271	8.077E+02	5.411E+01	-6.169E-05	5.681E-01	4.830E+00	-2.051E-07
277	8.321E+02	4.845E+01	-5.097E-05	5.964E-01	4.474E+00	-1.761E-07
283	8.534E+02	4.413E+01	-4.405E-05	6.048E-01	4.189E+00	-1.670E-07
289	8.687E+02	4.132E+01	-5.783E-05	6.107E-01	4.006E+00	-1.423E-07
295	8.763E+02	3.998E+01	-5.783E-05	6.249E-01	3.917E+00	2.112E-07

Table A-7. PRISCILLA for ideal surface - station locations at height of 0 ft (0 m) (concluded).

sta	xcord (m)	hdpp (kpa)	vdpp (kpa)	ppd (s)	dpih (kpa-s)	dpiv (kpa-s)
301	8.839E+02	3.875E+01	-3.360E-05	6.273E-01	3.835E+00	3.440E-07
307	8.915E+02	3.750E+01	4.975E-05	6.321E-01	3.749E+00	-1.247E-07
313	8.992E+02	3.637E+01	-4.616E-05	6.303E-01	3.670E+00	-1.408E-07
319	9.144E+02	3.417E+01	3.480E-05	6.454E-01	3.513E+00	-1.107E-07
325	9.906E+02	2.549E+01	3.123E-05	6.832E-01	2.865E+00	8.281E-08
331	1.067E+03	1.950E+01	-1.081E-05	7.186E-01	2.373E+00	-5.633E-08
337	1.074E+03	1.900E+01	-9.690E-06	7.333E-01	2.328E+00	-5.427E-08
343	1.082E+03	1.854E+01	-9.793E-06	7.395E-01	2.289E+00	-5.291E-08
349	1.090E+03	1.809E+01	-8.986E-06	7.376E-01	2.252E+00	-5.086E-08
355	1.097E+03	1.764E+01	-8.587E-06	7.455E-01	2.213E+00	-4.942E-08
361	1.105E+03	1.722E+01	-8.277E-06	7.423E-01	2.177E+00	-4.794E-08
367	1.113E+03	1.682E+01	-7.843E-06	7.417E-01	2.140E+00	-4.667E-08
373	1.120E+03	1.641E+01	-7.524E-06	7.562E-01	2.106E+00	-4.495E-08
379	1.128E+03	1.602E+01	-7.397E-06	7.577E-01	2.072E+00	-4.375E-08
385	1.158E+03	1.456E+01	-6.510E-06	7.707E-01	1.942E+00	-3.895E-08
391	1.189E+03	1.331E+01	-5.416E-06	7.835E-01	1.831E+00	-3.482E-08
397	1.198E+03	1.296E+01	-5.331E-06	7.861E-01	1.803E+00	-3.367E-08
403	1.219E+03	1.219E+01	-4.791E-06	7.965E-01	1.735E+00	-3.087E-08
409	1.234E+03	1.168E+01	-4.426E-06	7.994E-01	1.697E+00	-3.053E-08
415	1.250E+03	1.118E+01	-4.112E-06	8.050E-01	1.658E+00	2.879E-08
421	1.265E+03	1.058E+01	-1.241E-05	8.141E-01	1.624E+00	-3.040E-08
427	1.273E+03	1.057E+01	-3.135E-06	8.148E-01	1.609E+00	-2.557E-08
433	1.280E+03	1.032E+01	-2.853E-06	8.230E-01	1.593E+00	-2.795E-08
439	1.288E+03	1.002E+01	-2.754E-05	8.245E-01	1.579E+00	-4.005E-08
445	1.295E+03	9.940E+00	-3.638E-06	8.246E-01	1.563E+00	-2.442E-08
451	1.311E+03	9.532E+00	8.631E-06	8.385E-01	1.534E+00	3.370E-08
457	1.341E+03	8.770E+00	-2.146E-06	8.474E-01	1.473E+00	-2.356E-08
463	1.372E+03	8.097E+00	-1.422E-06	8.559E-01	1.413E+00	-1.947E-08
469	1.402E+03	7.560E+00	-1.540E-06	8.711E-01	1.360E+00	-1.650E-08
475	1.454E+03	6.651E+00	-1.067E-06	8.866E-01	1.268E+00	-1.082E-08
481	1.494E+03	6.058E+00	-8.440E-07	9.016E-01	1.198E+00	-9.598E-09
487	1.524E+03	5.891E+00	-8.697E-06	9.108E-01	1.152E+00	-1.085E-08
493	1.554E+03	5.257E+00	-4.976E-07	9.210E-01	1.101E+00	-8.188E-09
499	1.585E+03	4.933E+00	-4.519E-07	9.299E-01	1.055E+00	-6.158E-09
505	1.600E+03	4.748E+00	-6.380E-04	9.374E-01	1.036E+00	-6.496E-07
511	1.615E+03	4.630E+00	-3.863E-07	9.403E-01	1.016E+00	-5.094E-09
517	1.622E+03	4.576E+00	-4.103E-07	9.415E-01	1.006E+00	-6.561E-09
523	1.631E+03	4.451E+00	-4.098E-06	9.446E-01	9.965E-01	9.683E-09
529	1.646E+03	4.347E+00	-3.476E-07	9.476E-01	9.718E-01	-4.279E-09
535	1.676E+03	4.095E+00	-2.845E-07	9.575E-01	9.375E-01	-3.489E-09
541	1.707E+03	3.854E+00	-2.326E-07	8.781E-01	8.944E-01	-2.859E-09
547	1.737E+03	3.632E+00	-1.850E-07	7.994E-01	8.542E-01	-2.619E-09
553	1.829E+03	3.059E+00	1.554E-05	5.628E-01	7.151E-01	6.450E-08
559	1.865E+03	2.890E+00	5.349E-04	4.672E-01	6.402E-01	7.858E-07

Table A-8. PRISCILLA for ideal surface - station locations at height of 3 ft (0.9144 m).

sta	xcord (m)	at (s)	fop (kpa)	opmax (kpa)	opi (kpa-s)
8	1.524E+01	6.644E-02	1.672E+03	1.008E+04	1.225E+02
14	3.048E+01	6.773E-02	1.607E+03	1.008E+04	1.220E+02
20	4.572E+01	6.973E-02	1.553E+03	1.001E+04	1.222E+02
26	6.096E+01	7.259E-02	1.497E+03	8.654E+03	1.209E+02
32	7.620E+01	7.632E-02	1.544E+03	7.406E+03	1.156E+02
38	1.067E+02	8.607E-02	1.233E+03	5.890E+03	1.082E+02
44	1.372E+02	9.937E-02	1.029E+03	5.822E+03	9.810E+01
50	1.676E+02	1.162E-01	8.710E+02	4.150E+03	8.803E+01
56	1.981E+02	1.366E-01	7.870E+02	2.621E+03	7.937E+01
62	2.286E+02	1.590E-01	1.491E+03	1.856E+03	6.972E+01
68	2.591E+02	1.838E-01	1.197E+03	1.241E+03	6.180E+01
74	2.621E+02	1.864E-01	1.161E+03	1.195E+03	6.123E+01
80	2.957E+02	2.170E-01	9.310E+02	9.310E+02	5.463E+01
86	3.048E+02	2.259E-01	8.765E+02	8.765E+02	5.313E+01
92	3.170E+02	2.380E-01	8.127E+02	8.127E+02	5.135E+01
98	3.200E+02	2.412E-01	7.975E+02	7.975E+02	5.086E+01
104	3.505E+02	2.737E-01	6.765E+02	6.765E+02	4.704E+01
110	3.810E+02	3.086E-01	5.855E+02	5.855E+02	4.387E+01
116	4.115E+02	3.454E-01	5.087E+02	5.087E+02	4.129E+01
122	4.145E+02	3.491E-01	5.015E+02	5.015E+02	4.111E+01
128	4.359E+02	3.763E-01	4.780E+02	4.780E+02	3.902E+01
134	4.420E+02	3.840E-01	4.672E+02	4.672E+02	3.845E+01
140	4.679E+02	4.180E-01	4.237E+02	4.237E+02	3.664E+01
146	4.755E+02	4.282E-01	4.100E+02	4.100E+02	3.617E+01
152	5.029E+02	4.664E-01	3.598E+02	3.598E+02	3.430E+01
158	5.182E+02	4.884E-01	3.367E+02	3.367E+02	3.319E+01
164	5.243E+02	4.975E-01	3.285E+02	3.285E+02	3.283E+01
170	5.334E+02	5.112E-01	3.162E+02	3.162E+02	3.233E+01
176	5.486E+02	5.342E-01	2.976E+02	2.976E+02	3.163E+01
182	5.791E+02	5.818E-01	2.646E+02	2.646E+02	3.037E+01
188	6.096E+02	6.318E-01	2.368E+02	2.368E+02	2.917E+01
194	6.187E+02	6.469E-01	2.291E+02	2.291E+02	2.888E+01
200	6.401E+02	6.834E-01	2.128E+02	2.128E+02	2.810E+01
206	6.858E+02	7.643E-01	1.805E+02	1.805E+02	2.667E+01
212	6.949E+02	7.807E-01	1.753E+02	1.753E+02	2.645E+01
218	7.010E+02	7.921E-01	1.731E+02	1.731E+02	2.620E+01
224	7.163E+02	8.202E-01	1.661E+02	1.661E+02	2.582E+01
230	7.315E+02	8.487E-01	1.591E+02	1.591E+02	2.539E+01
236	7.468E+02	8.775E-01	1.521E+02	1.521E+02	2.496E+01
242	7.544E+02	8.921E-01	1.487E+02	1.487E+02	2.481E+01
248	7.620E+02	9.072E-01	1.455E+02	1.455E+02	2.457E+01
254	7.696E+02	9.219E-01	1.426E+02	1.426E+02	2.436E+01
260	7.772E+02	9.367E-01	1.397E+02	1.397E+02	2.421E+01
266	7.925E+02	9.666E-01	1.342E+02	1.342E+02	2.388E+01
272	8.077E+02	9.969E-01	1.288E+02	1.288E+02	2.354E+01
278	8.321E+02	1.046E+00	1.213E+02	1.213E+02	2.296E+01
284	8.534E+02	1.090E+00	1.153E+02	1.153E+02	2.246E+01
290	8.687E+02	1.121E+00	1.113E+02	1.113E+02	2.217E+01
296	8.763E+02	1.137E+00	1.093E+02	1.093E+02	2.201E+01
302	8.839E+02	1.153E+00	1.075E+02	1.075E+02	2.189E+01

Table A-8. PRISCILLA for ideal surface - station locations at height of 3 ft (0.9144 m) (continued).

sta	xcord (m)	at (s)	fop (kpa)	opmax (kpa)	opi (kpa-s)
308	8.915E+02	1.169E+00	1.056E+02	1.056E+02	2.170E+01
314	8.992E+02	1.185E+00	1.039E+02	1.039E+02	2.156E+01
320	9.144E+02	1.218E+00	1.004E+02	1.004E+02	2.127E+01
326	9.906E+02	1.383E+00	8.589E+01	8.589E+01	1.987E+01
332	1.067E+03	1.553E+00	7.451E+01	7.451E+01	1.864E+01
338	1.074E+03	1.571E+00	7.350E+01	7.350E+01	1.853E+01
344	1.082E+03	1.588E+00	7.256E+01	7.256E+01	1.841E+01
350	1.090E+03	1.605E+00	7.162E+01	7.162E+01	1.834E+01
356	1.097E+03	1.623E+00	7.067E+01	7.067E+01	1.819E+01
362	1.105E+03	1.640E+00	6.978E+01	6.978E+01	1.810E+01
368	1.113E+03	1.658E+00	6.893E+01	6.893E+01	1.799E+01
374	1.120E+03	1.675E+00	6.805E+01	6.805E+01	1.788E+01
380	1.128E+03	1.693E+00	6.720E+01	6.720E+01	1.780E+01
386	1.158E+03	1.764E+00	6.393E+01	6.393E+01	1.736E+01
392	1.189E+03	1.836E+00	6.097E+01	6.097E+01	1.695E+01
398	1.198E+03	1.857E+00	6.015E+01	6.015E+01	1.685E+01
404	1.219E+03	1.908E+00	5.825E+01	5.825E+01	1.656E+01
410	1.234E+03	1.944E+00	5.695E+01	5.695E+01	1.640E+01
416	1.250E+03	1.980E+00	5.568E+01	5.568E+01	1.620E+01
422	1.265E+03	2.017E+00	5.411E+01	5.411E+01	1.600E+01
428	1.273E+03	2.035E+00	5.406E+01	5.406E+01	1.595E+01
434	1.280E+03	2.053E+00	5.337E+01	5.337E+01	1.585E+01
440	1.288E+03	2.072E+00	5.268E+01	5.268E+01	1.578E+01
446	1.295E+03	2.090E+00	5.235E+01	5.235E+01	1.569E+01
452	1.311E+03	2.127E+00	5.119E+01	5.119E+01	1.553E+01
458	1.341E+03	2.201E+00	4.894E+01	4.894E+01	1.520E+01
464	1.372E+03	2.276E+00	4.702E+01	4.702E+01	1.486E+01
470	1.402E+03	2.351E+00	4.537E+01	4.537E+01	1.459E+01
476	1.454E+03	2.479E+00	4.246E+01	4.246E+01	1.410E+01
482	1.494E+03	2.578E+00	4.046E+01	4.046E+01	1.373E+01
488	1.524E+03	2.654E+00	3.712E+01	3.712E+01	1.348E+01
494	1.554E+03	2.732E+00	3.760E+01	3.760E+01	1.320E+01
500	1.585E+03	2.809E+00	3.639E+01	3.639E+01	1.295E+01
506	1.600E+03	2.848E+00	3.585E+01	3.585E+01	1.285E+01
512	1.615E+03	2.886E+00	3.522E+01	3.522E+01	1.274E+01
518	1.622E+03	2.902E+00	3.501E+01	3.501E+01	1.268E+01
524	1.631E+03	2.925E+00	3.456E+01	3.456E+01	1.264E+01
530	1.646E+03	2.964E+00	3.409E+01	3.409E+01	1.249E+01
536	1.676E+03	3.041E+00	3.305E+01	3.305E+01	1.231E+01
542	1.707E+03	3.121E+00	3.206E+01	3.206E+01	1.199E+01
548	1.737E+03	3.200E+00	3.110E+01	3.110E+01	1.158E+01
554	1.829E+03	3.436E+00	2.845E+01	2.845E+01	9.594E+00
560	1.865E+03	3.532E+00	2.746E+01	2.746E+01	8.433E+00

Table A-8. PRISCILLA for ideal surface - station locations at height of 3 ft (0.9144 m) (continued).

sta	xcord (m)	hdpp (kpa)	vdpp (kpa)	ppd (s)	dpih (kpa-s)	dpiv (kpa-s)
2	0.000E+00	3.401E-01	-3.762E+03	1.378E-01	1.246E-01	-9.625E+00
8	1.524E+01	7.590E+01	-3.675E+03	1.396E-01	7.852E-01	-9.477E+00
14	3.048E+01	3.147E+02	-3.451E+03	1.404E-01	2.995E+00	-8.755E+00
20	4.572E+01	6.958E+02	-3.198E+03	1.447E-01	7.002E+00	-7.146E+00
26	6.096E+01	1.065E+03	-3.002E+03	1.420E-01	1.159E+01	-5.692E+00
32	7.620E+01	1.396E+03	-2.770E+03	9.799E-02	1.697E+01	-4.820E+00
38	1.067E+02	2.191E+03	-2.309E+03	1.531E-01	2.715E+01	-3.446E+00
44	1.372E+02	2.982E+03	-1.328E+03	1.506E-01	3.617E+01	-2.371E+00
50	1.676E+02	2.986E+03	-9.477E+02	1.508E-01	4.164E+01	-1.374E+00
56	1.981E+02	2.470E+03	-6.405E+02	1.546E-01	4.489E+01	-3.920E-01
62	2.286E+02	2.858E+03	-2.034E+02	1.631E-01	5.202E+01	-2.011E-01
68	2.591E+02	2.314E+03	1.230E+02	1.795E-01	6.053E+01	1.171E-01
74	2.621E+02	2.421E+03	1.208E+02	1.804E-01	6.152E+01	1.183E-01
80	2.957E+02	2.144E+03	1.062E+02	2.010E-01	6.801E+01	1.308E-01
86	3.048E+02	2.010E+03	1.108E+02	2.063E-01	6.902E+01	1.384E-01
92	3.170E+02	1.896E+03	5.338E+01	2.185E-01	7.028E+01	1.192E-01
98	3.200E+02	1.821E+03	8.834E+01	2.217E-01	6.977E+01	1.320E-01
104	3.505E+02	1.749E+03	4.178E+01	2.429E-01	6.541E+01	8.009E-02
110	3.810E+02	1.157E+03	1.361E+01	2.636E-01	5.725E+01	5.721E-02
116	4.115E+02	5.917E+02	8.366E+00	2.942E-01	4.857E+01	3.024E-02
122	4.145E+02	5.760E+02	6.514E+00	2.956E-01	4.782E+01	2.863E-02
128	4.359E+02	5.271E+02	8.322E+00	3.145E-01	4.136E+01	3.035E-02
134	4.420E+02	5.097E+02	5.580E+00	3.135E-01	4.042E+01	2.366E-02
140	4.679E+02	4.352E+02	1.892E+00	3.441E-01	3.323E+01	1.956E-02
146	4.755E+02	4.121E+02	1.701E+00	3.501E-01	3.053E+01	1.971E-02
152	5.029E+02	3.321E+02	5.525E-01	3.759E-01	2.610E+01	6.073E-03
158	5.182E+02	2.971E+02	1.387E-01	3.772E-01	2.448E+01	2.836E-03
164	5.243E+02	2.855E+02	7.384E-02	3.861E-01	2.368E+01	2.666E-03
170	5.334E+02	2.671E+02	3.807E-02	3.829E-01	2.242E+01	2.229E-03
176	5.486E+02	2.415E+02	6.971E-03	3.977E-01	2.000E+01	1.258E-03
182	5.791E+02	1.976E+02	5.500E-04	4.216E-01	1.710E+01	1.616E-04
188	6.096E+02	1.628E+02	4.180E-04	4.400E-01	1.483E+01	9.302E-05
194	6.187E+02	1.541E+02	3.888E-04	4.509E-01	1.424E+01	7.903E-05
200	6.401E+02	1.351E+02	3.665E-04	4.543E-01	1.302E+01	5.711E-05
206	6.858E+02	1.010E+02	-3.655E-04	4.910E-01	1.092E+01	2.653E-05
212	6.949E+02	9.576E+01	3.471E-04	5.019E-01	1.057E+01	2.382E-05
218	7.010E+02	9.373E+01	-2.505E-04	5.059E-01	1.031E+01	2.396E-05
224	7.163E+02	8.692E+01	3.387E-04	5.056E-01	9.776E+00	1.821E-05
230	7.315E+02	8.024E+01	-5.950E-04	5.262E-01	9.257E+00	1.716E-05
236	7.468E+02	7.408E+01	-2.163E-04	5.439E-01	8.774E+00	1.617E-05
242	7.544E+02	7.118E+01	-2.163E-04	5.424E-01	8.555E+00	1.653E-05
248	7.620E+02	6.841E+01	2.702E-04	5.429E-01	8.321E+00	1.345E-05
254	7.696E+02	6.592E+01	2.702E-04	5.439E-01	8.107E+00	1.233E-05
260	7.772E+02	6.357E+01	-1.374E-04	5.478E-01	7.909E+00	1.219E-05
266	7.925E+02	5.907E+01	-1.646E-04	5.642E-01	7.530E+00	1.012E-05
272	8.077E+02	5.475E+01	-2.198E-04	5.689E-01	7.170E+00	9.831E-06
278	8.321E+02	4.901E+01	-1.997E-04	5.953E-01	6.629E+00	1.065E-05
284	8.534E+02	4.463E+01	2.032E-04	6.051E-01	6.203E+00	6.895E-06
290	8.687E+02	4.177E+01	1.477E-04	6.099E-01	5.926E+00	6.880E-06
296	8.763E+02	4.040E+01	-1.507E-04	6.249E-01	5.790E+00	7.220E-06

Table A-8. PRISCILLA for ideal surface - station locations at height of 3 ft (0.9144 m) (concluded).

sta	xcord (m)	hdpp (kpa)	vdpp (kpa)	ppd (s)	dpih (kpa-s)	dpiv (kpa-s)
302	8.839E+02	3.918E+01	-2.186E-04	6.266E-01	5.665E+00	6.070E-06
308	8.915E+02	3.790E+01	-2.186E-04	6.310E-01	5.538E+00	5.735E-06
314	8.992E+02	3.676E+01	1.945E-04	6.296E-01	5.417E+00	6.712E-06
320	9.144E+02	3.452E+01	1.726E-04	6.450E-01	5.179E+00	5.032E-06
326	9.906E+02	2.574E+01	1.016E-04	6.825E-01	4.203E+00	3.342E-06
332	1.067E+03	1.967E+01	6.646E-05	7.197E-01	3.456E+00	2.351E-06
338	1.074E+03	1.918E+01	4.159E-05	7.329E-01	3.387E+00	1.907E-06
344	1.082E+03	1.871E+01	5.494E-05	7.377E-01	3.325E+00	1.677E-06
350	1.090E+03	1.825E+01	2.564E-05	7.374E-01	3.272E+00	1.968E-06
356	1.097E+03	1.780E+01	2.539E-05	7.455E-01	3.211E+00	2.272E-06
362	1.105E+03	1.737E+01	1.718E-05	7.426E-01	3.154E+00	2.103E-06
368	1.113E+03	1.697E+01	-1.879E-05	7.417E-01	3.098E+00	1.269E-06
374	1.120E+03	1.656E+01	-4.096E-05	7.558E-01	3.044E+00	1.482E-06
380	1.128E+03	1.616E+01	2.568E-05	7.577E-01	2.992E+00	1.433E-06
386	1.158E+03	1.469E+01	-2.394E-05	7.707E-01	2.787E+00	1.230E-06
392	1.189E+03	1.342E+01	7.504E-06	7.824E-01	2.603E+00	8.753E-07
398	1.198E+03	1.307E+01	1.192E-05	7.856E-01	2.553E+00	9.170E-07
404	1.219E+03	1.229E+01	8.479E-06	7.981E-01	2.433E+00	8.825E-07
410	1.234E+03	1.178E+01	-5.753E-06	8.005E-01	2.359E+00	6.936E-07
416	1.250E+03	1.127E+01	-1.347E-05	8.070E-01	2.283E+00	8.554E-07
422	1.265E+03	1.067E+01	1.406E-04	8.132E-01	2.210E+00	6.117E-07
428	1.273E+03	1.065E+01	2.023E-05	8.151E-01	2.179E+00	6.802E-07
434	1.280E+03	1.040E+01	8.854E-06	8.218E-01	2.144E+00	6.288E-07
440	1.288E+03	1.015E+01	-3.731E-04	8.251E-01	2.113E+00	6.290E-07
446	1.295E+03	1.002E+01	-1.462E-05	8.255E-01	2.080E+00	5.870E-07
452	1.311E+03	9.602E+00	-8.750E-06	8.376E-01	2.020E+00	5.395E-07
458	1.341E+03	8.813E+00	3.253E-05	8.477E-01	1.899E+00	6.195E-07
464	1.372E+03	8.158E+00	6.776E-06	8.552E-01	1.789E+00	4.974E-07
470	1.402E+03	7.609E+00	-4.798E-05	8.711E-01	1.692E+00	4.180E-07
476	1.454E+03	6.693E+00	3.645E-06	8.857E-01	1.539E+00	3.437E-07
482	1.494E+03	6.095E+00	4.072E-06	9.021E-01	1.432E+00	3.231E-07
488	1.524E+03	6.046E+00	-3.747E-04	9.106E-01	1.362E+00	-5.496E-07
494	1.554E+03	5.287E+00	2.262E-06	9.224E-01	1.289E+00	2.534E-07
500	1.585E+03	4.962E+00	3.033E-06	9.294E-01	1.224E+00	2.655E-07
506	1.600E+03	4.791E+00	5.842E-04	9.369E-01	1.196E+00	9.582E-07
512	1.615E+03	4.656E+00	3.498E-06	9.398E-01	1.168E+00	2.768E-07
518	1.622E+03	4.602E+00	1.473E-06	9.415E-01	1.155E+00	2.202E-07
524	1.631E+03	4.500E+00	-2.324E-05	9.446E-01	1.141E+00	3.740E-07
530	1.646E+03	4.372E+00	1.737E-06	9.476E-01	1.109E+00	2.072E-07
536	1.676E+03	4.117E+00	1.653E-06	9.575E-01	1.061E+00	2.038E-07
542	1.707E+03	3.875E+00	1.580E-06	8.781E-01	1.004E+00	2.002E-07
548	1.737E+03	3.651E+00	2.213E-06	7.994E-01	9.505E-01	1.914E-07
554	1.829E+03	3.069E+00	-3.787E-05	5.628E-01	7.730E-01	2.582E-07
560	1.865E+03	2.880E+00	5.198E-04	4.672E-01	6.829E-01	1.880E-06

Table A-9. PRISCILLA for ideal surface - station locations at height of 10 ft (3.048 m).

sta	xcord (m)	at (s)	fop (kpa)	opmax (kpa)	opi (kpa-s)
4	0.000E+00	6.454E-02	1.757E+03	7.163E+03	1.051E+02
10	1.524E+01	6.491E-02	1.732E+03	7.158E+03	1.048E+02
16	3.048E+01	6.619E-02	1.667E+03	6.968E+03	1.034E+02
22	4.572E+01	6.817E-02	1.605E+03	6.359E+03	1.016E+02
28	6.096E+01	7.104E-02	1.522E+03	5.720E+03	9.963E+01
34	7.620E+01	7.476E-02	1.463E+03	5.247E+03	9.720E+01
40	1.067E+02	8.450E-02	1.411E+03	4.946E+03	8.488E+01
46	1.372E+02	9.785E-02	1.097E+03	4.710E+03	8.964E+01
52	1.676E+02	1.147E-01	8.681E+02	3.583E+03	8.235E+01
58	1.981E+02	1.350E-01	7.266E+02	2.661E+03	7.524E+01
64	2.286E+02	1.591E-01	1.570E+03	1.626E+03	6.949E+01
70	2.591E+02	1.838E-01	1.184E+03	1.184E+03	6.132E+01
76	2.621E+02	1.864E-01	1.169E+03	1.169E+03	6.069E+01
82	2.957E+02	2.171E-01	9.305E+02	9.305E+02	5.346E+01
88	3.048E+02	2.260E-01	8.782E+02	8.782E+02	5.178E+01
94	3.170E+02	2.380E-01	8.135E+02	8.135E+02	5.004E+01
100	3.200E+02	2.413E-01	7.965E+02	7.965E+02	4.954E+01
106	3.505E+02	2.737E-01	6.767E+02	6.767E+02	4.621E+01
112	3.810E+02	3.086E-01	5.853E+02	5.853E+02	4.302E+01
118	4.115E+02	3.454E-01	5.072E+02	5.072E+02	4.071E+01
124	4.145E+02	3.491E-01	5.016E+02	5.016E+02	4.055E+01
130	4.359E+02	3.763E-01	4.752E+02	4.752E+02	3.879E+01
136	4.420E+02	3.840E-01	4.687E+02	4.687E+02	3.825E+01
142	4.679E+02	4.180E-01	4.234E+02	4.234E+02	3.633E+01
148	4.755E+02	4.283E-01	4.106E+02	4.106E+02	3.588E+01
154	5.029E+02	4.664E-01	3.600E+02	3.600E+02	3.413E+01
160	5.182E+02	4.884E-01	3.367E+02	3.367E+02	3.315E+01
166	5.243E+02	4.975E-01	3.286E+02	3.286E+02	3.279E+01
172	5.334E+02	5.112E-01	3.156E+02	3.156E+02	3.232E+01
178	5.486E+02	5.342E-01	2.973E+02	2.973E+02	3.164E+01
184	5.791E+02	5.818E-01	2.646E+02	2.646E+02	3.038E+01
190	6.096E+02	6.318E-01	2.368E+02	2.368E+02	2.917E+01
196	6.187E+02	6.469E-01	2.291E+02	2.291E+02	2.888E+01
202	6.401E+02	6.834E-01	2.128E+02	2.128E+02	2.810E+01
208	6.858E+02	7.643E-01	1.805E+02	1.805E+02	2.667E+01
214	6.949E+02	7.807E-01	1.753E+02	1.753E+02	2.645E+01
220	7.010E+02	7.921E-01	1.731E+02	1.731E+02	2.620E+01
226	7.163E+02	8.202E-01	1.661E+02	1.661E+02	2.582E+01
232	7.315E+02	8.487E-01	1.591E+02	1.591E+02	2.539E+01
238	7.468E+02	8.776E-01	1.520E+02	1.520E+02	2.496E+01
244	7.544E+02	8.921E-01	1.487E+02	1.487E+02	2.481E+01
250	7.620E+02	9.072E-01	1.455E+02	1.455E+02	2.457E+01
256	7.696E+02	9.219E-01	1.426E+02	1.426E+02	2.436E+01
262	7.772E+02	9.367E-01	1.397E+02	1.397E+02	2.421E+01
268	7.925E+02	9.666E-01	1.342E+02	1.342E+02	2.388E+01
274	8.077E+02	9.969E-01	1.288E+02	1.288E+02	2.354E+01
280	8.321E+02	1.046E+00	1.212E+02	1.212E+02	2.296E+01
286	8.534E+02	1.090E+00	1.153E+02	1.153E+02	2.246E+01
292	8.687E+02	1.121E+00	1.112E+02	1.112E+02	2.217E+01
298	8.763E+02	1.137E+00	1.093E+02	1.093E+02	2.201E+01

Table A-9. PRISCILLA for ideal surface - station locations at height of 10 ft (3.048 m) (continued).

sta	xcord (m)	at (s)	fop (kpa)	opmax (kpa)	opi (kpa·s)
304	8.839E+02	1.153E+00	1.074E+02	1.074E+02	2.189E+01
310	8.915E+02	1.169E+00	1.056E+02	1.056E+02	2.170E+01
316	8.992E+02	1.185E+00	1.039E+02	1.039E+02	2.156E+01
322	9.144E+02	1.218E+00	1.004E+02	1.004E+02	2.127E+01
328	9.906E+02	1.383E+00	8.590E+01	8.590E+01	1.988E+01
334	1.067E+03	1.553E+00	7.451E+01	7.451E+01	1.864E+01
340	1.074E+03	1.571E+00	7.351E+01	7.351E+01	1.853E+01
346	1.082E+03	1.588E+00	7.256E+01	7.256E+01	1.840E+01
352	1.090E+03	1.605E+00	7.162E+01	7.162E+01	1.834E+01
358	1.097E+03	1.623E+00	7.068E+01	7.068E+01	1.819E+01
364	1.105E+03	1.640E+00	6.979E+01	6.979E+01	1.810E+01
370	1.113E+03	1.658E+00	6.893E+01	6.893E+01	1.799E+01
376	1.120E+03	1.675E+00	6.805E+01	6.805E+01	1.788E+01
382	1.128E+03	1.693E+00	6.720E+01	6.720E+01	1.780E+01
388	1.158E+03	1.764E+00	6.392E+01	6.392E+01	1.736E+01
394	1.189E+03	1.836E+00	6.097E+01	6.097E+01	1.695E+01
400	1.198E+03	1.857E+00	6.014E+01	6.014E+01	1.685E+01
406	1.219E+03	1.908E+00	5.824E+01	5.824E+01	1.656E+01
412	1.234E+03	1.944E+00	5.696E+01	5.696E+01	1.640E+01
418	1.250E+03	1.980E+00	5.567E+01	5.567E+01	1.620E+01
424	1.265E+03	2.017E+00	5.402E+01	5.402E+01	1.600E+01
430	1.273E+03	2.035E+00	5.405E+01	5.405E+01	1.595E+01
436	1.280E+03	2.053E+00	5.338E+01	5.338E+01	1.585E+01
442	1.288E+03	2.072E+00	5.246E+01	5.246E+01	1.578E+01
448	1.295E+03	2.090E+00	5.235E+01	5.235E+01	1.569E+01
454	1.311E+03	2.127E+00	5.118E+01	5.118E+01	1.553E+01
460	1.341E+03	2.201E+00	4.890E+01	4.890E+01	1.520E+01
466	1.372E+03	2.276E+00	4.697E+01	4.697E+01	1.486E+01
472	1.402E+03	2.351E+00	4.527E+01	4.527E+01	1.459E+01
478	1.454E+03	2.479E+00	4.247E+01	4.247E+01	1.410E+01
484	1.494E+03	2.578E+00	4.047E+01	4.047E+01	1.373E+01
490	1.524E+03	2.654E+00	3.875E+01	3.875E+01	1.348E+01
496	1.554E+03	2.732E+00	3.760E+01	3.760E+01	1.320E+01
502	1.585E+03	2.809E+00	3.639E+01	3.639E+01	1.295E+01
508	1.600E+03	2.848E+00	3.560E+01	3.562E+01	1.285E+01
514	1.615E+03	2.886E+00	3.522E+01	3.522E+01	1.274E+01
520	1.622E+03	2.902E+00	3.501E+01	3.501E+01	1.268E+01
526	1.631E+03	2.925E+00	3.453E+01	3.453E+01	1.264E+01
532	1.646E+03	2.964E+00	3.409E+01	3.409E+01	1.249E+01
538	1.676E+03	3.041E+00	3.305E+01	3.305E+01	1.231E+01
544	1.707E+03	3.121E+00	3.204E+01	3.204E+01	1.199E+01
550	1.737E+03	3.200E+00	3.111E+01	3.111E+01	1.158E+01
556	1.829E+03	3.436E+00	2.845E+01	2.845E+01	9.594E+00
562	1.865E+03	3.532E+00	2.751E+01	2.751E+01	8.433E+00

Table A-9. PRISCILLA for ideal surface - station locations at height of 10 ft (3.048 m) (continued).

sta	xcord (m)	hdpp (kpa)	vdpp (kpa)	ppd (s)	dpih (kpa-s)	dpiv (kpa-s)
4	0.000E+00	2.483E-01	-3.940E+03	1.372E-01	1.766E-01	-1.747E+01
10	1.524E+01	6.014E+01	-3.852E+03	1.388E-01	7.531E-01	-1.736E+01
16	3.048E+01	2.512E+02	-3.623E+03	1.371E-01	2.687E+00	-1.698E+01
22	4.572E+01	4.944E+02	-3.365E+03	1.412E-01	6.252E+00	-1.626E+01
28	6.096E+01	7.337E+02	-3.071E+03	1.442E-01	9.857E+00	-1.514E+01
34	7.620E+01	9.546E+02	-2.872E+03	1.456E-01	1.439E+01	-1.369E+01
40	1.067E+02	1.703E+03	-2.236E+03	6.074E-02	2.365E+01	-9.253E+00
46	1.372E+02	2.186E+03	-1.669E+03	1.531E-01	3.264E+01	-6.217E+00
52	1.676E+02	2.425E+03	-9.103E+02	1.516E-01	3.865E+01	-3.982E+00
58	1.981E+02	2.584E+03	-6.279E+02	1.562E-01	4.258E+01	-2.353E+00
64	2.286E+02	1.620E+03	-5.656E+01	1.629E-01	4.221E+01	-3.771E-01
70	2.591E+02	2.072E+03	-1.191E+02	1.800E-01	4.799E+01	-4.156E-01
76	2.621E+02	2.030E+03	-1.096E+02	1.804E-01	4.820E+01	-4.036E-01
82	2.957E+02	1.461E+03	1.471E+02	2.020E-01	5.122E+01	3.064E-01
88	3.048E+02	1.343E+03	1.520E+02	2.064E-01	5.170E+01	3.357E-01
94	3.170E+02	1.200E+03	1.694E+02	2.178E-01	5.332E+01	4.007E-01
100	3.200E+02	1.163E+03	1.425E+02	2.217E-01	5.324E+01	3.702E-01
106	3.505E+02	1.257E+03	1.184E+02	2.422E-01	5.462E+01	3.278E-01
112	3.810E+02	9.139E+02	9.374E+01	2.646E-01	5.044E+01	3.362E-01
118	4.115E+02	5.800E+02	4.305E+01	2.946E-01	4.422E+01	2.003E-01
124	4.145E+02	5.705E+02	3.311E+01	2.956E-01	4.404E+01	1.887E-01
130	4.359E+02	5.233E+02	1.600E+01	3.145E-01	3.869E+01	1.162E-01
136	4.420E+02	5.126E+02	1.537E+01	3.138E-01	3.839E+01	1.031E-01
142	4.679E+02	4.351E+02	6.310E+00	3.441E-01	3.375E+01	1.117E-01
148	4.755E+02	4.128E+02	5.249E+00	3.508E-01	3.240E+01	1.173E-01
154	5.029E+02	3.321E+02	3.184E+00	3.743E-01	2.632E+01	7.131E-02
160	5.182E+02	2.975E+02	9.054E-01	3.769E-01	2.495E+01	2.794E-02
166	5.243E+02	2.857E+02	5.645E-01	3.827E-01	2.430E+01	2.555E-02
172	5.334E+02	2.667E+02	2.501E-01	3.825E-01	2.319E+01	1.840E-02
178	5.486E+02	2.411E+02	5.418E-02	3.977E-01	2.069E+01	1.199E-02
184	5.791E+02	1.976E+02	1.048E-02	4.227E-01	1.763E+01	1.488E-03
190	6.096E+02	1.627E+02	6.745E-03	4.390E-01	1.529E+01	9.316E-04
196	6.187E+02	1.541E+02	6.885E-03	4.520E-01	1.467E+01	8.000E-04
202	6.401E+02	1.352E+02	4.709E-03	4.555E-01	1.331E+01	5.737E-04
208	6.858E+02	1.010E+02	2.667E-03	4.907E-01	1.104E+01	2.871E-04
214	6.949E+02	9.584E+01	2.415E-03	5.029E-01	1.068E+01	2.670E-04
220	7.010E+02	9.364E+01	2.418E-03	5.047E-01	1.041E+01	2.522E-04
226	7.163E+02	8.686E+01	2.028E-03	5.058E-01	9.856E+00	2.102E-04
232	7.315E+02	8.023E+01	1.925E-03	5.273E-01	9.324E+00	1.837E-04
238	7.468E+02	7.405E+01	1.552E-03	5.431E-01	8.829E+00	1.605E-04
244	7.544E+02	7.115E+01	1.380E-03	5.424E-01	8.610E+00	1.542E-04
250	7.620E+02	6.843E+01	1.170E-03	5.441E-01	8.369E+00	1.452E-04
256	7.696E+02	6.591E+01	1.115E-03	5.428E-01	8.155E+00	1.397E-04
262	7.772E+02	6.355E+01	1.003E-03	5.495E-01	7.950E+00	1.331E-04
268	7.925E+02	5.907E+01	1.020E-03	5.646E-01	7.563E+00	1.250E-04
274	8.077E+02	5.473E+01	9.796E-04	5.694E-01	7.199E+00	1.096E-04
280	8.321E+02	4.900E+01	5.392E-04	5.954E-01	6.659E+00	9.364E-05
286	8.534E+02	4.468E+01	5.816E-04	6.045E-01	6.216E+00	8.548E-05
292	8.687E+02	4.176E+01	5.598E-04	6.119E-01	5.941E+00	7.024E-05
298	8.763E+02	4.041E+01	5.598E-04	6.249E-01	5.802E+00	7.396E-05

Table A-9. PRISCILLA for ideal surface - station locations at height of 10 ft (3.048 m) (concluded).

sta	xcord (m)	hdpp (kpa)	vdpp (kpa)	ppd (s)	dpih (kpa-s)	dpiv (kpa-s)
304	8.839E+02	3.919E+01	4.372E-04	6.284E-01	5.679E+00	6.945E-05
310	8.915E+02	3.790E+01	5.311E-04	6.318E-01	5.551E+00	6.587E-05
316	8.992E+02	3.676E+01	4.601E-04	6.306E-01	5.430E+00	6.278E-05
322	9.144E+02	3.452E+01	3.770E-04	6.476E-01	5.189E+00	5.563E-05
328	9.906E+02	2.574E+01	2.387E-04	6.828E-01	4.206E+00	3.710E-05
334	1.067E+03	1.967E+01	1.568E-04	7.188E-01	3.457E+00	2.694E-05
340	1.074E+03	1.918E+01	1.502E-04	7.329E-01	3.394E+00	2.562E-05
346	1.082E+03	1.870E+01	1.440E-04	7.385E-01	3.327E+00	2.312E-05
352	1.090E+03	1.826E+01	1.388E-04	7.385E-01	3.273E+00	2.226E-05
358	1.097E+03	1.780E+01	1.330E-04	7.439E-01	3.213E+00	2.399E-05
364	1.105E+03	1.738E+01	1.302E-04	7.425E-01	3.157E+00	2.748E-05
370	1.113E+03	1.697E+01	1.235E-04	7.441E-01	3.099E+00	2.092E-05
376	1.120E+03	1.656E+01	1.201E-04	7.543E-01	3.046E+00	1.971E-05
382	1.128E+03	1.616E+01	1.159E-04	7.523E-01	2.994E+00	1.970E-05
388	1.158E+03	1.468E+01	1.000E-04	7.706E-01	2.789E+00	1.715E-05
394	1.189E+03	1.343E+01	8.644E-05	7.822E-01	2.604E+00	1.508E-05
400	1.198E+03	1.307E+01	8.443E-05	7.856E-01	2.554E+00	1.406E-05
406	1.219E+03	1.228E+01	7.779E-05	7.960E-01	2.434E+00	1.309E-05
412	1.234E+03	1.177E+01	7.258E-05	8.013E-01	2.360E+00	1.224E-05
418	1.250E+03	1.127E+01	6.767E-05	8.050E-01	2.284E+00	1.170E-05
424	1.265E+03	1.066E+01	6.171E-05	8.132E-01	2.211E+00	1.067E-05
430	1.273E+03	1.065E+01	6.194E-05	8.150E-01	2.180E+00	1.066E-05
436	1.280E+03	1.040E+01	4.786E-05	8.233E-01	2.145E+00	1.037E-05
442	1.288E+03	1.006E+01	6.044E-05	8.251E-01	2.114E+00	9.902E-06
448	1.295E+03	1.002E+01	5.429E-05	8.240E-01	2.080E+00	9.682E-06
454	1.311E+03	9.601E+00	5.695E-05	8.385E-01	2.020E+00	9.125E-06
460	1.341E+03	8.784E+00	4.663E-05	8.467E-01	1.900E+00	8.442E-06
466	1.372E+03	8.134E+00	3.783E-05	8.552E-01	1.789E+00	7.310E-06
472	1.402E+03	7.571E+00	3.703E-05	8.711E-01	1.692E+00	6.973E-06
478	1.454E+03	6.695E+00	3.453E-05	8.874E-01	1.540E+00	5.782E-06
484	1.494E+03	6.097E+00	2.951E-05	9.021E-01	1.433E+00	5.078E-06
490	1.524E+03	5.918E+00	3.705E-05	9.104E-01	1.362E+00	4.743E-06
496	1.554E+03	5.289E+00	2.535E-05	9.210E-01	1.290E+00	4.309E-06
502	1.585E+03	4.963E+00	2.705E-05	9.285E-01	1.225E+00	3.948E-06
508	1.600E+03	4.784E+00	3.205E-05	9.369E-01	1.197E+00	3.825E-06
514	1.615E+03	4.658E+00	2.215E-05	9.383E-01	1.169E+00	3.587E-06
520	1.622E+03	4.603E+00	1.913E-05	9.420E-01	1.156E+00	3.457E-06
526	1.631E+03	4.483E+00	3.832E-05	9.447E-01	1.142E+00	3.527E-06
532	1.646E+03	4.373E+00	1.728E-05	9.475E-01	1.110E+00	3.247E-06
538	1.676E+03	4.118E+00	1.754E-05	9.575E-01	1.062E+00	3.082E-06
544	1.707E+03	3.876E+00	1.434E-05	8.780E-01	1.005E+00	2.892E-06
550	1.737E+03	3.653E+00	1.494E-05	7.994E-01	9.512E-01	2.635E-06
556	1.829E+03	3.078E+00	2.829E-05	5.628E-01	7.731E-01	2.015E-06
562	1.865E+03	2.885E+00	5.061E-05	4.672E-01	6.829E-01	1.730E-06

INTENTIONALLY LEFT BLANK.

APPENDIX B

SUGGESTED PROGRAM FOR IMPROVEMENT OF THERMAL LAYER PREDICTIVE CAPABILITY

SSS-DTW-93-14208

A white paper prepared by

J. R. Barthel

25 August 1993 - Updated 20 April 1995

S-Cubed, a Division of Maxwell Laboratories
P. O. Box 1620, La Jolla, CA 92038-1620
3398 Carmel Mountain Road, San Diego, CA 92121-1095

SUGGESTED PROGRAM FOR IMPROVEMENT OF THERMAL LAYER PREDICTIVE CAPABILITY

J. R. Barthel

8/25/93 Updated 4/20/95 SSS-DTW-93-14208

OBJECTIVE

The objective of the suggested program is to achieve the capability in the S-Cubed THRML code to predict thermal layer evolution to an acceptable level of accuracy, given the following:

-- the burst scenario, in particular, the incident, specularly-resolved thermal flus as a function of ground range, wavelength, and time;

-- the relevant material properties:
- composition of soil and vegetation;
- equation of state (EOS) for each component, or composite;
- opacity as a function of temperature, wavelength, (and possibly pressure to a limited extent) for each component or composite.

PRESENT STATUS

The THRML code is highly developed and has many state-of-the-art features, as described below. The modeling of the response of vegetation has achieved a satisfactory degree of validation (references B-1 and B-2). However, modeling of the response of a bare soil surface has remained problematic. The basic symptom of the problem is the tendency to produce blowoff layer temperature profiles that are too strongly inverted (T increasing with height) along with a tendency toward too-high temperatures.

Capabilities of the THRML Code

The THRML code, after many years of evolution, is robust, relatively easy to operate, and has satisfactory models of a number of complex physical processes. For example, it includes:

-- multiple particle size groups, the number limited only by the capacity of the computer;
-- radiation transport including multiple frequency groups and multiple angular groups;
-- multi-phase motion allowing separate, interactive motion of air, steam, and particulates;
-- turbulent diffusion of species, particle size groups, and internal energy.

Needed Improvements in THRML

Despite these well-developed features, THRML's characterization of thermal layers over bare soil has exhibited certain shortcomings. Our careful assessment of the situation leads us to the conclusion that satisfactory thermal layer predictions are likely only after some or all of the following improvements have been implemented:

-- improved turbulent diffusion model, specifically, extending the diffusion into the region of stable stratification as a result of finite eddy size in the large-amplitude regime of Rayleigh-Taylor instability;

-- accounting for the volume of vaporized particulate material (this was not a problem in the low overpressure regime where the particulates did not vaporize; the particulate vapor enthalpy, but not volume, is now properly accounted for);

-- Improved representation of particle lofting, including (1) improved modeling of the drag on particles resulting from motion relative to the vapor, in particular, accounting for the effects of close spacing of particles, and (2) "popcorning"---the impulsive injection of fragments upward from the surface;

-- generalization to arbitrary pressures and explicit use of the momentum equation rather than the present isobaric approximation which currently limits THRML to the low-to-intermediate overpressure regime. (The S-Cubed PPML surface response code, used at high overpressure, is fully hydrodynamic but does not currently account for relative motion between the gas and particles.)

The first three of the above are considered the most likely to improve the results. In fact, the isobaric assumption may not become a significant limitation unless ranges where airblast overpressures reach the order of 1 kpsi or more are considered.

Material Properties

The opacity of a material determines how rapidly it is heated by thermal radiation, and its equation of state (EOS) describes its response to that heating. It is necessary to determine the opacity and EOS to reasonable accuracy for any material considered. The currently available store of information on the spectral opacity and EOS of materials of interest is generally quite inadequate. In particular, opacity and EOS tables exist for only a few surface materials such as MJ2 ground and Frenchman's Flat soil. Unfortunately, the soils, vegetation types (if any), and vegetation coverage in various above-ground nuclear events have varied widely, and the compilation of the properties for all the materials that will eventually be of interest is expected to be a very significant fraction of the effort needed to produce satisfactory predictions.

SUGGESTED APPROACH

The following suggested efforts include both the modeling and computational realms, as well as supporting experiments that may be required to provide data for validation calculations and/or to determine material properties that cannot be determined within reasonable accuracy by theoretical computations. This white paper deals primarily with an analytical/computational program that S-Cubed is prepared to carry forward, but it is important to recognize the need for related experimental work.

The experimental component could be supported through either separate procurements or subcontracts from S-Cubed. The program outlined below is an effort totaling an estimated 1.7 man years (MY) of which 0.2 MY is for opacity measurements.

Code improvements

The turbulent diffusion model should be upgraded by including the effect of larger "eddies", of sizes up to the order of gtt/2 that are attainable but not adequately represented in the present formulation in which the influence of the turbulence is strictly limited to the region of unstable density gradient (references B-3, B-4). This improvement would be largely hueristic, but would be amenable to further calibration and refinement on the basis of comparisons of calculations with data (see below). Any improvements must not degrade the level of agreement with DTI helium data as presented in reference B-4.

The kinematic equations should be extended to include the volume occupied by the vaporized soil components (in addition to water). This is expected to be straightforward, at least in principle.

The particle drag model is currently based on expressions that apply to isolated spherical particles. Close-spacing effects can be represented by applying a well-known result on pressure losses in beds of porous solids (reference B-5). We have developed the concept; the application should be a straightforward extension of the existing coding. At this point, we are uncertain whether this will even be needed, but will reserve judgement until we learn the effects of the above improvements on predictions.

Generalization of the code to allow significant deviation from ambient pressure would also be straightforward, though tedious; this would probably be worth undertaking only if there is interest in extending the code well into the high overpressure regime (order of 1 kbar and up). If needed, it would probably require an increase in the above estimated level of effort.

Material Properties

The EOS for a material of given chemical constituents can generally be characterized to an acceptable accuracy by chemical equilibrium thermodynamic calculations. Powerful tools for calculating atomic, molecular, and ionic opacity contributions of materials in the vapor phase are available (see below); however, theoretical calculations of spectral opacity are very difficult for condensed materials. The regime of cold, condensed states typical of ambient surface material is fortunately also the regime where opacity measurmenets are the most economical. Therefore, a combined calculational/experimental approach should be the most cost-effective way to characterize the spectral opacity over the range of states of interest.

Theoretical

Several surface materials of interest to validation calculations should be

selected. Their EOS's should be determined using our robust chemical equilibrium thermodynamic code, ORAKL, a descendant of the LLNL TIGER code. The temperatures of interest range to 3000 degrees K or more. The opacities in largely-vaporized states should be determined using an available atomic and molecular opacity code; for this we recommend the unique computational codes of Dr. Christopher Sharp (reference B-6), who is renowned for this capability within the astrophysical and nuclear effects communities. He has performed similar work as a consultant to S-Cubed in the past, and we suggest that such an arrangement be used here. We have found this approach to be very cost-effective.

Experimental

The opacities of the materials selected above should be measured in the cool, condensed regime using economical approaches, e. g., laser beam attenuation. This could be a separate procurement, but is probably more conveniently handled as a subcontract.

Validation Calculations

Comparison with Direct Thermal Layer Measurements

These comparisons are the most direct and therefore most meaningful measure of the validity of THRML's predictions. The most useful data would be temperature histories and flux histories at various heights above the surface. However, the available data are sparse. Candidates for this exercise include Flashlamp Thermal Simulator (FTS) data, Thermal Radiation Chamber (TRC) data, and solar furnace data. Each has certain limitations in terms of 3-D geometry, finite height, wall effects, available flux or fluence, etc. Any new simulation work carried out in parallel with this program will also be considered. There are also useful nuclear above-ground test data, although no nuclear event was as well-diagnosed as the simulations cited above. Emphasis should be given to those few nuclear events, such as the TUMBLER series, that produced temperature and sound speed history measurements at various heights. Nuclear events that were only slightly precursed should not be ignored because it is important to be able to represent the threshold of thermal precursing with sufficient confidence.

Comparison with Precursed Airblast Data

These comparisons would involve airblast environment calculations for nuclear events which indicated significant precursing. The calculations would be initialized with THRML's prediction of the thermal layer as a function of range and height at local time-of- arrival. The objective would be comparison of the calculated and measured pressure histories as well as any other available measurements. Events that should be considered include PRISCILLA, HOOD, MET, GRABLE, and TUMBLER 1,2,3,4. The most valuable events would be those that include temperature and thermal flux measurements in addition to pressure measurements. These events should receive priority consideration.

REFERENCES

B-1. Rogers, S. H., "Stressing Thermal Layer Sensitivity to Parameters in the THRML Code", DNA-TR-90-10, June 1990.

B-2. Patnaik, P. C., "TRC Modeling Calculations", presentation at Rail Garrison Review, S-Cubed document SSS-DVR-90-11390, March 7, 1990.

B-3. Freeman, B. E., "A Turbulence Model Incorporating Transients for Thermal Layer Application", DNA-TR-88-273, October 1988.

B-4. Rogers, S. H., "Verification of the New Turbulence Model Used in the THRML Code", DNA-TR-89-110, May 1990.

B-5. Ergun, S., "Fluid Flow Through Packed Columns", Chem. E. Progress, Volume 48, pp.89-94, 1952.

B-6. Sharp, C. M., "Molecular Opacities for Solar and Enhanced CNO Abundances: Relevance for Accretion Disks", Astron. Astroph. Suppl. Ser. 94, 1, 1992. (plus more than 30 other papers, LANL reports, and invited presentations).

APPENDIX C

PRISCILLA BLAST DATA

The air blast records presented in this appendix were taken from the weapons tests reports that were published following the PRISCILLA event in 1957. The report numbers are listed in the tabulations of data. A number of corrections were made.

The primary data presented were from gages on or within 200 feet of the main blast line. Precursor conditions vary along an arc and can differ significantly over such a width. In other areas many of the gages were affected by reflections from above-ground structures or, in the project 6.1 area, by exploding army mines.

These records increase in quality at the lower pressure levels. Exceptions to this are dynamic pressure waveforms derived from total head (stagnation) and overpressure records obtained below 10 psi overpressure.

In close, the total head pressure gages were bombarded with melted sand caused by the high thermal flux. The front of the gages and gage mounts were coated with green glass. In many cases this sealed or partially closed the total head pressure input port and caused the total head sensor to no longer record the total head pressure accurately. On some flat surfaces like cable anchors this green glass, known as trinitite, coated the surfaces with layers 1/4 centimeter to 1/2 centimeter in thickness.

Another observation was that in most cases the record baseline shifted gradually in the negative direction before the arrival of the shock wave. This shift between the time of detonation and the arrival of the shock wave at the gage stations varied with distance of the gage from ground zero. This shift was just a few kPa and was most apparent on the low pressure records. This shift was taken into account when the records were read.

The total head and dynamic pressure gages used on the PRISCILLA event are shown in Figure C-1.

Table C-1. Symbols for subsonic and supersonic flows in clean and dirty blast waves.

q = dynamic air pressure = $\frac{1}{2} \rho u^2$

q_c = $(P_p - P_s)$

M = u/c = local free-stream Mach number of flow behind blast front - $\frac{\text{particle velocity}}{\text{sound velocity}}$

P_t = free stream total pressure (absolute)

P_p = total head pitot pressure (absolute) $M < 1$ $P_p = P_t$; $M > 1$ $P_p \neq P_t$

P_s = free stream static pressure (absolute)

P_o = ambient preshock static pressure (absolute)

ΔP = free stream static overpressure = $P_s - P_o$

ΔP_p = total head overpressure = $P_p - P_o$

ρ = air density (local)

u = particle speed of air (local)

c = speed of sound in air (local)

t = ratio of specific heats

Primes are used to denote uncorrected, "as read" gage values, thus

$q_c' = (P_p - P_s)'$

Additional Symbols in Dirty Airblast Flows (*)

q^* = dynamic air-plus-dust pressure in free stream = $q + \phi_d$

$q_c^* = q_c + \phi_d$

$q_c^{*\prime} = (q_c + n\phi_d)'$

ϕ_d = momentum flux of dust = $\rho_d u_d^2$

n = dust registry coefficient of gage, $o \leq n \leq 1$

ρ_d = mass of suspended dust per unit volume of mixture (local)

u_d = particle speed of dust (local)

δ = specific gravity of dust particles = 2.5

SANDIA PITOT-STATIC DIFFERENTIAL GAGE

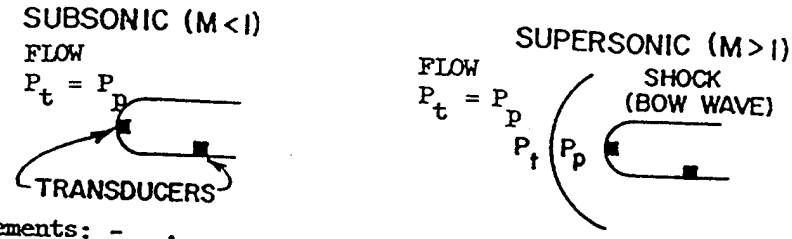

Direct Measurements: -

Clean Blast: $(\Delta p_p - \Delta p)'$ and $\Delta p'$. First Term = q_c'.

Dusty Blast: $(q_c + n\phi_d)'$ and $\Delta p'$. n and ϕ_d unknown.

SANDIA SNOB GAGE

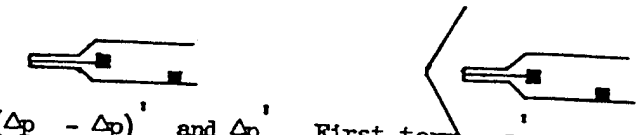

Clean Blast: $(\Delta p_p - \Delta p)'$ and $\Delta p'$. First term = q_c'.

Dusty Blast: $(q_c + n\phi_d)'$ and $\Delta p'$. n = 0.15, ϕ_d unknown.

SANDIA GREG GAGE

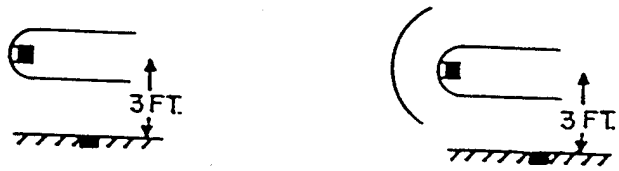

Clean Blast: $\Delta p_p'$ and $\Delta p'$. Difference = q_c'.

Dusty Blast: $\Delta p_p^{*\prime}$ and $\Delta p'$. Difference = $q_c^{*\prime} = (q_c + n\phi_d)'$.

n = 0.9, ϕ_d unknown.

BRL "q" GAGE

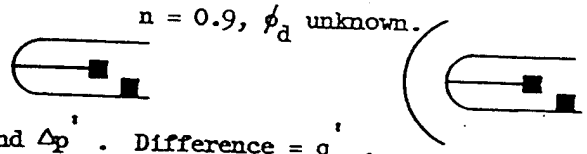

Clean Blast: $\Delta p_p'$ and $\Delta p'$. Difference = q_c'.

Dusty Blast: $\Delta p_p^{*\prime}$ and $\Delta p'$. Difference = $q_c^{*\prime} = (q_c + n\phi_d)'$.

n, ϕ_d unknown.

SRI TOTAL HEAD GAGE

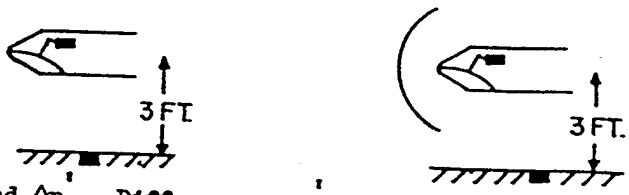

Clean Blast: $\Delta p_p'$ and $\Delta p'$. Difference = q_c'.

Dusty Blast: $\Delta p_p^{*\prime}$ and $\Delta p'$. Difference = $q_c^{*\prime} = (q_c + n\phi_d)'$.

n, ϕ_d unknown.

Figure C-1 Gages used on the PRISCILLA Event.

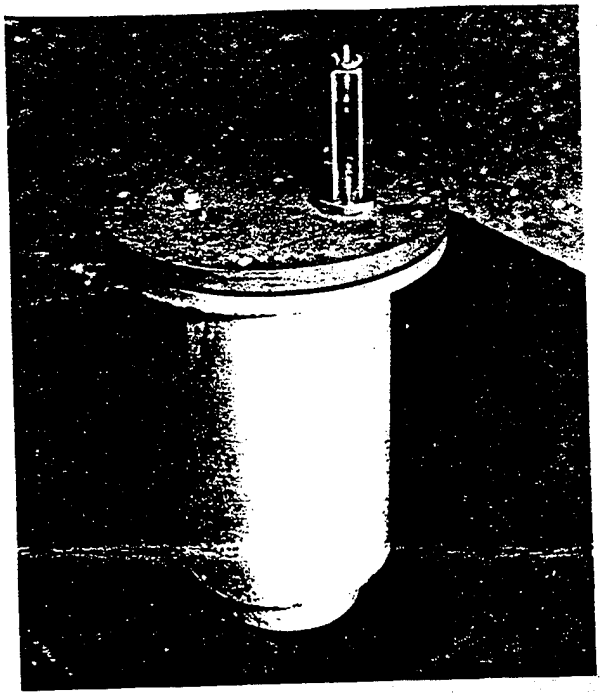

Figure C-2. BRL standard self-recording Pt-gage.

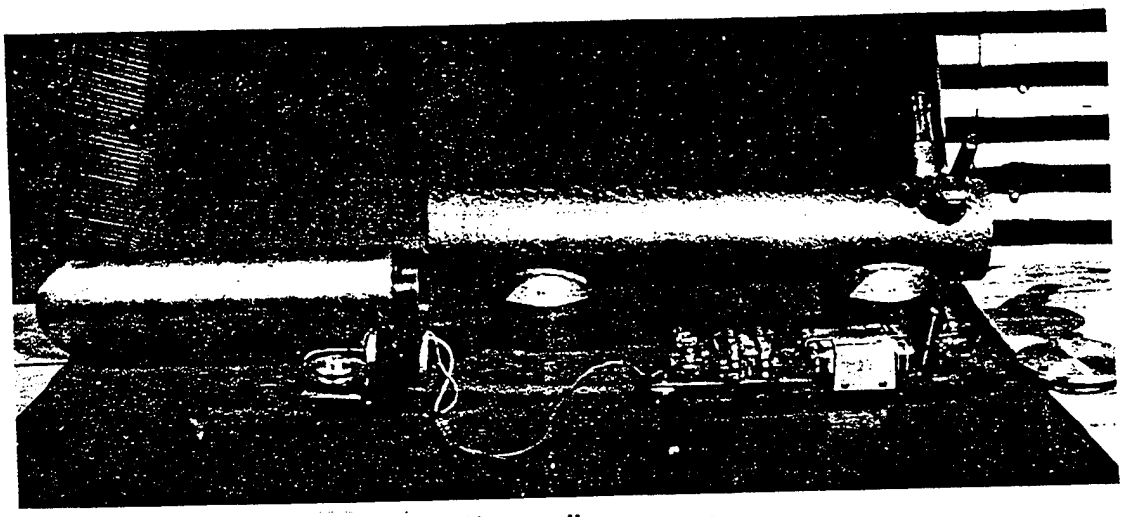

Figure C-3. BRL standard self-recording q-gage.

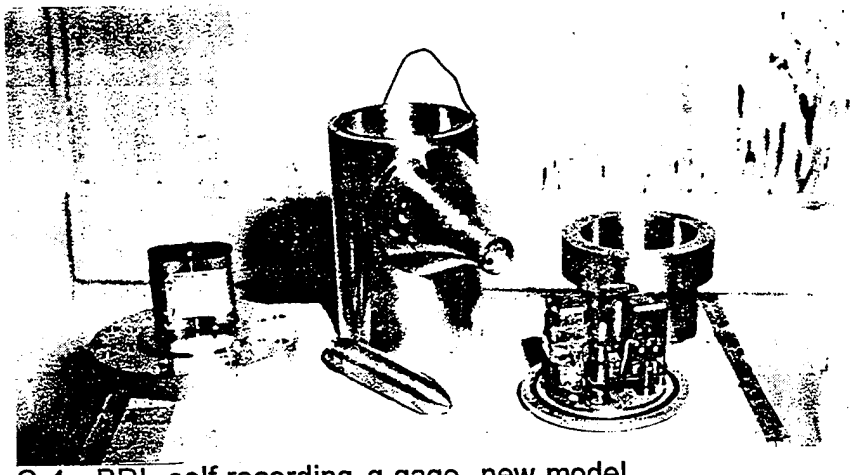

Figure C-4. BRL self-recording q-gage, new model.

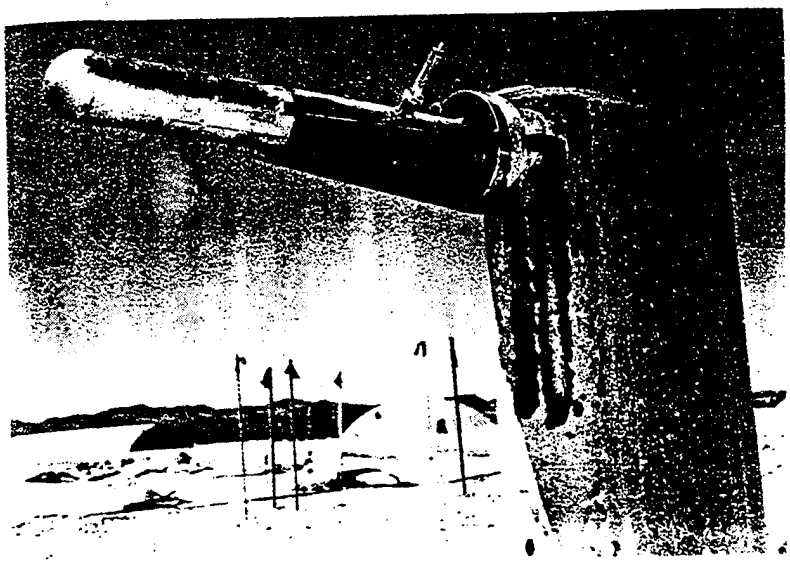

Figure C-5. Contractor-installed q-gage tower with new midbody for standard BRL q-gage.

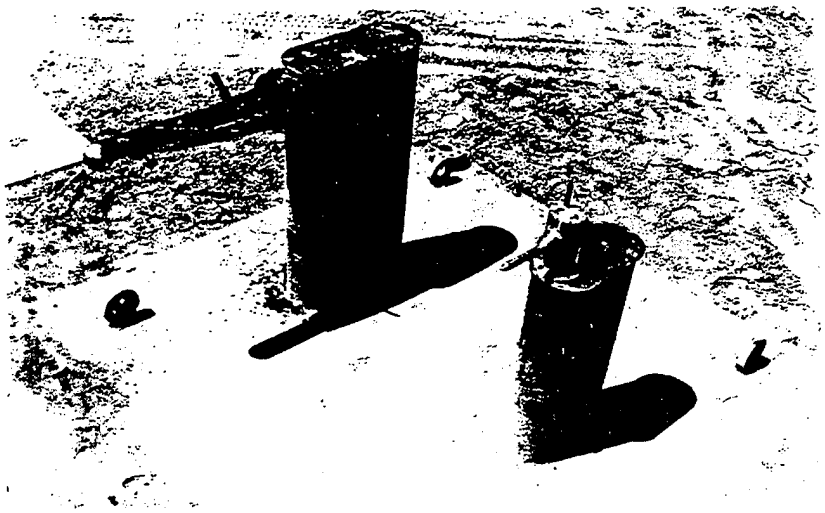

Figure C-6. Contractor-installed towers for standard and new model BRL q-gages.

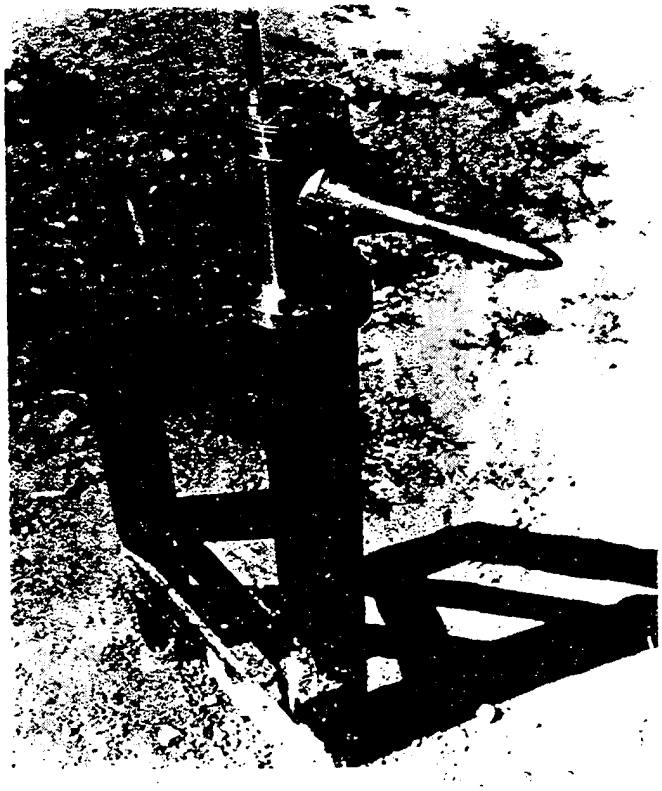

Figure C-7. BRL-installed q-gage mount, new model.

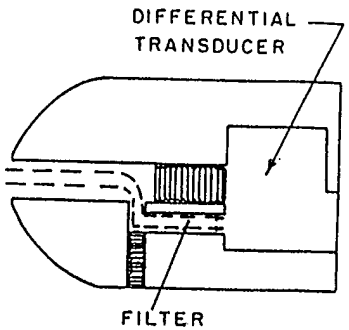

Figure C-8. Modified Sandia-Wiancko subsonic pitot-tube gage.

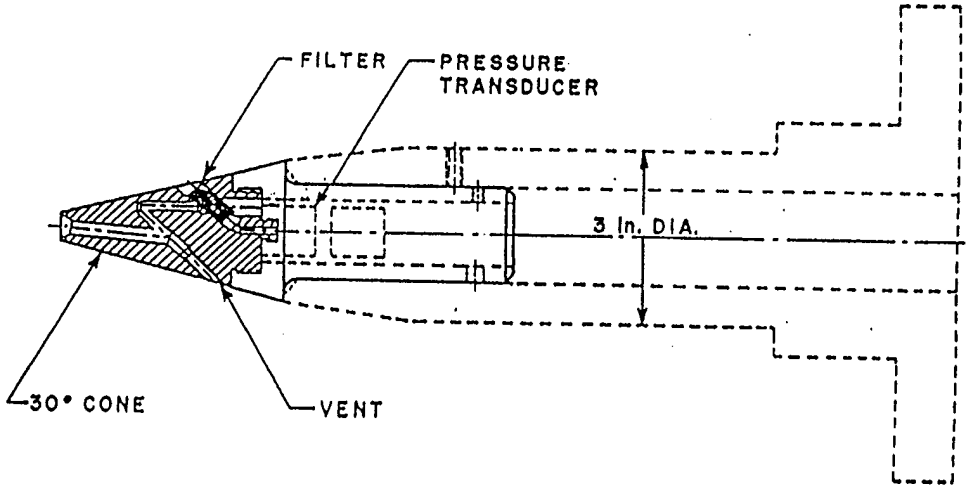

Figure C-9. SRI supersonic total-head gage (Z-gage)

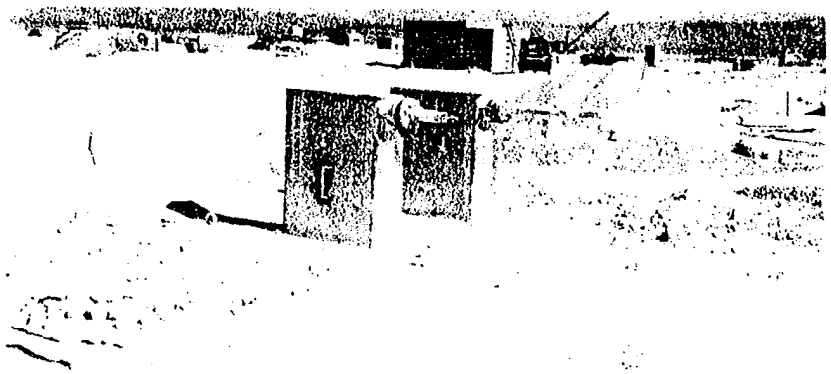

Figure C-10. Typical gage installation: ground baffle, SRI total-head gage, and Sandia-Wiancko pitot-tube.

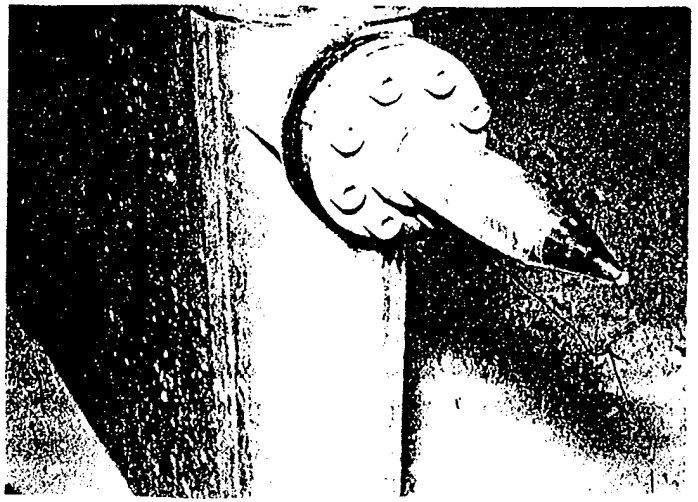

Figure C-11. Close-up of SRI total-head installed on tower.

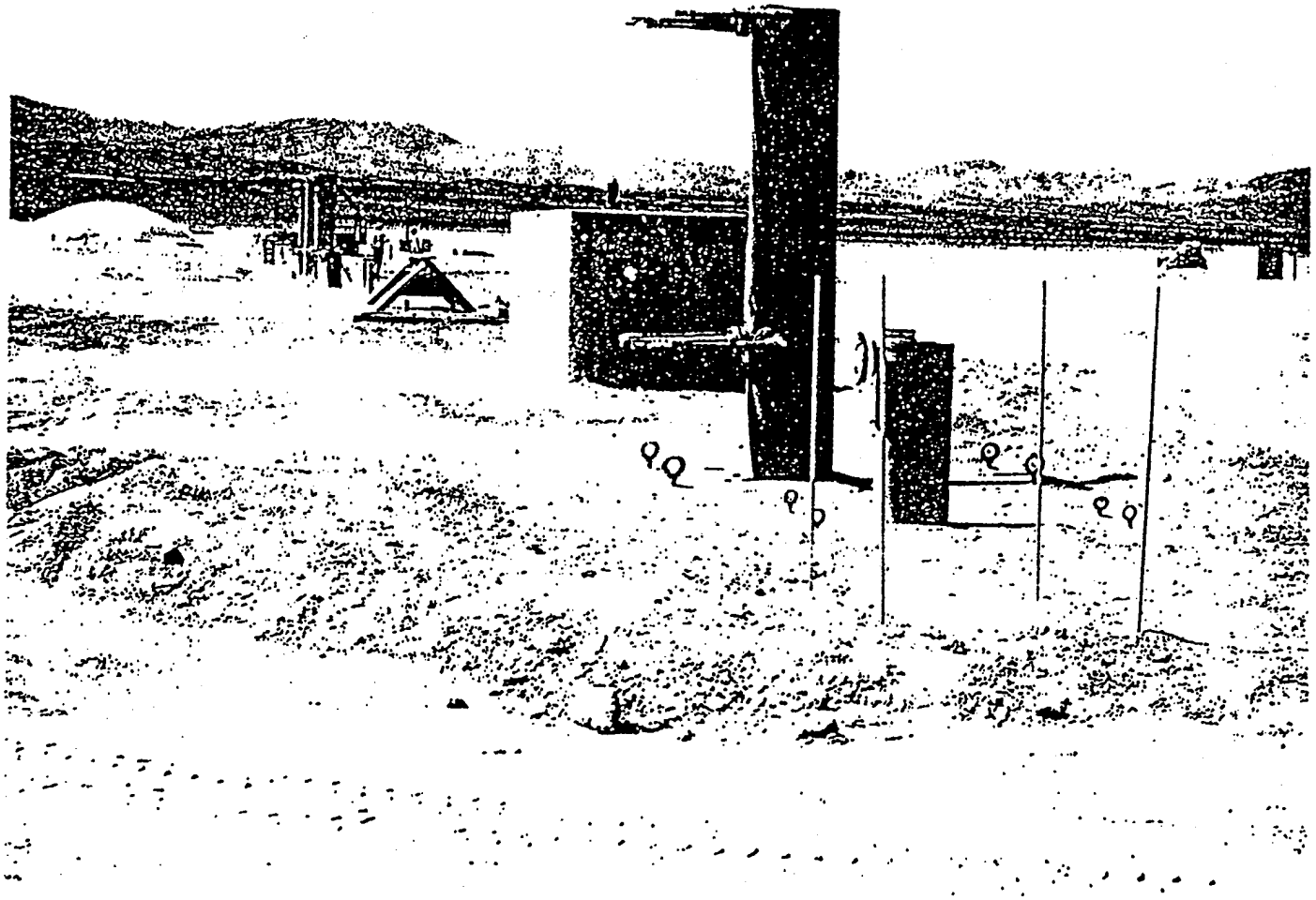

Figure C-12. Gage installation along a Station arc. The gages are well separated and may experience different precursor environments.

Table C-2. PRISCILLA overpressure data - as-read values from original records.

Station Number	Horizontal Distance	Maximum Overpressure	Arrival Time	Positive Duration	Positive Impulse	Wave Type	Agency and Source	Record Quality
	feet	psi	msec	msec	psi-msec			
9039.01	350	1,030	-	-	-	-	BRL WT 1401	Poor
9039.02	450	760	-	-	-	-	BRL WT 1401	Peak
	450	750	-	175	-	I	BRL WT 1401	Good
9039.03	650	480	364	95	10,563	II	BRL WT 1401	Poor
	650	400	676	162	8,896	II	BRL WT 1401	Good
9040.01	850	225	-	236	11,957	II	BRL WT 1401	Good
	850	206	-	-	-	II	BRL WT 1401	Peak
9040.02	1,050	125	-	233	6,156	II	BRL WT 1401	Good
	1,050	138	-	195	5,613	II	BRL WT 1401	Good
9041.00	1,350	60	-	343	4,503	II	BRL WT 1401	Good
	1,350	62	512	280	4,501	II	BRL WT 1401	Good
9042.01	1,650	31	-	467	3,973	II	BRL WT 1401	Good
9042.02	2,000	16.3	-	-	-	-	BRL WT 1401	Peak
9042.05	2,250	12.4	570	687	4,039	III	BRL WT 1401	Good
9042.06	2,500	9.2	523	852	4,179	III	BRL WT 1401	Good
9042.07	3,000	9.1	912	727	2,849	IV	BRL WT 1401	Good
9042.03	3,500	9.9	-	-	-	-	BRL WT 1401	Peak
9042.08	4,000	8.8	1,729	818	2,595	IV	BRL WT 1401	Good
9042.04	4,500	7.4	-	-	-	-	BRL WT 1401	Peak
9043.01	5,000	5.9	2,485	916	-	V	BRL WT 1401	Good
9014.01A	860	175	148	260	11,516	II	BRL WT 1426	Good
9014.02A	1,040	118	1,155	254	5,513	II	BRL WT 1426	Good
9014.03A	1,360	56	-	-	-	-	BRL WT 1426	Peak
9016.01A	970	145	603	234	6,797	II	BRL WT 1426	Good
9016.04C	1,040	122	116	206	4,883	II	BRL WT 1426	Good
9016.05	1,150	98	128	336	6,919	II	BRL WT 1426	Good
9019.01A	1,150	101	-	-	-	-	BRL WT 1426	Peak
9019.03B	1,360	56	-	361	5,703	II	BRL WT 1426	Good
8002.00	1,650	37	222	476	5,607	II	BRL WT 1426	Good
8003.01	1,250	97	-	-	-	-	BRL WT 1426	Peak
8003.02	1,450	49	-	-	-	-	BRL WT 1426	Peak
8003.03	1,750	33	304	529	5,118	II	BRL WT 1426	Good
8015.01	2,030	13.0	317	610	4,227	III	BRL WT 1426	Good
8015.02	2,280	13.8	433	661	3,830	III	BRL WT 1426	Good
8015.03	2,730	9.0	826	737	3,329	III	BRL WT 1426	Good
8015.04	3,930	8.8	1,764	823	2,574	V	BRL WT 1426	Good
8015.05	4,770	6.3	2,297	920	2,202	V	BRL WT 1426	Good
8015.06	5,320	4.9	-	-	-	-	BRL WT 1426	Peak

Table C-2. PRISCILLA overpressure data - as-read values from original records, (continued).

Station Number	Horizontal Distance	Maximum Overpressure	Arrival Time	Positive Duration	Positive Impulse	Wave Type	Agency and Source	Record Quality
	feet	psi	msec	msec	psi-msec			
1B	450	554	103	-	-	I	SRI WT 1403	Poor
2B	550	366	116	-	-	II	SRI WT 1403	Peak
3B	650	342	131	149	12,200	II	SRI WT 1403	Good
4B	750	229	146	164	10,100	II	SRI WT 1403	Good
5B	850	221	163	197	11,200	II	SRI WT 1403	Good
6B	1,050	101	201	314	9,150	II	SRI WT 1403	Good
7B	1,350	59.1	268	357	6,620	II	SRI WT 1403	Good
8B	1,650	37.2	350	395	5,020	II	SRI WT 1403	Good
9B	2,000	31.9	475	510	5,820	II	SR WT 1403	Good
10B	2,500	11.3	716	774	4,540	III	SRI WT 1403	Good
11B	3,000	10.9	1,049	789	3,660	IV	SRI WT 1403	Good
12B	3,500	7.7	1,445	490	1,670	IV	SRI WT 1403	Poor
F-1.5-9012.01	650	270	130	211	14,200	II	SC WT 1405	Good
F-1.5-9012.02	850	187	164	235	9,700	II	SC WT 1405	Good
F-1.5-9012.03	1,050	120	203	307	7,800	II	SC WT 1405	Good
F-1.5-9012.04	1,350	59.1	270	442	6,500	II	SC WT 1405	Good
PGB	1,150	85.0	223	406	8,140	II	SC WT 1472	Good
PGB	1,700	32.0	370	445	5,680	II	SC WT 1472	Good
PGBU	1,700	35.0	369	710	6,920	II	SC WT 1472	Good
PGBU	1,800	22.0	403	720	5,640	II	SC WT 1472	Good
PGBU	1,800	21.5	402	558	5,180	II	SC WT 1472	Good
PGB	1,900	27.5	439	573	4,200	II	SC WT 1472	Good
PGBa	2,000	25.5	483	549	4,960	II	SC WT 1472	Good
PGBb	2,000	24.5	484	595	4,240	II	SC WT 1472	Good
PGB	2,100	15./	524	575	3,810	III	SC WT 1472	Good
9031.01A	760	235	81	-	-	II	BRL WT 1426	Poor
B	760	225	101	178	7,048	II	BRL WT 1426	Good
C	760	210	54	-	-	II	BRL WT 1426	Poor
9031.02A	1,040	115	136	253	5,358	II	BRL WT 1426	Good
B	1,040	105	131	285	6,219	II	BRL WT 1426	Good
C	1,040	112	147	307	7,367	II	BRL WT 1426	Good
D	1,040	110	189	256	6,523	II	BRL WT 1426	Good
9031.03A	1,360	60	200	404	6,414	II	BRL WT 1426	Good
B	1,360	40	255	-	-	-	BRL WT 1426	Poor
1A	1,430	40	927	403	4,766	II	BRL WT 1426	Good
2A	1,720	28	1,901	401	3,326	II	BRL WT 1426	Good
3A	2,280	11	300	600	3,719	III	BRL WT 1426	Good
5B	3,900	9.2	-	842	3,286	V	BRL WT 1426	Good

Table C-3. Mach number and dynamic pressure from SRI gages on PRISCILLA.

Station	Ground Range (ft.)	Gage Height (ft.)	Mach No. Calculation Method	Maximum Mach No.	Time of Maximum Mach No. (sec.)	Maximum Dynamic Pressure (psi)	Time of Maximum Dynamic Pressure (sec)	Maximum Differential Pressure (pitot) (psi)	Time of Maximum Differential Pressure (pitot) (sec)	Maximum Total-Head Minus Static Pressure (psi)	Time of Maximum Total-Head Minus Static Pressure (sec)	Dynamic Pressure Impulse (psi-sec)	Remarks
As-read from original records													
1	450	3	Z	0.93*	0.124	258	0.109	--	--	310	0.112	--	Partial record
2	550	3	Z	1.89*	0.119	287	0.126	--	--	373	0.126	--	Partial record
3	650	3	Z	1.73*	0.139	211	0.150	--	--	270	0.150	--	Partial record
4	750	3	Z	1.63*	0.163	211	0.169	--	--	308	0.169	--	Partial record
5	850	3	Z	1.88	0.192	309	0.201	--	--	498	0.200	9.3	Good record
6	1,050	3	Z	2.17	0.257	225	0.271	--	--	519	0.266	8.3	Good record
7	1,350	3	Z	2.33	0.382	143	0.390	--	--	412	0.386	6.8	Good record
8	1,650	3	$\Delta p + Q$	1.81	0.480	44.1	0.475	98.1	0.480	--	--	9.2	Record did not return to the base line
8	1,650	10	$\Delta p + Q$	2.27	0.525	72.6	0.545	193	0.525	--	--	11.6	Good record
9	2,000	3	$\Delta p + Q$	1.42	0.740	29.0	0.530	42.3	0.530	--	--	8.9	Good record
10	2,500	3	Z	1.26	1.230	23.1	0.758	19.9	0.746	32.51	0.758	8.1	Good record
10	2,500	3	$\Delta p + Q$	1.09	1.260	18.0	0.750	19.9	0.746	--	--	8.1	Good record
10	2,500	10	$\Delta p + Q$	1.36	1.110	27.7	0.825	28.2	0.865	--	--	11.0	Good record
11	3,000	10	$\Delta p + Q$	1.15	1.370	17.5	0.370	20.6	1.370	--	--	5.2	Good record
12	3,500	3	$\Delta p + Q$	0.74	1.890	5.31	1.890	2.81	1.890	--	--	2.9	Good small record

Table C-4. BRL Q-gage results, main blast line, maximum values.

Station	Ground Range (ft.)	Gage Height (ft.)	Total Pressure (psi)	Static Overpressure (psi)	Pressure Difference $(P_p - P_o)^{*'}$ (psi)	Dynamic Pressure q* (psi)	Mach No. (u/a)	Dynamic Pressure Impulse DPI (psi)	Remarks
F1.1-9040.01	850	3	--	--	--	--	--	--	Record destroyed by acceleration effects.
F1.1-9040.02	1050	3	470.0	125.0	445.0	240.0	3.3	--	Total head is a partial record. May not be maximum.
F1.1-9041.00	1350	3	275.0	60.0	255.0	150.0	3.6	--	Partial record.
F1.1-9041.00N[x]	1350	3	--	--	--	--	--	--	New prototype gage was effected by acceleration.
F1.1-9042.01	1650	3	143.5	31.0	150.0	80.0	2.3	--	Total head had only a partial record.
F1.1-9042.02	2000	3	58.5	23.0x	44.0	32.0	1.3	--	Gage failed at 240 msec.
F1.1-9042.05N	2250	3	48.0	12.4	36.0	27.0	1.4	--	Acceleration effected prototype gage.
F1.1-9042.06	2500	3	47.0	9.2	38.0	25.0	1.3	5.45	Good record.
F1.1-9042.06Nx	2500	3	35.0	9.2	28.0	19.0	1.2	--	Total head plug by dust.
F1.1-9042.07	3000	3	29.0	9.1	20.0	15.1	1.0	3.18	Good record.
F1.1-9042.07Nx	3000	3	26.5	9.1	20.5	17.0	1.04	3.37	Gage plugs on arrival of main shock.
F1.1-9042.03	3500	3	11.2	8.6x	3.4	2.8	0.45	0.79	Good record.
F1.1-9042.08	4000	3	10.0	9.0	1.3	1.3	0.29	--	Ratio of two small numbers. Good records.
F1.1-9042.08N	4000	3	--	--	--	--	--	--	
F1.1-9042.04	4500	3	7.8	6.5x	1.7	1.2	0.29	0.33	Ratio of two small numbers. Good records.

N, refers to new q-gage. x, values from q-gage.

Table C-5. BRL Q-gage results, Project 3.4, maximum values.

Station	Ground Range (ft.)	Gage Height (ft.)	Total Pressure (psi)	Static Overpressure (psi)	Pressure Difference $(P_p - P_o)^{*'}$ (psi)	Dynamic Pressure q* (psi)	Mach No. (u/a)	Dynamic Pressure Impulse DPI (psi)	Remarks
F3.4-9021	900	3	--	--	--	--	--	--	No record.
F3.4-9024.01	4200	3	8.2	6.7x	1.3	1.2	0.28	0.20	Good record but ratio of two small numbers.
F3.4-9022.01	3600	10	13.0	10.2x	3.8	3.7	0.47	0.68	Good record.
F3.4-9022.02	5000	10	6.7	6.0x	1.9	1.8	0.38	0.18	Good record but ratio of two small numbers.

x Obtained from q-gage as opposed to ground baffle gages.

Table C-6. BRL Q-gage results, Project 4.3/33.2, maximum values.

Station	Ground Range (ft.)	Gage Height (ft.)	Total Pressure (psi)	Static Overpressure (psi)	Pressure Difference $(P_p - P_o)^{*'}$ (psi)	Dynamic Pressure q* (psi)	Mach No. (u/a)	Dynamic Pressure Impulse DPI (psi)	Remarks
F33.2-8015.01	2030	3	61.0	13.0	51.0	37.0	1.6	--	Partial record.
F33.2-8015.02	2280	3	50.0	13.8	41.0	28.0	1.3	3.5	Good record. Max. corresponds to main shock.
F33.2-8015.03	2730	3	23.7	9.0	14.5	11.5	0.89	2.6	Good record.
F33.2-8015.04	3930	3	11.0	8.8	2.4	2.3	0.39	0.26	Good record. End of precursor.
F33.2-8015.05	4770	3	6.8	6.3	0.9	0.9	0.23	0.26	Good record.
F33.2-8015.06	5320	3	6.4	5.1x	1.2	1.2	0.31	0.28	Good record.
F33.2-8015.07	6120	3	4.9	4.7x	0.3	0.35	0.18	--	Ratio of two small numbers.

x, obtained from q-gage as opposed to ground baffle gage.

Table C-7. Summary of free-field gauge results by Sandia Corporation (WT-1472).

Distance (ft)	Gauge	Location	Calibration Pressure (psi)	Time of Arrival (msec)	First Peak Overpressure (psi)	Time of Arrival of First Peak (msec)	Second Peak Overpressure (psi)	Time of Arrival of Second Peak (msec)	Positive-Phase Duration (msec)	Positive-Phase Impulse (psi-msec)	Dynamic Pressure Impulse (psi-sec)	Remarks
1150	PGB-1150-0	Ground baffle	75	222	17	268	87	312	462	8.14		Good record
1150	Q-1150-3	3 ft.	375	223	518	305	-	-	-	-	-	Baseline shift
1700	PGB-1700-0	Ground baffle	30	369	9.3	485	31.8	592	598	4.86		Good record
1700	PGBU-1700-0	Ground baffle	30	369	14	467	37.2	594	806	7.21		Good record
1800	PGB-1800-0	Ground baffle	27	401	8.6	465	23	653	720	4.50		Pressure scale error in WT1472 - good record
1800	PGBU-1800-0	Ground baffle	27	402	12.6	444	23	653	540	4.48		Good record
1900	PGB-1900-0	Ground baffle	24	438	10.4	463	27.3	713	619	4.70		Good record
2000	PGB-2000a-0	Ground baffle	21	483	19.2	663	25.8	805	552	5.17		Good record
2000	PGB-2000b-0	Ground baffle	21	484	11.8	645	24.2	822	578	4.05		Good record
2100	PGB-2100-0	Ground baffle	15	524	15.1	588	12.6	883	578	3.75		Good record
2000	G-2000-3		162	486	140 (spike to 165)	661	145 (spike to 167)	764	-	-		Gauge damaged after blast-wave passage
2000	G-2000-10		162	486	170	628	145	743	-	-		Gauge damaged after second maximum
2000	S-2000-3		90	487	42	545	65	753	-	-		Gauge damaged after second maximum
2000	S-2000-10		90	487	120	635	93	748	540	-		
2000	SS-2000-3		21	482	17	554	25	798	790	6.8		
2000	SS-2000-10		21	486	24	591	36	795	730	6.7		
2000	Q-2000-3		135	486	48	521	-	-			-	Gauge plugged after maximum
2000	Q-2000-10		135	486	140	632	108	755	790		-	Baseline shift
2000	FP-2000-3		120	485	117 (spike to 129)	662	110 (spike to 117)	746	-	-		Baseline shift

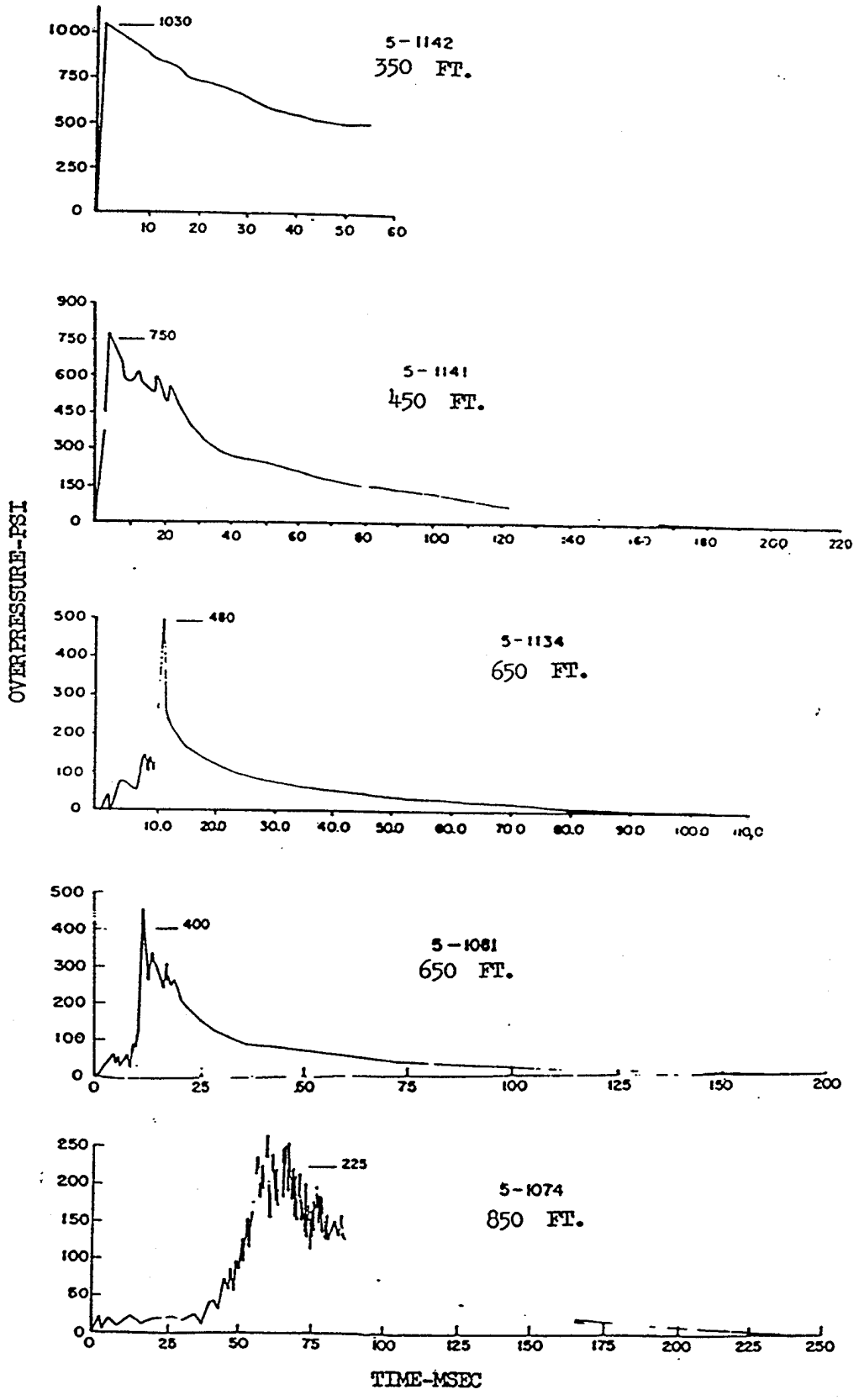

Figure C-13. Overpressure-time histories, main blast line, at distances of 350, 450, 650, and 850 feet. BRL data, WT-1401.

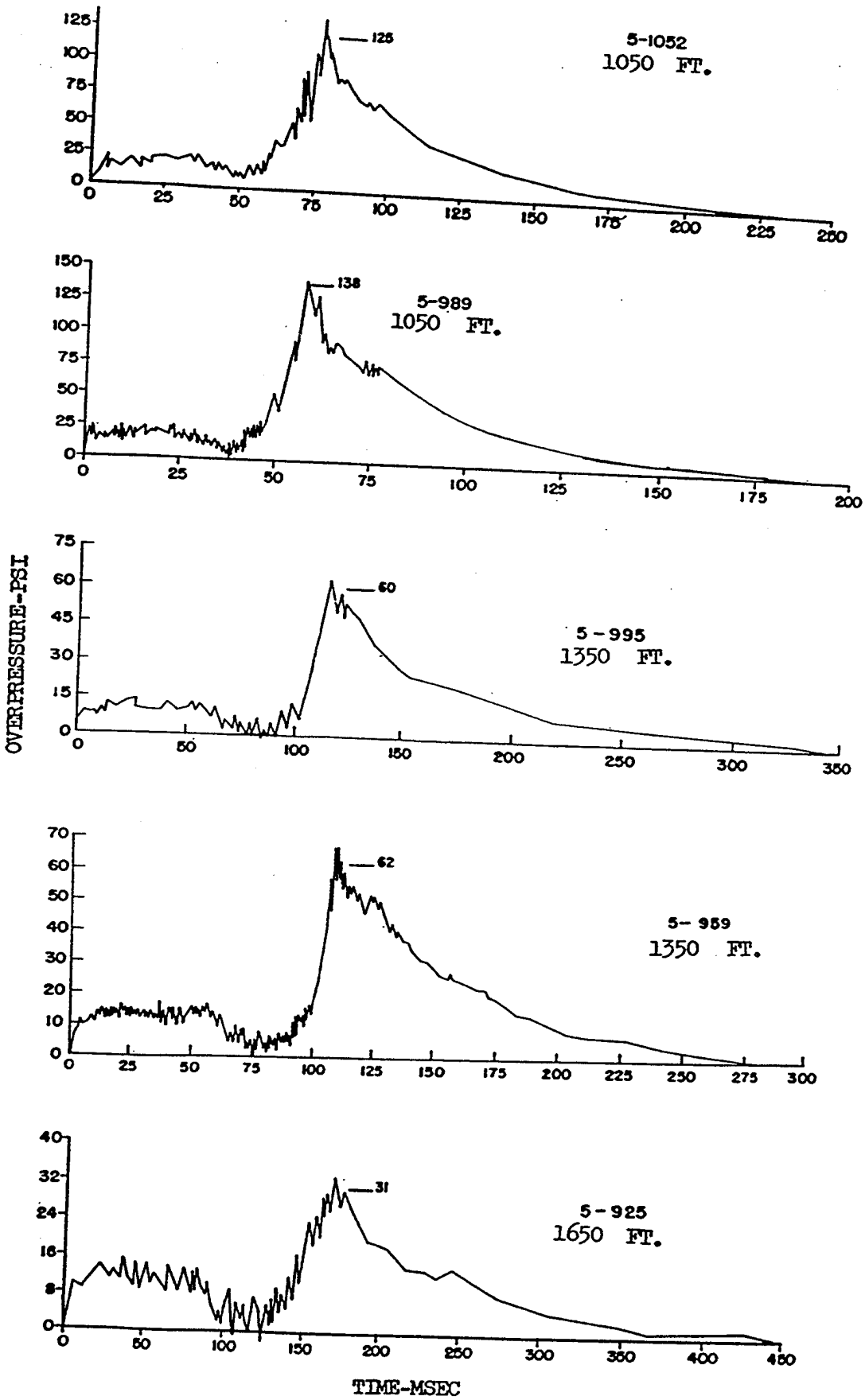

Figure C-14. Overpressure-time histories, main blast line, at distances of 1050, 1350, and 1650 feet. BRL data, WT-1401.

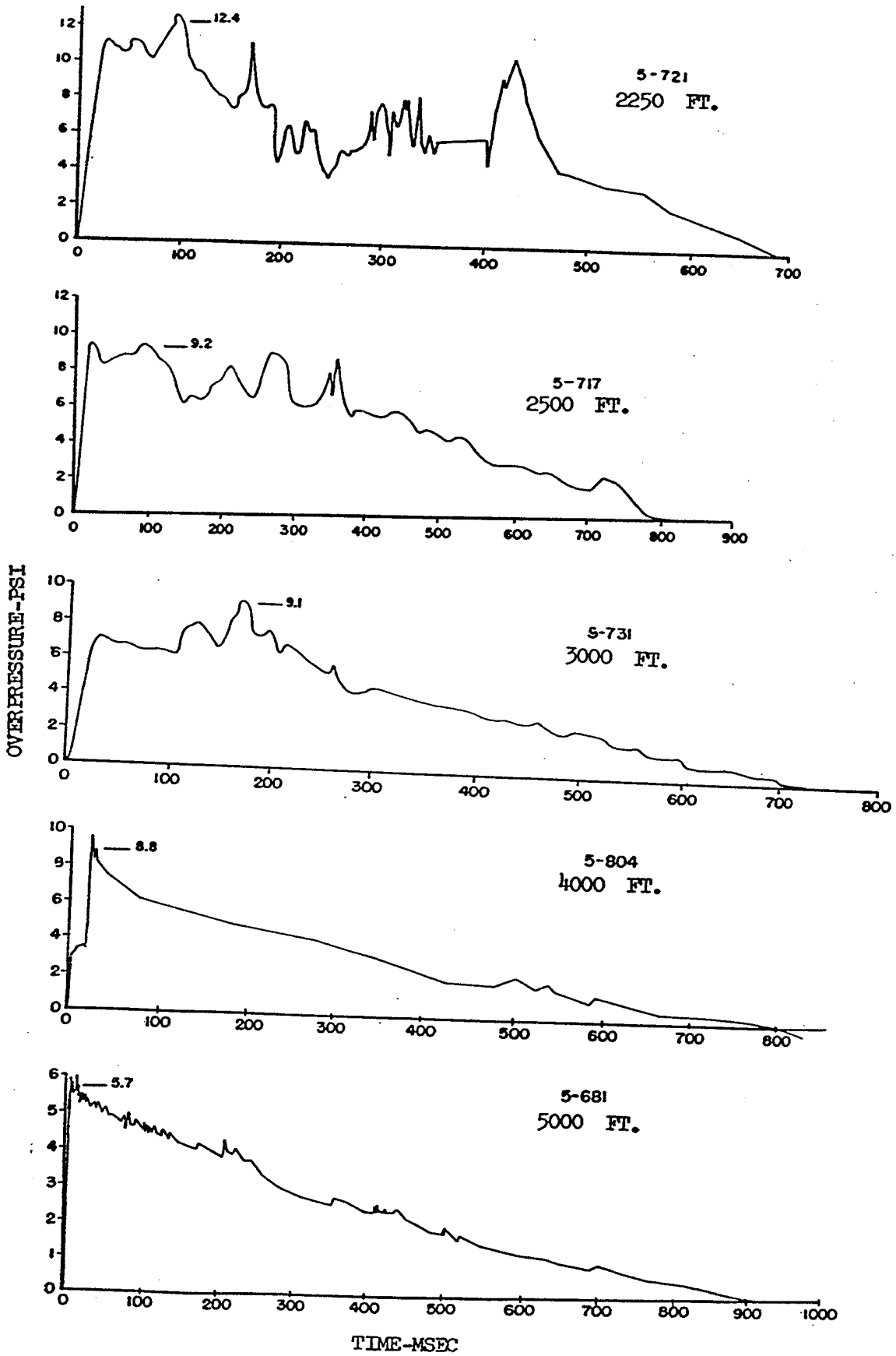

Figure C-15. Overpressure-time histories, main blast line, at distances of 2250, 2500, 3000, 4000, and 5000 feet. BRL data, WT-1401.

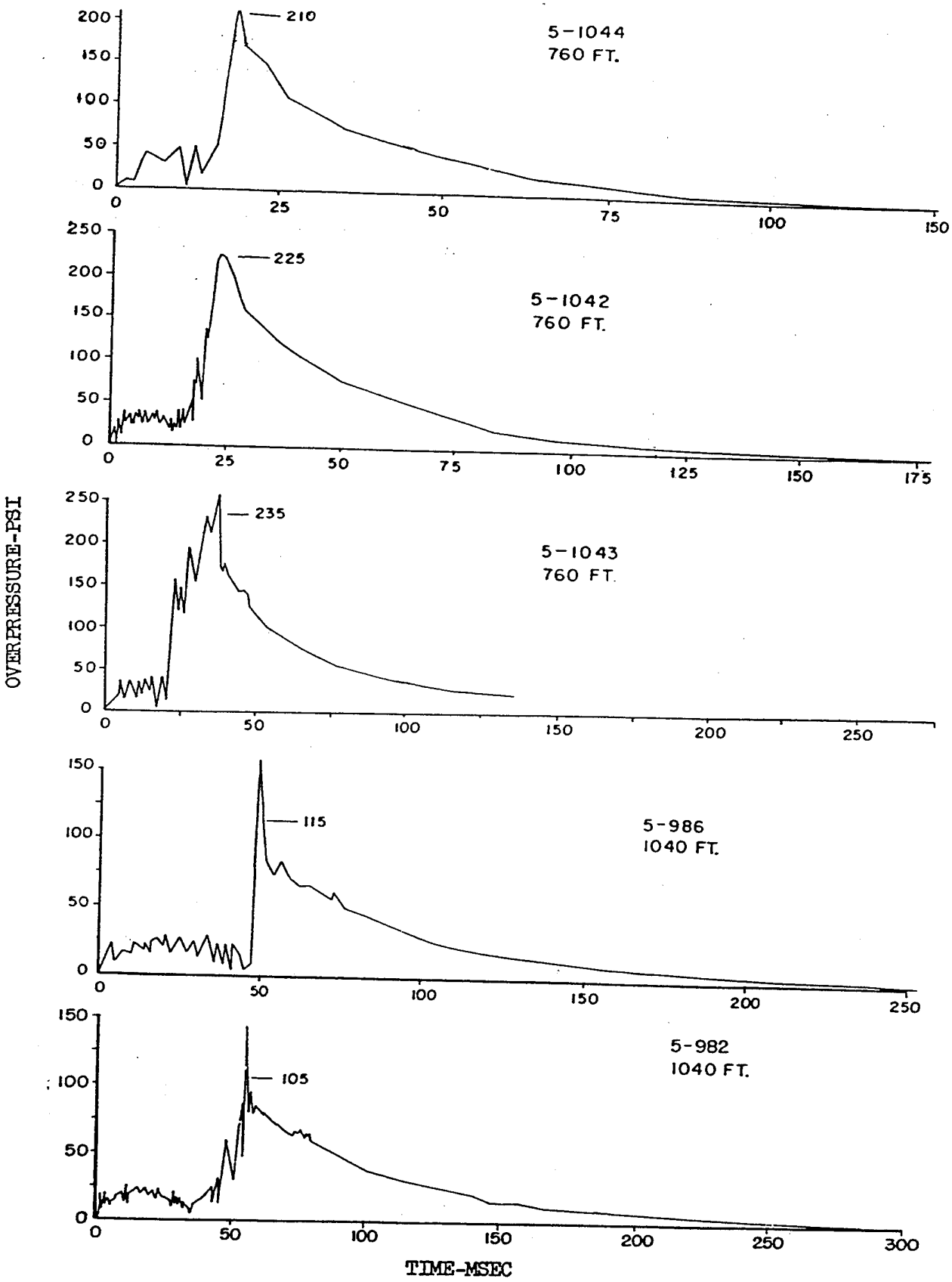

Figure C-16. Overpressure-time histories, Project 1.7 at distances of 760 and 1040 feet. BRL data, WT-1401.

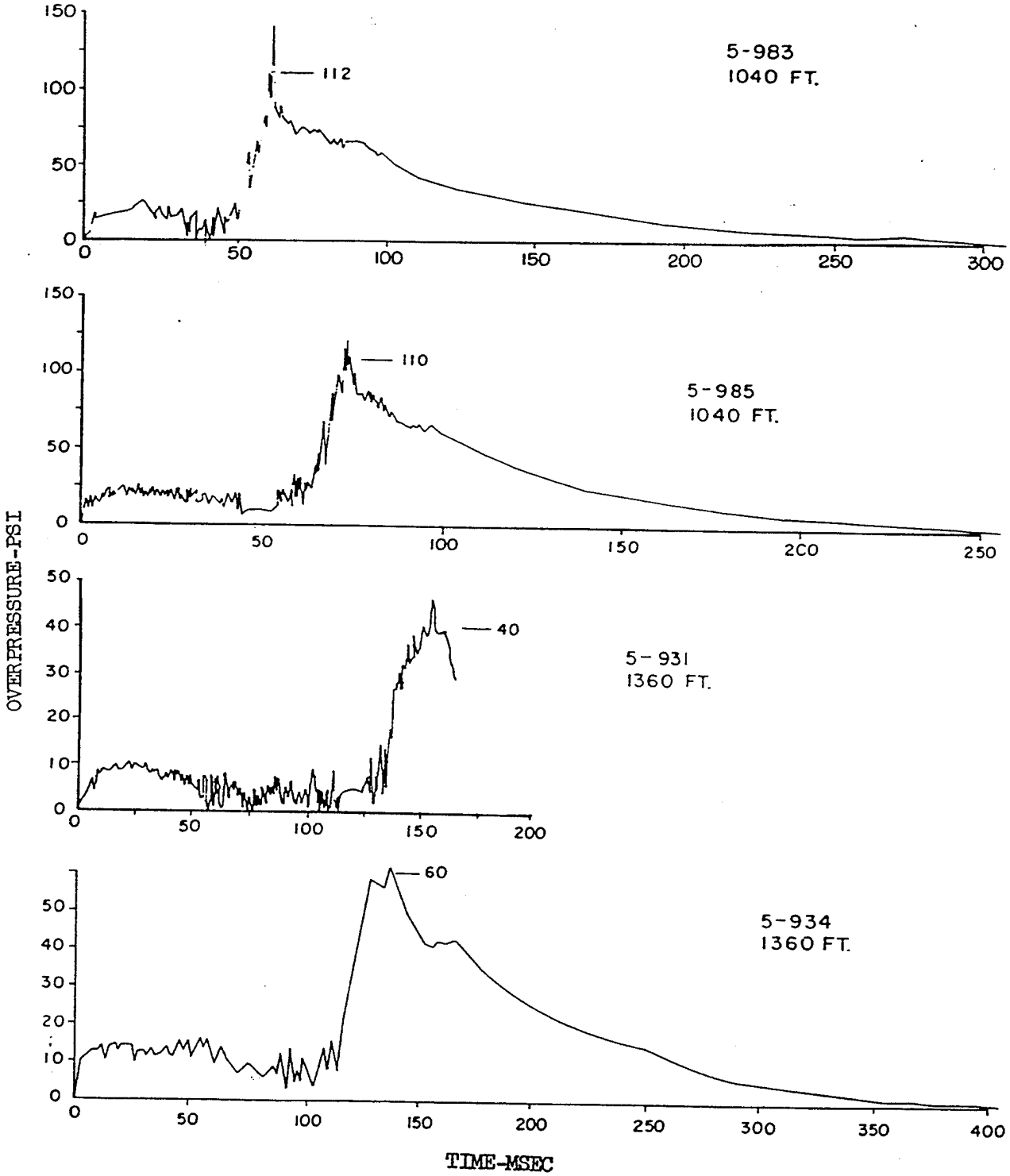

Figure C-17. Overpressure-time histories, Project 1.7 at distances of 1040 and 1360 feet. BRL data, WT-1401.

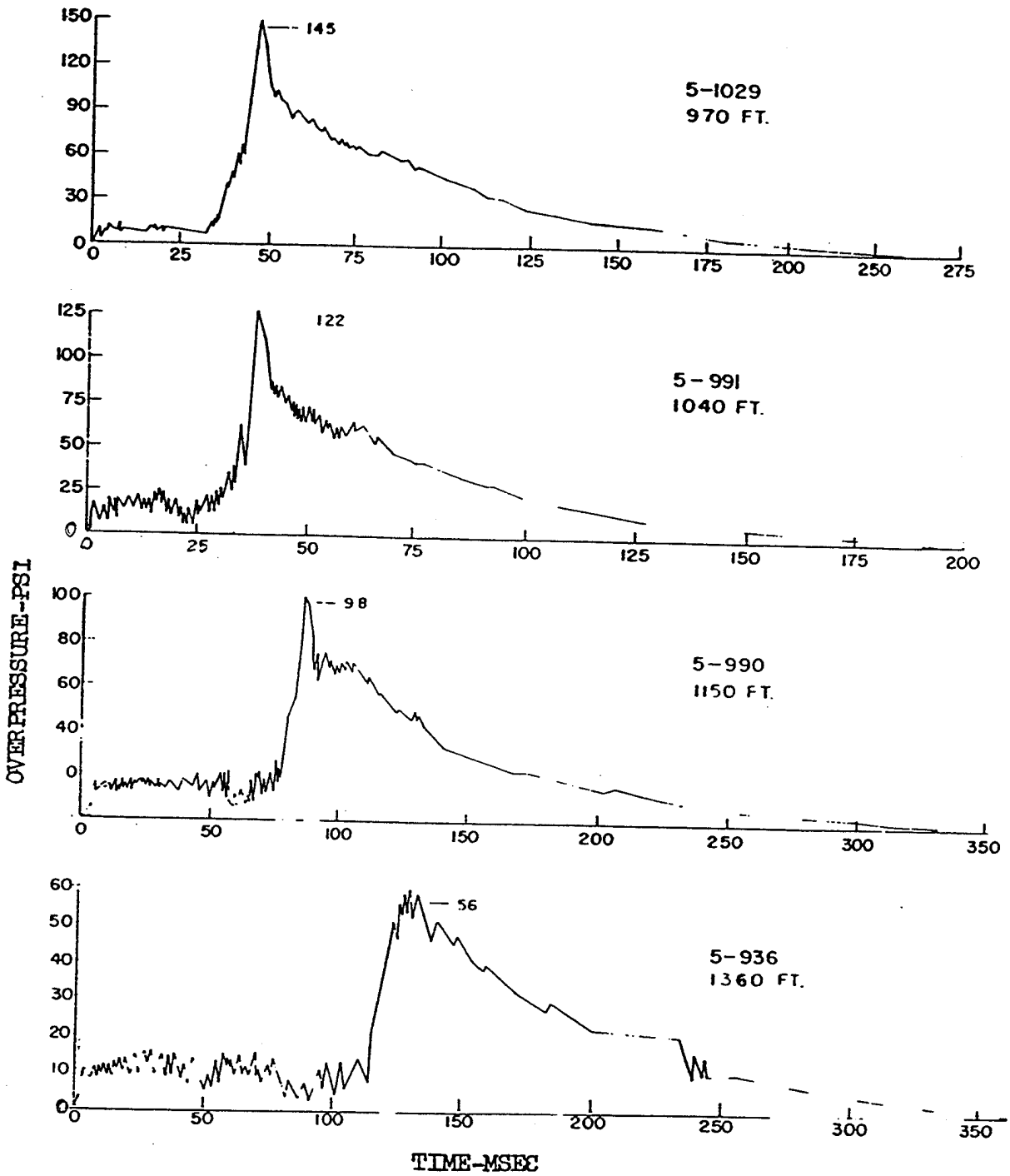

Figure C-18. Overpressure-time histories, Projects 3.2 and 3.3 at distances of 970, 1040, 1150, and 1360 feet. BRL data, WT-1401.

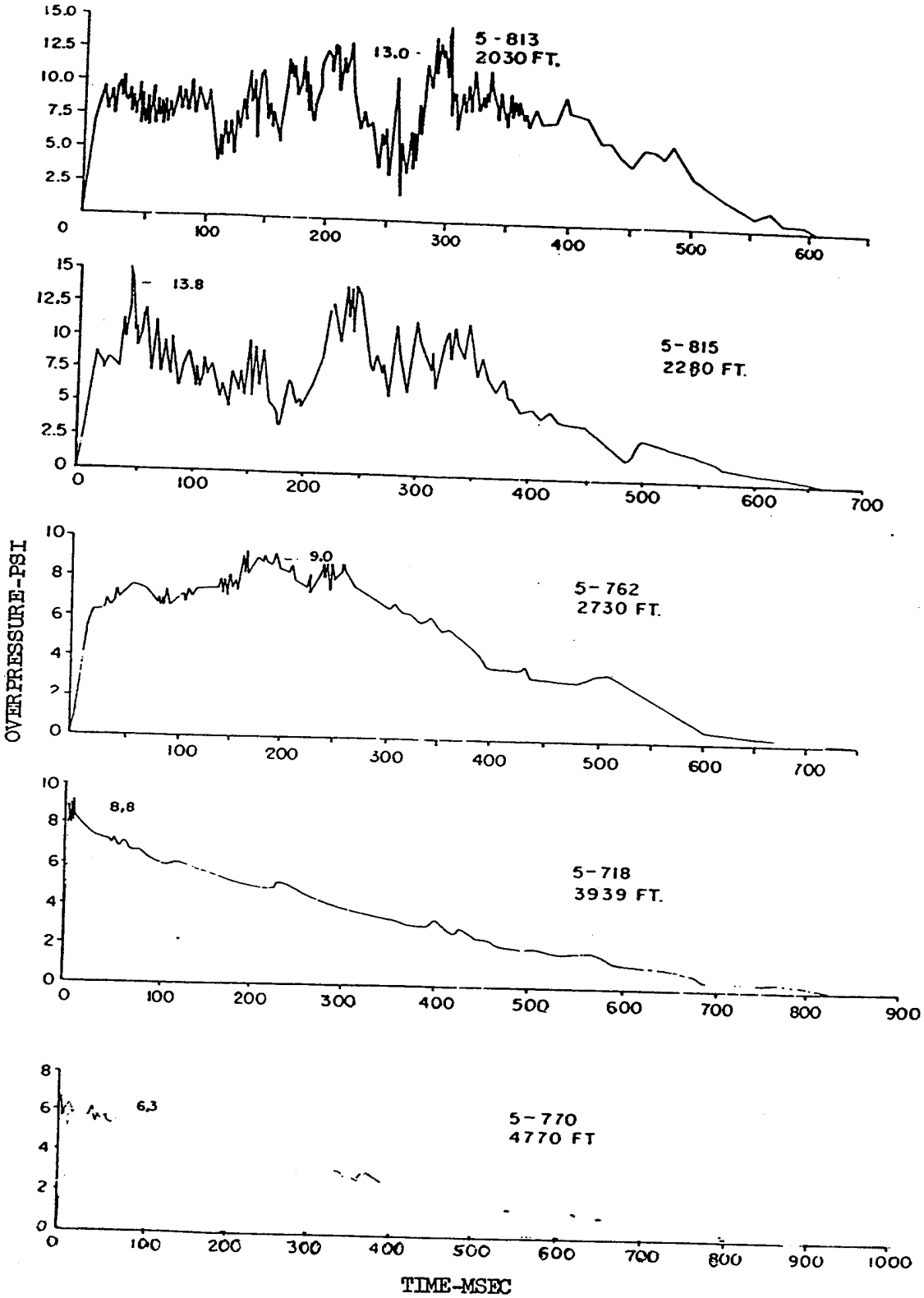

Figure C-19. Overpressure-time histories, Project 4.3/33.2 at distances of 2030, 2280, 2730, 3939, and 4770 feet. BRL data, WT-1401.

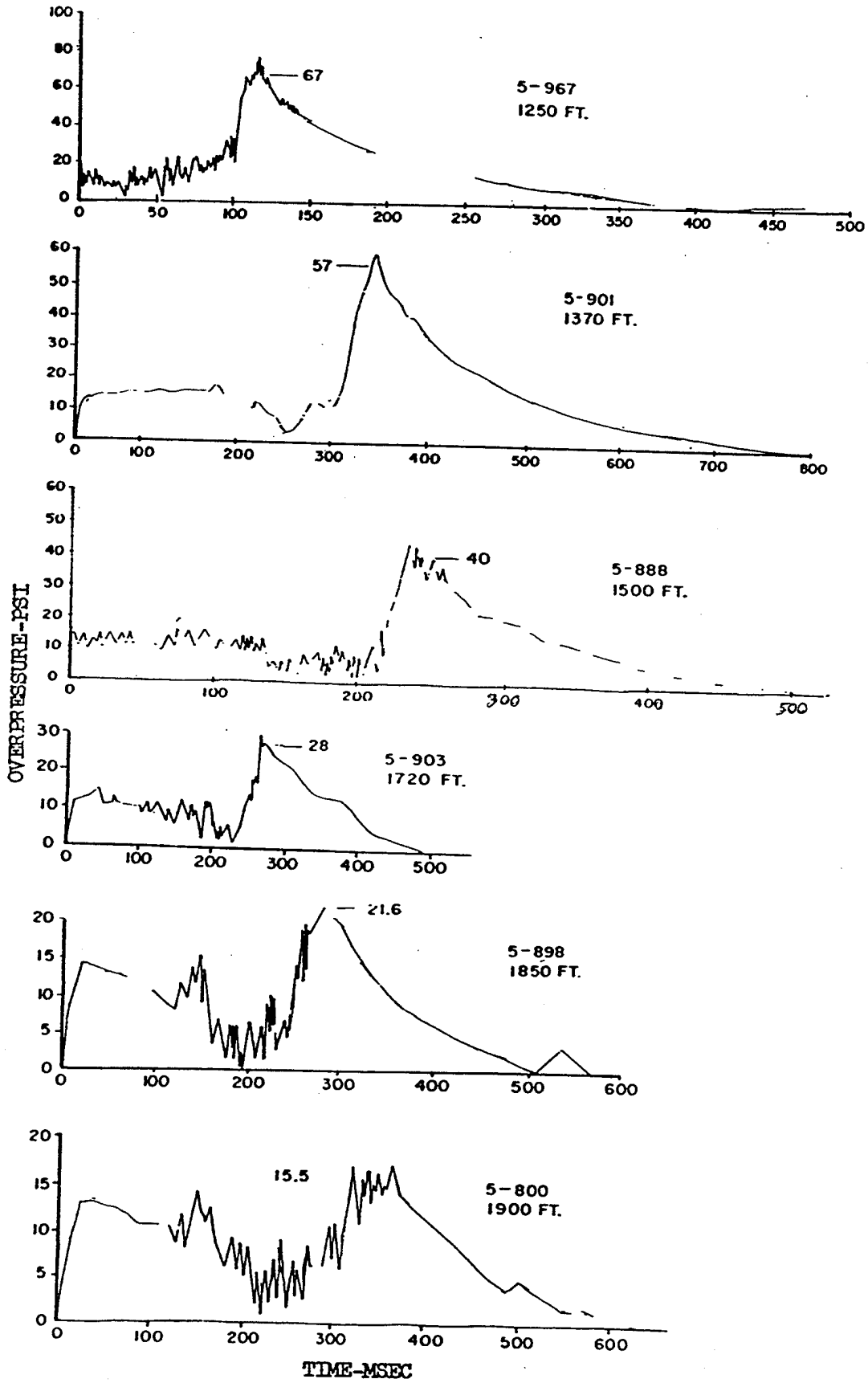

Figure C-20. Overpressure-time histories, Project 6.1 at distances of 1250, 1370, 1500, 1720, 1850, and 1900 feet. BRL data, WT-1401.

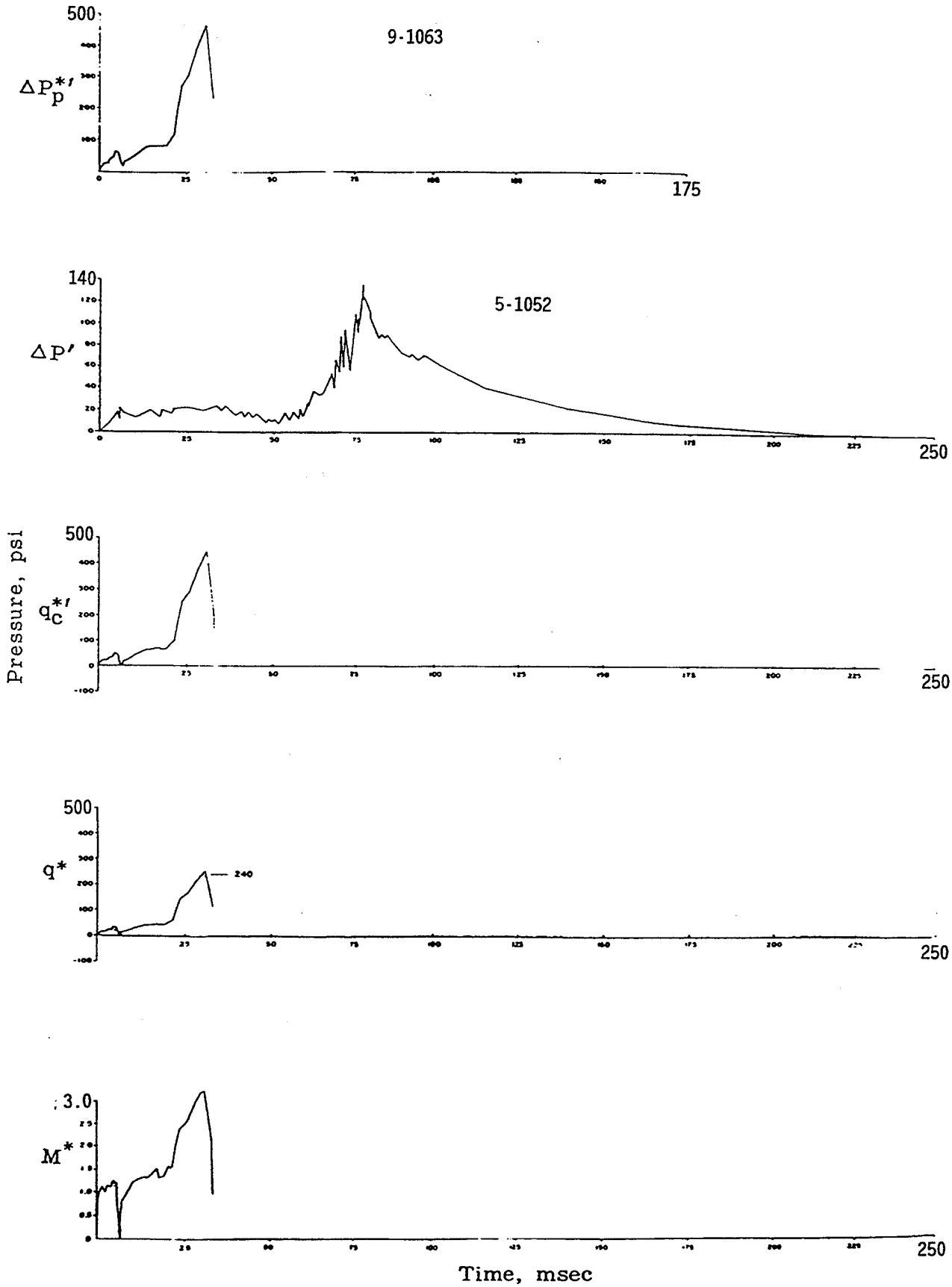

Figure C-21. Pressure and Mach number versus time, main blast line at 1050 feet. BRL standard Q-gage data, WT-1401.

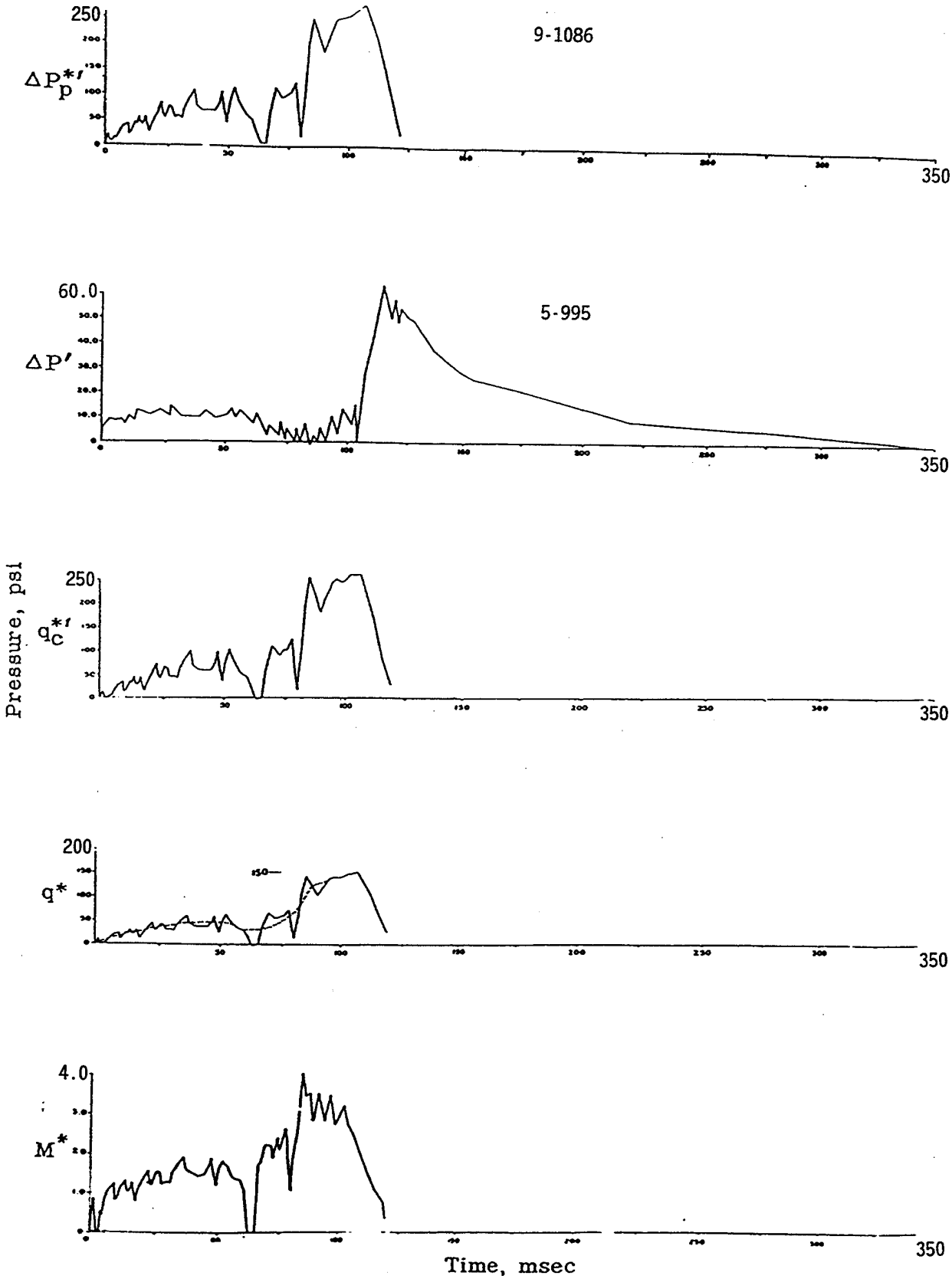

Figure C-22. Pressure and Mach number versus time, main blast line at 1350 feet. BRL standard Q-gage data, WT-1401.

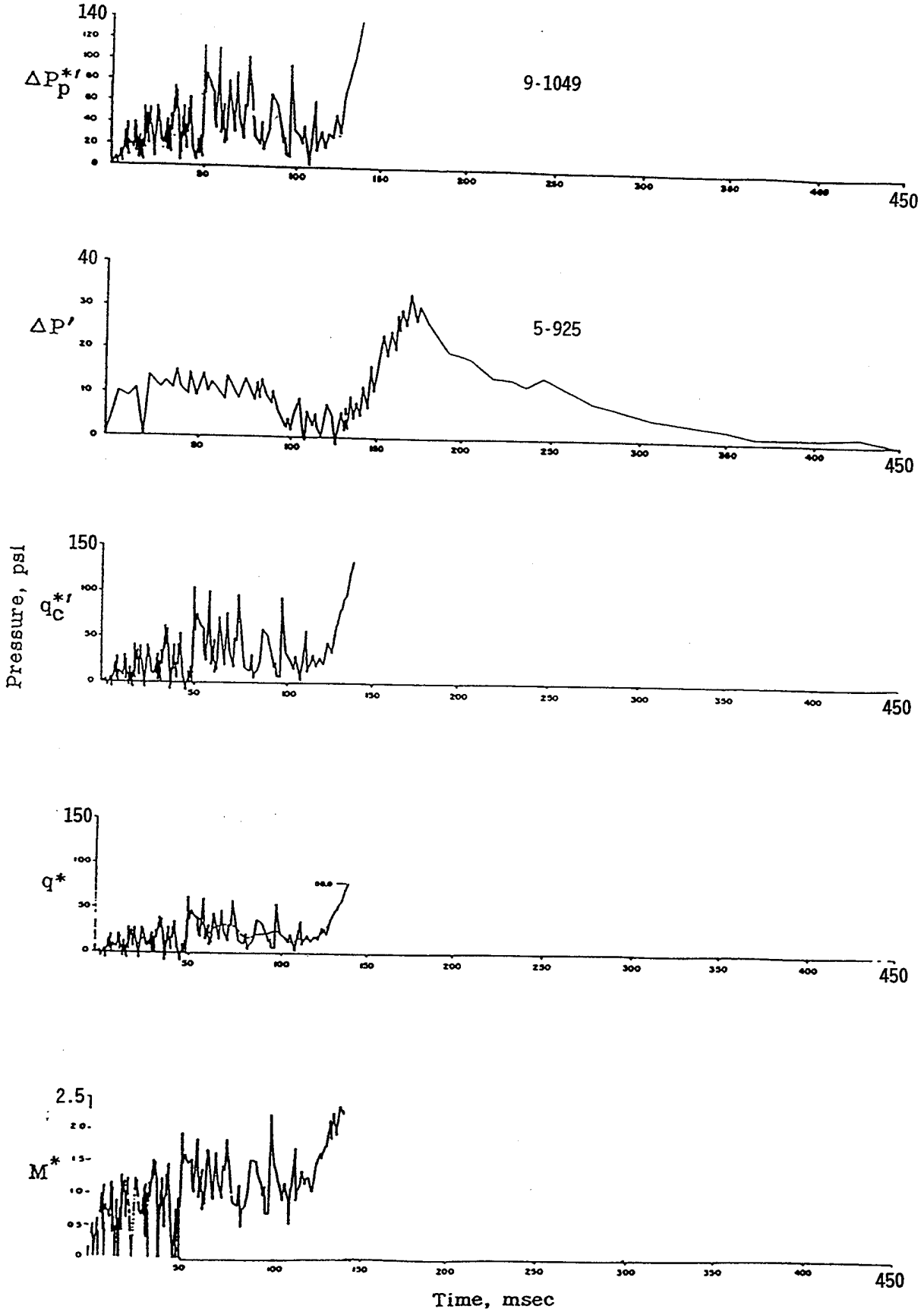

Figure C-23. Pressure and Mach number versus time, main blast line at 1650 feet. BRL standard Q-gage data, WT-1401.

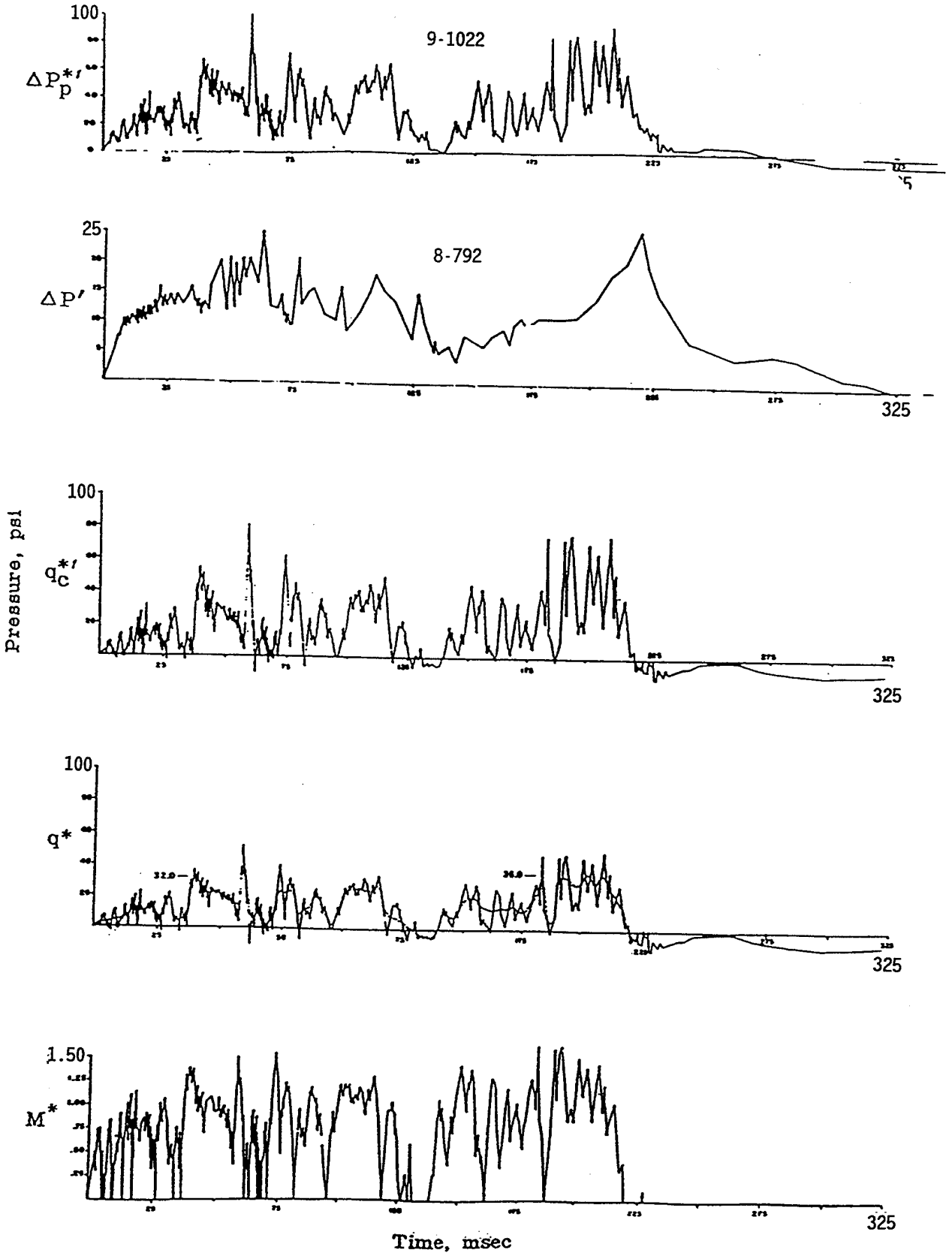

Figure C-24. Pressure and Mach number versus time, main blast line at 2000 feet. BRL standard Q-gage data, WT-1401.

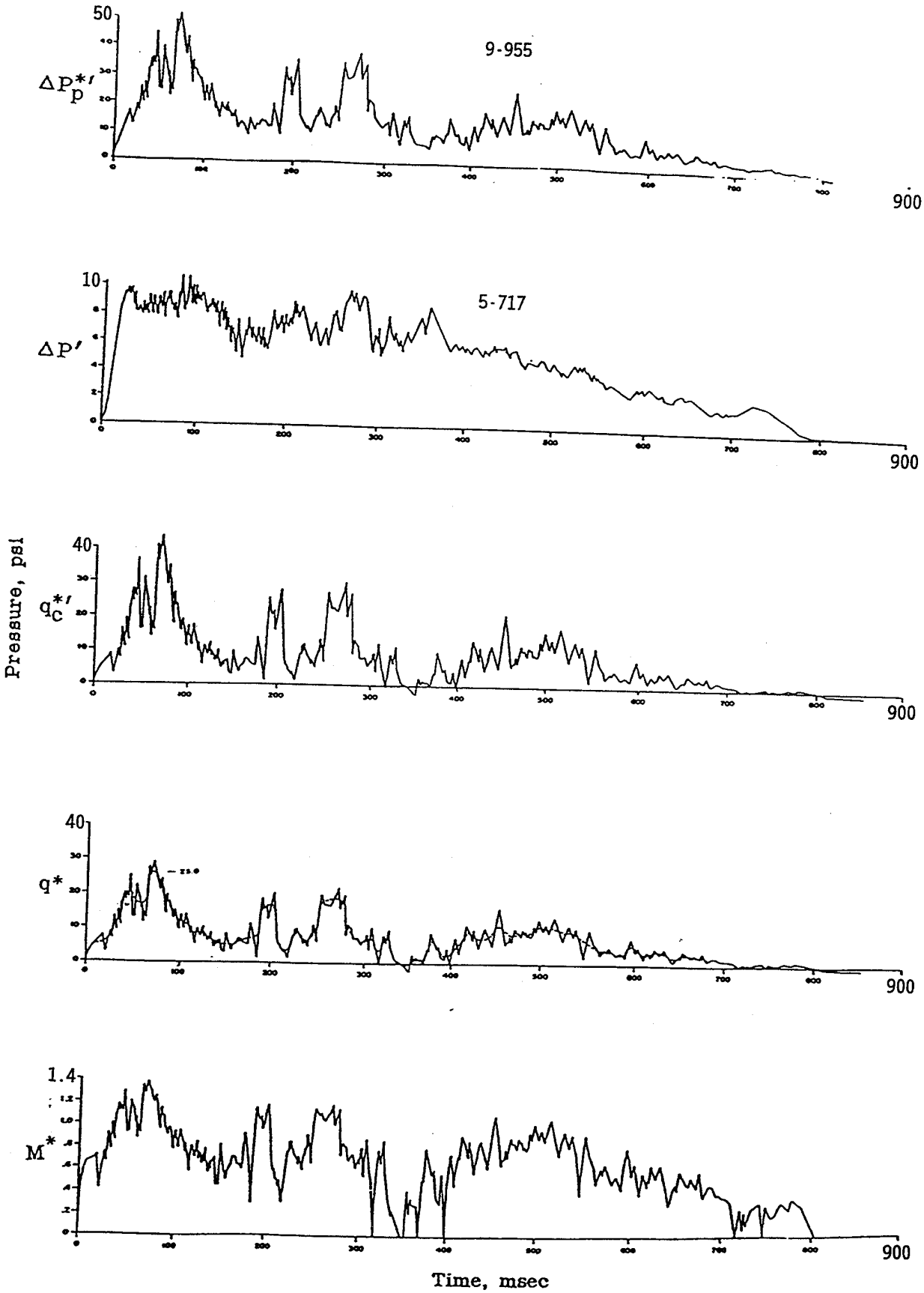

Figure C-25. Pressure and Mach number versus time, main blast line at 2500 feet. BRL standard Q-gage data, WT-1401.

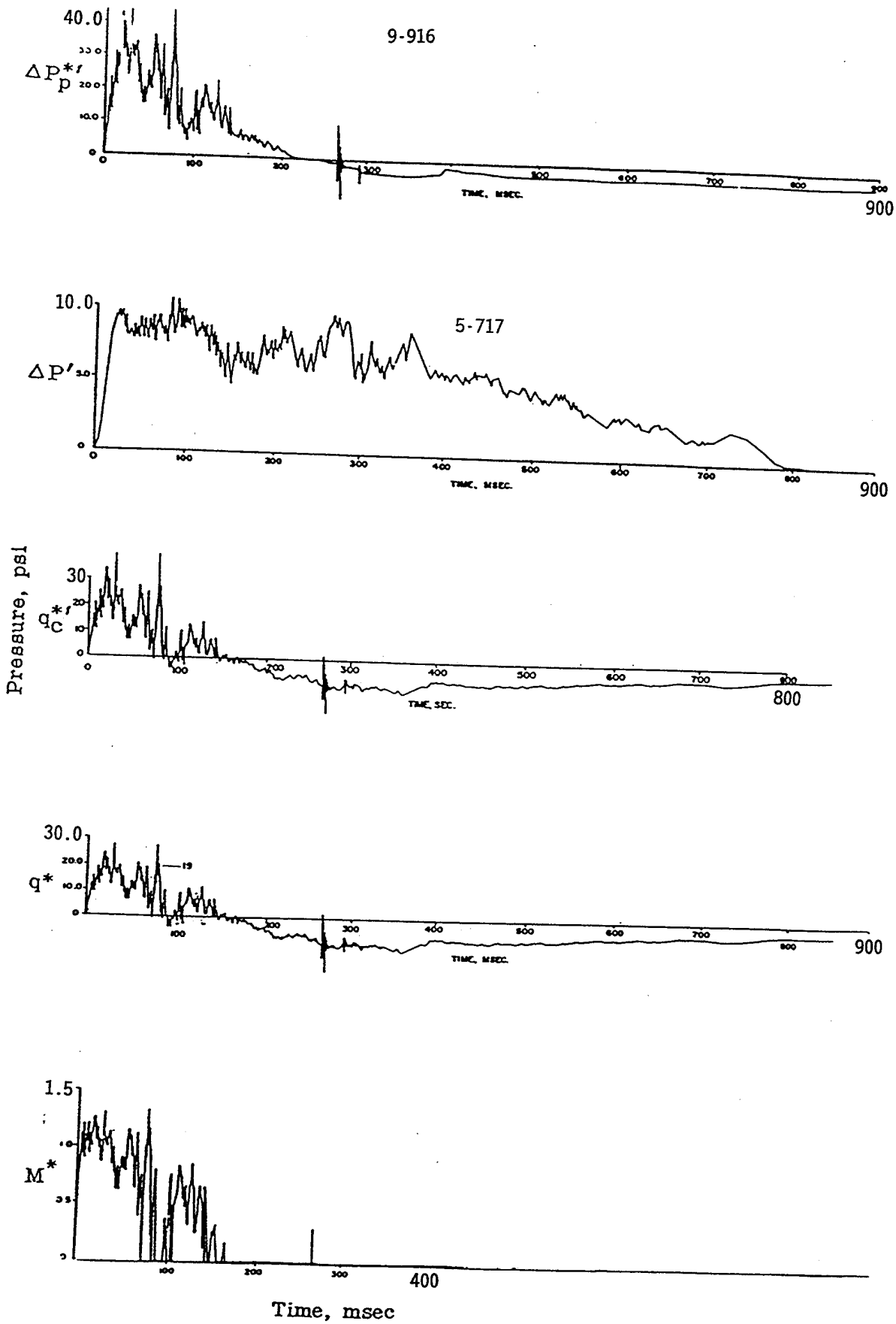

Figure C-26. Pressure and Mach number versus time, main blast line at 2500 feet. BRL new Q-gage data, WT-1401.

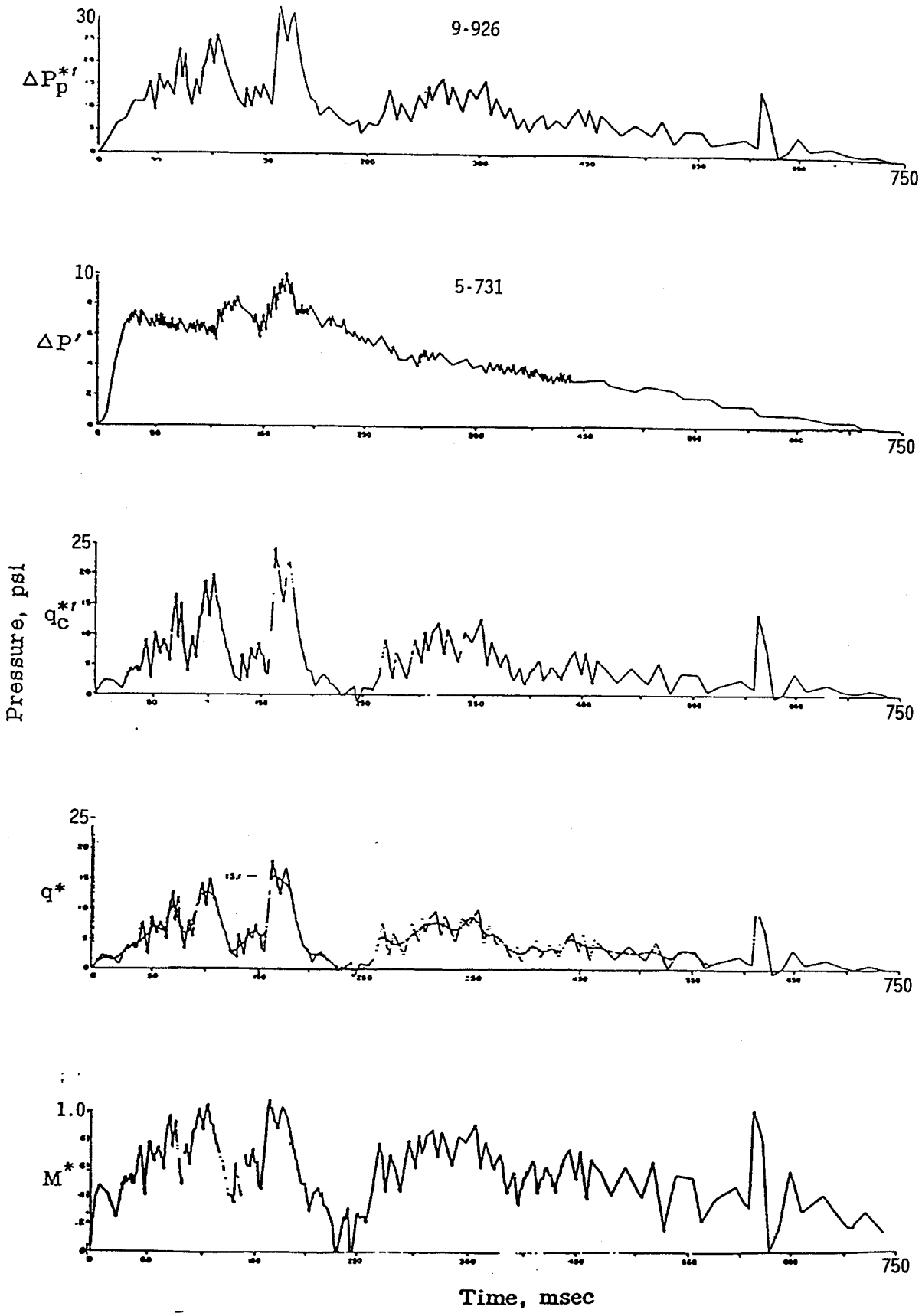

Figure C-27. Pressure and Mach number versus time, main blast line at 3000 feet. BRL standard Q-gage data, WT-1401.

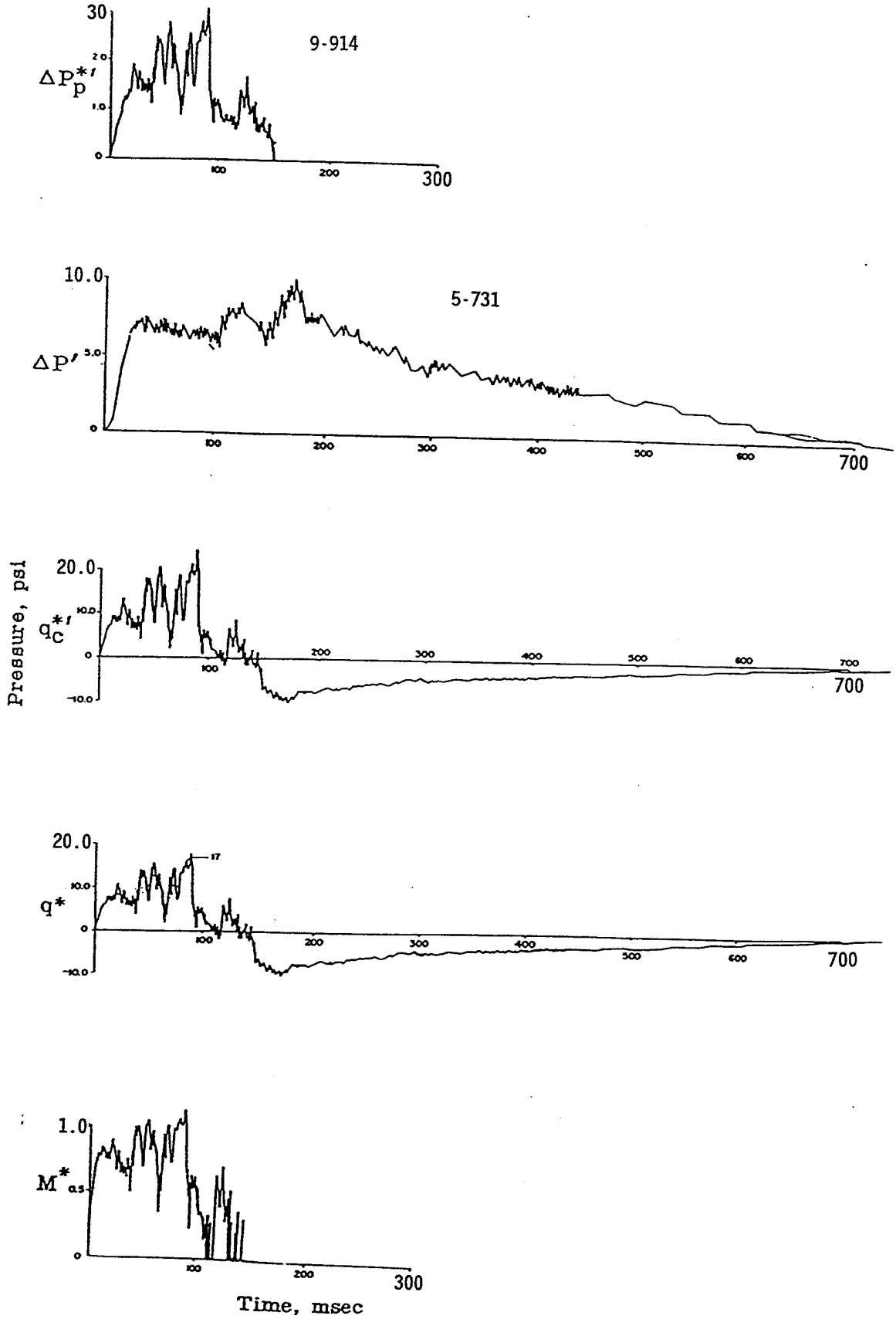

Figure C-28. Pressure and Mach number versus time, main blast line at 3000 feet. BRL new Q-gage data, WT-1401.

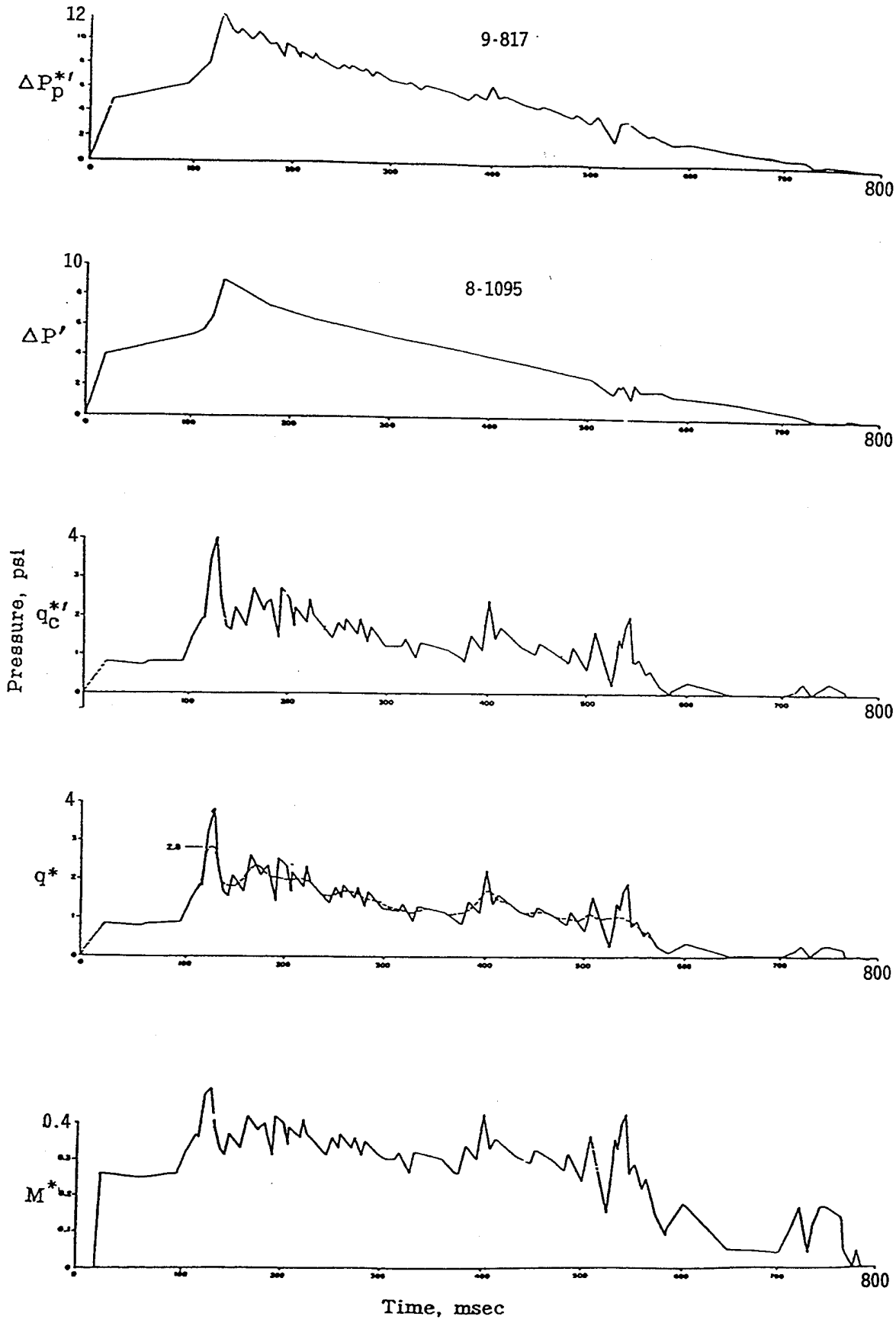

Figure C-29. Pressure and Mach number versus time, main blast line at 3500 feet. BRL standard Q-gage data, WT-1401.

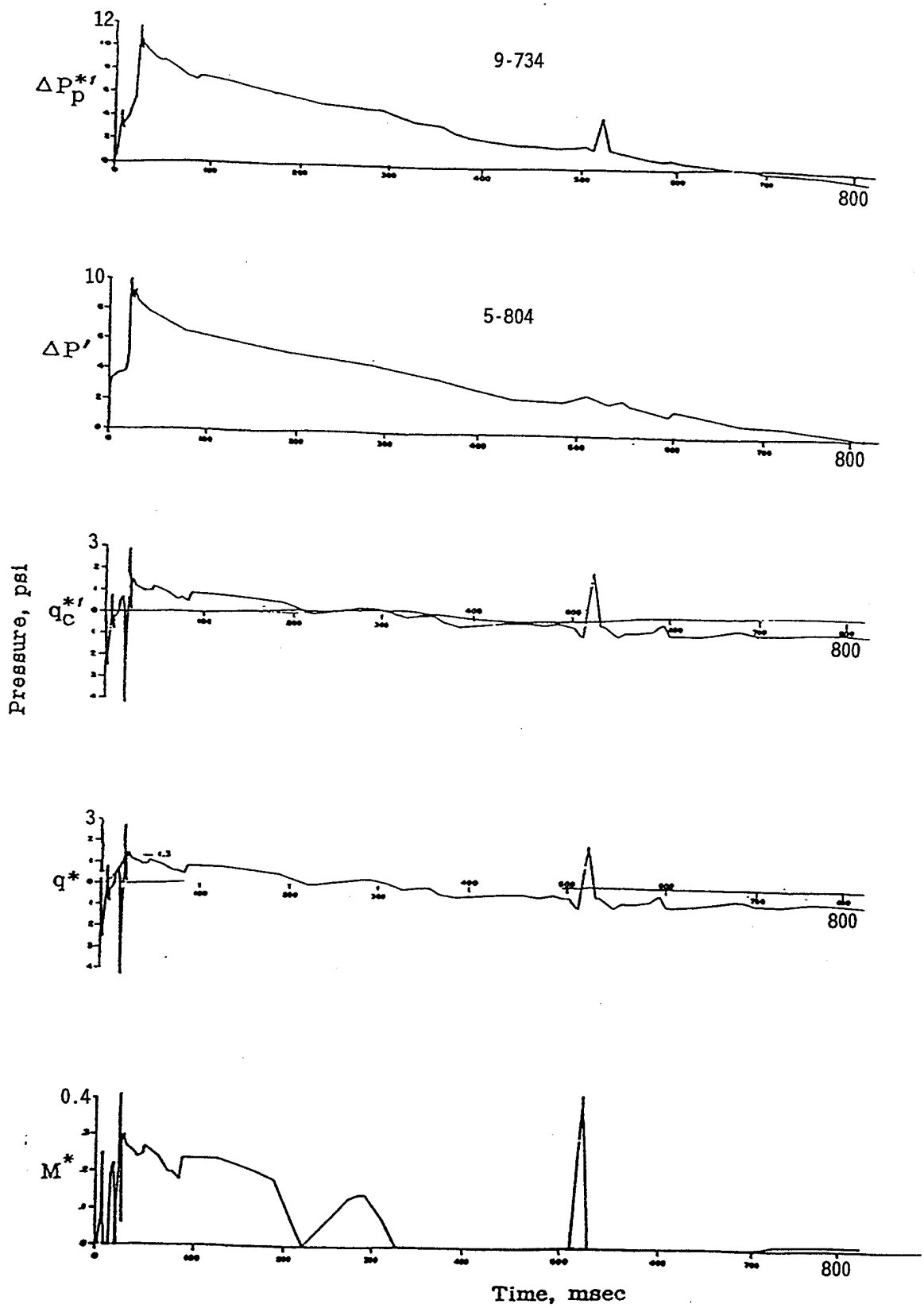

Figure C-30. Pressure and Mach number versus time, main blast line at 4000 feet. BRL standard Q-gage data, WT-1401.

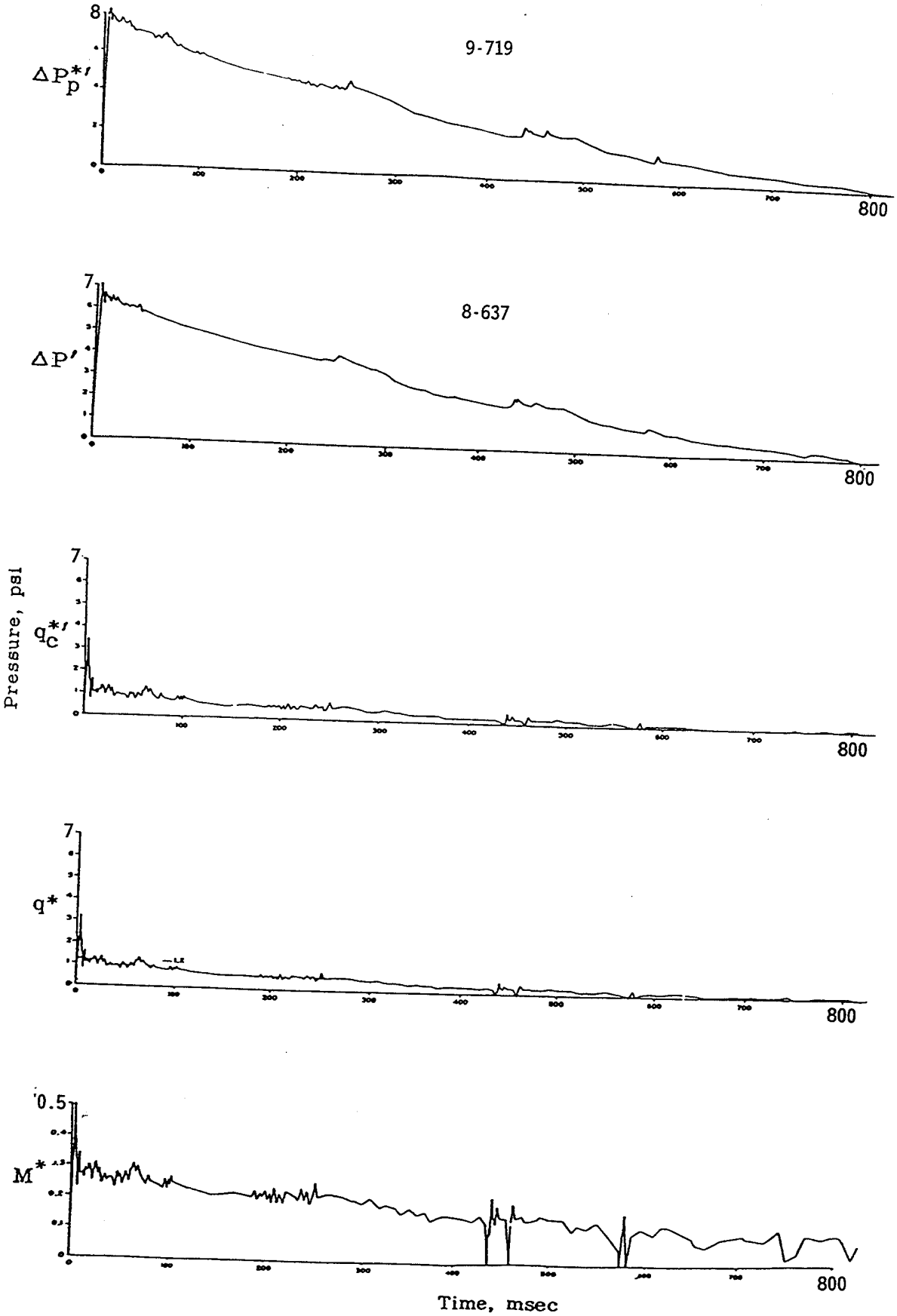

Figure C-31. Pressure and Mach number versus time, main blast line at 4500 feet. BRL standard Q-gage data, WT-1401.

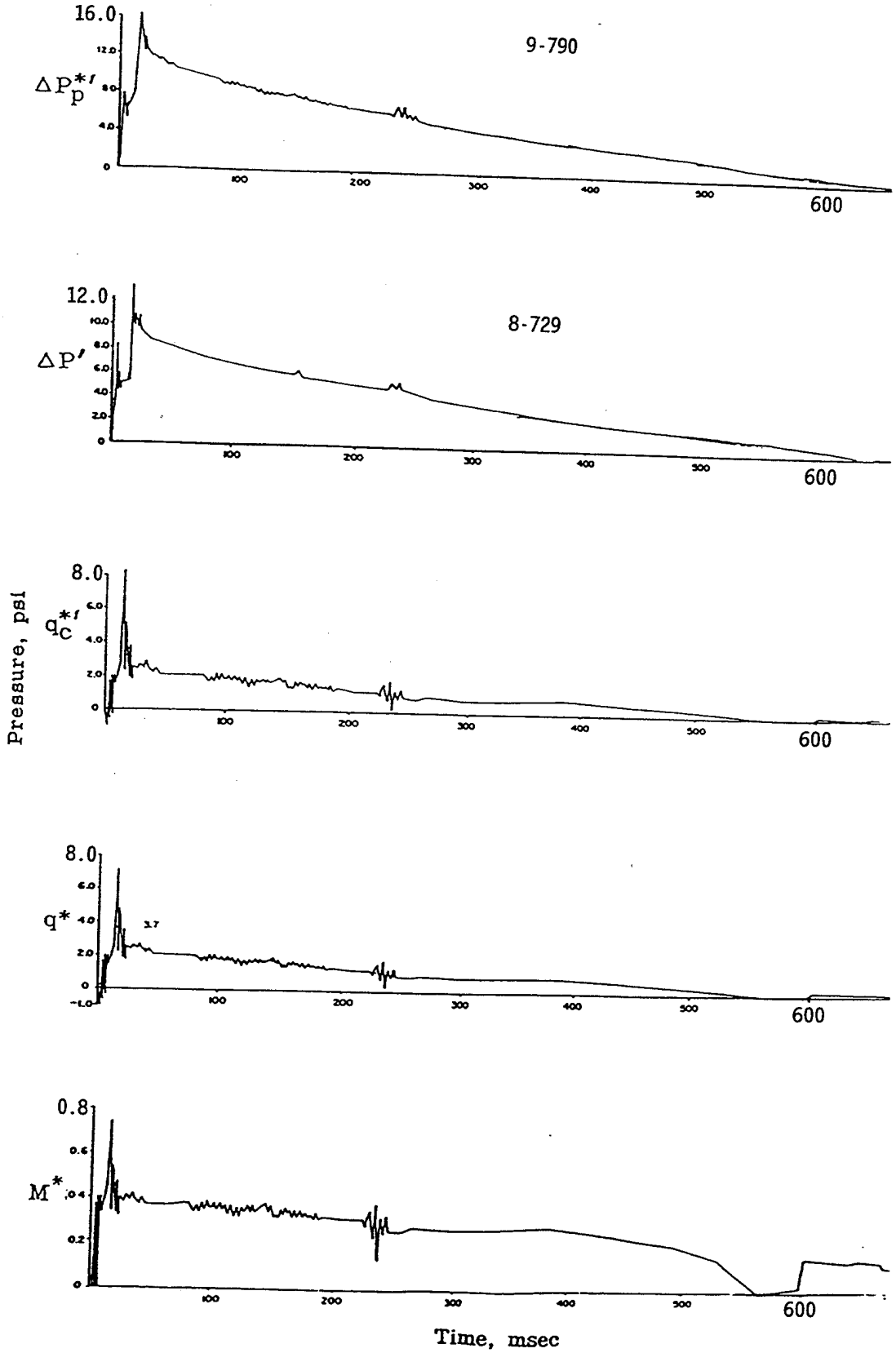

Figure C-32. Pressure and Mach number versus time, Project 3.4 at 3600 feet. BRL standard Q-gage data, WT-1401. Gage elevation of 10 feet, overpressure obtained from Q-gage as opposed to ground baffle gages.

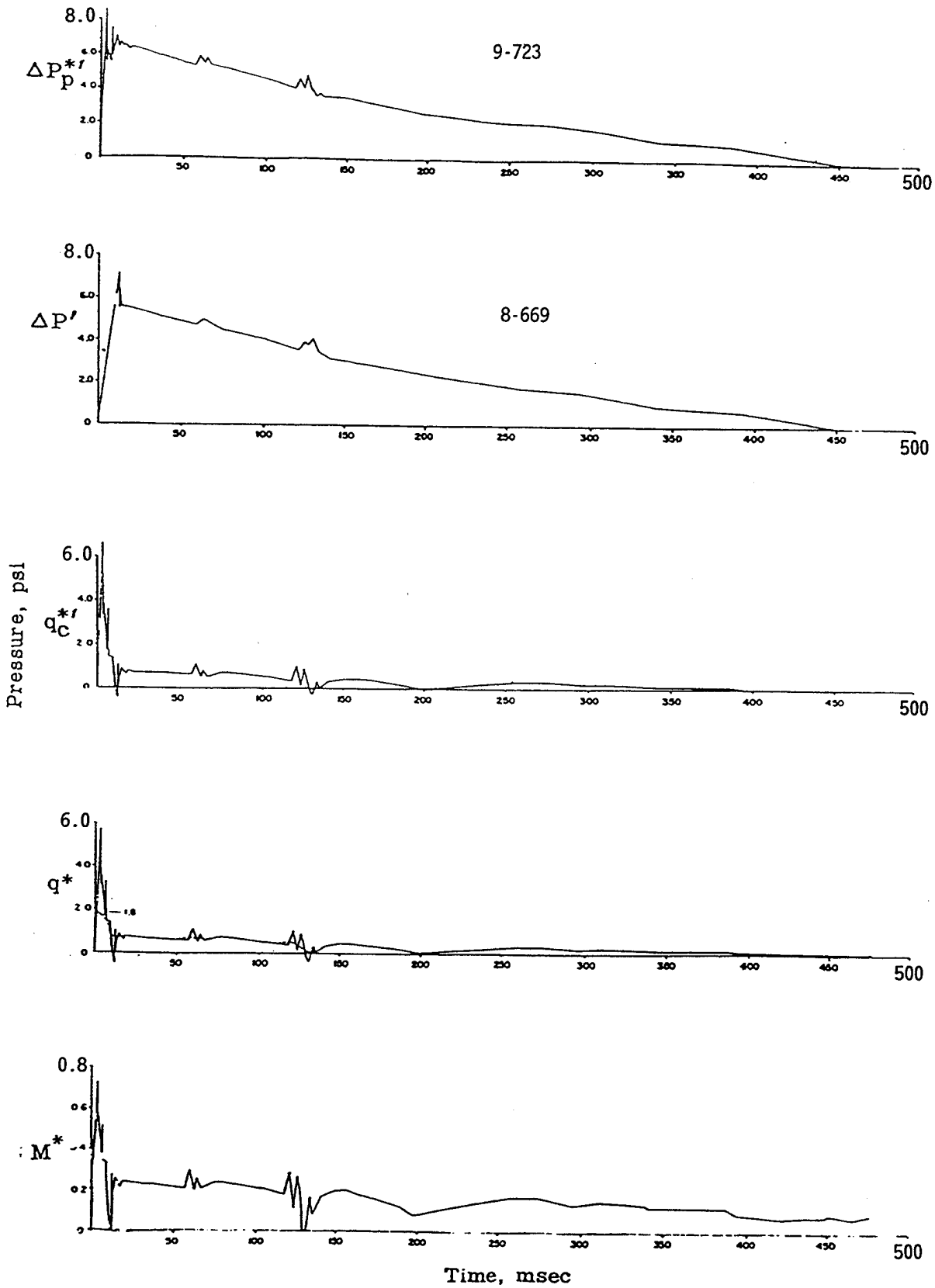

Figure C-33. Pressure and Mach number versus time, Project 3.4 at 5000 feet. BRL standard Q-gage data, WT-1401. Gage elevation of 10 feet, overpressure obtained from Q-gage as opposed to ground baffle gages.

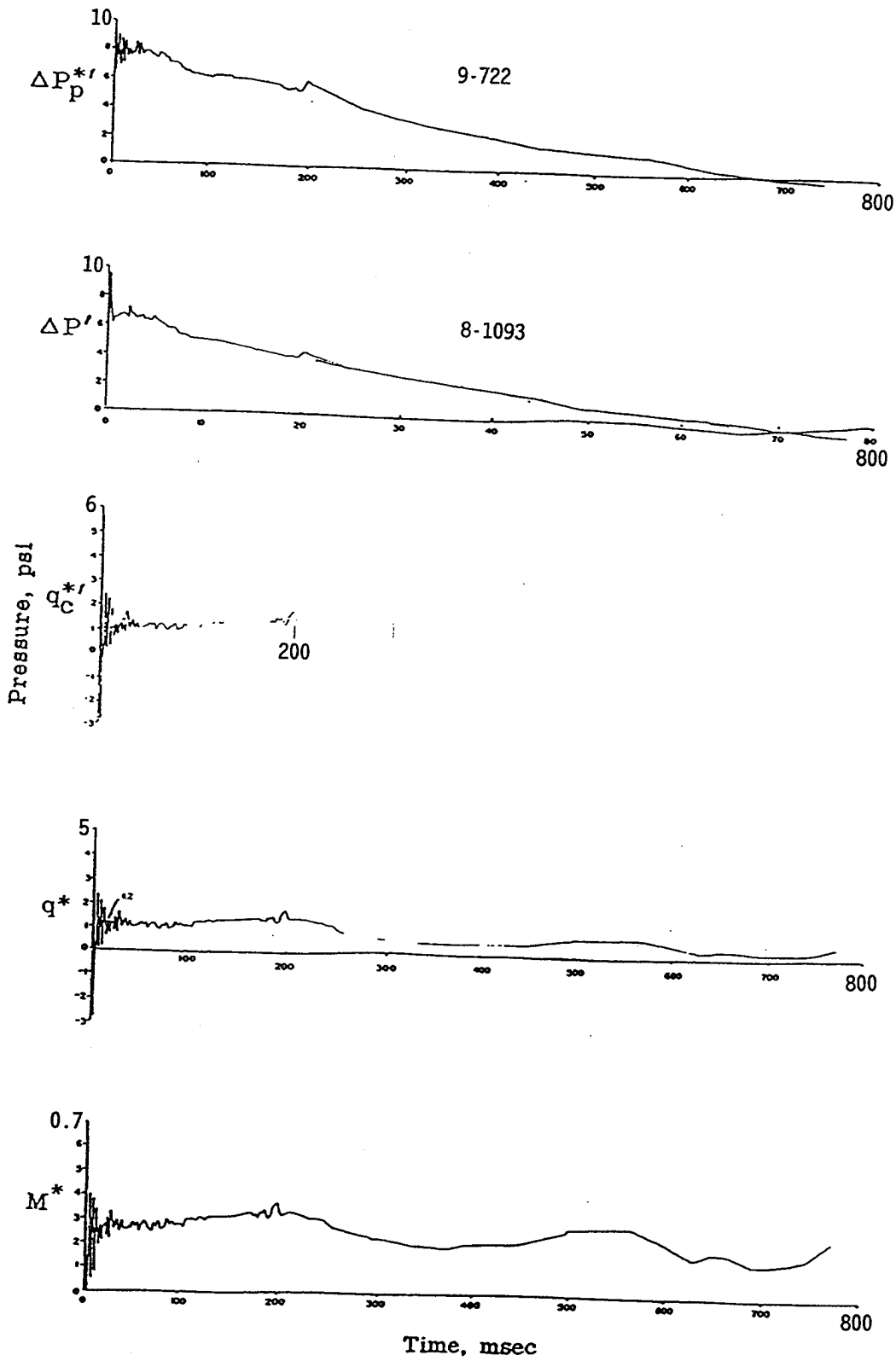

Figure C-34. Pressure and Mach number versus time, Project 3.4 at 4200 feet. BRL standard Q-gage data, WT-1401. Overpressure obtained from Q-gage as opposed to ground baffle gages.

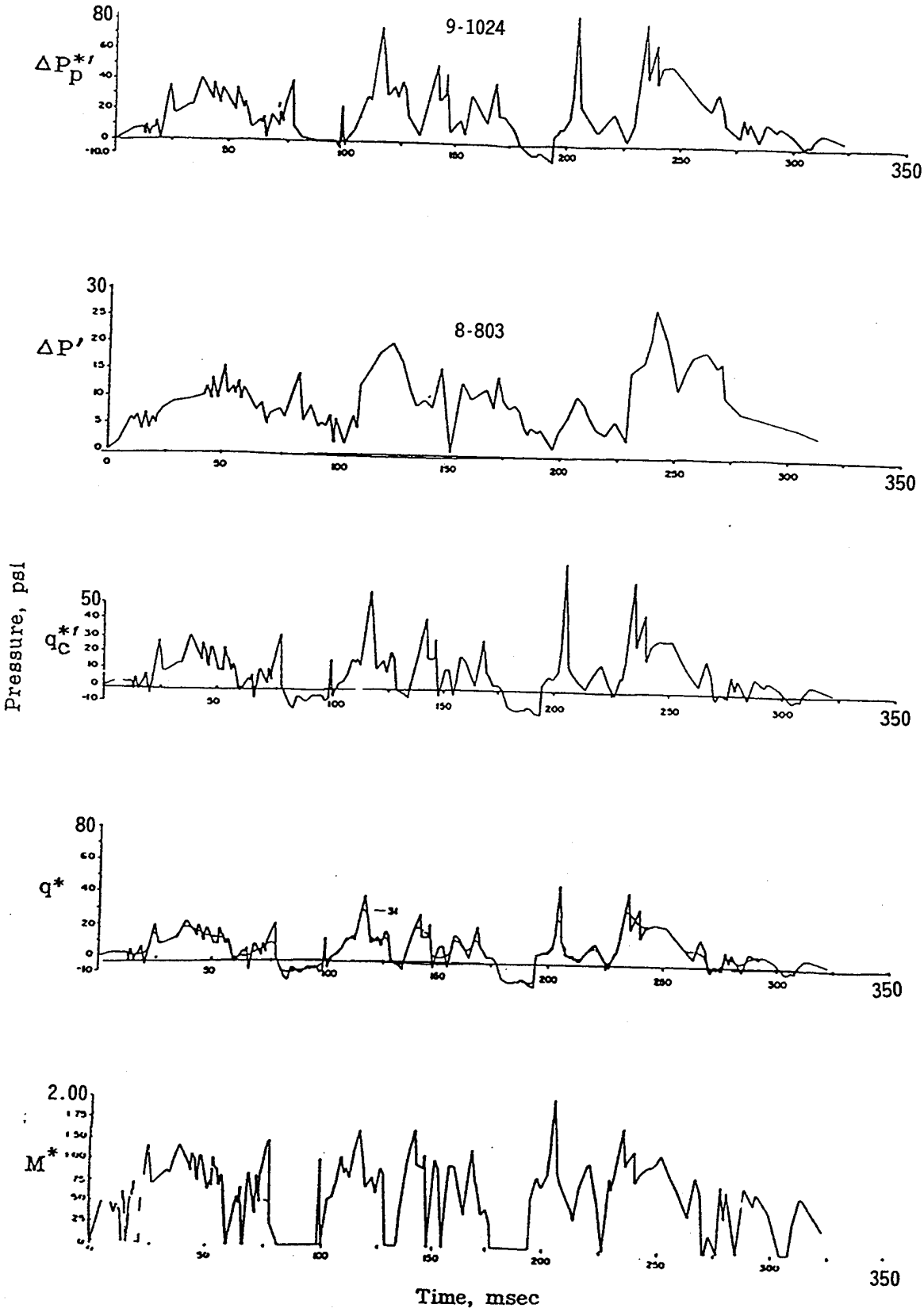

Figure C-35. Pressure and Mach number versus time, Project 4.3/33.2 at 2030 feet. BRL standard Q-gage data, WT-1401.

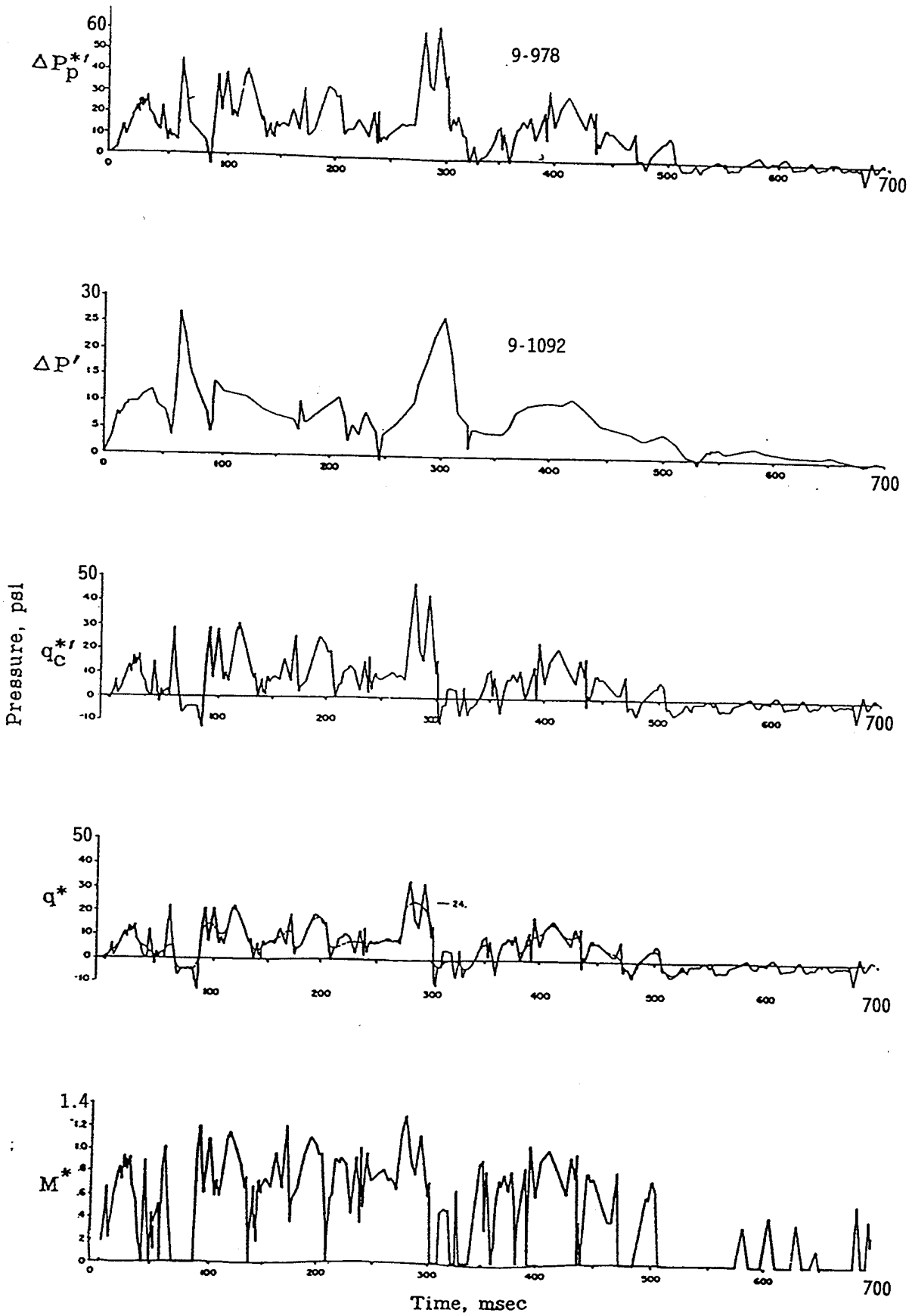

Figure C-36. Pressure and Mach number versus time, Project 4.3/33.2 at 2280 feet. BRL standard Q-gage data, WT-1401.

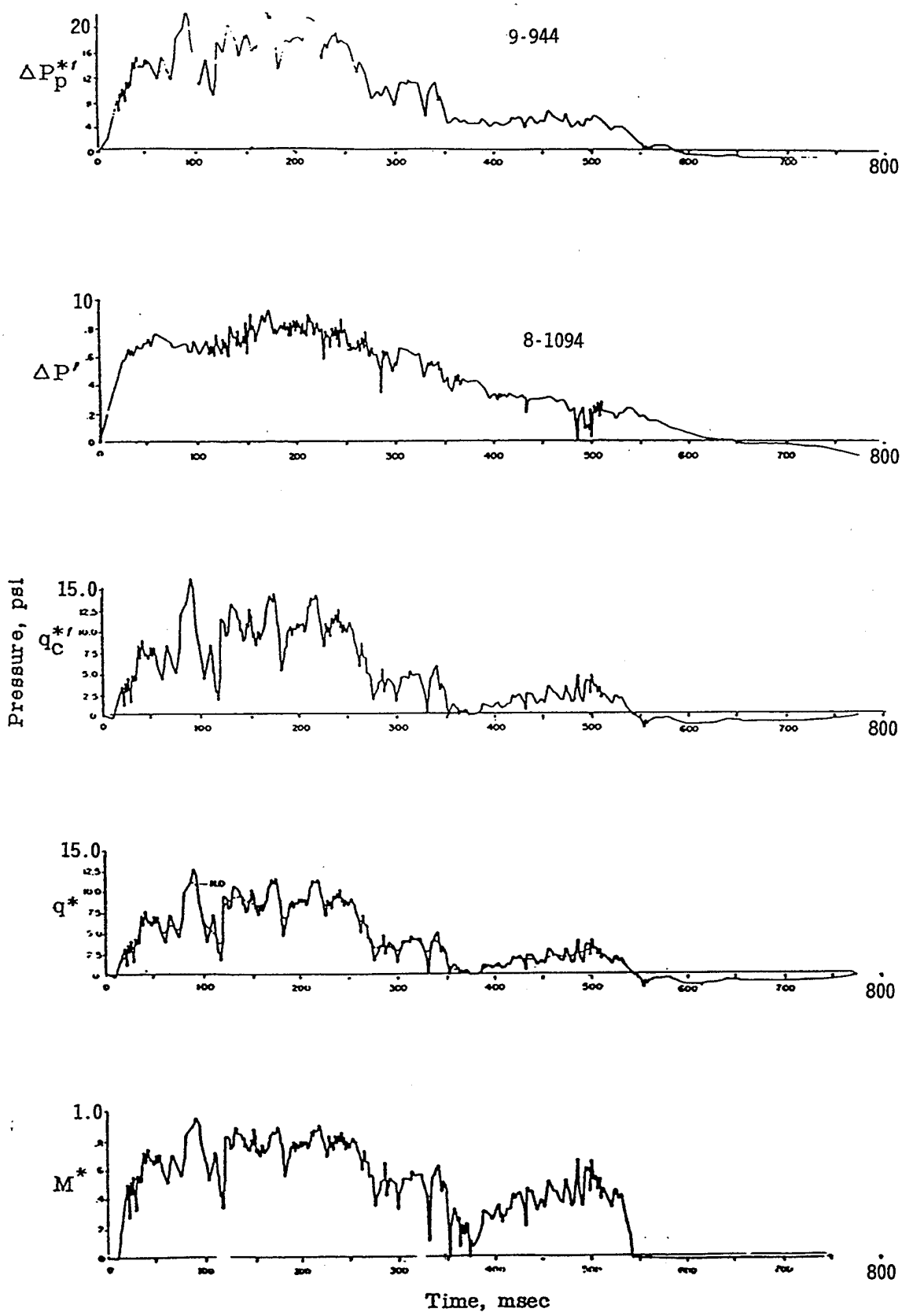

Figure C-37. Pressure and Mach number versus time, Project 4.3/33.2 at 2730 feet. BRL standard Q-gage data, WT-1401.

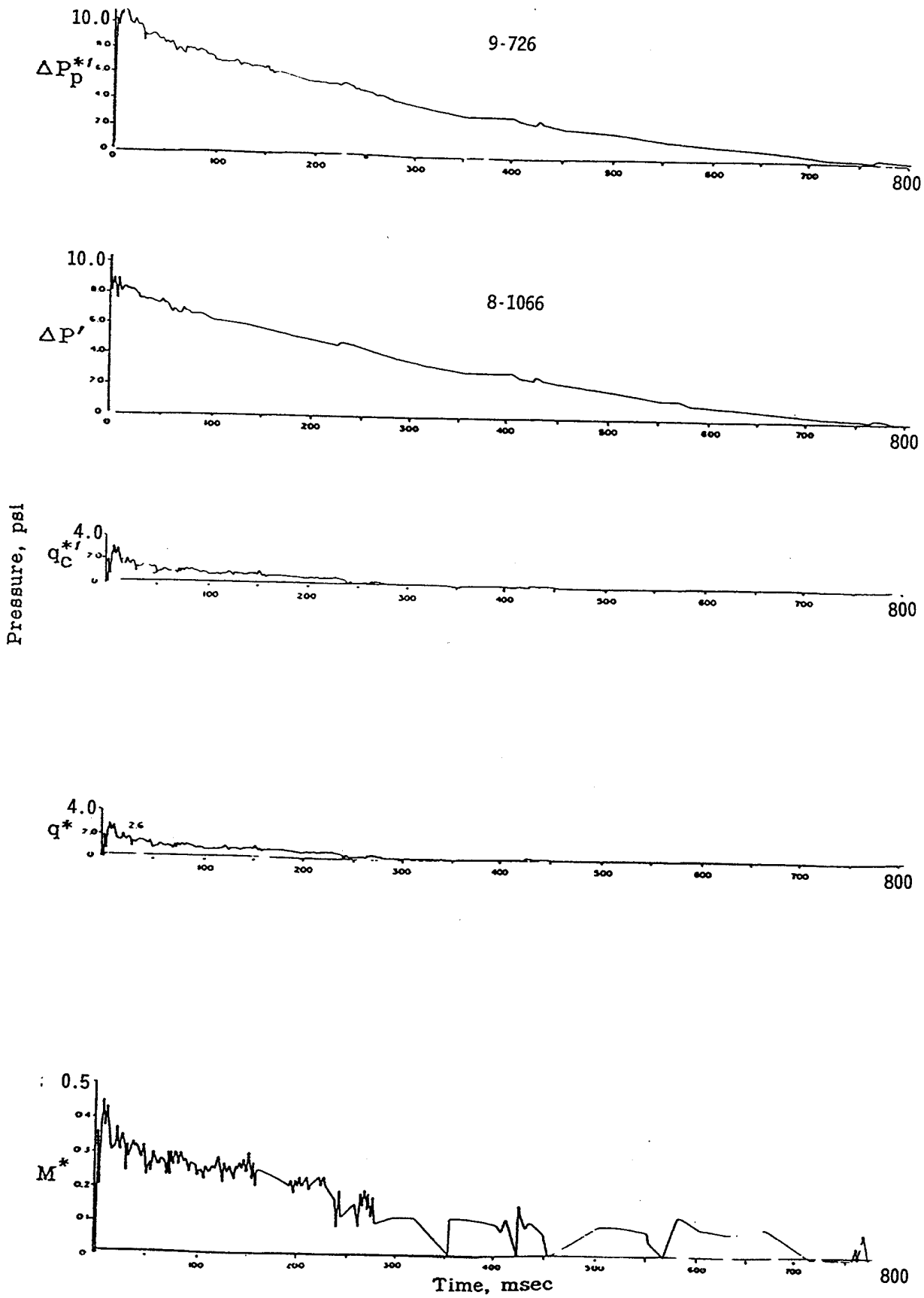

Figure C-38. Pressure and Mach number versus time, Project 4.3/33.2 at 3930 feet. BRL standard Q-gage data, WT-1401.

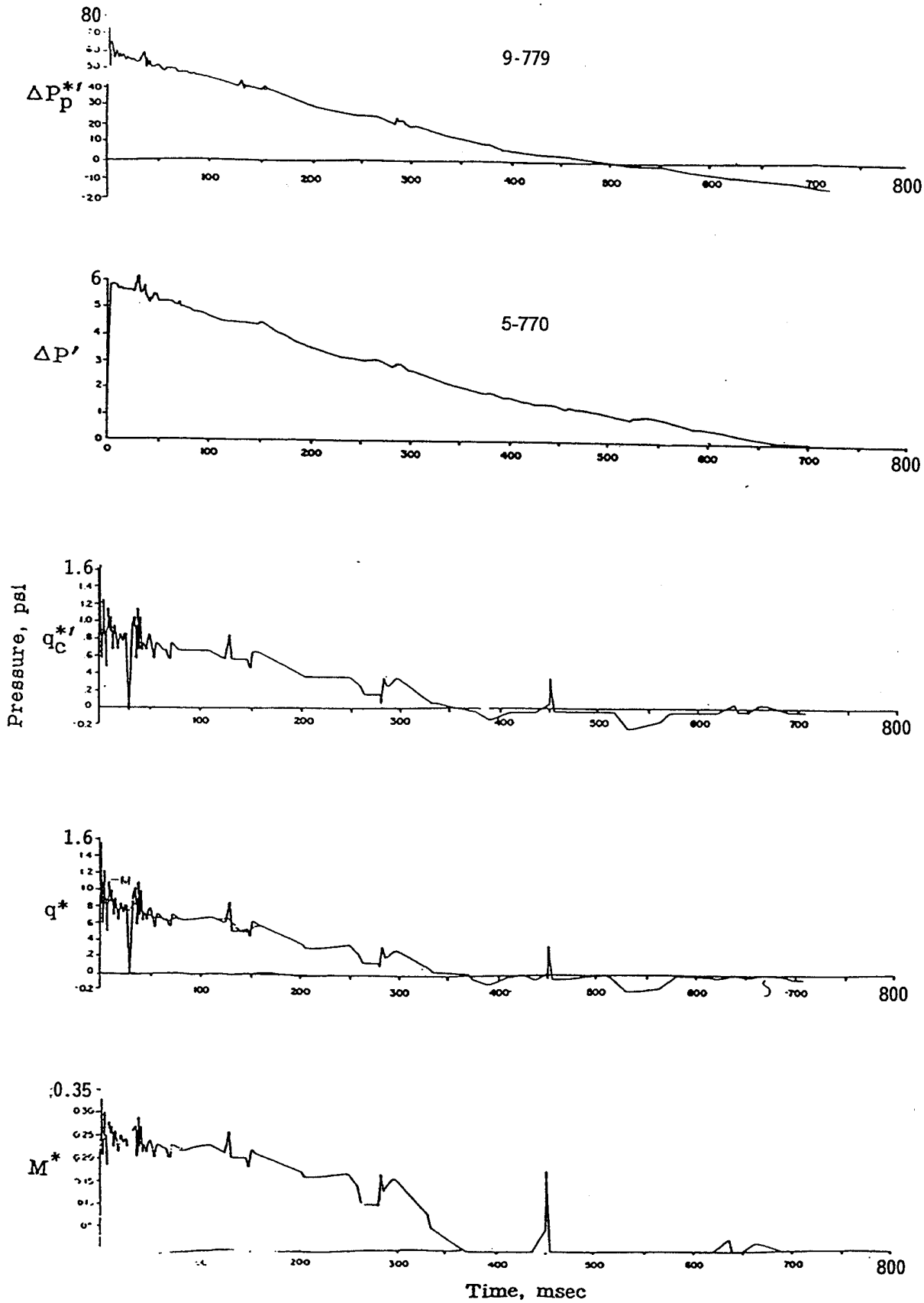

Figure C-39. Pressure and Mach number versus time, Project 4.3/33.2 at 4770 feet. BRL standard Q-gage data, WT-1401.

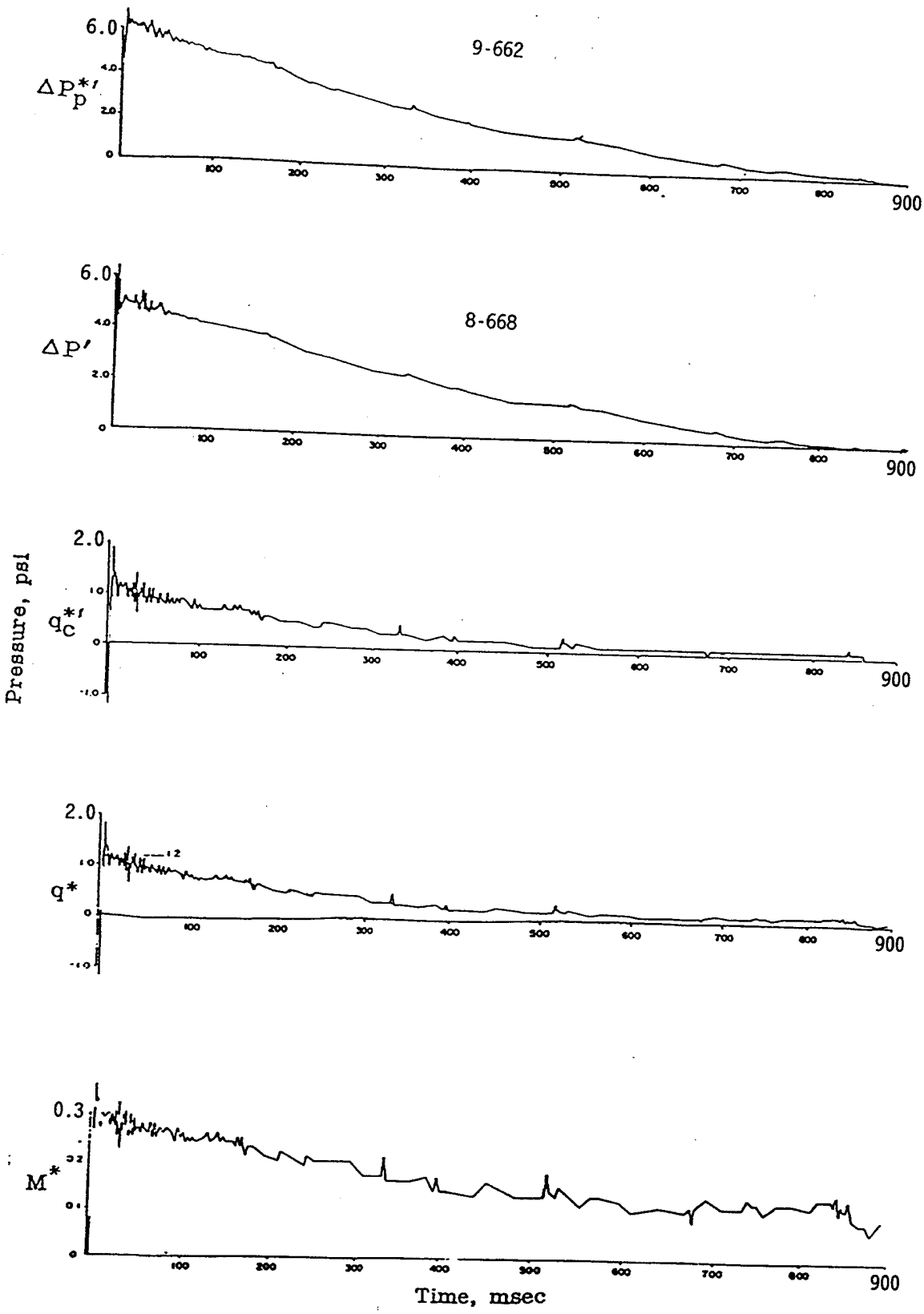

Figure C-40. Pressure and Mach number versus time, Project 4.3/33.2 at 5320 feet. BRL standard Q-gage data, WT-1401. Overpressure obtained from Q-gage as opposed to ground baffle gages.

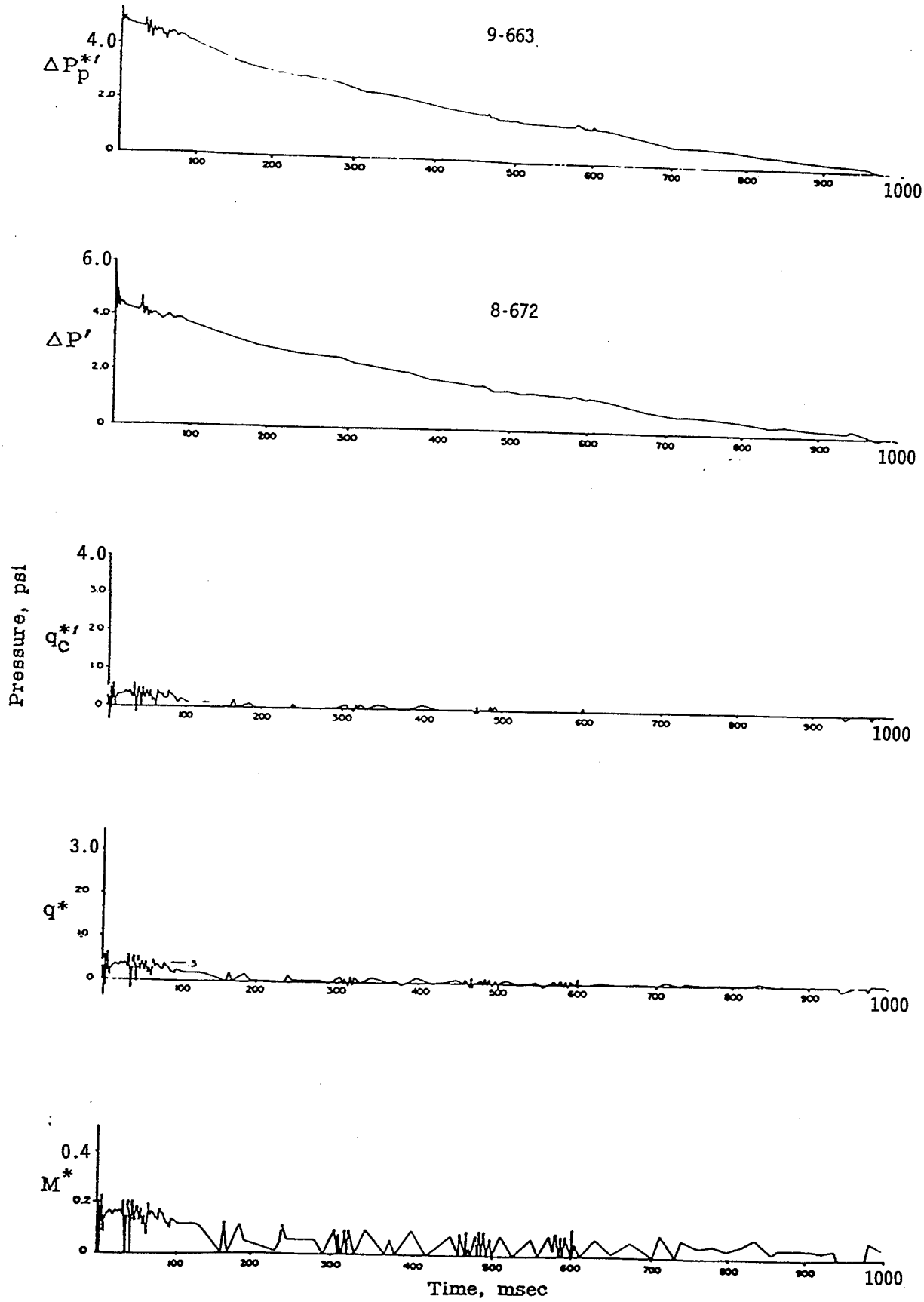

Figure C-41. Pressure and Mach number versus time, Project 4.3/33.2 at 6120 feet. BRL standard Q-gage data, WT-1401. Overpressure obtained from Q-gage as opposed to ground baffle gages

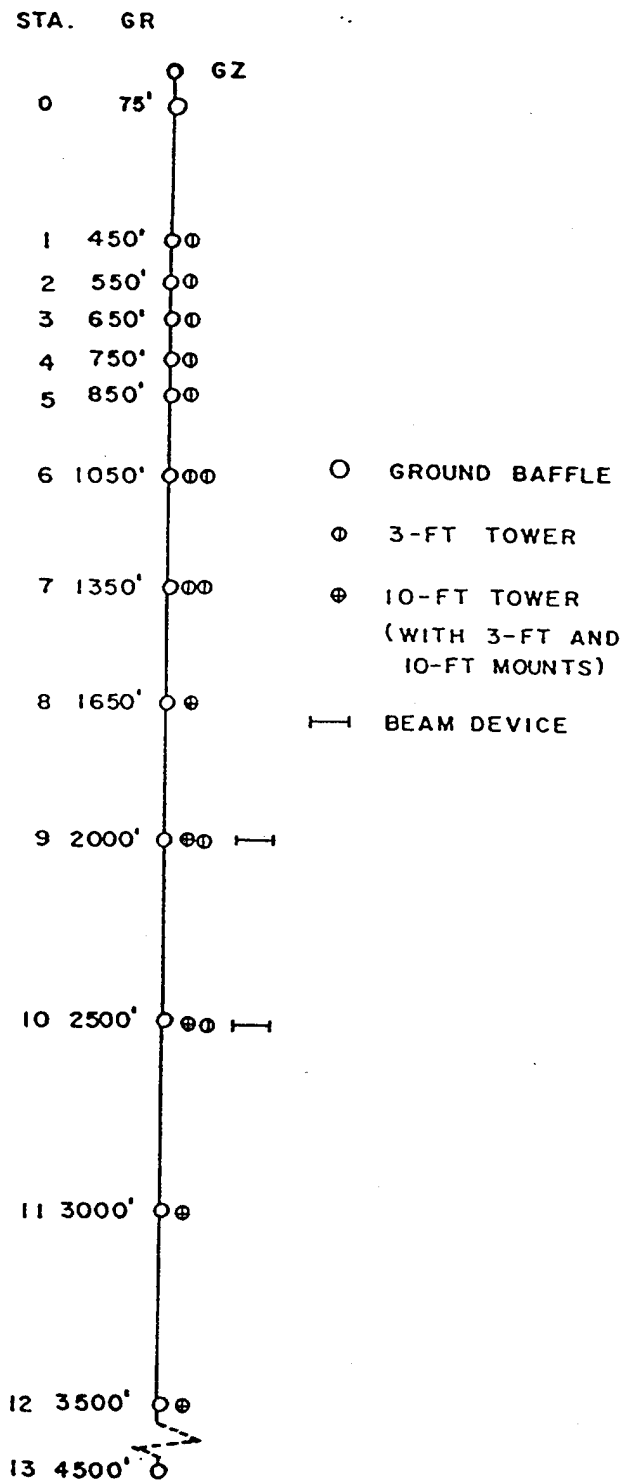

Figure C-42. Main blast line gage layout for Project 1.3, SRI, WT-1403.

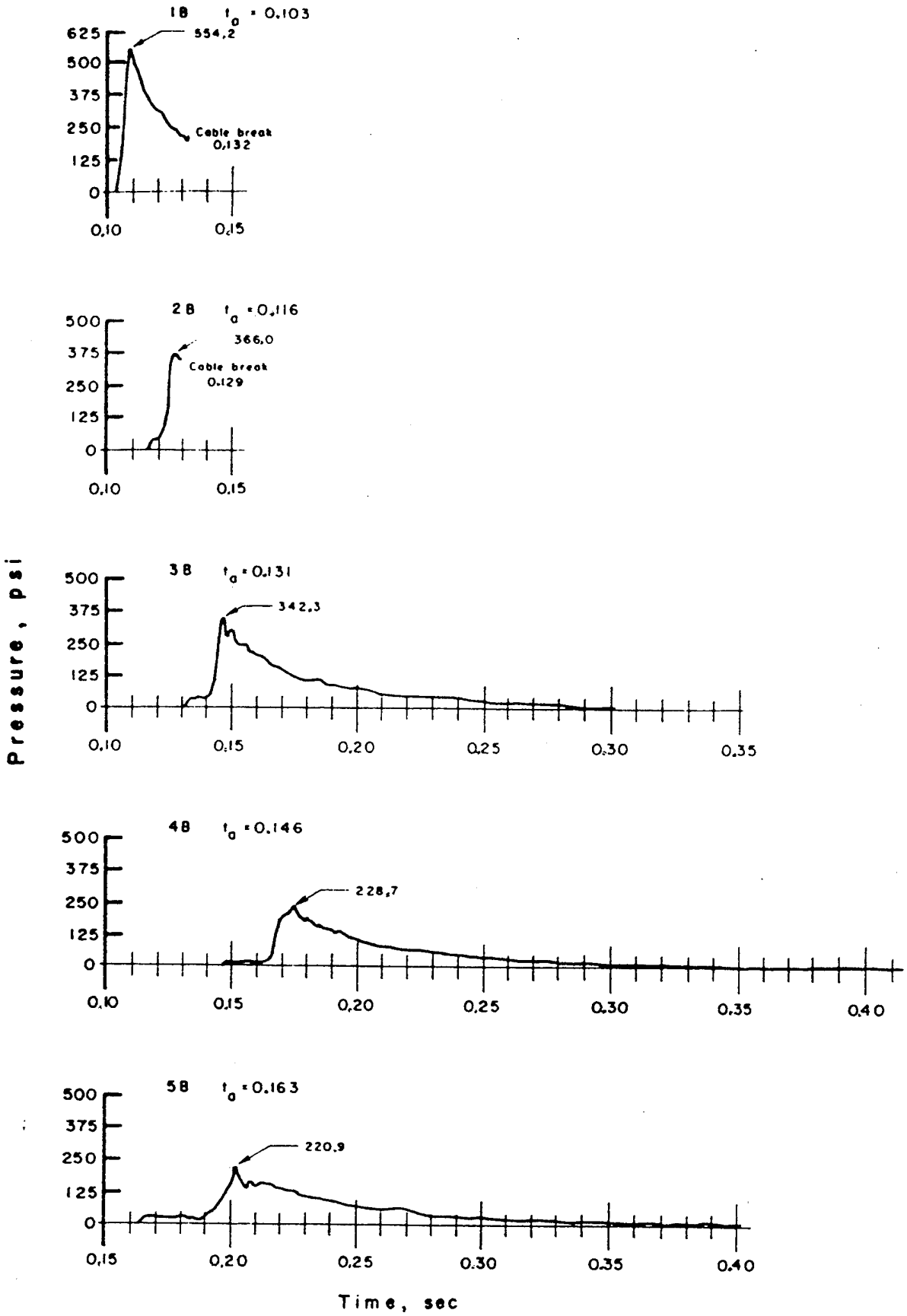

Figure C-43. Surface-level overpressure versus time from Stations 1 B to 5 B, SRI gage data, WT-1403.

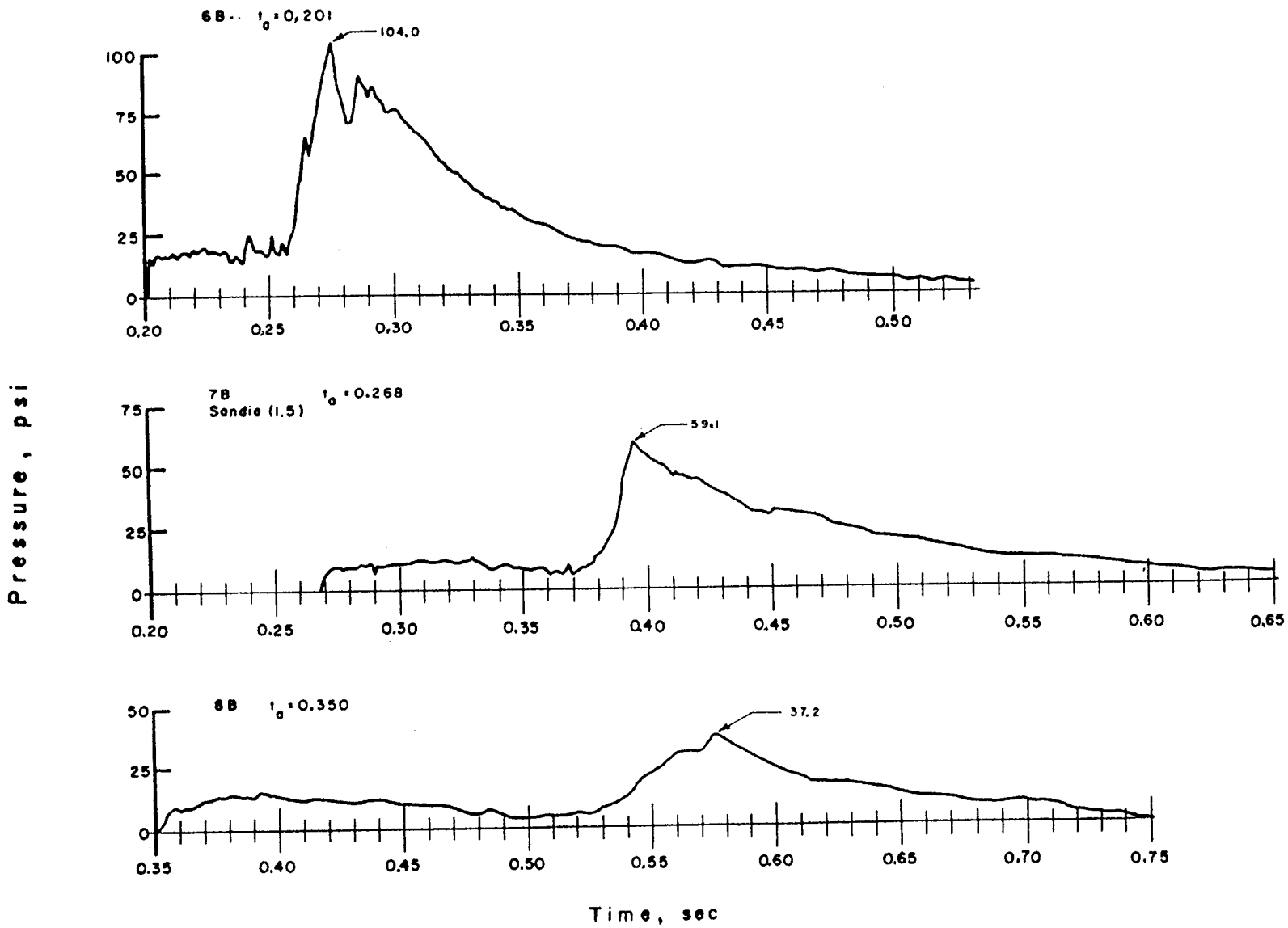

Figure C-44. Surface-level overpressure versus time from Stations 6 B through 8 B, SRI gage data, WT-1403.

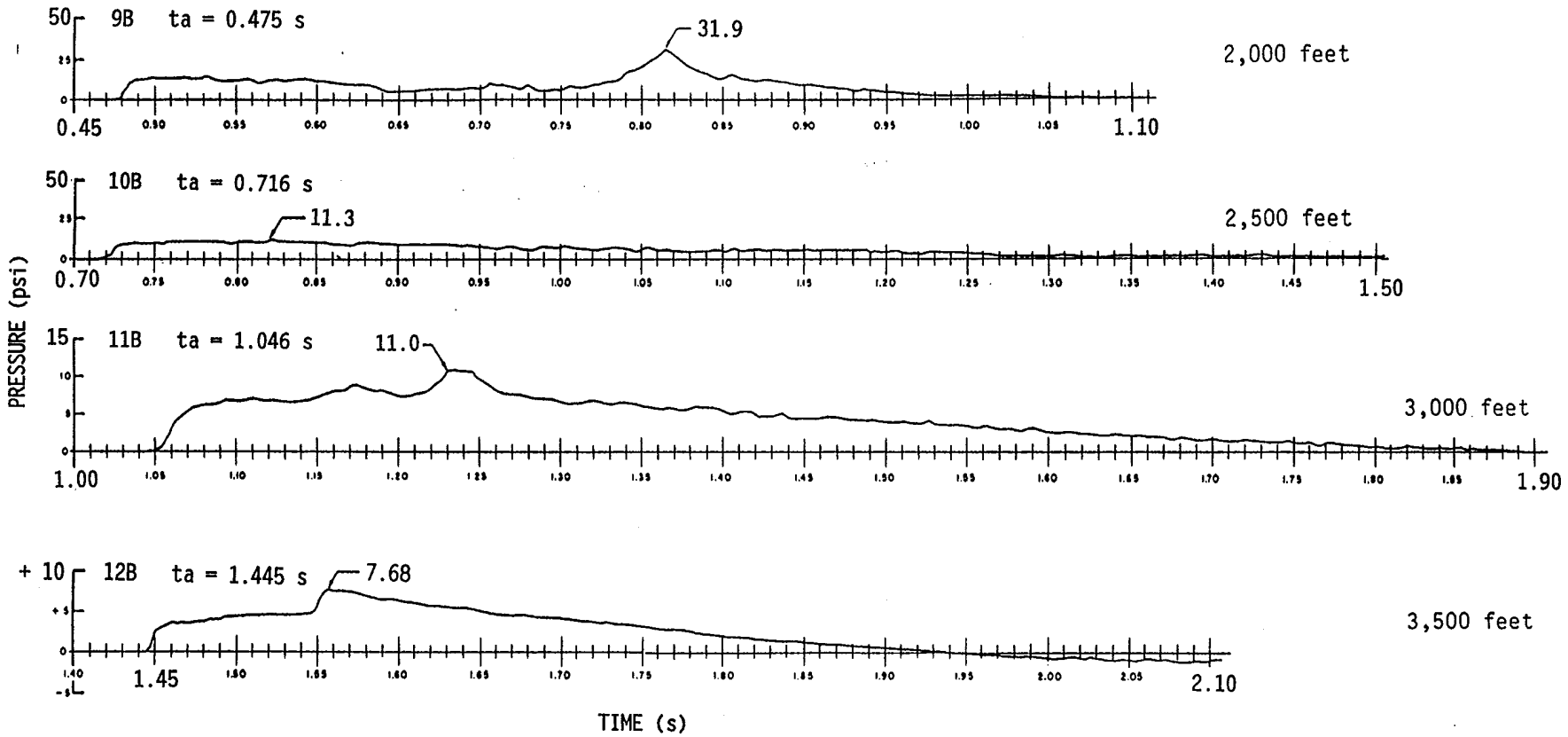

13B No Record

Figure C-45. Surface-level overpressure versus time from Stations 9 B through 12 B, SRI gage data, WT-1403.

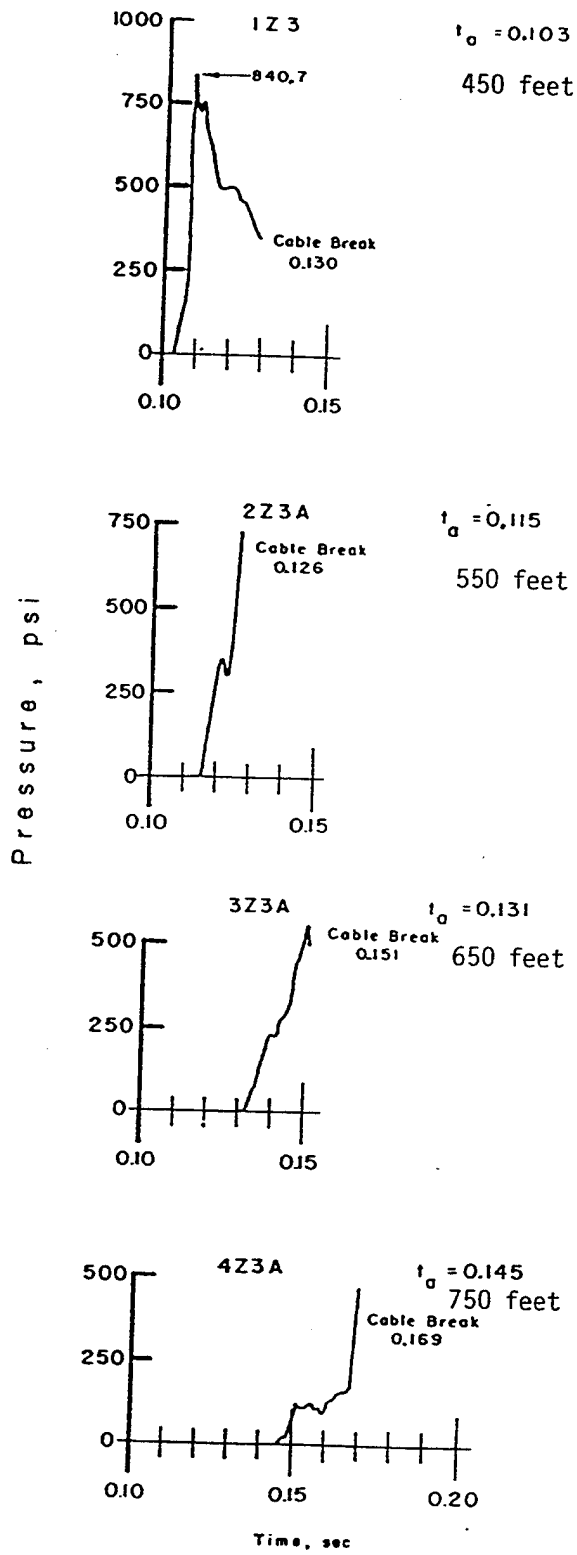

Figure C-46. Total-head pressure versus time, 3-foot level, Stations 1 to 4, SRI Z-gage data, WT-1403.

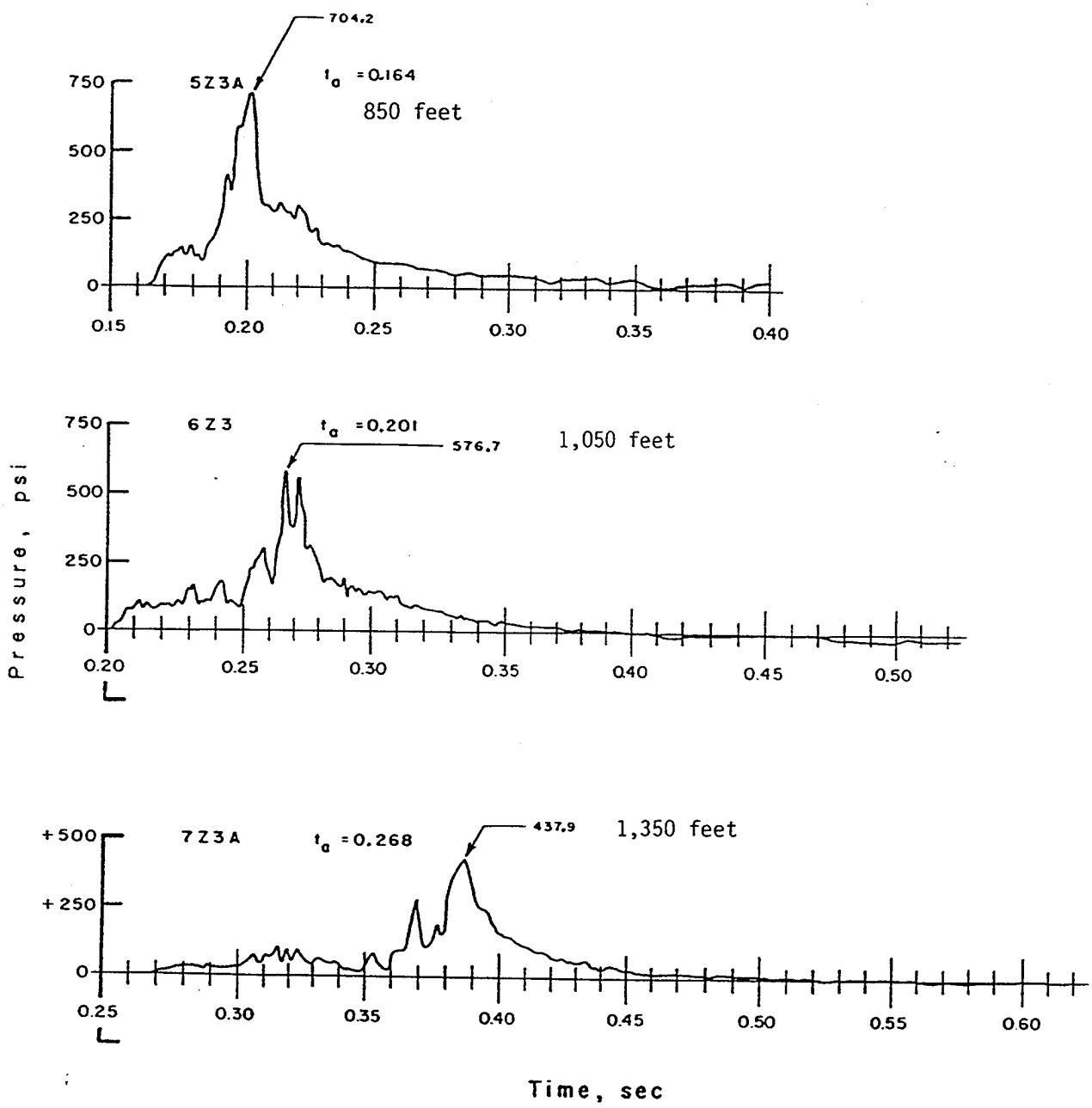

Figure C-47. Total-head pressure versus time, 3-foot level, Stations 5 t0 7, SRI Z-gage data, WT-1403.

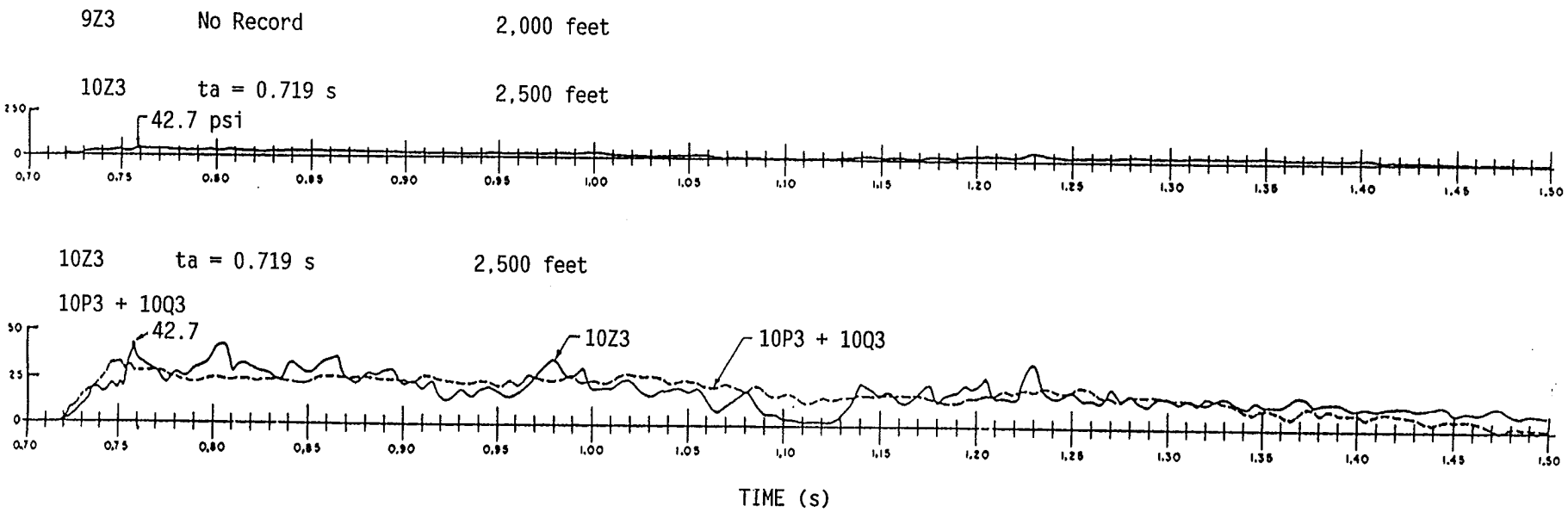

Figure C-48. Total-head pressure versus time, 3-foot level, Stations 9 and 10, SRI Z-gage data, WT-1403.

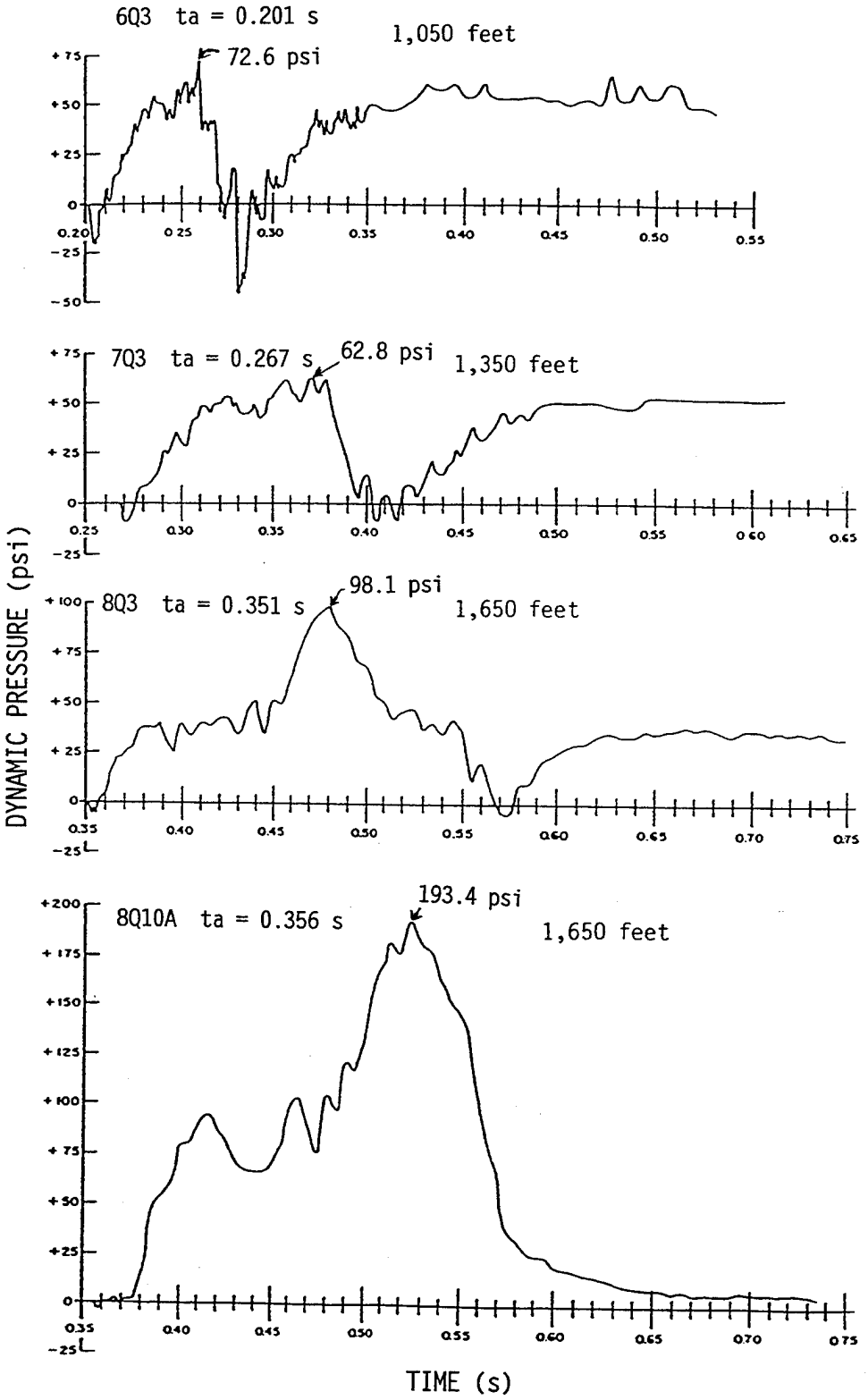

Figure C-49. Dynamic pressure versus time, 3- and 10-foot levels, Stations 6 to 8, SRI data, WT-1403.

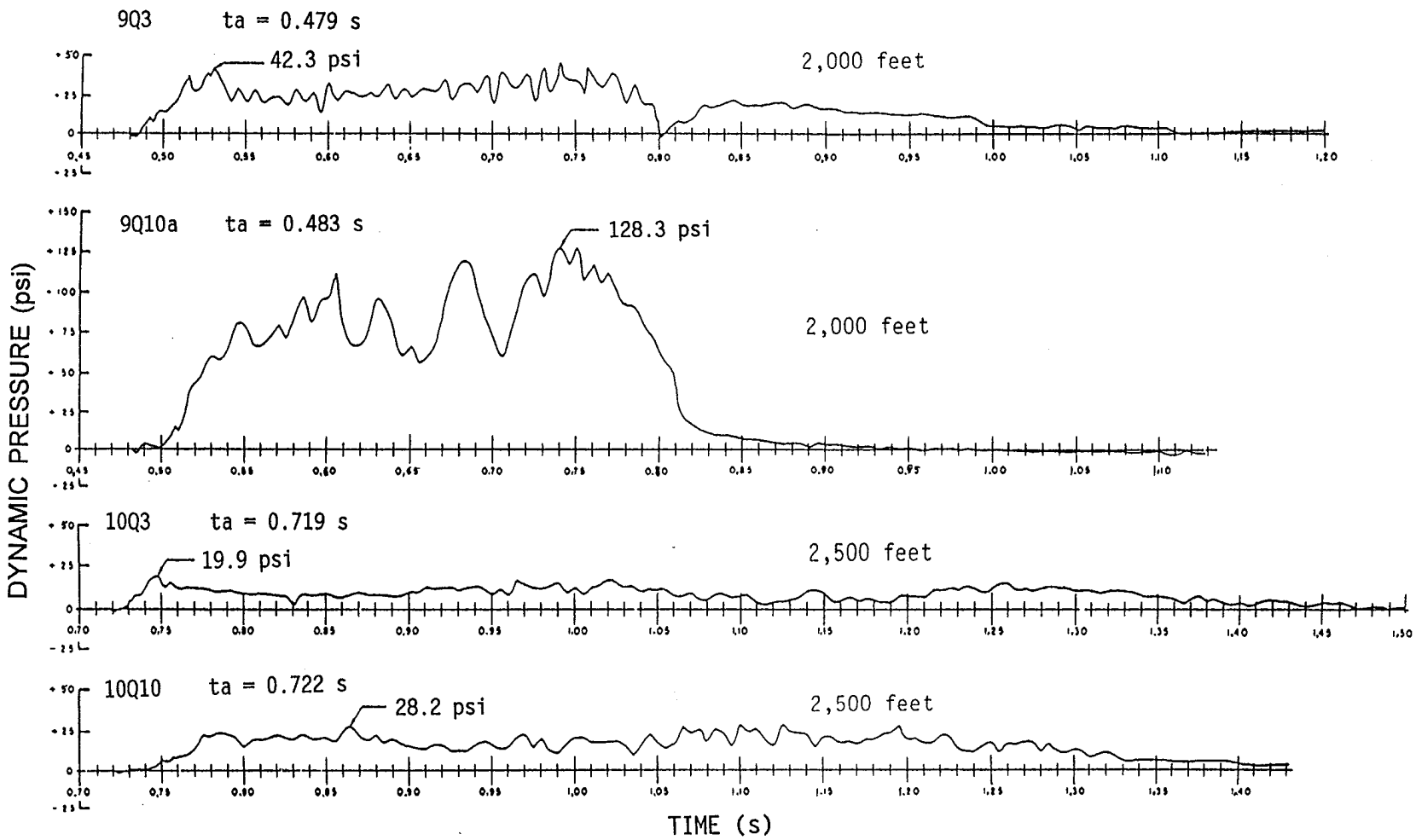

Figure C-50. Dynamic pressure versus time, 3- and 10-foot levels, Stations 9 and 10, SRI data, WT-1403.

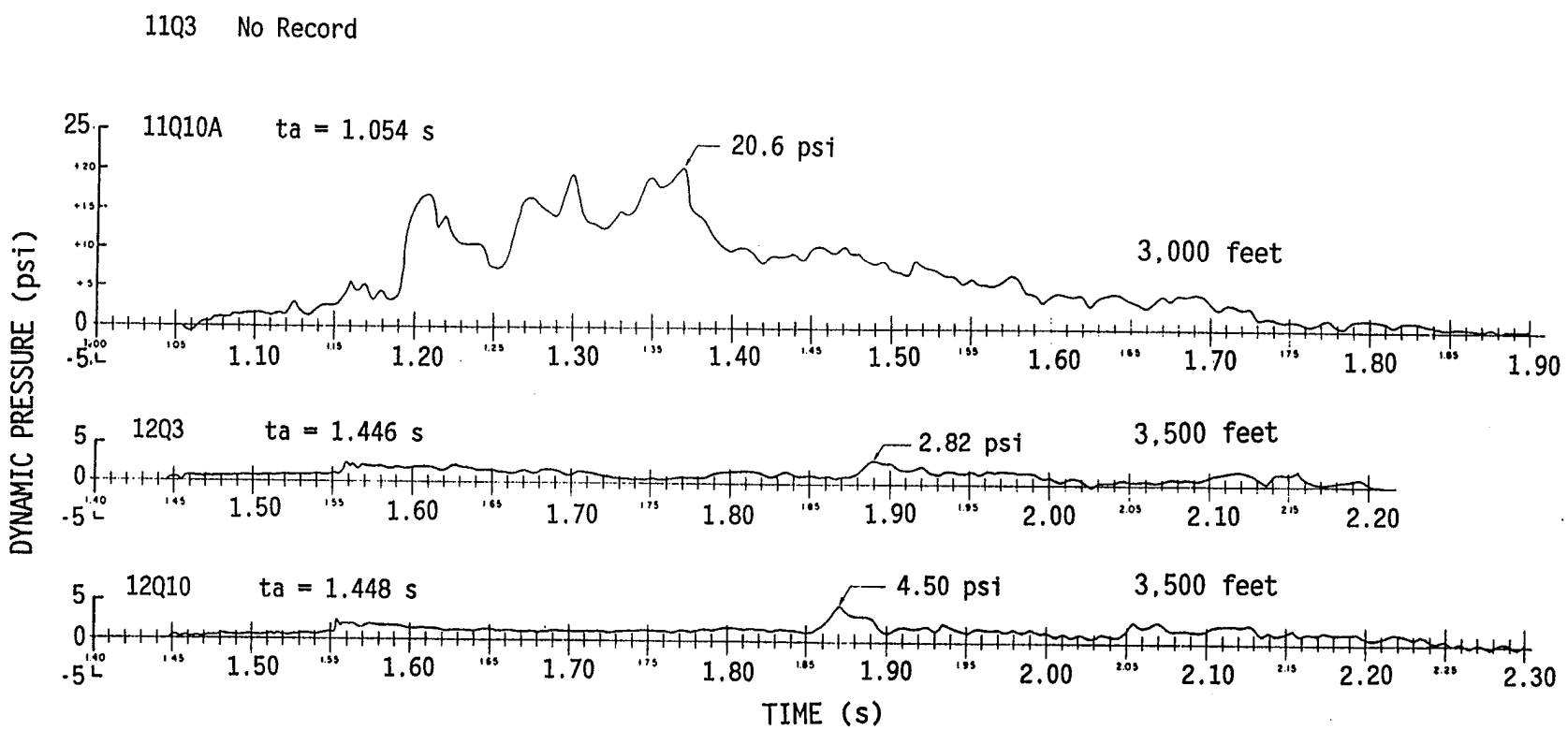

Figure C-51. Dynamic pressure versus time, 3- and 10-foot levels, Stations 11 and 12, SRI data, WT-1403.

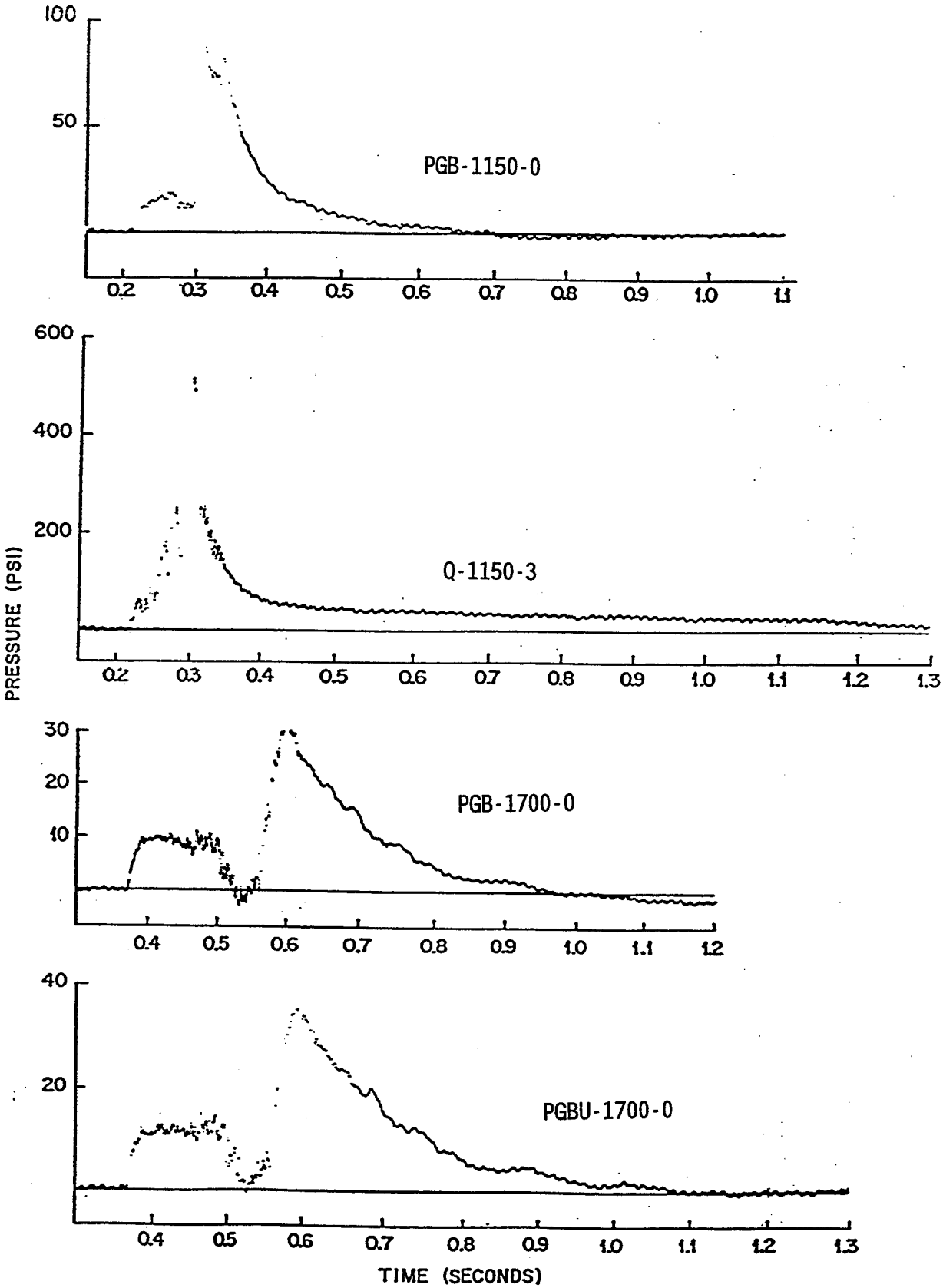

Figure C-52. Incident overpressure gage records, Sandia Corporation.

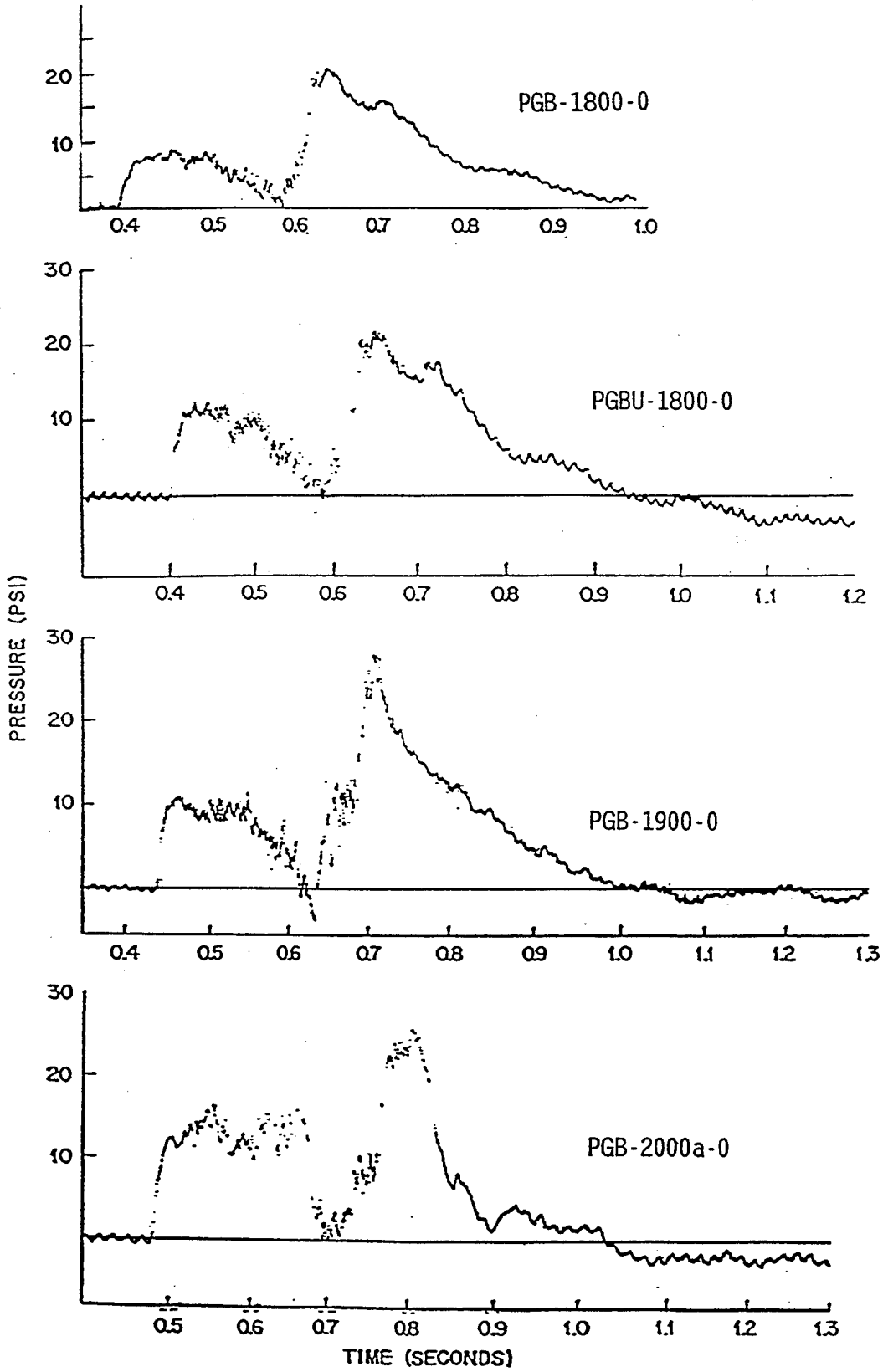

Figure C-53. Incident overpressure gage records, Sandia Corporation.

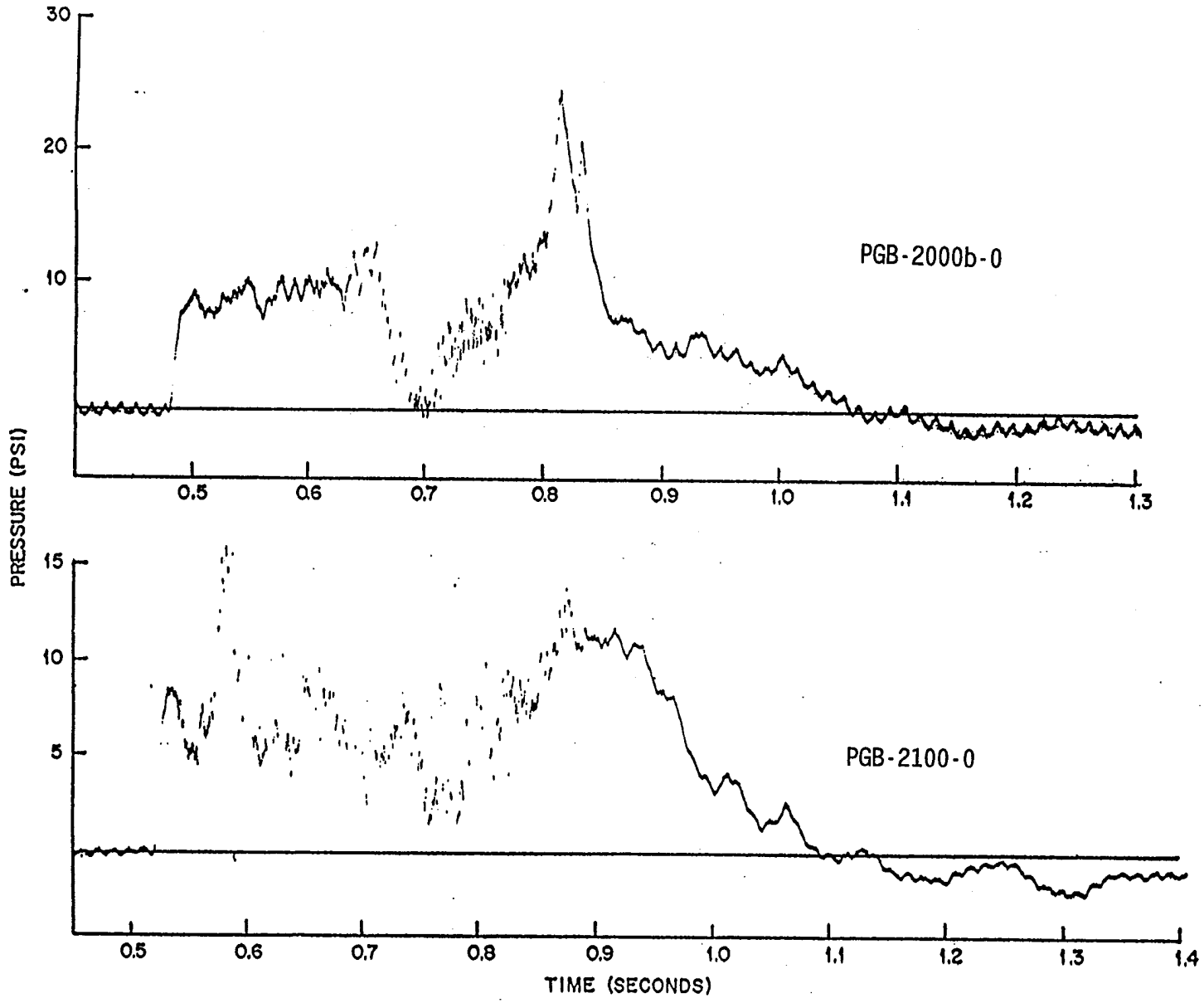

Figure C-54. Incident overpressure gage records, Sandia Corporation.

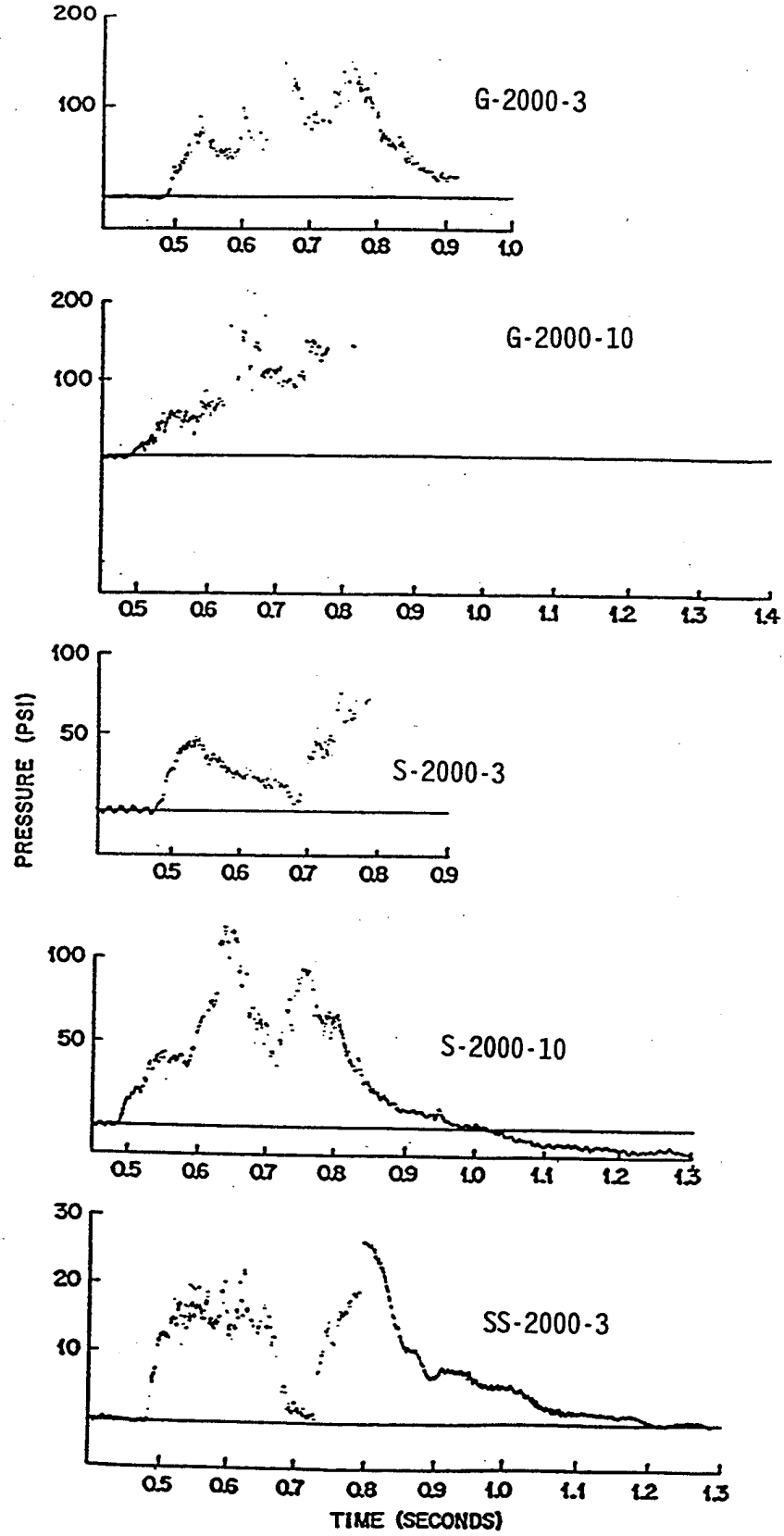

Figure C-55. Incident overpressure gage records, Sandia Corporation.

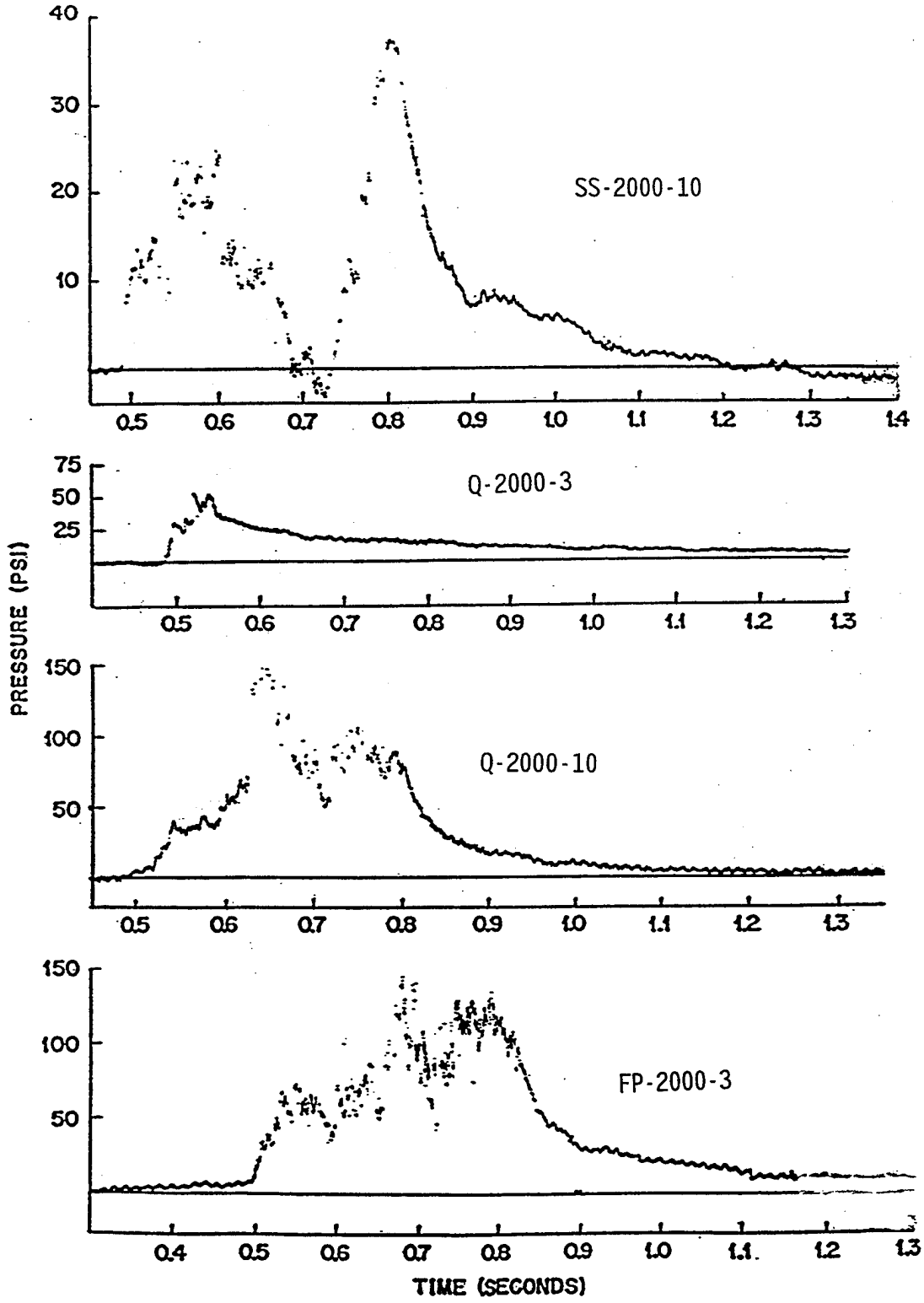

Figure C-56. Incident overpressure gage records, Sandia Corporation.

APPENDIX D:

CONVERSION TABLE

Conversion factors for U.S. Customary to metric (SI) units of measurement

MULTIPLY → BY → TO GET

TO GET ← BY ← DIVIDE

angstrom	1.000 000 X E -10	meters (m)
atmosphere (normal)	1.013 25 X E +2	kilo pascal (kPa)
bar	1.000 000 X E +2	kilo pascal (kPa)
barn	1.000 000 X E -28	meter ^{2} (m^2)
British thermal unit (thermochemical)	1.054 350 X E +3	joule (J)
calorie (thermochemical)	4.184 000	joule (J)
cal (thermochemical)/cm^2	4.184 000 X E -2	mega joule/m^2 (MJ/m^2)
curie	3.700 000 X E +1	* giga becquerel (GBq)
degree (angle)	1.745 329 X E -2	radian (rad)
degree Fahrenheit	$t_K = (t^\circ f + 459.67)/1.8$	degree kelvin (K)
electron volt	1.602 19 X E -19	joule (J)
erg	1.000 000 X E -7	joule (J)
erg/second	1.000 000 X E -7	watt (W)
foot	3.048 000 X E -1	meter (m)
foot-pound-force	1.355 818	joule (J)
gallon (U.S. liquid)	3.785 412 X E -3	meter ^{3} (m^3)
inch	2.540 000 X E -2	meter (m)
jerk	1.000 000 X E +9	joule (J)
joule/kilogram (J/kg) (radiation dose absorbed)	1.000 000	Gray (Gy)
kilotons	4.183	terajoules
kip (1000 lbf)	4.448 222 X E +3	newton (N)
kip/inch^2 (ksi)	6.894 757 X E +3	kilo pascal (kPa)
ktap	1.000 000 X E +2	newton-second/m^2 (N-s/m^2)
micron	1.000 000 X E -6	meter (m)
mil	2.540 000 X E -5	meter (m)
mile (international)	1.609 344 X E +3	meter (m)
ounce	2.834 952 X E -2	kilogram (kg)
pound-force (lbs avoirdupois)	4.448 222	newton (N)
pound-force inch	1.129 848 X E -1	newton-meter (N•m)
pound-force/inch	1.751 268 X E +2	newton/meter (N/m)
pound-force/foot^2	4.788 026 X E -2	kilo pascal (kPa)
pound-force/inch^2 (psi)	6.894 757	kilo pascal (kPa)
pound-mass (lbm avoirdupois)	4.535 924 X E -1	kilogram (kg)
pound-mass-foot^2 (moment of intertia)	4.214 011 X E -2	kilogram-meter^2 (kg•m^2)
pound-mass/foot^3	1.601 846 X E +1	kilogram/meter^3 (kg/m^3)
rad (radiation dose absorbed)	1.000 000 X E -2	** Gray (Gy)
roentgen	2.579 760 X E -4	coulomb/kilogram (C/kg)
shake	1.000 000 X E -8	second (s)
slug	1.459 390 X E +1	kilogram (kg)
torr (mm HG, O C)	1.333 22 X E -1	kilo pascal (kPa)

* The becquerel (Bq) is the SI unit of radioactivity; 1 Bq = 1 event/s.
** The Gray (GY) is the SI unit of absorbed radiation.

A more complete listing of conversions may be found in "Metric Practice Guide E 380-74," American Society for Testing and Materials.

INTENTIONALLY LEFT BLANK.

REAL SURFACE (NON-IDEAL) EFFECTS ON NUCLEAR EXPLOSION AIRBLAST FROM PRISCILLA-TYPE EVENTS

PART II: SHARC Hydrocode Calculations of the PRISCILLA Event (Phase I)

Joseph E. Crepeau
Robert G. Ekler
Lynn W. Kennedy
Charles E. Needham
Shelley H. Rogers

1 October 1993

Work Performed under Subcontract to
Applied Research Associates, Inc., under
Contract Number DAAL03-91-C-0034

S-Cubed, a Division of Maxwell Laboratories
2501 Yale Boulevard, SE, Suite 300
Albuquerque, New Mexico 87106

INTENTIONALLY LEFT BLANK.

PREFACE

In support of the non-ideal airblast program of the Army Research Laboratory, S-Cubed was engaged under a subcontract to Applied Research Associates, Inc., to perform three state-of-the-art hydrocode computations of blast from the nuclear explosion PRISCILLA over three surfaces: ideal; desert, simulating the PRISCILLA event; and grassland, which was expected to produce a very non-ideal blast wave.

The computations were to carry the blast wave to a time of four seconds after detonation and to define the full positive phase of the five psi overpressure waveform. The computations were performed in two phases. In the first phase, the computations were carried to two seconds for all three cases. The second phase was performed when additional funding became available, and the three cases were run to completion at four seconds.

Part II of this reports presents the results of the Phase I computations. They have been superseded by the reports of the completed computations listed below. The Phase I report is included because it describes the initiation of the computations and material not presented in the later reports.

In Phase II, the ideal and desert computations were run to completion under Contract DAAL01-94-P-1217 with the ARL. The results are presented in the following report:

Needham, C. E., R. G. Ekler, and L. W. Kennedy. "Extended Desert Calculation Results with Comparisons to PRISCILLA Experimental Data and a Near-Ideal Calculation." S-Cubed Report No. SSS-DTR-94-14802. This report was published as an ARL contractor report, ARL-CR-235, in July 1995.

The grassland computation was completed under Contract DAAL01-94-P-2257 with the ARL. The work is contained in the following report:

Ekler, R. G., C. E. Needham, and L. W. Kennedy. "Extended Grassland Calculation Results With Comparisons to PRISCILLA Experimental Data and a Near-Ideal Calculation." S-Cubed Report

No. SSS-DFR-94-14920. This report was published as an ARL contractor report, ARL-CR-236, in July 1995.

Part I of this report was prepared utilizing the material presented in the three S-Cubed reports and in supplementary communications.

TABLE OF CONTENTS

		Page
	PREFACE	iii
	LIST OF FIGURES	vii
1.	INTRODUCTION	1
2.	DESCRIPTION OF FEATURES COMMON TO ALL CALCULATIONS; ZONING	2
3.	SPECIFIC FEATURES AND RESULTS FROM IDEAL CALCULATION	8
4.	SPECIFIC FEATURES AND RESULTS FROM GRASSLAND CALCULATION	9
5.	SPECIFIC FEATURES AND RESULTS FROM DESERT CALCULATION	13
	APPENDIX A: STATION LOCATIONS	A-1
	APPENDIX B: CONTOUR PLOTS OF PRESSURE AND DENSITY FROM IDEAL SURFACE CALCULATION (75 TO 500 MSEC)	B-1
	APPENDIX C: GROUND-LEVEL STATION OVERPRESSURE AND OVERPRESSURE IMPULSE PLOTS	C-1
	APPENDIX D: COMPARISON OF FINE- AND COARSE-ZONED GRASSLAND CALCULATION	D-1
	APPENDIX E: COMMENTARY ON DEVELOPMENT OF PRECURSOR IN GRASSLAND CALCULATION	E-1
	APPENDIX F: SURFACE-LEVEL OVERPRESSURE AND OVERPRESSURE IMPULSE STATION PLOTS FROM GRASSLAND CALCULATION	F-1
	APPENDIX G: CONTOUR PLOTS AND STATION RECORDS FROM DESERT CALCULATION	G-1
	APPENDIX H: COMPARISON OF CALCULATIONAL RESULTS	H-1
	APPENDIX I: COMPARISON OF PRISCILLA EXPERIMENTAL WAVEFORMS WITH DESERT CALCULATION	I-1
	APPENDIX J: CONVERSION TABLE	J-1

INTENTIONALLY LEFT BLANK.

LIST OF FIGURES

Figure		Page
1.	Mesh configuration at initiation of first phase, ideal surface calculation	3
2.	Mesh configuration at initiation of second phase, ideal surface calculation	4
3.	Initial configuration for grassland and desert surface calculations	5
4.	Station locations for all three calculations	7
5.	Thermal layer as obtained from THRML for grassland calculation	12
6.	Sound speed vs. range as derived by Carpenter from experimental data	14

INTENTIONALLY LEFT BLANK.

SECTION 1
INTRODUCTION

1.1 Rationale

Three calculations were undertaken to simulate the PRISCILLA nuclear test event, a 36.6-KT detonation at a height-of-burst of 700 ft. PRISCILLA was part of the Plumbbob series, and occurred on 24 June, 1957, at Frenchman's Flat at the Nevada Test Site. Frenchman's Flat is a dry lake bed notable because of its flat surface and its fine dust soil. The PRISCILLA event surface is generally described as "desert-like".

A new simulation of the PRISCILLA event was undertaken because of recent improvements in the handling of turbulence and dust-lofting in hydrodynamic codes. Specifically, the SHARC hydrocode with a K–ε turbulence model was used for all calculations in the series. The calculations included one with an ideal surface, used as a baseline against which to compare results from the other simulations, one with a "grassland" thermal layer at the surface, derived from S-Cubed's THRML code, and one with a "desert" thermal layer, obtained by backing out the appropriate sound speed ratios near the surface from experimental data[1]. The ideal and desert calculations were performed under a subcontract (#5709S) to Applied Research Associates (ARA), whose prime contract (DAAL03-91-C-0034) is with the Army Research Laboratories (ARL). Technical monitors are Noel Ethridge at ARA and Richard Lottero at ARL. The grassland calculation was done under Defense Nuclear Agency sponsorship on Contract DNA001-92-C-0165, CTM Maj. E.B. Tucker. Because the calculations are closely related, a combined final report covering all three calculations is being submitted. We appreciate the assistance and guidance provided by our sponsors during the course of this work.

[1] The derivation of the thermal layer from the experimental data was performed by H.J. Carpenter, of Carpenter Research Corporation.

SECTION 2
DESCRIPTION OF FEATURES COMMON TO ALL CALCULATIONS; ZONING

All of the PRISCILLA calculations in this series were run in a two-dimensional, cylindrical coordinate system, with the axis of symmetry passing through the detonation point and normal to the ground surface. The calculations were initiated at a problem time of 55 ms after detonation, with scaled conditions from FB14, a one-dimensional SPUTTER[2] radiation-hydrodynamic calculation, used as input to the SHARC mesh. The ideal calculation was run in two phases. The first phase was initiated with the SPUTTER result and run from 55 ms to 250 ms; the second phase was picked up from the first at 250 ms. Conditions from the first phase were read into the expanded mesh for the second phase, and this second part was run to completion of the calculation at 2 seconds.

Details of the mesh configuration for the two phases of the ideal calculation are described below, and diagrams are shown in Figures 1 and 2. It was intended at the outset that this zoning configuration would be used for all of the calculations. However, during performance of the grassland calculation, it was found that the zoning used for the ideal case would require too much computer time (several hundred Cray cpu hours) with the multi-material grassland surface. Therefore, a compromise zoning configuration was constructed under which the grassland and desert calculations were run. This coarser zoning configuration is shown in Figure 3.

For the ideal-surface calculation, a constant-mesh subgrid, in which zones sizes are 20 cm (horizontal) by 10 cm (vertical), was placed at the surface. For the first phase, the subgrid was 5 m high and was initially placed at range 220 to 250 m. For the second phase, the subgrid was 90 m wide by 12 m high, and was initially placed at range 240 to 330 m. Geometrically-expanding zones were placed above and to the left (and also to the right, in the second phase) of this subgrid. Radius of the SPUTTER input region was 210 m, just short of the height-of-burst, so that the shock front had not yet interacted with the ground surface or intruded into the region where the thermal layer would be placed in the grassland and desert calculations at time of initiation. As the calculation proceeded, the subgrid was allowed to move outward, following the progress of the shock along the surface. Rezoning was accomplished to adjust the mesh automatically each time the subgrid moved.

In the second phase, the grid extended upward to 703 m, rather than to 500 m as in the first phase, and outward to 390 m. As the upper portion of the shock perimeter approached the top of the mesh, a vertical rezone expanded the vertical zones above the subgrid without affecting conditions near the surface. In the horizontal direction, cells were shifted from the right side of the subgrid to the left as the subgrid moves outward. When it approached the left boundary of the mesh, expansion of horizontal zoning

---

[2] SPUTTER is a one-dimensional, multi-group, radiation hydrocode. Results of a number of calculations have been saved and are used to initiate other types of calculations. The yield of FB14, which was scaled to appropriate values for these calculations, is 30 KT. The reference for SPUTTER is: Sharp, A.L., "A Thermal Source Model from SPUTTER Calculations," Phillips Laboratory AFWL-TR-72-49, March 1973.

toward the axis allowed the left boundary to be displaced outward. Thus, the entire active region was maintained within the grid at all times.

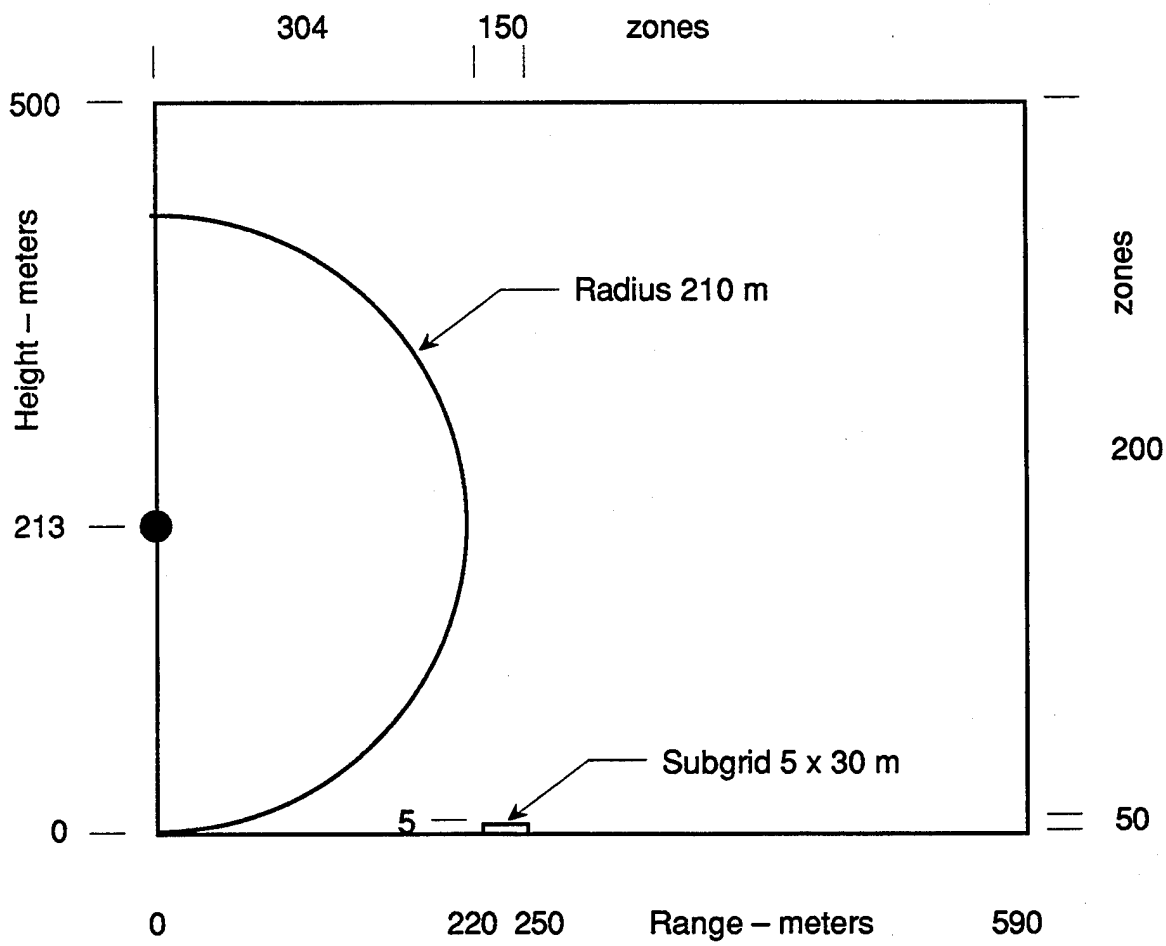

Figure 1. Mesh configuration at initiation of first phase, ideal surface calculation.

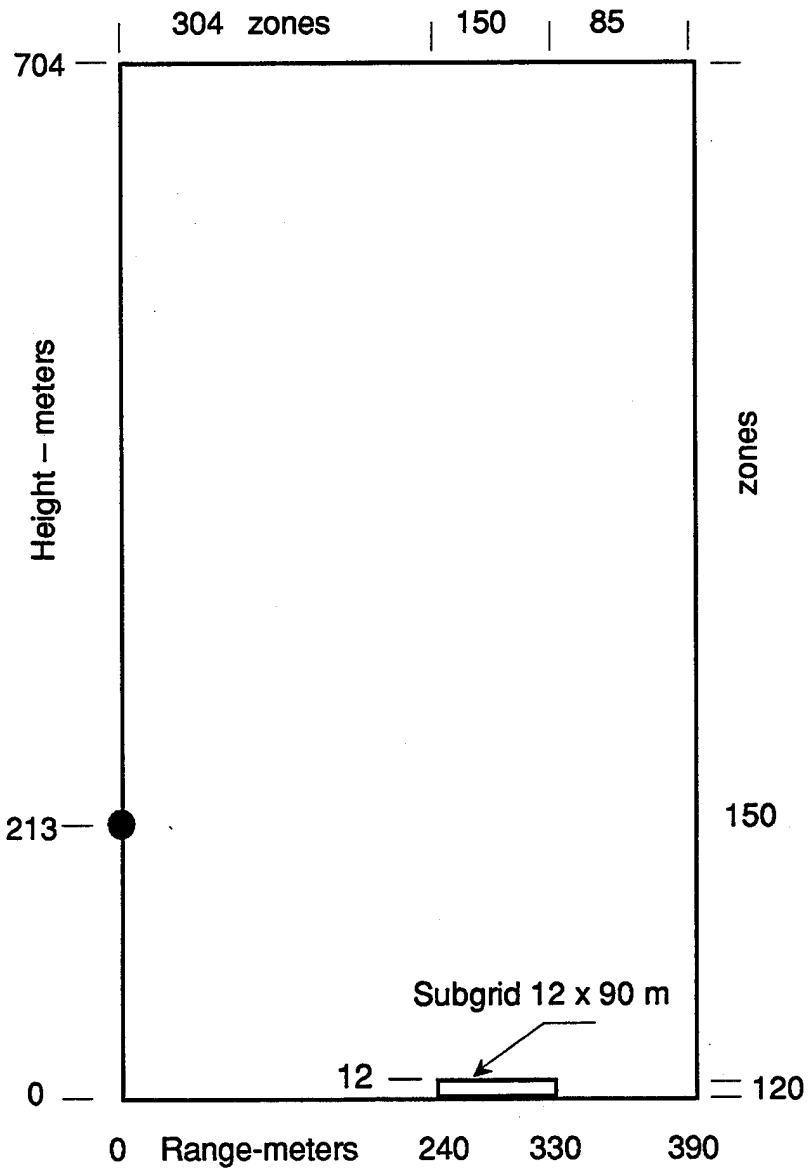

Figure 2. Mesh configuration at initiation of second phase, ideal surface calculation.

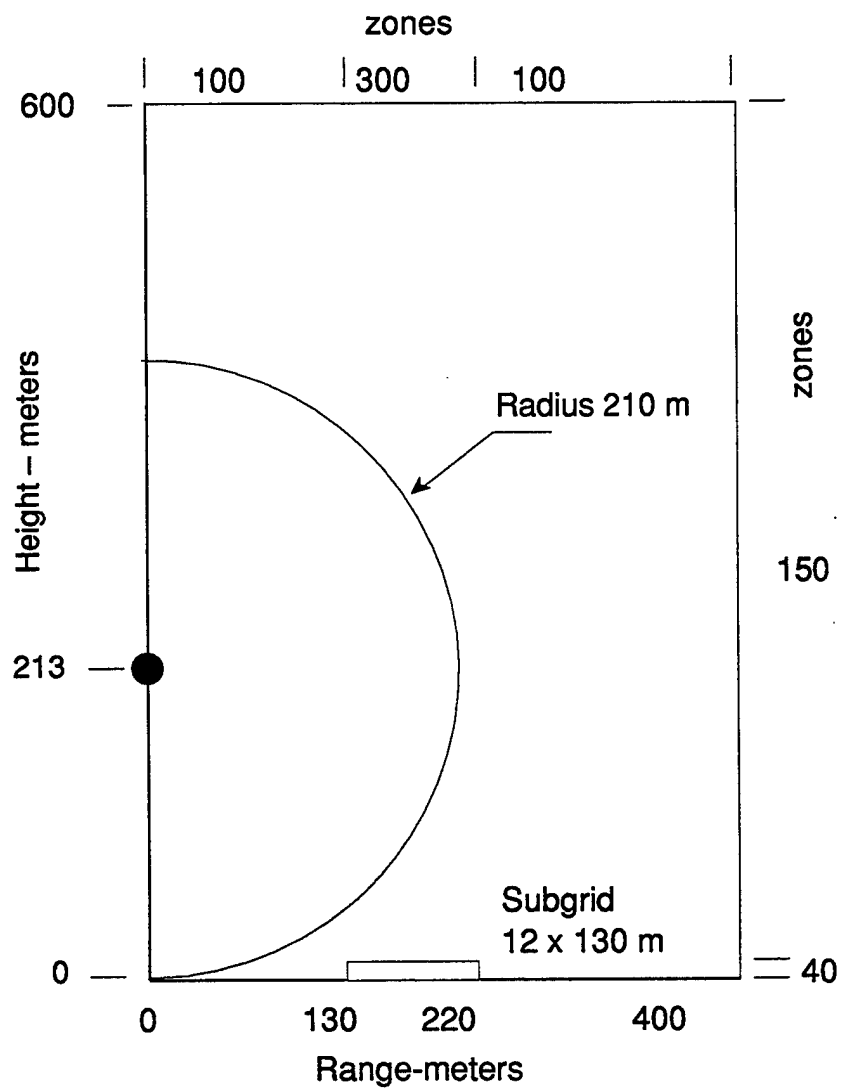

Figure 3. Initial configuration for grassland and desert surface calculations.

The grassland and desert calculations were each run in a single phase with the coarser zoning configuration shown in Figure 3. This zoning was initiated when it was found that the finer-zoned version would not run to completion in a reasonable amount of computer time. The complications added by diffusion of the different grass materials and by the dust being swept into the mesh slow the progress of the computation. The grassland and desert zoning included a subgrid with 30-cm zones in both the vertical and horizontal directions. The subgrid was initially placed between ranges 130 and 220 m, and was 12 m high. It was allowed to move outward to follow the shock as the calculations progressed.

1010 stations, or stationary recording locations at which conditions are recorded as functions of time, were incorporated into all three calculations. Stations were placed from the axis of symmetry to a range of 2286 m, and from the surface to 12.2 m. All

station locations are shown as dots in Figure 4, and are listed in the table of Appendix A. Many of the stations are beyond the range of the initial grid as shown in Figures 1, 2, and 3. However, these stations are activated as the grid expands to the right to follow the expanding shock system.

Because interest for these calculations was primarily in surface effects, including thermal interactions and dust, and the influence of these effects on the precursor and boundary layer, a constant ambient atmosphere was used for all of the calculations. This corresponds to conditions of the U.S. Standard Atmosphere at an elevation of approximately 3100 ft above sea level. The constant atmosphere simplifies the calculation and affects only late-time, gravity-related phenomena, such as cloud rise. All calculations were run to a time of completion at 2 sec after detonation.

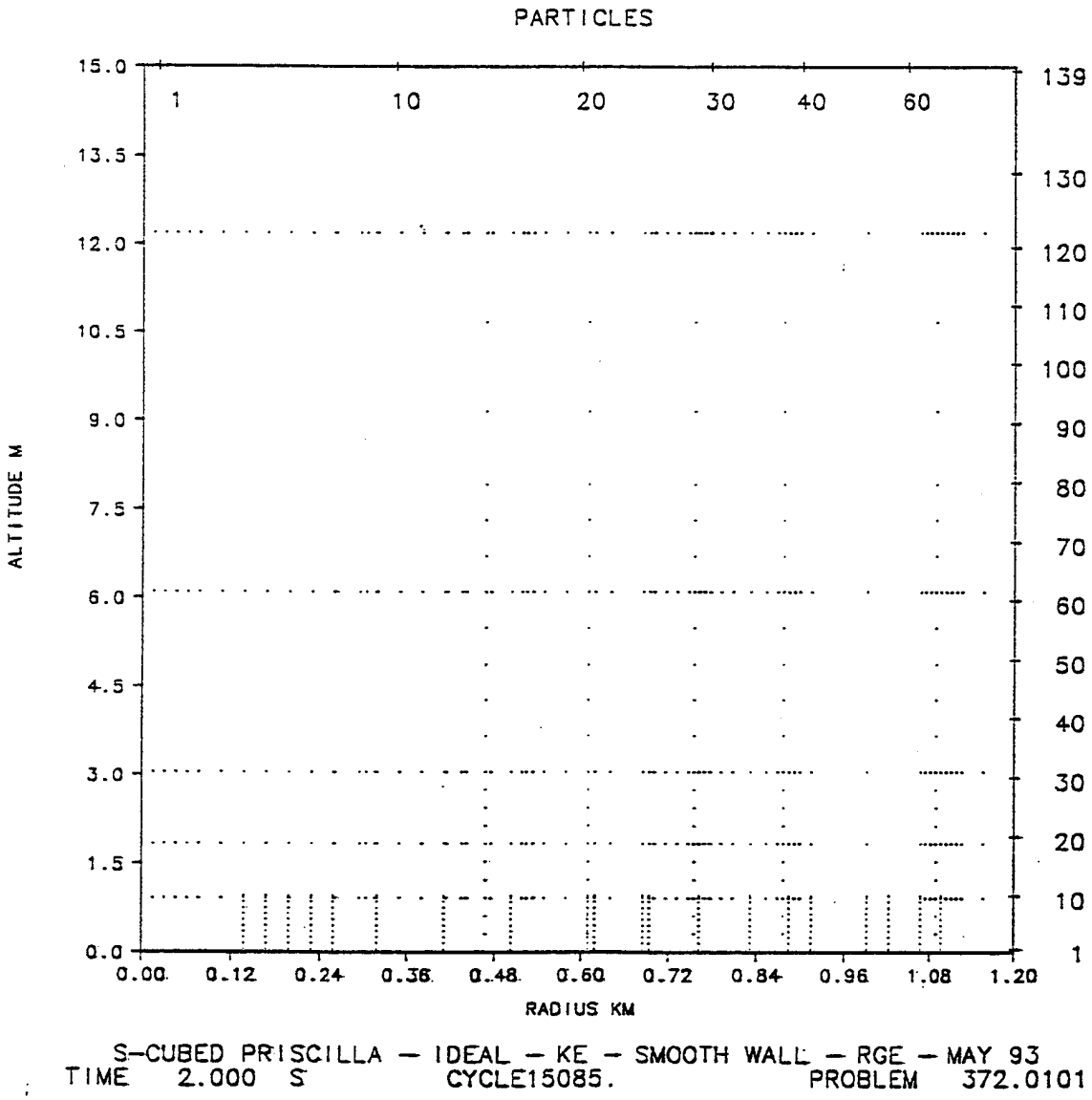

Figure 4. Station locations for all three calculations.

SECTION 3
SPECIFIC FEATURES AND RESULTS FROM IDEAL CALCULATION

For the ideal calculation, we used the K-ε turbulence modeling[3], but specified a smooth-wall Clauser "law-of-the-wall"[4] at the surface. No thermal layer or dust sweep-up was included in this calculation, which is to be used as a baseline against which to compare results of the other calculations.

Appendix B contains a series of pressure and density contour plots from the ideal surface calculation between 75 and 500 msec. Most of the plots include the entire calculation; a few concentrate on the area of interest where the shock wave interacts with the ground surface. The development and growth of the Mach stem is clearly demonstrated in this series. A few ground-level station overpressure and overpressure impulse plots are given in Appendix C. These are at ranges of from 350 to 1650 ft. Other parameters, or other station locations, are available and can be provided to answer specific questions or to further explore specific regions of interest.

---

[3] Pierce, T.H., "Numerical Boundary Layer Analysis with K-ε Turbulence Model and Wall Functions," Defense Nuclear Agency Report DNA-TR-87-15, September 1986.

[4] Barthel, J.R., Needham, C.E., Pierce, T.H., and Schneyer, G.P., "A Computational Model for Precursed Airblasts over Rough Surfaces," S-Cubed Report SSS-R-89-10003, August 1989.

SECTION 4
SPECIFIC FEATURES AND RESULTS FROM GRASSLAND CALCULATION

The grassland calculation was initialized from FB14 in the same manner as the ideal calculation. Initially, a grassland calculation was attempted with the same zoning as was used for the ideal calculation. This was found to be impractical, so the coarser zoning illustrated in Figure 3 was finally used. The first, fine-zoned calculation was continued to 200 msec, and some results comparing these two versions of the same calculation at that time are shown in Appendix D. The direct comparison of fine- and coarse-zoned results shows the effects of the zone-size differences. These include a slight reduction in precursor propagation velocity and the consequent reduction in size of the precursor toe. The tip of the precursor toe is slightly further advanced in range in the fine-zoned calculation— to 333 m as opposed to 330 m at 200 msec for the coarse-zoned version. Otherwise, the two versions produce nearly identical contour plots. As in the ideal calculation, rezone boundary conditions, constant-subgrid rezone, and constant atmosphere were incorporated for both versions of the grassland simulation.

The thermal layer used in the grassland calculation was generated using S-Cubed's THRML code. THRML is a one-dimensional code which provides the response of a surface to a time-dependent incident thermal flux. Characteristics of the surface soil, such as density and particle-size-distribution, and characteristics of the vegetative ground cover, such as mass distribution, water content, and heat of combustion and vaporization, are used to calculate the time evolution of the thermal layer at a given range. Characteristics of the grassland surface used as input to THRML were the same as those used in an earlier study[5] (except for soil melt temperature and amount of soil in loftable particles), and were chosen as those thought to produce a "most stressing" thermal layer; that is, the thermal layer which would generate the precursed waveform most damaging to equipment. THRML was modified for this set of calculations to incorporate ambient atmospheric conditions other than those a sea level, and the standard conditions at an elevation of 3100 ft were used. Vegetation and soil characteristics used as input to THRML are given in Table 1.

At the expected time-of-arrival of the blast wave at a given range, information about the temperature and density distribution with height is saved. This information is combined with profiles from other ranges at appropriate times and processed for reading into the SHARC mesh. THRML runs for the PRISCILLA grassland calculation were made every 50 ft/$KT^{1/3}$ (about every 52 m) from 0 to 1570 m. Experimental times-of-arrival from the PRISCILLA event (which was of course over a dry lakebed rather than a grassland surface) were used to determine the times to freeze the THRML results for SHARC. The THRML layer as provided for SHARC processing is shown in Figure 5. A banded grayscale color table has been assigned to the data array to emphasize variations, and there is some interpolation and smoothing generated by the contouring routines used to make this plot.

---

[5] Kennedy, Lynn W. and Rogers, Shelley H., "Thermal Layer Computations for Non-Ideal Airblast Scenario Assessment," S-Cubed Report SSS-DFR-92-13512, September 1992.

Table 1. Vegetation and soil parameters used in THRML for PRISCILLA grassland thermal layer.

Vegetation Characteristics:

Vegetation height (top and bottom)	30 cm, 0 cm (ground surface)
Mass Distribution	Uniform
Dry Mass Load	0.022 gm/cm^2
Bound Water Content	0.003 gm/cm^2 (14% of dry mass load)
Free Water Content	none
Bound Water Release Temperature	375° K
Heat of Combustion	3600 cal/gm
Onset and Completion of Pyrolysis	475° K, 800° K
Plant Residue in Ash and Soot	2.97% and 0.03%, respectively, of burned mass
Leaf Index	3.56
Density of Dry, Compacted Plant	0.35 gm/cm^3

Soil:

Particle Categories	2, loftable and immobile
Amount in Loftable Particles	1% by mass
Particle Diameters	10 microns, 400 microns
Bound Water Content	13.8% of dry mass
Bound Water Release Temperature	600° K
Void Space	30%
Density of Dry, Compacted Soil	2.2 gm/cm^3
Melt Temperature	2000° K

The obvious problem with this approach for insertion of the thermal layer is that the predetermined times-of-arrival may not be the same as the actual times-of-arrival. For example, as shown in the time-of-arrival comparison in Appendix H, the grassland TOAs are as much as 200 ms earlier than the desert TOAs at ranges beyond about 900 m. The thermal layer structure used at these ranges is thus more time-evolved than it would be in a nuclear detonation. This situation could be improved by incorporating a semi-automatic link between THRML and SHARC, so that when the shock arrives at a given range, the THRML results for the appropriate time are inserted into the region just ahead of the shock.

The finely-resolved (in the vertical direction) thermal layer profiles generated by THRML were averaged over each vertical region corresponding to a SHARC zone. The thermal layer average value for the cell was assigned to the center of that cell. This averaging could account for the slight difference in precursor toe position noted between the fine- and coarse-zoned calculations. The THRML results averaged over a 30-cm zone rather than a 10-cm zone may produce a slightly lower peak temperature in the thermal layer for the coarse-zoned case. It is the thermal layer peak temperature, even if it occurs over only a very thin region, which apparently governs precursor toe development.

For a smooth variation of thermal parameters with range, values were obtained by linear interpolation. Prior to insertion into the computational grid, the averaged density data was processed through the equation-of-state routine to obtain specific energy at

pressure equilibrium. Pressure equilibrium is necessary so that the layer will not continue to evolve hydrodynamically during the pre-shock-arrival part of the calculation.

A two-material, or multi-phase, dust equation-of-state was included in the SHARC calculation, and the plant and soil material from THRML was treated with this dust equation. Both vaporized and solid dust are allowed in the calculation, and mass can be transformed from one phase to the other as it is heated or cooled by its surroundings. Dust scouring by the shock structure, beyond that lofted pre-shock by THRML and existing in the added thermal layer, was not considered. Also, additional thermal radiation from the fireball after shock arrival was not considered.

The K-ε turbulence model was used for this calculation as well as for the ideal case. Instead of the "smooth wall" used for the ideal simulation, a "rough wall" was incorporated for the soil surface under the vegetation. The parameters chosen provided for 35 percent coverage by roughness elements, with an average height for these elements of 2 cm.

Appendix E contains a series of contour plots illustrating detail at various calculation times. Both fine- and coarse-zoned results are included in this series. Of particular interest in this series is the development of the precursor, and a commentary describing this development is included with the plots in the Appendix. A selected group of surface-level overpressure and overpressure impulse station plots, from both the fine-zoned and coarse-zoned calculations where applicable, is given in Appendix F.

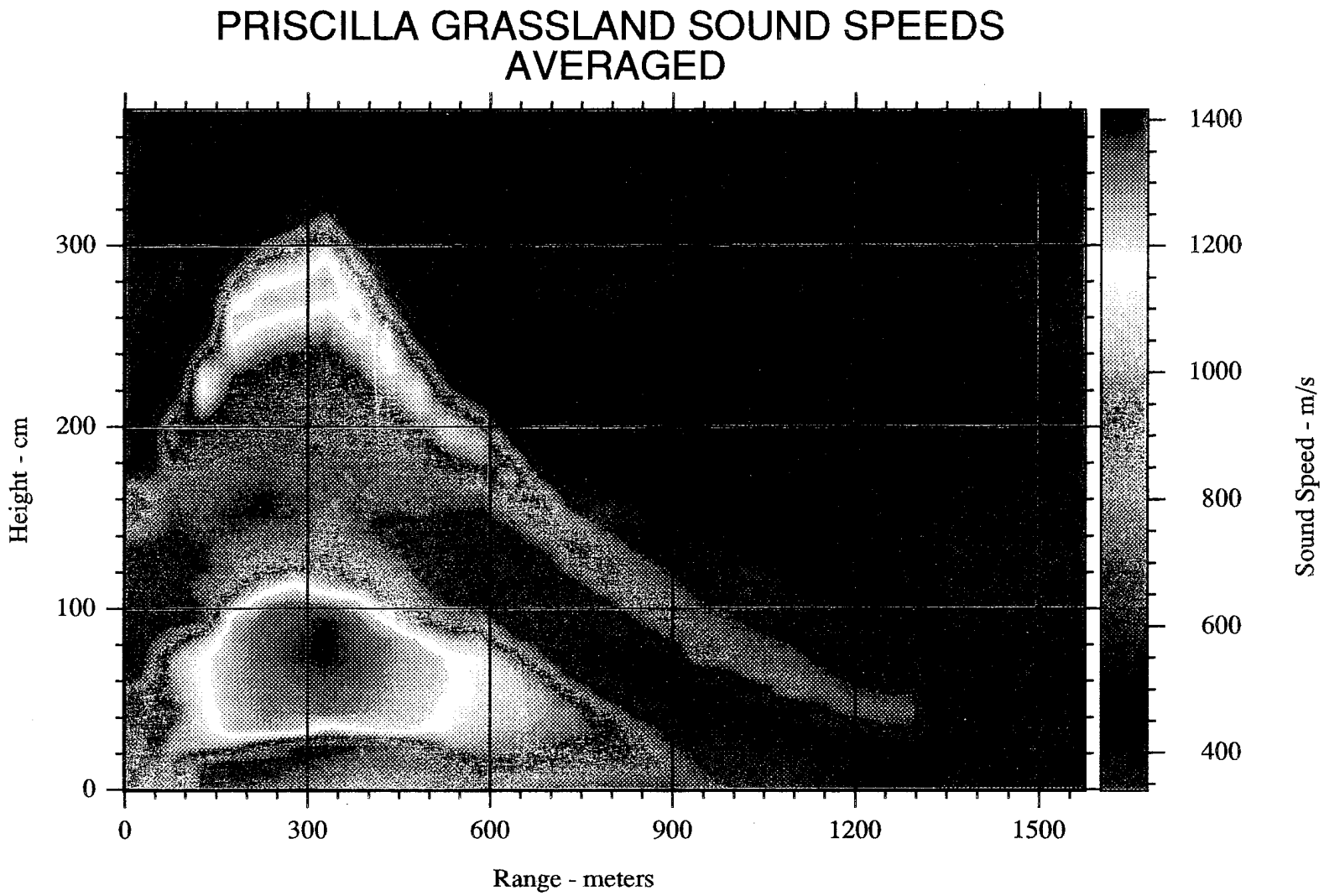

Figure 5. Thermal layer as obtained from THRML for grassland calculation.

SECTION 5
SPECIFIC FEATURES AND RESULTS FROM DESERT CALCULATION

The PRISCILLA desert calculation was constructed and initialized in exactly the same manner as the coarse-zoned grassland calculation described above, with exceptions in wall roughness parameters, construction of the thermal layer, and the dust lofting mechanism. For the desert, the K-ε turbulence model was used as before, but this time with a smooth wall as described for the ideal surface. Because the desert surface is not covered by vegetation, coding for a dust lofting mechanism was included. In this model, the dust mass is injected into the surface-level zones of the calculation depending on the shear layer strength as determined by the wall/boundary layer model.

Considerable effort was expended during this program in obtaining the best representation of the thermal layer which actually existed for the PRISCILLA event. Because the Frenchman's Flat dry lakebed surface is generally considered to be desert-like, it was the authors' intent that the hydrocode results would validate the calculational technique by producing overpressure station records that could be compared favorably with actual experimental data from PRISCILLA. We expended considerable effort in attempting to improve the THRML code so that it would produce a thermal layer that is in agreement with the experimental information. Although THRML is highly developed, has many state-of-the-art features, and has been well validated against experimental data for vegetation-covered surfaces, it continues to generate unrealistic thermal layers when applied to bare soils. Its problems in these cases include the tendency to produce blowoff layer temperature profiles that are too strongly inverted (temperature increases with height within the extent of the layer, whereas experimental data indicates that the hottest region is near the surface) and too hot. Efforts are underway elsewhere[6] to upgrade THRML and to incorporate surface blowoff modeling that will overcome these problems.

Ultimately, we found that the most reasonable approach was to use a thermal layer derived from the experimental data by Carpenter. This data involves only sound-speed (or temperature) vs. range information, with no vertical structure. Therefore, the thermal layer used in the SHARC calculation was given a uniform thickness of 60 cm, encompassing two of the 30-cm calculational zones. Above 60 cm, the thermal layer was allowed to decay exponentially with height in a manner prescribed by the FDOT model[7]. The Carpenter sound speed vs. range curve is given in Figure 6. In the acoustic region, between 1500 and 3500 ft, the precursor is thought to be an acoustic wave rather than a shock. (The curve shown and used assumes a precursor shock front. Note added in proof.)

Appendix G is a series of contour plots and station records from the desert calculation. At 200 ms, the precursor is well developed and there is a double Mach stem structure at the top of the precursor toe. Comparing this plot to the one for the ideal surface

---

[6] Barthel, J.R., private communication, and Needham, C.E., private communication, September 1993.

[7] Needham, C.E., and Crepeau, J.E., "A Flux Dependent Thermal Layer Model (FDOT)," Defense Nuclear Agency Report DNA 5538T, October 1980.

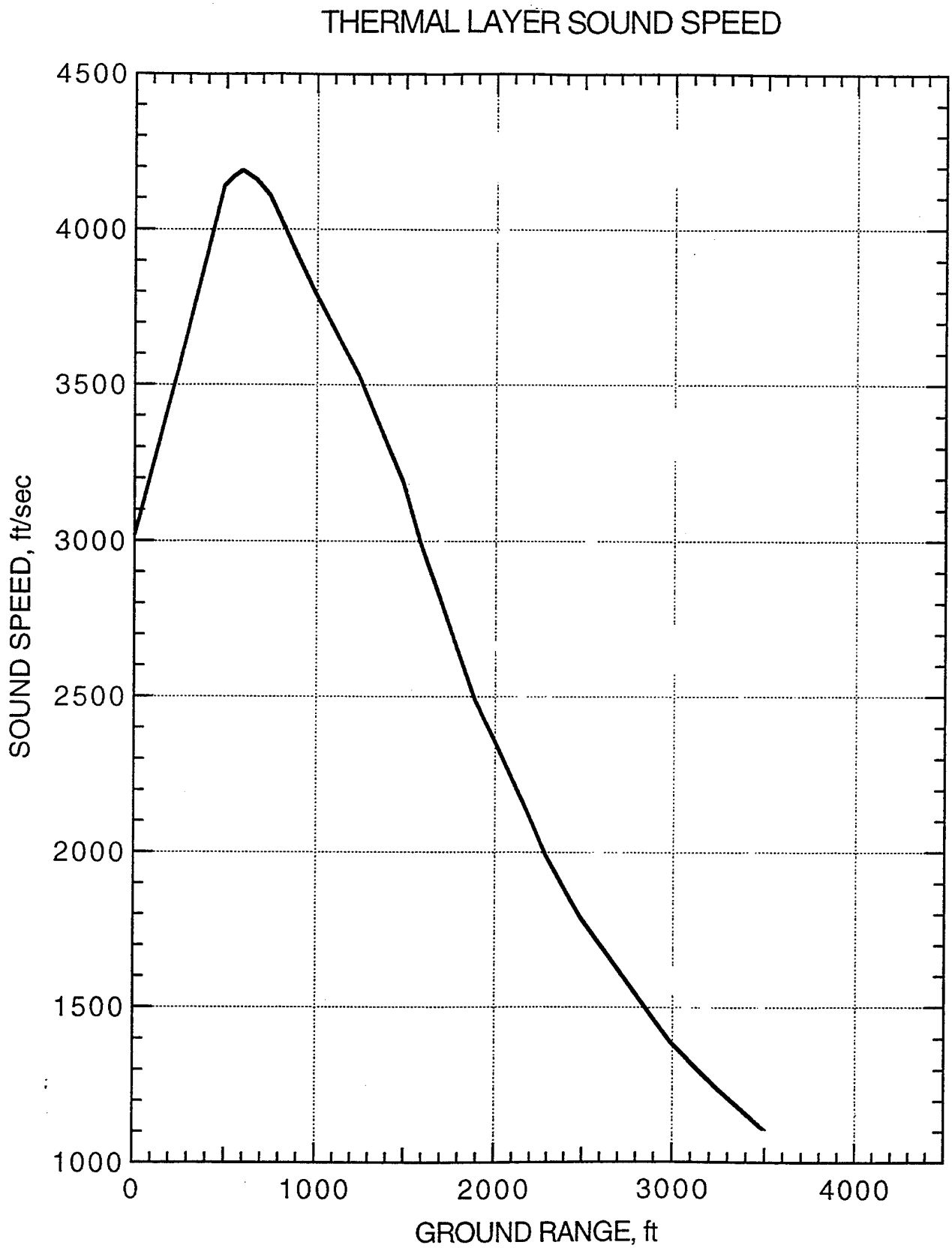

Figure 6. PRISCILLA sound speed versus range.

(Appendix B) however, it is clear that this is not the same as the classical Mach stem, which is back at range 278 m and rises less than 10 m above the surface at this time. The growth of this structure and its eventual re-attachment to the reflected wave are shown in the subsequent plots. In the last pressure contour plot, at 800 ms, it is evident that the precursor is beginning to clean up. The "density material 3" contour plots illustrate the scouring of solid dust from the surface into the precursor structure. Vaporized dust is also allowed in the calculation, but a very small amount is observed.

The series of station plots, also in Appendix G, illustrates the development of the precursed waveform with range. The stations for which plots are included are all at ground level. The last one, at range 2,500 ft, shows the round-topped shape typical of a nearly cleaned-up precursor. The waveform is similar to that of an ideal waveform, but does not have the fast rise and sharp peak of the ideal shock.

SECTION 6
COMPARISONS AMONG THE THREE CALCULATIONS, AND COMPARISONS WITH EXPERIMENTAL DATA

Appendix H consists of a series of summary plots comparing all three calculations with each other and with some of the PRISCILLA desert line data. The arrival-time plot illustrates that the desert calculation produces results in closest correspondence with the data. This is to be expected in that the desert thermal layer used for the calculation was developed from experimental information. The calculated desert overpressure peaks at ground level compare most closely with 0-ft data. Overpressure impulses are nearly the same in all calculations. The development of a precursor modifies the timing of impulse delivery, but does not change its total value significantly.

The most interesting results are in the dynamic pressure and dynamic pressure impulses. Calculated dynamic pressure impulses at the surface are up to an order of magnitude larger for the desert calculation than for the grassland or ideal calculations. This is because a large amount of scoured dust mass is moving at a high velocity near the surface. At the 3-ft level, the grassland calculation produces the highest dynamic pressure impulse. Because the grassland vegetative mass pre-existed (from THRML) at these greater heights and because the grassland thermal layer temperature is higher, more dynamic pressure impulse is produced at this level.

Several of the PRISCILLA experimental waveforms have been compared with those from the desert calculation in Appendix I. The correspondence is generally good. We believe that this is the most comprehensive calculation attempted so far to simulate the much-calculated PRISCILLA event. Improvements now contemplated for the THRML code will allow a more "first principles" simulation. The development of the K-ε turbulence modeling, together with rough/smooth wall effects for the surface interactions, appears to be allowing improvements in the calculational reproduction of real-surface nuclear effects.

APPENDIX A
STATION LOCATIONS

Locations of stations generated are ...

Station	1	xp =	0.000000E+00	yp =	0.000000E+00
Station	2	xp =	0.000000E+00	yp =	9.144000E+01
Station	3	xp =	0.000000E+00	yp =	1.828800E+02
Station	4	xp =	0.000000E+00	yp =	3.048000E+02
Station	5	xp =	0.000000E+00	yp =	6.096000E+02
Station	6	xp =	0.000000E+00	yp =	1.219200E+03
Station	7	xp =	1.524000E+03	yp =	0.000000E+00
Station	8	xp =	1.524000E+03	yp =	9.144000E+01
Station	9	xp =	1.524000E+03	yp =	1.828800E+02
Station	10	xp =	1.524000E+03	yp =	3.048000E+02
Station	11	xp =	1.524000E+03	yp =	6.096000E+02
Station	12	xp =	1.524000E+03	yp =	1.219200E+03
Station	13	xp =	3.048000E+03	yp =	0.000000E+00
Station	14	xp =	3.048000E+03	yp =	9.144000E+01
Station	15	xp =	3.048000E+03	yp =	1.828800E+02
Station	16	xp =	3.048000E+03	yp =	3.048000E+02
Station	17	xp =	3.048000E+03	yp =	6.096000E+02
Station	18	xp =	3.048000E+03	yp =	1.219200E+03
Station	19	xp =	4.572000E+03	yp =	0.000000E+00
Station	20	xp =	4.572000E+03	yp =	9.144000E+01
Station	21	xp =	4.572000E+03	yp =	1.828800E+02
Station	22	xp =	4.572000E+03	yp =	3.048000E+02
Station	23	xp =	4.572000E+03	yp =	6.096000E+02
Station	24	xp =	4.572000E+03	yp =	1.219200E+03
Station	25	xp =	6.096000E+03	yp =	0.000000E+00
Station	26	xp =	6.096000E+03	yp =	9.144000E+01
Station	27	xp =	6.096000E+03	yp =	1.828800E+02
Station	28	xp =	6.096000E+03	yp =	3.048000E+02
Station	29	xp =	6.096000E+03	yp =	6.096000E+02
Station	30	xp =	6.096000E+03	yp =	1.219200E+03
Station	31	xp =	7.620000E+03	yp =	0.000000E+00
Station	32	xp =	7.620000E+03	yp =	9.144000E+01
Station	33	xp =	7.620000E+03	yp =	1.828800E+02
Station	34	xp =	7.620000E+03	yp =	3.048000E+02
Station	35	xp =	7.620000E+03	yp =	6.096000E+02
Station	36	xp =	7.620000E+03	yp =	1.219200E+03
Station	37	xp =	1.066800E+04	yp =	0.000000E+00
Station	38	xp =	1.066800E+04	yp =	9.144000E+01
Station	39	xp =	1.066800E+04	yp =	1.828800E+02
Station	40	xp =	1.066800E+04	yp =	3.048000E+02
Station	41	xp =	1.066800E+04	yp =	6.096000E+02
Station	42	xp =	1.066800E+04	yp =	1.219200E+03
Station	43	xp =	1.371600E+04	yp =	0.000000E+00
Station	44	xp =	1.371600E+04	yp =	9.144000E+01
Station	45	xp =	1.371600E+04	yp =	1.828800E+02
Station	46	xp =	1.371600E+04	yp =	3.048000E+02
Station	47	xp =	1.371600E+04	yp =	6.096000E+02
Station	48	xp =	1.371600E+04	yp =	1.219200E+03
Station	49	xp =	1.676400E+04	yp =	0.000000E+00
Station	50	xp =	1.676400E+04	yp =	9.144000E+01
Station	51	xp =	1.676400E+04	yp =	1.828800E+02
Station	52	xp =	1.676400E+04	yp =	3.048000E+02
Station	53	xp =	1.676400E+04	yp =	6.096000E+02
Station	54	xp =	1.676400E+04	yp =	1.219200E+03
Station	55	xp =	1.981200E+04	yp =	0.000000E+00
Station	56	xp =	1.981200E+04	yp =	9.144000E+01
Station	57	xp =	1.981200E+04	yp =	1.828800E+02
Station	58	xp =	1.981200E+04	yp =	3.048000E+02
Station	59	xp =	1.981200E+04	yp =	6.096000E+02
Station	60	xp =	1.981200E+04	yp =	1.219200E+03
Station	61	xp =	2.286000E+04	yp =	0.000000E+00
Station	62	xp =	2.286000E+04	yp =	9.144000E+01
Station	63	xp =	2.286000E+04	yp =	1.828800E+02

Station	64	xp =	2.286000E+04	yp =	3.048000E+02
Station	65	xp =	2.286000E+04	yp =	6.096000E+02
Station	66	xp =	2.286000E+04	yp =	1.219200E+03
Station	67	xp =	2.590800E+04	yp =	0.000000E+00
Station	68	xp =	2.590800E+04	yp =	9.144000E+01
Station	69	xp =	2.590800E+04	yp =	1.828800E+02
Station	70	xp =	2.590800E+04	yp =	3.048000E+02
Station	71	xp =	2.590800E+04	yp =	6.096000E+02
Station	72	xp =	2.590800E+04	yp =	1.219200E+03
Station	73	xp =	2.621280E+04	yp =	0.000000E+00
Station	74	xp =	2.621280E+04	yp =	9.144000E+01
Station	75	xp =	2.621280E+04	yp =	1.828800E+02
Station	76	xp =	2.621280E+04	yp =	3.048000E+02
Station	77	xp =	2.621280E+04	yp =	6.096000E+02
Station	78	xp =	2.621280E+04	yp =	1.219200E+03
Station	79	xp =	2.956560E+04	yp =	0.000000E+00
Station	80	xp =	2.956560E+04	yp =	9.144000E+01
Station	81	xp =	2.956560E+04	yp =	1.828800E+02
Station	82	xp =	2.956560E+04	yp =	3.048000E+02
Station	83	xp =	2.956560E+04	yp =	6.096000E+02
Station	84	xp =	2.956560E+04	yp =	1.219200E+03
Station	85	xp =	3.048000E+04	yp =	0.000000E+00
Station	86	xp =	3.048000E+04	yp =	9.144000E+01
Station	87	xp =	3.048000E+04	yp =	1.828800E+02
Station	88	xp =	3.048000E+04	yp =	3.048000E+02
Station	89	xp =	3.048000E+04	yp =	6.096000E+02
Station	90	xp =	3.048000E+04	yp =	1.219200E+03
Station	91	xp =	3.169920E+04	yp =	0.000000E+00
Station	92	xp =	3.169920E+04	yp =	9.144000E+01
Station	93	xp =	3.169920E+04	yp =	1.828800E+02
Station	94	xp =	3.169920E+04	yp =	3.048000E+02
Station	95	xp =	3.169920E+04	yp =	6.096000E+02
Station	96	xp =	3.169920E+04	yp =	1.219200E+03
Station	97	xp =	3.200400E+04	yp =	0.000000E+00
Station	98	xp =	3.200400E+04	yp =	9.144000E+01
Station	99	xp =	3.200400E+04	yp =	1.828800E+02
Station	100	xp =	3.200400E+04	yp =	3.048000E+02
Station	101	xp =	3.200400E+04	yp =	6.096000E+02
Station	102	xp =	3.200400E+04	yp =	1.219200E+03
Station	103	xp =	3.505200E+04	yp =	0.000000E+00
Station	104	xp =	3.505200E+04	yp =	9.144000E+01
Station	105	xp =	3.505200E+04	yp =	1.828800E+02
Station	106	xp =	3.505200E+04	yp =	3.048000E+02
Station	107	xp =	3.505200E+04	yp =	6.096000E+02
Station	108	xp =	3.505200E+04	yp =	1.219200E+03
Station	109	xp =	3.810000E+04	yp =	0.000000E+00
Station	110	xp =	3.810000E+04	yp =	9.144000E+01
Station	111	xp =	3.810000E+04	yp =	1.828800E+02
Station	112	xp =	3.810000E+04	yp =	3.048000E+02
Station	113	xp =	3.810000E+04	yp =	6.096000E+02
Station	114	xp =	3.810000E+04	yp =	1.219200E+03
Station	115	xp =	4.114800E+04	yp =	0.000000E+00
Station	116	xp =	4.114800E+04	yp =	9.144000E+01
Station	117	xp =	4.114800E+04	yp =	1.828800E+02
Station	118	xp =	4.114800E+04	yp =	3.048000E+02
Station	119	xp =	4.114800E+04	yp =	6.096000E+02
Station	120	xp =	4.114800E+04	yp =	1.219200E+03
Station	121	xp =	4.145280E+04	yp =	0.000000E+00
Station	122	xp =	4.145280E+04	yp =	9.144000E+01
Station	123	xp =	4.145280E+04	yp =	1.828800E+02
Station	124	xp =	4.145280E+04	yp =	3.048000E+02
Station	125	xp =	4.145280E+04	yp =	6.096000E+02
Station	126	xp =	4.145280E+04	yp =	1.219200E+03
Station	127	xp =	4.358640E+04	yp =	0.000000E+00
Station	128	xp =	4.358640E+04	yp =	9.144000E+01
Station	129	xp =	4.358640E+04	yp =	1.828800E+02

```
Station  130 xp =  4.358640E+04 yp =  3.048000E+02
Station  131 xp =  4.358640E+04 yp =  6.096000E+02
Station  132 xp =  4.358640E+04 yp =  1.219200E+03
Station  133 xp =  4.419600E+04 yp =  0.000000E+00
Station  134 xp =  4.419600E+04 yp =  9.144000E+01
Station  135 xp =  4.419600E+04 yp =  1.828800E+02
Station  136 xp =  4.419600E+04 yp =  3.048000E+02
Station  137 xp =  4.419600E+04 yp =  6.096000E+02
Station  138 xp =  4.419600E+04 yp =  1.219200E+03
Station  139 xp =  4.678680E+04 yp =  0.000000E+00
Station  140 xp =  4.678680E+04 yp =  9.144000E+01
Station  141 xp =  4.678680E+04 yp =  1.828800E+02
Station  142 xp =  4.678680E+04 yp =  3.048000E+02
Station  143 xp =  4.678680E+04 yp =  6.096000E+02
Station  144 xp =  4.678680E+04 yp =  1.219200E+03
Station  145 xp =  4.754880E+04 yp =  0.000000E+00
Station  146 xp =  4.754880E+04 yp =  9.144000E+01
Station  147 xp =  4.754880E+04 yp =  1.828800E+02
Station  148 xp =  4.754880E+04 yp =  3.048000E+02
Station  149 xp =  4.754880E+04 yp =  6.096000E+02
Station  150 xp =  4.754880E+04 yp =  1.219200E+03
Station  151 xp =  5.029200E+04 yp =  0.000000E+00
Station  152 xp =  5.029200E+04 yp =  9.144000E+01
Station  153 xp =  5.029200E+04 yp =  1.828800E+02
Station  154 xp =  5.029200E+04 yp =  3.048000E+02
Station  155 xp =  5.029200E+04 yp =  6.096000E+02
Station  156 xp =  5.029200E+04 yp =  1.219200E+03
Station  157 xp =  5.181600E+04 yp =  0.000000E+00
Station  158 xp =  5.181600E+04 yp =  9.144000E+01
Station  159 xp =  5.181600E+04 yp =  1.828800E+02
Station  160 xp =  5.181600E+04 yp =  3.048000E+02
Station  161 xp =  5.181600E+04 yp =  6.096000E+02
Station  162 xp =  5.181600E+04 yp =  1.219200E+03
Station  163 xp =  5.242560E+04 yp =  0.000000E+00
Station  164 xp =  5.242560E+04 yp =  9.144000E+01
Station  165 xp =  5.242560E+04 yp =  1.828800E+02
Station  166 xp =  5.242560E+04 yp =  3.048000E+02
Station  167 xp =  5.242560E+04 yp =  6.096000E+02
Station  168 xp =  5.242560E+04 yp =  1.219200E+03
Station  169 xp =  5.334000E+04 yp =  0.000000E+00
Station  170 xp =  5.334000E+04 yp =  9.144000E+01
Station  171 xp =  5.334000E+04 yp =  1.828800E+02
Station  172 xp =  5.334000E+04 yp =  3.048000E+02
Station  173 xp =  5.334000E+04 yp =  6.096000E+02
Station  174 xp =  5.334000E+04 yp =  1.219200E+03
Station  175 xp =  5.486400E+04 yp =  0.000000E+00
Station  176 xp =  5.486400E+04 yp =  9.144000E+01
Station  177 xp =  5.486400E+04 yp =  1.828800E+02
Station  178 xp =  5.486400E+04 yp =  3.048000E+02
Station  179 xp =  5.486400E+04 yp =  6.096000E+02
Station  180 xp =  5.486400E+04 yp =  1.219200E+03
Station  181 xp =  5.791200E+04 yp =  0.000000E+00
Station  182 xp =  5.791200E+04 yp =  9.144000E+01
Station  183 xp =  5.791200E+04 yp =  1.828800E+02
Station  184 xp =  5.791200E+04 yp =  3.048000E+02
Station  185 xp =  5.791200E+04 yp =  6.096000E+02
Station  186 xp =  5.791200E+04 yp =  1.219200E+03
Station  187 xp =  6.096000E+04 yp =  0.000000E+00
Station  188 xp =  6.096000E+04 yp =  9.144000E+01
Station  189 xp =  6.096000E+04 yp =  1.828800E+02
Station  190 xp =  6.096000E+04 yp =  3.048000E+02
Station  191 xp =  6.096000E+04 yp =  6.096000E+02
Station  192 xp =  6.096000E+04 yp =  1.219200E+03
Station  193 xp =  6.187440E+04 yp =  0.000000E+00
Station  194 xp =  6.187440E+04 yp =  9.144000E+01
Station  195 xp =  6.187440E+04 yp =  1.828800E+02
```

Station	196	xp =	6.187440E+04	yp =	3.048000E+02
Station	197	xp =	6.187440E+04	yp =	6.096000E+02
Station	198	xp =	6.187440E+04	yp =	1.219200E+03
Station	199	xp =	6.400800E+04	yp =	0.000000E+00
Station	200	xp =	6.400800E+04	yp =	9.144000E+01
Station	201	xp =	6.400800E+04	yp =	1.828800E+02
Station	202	xp =	6.400800E+04	yp =	3.048000E+02
Station	203	xp =	6.400800E+04	yp =	6.096000E+02
Station	204	xp =	6.400800E+04	yp =	1.219200E+03
Station	205	xp =	6.858000E+04	yp =	0.000000E+00
Station	206	xp =	6.858000E+04	yp =	9.144000E+01
Station	207	xp =	6.858000E+04	yp =	1.828800E+02
Station	208	xp =	6.858000E+04	yp =	3.048000E+02
Station	209	xp =	6.858000E+04	yp =	6.096000E+02
Station	210	xp =	6.858000E+04	yp =	1.219200E+03
Station	211	xp =	6.949440E+04	yp =	0.000000E+00
Station	212	xp =	6.949440E+04	yp =	9.144000E+01
Station	213	xp =	6.949440E+04	yp =	1.828800E+02
Station	214	xp =	6.949440E+04	yp =	3.048000E+02
Station	215	xp =	6.949440E+04	yp =	6.096000E+02
Station	216	xp =	6.949440E+04	yp =	1.219200E+03
Station	217	xp =	7.010400E+04	yp =	0.000000E+00
Station	218	xp =	7.010400E+04	yp =	9.144000E+01
Station	219	xp =	7.010400E+04	yp =	1.828800E+02
Station	220	xp =	7.010400E+04	yp =	3.048000E+02
Station	221	xp =	7.010400E+04	yp =	6.096000E+02
Station	222	xp =	7.010400E+04	yp =	1.219200E+03
Station	223	xp =	7.162800E+04	yp =	0.000000E+00
Station	224	xp =	7.162800E+04	yp =	9.144000E+01
Station	225	xp =	7.162800E+04	yp =	1.828800E+02
Station	226	xp =	7.162800E+04	yp =	3.048000E+02
Station	227	xp =	7.162800E+04	yp =	6.096000E+02
Station	228	xp =	7.162800E+04	yp =	1.219200E+03
Station	229	xp =	7.315200E+04	yp =	0.000000E+00
Station	230	xp =	7.315200E+04	yp =	9.144000E+01
Station	231	xp =	7.315200E+04	yp =	1.828800E+02
Station	232	xp =	7.315200E+04	yp =	3.048000E+02
Station	233	xp =	7.315200E+04	yp =	6.096000E+02
Station	234	xp =	7.315200E+04	yp =	1.219200E+03
Station	235	xp =	7.467600E+04	yp =	0.000000E+00
Station	236	xp =	7.467600E+04	yp =	9.144000E+01
Station	237	xp =	7.467600E+04	yp =	1.828800E+02
Station	238	xp =	7.467600E+04	yp =	3.048000E+02
Station	239	xp =	7.467600E+04	yp =	6.096000E+02
Station	240	xp =	7.467600E+04	yp =	1.219200E+03
Station	241	xp =	7.543800E+04	yp =	0.000000E+00
Station	242	xp =	7.543800E+04	yp =	9.144000E+01
Station	243	xp =	7.543800E+04	yp =	1.828800E+02
Station	244	xp =	7.543800E+04	yp =	3.048000E+02
Station	245	xp =	7.543800E+04	yp =	6.096000E+02
Station	246	xp =	7.543800E+04	yp =	1.219200E+03
Station	247	xp =	7.620000E+04	yp =	0.000000E+00
Station	248	xp =	7.620000E+04	yp =	9.144000E+01
Station	249	xp =	7.620000E+04	yp =	1.828800E+02
Station	250	xp =	7.620000E+04	yp =	3.048000E+02
Station	251	xp =	7.620000E+04	yp =	6.096000E+02
Station	252	xp =	7.620000E+04	yp =	1.219200E+03
Station	253	xp =	7.696200E+04	yp =	0.000000E+00
Station	254	xp =	7.696200E+04	yp =	9.144000E+01
Station	255	xp =	7.696200E+04	yp =	1.828800E+02
Station	256	xp =	7.696200E+04	yp =	3.048000E+02
Station	257	xp =	7.696200E+04	yp =	6.096000E+02
Station	258	xp =	7.696200E+04	yp =	1.219200E+03
Station	259	xp =	7.772400E+04	yp =	0.000000E+00
Station	260	xp =	7.772400E+04	yp =	9.144000E+01
Station	261	xp =	7.772400E+04	yp =	1.828800E+02

Station	262	xp =	7.772400E+04	yp =	3.048000E+02
Station	263	xp =	7.772400E+04	yp =	6.096000E+02
Station	264	xp =	7.772400E+04	yp =	1.219200E+03
Station	265	xp =	7.924800E+04	yp =	0.000000E+00
Station	266	xp =	7.924800E+04	yp =	9.144000E+01
Station	267	xp =	7.924800E+04	yp =	1.828800E+02
Station	268	xp =	7.924800E+04	yp =	3.048000E+02
Station	269	xp =	7.924800E+04	yp =	6.096000E+02
Station	270	xp =	7.924800E+04	yp =	1.219200E+03
Station	271	xp =	8.077200E+04	yp =	0.000000E+00
Station	272	xp =	8.077200E+04	yp =	9.144000E+01
Station	273	xp =	8.077200E+04	yp =	1.828800E+02
Station	274	xp =	8.077200E+04	yp =	3.048000E+02
Station	275	xp =	8.077200E+04	yp =	6.096000E+02
Station	276	xp =	8.077200E+04	yp =	1.219200E+03
Station	277	xp =	8.321040E+04	yp =	0.000000E+00
Station	278	xp =	8.321040E+04	yp =	9.144000E+01
Station	279	xp =	8.321040E+04	yp =	1.828800E+02
Station	280	xp =	8.321040E+04	yp =	3.048000E+02
Station	281	xp =	8.321040E+04	yp =	6.096000E+02
Station	282	xp =	8.321040E+04	yp =	1.219200E+03
Station	283	xp =	8.534400E+04	yp =	0.000000E+00
Station	284	xp =	8.534400E+04	yp =	9.144000E+01
Station	285	xp =	8.534400E+04	yp =	1.828800E+02
Station	286	xp =	8.534400E+04	yp =	3.048000E+02
Station	287	xp =	8.534400E+04	yp =	6.096000E+02
Station	288	xp =	8.534400E+04	yp =	1.219200E+03
Station	289	xp =	8.686800E+04	yp =	0.000000E+00
Station	290	xp =	8.686800E+04	yp =	9.144000E+01
Station	291	xp =	8.686800E+04	yp =	1.828800E+02
Station	292	xp =	8.686800E+04	yp =	3.048000E+02
Station	293	xp =	8.686800E+04	yp =	6.096000E+02
Station	294	xp =	8.686800E+04	yp =	1.219200E+03
Station	295	xp =	8.763000E+04	yp =	0.000000E+00
Station	296	xp =	8.763000E+04	yp =	9.144000E+01
Station	297	xp =	8.763000E+04	yp =	1.828800E+02
Station	298	xp =	8.763000E+04	yp =	3.048000E+02
Station	299	xp =	8.763000E+04	yp =	6.096000E+02
Station	300	xp =	8.763000E+04	yp =	1.219200E+03
Station	301	xp =	8.839200E+04	yp =	0.000000E+00
Station	302	xp =	8.839200E+04	yp =	9.144000E+01
Station	303	xp =	8.839200E+04	yp =	1.828800E+02
Station	304	xp =	8.839200E+04	yp =	3.048000E+02
Station	305	xp =	8.839200E+04	yp =	6.096000E+02
Station	306	xp =	8.839200E+04	yp =	1.219200E+03
Station	307	xp =	8.915400E+04	yp =	0.000000E+00
Station	308	xp =	8.915400E+04	yp =	9.144000E+01
Station	309	xp =	8.915400E+04	yp =	1.828800E+02
Station	310	xp =	8.915400E+04	yp =	3.048000E+02
Station	311	xp =	8.915400E+04	yp =	6.096000E+02
Station	312	xp =	8.915400E+04	yp =	1.219200E+03
Station	313	xp =	8.991600E+04	yp =	0.000000E+00
Station	314	xp =	8.991600E+04	yp =	9.144000E+01
Station	315	xp =	8.991600E+04	yp =	1.828800E+02
Station	316	xp =	8.991600E+04	yp =	3.048000E+02
Station	317	xp =	8.991600E+04	yp =	6.096000E+02
Station	318	xp =	8.991600E+04	yp =	1.219200E+03
Station	319	xp =	9.144000E+04	yp =	0.000000E+00
Station	320	xp =	9.144000E+04	yp =	9.144000E+01
Station	321	xp =	9.144000E+04	yp =	1.828800E+02
Station	322	xp =	9.144000E+04	yp =	3.048000E+02
Station	323	xp =	9.144000E+04	yp =	6.096000E+02
Station	324	xp =	9.144000E+04	yp =	1.219200E+03
Station	325	xp =	9.906000E+04	yp =	0.000000E+00
Station	326	xp =	9.906000E+04	yp =	9.144000E+01
Station	327	xp =	9.906000E+04	yp =	1.828800E+02

Station	328	xp =	9.906000E+04	yp =	3.048000E+02
Station	329	xp =	9.906000E+04	yp =	6.096000E+02
Station	330	xp =	9.906000E+04	yp =	1.219200E+03
Station	331	xp =	1.066800E+05	yp =	0.000000E+00
Station	332	xp =	1.066800E+05	yp =	9.144000E+01
Station	333	xp =	1.066800E+05	yp =	1.828800E+02
Station	334	xp =	1.066800E+05	yp =	3.048000E+02
Station	335	xp =	1.066800E+05	yp =	6.096000E+02
Station	336	xp =	1.066800E+05	yp =	1.219200E+03
Station	337	xp =	1.074420E+05	yp =	0.000000E+00
Station	338	xp =	1.074420E+05	yp =	9.144000E+01
Station	339	xp =	1.074420E+05	yp =	1.828800E+02
Station	340	xp =	1.074420E+05	yp =	3.048000E+02
Station	341	xp =	1.074420E+05	yp =	6.096000E+02
Station	342	xp =	1.074420E+05	yp =	1.219200E+03
Station	343	xp =	1.082040E+05	yp =	0.000000E+00
Station	344	xp =	1.082040E+05	yp =	9.144000E+01
Station	345	xp =	1.082040E+05	yp =	1.828800E+02
Station	346	xp =	1.082040E+05	yp =	3.048000E+02
Station	347	xp =	1.082040E+05	yp =	6.096000E+02
Station	348	xp =	1.082040E+05	yp =	1.219200E+03
Station	349	xp =	1.089660E+05	yp =	0.000000E+00
Station	350	xp =	1.089660E+05	yp =	9.144000E+01
Station	351	xp =	1.089660E+05	yp =	1.828800E+02
Station	352	xp =	1.089660E+05	yp =	3.048000E+02
Station	353	xp =	1.089660E+05	yp =	6.096000E+02
Station	354	xp =	1.089660E+05	yp =	1.219200E+03
Station	355	xp =	1.097280E+05	yp =	0.000000E+00
Station	356	xp =	1.097280E+05	yp =	9.144000E+01
Station	357	xp =	1.097280E+05	yp =	1.828800E+02
Station	358	xp =	1.097280E+05	yp =	3.048000E+02
Station	359	xp =	1.097280E+05	yp =	6.096000E+02
Station	360	xp =	1.097280E+05	yp =	1.219200E+03
Station	361	xp =	1.104900E+05	yp =	0.000000E+00
Station	362	xp =	1.104900E+05	yp =	9.144000E+01
Station	363	xp =	1.104900E+05	yp =	1.828800E+02
Station	364	xp =	1.104900E+05	yp =	3.048000E+02
Station	365	xp =	1.104900E+05	yp =	6.096000E+02
Station	366	xp =	1.104900E+05	yp =	1.219200E+03
Station	367	xp =	1.112520E+05	yp =	0.000000E+00
Station	368	xp =	1.112520E+05	yp =	9.144000E+01
Station	369	xp =	1.112520E+05	yp =	1.828800E+02
Station	370	xp =	1.112520E+05	yp =	3.048000E+02
Station	371	xp =	1.112520E+05	yp =	6.096000E+02
Station	372	xp =	1.112520E+05	yp =	1.219200E+03
Station	373	xp =	1.120140E+05	yp =	0.000000E+00
Station	374	xp =	1.120140E+05	yp =	9.144000E+01
Station	375	xp =	1.120140E+05	yp =	1.828800E+02
Station	376	xp =	1.120140E+05	yp =	3.048000E+02
Station	377	xp =	1.120140E+05	yp =	6.096000E+02
Station	378	xp =	1.120140E+05	yp =	1.219200E+03
Station	379	xp =	1.127760E+05	yp =	0.000000E+00
Station	380	xp =	1.127760E+05	yp =	9.144000E+01
Station	381	xp =	1.127760E+05	yp =	1.828800E+02
Station	382	xp =	1.127760E+05	yp =	3.048000E+02
Station	383	xp =	1.127760E+05	yp =	6.096000E+02
Station	384	xp =	1.127760E+05	yp =	1.219200E+03
Station	385	xp =	1.158240E+05	yp =	0.000000E+00
Station	386	xp =	1.158240E+05	yp =	9.144000E+01
Station	387	xp =	1.158240E+05	yp =	1.828800E+02
Station	388	xp =	1.158240E+05	yp =	3.048000E+02
Station	389	xp =	1.158240E+05	yp =	6.096000E+02
Station	390	xp =	1.158240E+05	yp =	1.219200E+03
Station	391	xp =	1.188720E+05	yp =	0.000000E+00
Station	392	xp =	1.188720E+05	yp =	9.144000E+01
Station	393	xp =	1.188720E+05	yp =	1.828800E+02

Station	394	xp =	1.188720E+05	yp =	3.048000E+02
Station	395	xp =	1.188720E+05	yp =	6.096000E+02
Station	396	xp =	1.188720E+05	yp =	1.219200E+03
Station	397	xp =	1.197864E+05	yp =	0.000000E+00
Station	398	xp =	1.197864E+05	yp =	9.144000E+01
Station	399	xp =	1.197864E+05	yp =	1.828800E+02
Station	400	xp =	1.197864E+05	yp =	3.048000E+02
Station	401	xp =	1.197864E+05	yp =	6.096000E+02
Station	402	xp =	1.197864E+05	yp =	1.219200E+03
Station	403	xp =	1.219200E+05	yp =	0.000000E+00
Station	404	xp =	1.219200E+05	yp =	9.144000E+01
Station	405	xp =	1.219200E+05	yp =	1.828800E+02
Station	406	xp =	1.219200E+05	yp =	3.048000E+02
Station	407	xp =	1.219200E+05	yp =	6.096000E+02
Station	408	xp =	1.219200E+05	yp =	1.219200E+03
Station	409	xp =	1.234440E+05	yp =	0.000000E+00
Station	410	xp =	1.234440E+05	yp =	9.144000E+01
Station	411	xp =	1.234440E+05	yp =	1.828800E+02
Station	412	xp =	1.234440E+05	yp =	3.048000E+02
Station	413	xp =	1.234440E+05	yp =	6.096000E+02
Station	414	xp =	1.234440E+05	yp =	1.219200E+03
Station	415	xp =	1.249680E+05	yp =	0.000000E+00
Station	416	xp =	1.249680E+05	yp =	9.144000E+01
Station	417	xp =	1.249680E+05	yp =	1.828800E+02
Station	418	xp =	1.249680E+05	yp =	3.048000E+02
Station	419	xp =	1.249680E+05	yp =	6.096000E+02
Station	420	xp =	1.249680E+05	yp =	1.219200E+03
Station	421	xp =	1.264920E+05	yp =	0.000000E+00
Station	422	xp =	1.264920E+05	yp =	9.144000E+01
Station	423	xp =	1.264920E+05	yp =	1.828800E+02
Station	424	xp =	1.264920E+05	yp =	3.048000E+02
Station	425	xp =	1.264920E+05	yp =	6.096000E+02
Station	426	xp =	1.264920E+05	yp =	1.219200E+03
Station	427	xp =	1.272540E+05	yp =	0.000000E+00
Station	428	xp =	1.272540E+05	yp =	9.144000E+01
Station	429	xp =	1.272540E+05	yp =	1.828800E+02
Station	430	xp =	1.272540E+05	yp =	3.048000E+02
Station	431	xp =	1.272540E+05	yp =	6.096000E+02
Station	432	xp =	1.272540E+05	yp =	1.219200E+03
Station	433	xp =	1.280160E+05	yp =	0.000000E+00
Station	434	xp =	1.280160E+05	yp =	9.144000E+01
Station	435	xp =	1.280160E+05	yp =	1.828800E+02
Station	436	xp =	1.280160E+05	yp =	3.048000E+02
Station	437	xp =	1.280160E+05	yp =	6.096000E+02
Station	438	xp =	1.280160E+05	yp =	1.219200E+03
Station	439	xp =	1.287780E+05	yp =	0.000000E+00
Station	440	xp =	1.287780E+05	yp =	9.144000E+01
Station	441	xp =	1.287780E+05	yp =	1.828800E+02
Station	442	xp =	1.287780E+05	yp =	3.048000E+02
Station	443	xp =	1.287780E+05	yp =	6.096000E+02
Station	444	xp =	1.287780E+05	yp =	1.219200E+03
Station	445	xp =	1.295400E+05	yp =	0.000000E+00
Station	446	xp =	1.295400E+05	yp =	9.144000E+01
Station	447	xp =	1.295400E+05	yp =	1.828800E+02
Station	448	xp =	1.295400E+05	yp =	3.048000E+02
Station	449	xp =	1.295400E+05	yp =	6.096000E+02
Station	450	xp =	1.295400E+05	yp =	1.219200E+03
Station	451	xp =	1.310640E+05	yp =	0.000000E+00
Station	452	xp =	1.310640E+05	yp =	9.144000E+01
Station	453	xp =	1.310640E+05	yp =	1.828800E+02
Station	454	xp =	1.310640E+05	yp =	3.048000E+02
Station	455	xp =	1.310640E+05	yp =	6.096000E+02
Station	456	xp =	1.310640E+05	yp =	1.219200E+03
Station	457	xp =	1.341120E+05	yp =	0.000000E+00
Station	458	xp =	1.341120E+05	yp =	9.144000E+01
Station	459	xp =	1.341120E+05	yp =	1.828800E+02

Station	460	xp =	1.341120E+05	yp =	3.048000E+02
Station	461	xp =	1.341120E+05	yp =	6.096000E+02
Station	462	xp =	1.341120E+05	yp =	1.219200E+03
Station	463	xp =	1.371600E+05	yp =	0.000000E+00
Station	464	xp =	1.371600E+05	yp =	9.144000E+01
Station	465	xp =	1.371600E+05	yp =	1.828800E+02
Station	466	xp =	1.371600E+05	yp =	3.048000E+02
Station	467	xp =	1.371600E+05	yp =	6.096000E+02
Station	468	xp =	1.371600E+05	yp =	1.219200E+03
Station	469	xp =	1.402080E+05	yp =	0.000000E+00
Station	470	xp =	1.402080E+05	yp =	9.144000E+01
Station	471	xp =	1.402080E+05	yp =	1.828800E+02
Station	472	xp =	1.402080E+05	yp =	3.048000E+02
Station	473	xp =	1.402080E+05	yp =	6.096000E+02
Station	474	xp =	1.402080E+05	yp =	1.219200E+03
Station	475	xp =	1.453896E+05	yp =	0.000000E+00
Station	476	xp =	1.453896E+05	yp =	9.144000E+01
Station	477	xp =	1.453896E+05	yp =	1.828800E+02
Station	478	xp =	1.453896E+05	yp =	3.048000E+02
Station	479	xp =	1.453896E+05	yp =	6.096000E+02
Station	480	xp =	1.453896E+05	yp =	1.219200E+03
Station	481	xp =	1.493520E+05	yp =	0.000000E+00
Station	482	xp =	1.493520E+05	yp =	9.144000E+01
Station	483	xp =	1.493520E+05	yp =	1.828800E+02
Station	484	xp =	1.493520E+05	yp =	3.048000E+02
Station	485	xp =	1.493520E+05	yp =	6.096000E+02
Station	486	xp =	1.493520E+05	yp =	1.219200E+03
Station	487	xp =	1.524000E+05	yp =	0.000000E+00
Station	488	xp =	1.524000E+05	yp =	9.144000E+01
Station	489	xp =	1.524000E+05	yp =	1.828800E+02
Station	490	xp =	1.524000E+05	yp =	3.048000E+02
Station	491	xp =	1.524000E+05	yp =	6.096000E+02
Station	492	xp =	1.524000E+05	yp =	1.219200E+03
Station	493	xp =	1.554480E+05	yp =	0.000000E+00
Station	494	xp =	1.554480E+05	yp =	9.144000E+01
Station	495	xp =	1.554480E+05	yp =	1.828800E+02
Station	496	xp =	1.554480E+05	yp =	3.048000E+02
Station	497	xp =	1.554480E+05	yp =	6.096000E+02
Station	498	xp =	1.554480E+05	yp =	1.219200E+03
Station	499	xp =	1.584960E+05	yp =	0.000000E+00
Station	500	xp =	1.584960E+05	yp =	9.144000E+01
Station	501	xp =	1.584960E+05	yp =	1.828800E+02
Station	502	xp =	1.584960E+05	yp =	3.048000E+02
Station	503	xp =	1.584960E+05	yp =	6.096000E+02
Station	504	xp =	1.584960E+05	yp =	1.219200E+03
Station	505	xp =	1.600200E+05	yp =	0.000000E+00
Station	506	xp =	1.600200E+05	yp =	9.144000E+01
Station	507	xp =	1.600200E+05	yp =	1.828800E+02
Station	508	xp =	1.600200E+05	yp =	3.048000E+02
Station	509	xp =	1.600200E+05	yp =	6.096000E+02
Station	510	xp =	1.600200E+05	yp =	1.219200E+03
Station	511	xp =	1.615440E+05	yp =	0.000000E+00
Station	512	xp =	1.615440E+05	yp =	9.144000E+01
Station	513	xp =	1.615440E+05	yp =	1.828800E+02
Station	514	xp =	1.615440E+05	yp =	3.048000E+02
Station	515	xp =	1.615440E+05	yp =	6.096000E+02
Station	516	xp =	1.615440E+05	yp =	1.219200E+03
Station	517	xp =	1.621536E+05	yp =	0.000000E+00
Station	518	xp =	1.621536E+05	yp =	9.144000E+01
Station	519	xp =	1.621536E+05	yp =	1.828800E+02
Station	520	xp =	1.621536E+05	yp =	3.048000E+02
Station	521	xp =	1.621536E+05	yp =	6.096000E+02
Station	522	xp =	1.621536E+05	yp =	1.219200E+03
Station	523	xp =	1.630680E+05	yp =	0.000000E+00
Station	524	xp =	1.630680E+05	yp =	9.144000E+01
Station	525	xp =	1.630680E+05	yp =	1.828800E+02

```
Station  526 xp =  1.630680E+05 yp =  3.048000E+02
Station  527 xp =  1.630680E+05 yp =  6.096000E+02
Station  528 xp =  1.630680E+05 yp =  1.219200E+03
Station  529 xp =  1.645920E+05 yp =  0.000000E+00
Station  530 xp =  1.645920E+05 yp =  9.144000E+01
Station  531 xp =  1.645920E+05 yp =  1.828800E+02
Station  532 xp =  1.645920E+05 yp =  3.048000E+02
Station  533 xp =  1.645920E+05 yp =  6.096000E+02
Station  534 xp =  1.645920E+05 yp =  1.219200E+03
Station  535 xp =  1.676400E+05 yp =  0.000000E+00
Station  536 xp =  1.676400E+05 yp =  9.144000E+01
Station  537 xp =  1.676400E+05 yp =  1.828800E+02
Station  538 xp =  1.676400E+05 yp =  3.048000E+02
Station  539 xp =  1.676400E+05 yp =  6.096000E+02
Station  540 xp =  1.676400E+05 yp =  1.219200E+03
Station  541 xp =  1.706880E+05 yp =  0.000000E+00
Station  542 xp =  1.706880E+05 yp =  9.144000E+01
Station  543 xp =  1.706880E+05 yp =  1.828800E+02
Station  544 xp =  1.706880E+05 yp =  3.048000E+02
Station  545 xp =  1.706880E+05 yp =  6.096000E+02
Station  546 xp =  1.706880E+05 yp =  1.219200E+03
Station  547 xp =  1.737360E+05 yp =  0.000000E+00
Station  548 xp =  1.737360E+05 yp =  9.144000E+01
Station  549 xp =  1.737360E+05 yp =  1.828800E+02
Station  550 xp =  1.737360E+05 yp =  3.048000E+02
Station  551 xp =  1.737360E+05 yp =  6.096000E+02
Station  552 xp =  1.737360E+05 yp =  1.219200E+03
Station  553 xp =  1.828800E+05 yp =  0.000000E+00
Station  554 xp =  1.828800E+05 yp =  9.144000E+01
Station  555 xp =  1.828800E+05 yp =  1.828800E+02
Station  556 xp =  1.828800E+05 yp =  3.048000E+02
Station  557 xp =  1.828800E+05 yp =  6.096000E+02
Station  558 xp =  1.828800E+05 yp =  1.219200E+03
Station  559 xp =  1.865376E+05 yp =  0.000000E+00
Station  560 xp =  1.865376E+05 yp =  9.144000E+01
Station  561 xp =  1.865376E+05 yp =  1.828800E+02
Station  562 xp =  1.865376E+05 yp =  3.048000E+02
Station  563 xp =  1.865376E+05 yp =  6.096000E+02
Station  564 xp =  1.865376E+05 yp =  1.219200E+03
Station  565 xp =  2.133600E+05 yp =  0.000000E+00
Station  566 xp =  2.133600E+05 yp =  9.144000E+01
Station  567 xp =  2.133600E+05 yp =  1.828800E+02
Station  568 xp =  2.133600E+05 yp =  3.048000E+02
Station  569 xp =  2.133600E+05 yp =  6.096000E+02
Station  570 xp =  2.133600E+05 yp =  1.219200E+03
Station  571 xp =  2.286000E+05 yp =  0.000000E+00
Station  572 xp =  2.286000E+05 yp =  9.144000E+01
Station  573 xp =  2.286000E+05 yp =  1.828800E+02
Station  574 xp =  2.286000E+05 yp =  3.048000E+02
Station  575 xp =  2.286000E+05 yp =  6.096000E+02
Station  576 xp =  2.286000E+05 yp =  1.219200E+03

Locations of stations generated are ...

Station  577 xp =  4.678680E+04 yp =  0.000000E+00
Station  578 xp =  4.678680E+04 yp =  3.048000E+01
Station  579 xp =  4.678680E+04 yp =  6.096000E+01
Station  580 xp =  4.678680E+04 yp =  9.144000E+01
Station  581 xp =  4.678680E+04 yp =  1.219200E+02
Station  582 xp =  4.678680E+04 yp =  1.524000E+02
Station  583 xp =  4.678680E+04 yp =  1.828800E+02
Station  584 xp =  4.678680E+04 yp =  2.133600E+02
Station  585 xp =  4.678680E+04 yp =  2.438400E+02
Station  586 xp =  4.678680E+04 yp =  2.743200E+02
Station  587 xp =  4.678680E+04 yp =  3.048000E+02
Station  588 xp =  4.678680E+04 yp =  3.657600E+02
```

Station	589	xp =	4.678680E+04	yp =	4.267200E+02
Station	590	xp =	4.678680E+04	yp =	4.876800E+02
Station	591	xp =	4.678680E+04	yp =	5.486400E+02
Station	592	xp =	4.678680E+04	yp =	6.096000E+02
Station	593	xp =	4.678680E+04	yp =	6.705600E+02
Station	594	xp =	4.678680E+04	yp =	7.315200E+02
Station	595	xp =	4.678680E+04	yp =	7.924800E+02
Station	596	xp =	4.678680E+04	yp =	9.144000E+02
Station	597	xp =	4.678680E+04	yp =	1.066800E+03
Station	598	xp =	4.678680E+04	yp =	1.219200E+03
Station	599	xp =	6.096000E+04	yp =	0.000000E+00
Station	600	xp =	6.096000E+04	yp =	3.048000E+01
Station	601	xp =	6.096000E+04	yp =	6.096000E+01
Station	602	xp =	6.096000E+04	yp =	9.144000E+01
Station	603	xp =	6.096000E+04	yp =	1.219200E+02
Station	604	xp =	6.096000E+04	yp =	1.524000E+02
Station	605	xp =	6.096000E+04	yp =	1.828800E+02
Station	606	xp =	6.096000E+04	yp =	2.133600E+02
Station	607	xp =	6.096000E+04	yp =	2.438400E+02
Station	608	xp =	6.096000E+04	yp =	2.743200E+02
Station	609	xp =	6.096000E+04	yp =	3.048000E+02
Station	610	xp =	6.096000E+04	yp =	3.657600E+02
Station	611	xp =	6.096000E+04	yp =	4.267200E+02
Station	612	xp =	6.096000E+04	yp =	4.876800E+02
Station	613	xp =	6.096000E+04	yp =	5.486400E+02
Station	614	xp =	6.096000E+04	yp =	6.096000E+02
Station	615	xp =	6.096000E+04	yp =	6.705600E+02
Station	616	xp =	6.096000E+04	yp =	7.315200E+02
Station	617	xp =	6.096000E+04	yp =	7.924800E+02
Station	618	xp =	6.096000E+04	yp =	9.144000E+02
Station	619	xp =	6.096000E+04	yp =	1.066800E+03
Station	620	xp =	6.096000E+04	yp =	1.219200E+03
Station	621	xp =	7.543800E+04	yp =	0.000000E+00
Station	622	xp =	7.543800E+04	yp =	3.048000E+01
Station	623	xp =	7.543800E+04	yp =	6.096000E+01
Station	624	xp =	7.543800E+04	yp =	9.144000E+01
Station	625	xp =	7.543800E+04	yp =	1.219200E+02
Station	626	xp =	7.543800E+04	yp =	1.524000E+02
Station	627	xp =	7.543800E+04	yp =	1.828800E+02
Station	628	xp =	7.543800E+04	yp =	2.133600E+02
Station	629	xp =	7.543800E+04	yp =	2.438400E+02
Station	630	xp =	7.543800E+04	yp =	2.743200E+02
Station	631	xp =	7.543800E+04	yp =	3.048000E+02
Station	632	xp =	7.543800E+04	yp =	3.657600E+02
Station	633	xp =	7.543800E+04	yp =	4.267200E+02
Station	634	xp =	7.543800E+04	yp =	4.876800E+02
Station	635	xp =	7.543800E+04	yp =	5.486400E+02
Station	636	xp =	7.543800E+04	yp =	6.096000E+02
Station	637	xp =	7.543800E+04	yp =	6.705600E+02
Station	638	xp =	7.543800E+04	yp =	7.315200E+02
Station	639	xp =	7.543800E+04	yp =	7.924800E+02
Station	640	xp =	7.543800E+04	yp =	9.144000E+02
Station	641	xp =	7.543800E+04	yp =	1.066800E+03
Station	642	xp =	7.543800E+04	yp =	1.219200E+03
Station	643	xp =	8.763000E+04	yp =	0.000000E+00
Station	644	xp =	8.763000E+04	yp =	3.048000E+01
Station	645	xp =	8.763000E+04	yp =	6.096000E+01
Station	646	xp =	8.763000E+04	yp =	9.144000E+01
Station	647	xp =	8.763000E+04	yp =	1.219200E+02
Station	648	xp =	8.763000E+04	yp =	1.524000E+02
Station	649	xp =	8.763000E+04	yp =	1.828800E+02
Station	650	xp =	8.763000E+04	yp =	2.133600E+02
Station	651	xp =	8.763000E+04	yp =	2.438400E+02
Station	652	xp =	8.763000E+04	yp =	2.743200E+02
Station	653	xp =	8.763000E+04	yp =	3.048000E+02
Station	654	xp =	8.763000E+04	yp =	3.657600E+02

Station	655	xp =	8.763000E+04	yp =	4.267200E+02
Station	656	xp =	8.763000E+04	yp =	4.876800E+02
Station	657	xp =	8.763000E+04	yp =	5.486400E+02
Station	658	xp =	8.763000E+04	yp =	6.096000E+02
Station	659	xp =	8.763000E+04	yp =	6.705600E+02
Station	660	xp =	8.763000E+04	yp =	7.315200E+02
Station	661	xp =	8.763000E+04	yp =	7.924800E+02
Station	662	xp =	8.763000E+04	yp =	9.144000E+02
Station	663	xp =	8.763000E+04	yp =	1.066800E+03
Station	664	xp =	8.763000E+04	yp =	1.219200E+03
Station	665	xp =	1.089660E+05	yp =	0.000000E+00
Station	666	xp =	1.089660E+05	yp =	3.048000E+01
Station	667	xp =	1.089660E+05	yp =	6.096000E+01
Station	668	xp =	1.089660E+05	yp =	9.144000E+01
Station	669	xp =	1.089660E+05	yp =	1.219200E+02
Station	670	xp =	1.089660E+05	yp =	1.524000E+02
Station	671	xp =	1.089660E+05	yp =	1.828800E+02
Station	672	xp =	1.089660E+05	yp =	2.133600E+02
Station	673	xp =	1.089660E+05	yp =	2.438400E+02
Station	674	xp =	1.089660E+05	yp =	2.743200E+02
Station	675	xp =	1.089660E+05	yp =	3.048000E+02
Station	676	xp =	1.089660E+05	yp =	3.657600E+02
Station	677	xp =	1.089660E+05	yp =	4.267200E+02
Station	678	xp =	1.089660E+05	yp =	4.876800E+02
Station	679	xp =	1.089660E+05	yp =	5.486400E+02
Station	680	xp =	1.089660E+05	yp =	6.096000E+02
Station	681	xp =	1.089660E+05	yp =	6.705600E+02
Station	682	xp =	1.089660E+05	yp =	7.315200E+02
Station	683	xp =	1.089660E+05	yp =	7.924800E+02
Station	684	xp =	1.089660E+05	yp =	9.144000E+02
Station	685	xp =	1.089660E+05	yp =	1.066800E+03
Station	686	xp =	1.089660E+05	yp =	1.219200E+03
Station	687	xp =	1.272540E+05	yp =	0.000000E+00
Station	688	xp =	1.272540E+05	yp =	3.048000E+01
Station	689	xp =	1.272540E+05	yp =	6.096000E+01
Station	690	xp =	1.272540E+05	yp =	9.144000E+01
Station	691	xp =	1.272540E+05	yp =	1.219200E+02
Station	692	xp =	1.272540E+05	yp =	1.524000E+02
Station	693	xp =	1.272540E+05	yp =	1.828800E+02
Station	694	xp =	1.272540E+05	yp =	2.133600E+02
Station	695	xp =	1.272540E+05	yp =	2.438400E+02
Station	696	xp =	1.272540E+05	yp =	2.743200E+02
Station	697	xp =	1.272540E+05	yp =	3.048000E+02
Station	698	xp =	1.272540E+05	yp =	3.657600E+02
Station	699	xp =	1.272540E+05	yp =	4.267200E+02
Station	700	xp =	1.272540E+05	yp =	4.876800E+02
Station	701	xp =	1.272540E+05	yp =	5.486400E+02
Station	702	xp =	1.272540E+05	yp =	6.096000E+02
Station	703	xp =	1.272540E+05	yp =	6.705600E+02
Station	704	xp =	1.272540E+05	yp =	7.315200E+02
Station	705	xp =	1.272540E+05	yp =	7.924800E+02
Station	706	xp =	1.272540E+05	yp =	9.144000E+02
Station	707	xp =	1.272540E+05	yp =	1.066800E+03
Station	708	xp =	1.272540E+05	yp =	1.219200E+03
Station	709	xp =	1.615440E+05	yp =	0.000000E+00
Station	710	xp =	1.615440E+05	yp =	3.048000E+01
Station	711	xp =	1.615440E+05	yp =	6.096000E+01
Station	712	xp =	1.615440E+05	yp =	9.144000E+01
Station	713	xp =	1.615440E+05	yp =	1.219200E+02
Station	714	xp =	1.615440E+05	yp =	1.524000E+02
Station	715	xp =	1.615440E+05	yp =	1.828800E+02
Station	716	xp =	1.615440E+05	yp =	2.133600E+02
Station	717	xp =	1.615440E+05	yp =	2.438400E+02
Station	718	xp =	1.615440E+05	yp =	2.743200E+02
Station	719	xp =	1.615440E+05	yp =	3.048000E+02
Station	720	xp =	1.615440E+05	yp =	3.657600E+02

```
Station  721 xp =  1.615440E+05 yp =  4.267200E+02
Station  722 xp =  1.615440E+05 yp =  4.876800E+02
Station  723 xp =  1.615440E+05 yp =  5.486400E+02
Station  724 xp =  1.615440E+05 yp =  6.096000E+02
Station  725 xp =  1.615440E+05 yp =  6.705600E+02
Station  726 xp =  1.615440E+05 yp =  7.315200E+02
Station  727 xp =  1.615440E+05 yp =  7.924800E+02
Station  728 xp =  1.615440E+05 yp =  9.144000E+02
Station  729 xp =  1.615440E+05 yp =  1.066800E+03
Station  730 xp =  1.615440E+05 yp =  1.219200E+03
```

Locations of stations generated are ...

```
Station  731 xp =  1.371600E+04 yp =  5.000000E+00
Station  732 xp =  1.371600E+04 yp =  1.500000E+01
Station  733 xp =  1.371600E+04 yp =  2.500000E+01
Station  734 xp =  1.371600E+04 yp =  3.500000E+01
Station  735 xp =  1.371600E+04 yp =  4.500000E+01
Station  736 xp =  1.371600E+04 yp =  5.500000E+01
Station  737 xp =  1.371600E+04 yp =  6.500000E+01
Station  738 xp =  1.371600E+04 yp =  7.500000E+01
Station  739 xp =  1.371600E+04 yp =  8.500000E+01
Station  740 xp =  1.371600E+04 yp =  9.500000E+01
Station  741 xp =  1.676400E+04 yp =  5.000000E+00
Station  742 xp =  1.676400E+04 yp =  1.500000E+01
Station  743 xp =  1.676400E+04 yp =  2.500000E+01
Station  744 xp =  1.676400E+04 yp =  3.500000E+01
Station  745 xp =  1.676400E+04 yp =  4.500000E+01
Station  746 xp =  1.676400E+04 yp =  5.500000E+01
Station  747 xp =  1.676400E+04 yp =  6.500000E+01
Station  748 xp =  1.676400E+04 yp =  7.500000E+01
Station  749 xp =  1.676400E+04 yp =  8.500000E+01
Station  750 xp =  1.676400E+04 yp =  9.500000E+01
Station  751 xp =  1.981200E+04 yp =  5.000000E+00
Station  752 xp =  1.981200E+04 yp =  1.500000E+01
Station  753 xp =  1.981200E+04 yp =  2.500000E+01
Station  754 xp =  1.981200E+04 yp =  3.500000E+01
Station  755 xp =  1.981200E+04 yp =  4.500000E+01
Station  756 xp =  1.981200E+04 yp =  5.500000E+01
Station  757 xp =  1.981200E+04 yp =  6.500000E+01
Station  758 xp =  1.981200E+04 yp =  7.500000E+01
Station  759 xp =  1.981200E+04 yp =  8.500000E+01
Station  760 xp =  1.981200E+04 yp =  9.500000E+01
Station  761 xp =  2.286000E+04 yp =  5.000000E+00
Station  762 xp =  2.286000E+04 yp =  1.500000E+01
Station  763 xp =  2.286000E+04 yp =  2.500000E+01
Station  764 xp =  2.286000E+04 yp =  3.500000E+01
Station  765 xp =  2.286000E+04 yp =  4.500000E+01
Station  766 xp =  2.286000E+04 yp =  5.500000E+01
Station  767 xp =  2.286000E+04 yp =  6.500000E+01
Station  768 xp =  2.286000E+04 yp =  7.500000E+01
Station  769 xp =  2.286000E+04 yp =  8.500000E+01
Station  770 xp =  2.286000E+04 yp =  9.500000E+01
Station  771 xp =  2.590800E+04 yp =  5.000000E+00
Station  772 xp =  2.590800E+04 yp =  1.500000E+01
Station  773 xp =  2.590800E+04 yp =  2.500000E+01
Station  774 xp =  2.590800E+04 yp =  3.500000E+01
Station  775 xp =  2.590800E+04 yp =  4.500000E+01
Station  776 xp =  2.590800E+04 yp =  5.500000E+01
Station  777 xp =  2.590800E+04 yp =  6.500000E+01
Station  778 xp =  2.590800E+04 yp =  7.500000E+01
Station  779 xp =  2.590800E+04 yp =  8.500000E+01
Station  780 xp =  2.590800E+04 yp =  9.500000E+01
Station  781 xp =  3.200400E+04 yp =  5.000000E+00
Station  782 xp =  3.200400E+04 yp =  1.500000E+01
Station  783 xp =  3.200400E+04 yp =  2.500000E+01
```

```
Station  784 xp =  3.200400E+04 yp =  3.500000E+01
Station  785 xp =  3.200400E+04 yp =  4.500000E+01
Station  786 xp =  3.200400E+04 yp =  5.500000E+01
Station  787 xp =  3.200400E+04 yp =  6.500000E+01
Station  788 xp =  3.200400E+04 yp =  7.500000E+01
Station  789 xp =  3.200400E+04 yp =  8.500000E+01
Station  790 xp =  3.200400E+04 yp =  9.500000E+01
Station  791 xp =  4.114800E+04 yp =  5.000000E+00
Station  792 xp =  4.114800E+04 yp =  1.500000E+01
Station  793 xp =  4.114800E+04 yp =  2.500000E+01
Station  794 xp =  4.114800E+04 yp =  3.500000E+01
Station  795 xp =  4.114800E+04 yp =  4.500000E+01
Station  796 xp =  4.114800E+04 yp =  5.500000E+01
Station  797 xp =  4.114800E+04 yp =  6.500000E+01
Station  798 xp =  4.114800E+04 yp =  7.500000E+01
Station  799 xp =  4.114800E+04 yp =  8.500000E+01
Station  800 xp =  4.114800E+04 yp =  9.500000E+01
Station  801 xp =  5.029200E+04 yp =  5.000000E+00
Station  802 xp =  5.029200E+04 yp =  1.500000E+01
Station  803 xp =  5.029200E+04 yp =  2.500000E+01
Station  804 xp =  5.029200E+04 yp =  3.500000E+01
Station  805 xp =  5.029200E+04 yp =  4.500000E+01
Station  806 xp =  5.029200E+04 yp =  5.500000E+01
Station  807 xp =  5.029200E+04 yp =  6.500000E+01
Station  808 xp =  5.029200E+04 yp =  7.500000E+01
Station  809 xp =  5.029200E+04 yp =  8.500000E+01
Station  810 xp =  5.029200E+04 yp =  9.500000E+01
Station  811 xp =  6.096000E+04 yp =  5.000000E+00
Station  812 xp =  6.096000E+04 yp =  1.500000E+01
Station  813 xp =  6.096000E+04 yp =  2.500000E+01
Station  814 xp =  6.096000E+04 yp =  3.500000E+01
Station  815 xp =  6.096000E+04 yp =  4.500000E+01
Station  816 xp =  6.096000E+04 yp =  5.500000E+01
Station  817 xp =  6.096000E+04 yp =  6.500000E+01
Station  818 xp =  6.096000E+04 yp =  7.500000E+01
Station  819 xp =  6.096000E+04 yp =  8.500000E+01
Station  820 xp =  6.096000E+04 yp =  9.500000E+01
Station  821 xp =  6.187440E+04 yp =  5.000000E+00
Station  822 xp =  6.187440E+04 yp =  1.500000E+01
Station  823 xp =  6.187440E+04 yp =  2.500000E+01
Station  824 xp =  6.187440E+04 yp =  3.500000E+01
Station  825 xp =  6.187440E+04 yp =  4.500000E+01
Station  826 xp =  6.187440E+04 yp =  5.500000E+01
Station  827 xp =  6.187440E+04 yp =  6.500000E+01
Station  828 xp =  6.187440E+04 yp =  7.500000E+01
Station  829 xp =  6.187440E+04 yp =  8.500000E+01
Station  830 xp =  6.187440E+04 yp =  9.500000E+01
Station  831 xp =  6.858000E+04 yp =  5.000000E+00
Station  832 xp =  6.858000E+04 yp =  1.500000E+01
Station  833 xp =  6.858000E+04 yp =  2.500000E+01
Station  834 xp =  6.858000E+04 yp =  3.500000E+01
Station  835 xp =  6.858000E+04 yp =  4.500000E+01
Station  836 xp =  6.858000E+04 yp =  5.500000E+01
Station  837 xp =  6.858000E+04 yp =  6.500000E+01
Station  838 xp =  6.858000E+04 yp =  7.500000E+01
Station  839 xp =  6.858000E+04 yp =  8.500000E+01
Station  840 xp =  6.858000E+04 yp =  9.500000E+01
Station  841 xp =  6.949440E+04 yp =  5.000000E+00
Station  842 xp =  6.949440E+04 yp =  1.500000E+01
Station  843 xp =  6.949440E+04 yp =  2.500000E+01
Station  844 xp =  6.949440E+04 yp =  3.500000E+01
Station  845 xp =  6.949440E+04 yp =  4.500000E+01
Station  846 xp =  6.949440E+04 yp =  5.500000E+01
Station  847 xp =  6.949440E+04 yp =  6.500000E+01
Station  848 xp =  6.949440E+04 yp =  7.500000E+01
Station  849 xp =  6.949440E+04 yp =  8.500000E+01
```

```
Station  850 xp =  6.949440E+04 yp =  9.500000E+01
Station  851 xp =  7.620000E+04 yp =  5.000000E+00
Station  852 xp =  7.620000E+04 yp =  1.500000E+01
Station  853 xp =  7.620000E+04 yp =  2.500000E+01
Station  854 xp =  7.620000E+04 yp =  3.500000E+01
Station  855 xp =  7.620000E+04 yp =  4.500000E+01
Station  856 xp =  7.620000E+04 yp =  5.500000E+01
Station  857 xp =  7.620000E+04 yp =  6.500000E+01
Station  858 xp =  7.620000E+04 yp =  7.500000E+01
Station  859 xp =  7.620000E+04 yp =  8.500000E+01
Station  860 xp =  7.620000E+04 yp =  9.500000E+01
Station  861 xp =  8.321040E+04 yp =  5.000000E+00
Station  862 xp =  8.321040E+04 yp =  1.500000E+01
Station  863 xp =  8.321040E+04 yp =  2.500000E+01
Station  864 xp =  8.321040E+04 yp =  3.500000E+01
Station  865 xp =  8.321040E+04 yp =  4.500000E+01
Station  866 xp =  8.321040E+04 yp =  5.500000E+01
Station  867 xp =  8.321040E+04 yp =  6.500000E+01
Station  868 xp =  8.321040E+04 yp =  7.500000E+01
Station  869 xp =  8.321040E+04 yp =  8.500000E+01
Station  870 xp =  8.321040E+04 yp =  9.500000E+01
Station  871 xp =  8.839200E+04 yp =  5.000000E+00
Station  872 xp =  8.839200E+04 yp =  1.500000E+01
Station  873 xp =  8.839200E+04 yp =  2.500000E+01
Station  874 xp =  8.839200E+04 yp =  3.500000E+01
Station  875 xp =  8.839200E+04 yp =  4.500000E+01
Station  876 xp =  8.839200E+04 yp =  5.500000E+01
Station  877 xp =  8.839200E+04 yp =  6.500000E+01
Station  878 xp =  8.839200E+04 yp =  7.500000E+01
Station  879 xp =  8.839200E+04 yp =  8.500000E+01
Station  880 xp =  8.839200E+04 yp =  9.500000E+01
Station  881 xp =  9.144000E+04 yp =  5.000000E+00
Station  882 xp =  9.144000E+04 yp =  1.500000E+01
Station  883 xp =  9.144000E+04 yp =  2.500000E+01
Station  884 xp =  9.144000E+04 yp =  3.500000E+01
Station  885 xp =  9.144000E+04 yp =  4.500000E+01
Station  886 xp =  9.144000E+04 yp =  5.500000E+01
Station  887 xp =  9.144000E+04 yp =  6.500000E+01
Station  888 xp =  9.144000E+04 yp =  7.500000E+01
Station  889 xp =  9.144000E+04 yp =  8.500000E+01
Station  890 xp =  9.144000E+04 yp =  9.500000E+01
Station  891 xp =  9.906000E+04 yp =  5.000000E+00
Station  892 xp =  9.906000E+04 yp =  1.500000E+01
Station  893 xp =  9.906000E+04 yp =  2.500000E+01
Station  894 xp =  9.906000E+04 yp =  3.500000E+01
Station  895 xp =  9.906000E+04 yp =  4.500000E+01
Station  896 xp =  9.906000E+04 yp =  5.500000E+01
Station  897 xp =  9.906000E+04 yp =  6.500000E+01
Station  898 xp =  9.906000E+04 yp =  7.500000E+01
Station  899 xp =  9.906000E+04 yp =  8.500000E+01
Station  900 xp =  9.906000E+04 yp =  9.500000E+01
Station  901 xp =  1.021080E+05 yp =  5.000000E+00
Station  902 xp =  1.021080E+05 yp =  1.500000E+01
Station  903 xp =  1.021080E+05 yp =  2.500000E+01
Station  904 xp =  1.021080E+05 yp =  3.500000E+01
Station  905 xp =  1.021080E+05 yp =  4.500000E+01
Station  906 xp =  1.021080E+05 yp =  5.500000E+01
Station  907 xp =  1.021080E+05 yp =  6.500000E+01
Station  908 xp =  1.021080E+05 yp =  7.500000E+01
Station  909 xp =  1.021080E+05 yp =  8.500000E+01
Station  910 xp =  1.021080E+05 yp =  9.500000E+01
Station  911 xp =  1.066800E+05 yp =  5.000000E+00
Station  912 xp =  1.066800E+05 yp =  1.500000E+01
Station  913 xp =  1.066800E+05 yp =  2.500000E+01
Station  914 xp =  1.066800E+05 yp =  3.500000E+01
Station  915 xp =  1.066800E+05 yp =  4.500000E+01
```

```
Station  916 xp =  1.066800E+05 yp =  5.500000E+01
Station  917 xp =  1.066800E+05 yp =  6.500000E+01
Station  918 xp =  1.066800E+05 yp =  7.500000E+01
Station  919 xp =  1.066800E+05 yp =  8.500000E+01
Station  920 xp =  1.066800E+05 yp =  9.500000E+01
Station  921 xp =  1.097280E+05 yp =  5.000000E+00
Station  922 xp =  1.097280E+05 yp =  1.500000E+01
Station  923 xp =  1.097280E+05 yp =  2.500000E+01
Station  924 xp =  1.097280E+05 yp =  3.500000E+01
Station  925 xp =  1.097280E+05 yp =  4.500000E+01
Station  926 xp =  1.097280E+05 yp =  5.500000E+01
Station  927 xp =  1.097280E+05 yp =  6.500000E+01
Station  928 xp =  1.097280E+05 yp =  7.500000E+01
Station  929 xp =  1.097280E+05 yp =  8.500000E+01
Station  930 xp =  1.097280E+05 yp =  9.500000E+01
Station  931 xp =  1.197864E+05 yp =  5.000000E+00
Station  932 xp =  1.197864E+05 yp =  1.500000E+01
Station  933 xp =  1.197864E+05 yp =  2.500000E+01
Station  934 xp =  1.197864E+05 yp =  3.500000E+01
Station  935 xp =  1.197864E+05 yp =  4.500000E+01
Station  936 xp =  1.197864E+05 yp =  5.500000E+01
Station  937 xp =  1.197864E+05 yp =  6.500000E+01
Station  938 xp =  1.197864E+05 yp =  7.500000E+01
Station  939 xp =  1.197864E+05 yp =  8.500000E+01
Station  940 xp =  1.197864E+05 yp =  9.500000E+01
Station  941 xp =  1.219200E+05 yp =  5.000000E+00
Station  942 xp =  1.219200E+05 yp =  1.500000E+01
Station  943 xp =  1.219200E+05 yp =  2.500000E+01
Station  944 xp =  1.219200E+05 yp =  3.500000E+01
Station  945 xp =  1.219200E+05 yp =  4.500000E+01
Station  946 xp =  1.219200E+05 yp =  5.500000E+01
Station  947 xp =  1.219200E+05 yp =  6.500000E+01
Station  948 xp =  1.219200E+05 yp =  7.500000E+01
Station  949 xp =  1.219200E+05 yp =  8.500000E+01
Station  950 xp =  1.219200E+05 yp =  9.500000E+01
Station  951 xp =  1.280160E+05 yp =  5.000000E+00
Station  952 xp =  1.280160E+05 yp =  1.500000E+01
Station  953 xp =  1.280160E+05 yp =  2.500000E+01
Station  954 xp =  1.280160E+05 yp =  3.500000E+01
Station  955 xp =  1.280160E+05 yp =  4.500000E+01
Station  956 xp =  1.280160E+05 yp =  5.500000E+01
Station  957 xp =  1.280160E+05 yp =  6.500000E+01
Station  958 xp =  1.280160E+05 yp =  7.500000E+01
Station  959 xp =  1.280160E+05 yp =  8.500000E+01
Station  960 xp =  1.280160E+05 yp =  9.500000E+01
Station  961 xp =  1.371600E+05 yp =  5.000000E+00
Station  962 xp =  1.371600E+05 yp =  1.500000E+01
Station  963 xp =  1.371600E+05 yp =  2.500000E+01
Station  964 xp =  1.371600E+05 yp =  3.500000E+01
Station  965 xp =  1.371600E+05 yp =  4.500000E+01
Station  966 xp =  1.371600E+05 yp =  5.500000E+01
Station  967 xp =  1.371600E+05 yp =  6.500000E+01
Station  968 xp =  1.371600E+05 yp =  7.500000E+01
Station  969 xp =  1.371600E+05 yp =  8.500000E+01
Station  970 xp =  1.371600E+05 yp =  9.500000E+01
Station  971 xp =  1.453896E+05 yp =  5.000000E+00
Station  972 xp =  1.453896E+05 yp =  1.500000E+01
Station  973 xp =  1.453896E+05 yp =  2.500000E+01
Station  974 xp =  1.453896E+05 yp =  3.500000E+01
Station  975 xp =  1.453896E+05 yp =  4.500000E+01
Station  976 xp =  1.453896E+05 yp =  5.500000E+01
Station  977 xp =  1.453896E+05 yp =  6.500000E+01
Station  978 xp =  1.453896E+05 yp =  7.500000E+01
Station  979 xp =  1.453896E+05 yp =  8.500000E+01
Station  980 xp =  1.453896E+05 yp =  9.500000E+01
Station  981 xp =  1.524000E+05 yp =  5.000000E+00
```

```
          Station  982 xp =  1.524000E+05 yp =  1.500000E+01
          Station  983 xp =  1.524000E+05 yp =  2.500000E+01
          Station  984 xp =  1.524000E+05 yp =  3.500000E+01
          Station  985 xp =  1.524000E+05 yp =  4.500000E+01
          Station  986 xp =  1.524000E+05 yp =  5.500000E+01
          Station  987 xp =  1.524000E+05 yp =  6.500000E+01
          Station  988 xp =  1.524000E+05 yp =  7.500000E+01
          Station  989 xp =  1.524000E+05 yp =  8.500000E+01
          Station  990 xp =  1.524000E+05 yp =  9.500000E+01
          Station  991 xp =  1.621536E+05 yp =  5.000000E+00
          Station  992 xp =  1.621536E+05 yp =  1.500000E+01
          Station  993 xp =  1.621536E+05 yp =  2.500000E+01
          Station  994 xp =  1.621536E+05 yp =  3.500000E+01
          Station  995 xp =  1.621536E+05 yp =  4.500000E+01
          Station  996 xp =  1.621536E+05 yp =  5.500000E+01
          Station  997 xp =  1.621536E+05 yp =  6.500000E+01
          Station  998 xp =  1.621536E+05 yp =  7.500000E+01
          Station  999 xp =  1.621536E+05 yp =  8.500000E+01
          Station 1000 xp =  1.621536E+05 yp =  9.500000E+01
          Station 1001 xp =  1.865376E+05 yp =  5.000000E+00
          Station 1002 xp =  1.865376E+05 yp =  1.500000E+01
          Station 1003 xp =  1.865376E+05 yp =  2.500000E+01
          Station 1004 xp =  1.865376E+05 yp =  3.500000E+01
          Station 1005 xp =  1.865376E+05 yp =  4.500000E+01
          Station 1006 xp =  1.865376E+05 yp =  5.500000E+01
          Station 1007 xp =  1.865376E+05 yp =  6.500000E+01
          Station 1008 xp =  1.865376E+05 yp =  7.500000E+01
          Station 1009 xp =  1.865376E+05 yp =  8.500000E+01
          Station 1010 xp =  1.865376E+05 yp =  9.500000E+01
0         0 particles and  1010 stations generated
0Filling remainder of mesh with air.
```

INTENTIONALLY LEFT BLANK.

APPENDIX B
CONTOUR PLOTS OF PRESSURE AND DENSITY FROM IDEAL SURFACE CALCULATION (75 TO 500 MSEC)

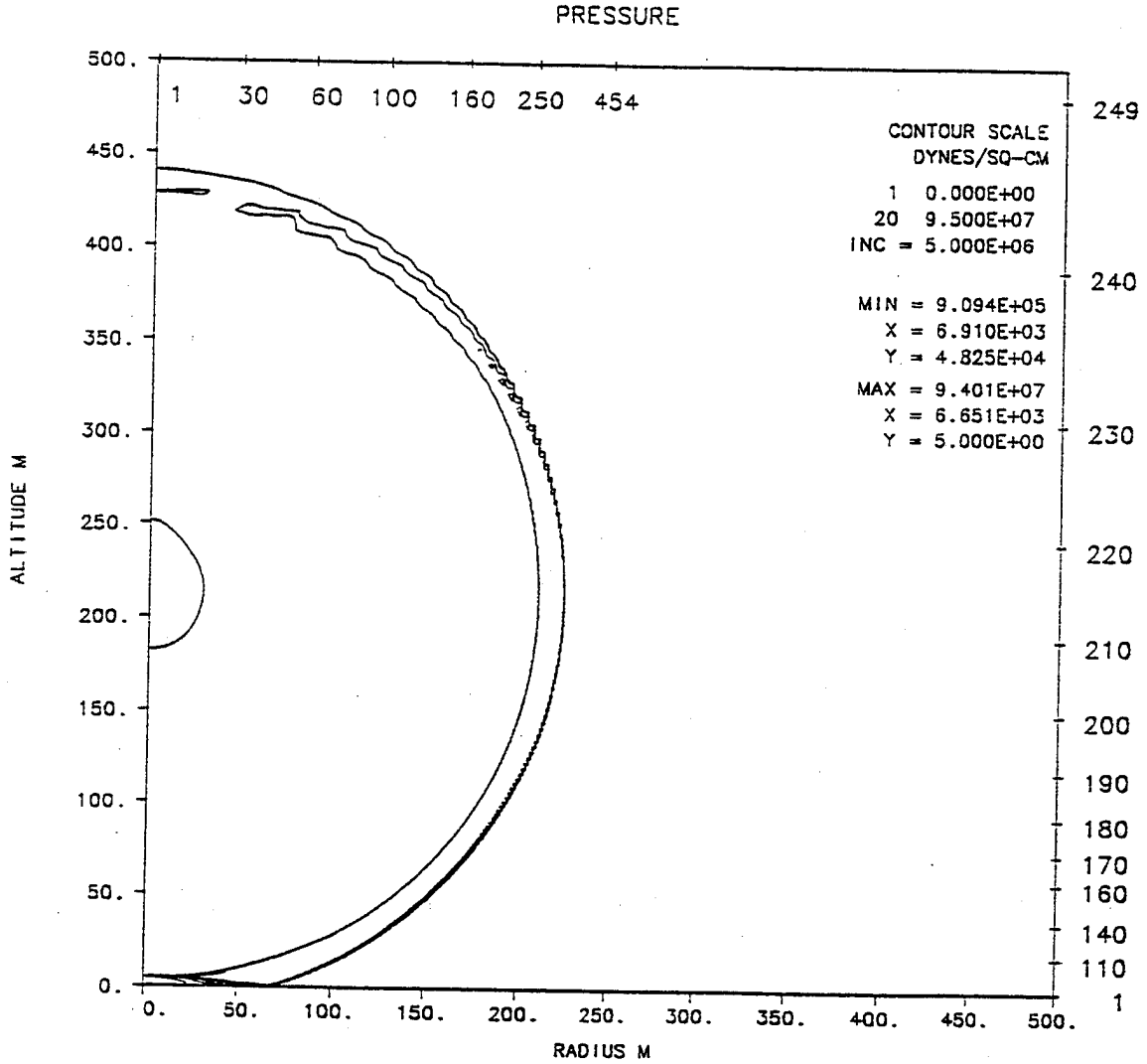

S-CUBED PRISCILLA - IDEAL - KE - SMOOTH WALL - RGE - MAY 93
TIME 75.030 MSEC CYCLE 281. PROBLEM 372.0100

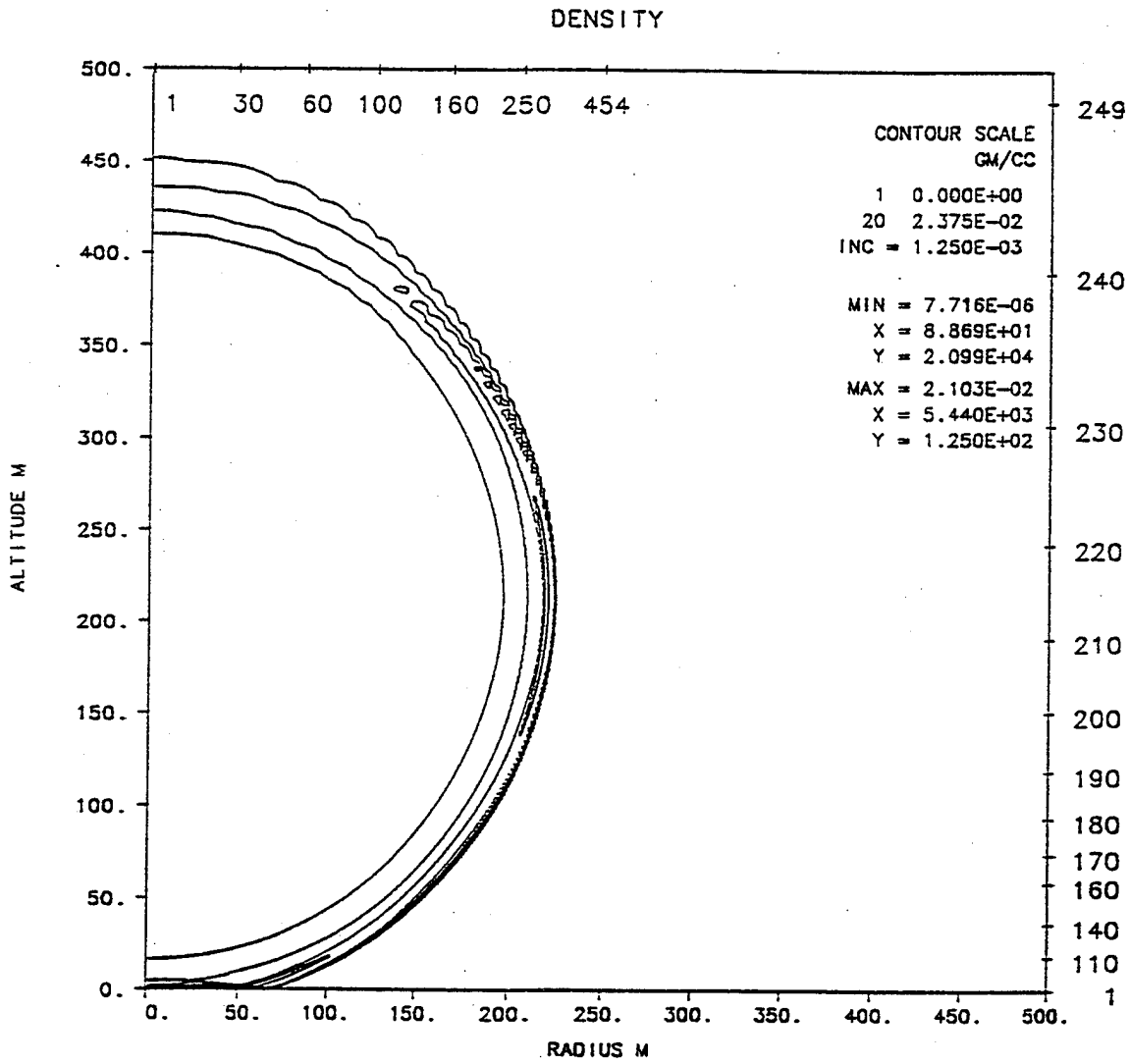

S-CUBED PRISCILLA - IDEAL - KE - SMOOTH WALL - RGE - MAY 93
TIME 75.030 MSEC CYCLE 281. PROBLEM 372.0100

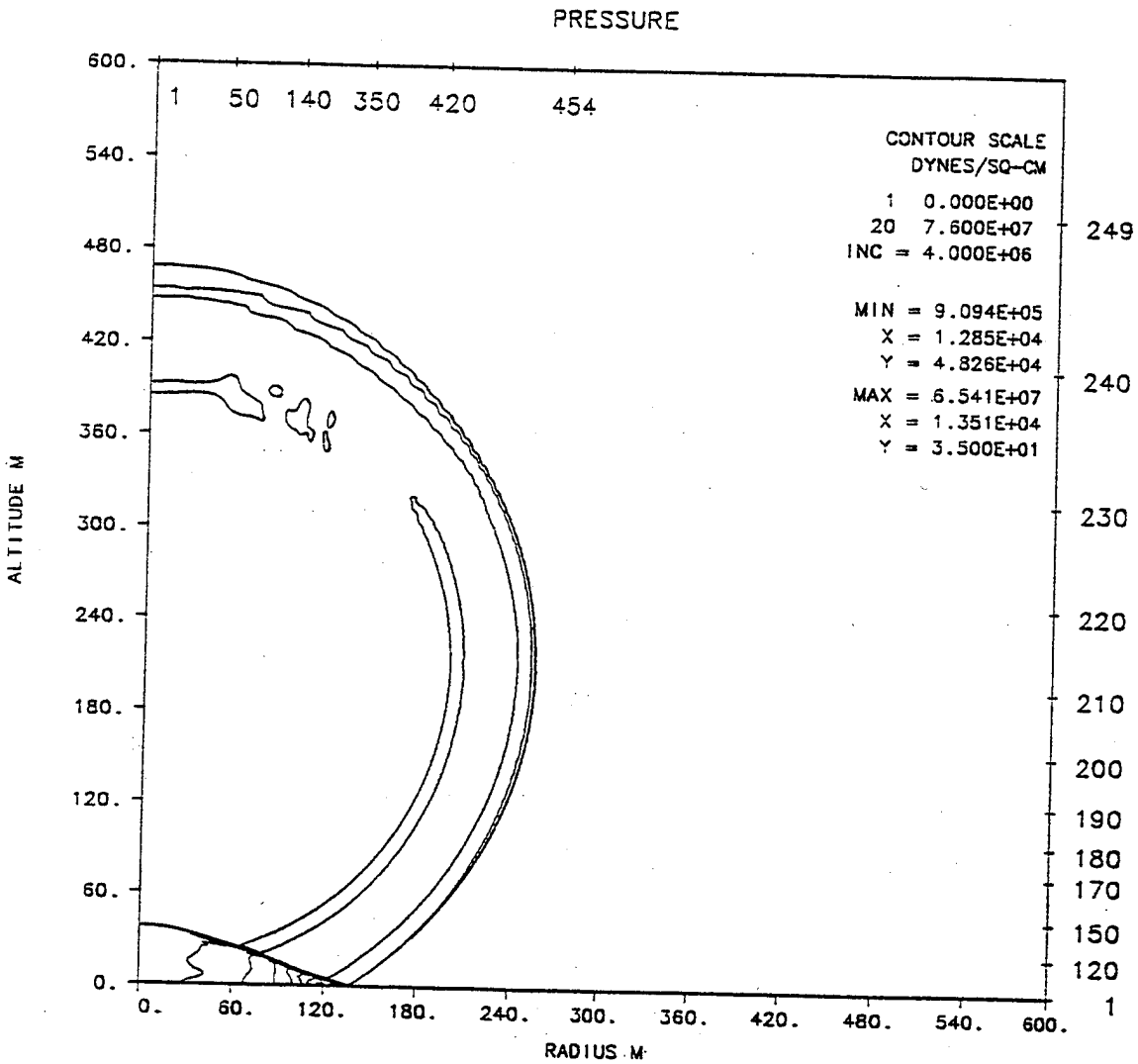

S-CUBED PRISCILLA - IDEAL - KE - SMOOTH WALL - RGE - MAY 93
TIME 100.000 MSEC CYCLE 771. PROBLEM 372.0100

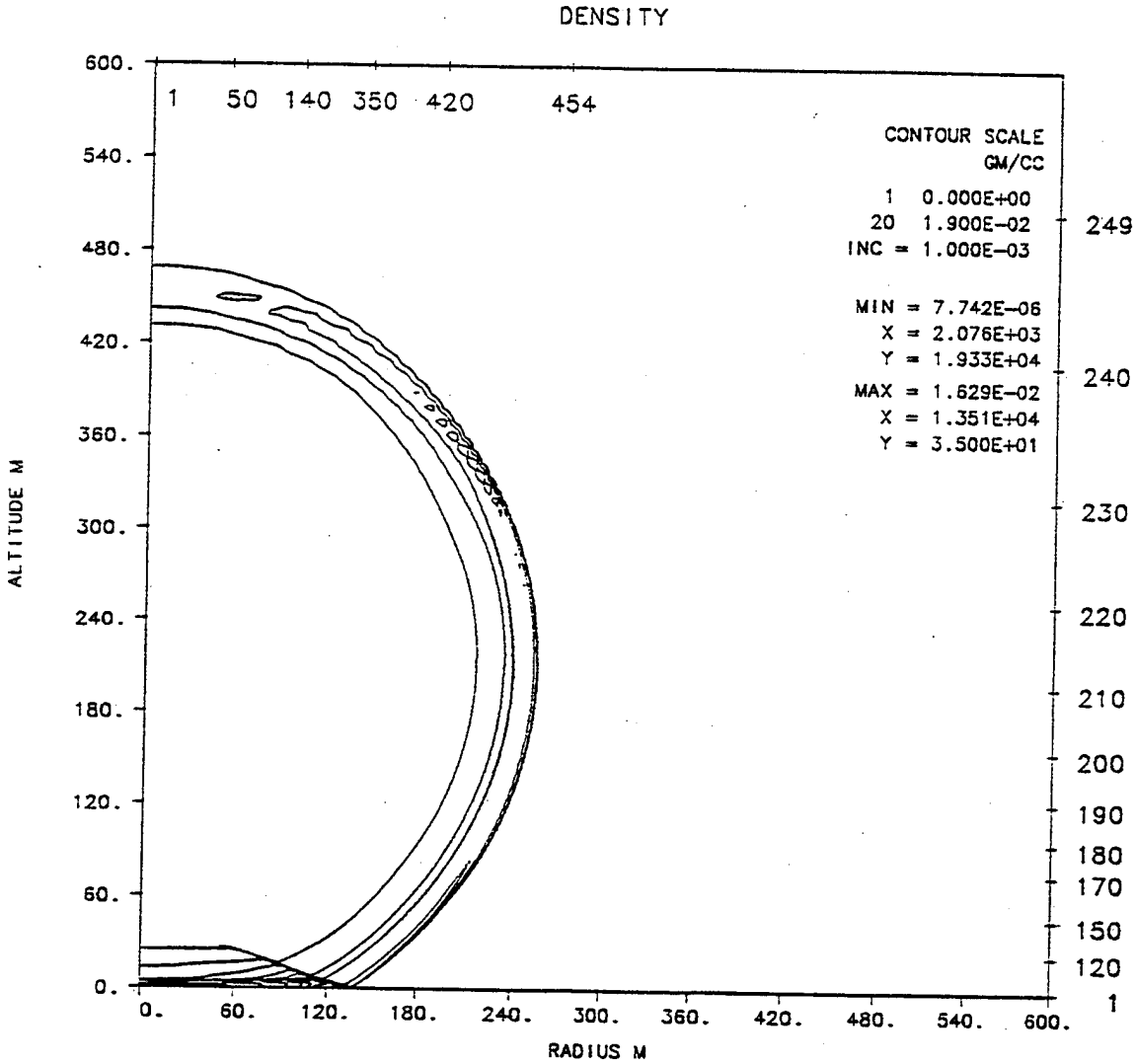

S-CUBED PRISCILLA - IDEAL - KE - SMOOTH WALL - RGE - MAY 93
TIME 100.000 MSEC CYCLE 771. PROBLEM 372.0100

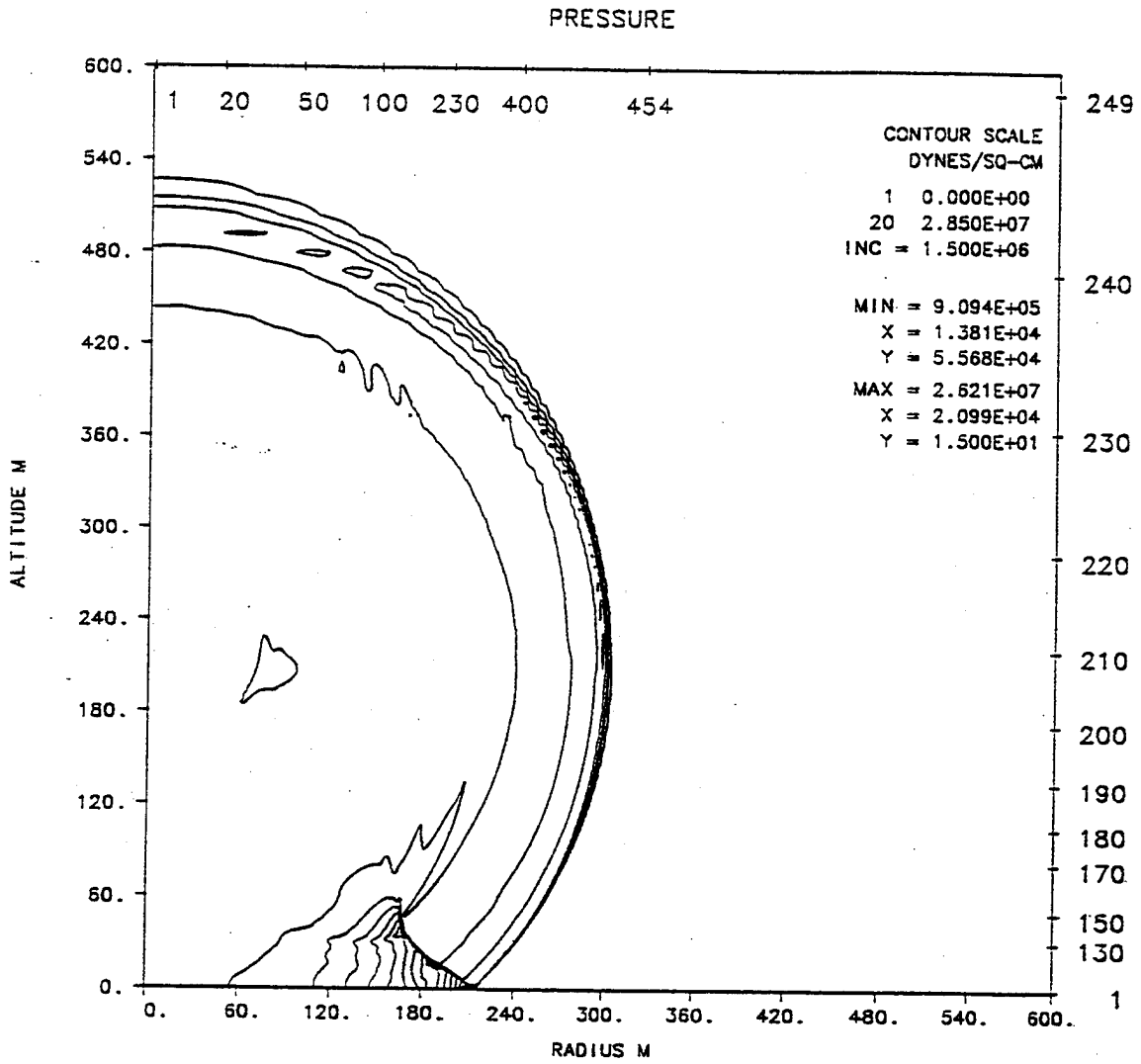

S-CUBED PRISCILLA – IDEAL – KE – SMOOTH WALL – RGE – MAY 93
TIME 150.000 MSEC CYCLE 2865. PROBLEM 372.0100

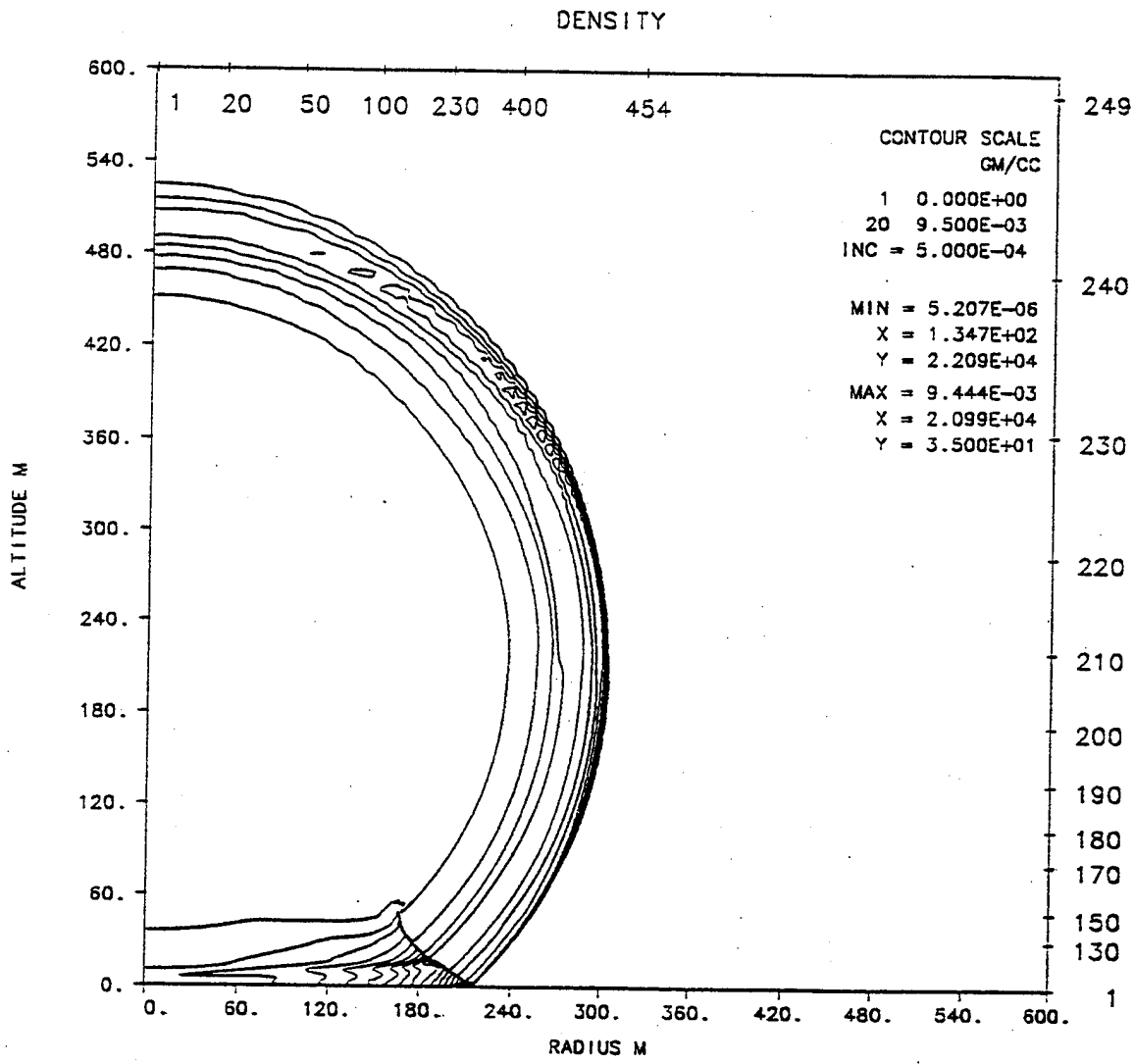

S-CUBED PRISCILLA - IDEAL - KE - SMOOTH WALL - RGE - MAY 93
TIME 150.000 MSEC CYCLE 2865. PROBLEM 372.0100

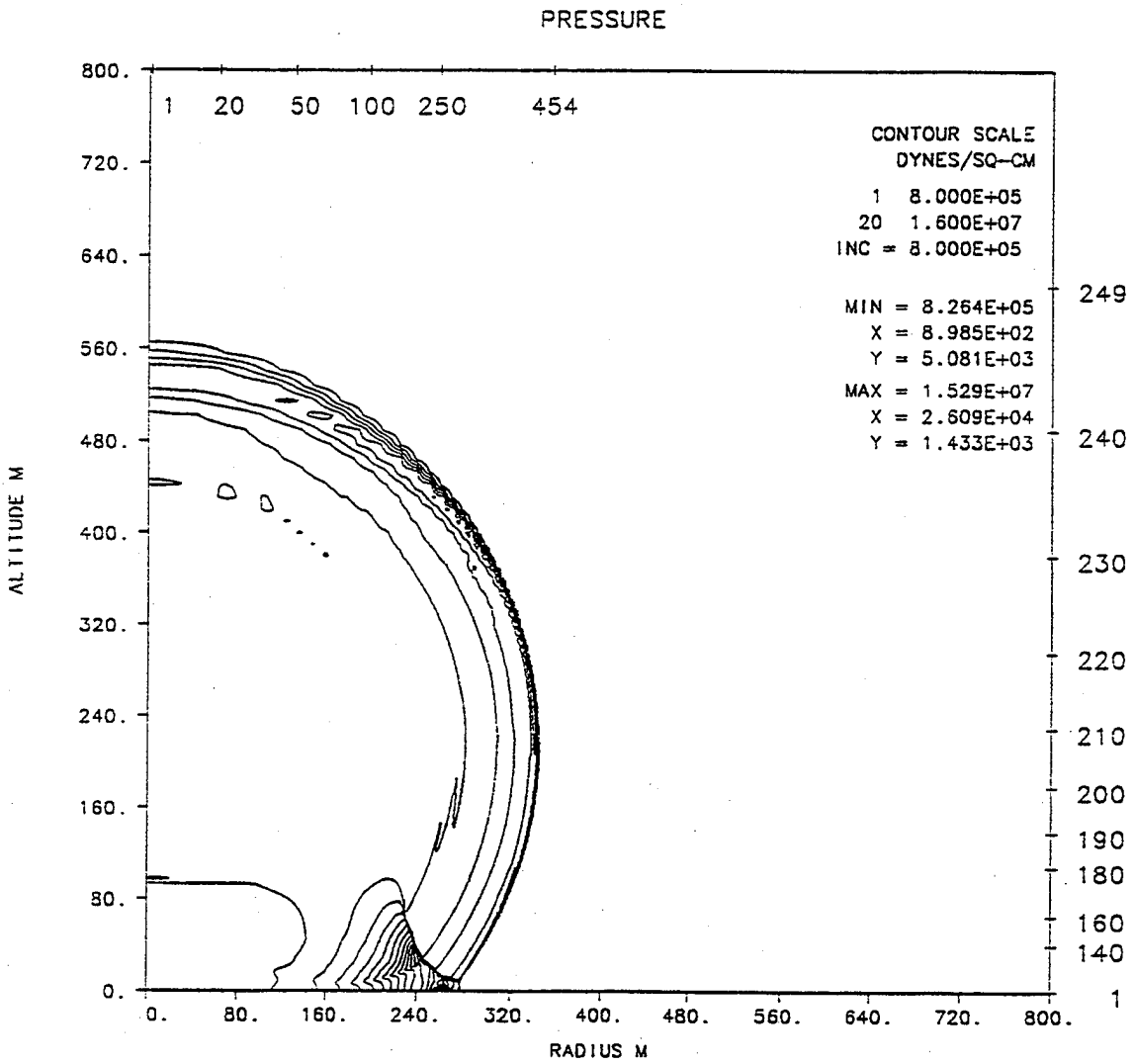

S-CUBED PRISCILLA - IDEAL - KE - SMOOTH WALL - RGE - MAY 93
TIME 200.000 MSEC CYCLE 3511. PROBLEM 372.0100

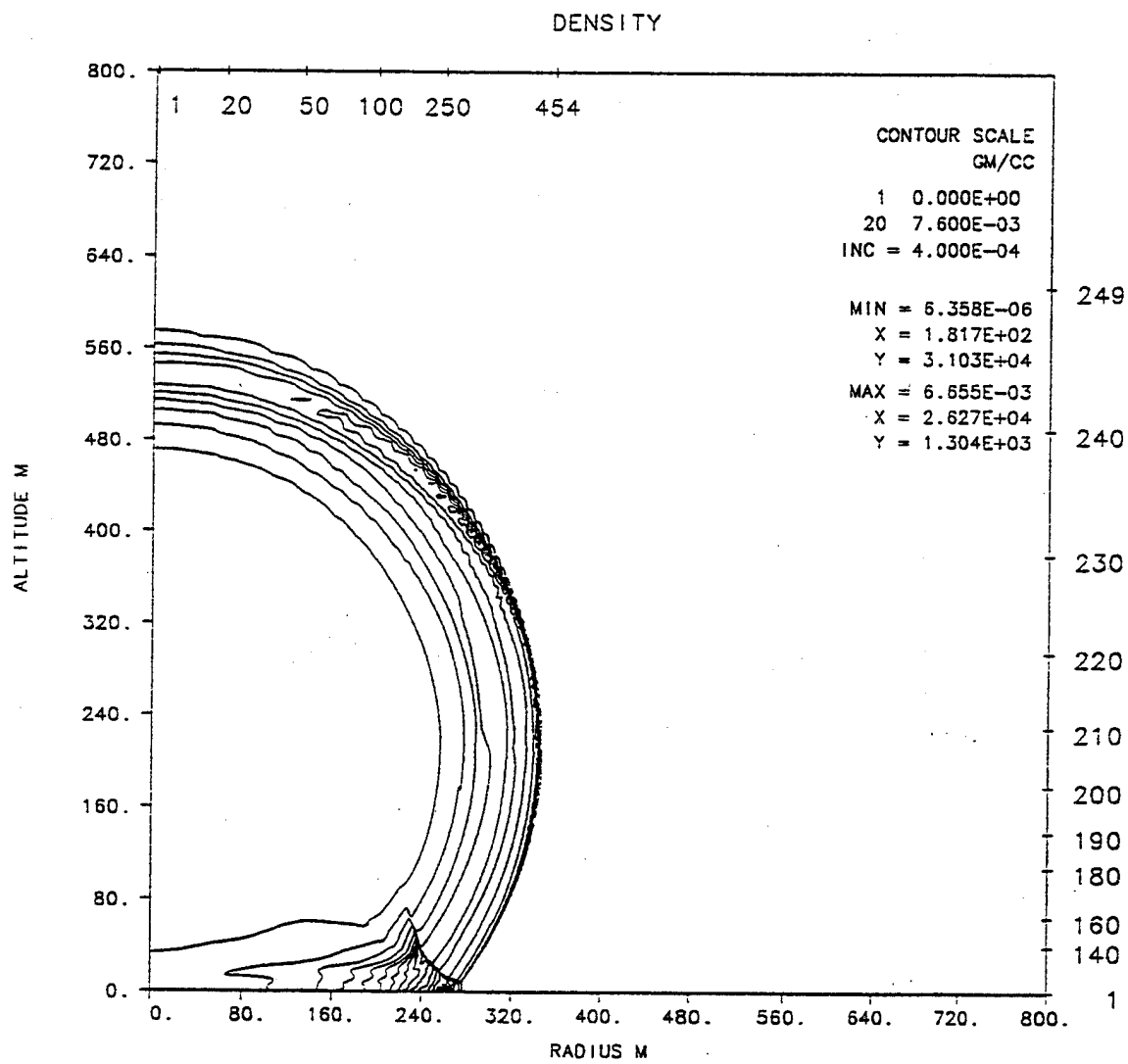

S-CUBED PRISCILLA - IDEAL - KE - SMOOTH WALL - RGE - MAY 93
TIME 200.000 MSEC CYCLE 3511. PROBLEM 372.0100

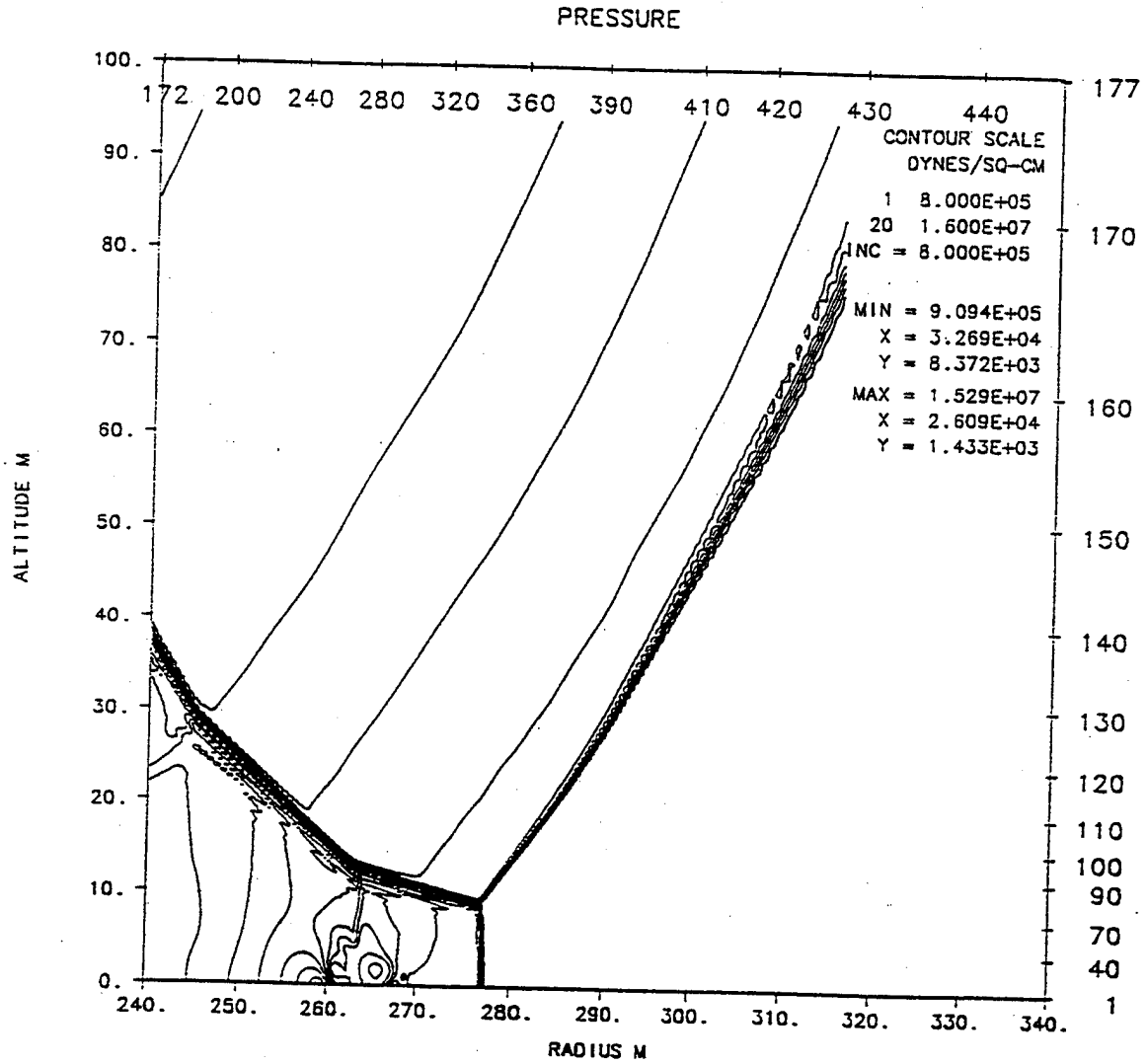

S-CUBED PRISCILLA - IDEAL - KE - SMOOTH WALL - RGE - MAY 93
TIME 200.000 MSEC CYCLE 3511. PROBLEM 372.0100

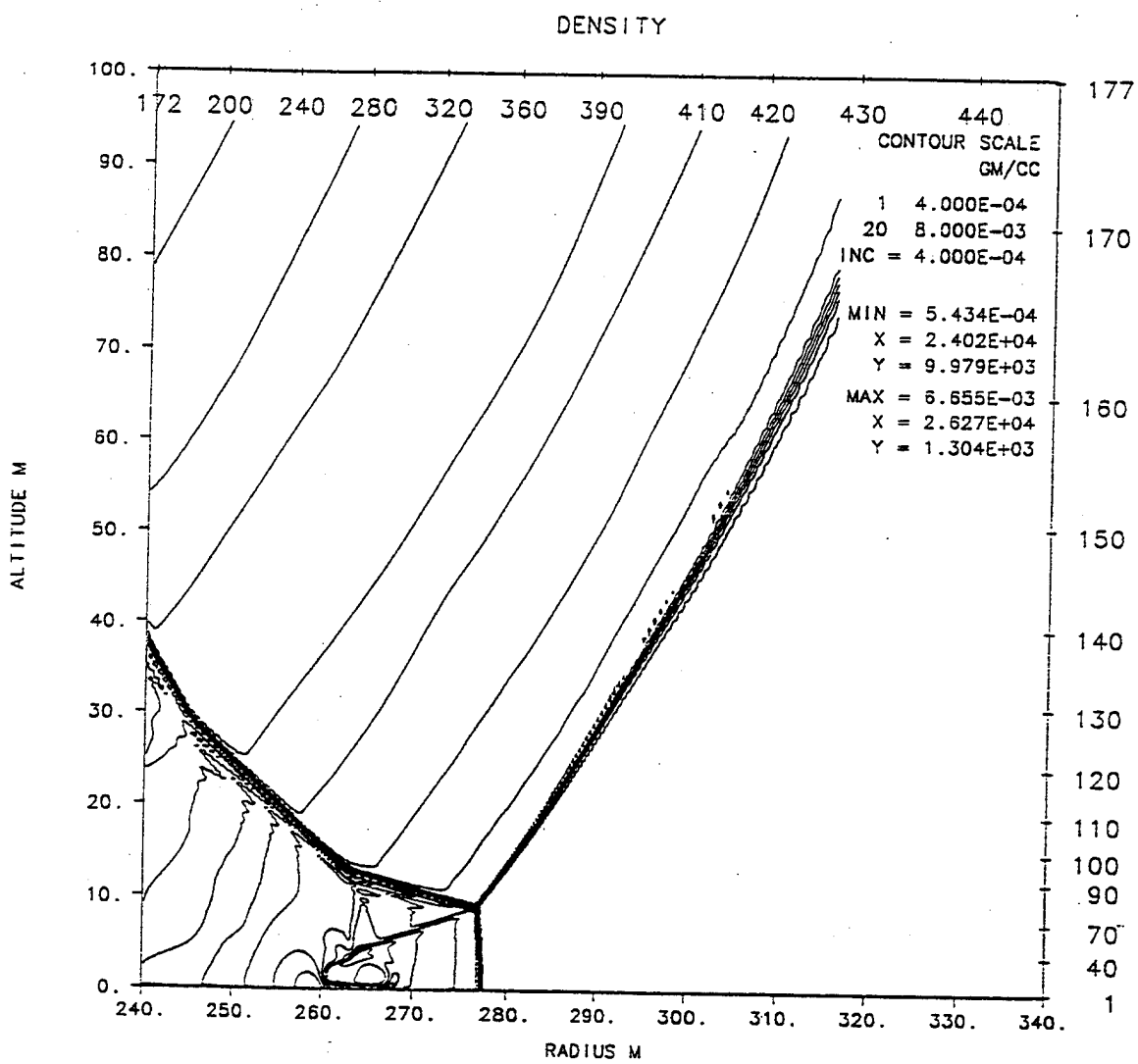

S-CUBED PRISCILLA - IDEAL - KE - SMOOTH WALL - RGE - MAY 93
TIME 200.000 MSEC CYCLE 3511. PROBLEM 372.0100

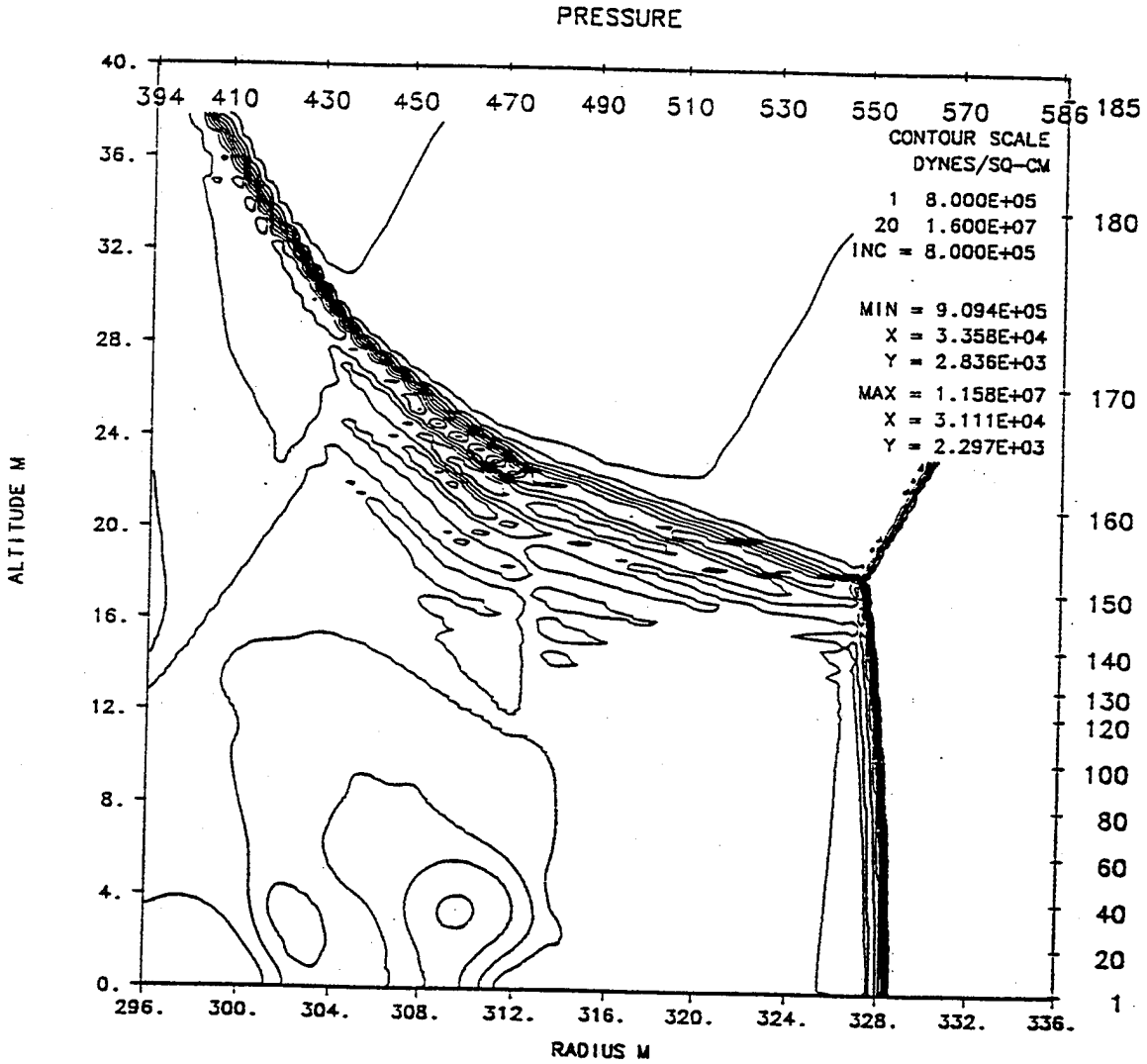

S-CUBED PRISCILLA - IDEAL - KE - SMOOTH WALL - RGE - MAY 93
TIME 250.000 MSEC CYCLE 0. PROBLEM 372.0101

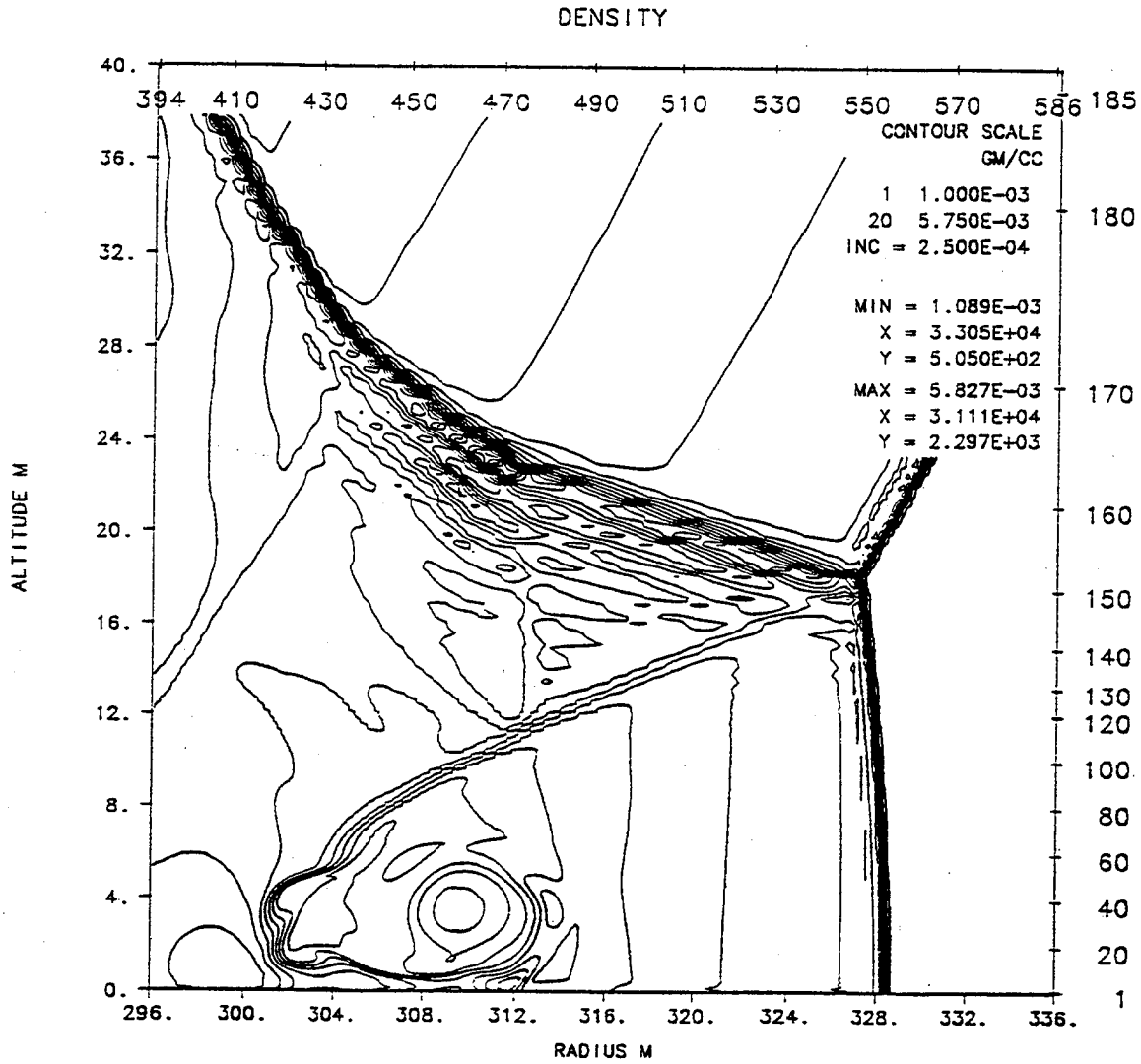

S-CUBED PRISCILLA - IDEAL - KE - SMOOTH WALL - RGE - MAY 93
TIME 250.000 MSEC CYCLE 0. PROBLEM 372.0101

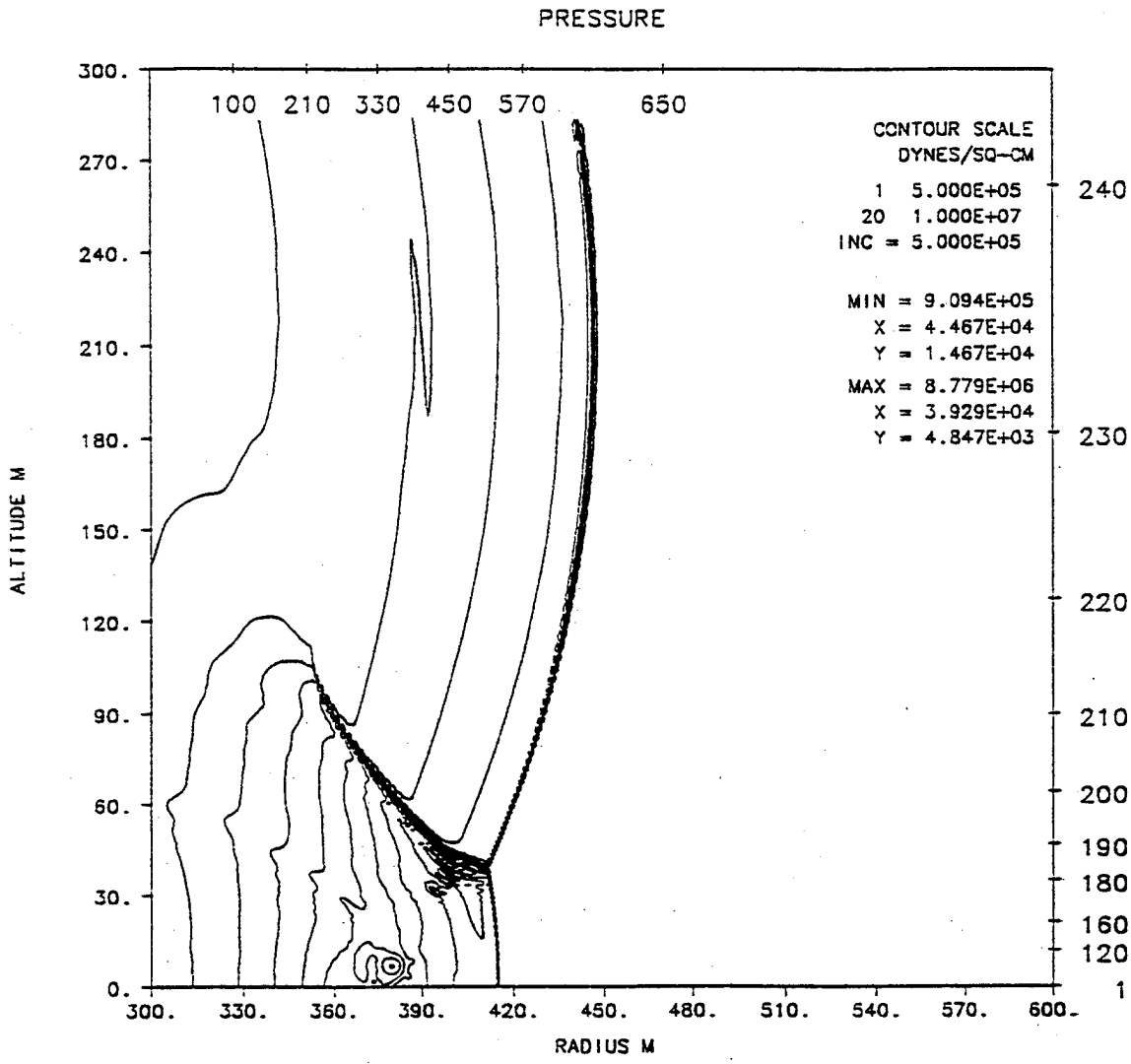

S-CUBED PRISCILLA - IDEAL - KE - SMOOTH WALL - RGE - MAY 93
TIME 350.000 MSEC CYCLE 1285. PROBLEM 372.0101

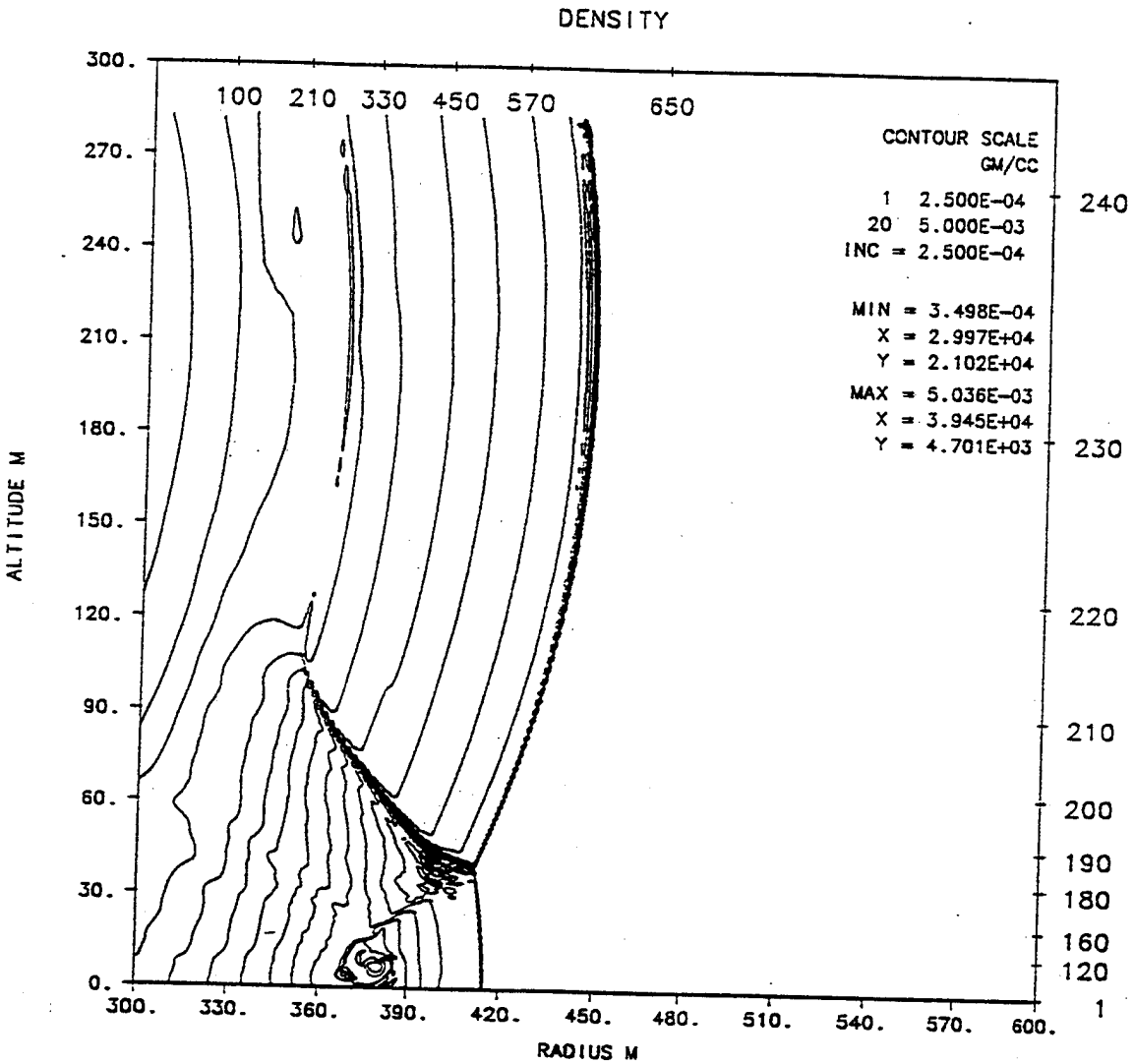

S-CUBED PRISCILLA - IDEAL - KE - SMOOTH WALL - RGE - MAY 93
TIME 350.000 MSEC CYCLE 1285. PROBLEM 372.0101

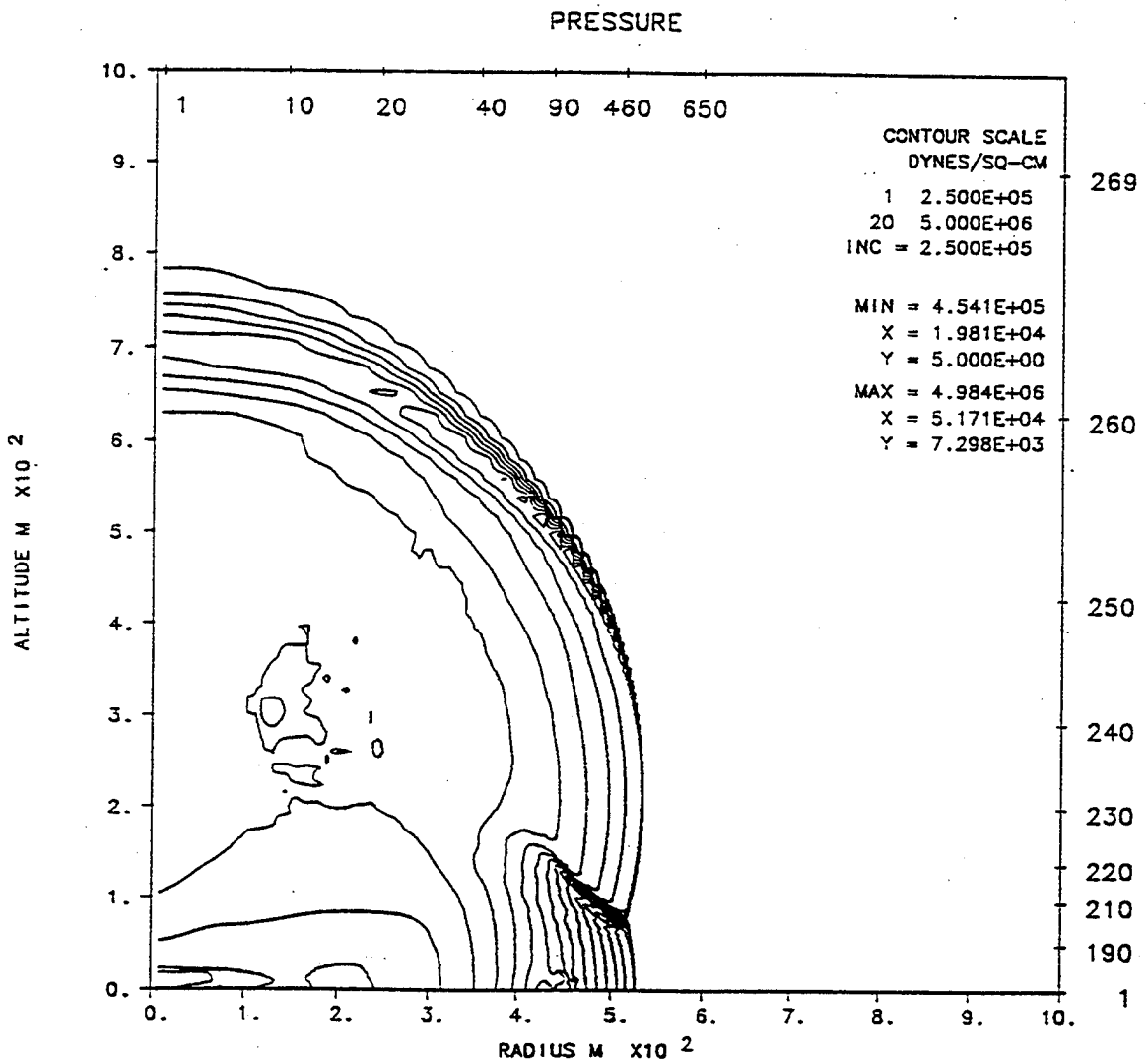

S-CUBED PRISCILLA - IDEAL - KE - SMOOTH WALL - RGE - MAY 93
TIME 500.000 MSEC CYCLE 2431. PROBLEM 372.0101

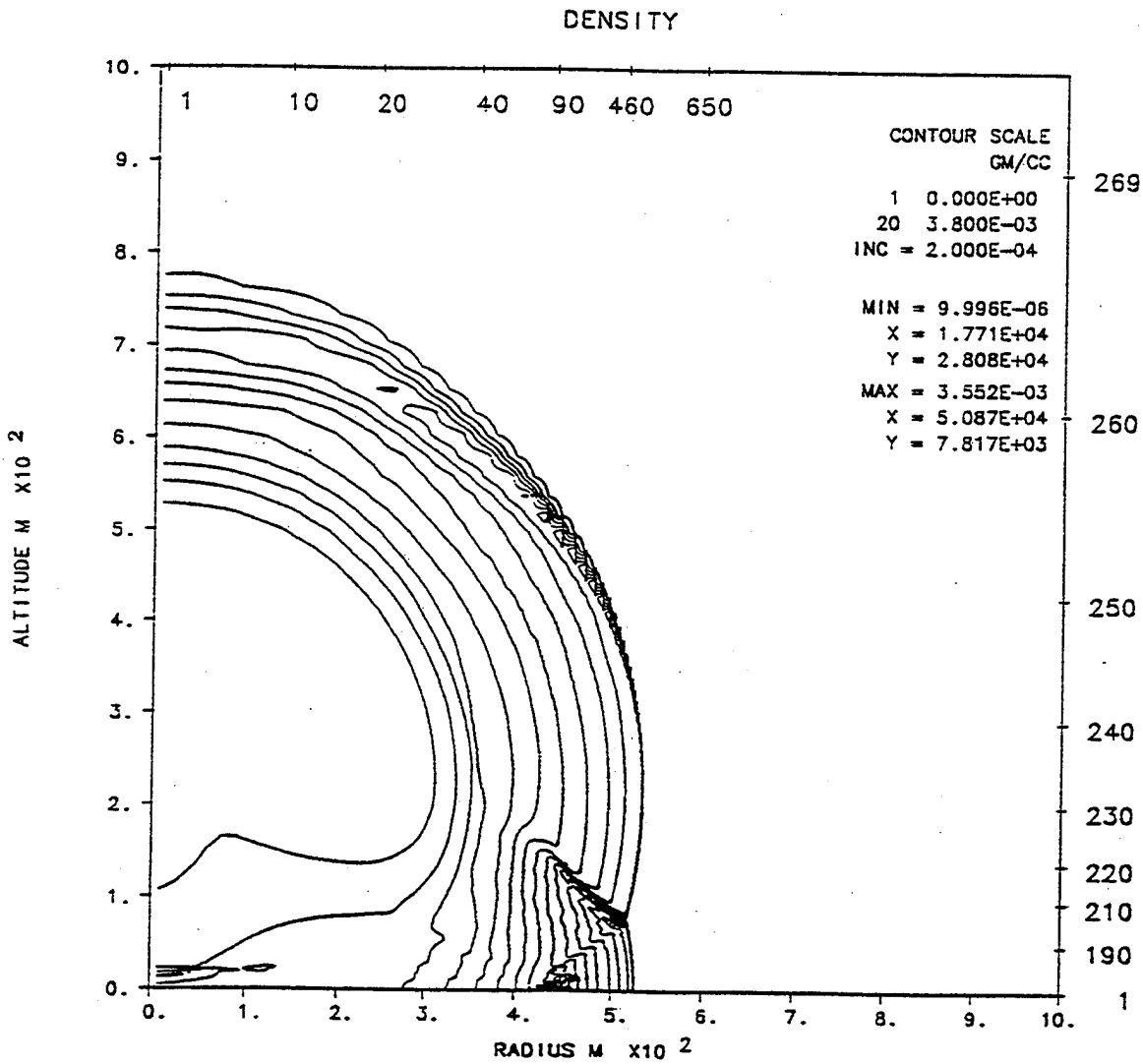

S-CUBED PRISCILLA - IDEAL - KE - SMOOTH WALL - RGE - MAY 93
TIME 500.000 MSEC CYCLE 2431. PROBLEM 372.0101

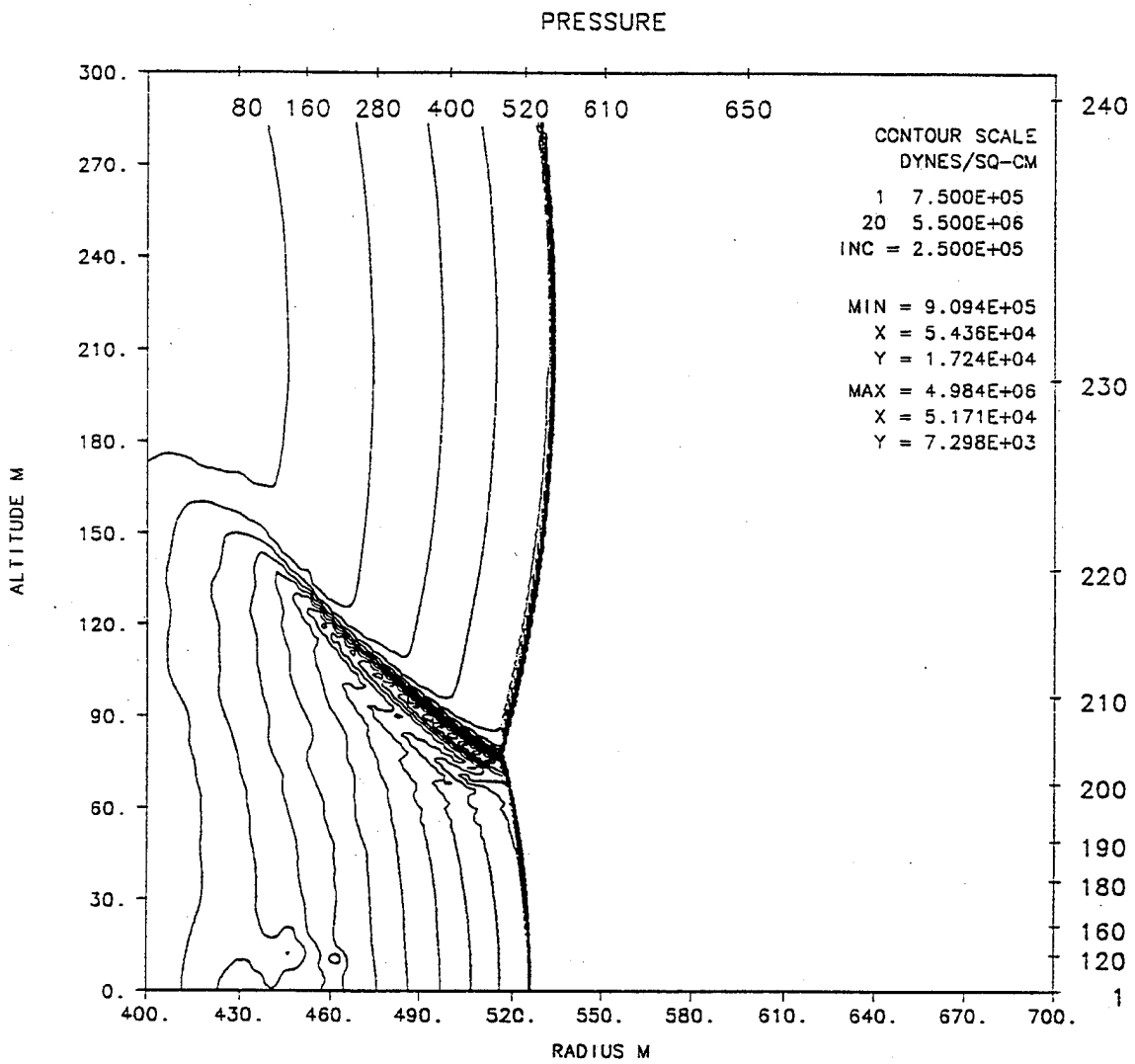

S-CUBED PRISCILLA - IDEAL - KE - SMOOTH WALL - RGE - MAY 93
TIME 500.000 MSEC CYCLE 2431. PROBLEM 372.0101

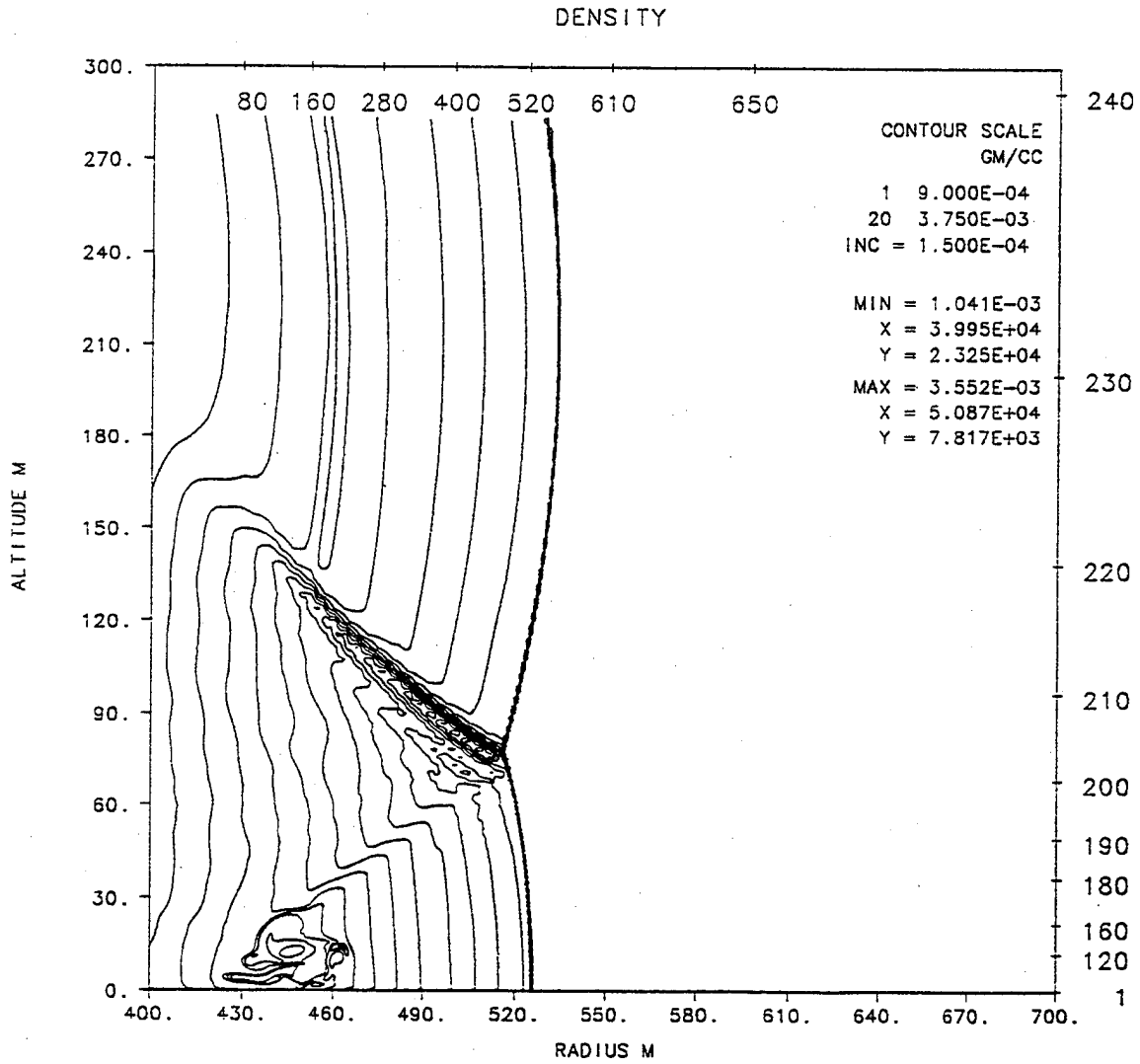

S-CUBED PRISCILLA - IDEAL - KE - SMOOTH WALL - RGE - MAY 93
TIME 500.000 MSEC CYCLE 2431. PROBLEM 372.0101

APPENDIX C
GROUND-LEVEL STATION OVERPRESSURE AND OVERPRESSURE IMPULSE PLOTS

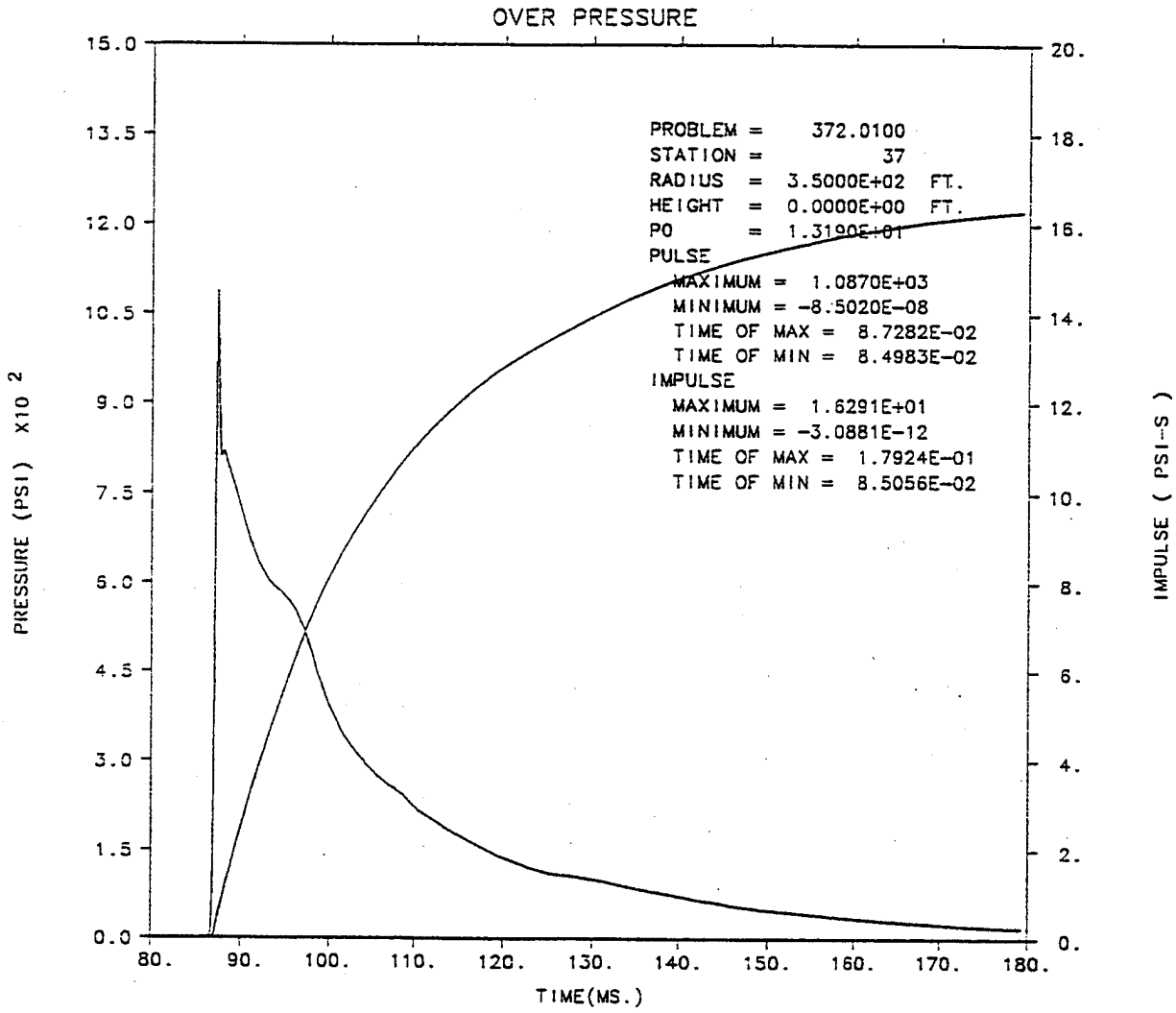

S-CUBED PRISCILLA - IDEAL - KE - SMOOTH WALL - RGE - MAY 93

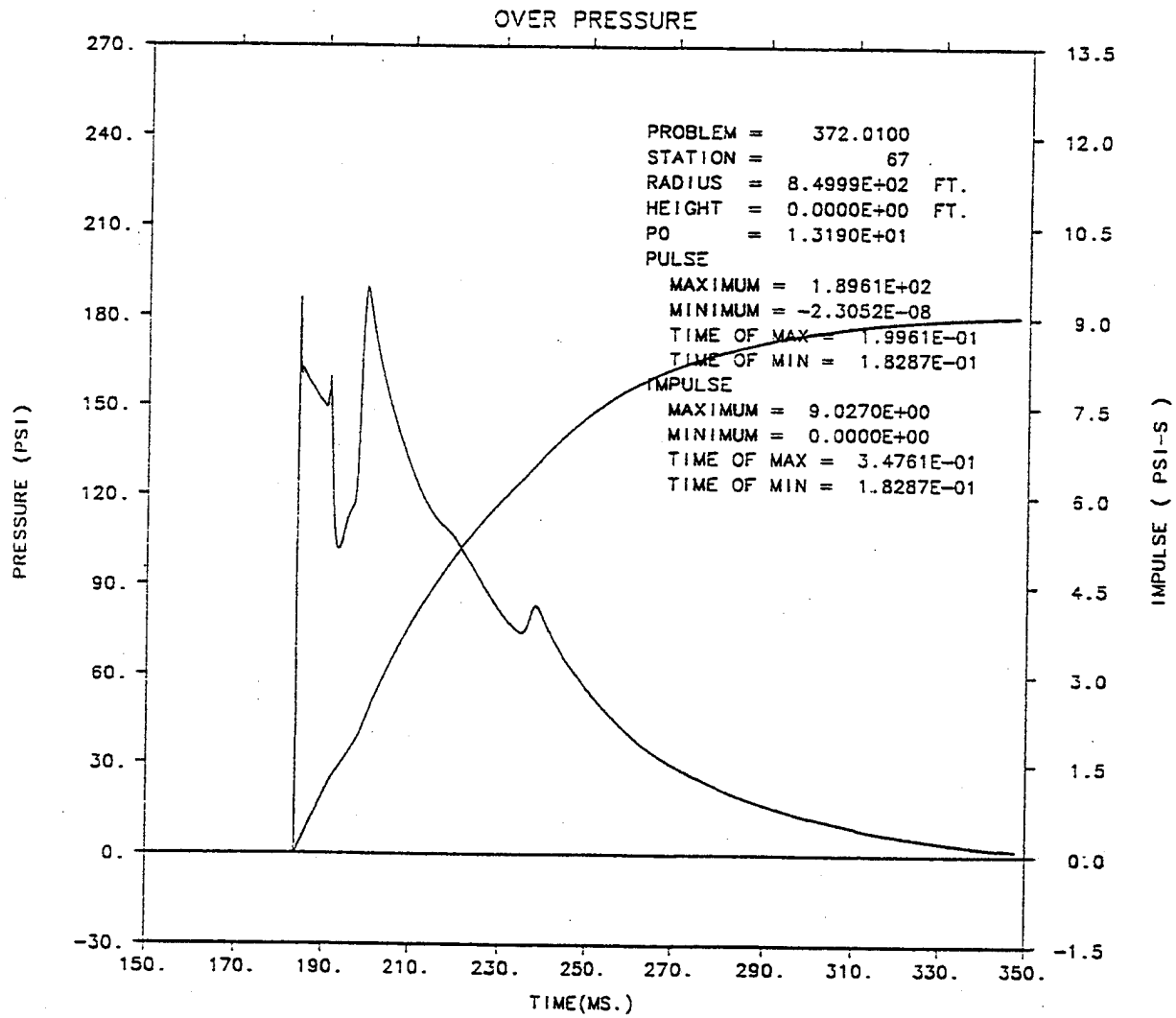

S-CUBED PRISCILLA - IDEAL - KE - SMOOTH WALL - RGE - MAY 93

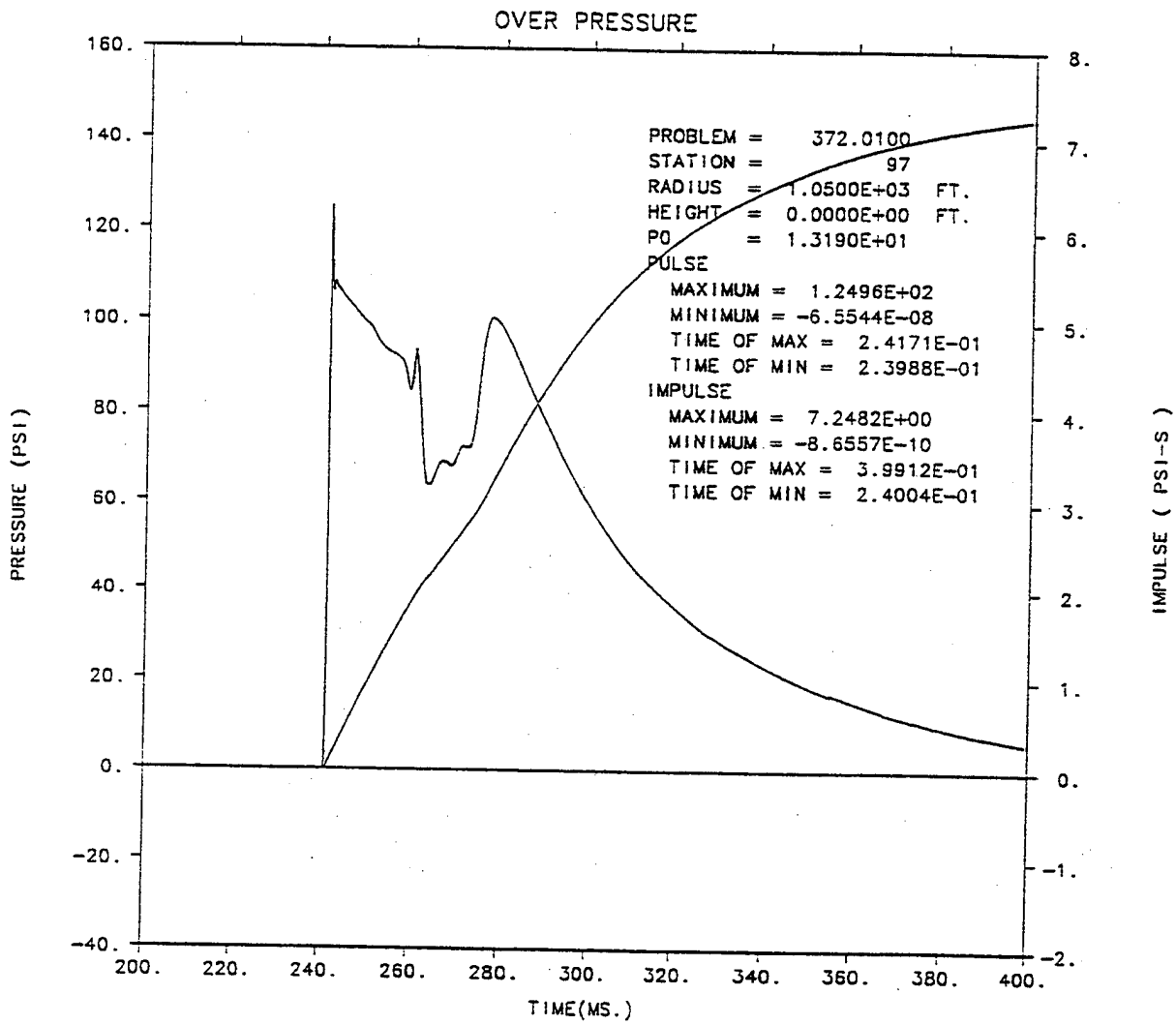

S-CUBED PRISCILLA - IDEAL - KE - SMOOTH WALL - RGE - MAY 93

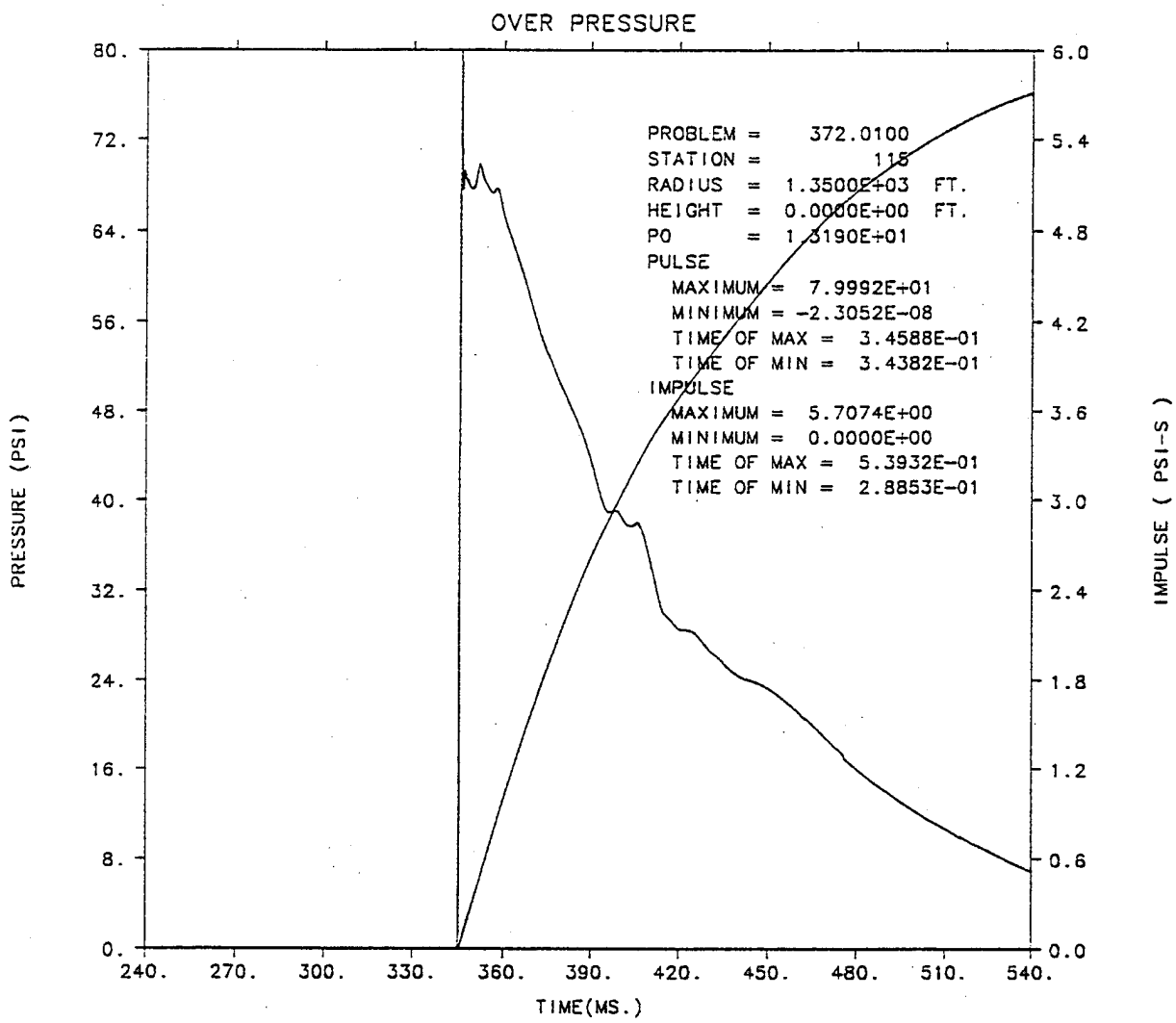

S-CUBED PRISCILLA - IDEAL - KE - SMOOTH WALL - RGE - MAY 93

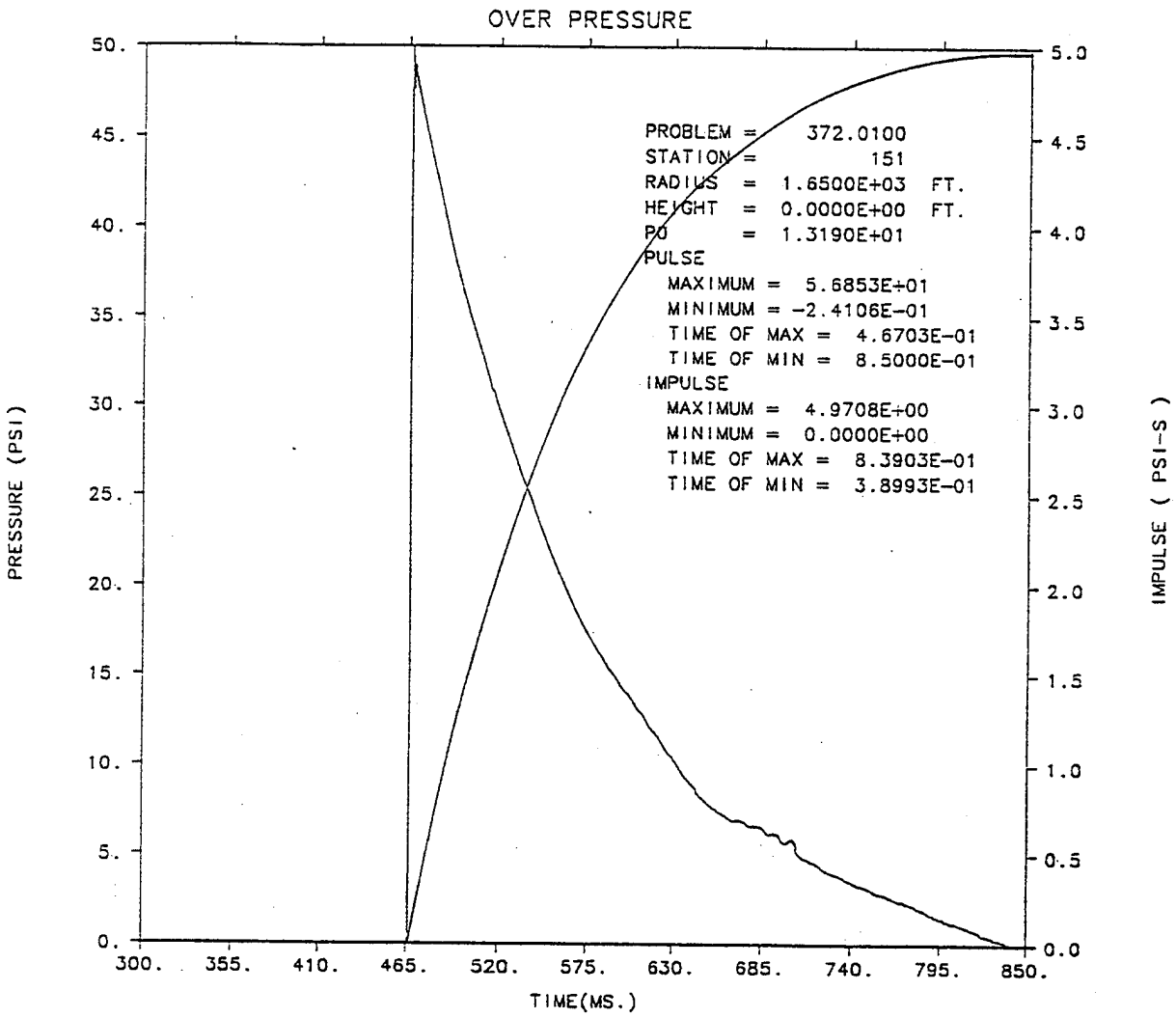

S-CUBED PRISCILLA - IDEAL - KE - SMOOTH WALL - RGE - MAY 93

INTENTIONALLY LEFT BLANK.

APPENDIX D
COMPARISON OF FINE- AND COARSE-ZONED GRASSLAND CALCULATIONS

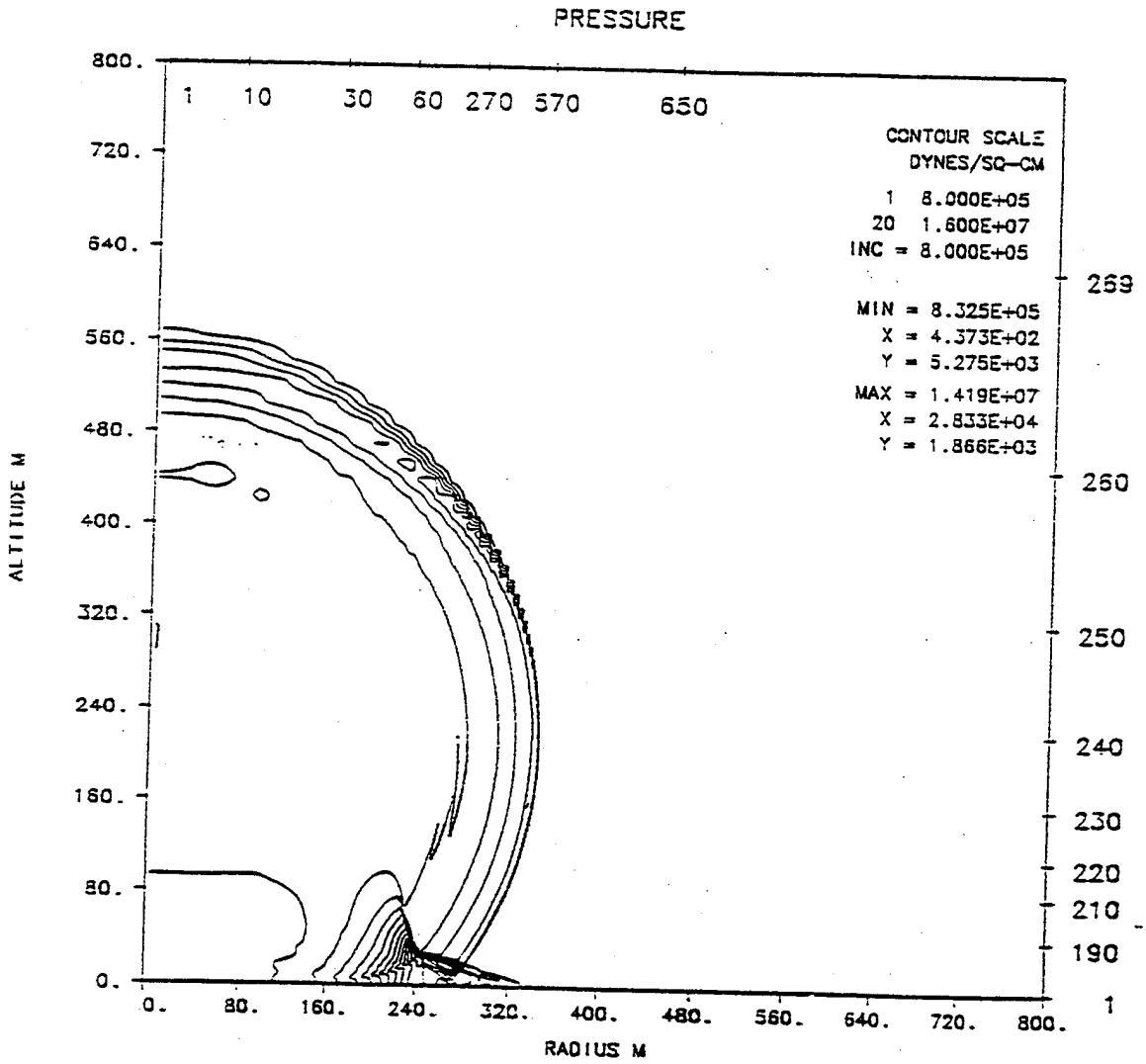

S-CUBED PRISCILLA - GRASSLAND THERMAL - KE - ROUGH WALL - RGE - JUNE 93
TIME 200.000 MSEC CYCLE13673. PROBLEM 372.0102

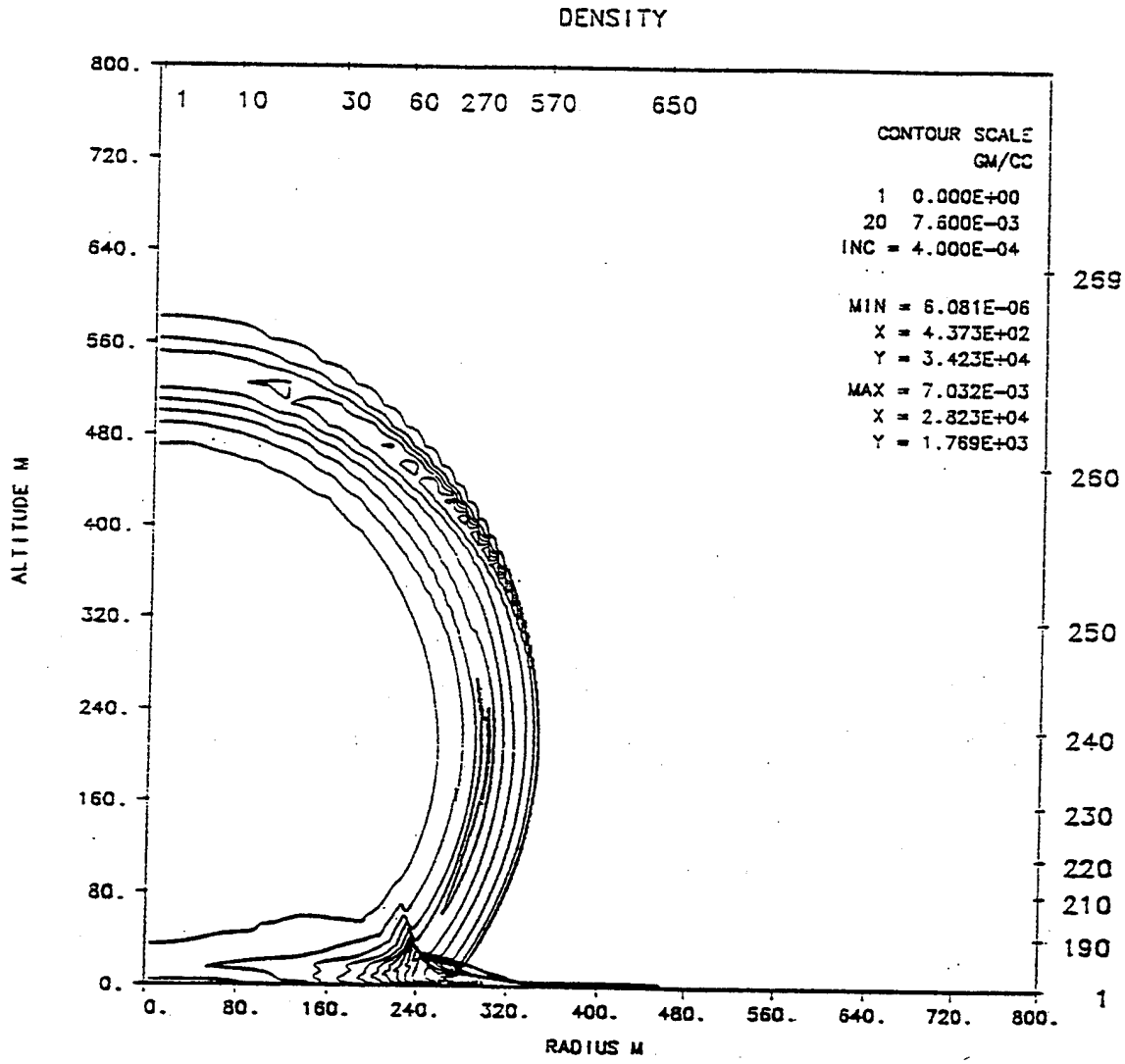

S-CUBED PRISCILLA - GRASSLAND THERMAL - KE - ROUGH WALL - RGE - JUNE 93
TIME 200.000 MSEC CYCLE13673. PROBLEM 372.0102

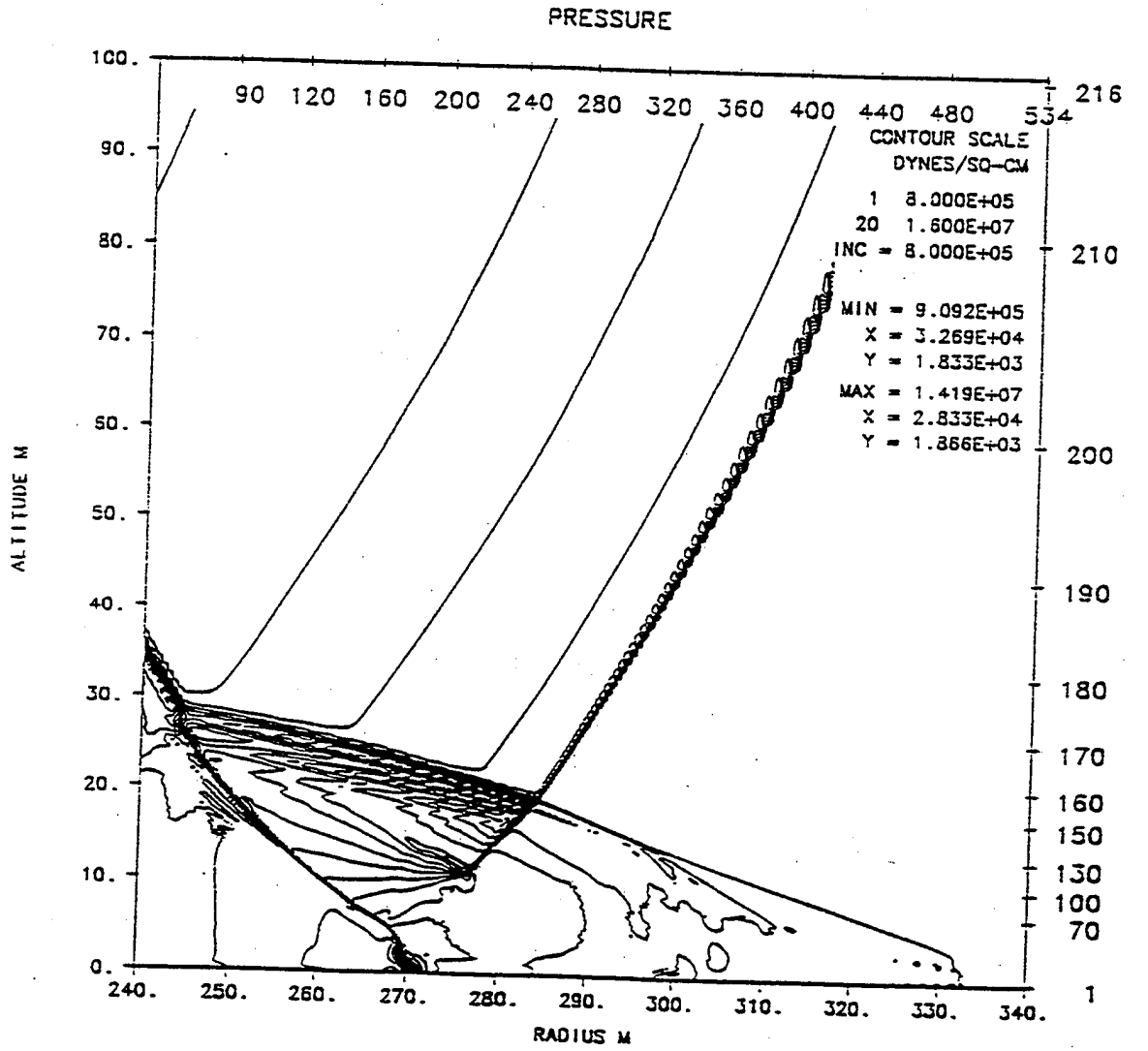

S-CUBED PRISCILLA - GRASSLAND THERMAL - KE - ROUGH WALL - RGE - JUNE 93
TIME 200.000 MSEC CYCLE13673. PROBLEM 372.0102

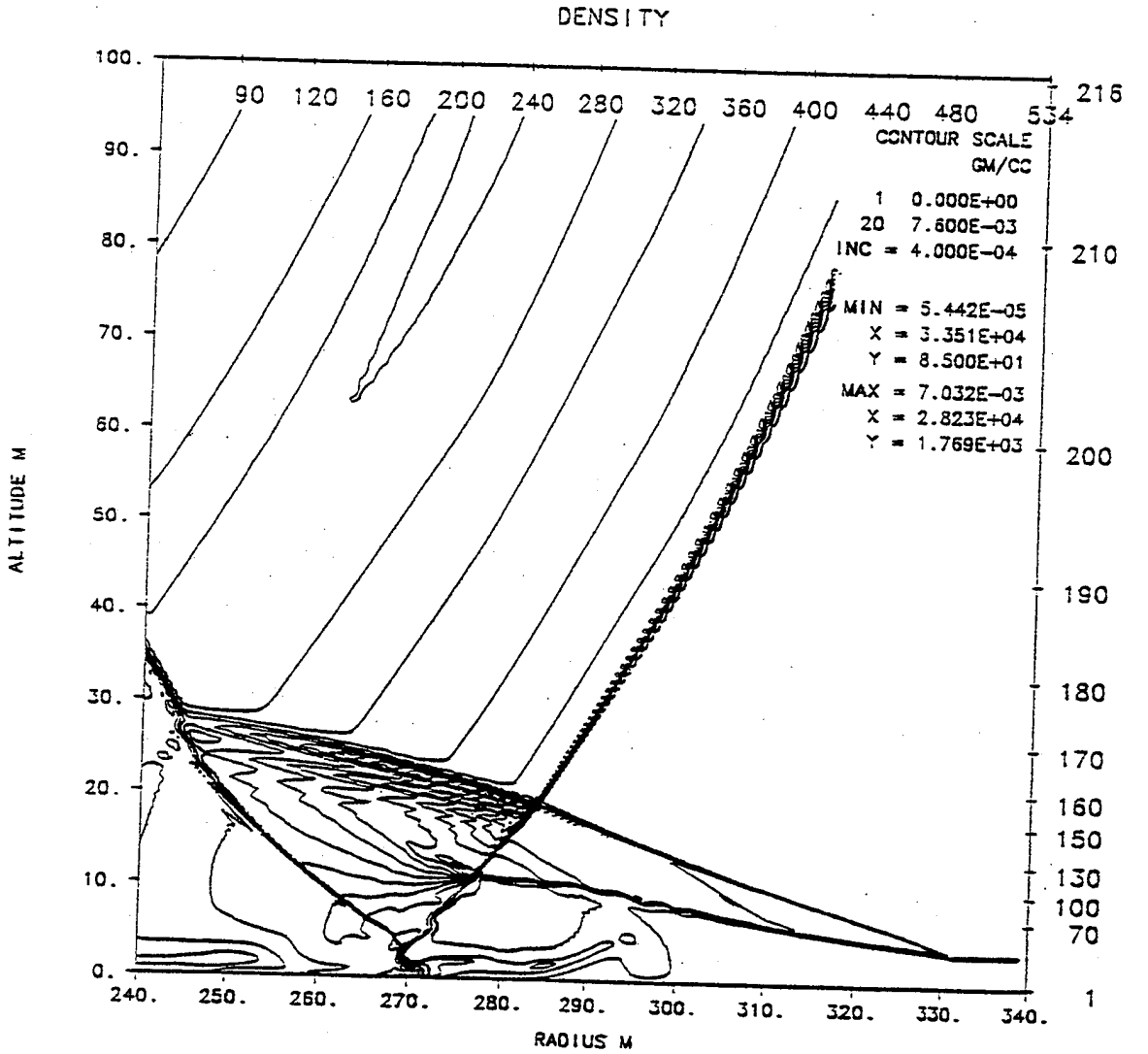

S-CUBED PRISCILLA - GRASSLAND THERMAL - KE - ROUGH WALL - RGE - JUNE 93
TIME 200.000 MSEC CYCLE13673. PROBLEM 372.0102

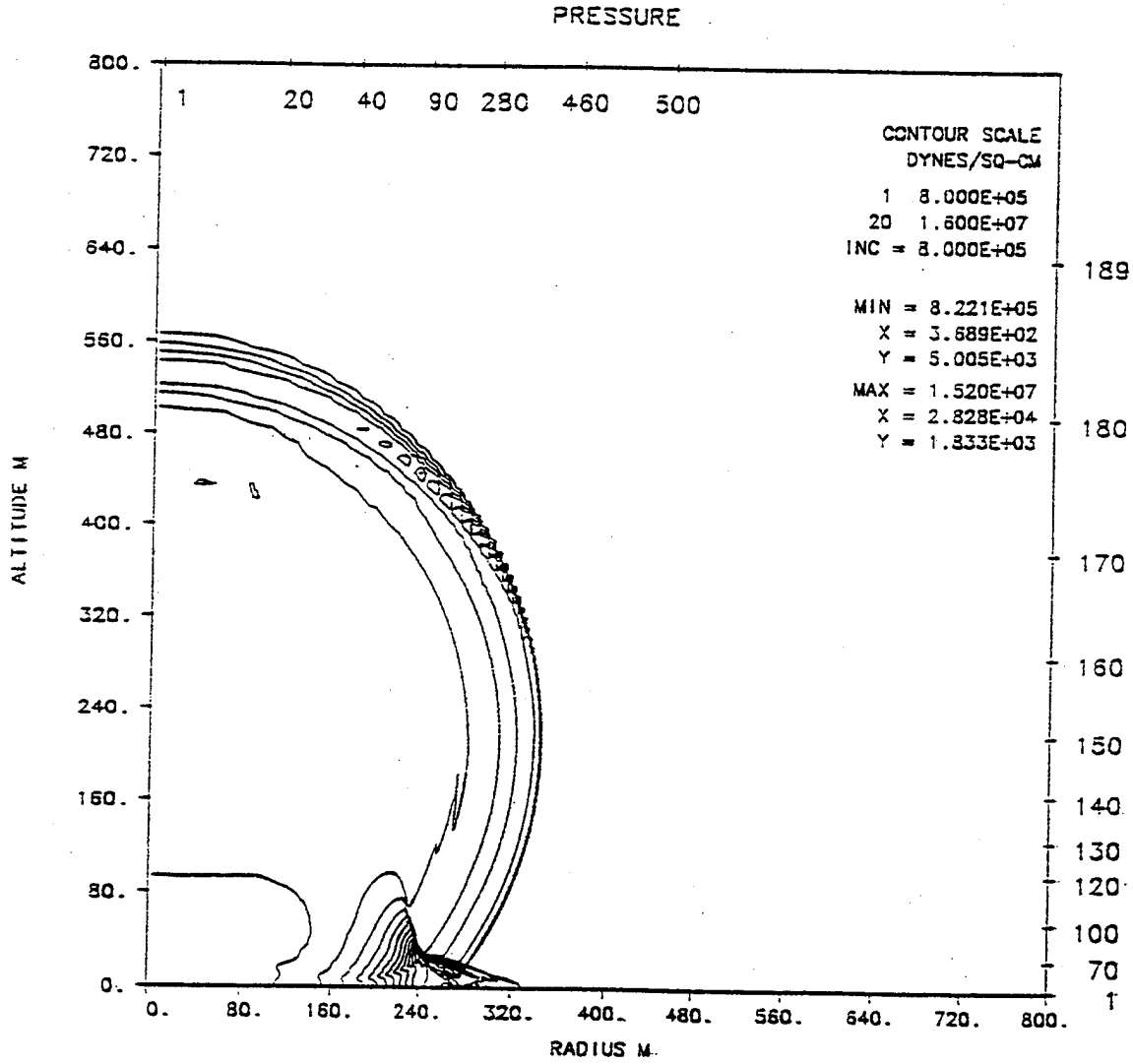

S-CUBED PRISCILLA - GRASSLAND COARSE THERMAL - KE - ROUGH WALL -RGE 7/93-
TIME 200.000 MSEC CYCLE 3877. PROBLEM 372.0104

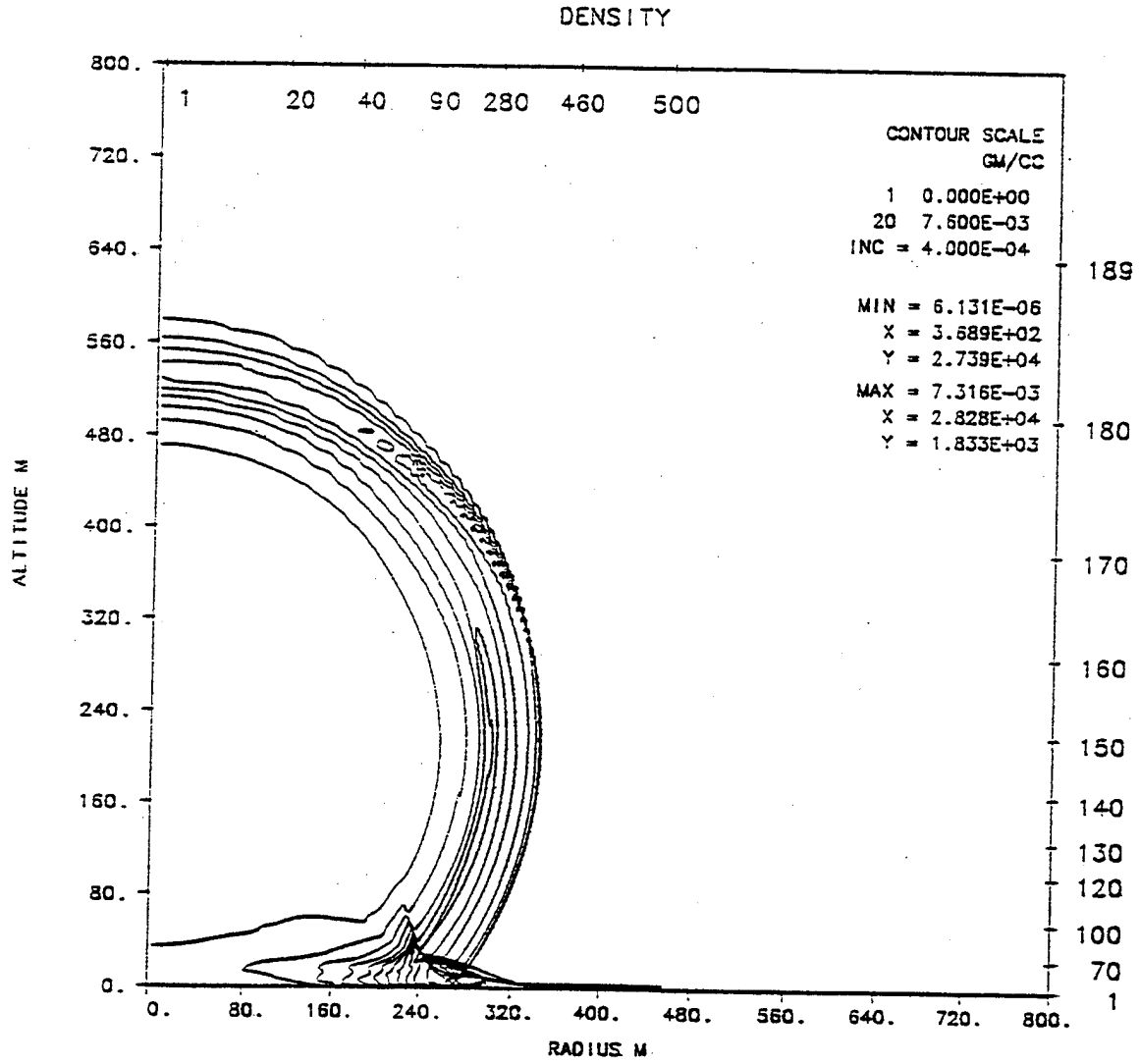

S-CUBED PRISCILLA - GRASSLAND COARSE THERMAL - KE - ROUGH WALL -RGE 7/93-
TIME 200.000 MSEC CYCLE 3877. PROBLEM 372.0104

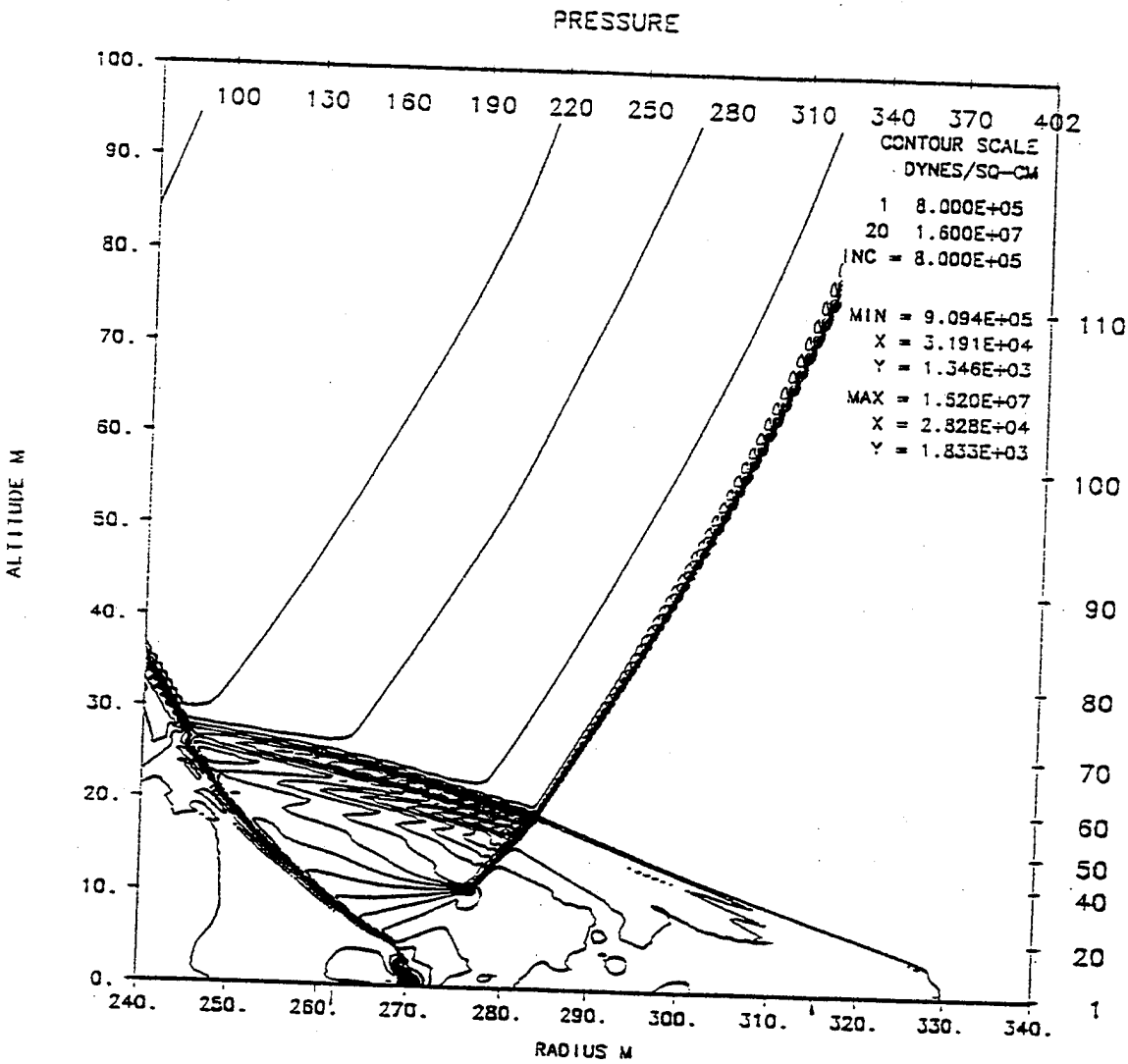

S-CUBED PRISCILLA - GRASSLAND COARSE THERMAL - KE - ROUGH WALL -RGE 7/93-
TIME 200.000 MSEC CYCLE 3877. PROBLEM 372.0104

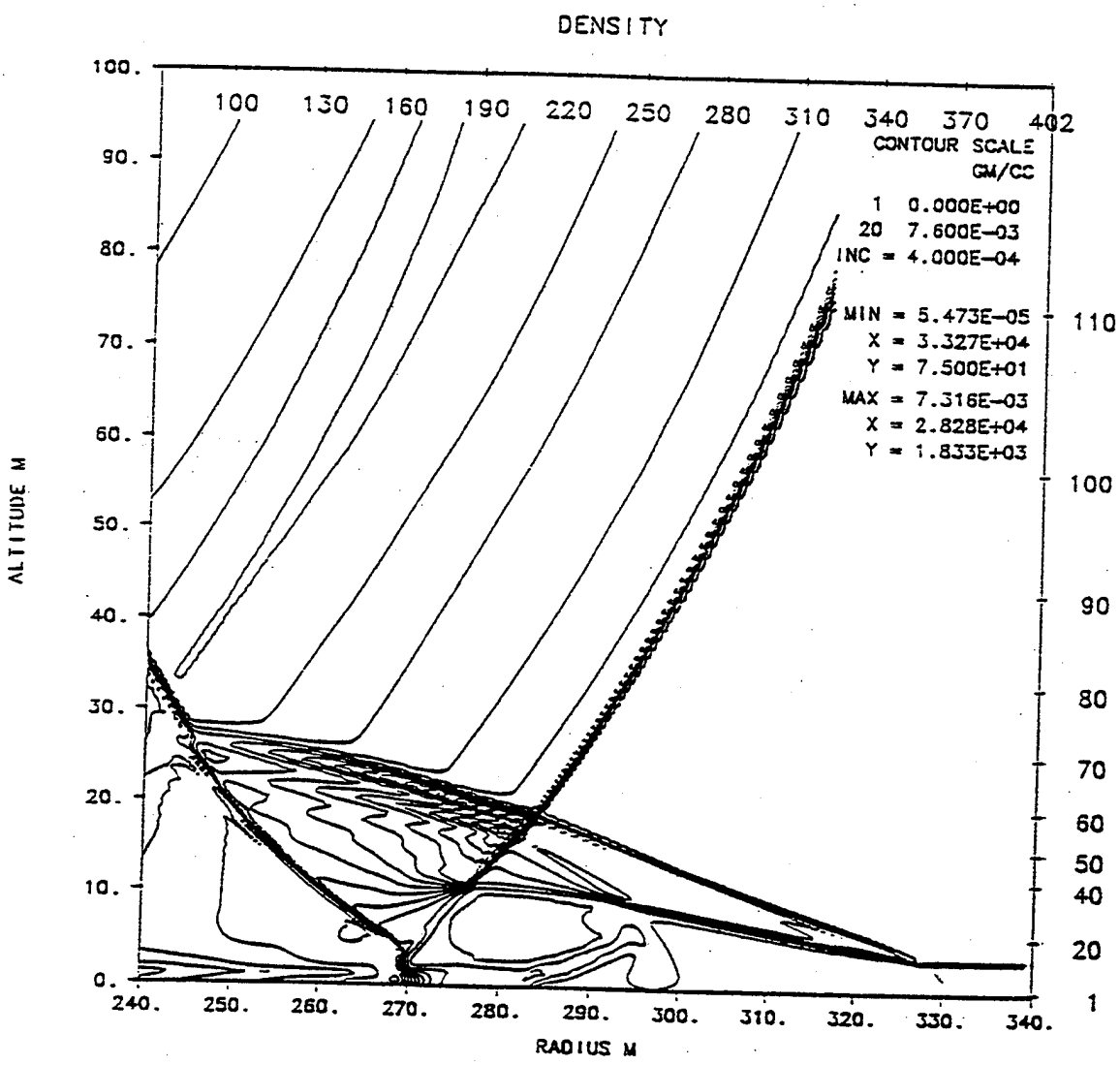

S-CUBED PRISCILLA – GRASSLAND COARSE THERMAL – KE – ROUGH WALL –RGE 7/93–
TIME 200.000 MSEC CYCLE 3877. PROBLEM 372.0104

APPENDIX E
COMMENTARY ON DEVELOPMENT OF PRECURSOR IN GRASSLAND CALCULATION

At 70 ms, the contours show reflection at approximately 45 meters. There is no indication at this early time of precursor formation.

At 80 ms, the contours show reflection to approximately 88 meters. There is a slight curvature of the incident shock in the bottom two to three meters. A weak upward-moving wave has appeared near the top of the thermal layer. The pressure histogram from the surface zone shows a weak outrunning wave to approximately 90 meters, with the peak pressure following behind the first shock at 65 meters.

At 90 ms, the contours show reflection out to 118 meters. In the lower two to three meters, the contours of the incident shock are approaching vertical. The upward-moving wave shows influence to approximately 105 meters, but it is difficult to see whether or not growth of this pre-precursor structure has occurred since the previous time.

At 100 ms, definite precursor formation is evident at approximately 145 meters. The vertically-moving signal is not visible in these plots, probably because of the way the contours fall.

At 110 ms, the precursor toe extends to 170 meters. The precursor intersects the top of the thermal layer at approximate range 168 meters and at height 3.5 meters. The upward-moving precursor wave intersects the incident wave at range 163 meters and at approximate height 5.5 meters. This is particularly apparent in the expanded scale contours from the fine-zoned calculation (E-16). This point corresponds also to the intersection of the upward-moving wave behind the incident shock with the incident shock. This upward-moving wave extends back to intersect the reflected shock at approximately 142 meters at a height of about 4 meters. The reflected wave displays a kink at the intersection point. The lower part of the reflected wave extends to about 156 meters. The incident wave changes rapidly from a shock at the precursor intersection point to a compressive wave by about meter below the intersection point.

At 120 ms, the precursor extends to about 194 meters. Results from the fine-zoned calculation show effects of the vertically-structured thermal layer at the precursor toe. The top of the thermal layer is distinct at a height of about 3.5 meters. The intersection of the precursor with the incident shock occurs at about range 181 meters and height 7 meters. The upward-moving wave is slightly rounded and convex upward. Its maximum height occurs at range 169 meters, and it intersects the reflected shock at range 155 meters, height 7 meters. The reflected shock in the expanded plots from the fine-zoned calculation shows structure similar to that of a double Mach reflection near ground at range 172 meters.

At 150 ms, the precursor extends to 248 meters. Intersection of the precursor shock with the incident shock is about 10 meters above the surface at range 225 meters. This

upward-moving wave is significantly stronger inside the region encompassed by the incident shockthan it is outside.

At 200 ms, the precursor extends to 333 meters. The intersection with the incident shock is at range 283 meters and height 20 meters. The incident shock extends through the precursor shock, but ends rather abruptly at a height of 11 meters. This corresponds closely to the Mach stem height of the ideal case at this time. The incident shock terminates at the top of lofted thermal layer. Some instabilities appear in the density contour plot along the interface between the top of the thermal layer and the precursor toe region.

At 500 ms, the inside, upward-moving shock has separated from the precursor shock outside of the incident shock region. The inside shock is attached to a triple-point-like structure, which is attached to the precursor-shock intersection point with a Mach-like stem.

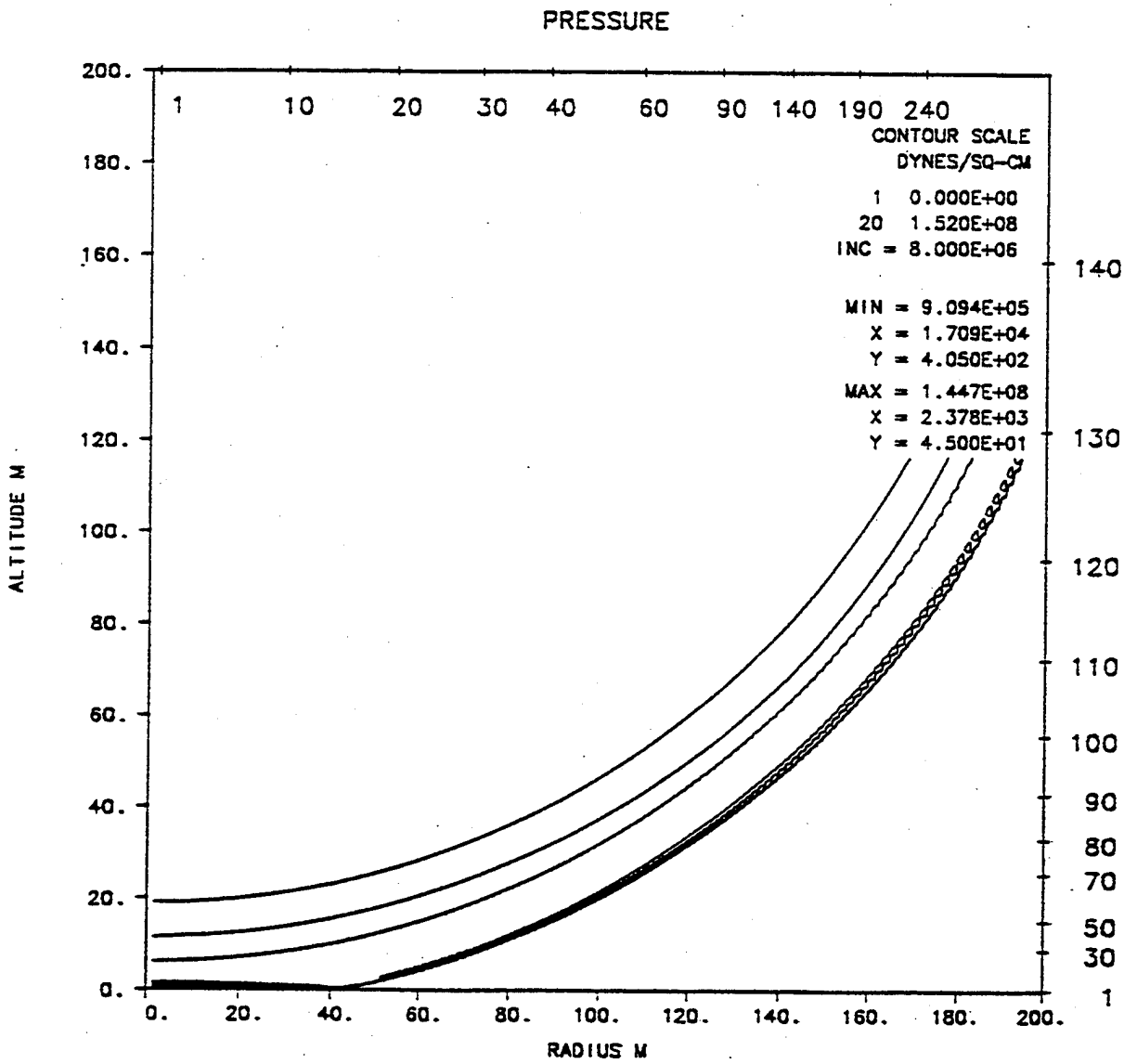

S-CUBED PRISCILLA - GRASSLAND COARSE THERMAL - KE - ROUGH WALL -RGE 7/93-
: TIME 70.000 MSEC CYCLE 453. PROBLEM 372.0104

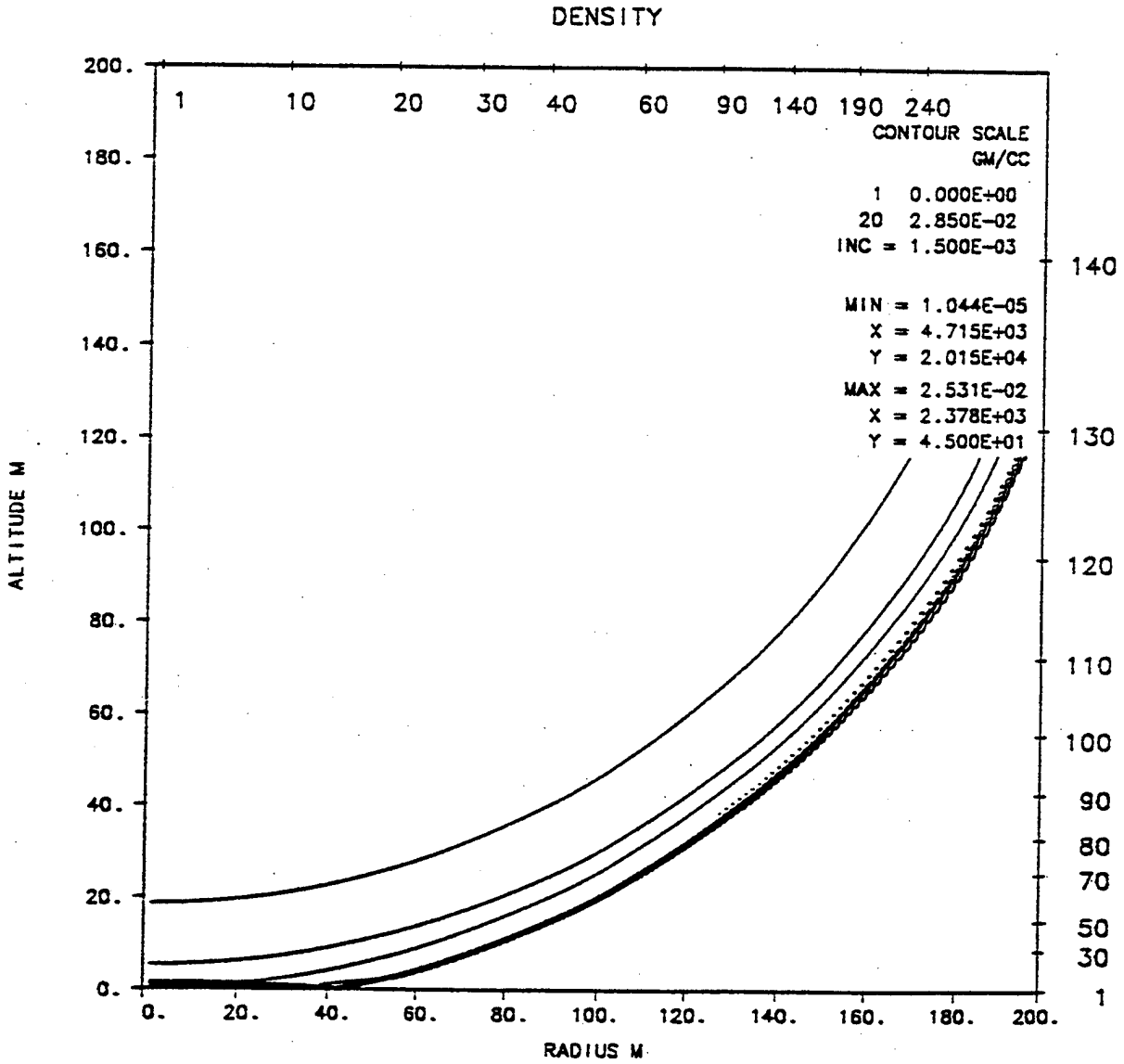

S-CUBED PRISCILLA – GRASSLAND COARSE THERMAL – KE – ROUGH WALL –RGE 7/93–
TIME 70.000 MSEC CYCLE 453. PROBLEM 372.0104

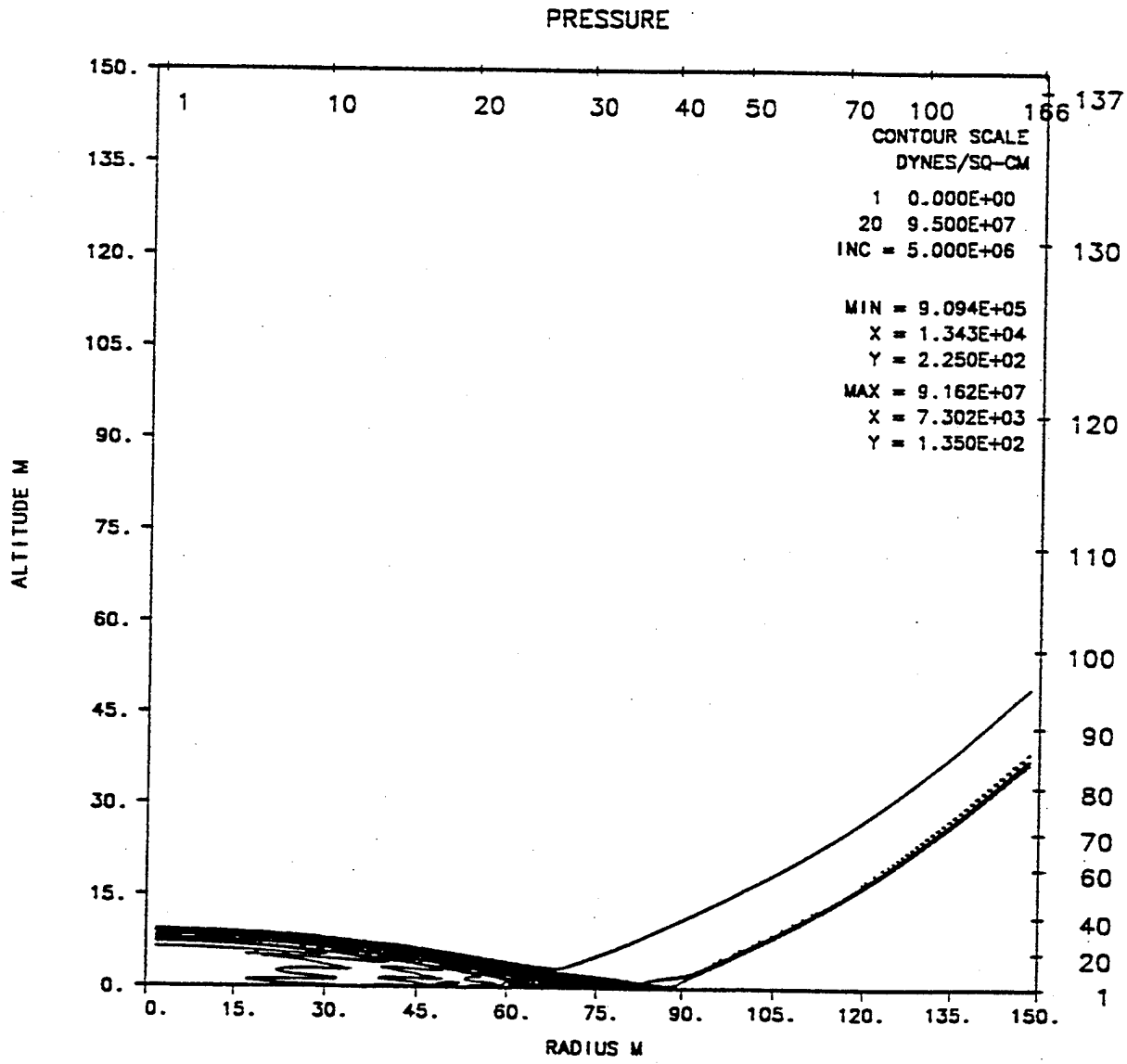

S-CUBED PRISCILLA - GRASSLAND COARSE THERMAL - KE - ROUGH WALL -RGE 7/93-
TIME 80.000 MSEC CYCLE 781. PROBLEM 372.0104

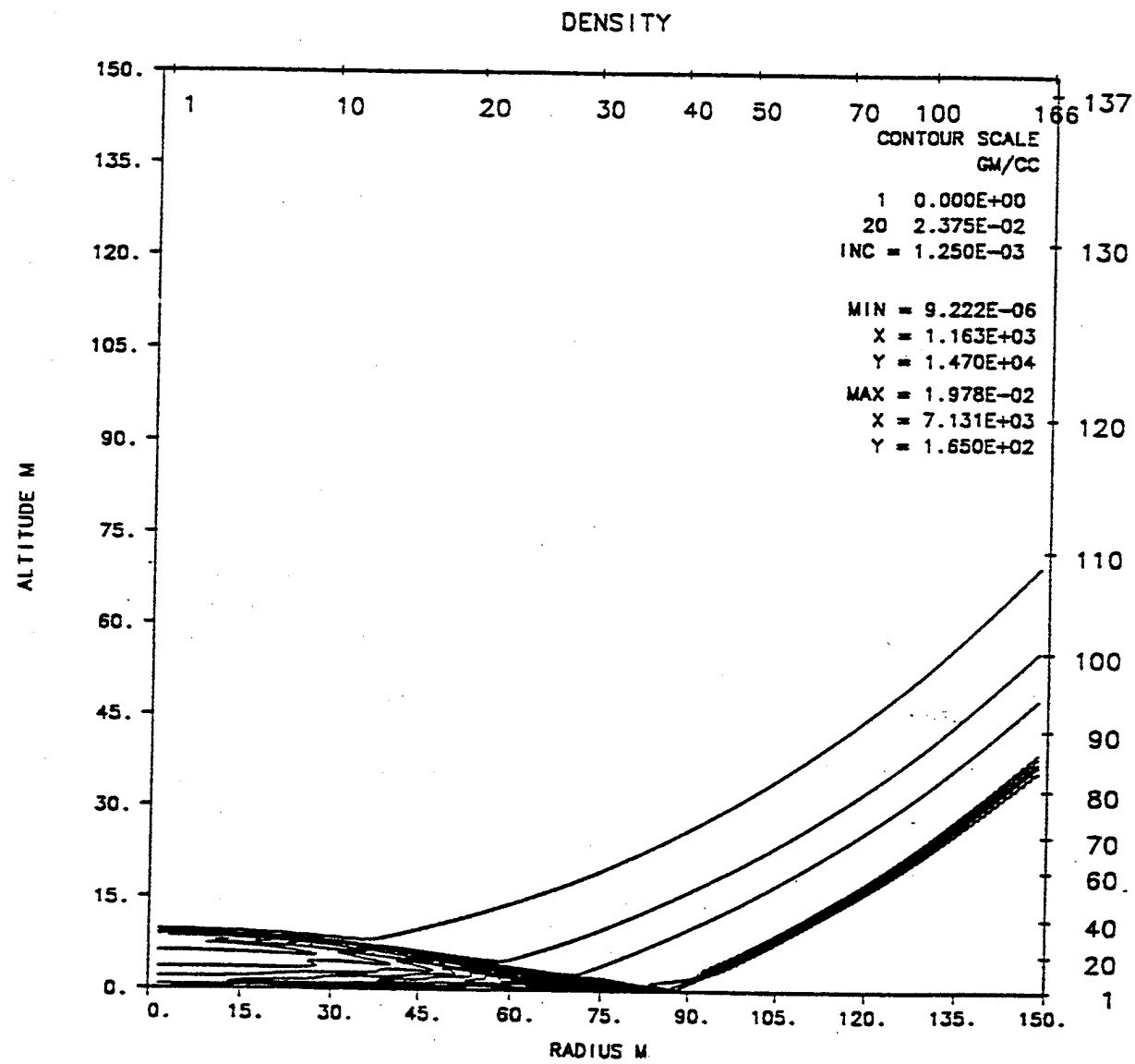

S-CUBED PRISCILLA - GRASSLAND COARSE THERMAL - KE - ROUGH WALL -RGE 7/93-
TIME 80.000 MSEC CYCLE 781. PROBLEM 372.0104

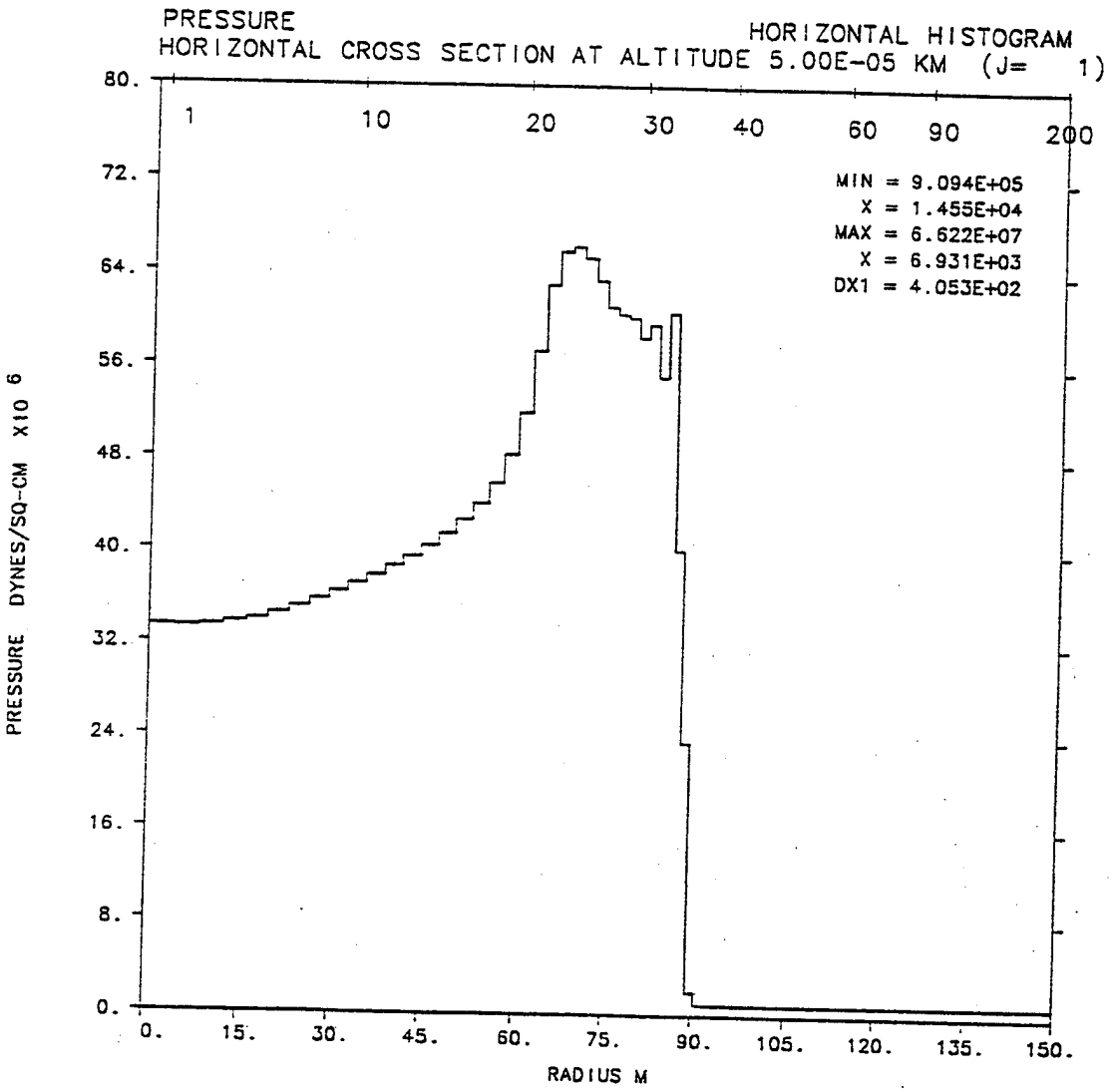

S-CUBED PRISCILLA - GRASSLAND THERMAL - KE - ROUGH WALL - RGE - JUNE 93
TIME 80.000 MSEC CYCLE 1171. PROBLEM 372.0102

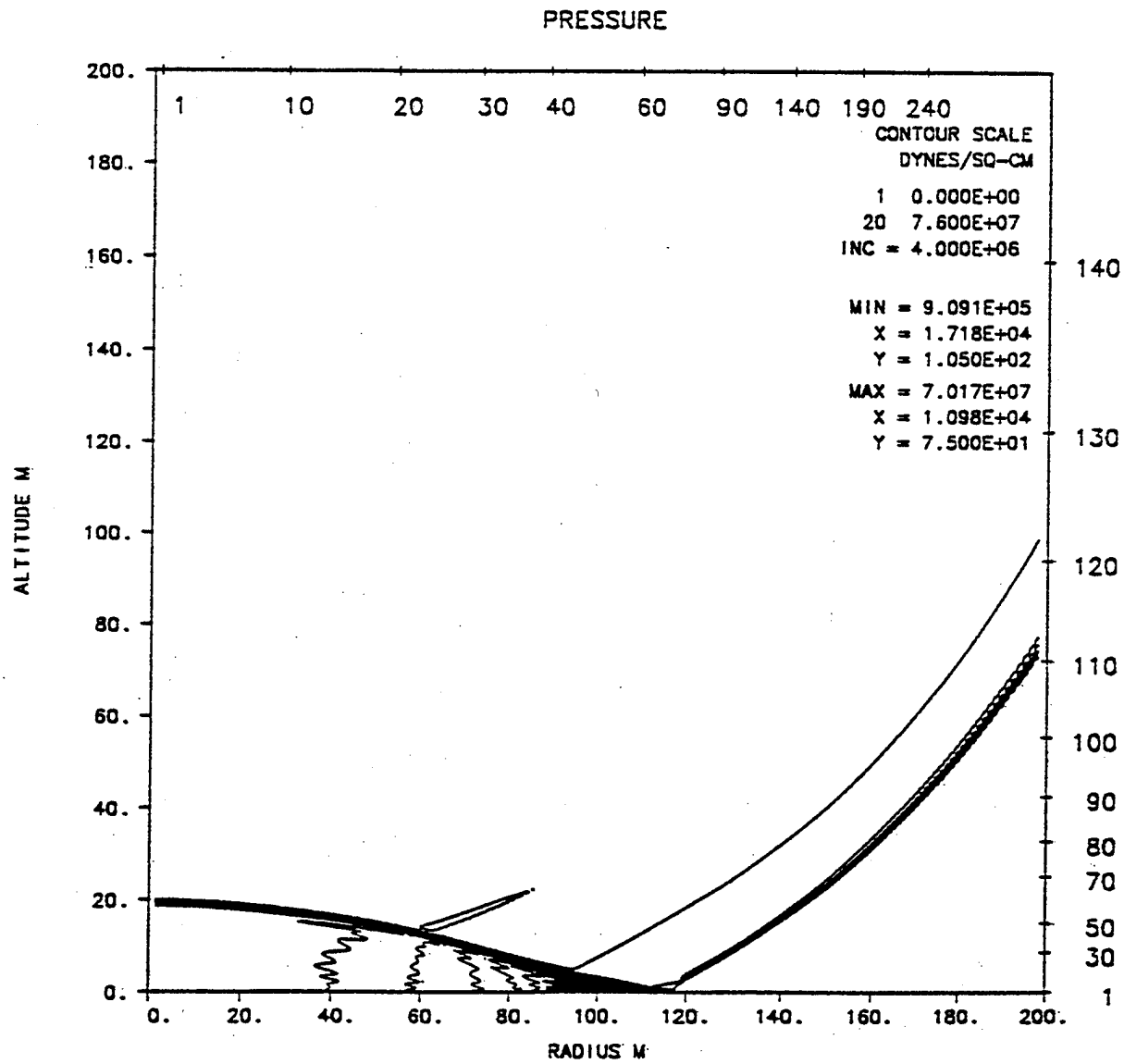

S-CUBED PRISCILLA - GRASSLAND COARSE THERMAL - KE - ROUGH WALL -RGE 7/93-
TIME 90.000 MSEC CYCLE 1117. PROBLEM 372.0104

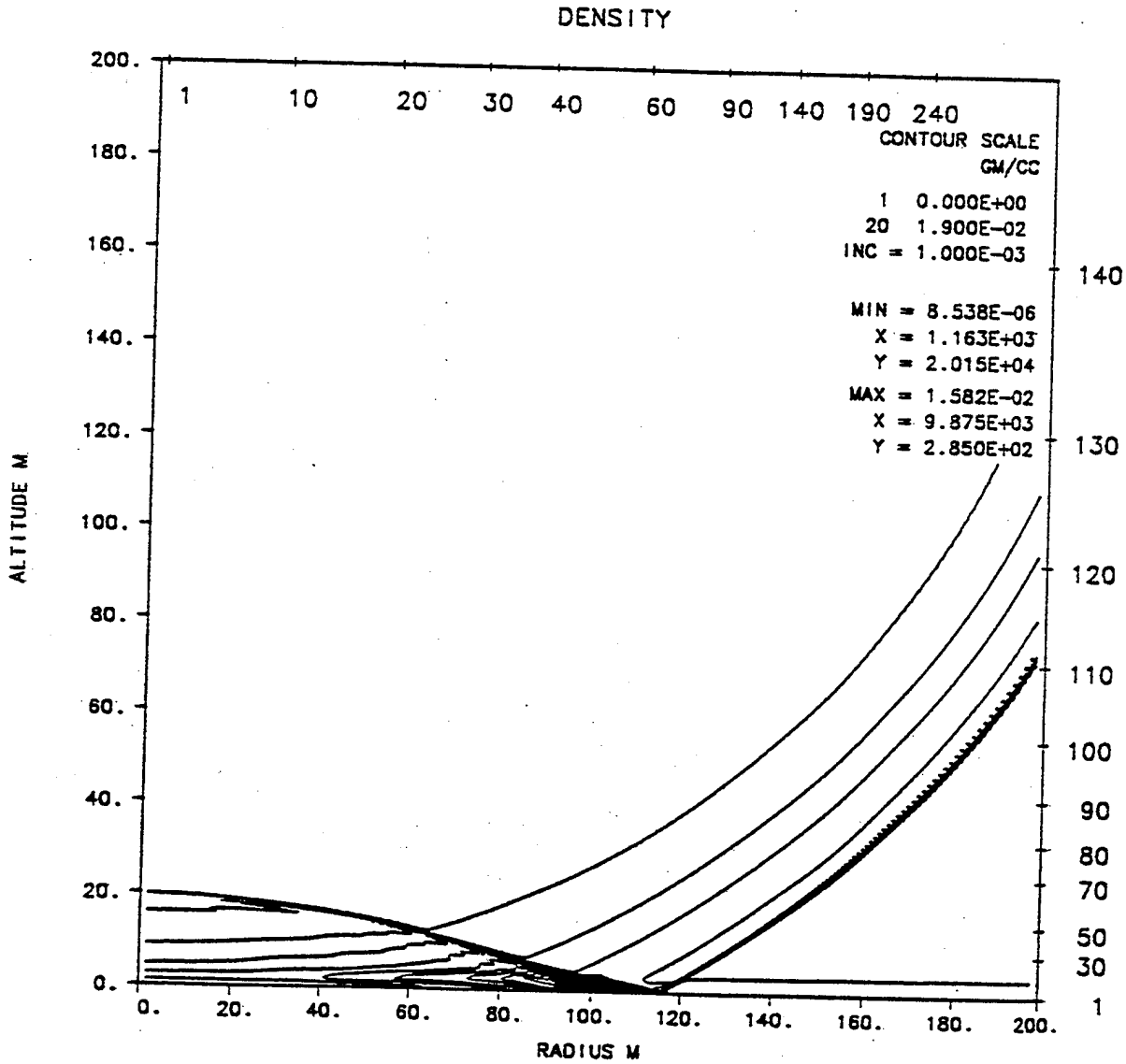

S-CUBED PRISCILLA - GRASSLAND COARSE THERMAL - KE - ROUGH WALL -RGE 7/93-
TIME 90.000 MSEC CYCLE 1117. PROBLEM 372.0104

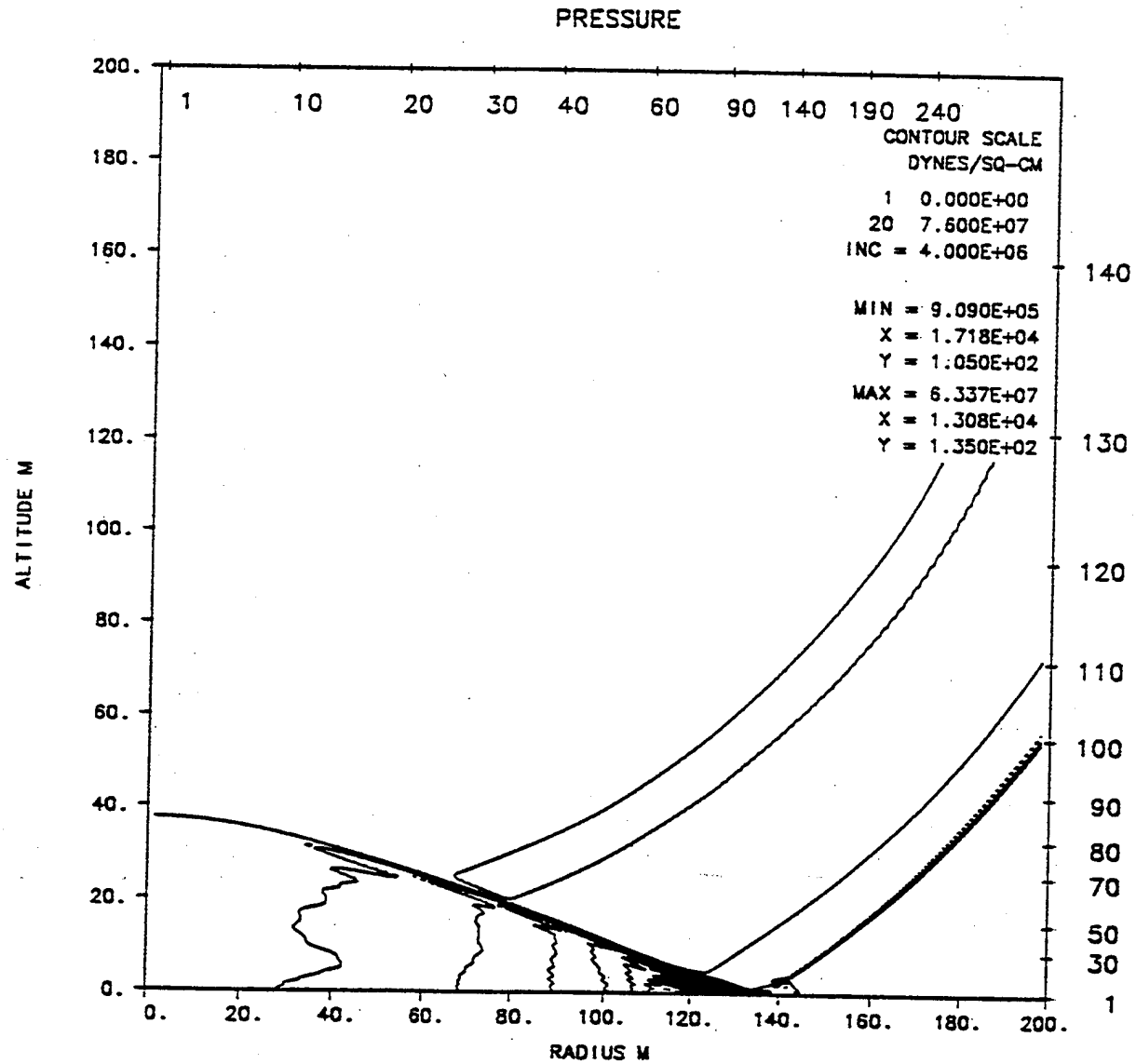

S-CUBED PRISCILLA - GRASSLAND COARSE THERMAL - KE - ROUGH WALL -RGE 7/93-
TIME 100.000 MSEC CYCLE 1453. PROBLEM 372.0104

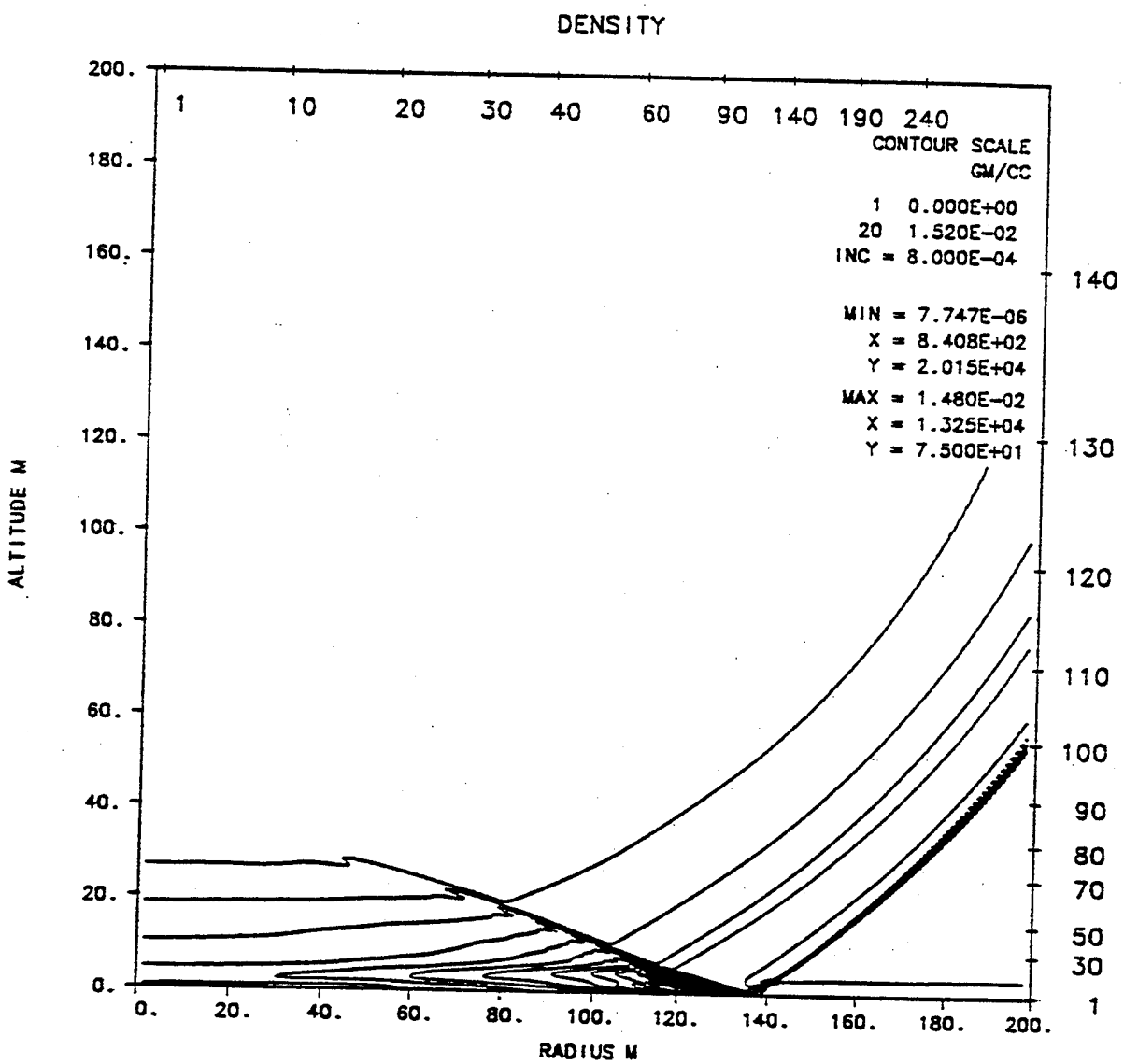

S-CUBED PRISCILLA – GRASSLAND COARSE THERMAL – KE – ROUGH WALL –RGE 7/93–
TIME 100.000 MSEC CYCLE 1453. PROBLEM 372.0104

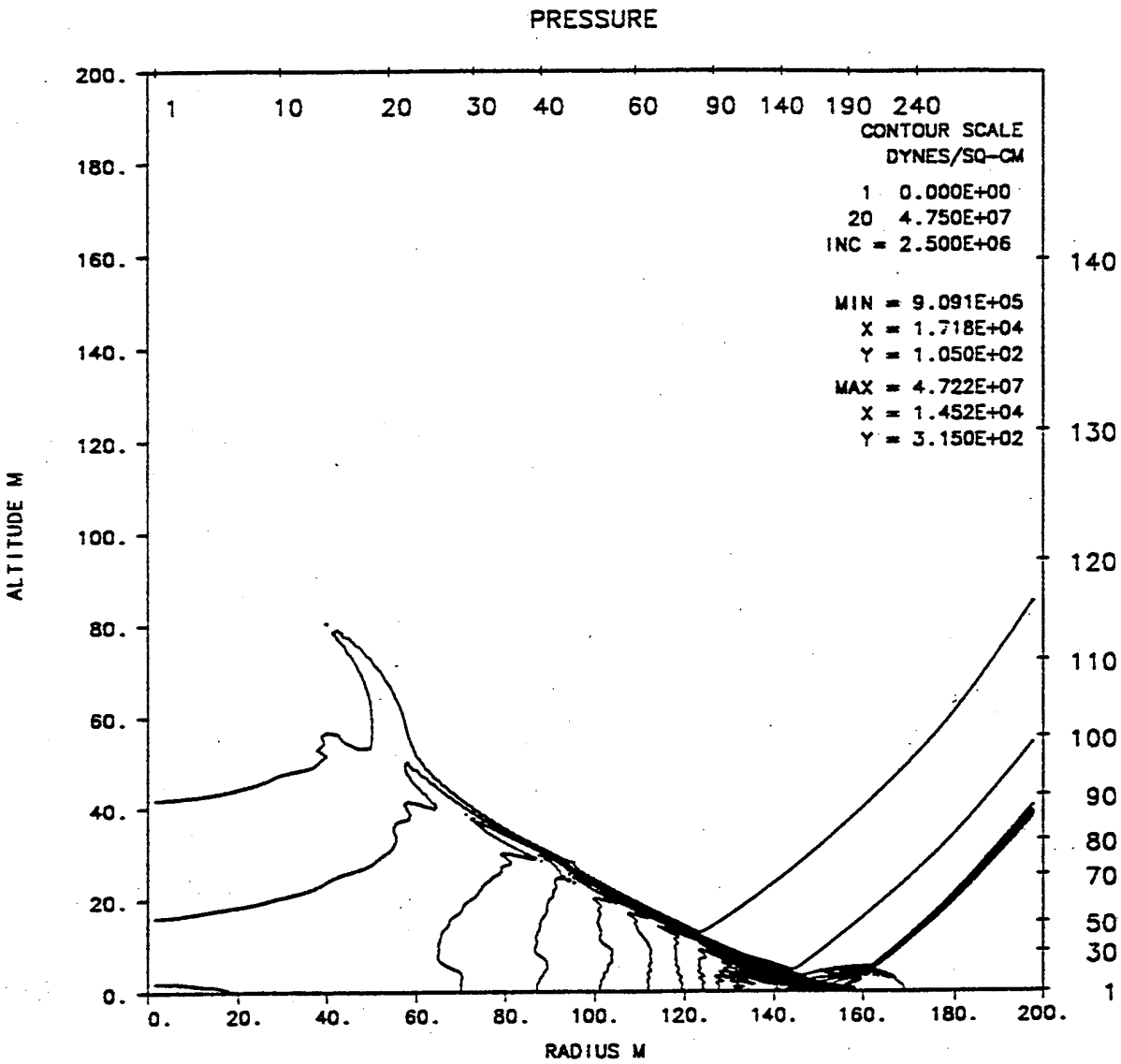

S-CUBED PRISCILLA - GRASSLAND COARSE THERMAL - KE - ROUGH WALL -RGE 7/93-
TIME 110.000 MSEC CYCLE 1789. PROBLEM 372.0104

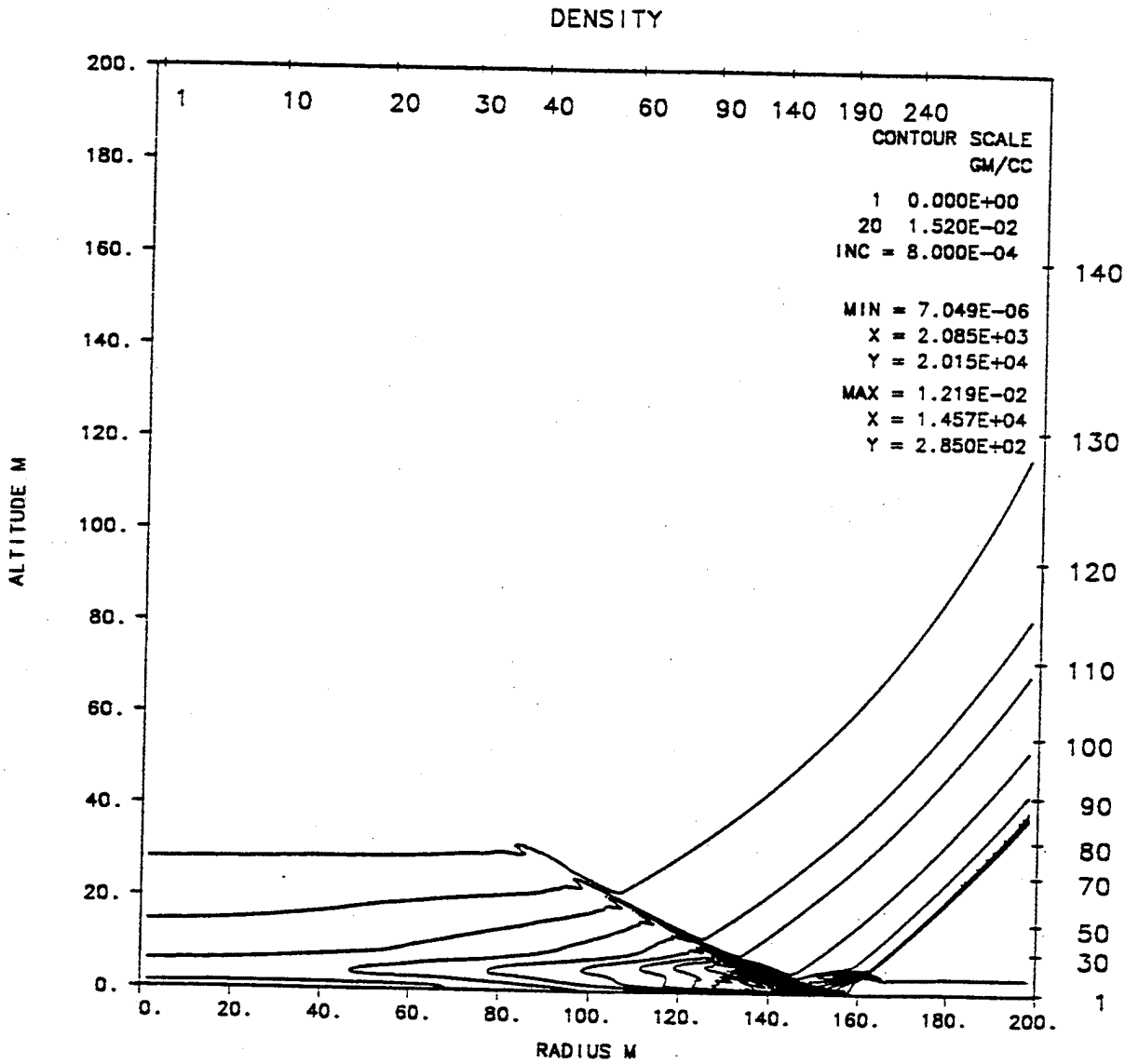

S-CUBED PRISCILLA - GRASSLAND COARSE THERMAL - KE - ROUGH WALL -RGE 7/93-
TIME 110.000 MSEC CYCLE 1789. PROBLEM 372.0104

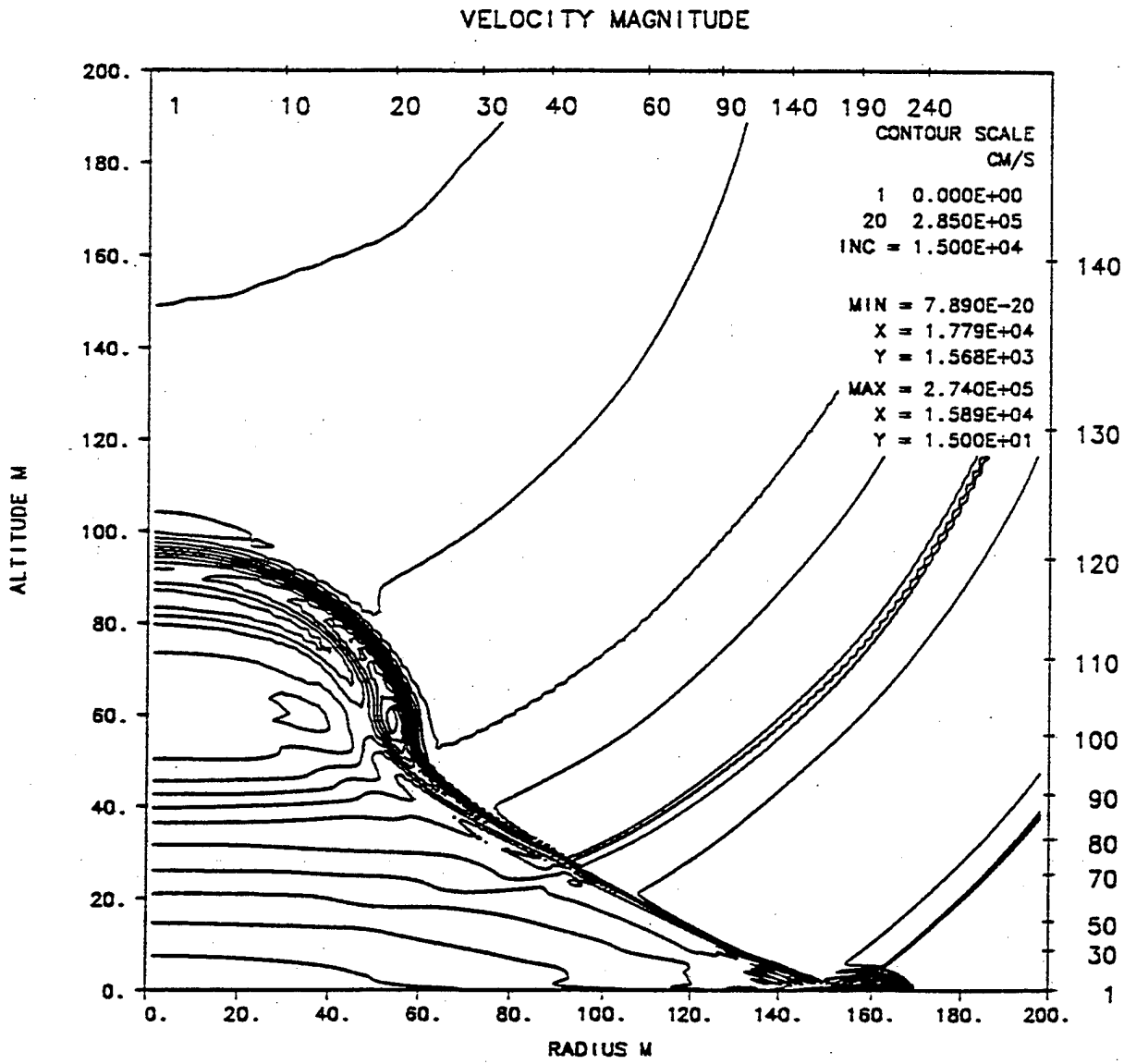

S-CUBED PRISCILLA - GRASSLAND COARSE THERMAL - KE - ROUGH WALL -RGE 7/93-
TIME 110.000 MSEC CYCLE 1789. PROBLEM 372.0104

VELOCITY VECTORS

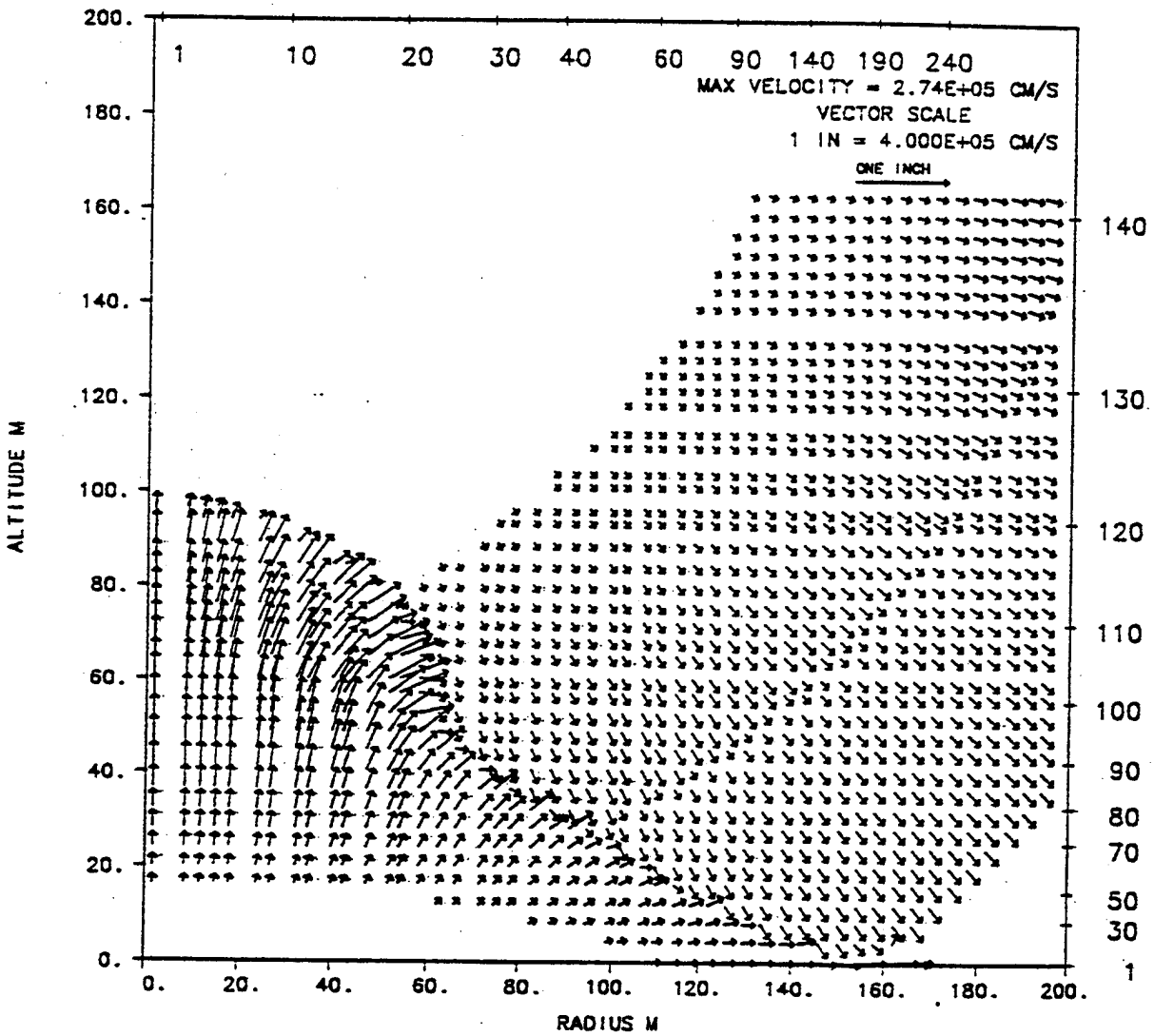

S-CUBED PRISCILLA - GRASSLAND COARSE THERMAL - KE - ROUGH WALL -RGE 7/93-
TIME 110.000 MSEC CYCLE 1789. PROBLEM 372.0104

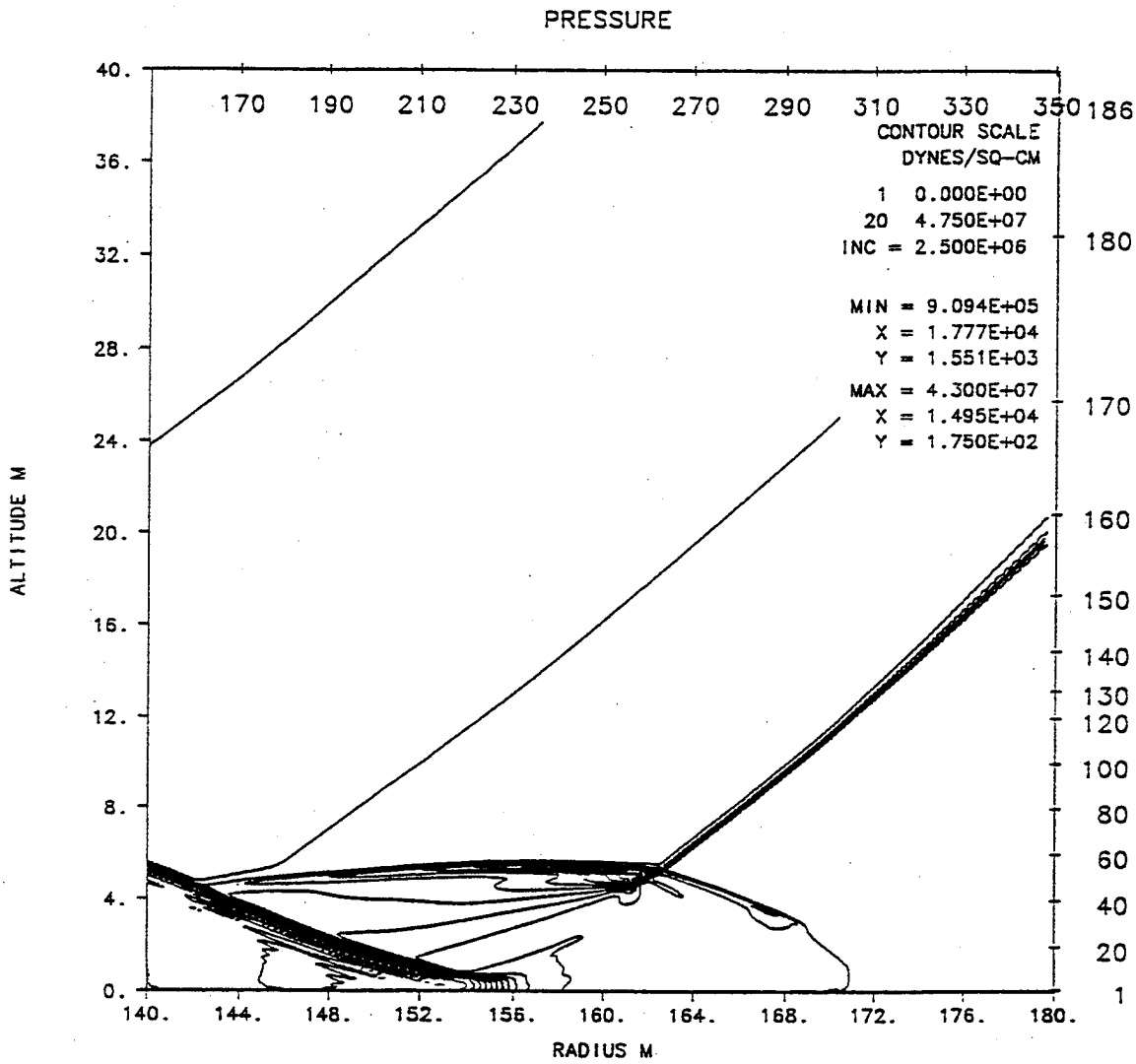

S-CUBED PRISCILLA - GRASSLAND THERMAL - KE - ROUGH WALL - RGE - JUNE 93
TIME 110.000 MSEC CYCLE 2787. PROBLEM 372.0102

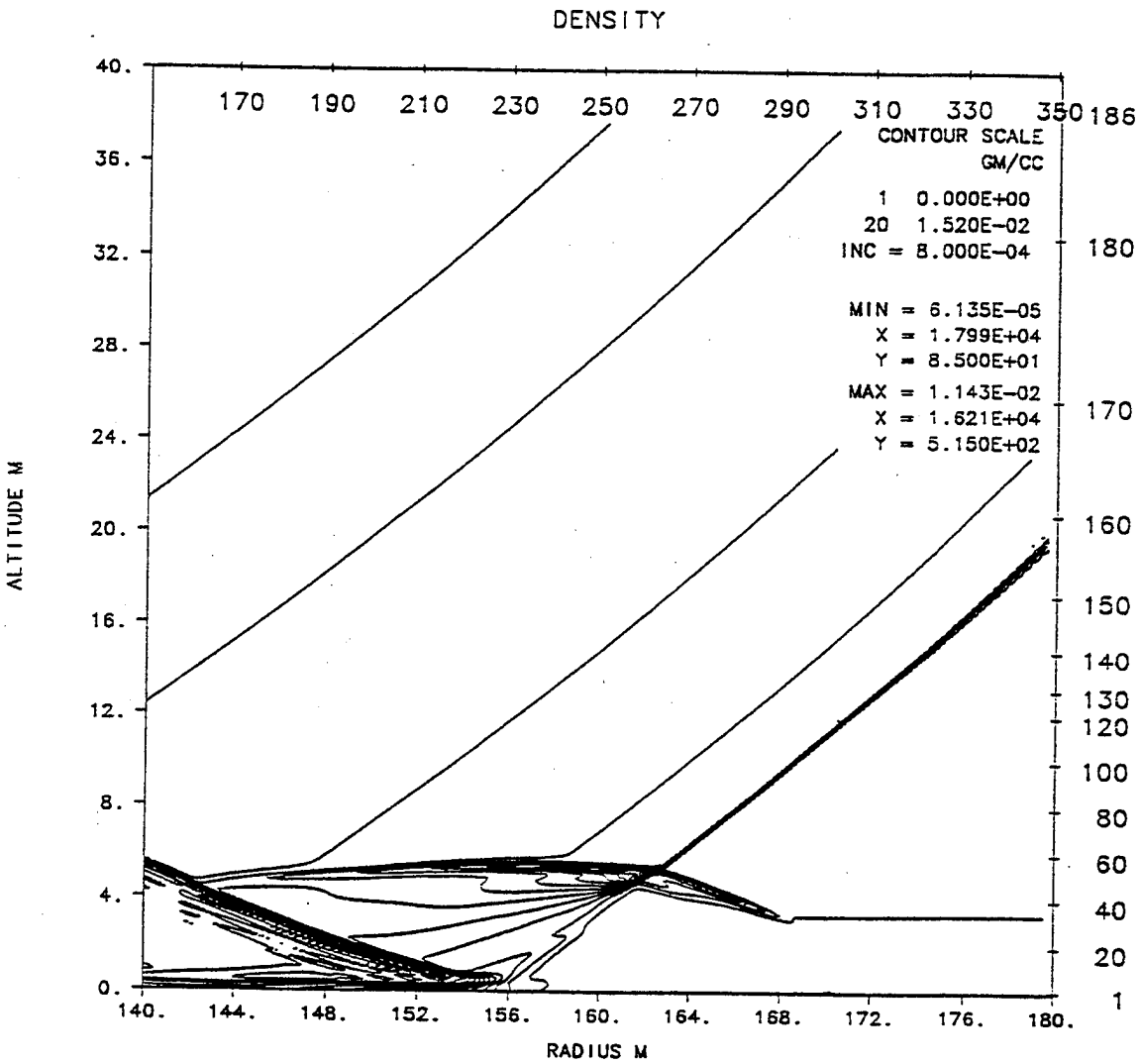

S-CUBED PRISCILLA - GRASSLAND THERMAL - KE - ROUGH WALL - RGE - JUNE 93
TIME 110.000 MSEC CYCLE 2787. PROBLEM 372.0102

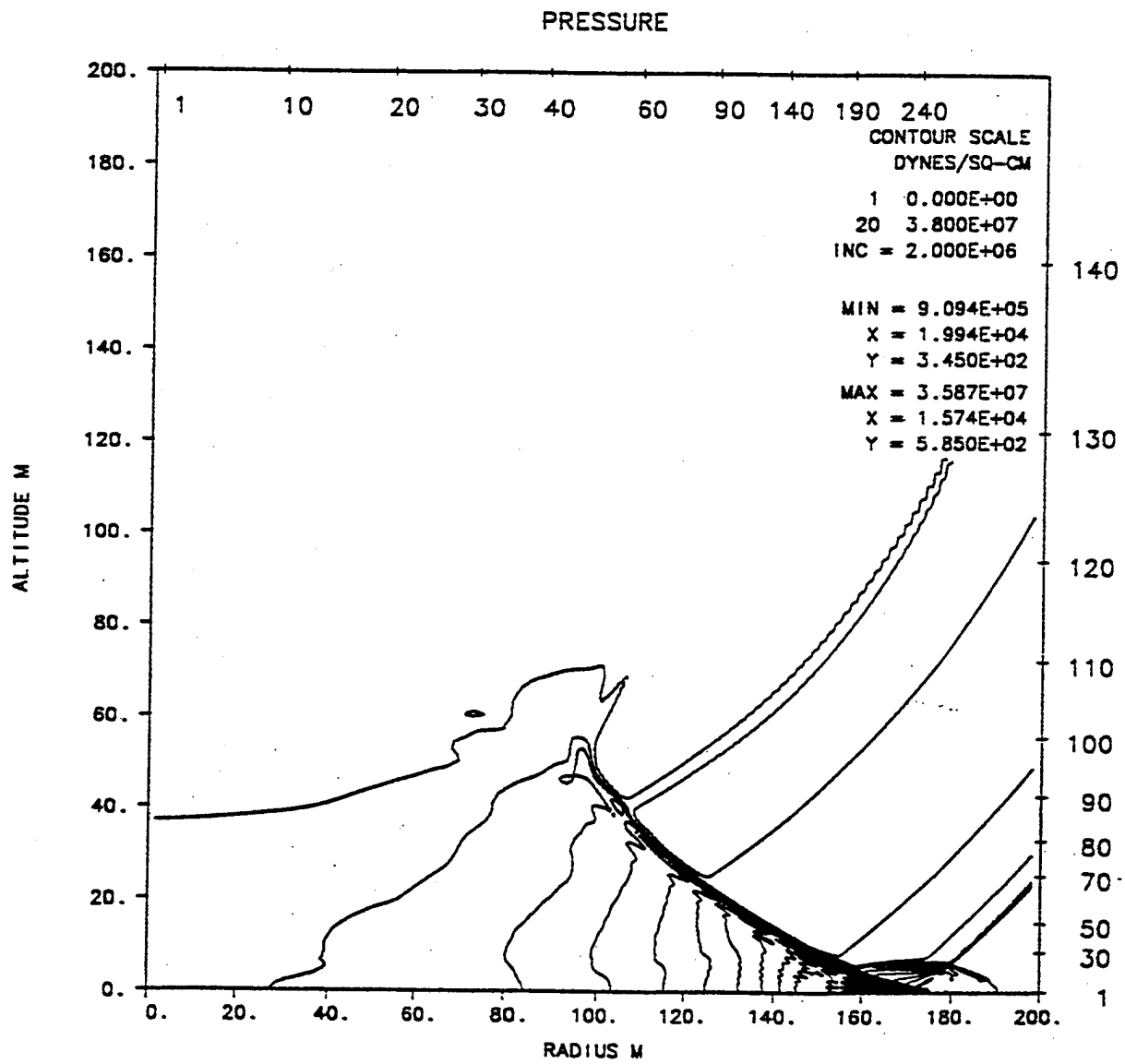

S-CUBED PRISCILLA - GRASSLAND COARSE THERMAL - KE - ROUGH WALL -RGE 7/93-
TIME 120.000 MSEC CYCLE 2121. PROBLEM 372.0104

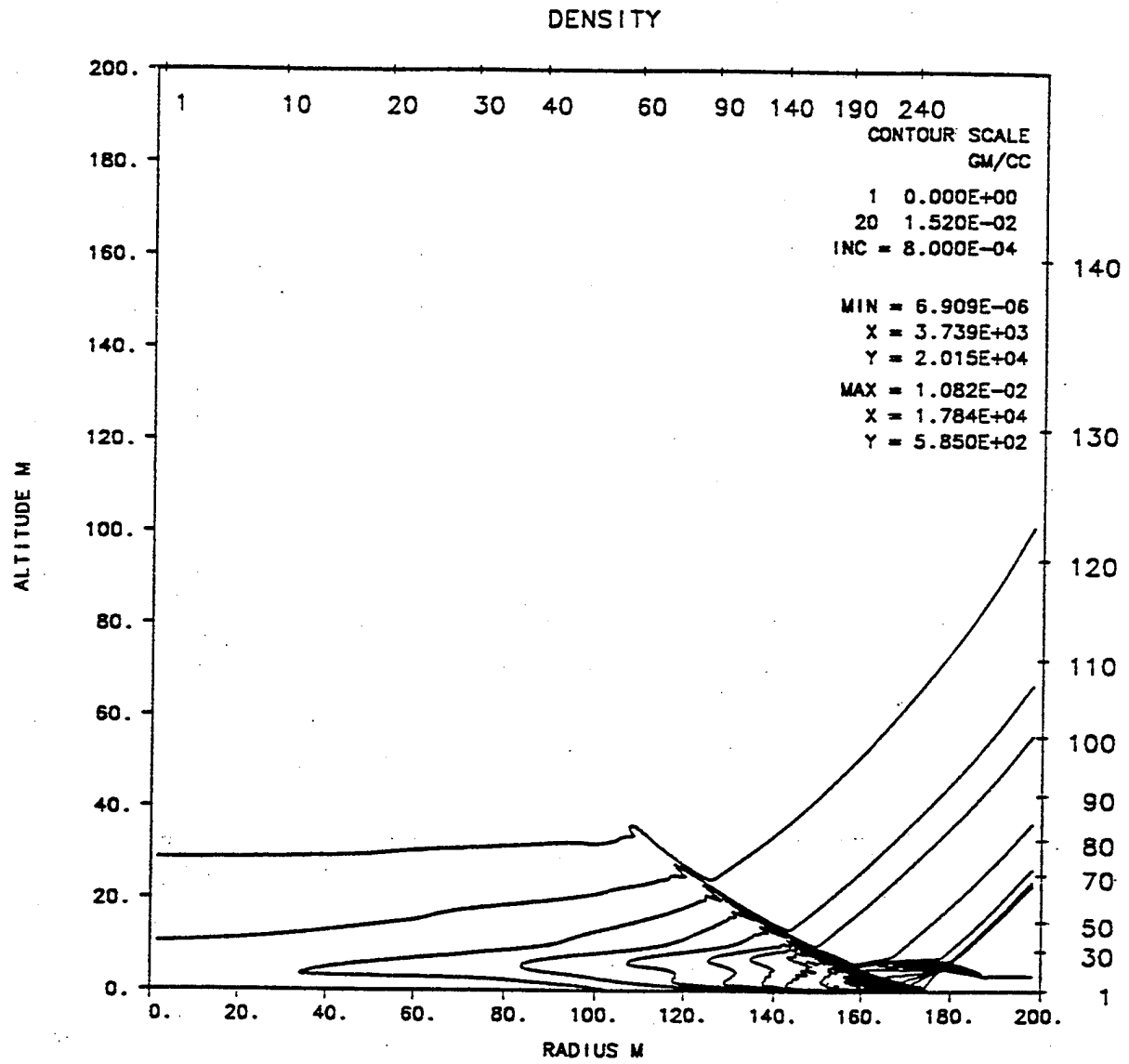

S-CUBED PRISCILLA - GRASSLAND COARSE THERMAL - KE - ROUGH WALL -RGE 7/93-
TIME 120.000 MSEC CYCLE 2121. PROBLEM 372.0104

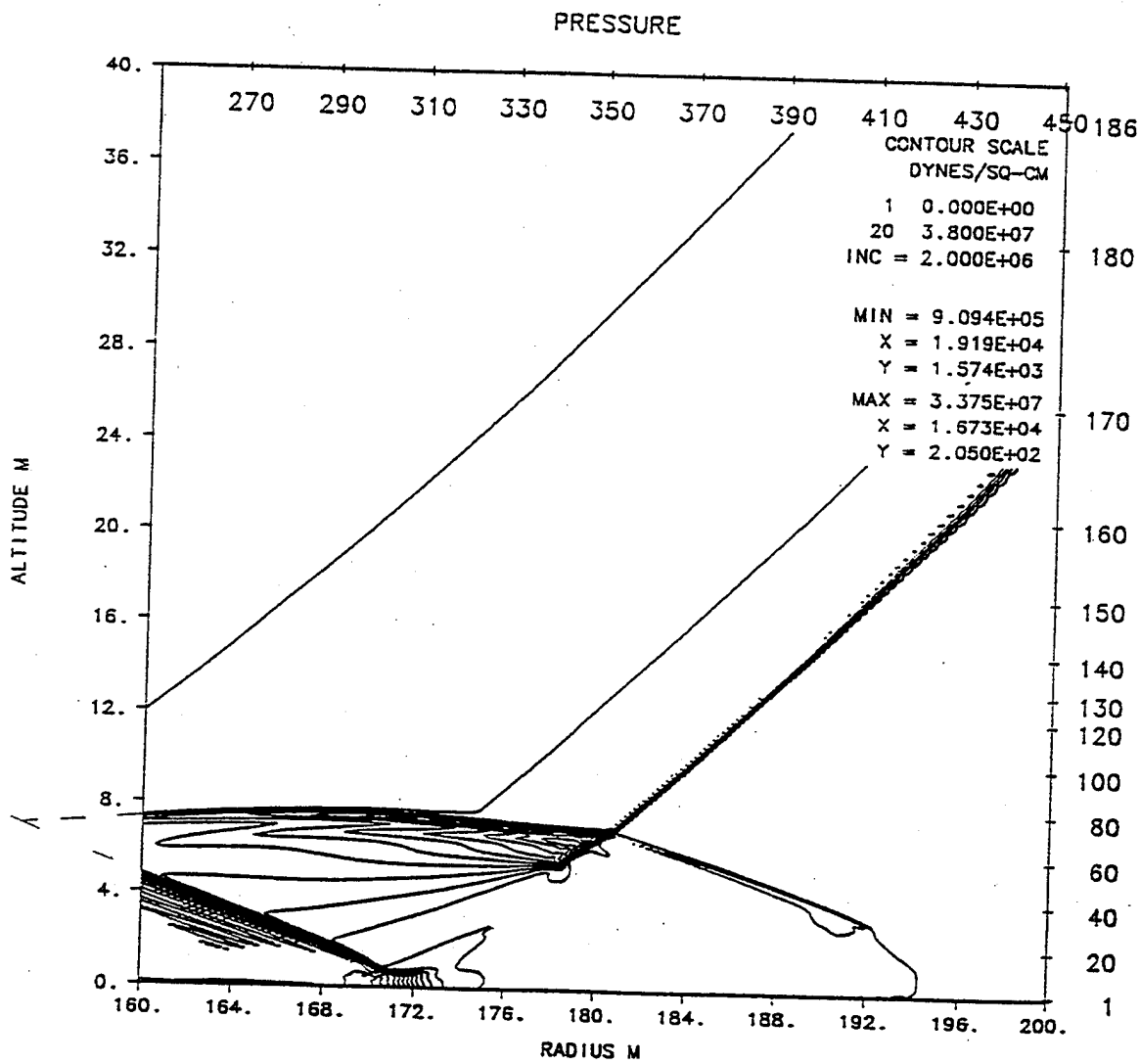

S-CUBED PRISCILLA – GRASSLAND THERMAL – KE – ROUGH WALL – RGE – JUNE 93
TIME 120.000 MSEC CYCLE 3505. PROBLEM 372.0102

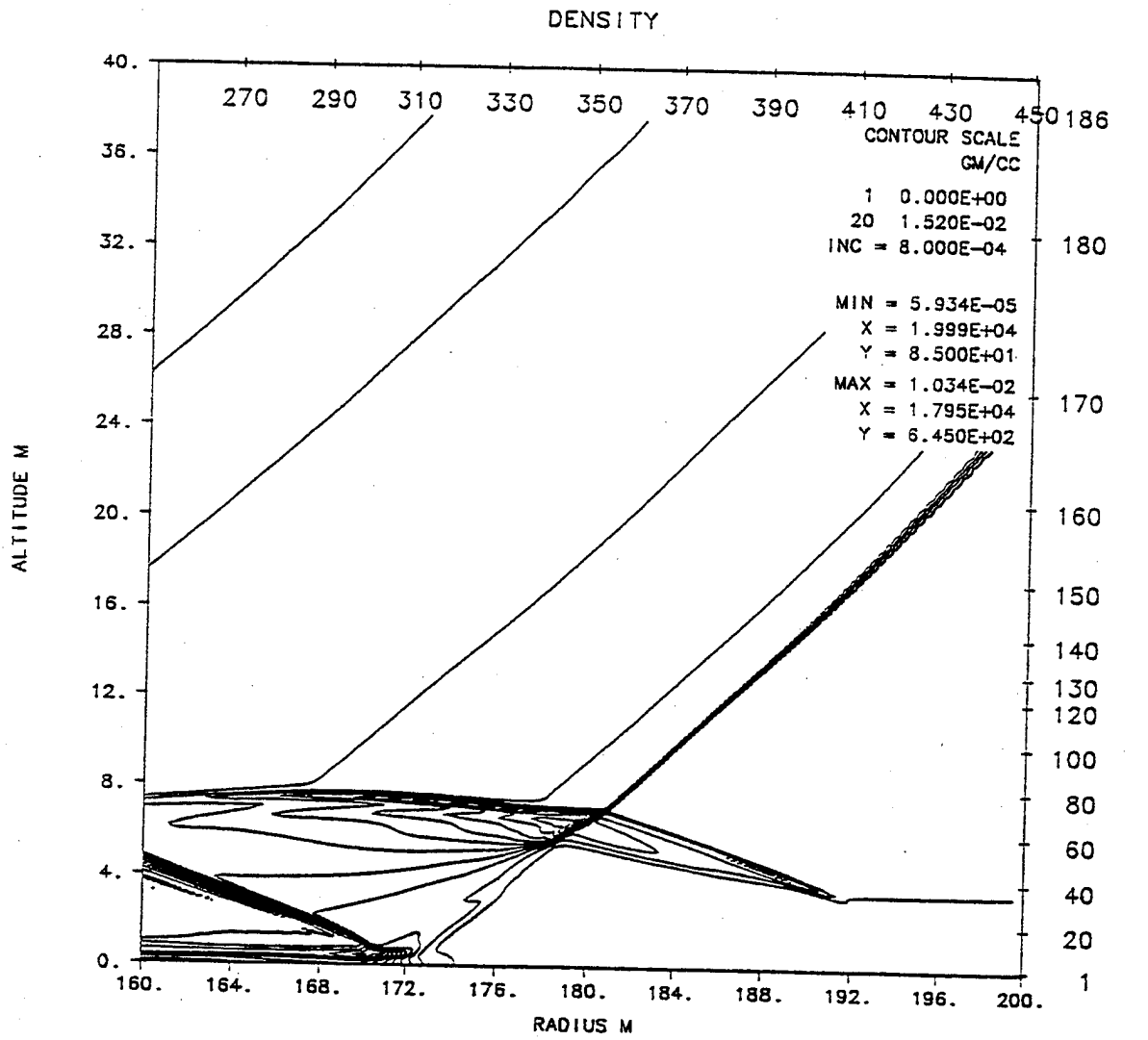

S-CUBED PRISCILLA - GRASSLAND THERMAL - KE - ROUGH WALL - RGE - JUNE 93
TIME 120.000 MSEC CYCLE 3505. PROBLEM 372.0102

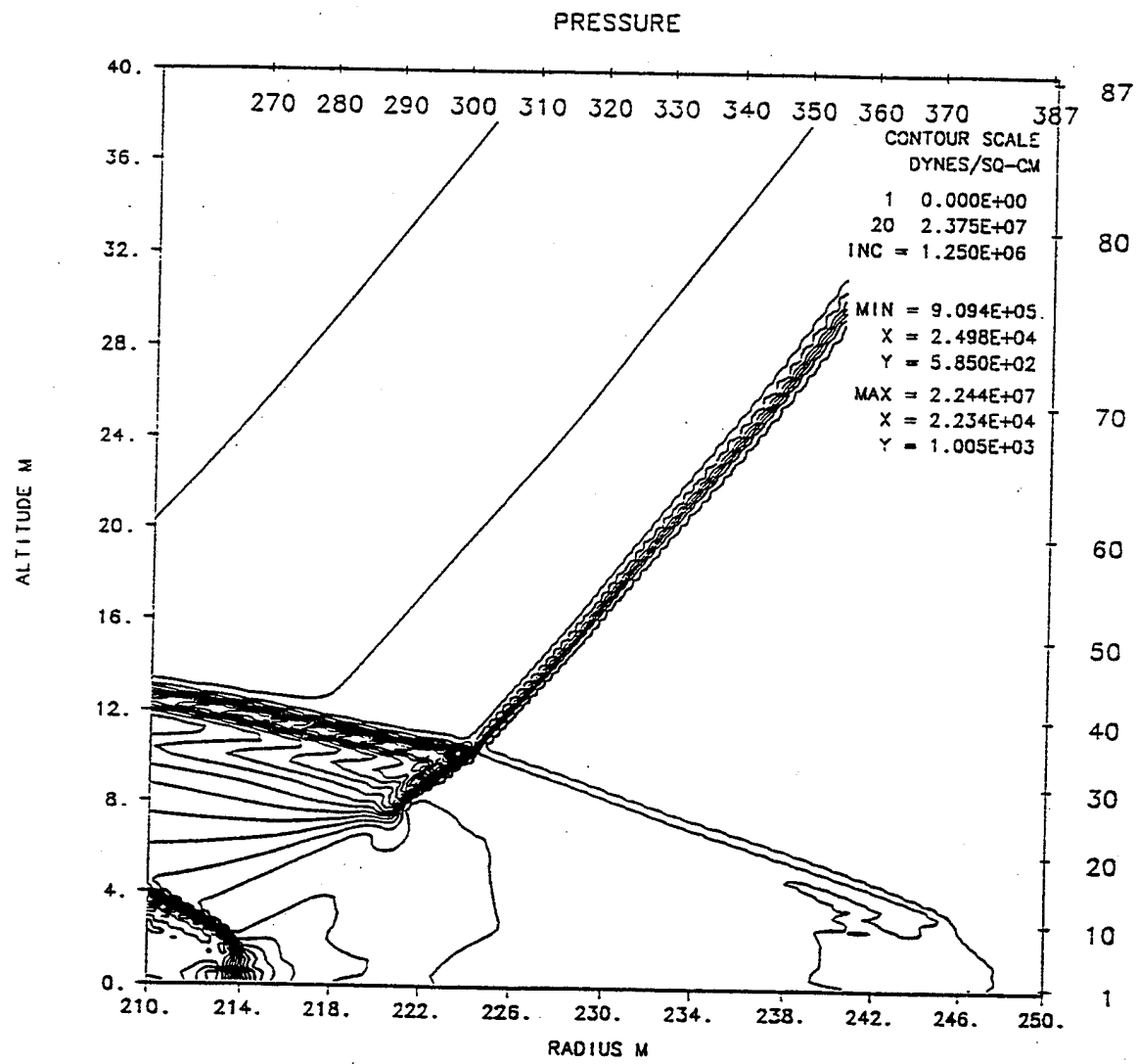

S-CUBED PRISCILLA - GRASSLAND COARSE THERMAL - KE - ROUGH WALL -RGE 7/93-
TIME 150.000 MSEC CYCLE 3063. PROBLEM 372.0104

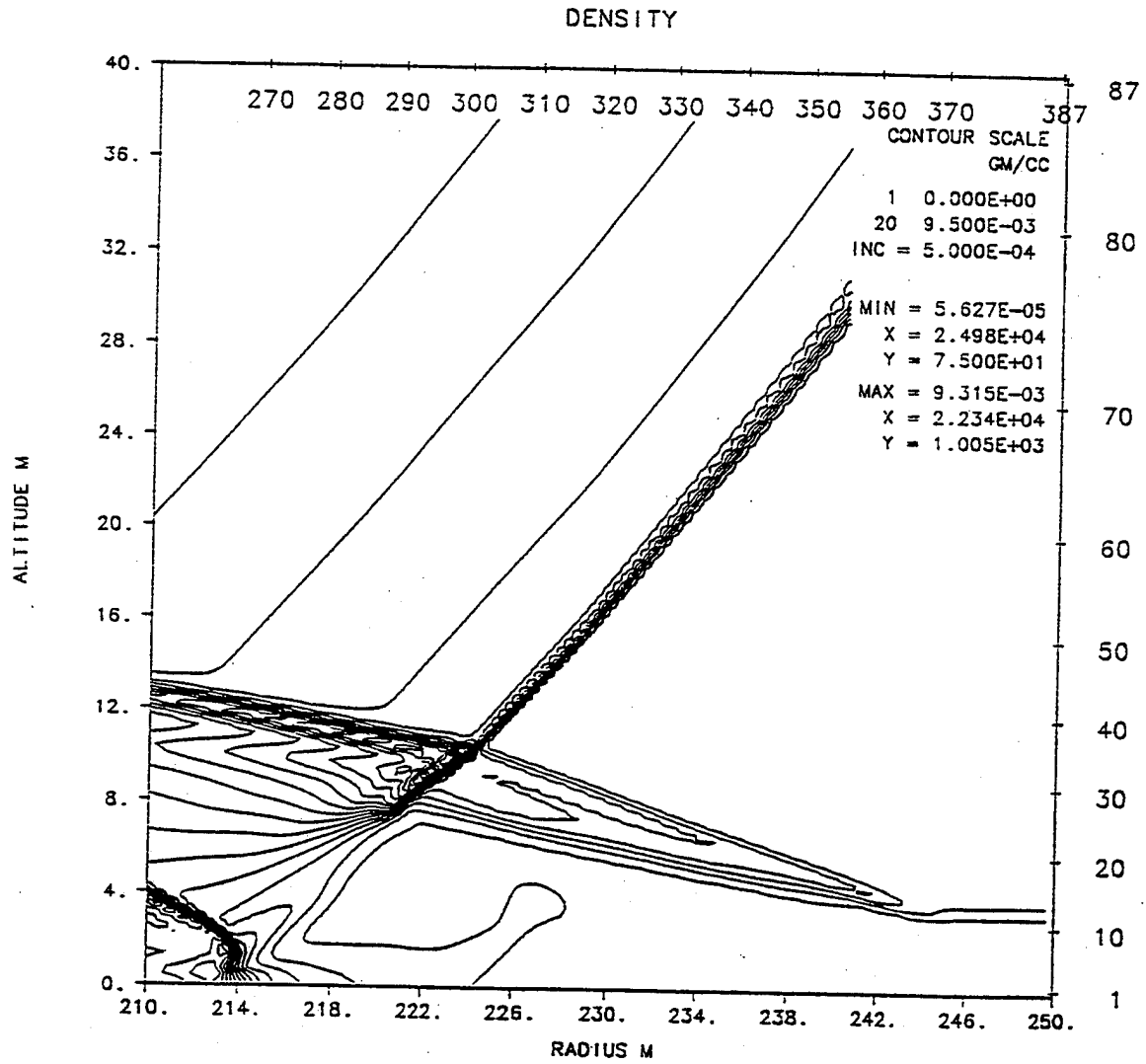

S-CUBED PRISCILLA - GRASSLAND COARSE THERMAL - KE - ROUGH WALL -RGE 7/93-
TIME 150.000 MSEC CYCLE 3063. PROBLEM 372.0104

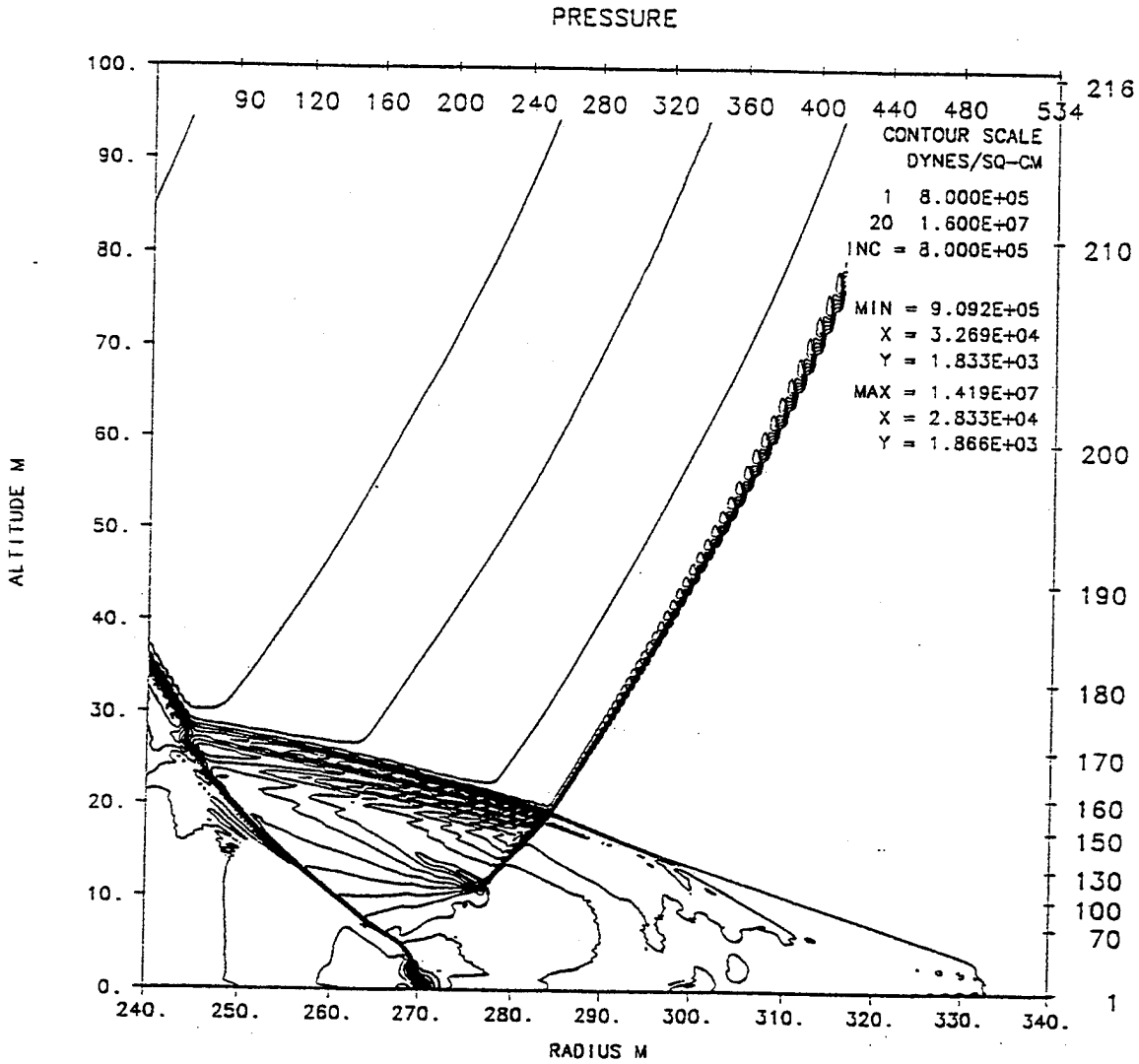

S-CUBED PRISCILLA - GRASSLAND THERMAL - KE - ROUGH WALL - RGE - JUNE 93
TIME 200.000 MSEC CYCLE13673. PROBLEM 372.0102

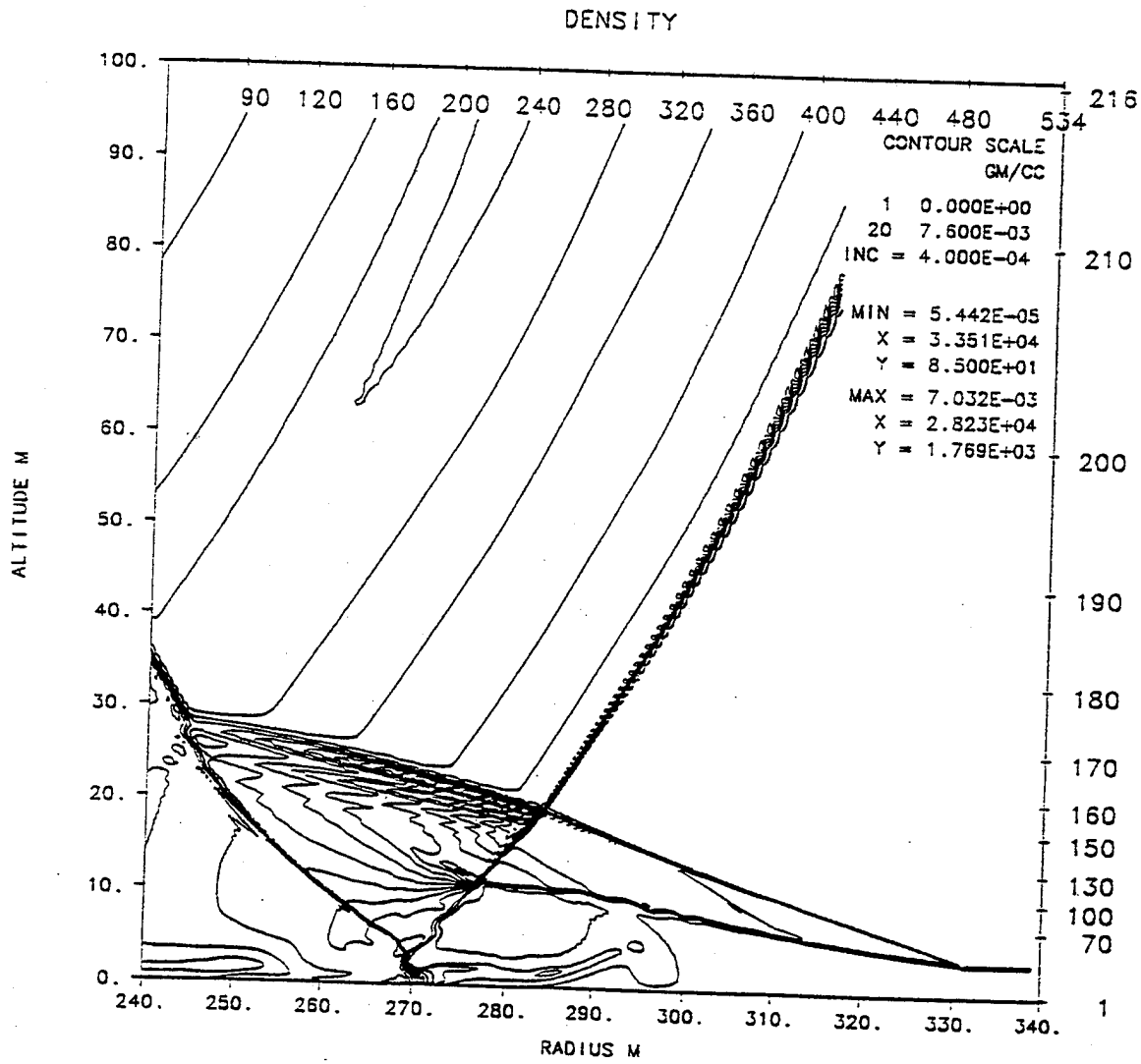

S-CUBED PRISCILLA - GRASSLAND THERMAL - KE - ROUGH WALL - RGE - JUNE 93
TIME 200.000 MSEC CYCLE13673. PROBLEM 372.0102

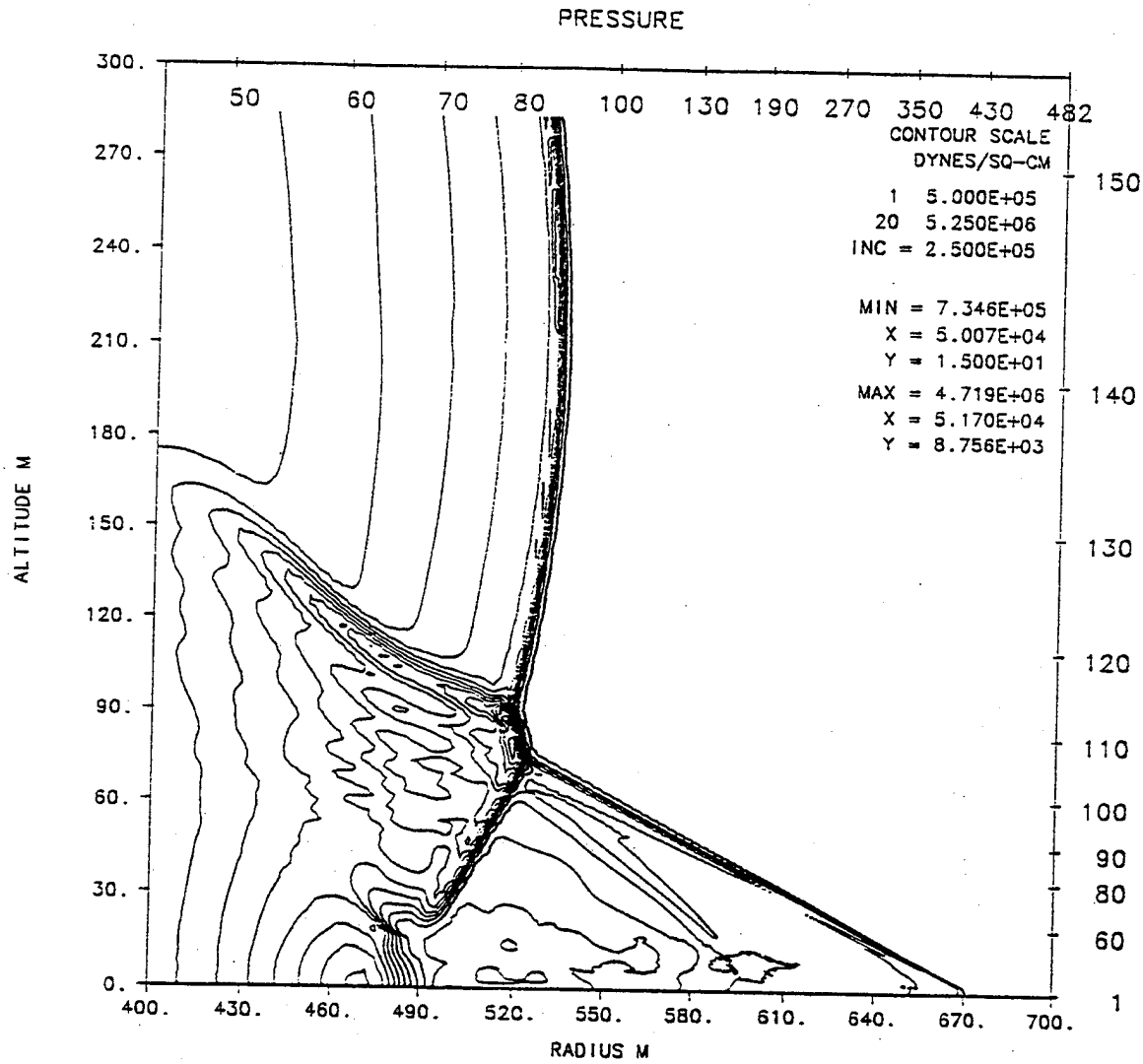

S-CUBED PRISCILLA - GRASSLAND COARSE THERMAL - KE - ROUGH WALL -RGE 7/93-
TIME 500.000 MSEC CYCLE 8117. PROBLEM 372.0104

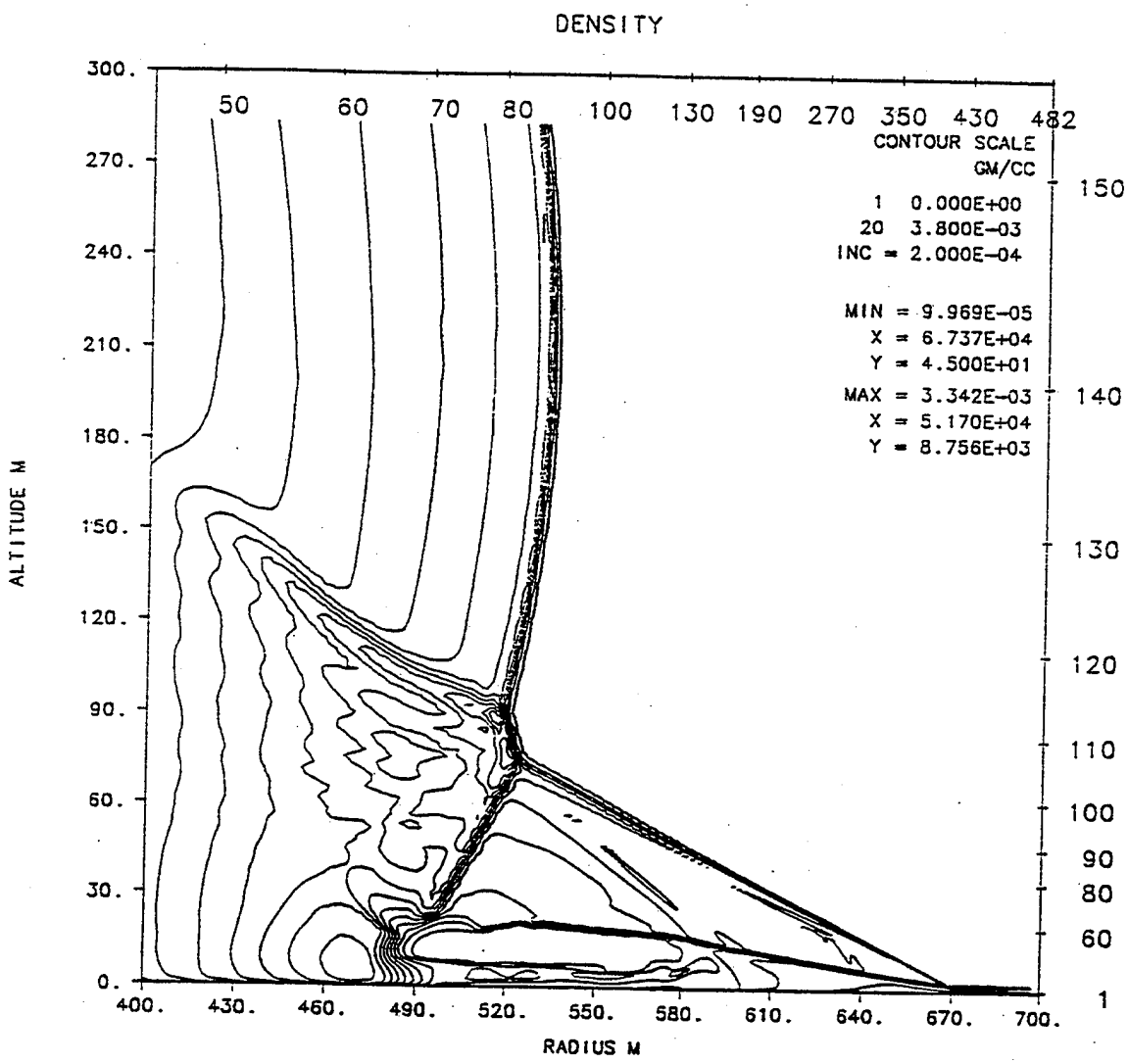

S-CUBED PRISCILLA - GRASSLAND COARSE THERMAL - KE - ROUGH WALL -RGE 7/93-
TIME 500.000 MSEC CYCLE 8117. PROBLEM 372.0104

INTENTIONALLY LEFT BLANK.

APPENDIX F
SURFACE-LEVEL OVERPRESSURE AND OVERPRESSURE IMPULSE STATION PLOTS FROM GRASSLAND CALCULATION

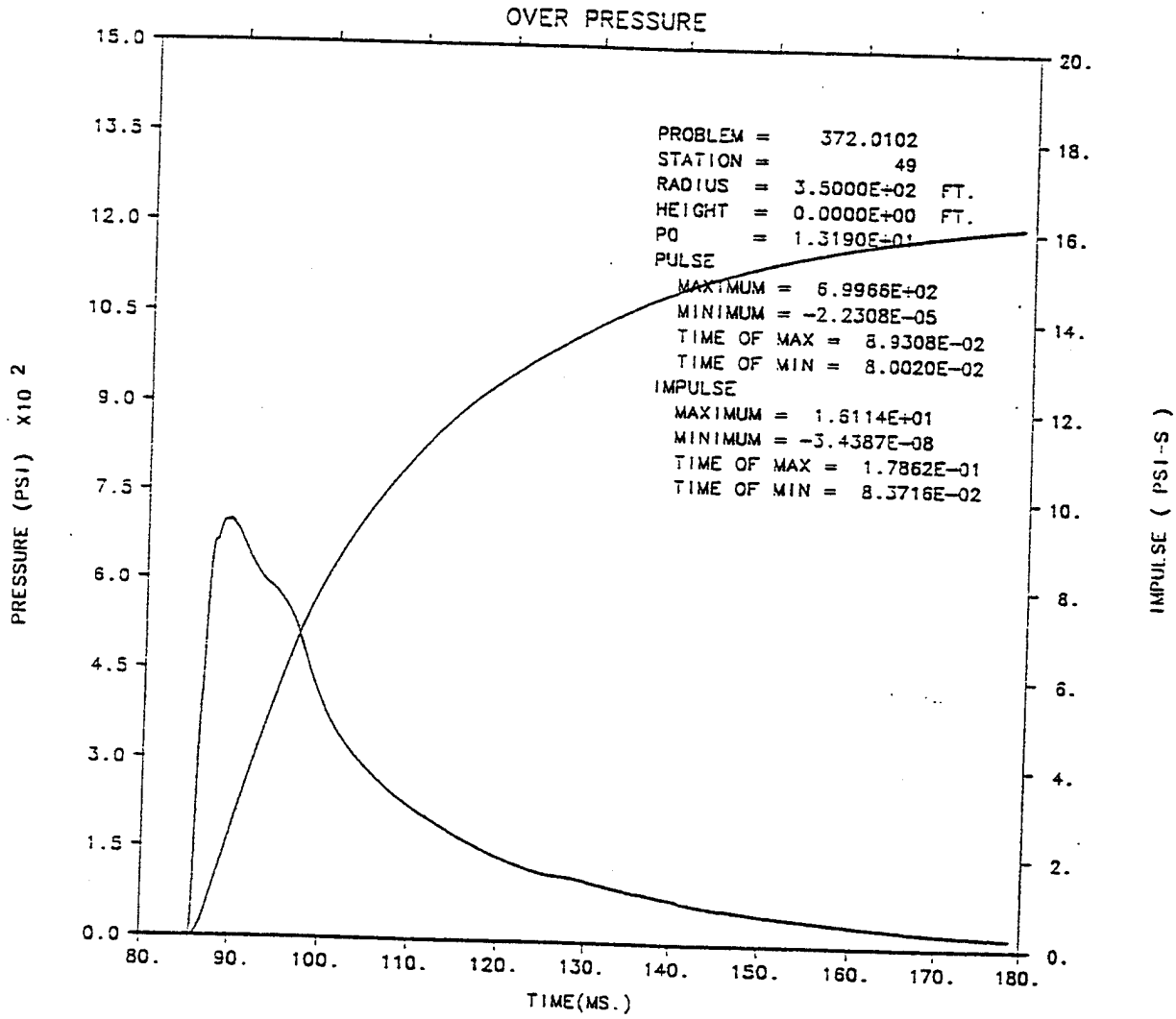

S-CUBED PRISCILLA – GRASSLAND THERMAL – KE – ROUGH WALL – RGE – JUNE 93

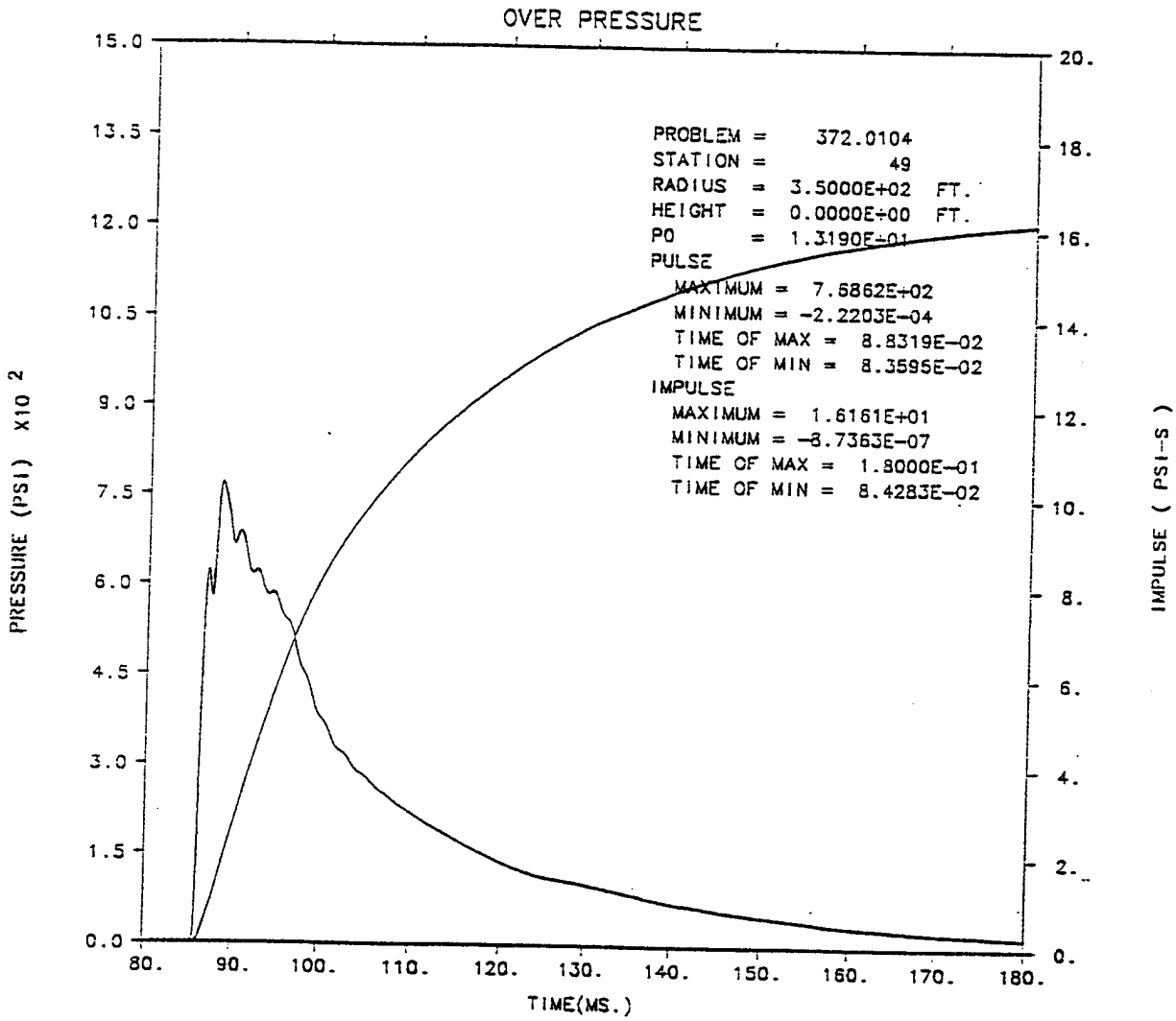

S-CUBED PRISCILLA - GRASSLAND COARSE THERMAL - KE - ROUGH WALL -RGE 7/93-

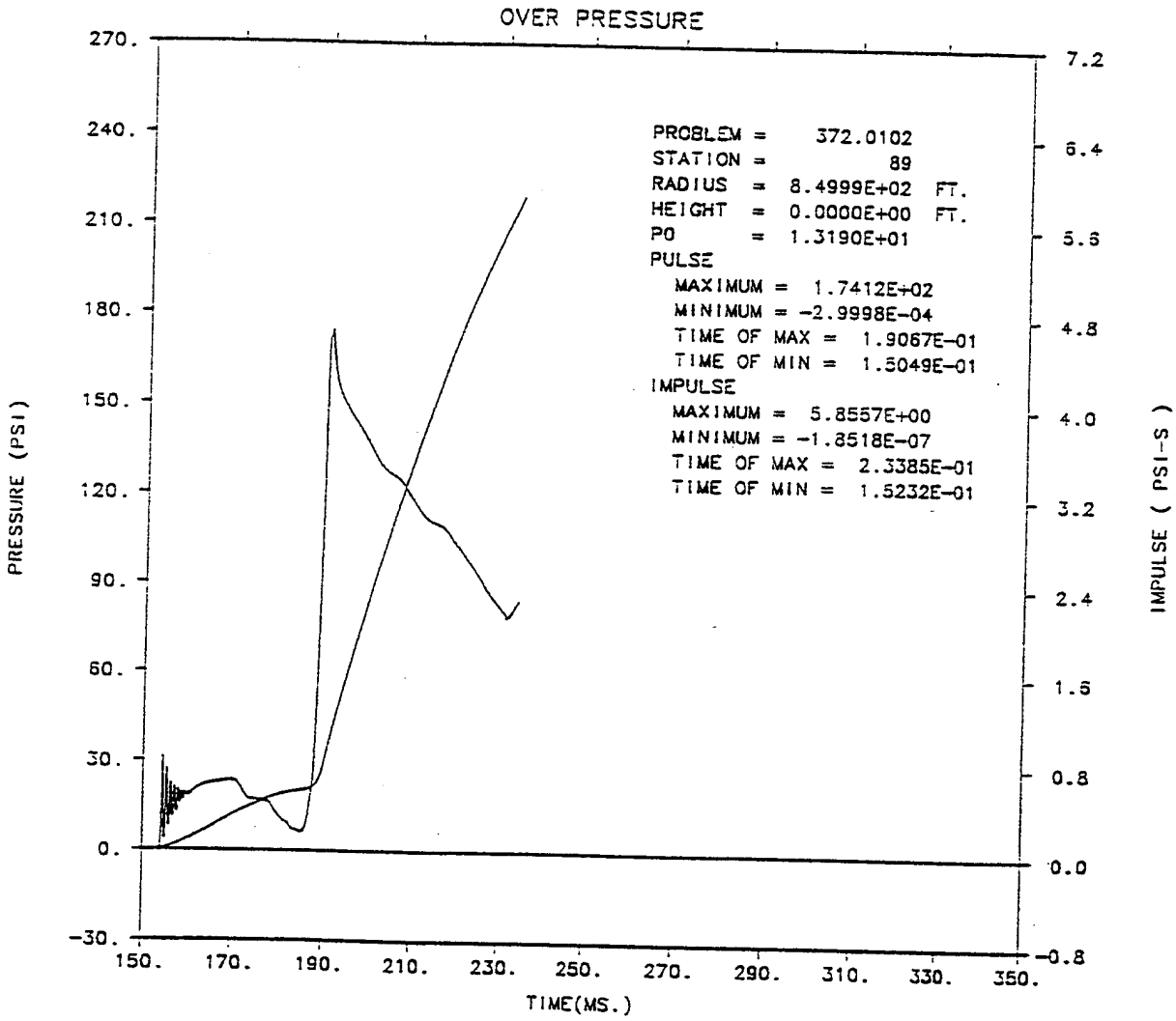

S-CUBED PRISCILLA – GRASSLAND THERMAL – KE – ROUGH WALL – RGE – JUNE 93

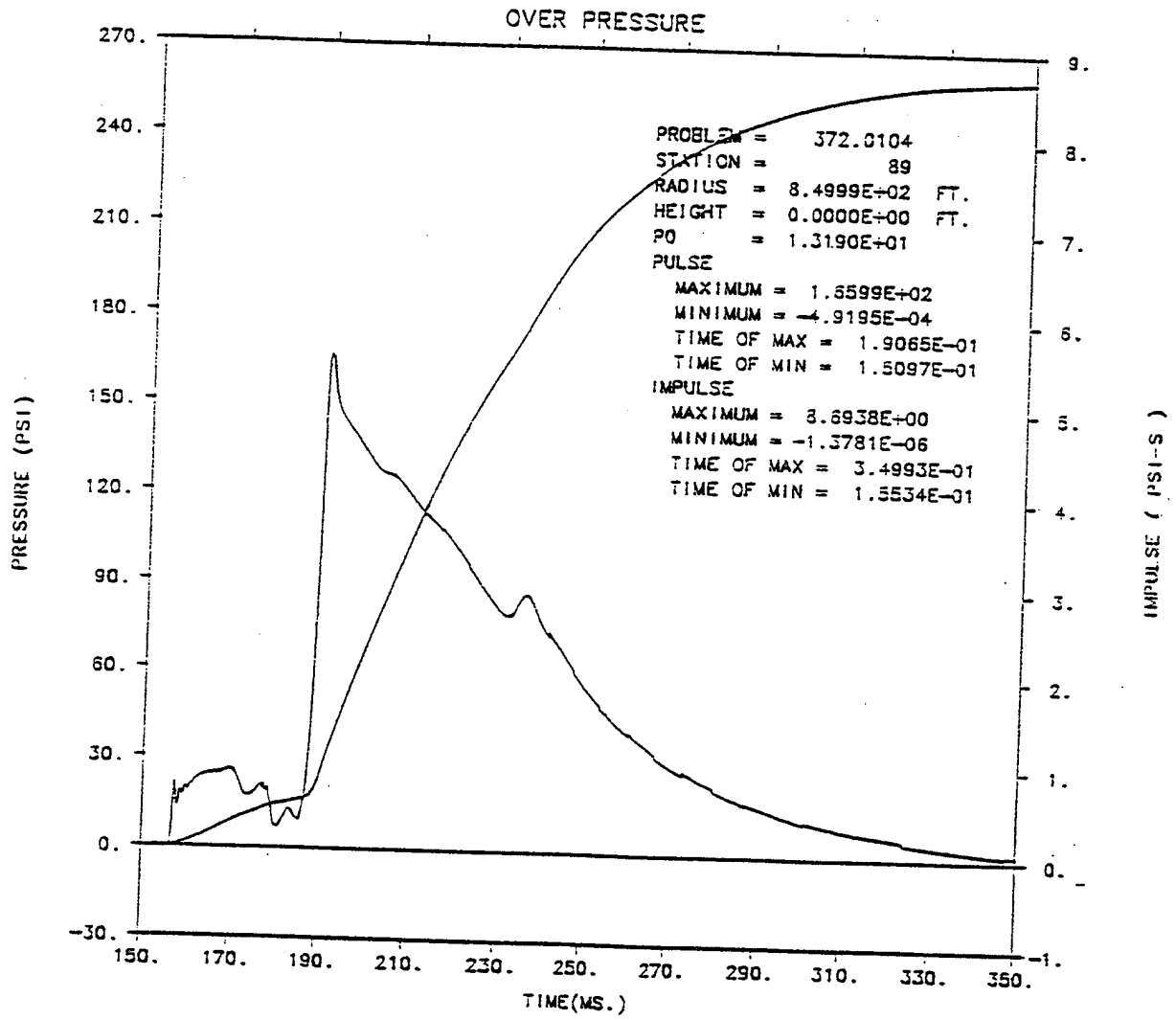

S-CUBED PRISCILLA - GRASSLAND COARSE THERMAL - KE - ROUGH WALL -RGE 7/93-

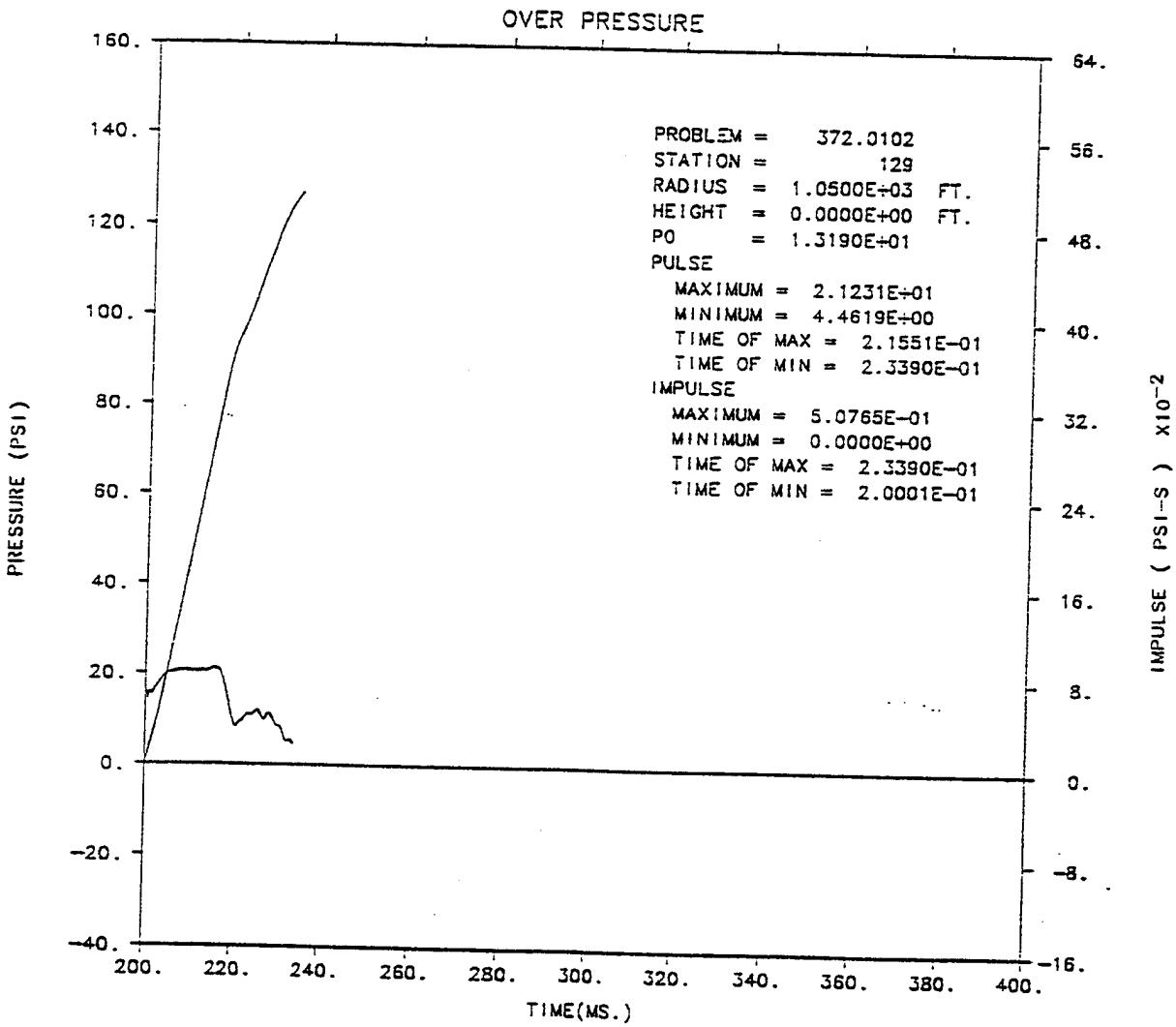

S-CUBED PRISCILLA – GRASSLAND THERMAL – KE – ROUGH WALL – RGE. – JUNE 93

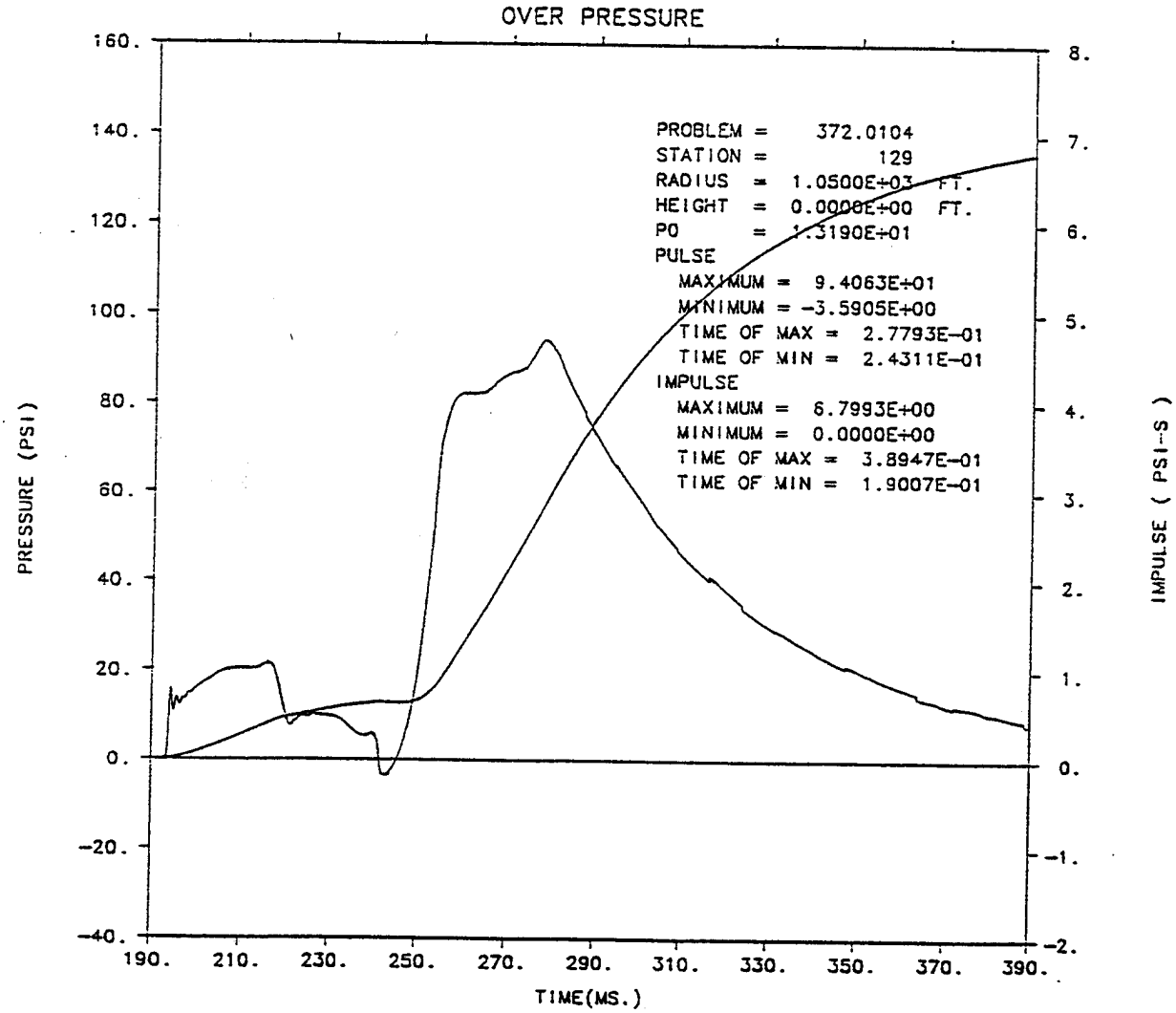

S-CUBED PRISCILLA – GRASSLAND COARSE THERMAL – KE – ROUGH WALL –RGE 7/93–

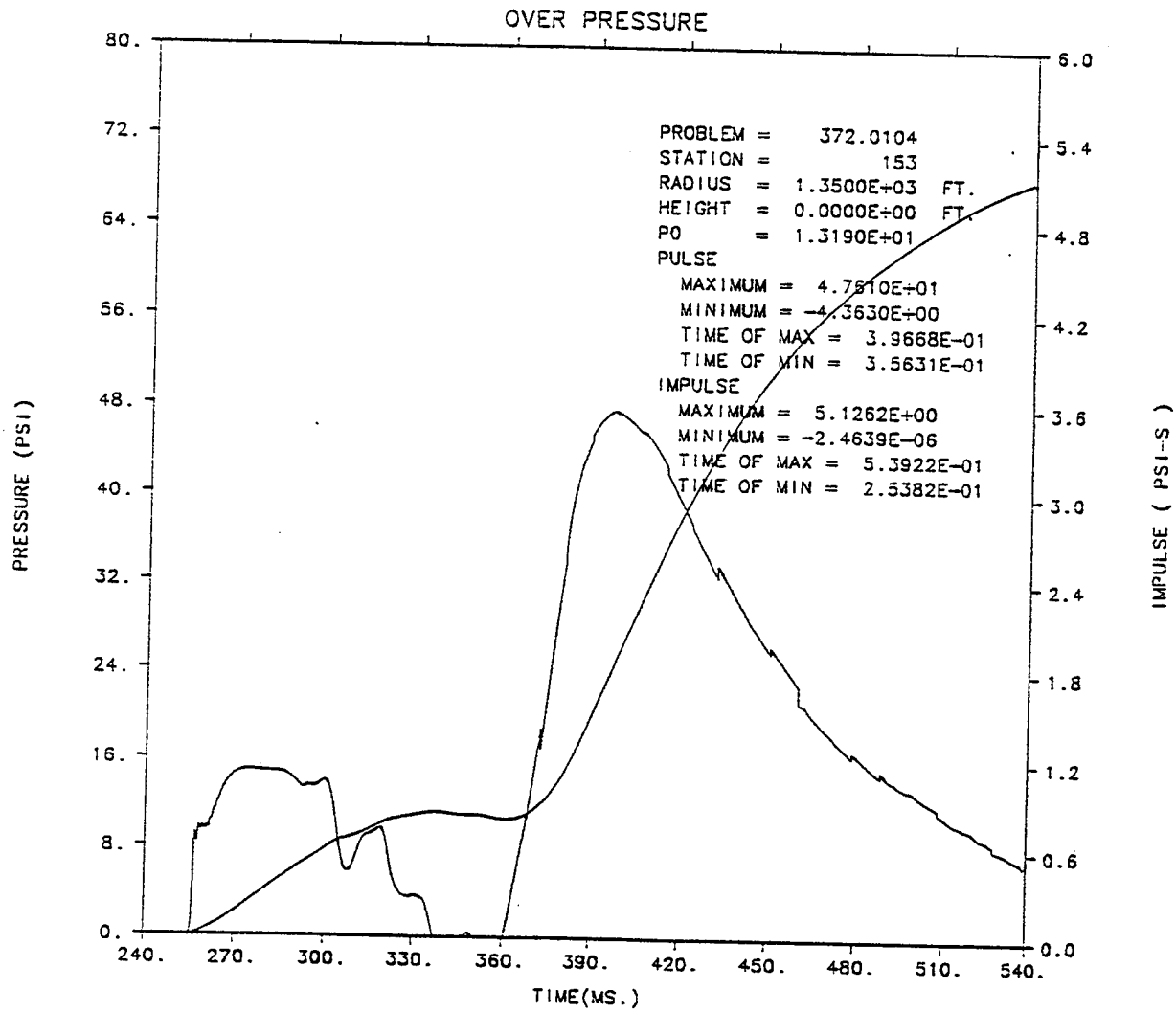

S-CUBED PRISCILLA – GRASSLAND COARSE THERMAL – KE – ROUGH WALL –RGE 7/93–

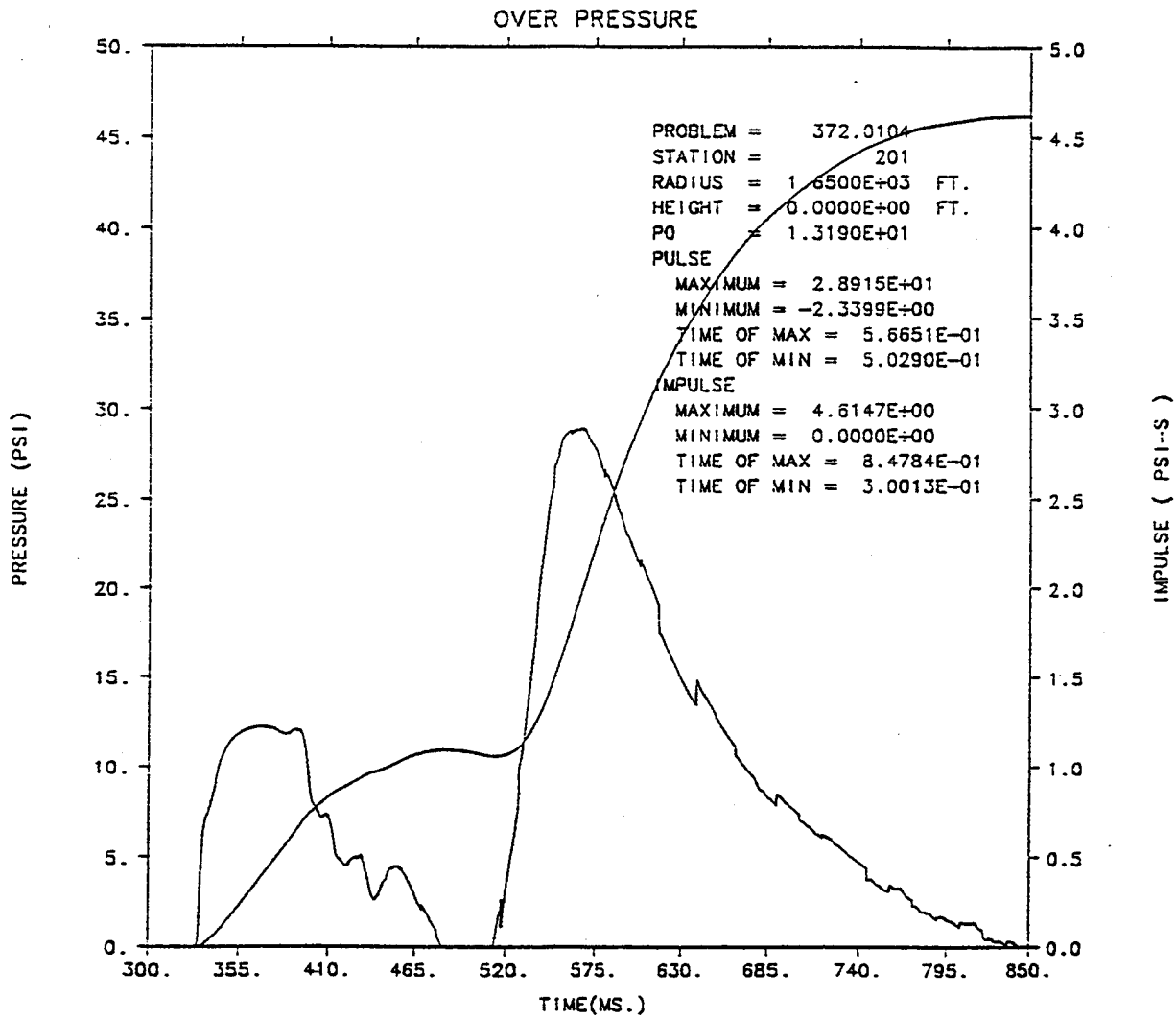

S-CUBED PRISCILLA - GRASSLAND COARSE THERMAL - KE - ROUGH WALL -RGE 7/93-

APPENDIX G
CONTOUR PLOTS AND STATION RECORDS FROM DESERT CALCULATION

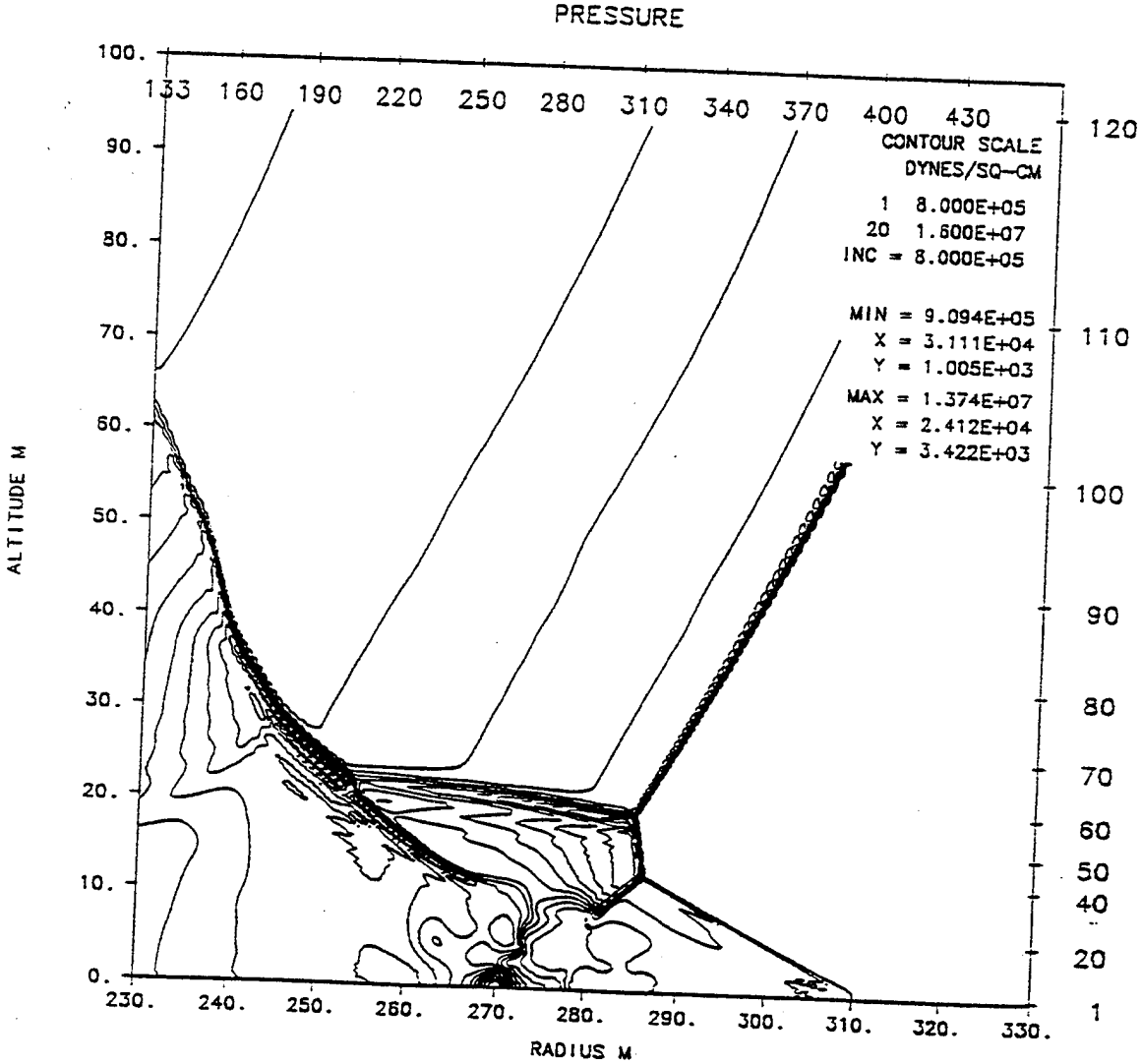

S-CUBED PRISCILLA - DESERT 30X30 CM THERMAL-KE- JEC 7/93
TIME 200.000 MSEC CYCLE 3917. PROBLEM 372.0050

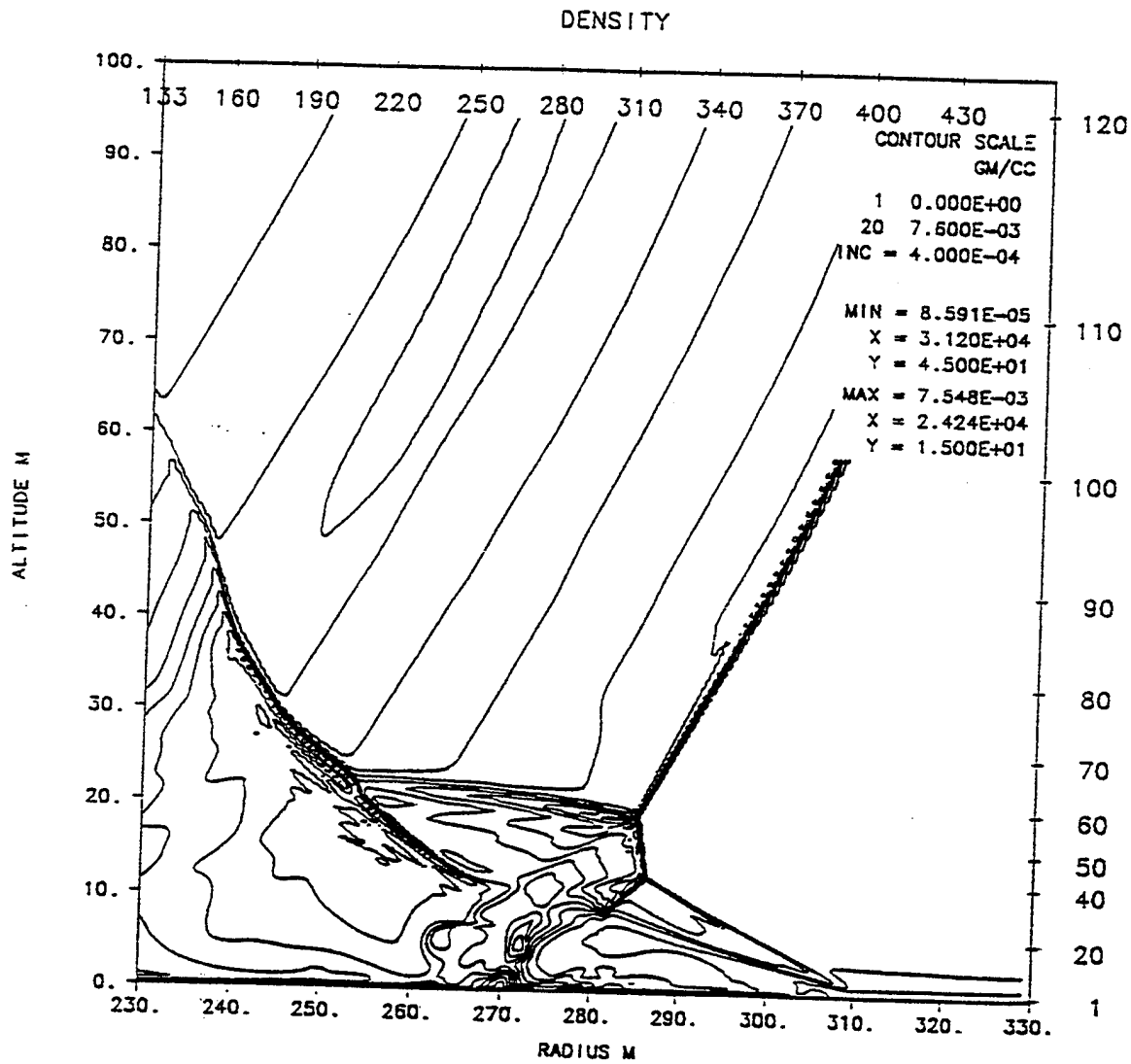

S-CUBED PRISCILLA - DESERT 30X30 CM THERMAL-KE- JEC 7/93
TIME 200.000 MSEC CYCLE 3917. PROBLEM 372.0050

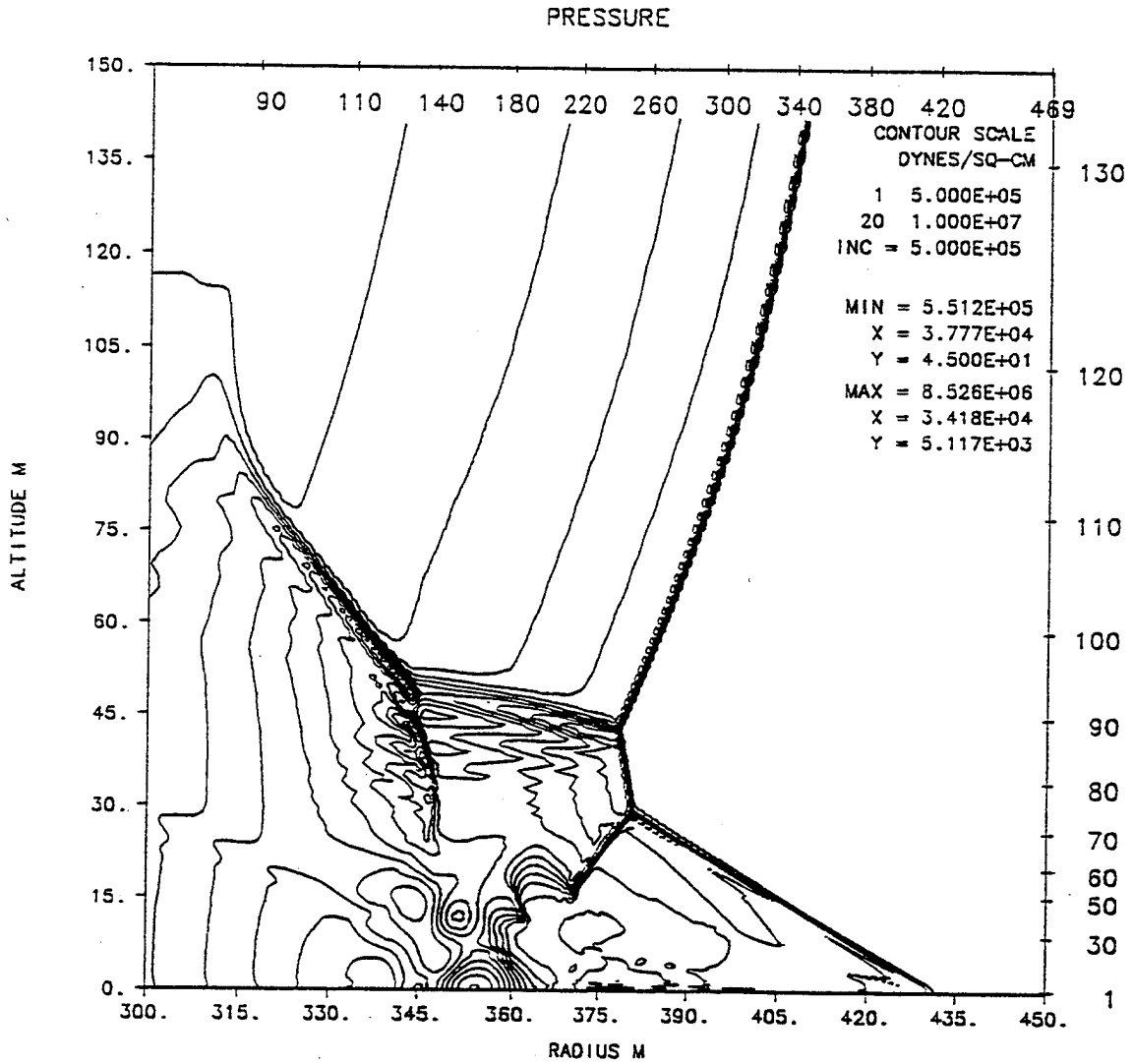

S-CUBED PRISCILLA - DESERT 30X30 CM THERMAL-KE- JEC 7/93
TIME 300.000 MSEC CYCLE 5495. PROBLEM 372.0050

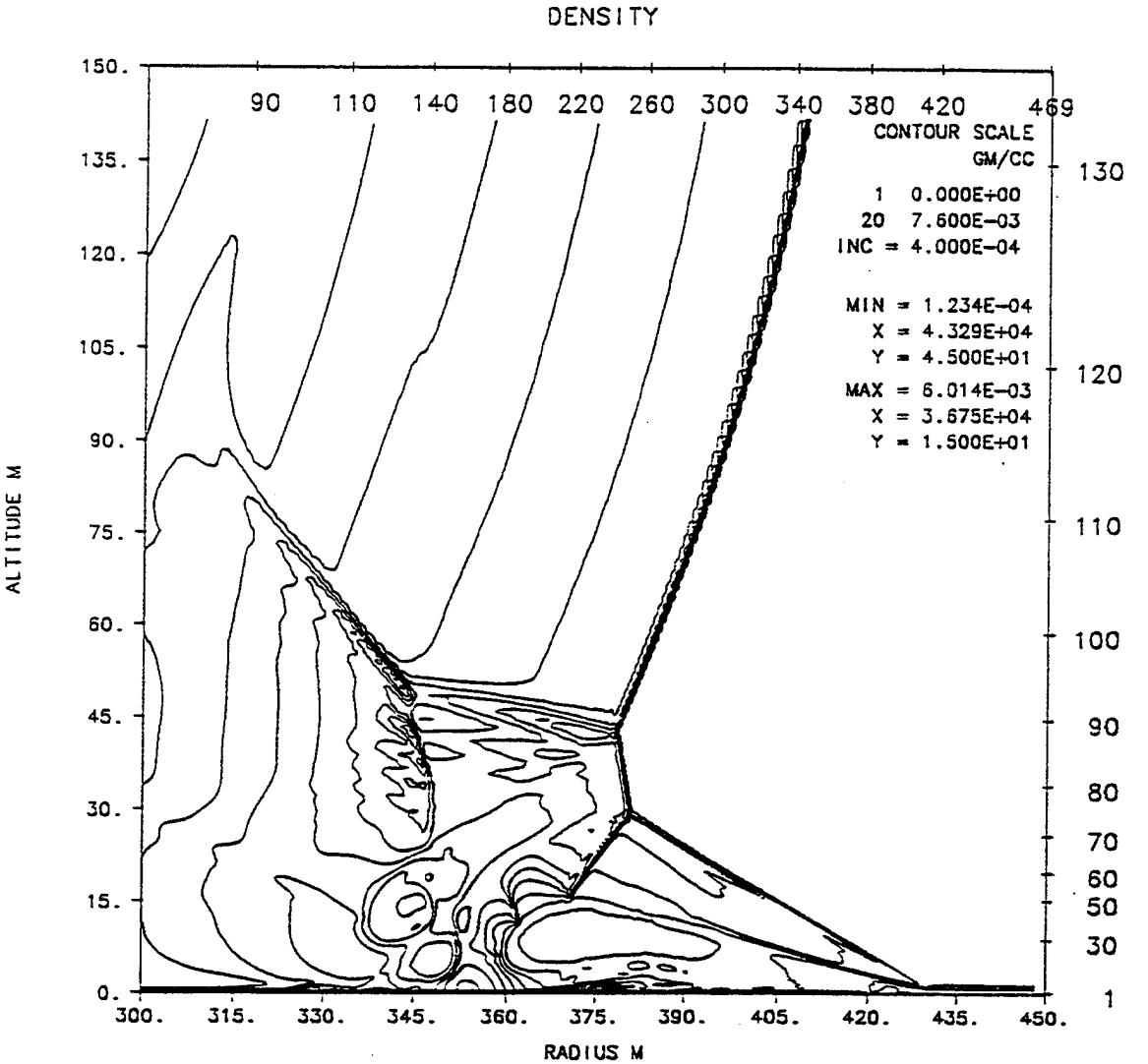

S-CUBED PRISCILLA - DESERT 30X30 CM THERMAL-KE- JEC 7/93
TIME 300.000 MSEC CYCLE 5495. PROBLEM 372.0050

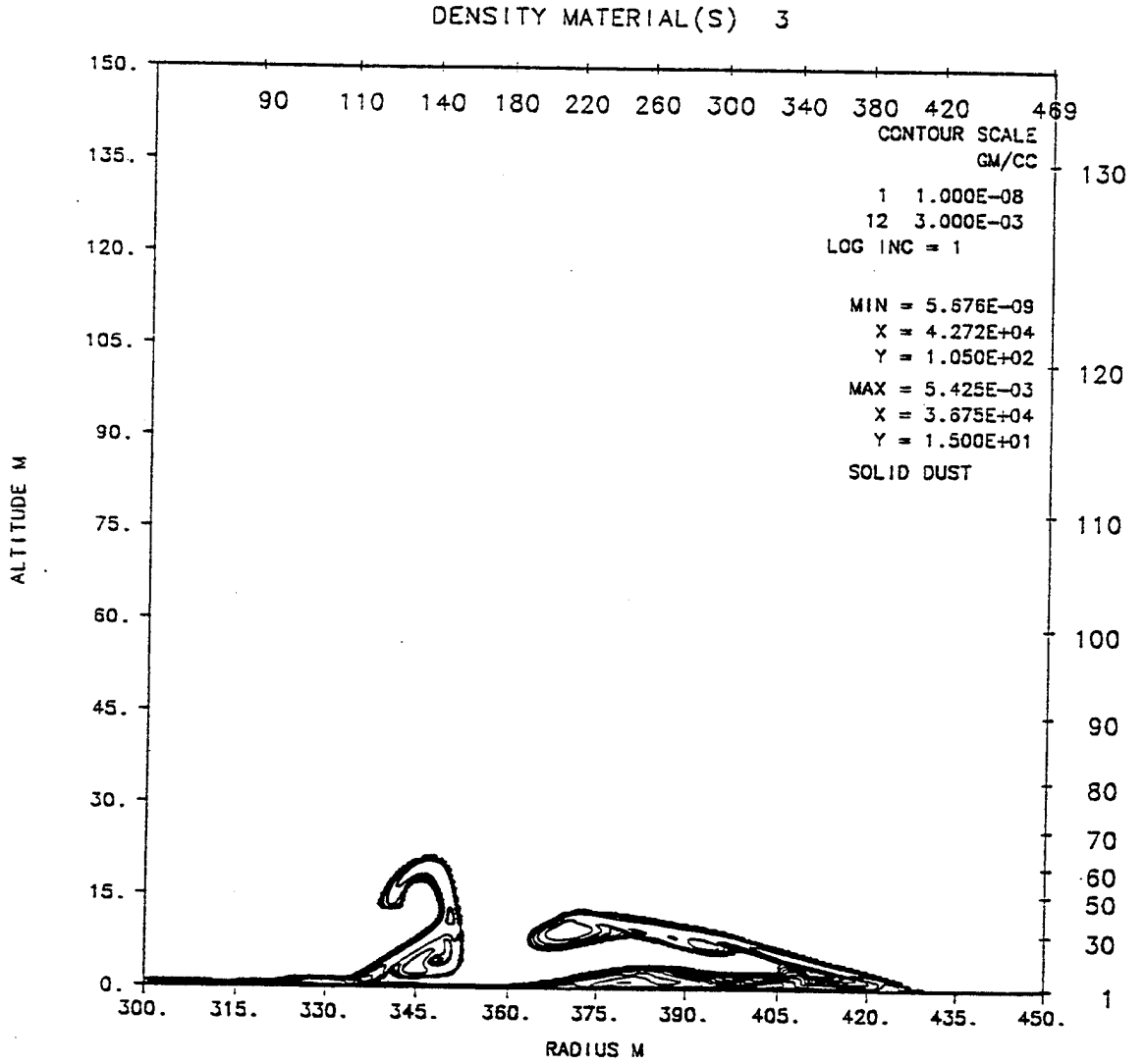

S-CUBED PRISCILLA - DESERT 30X30 CM THERMAL-KE- WALL JEC 7/93
TIME 300.000 MSEC CYCLE 5495. PROBLEM 372.0050

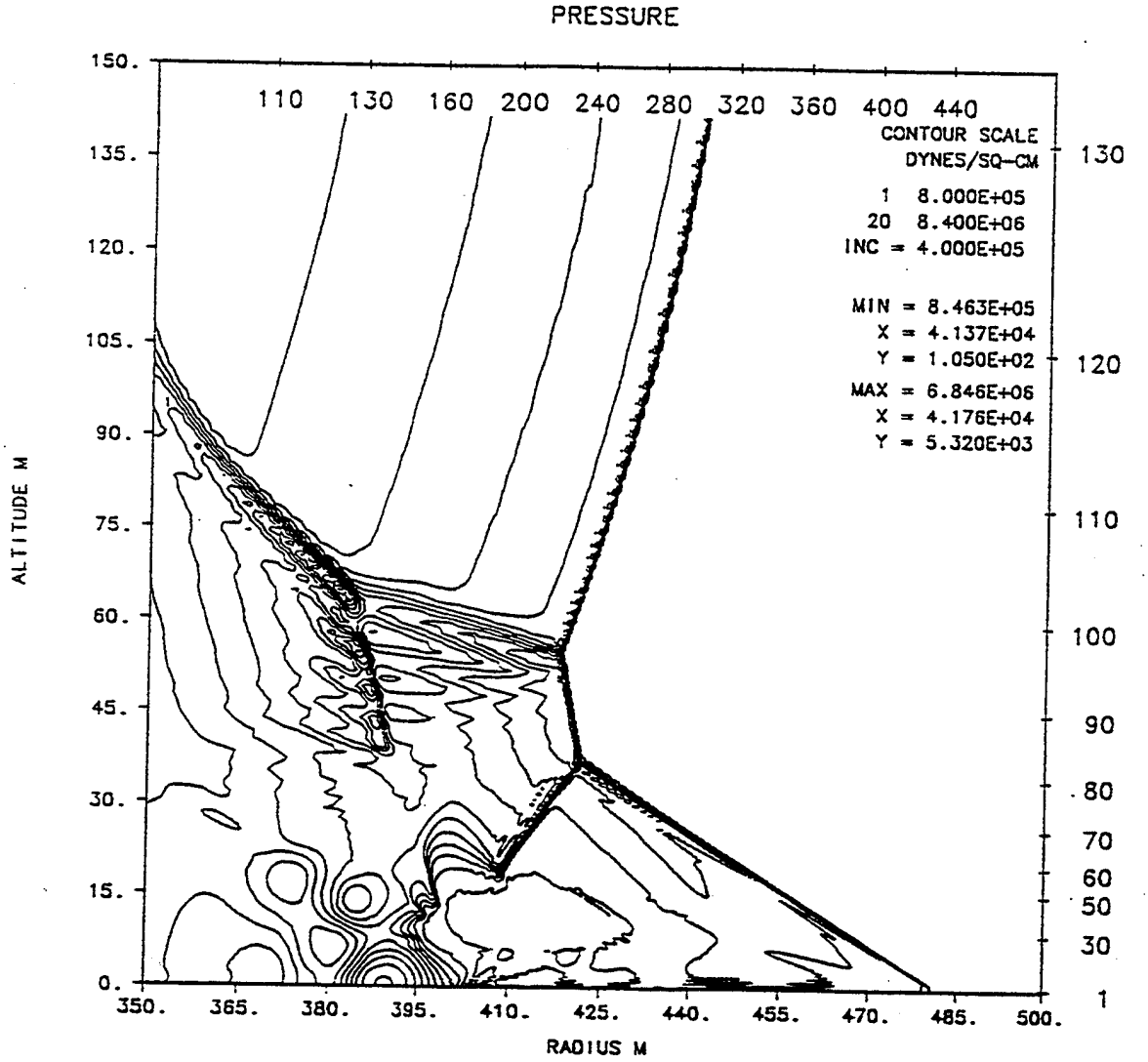

S-CUBED PRISCILLA - DESERT 30X30 CM THERMAL-KE- JEC 7/93
TIME 350.000 MSEC CYCLE 6587. PROBLEM 372.0050

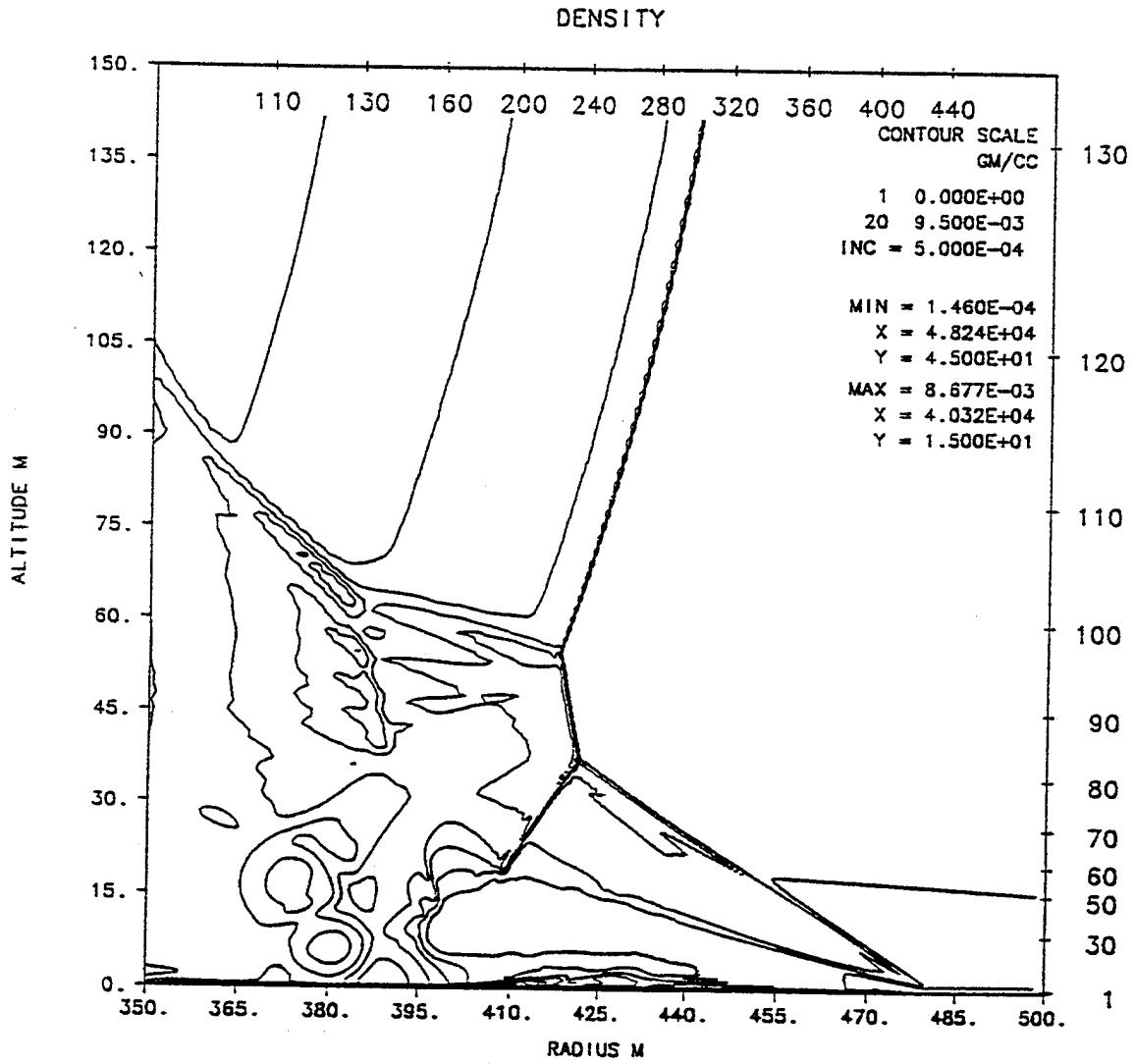

S-CUBED PRISCILLA - DESERT 30X30 CM THERMAL-KE- JEC 7/93
TIME 350.000 MSEC CYCLE 6587. PROBLEM 372.0050

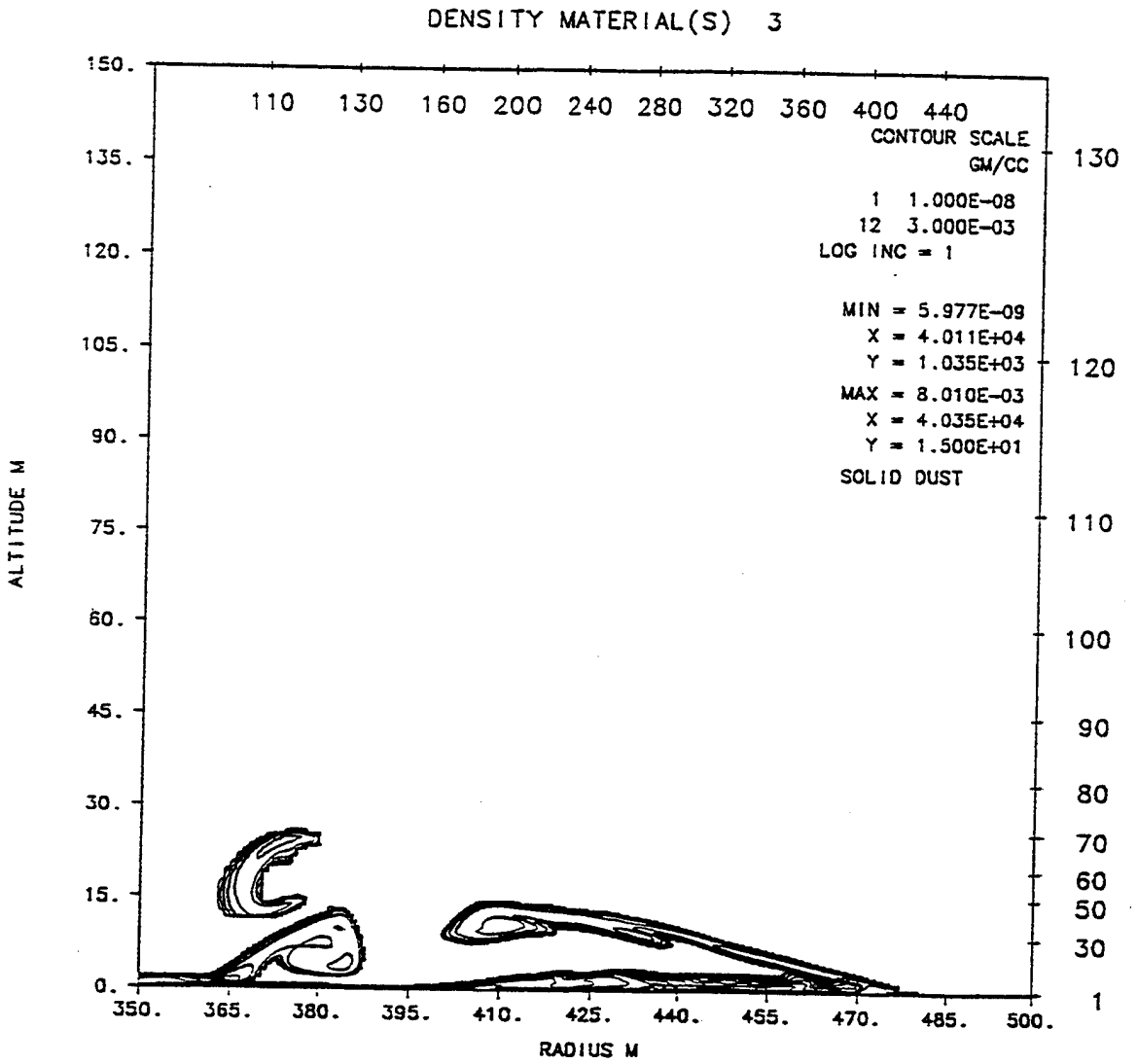

S-CUBED PRISCILLA – DESERT 30X30 CM THERMAL-KE- JEC 7/93
TIME 350.000 MSEC CYCLE 6587. PROBLEM 372.0050

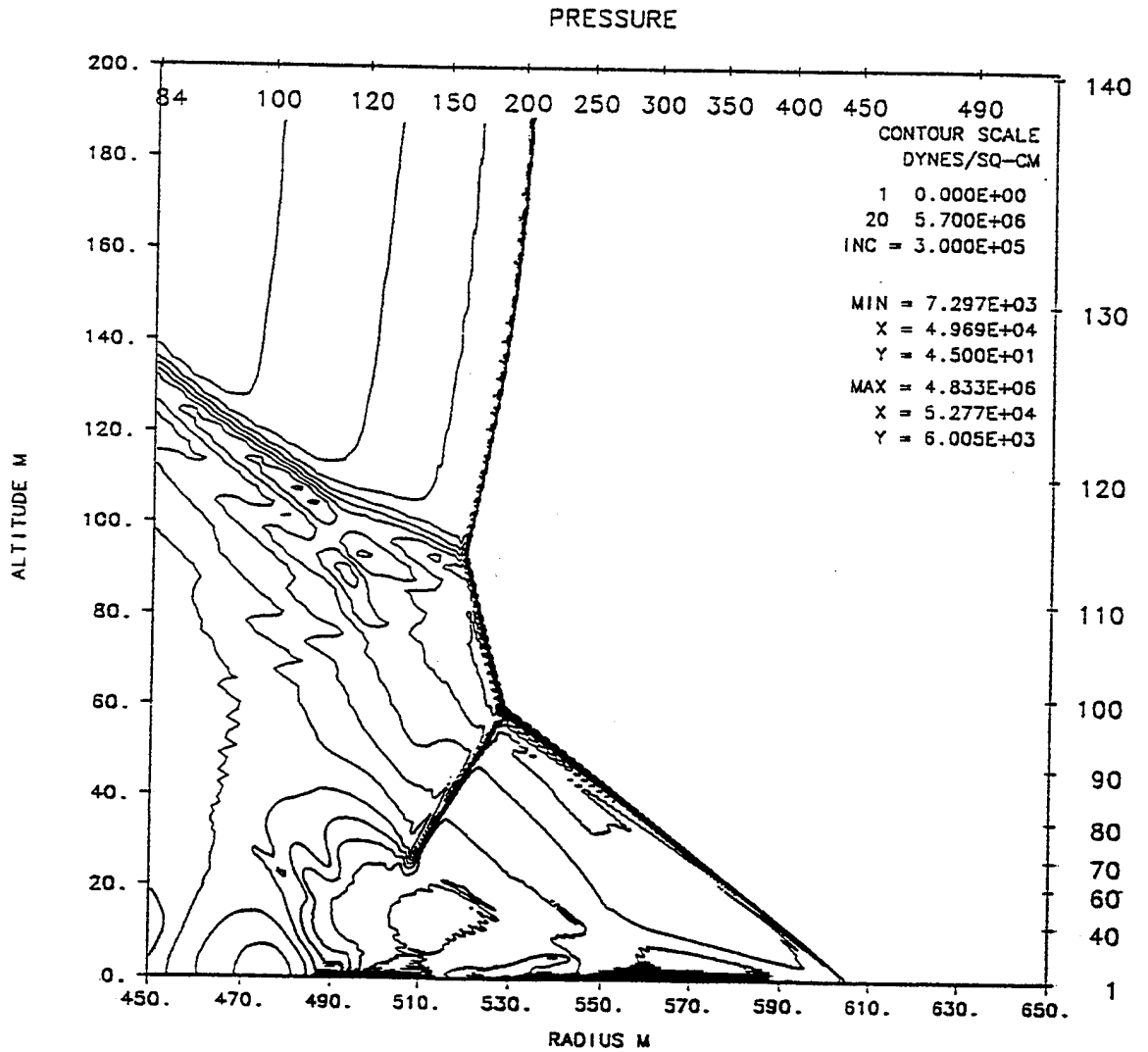

S-CUBED PRISCILLA - DESERT 30X30 CM THERMAL-KE- JEC 7/93
TIME 500.000 MSEC CYCLE10465. PROBLEM 372.0050

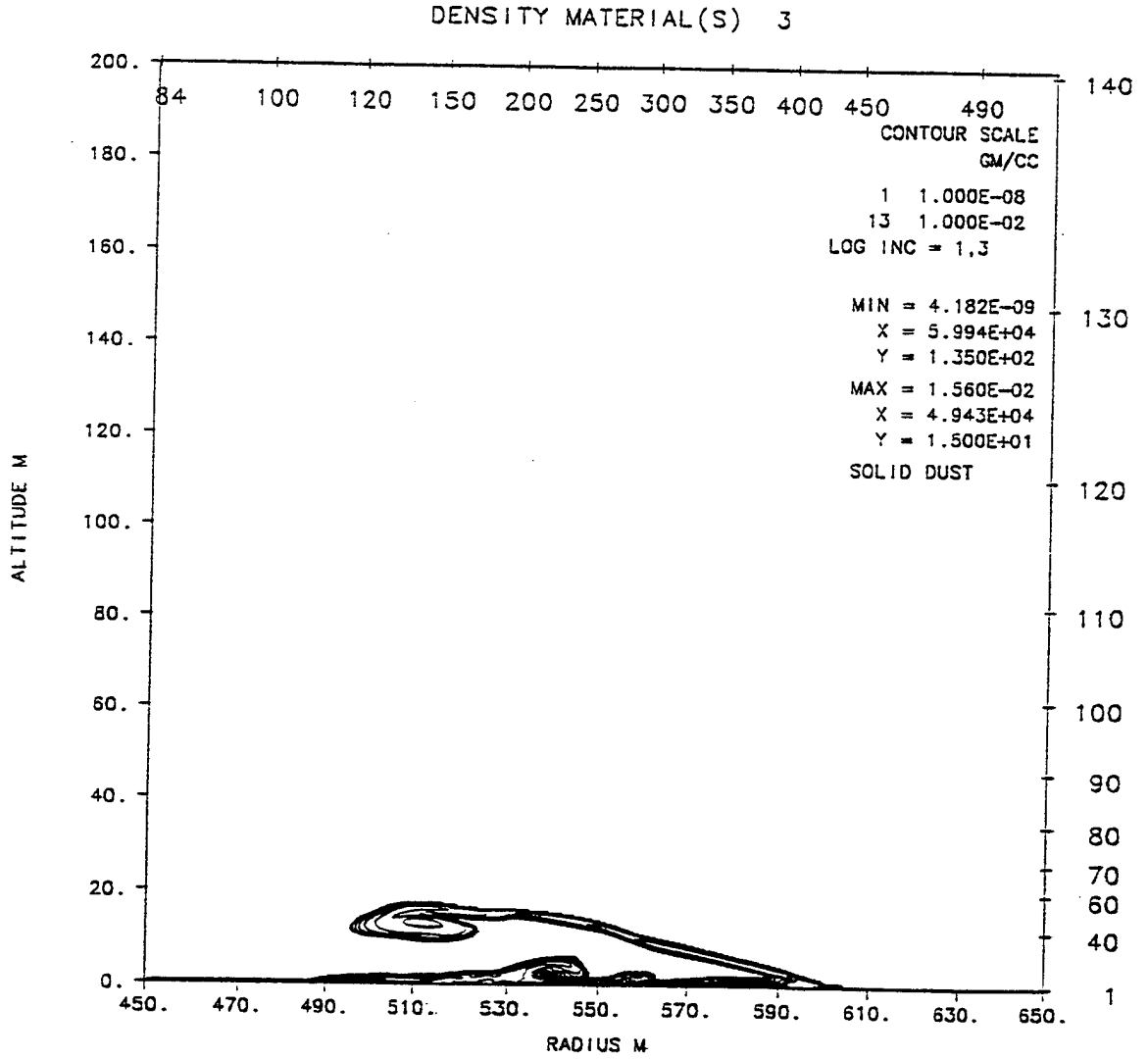

S-CUBED PRISCILLA - DESERT 30X30 CM THERMAL-KE- JEC 7/93
TIME 500.000 MSEC CYCLE10465. PROBLEM 372.0050

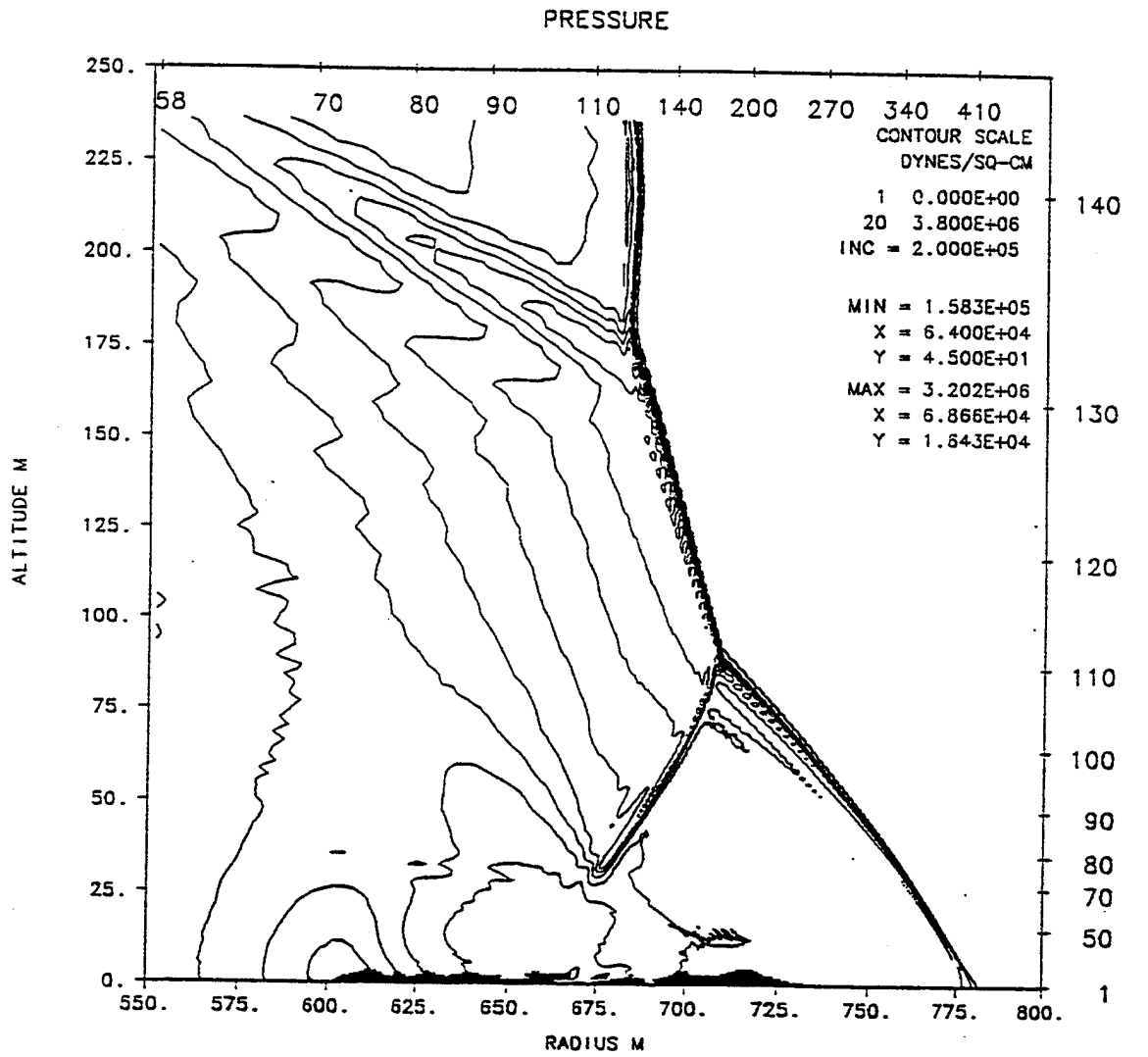

S-CUBED PRISCILLA - DESERT 30X30 CM THERMAL-KE- JEC 7/93
TIME 800.000 MSEC CYCLE18409. PROBLEM 372.0050

DENSITY MATERIAL(S) 3

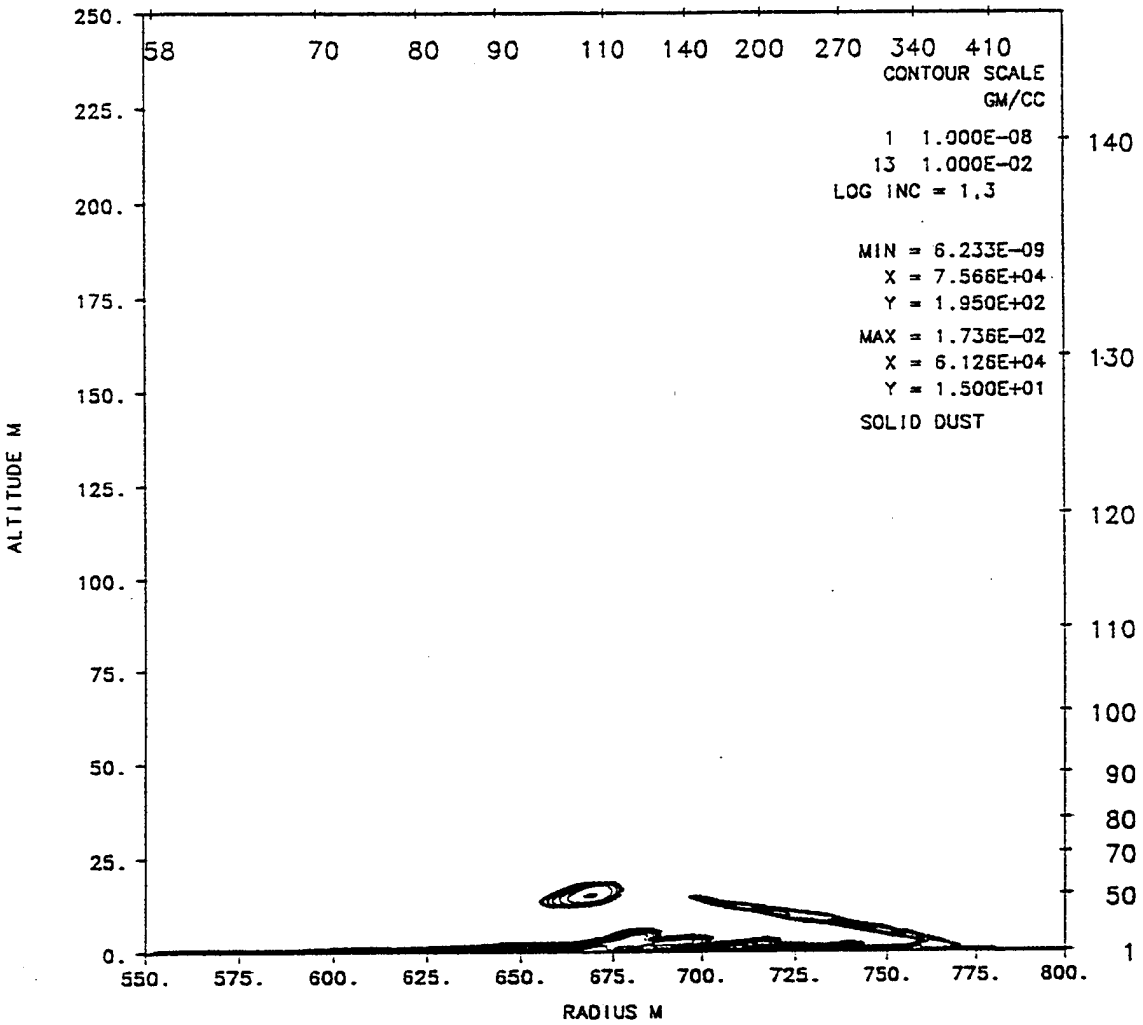

S-CUBED PRISCILLA - DESERT 30X30 CM THERMAL-KE- JEC 7/93
TIME 800.000 MSEC CYCLE18409. PROBLEM 372.0050

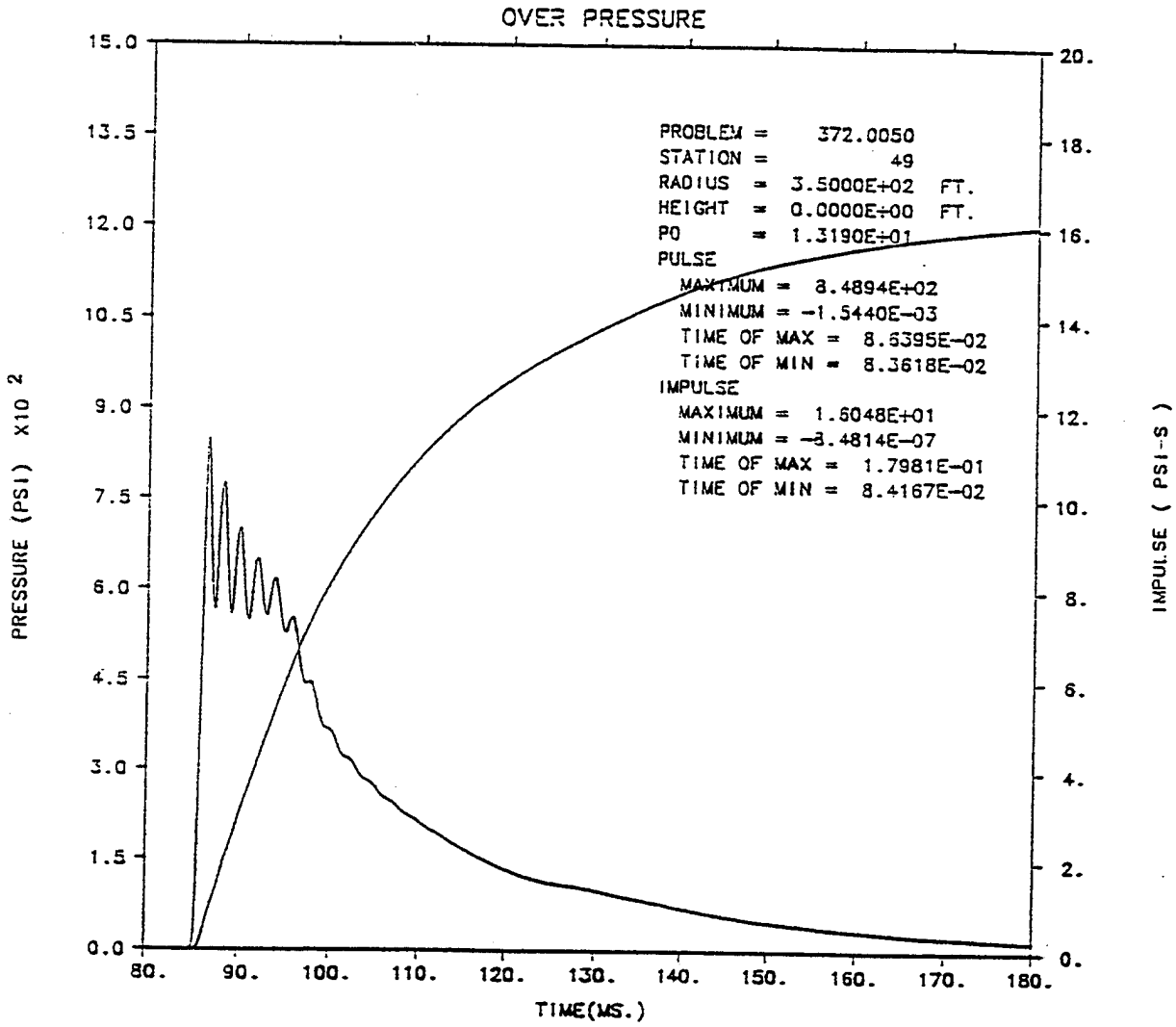

S-CUBED PRISCILLA – DESERT 30X30 CM THERMAL-KE- JEC 7/93

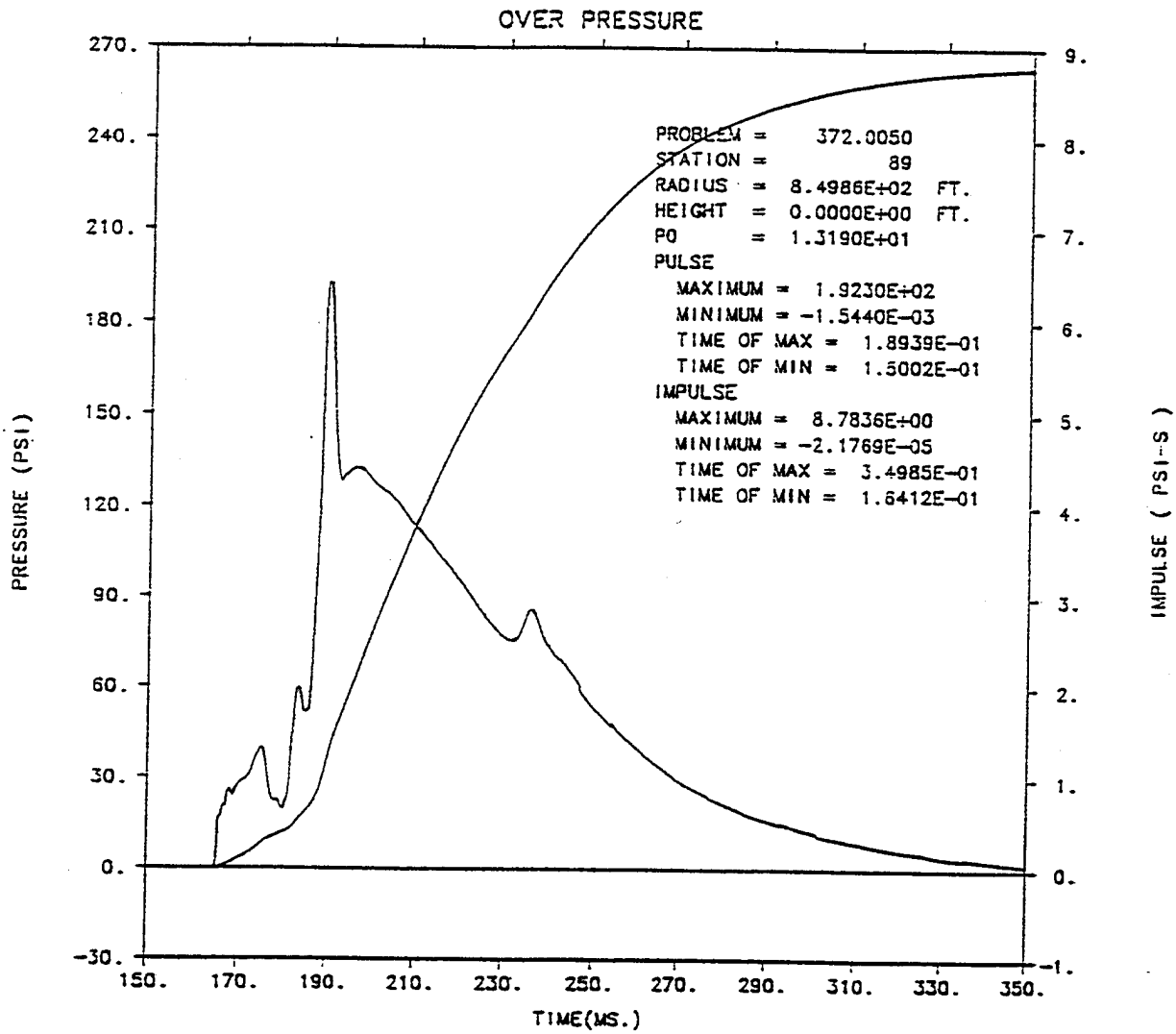

: S-CUBED PRISCILLA - DESERT 30X30 CM THERMAL-KE- JEC 7/93

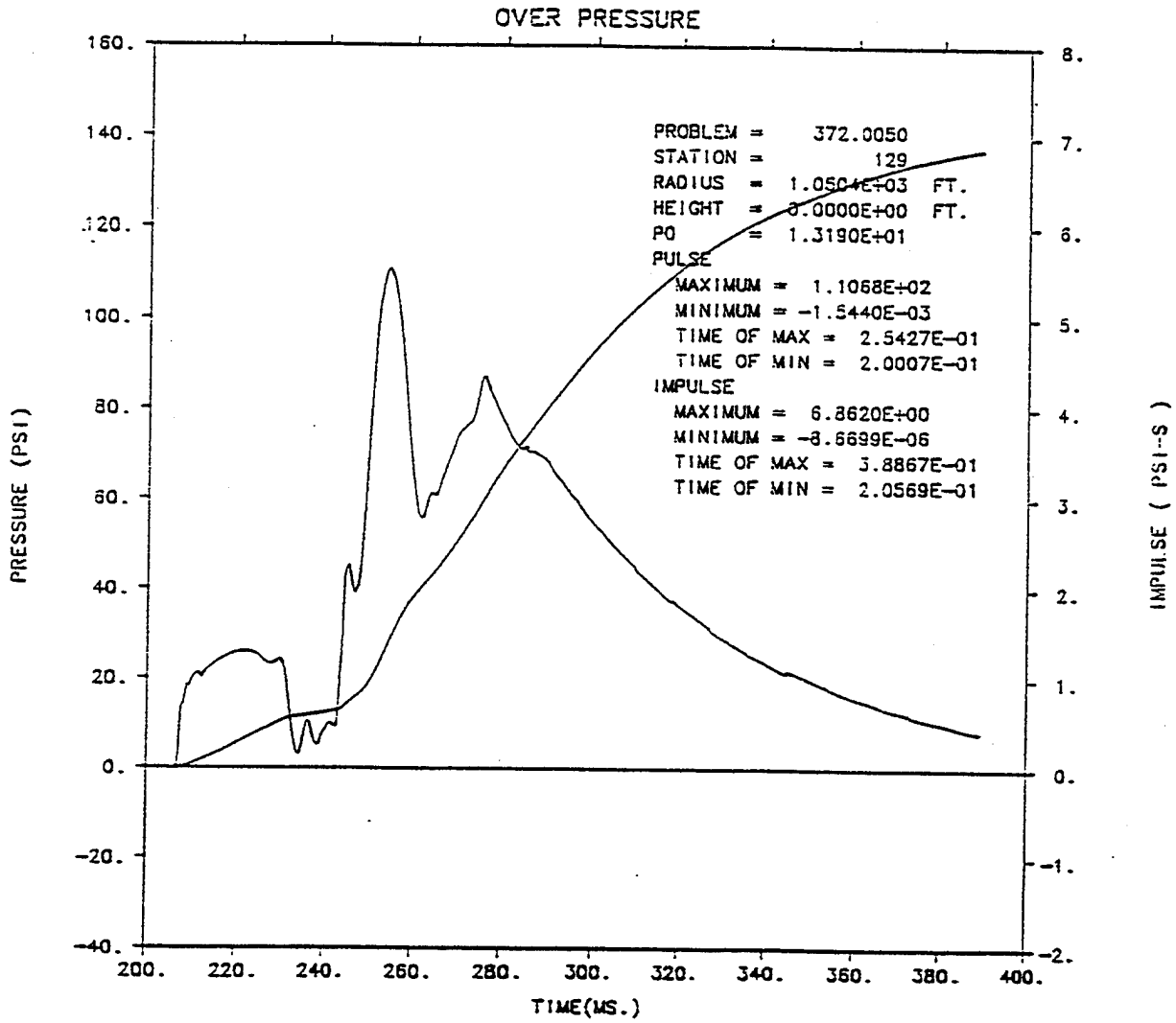

:S-CUBED PRISCILLA - DESERT 30X30 CM THERMAL-KE- JEC 7/93

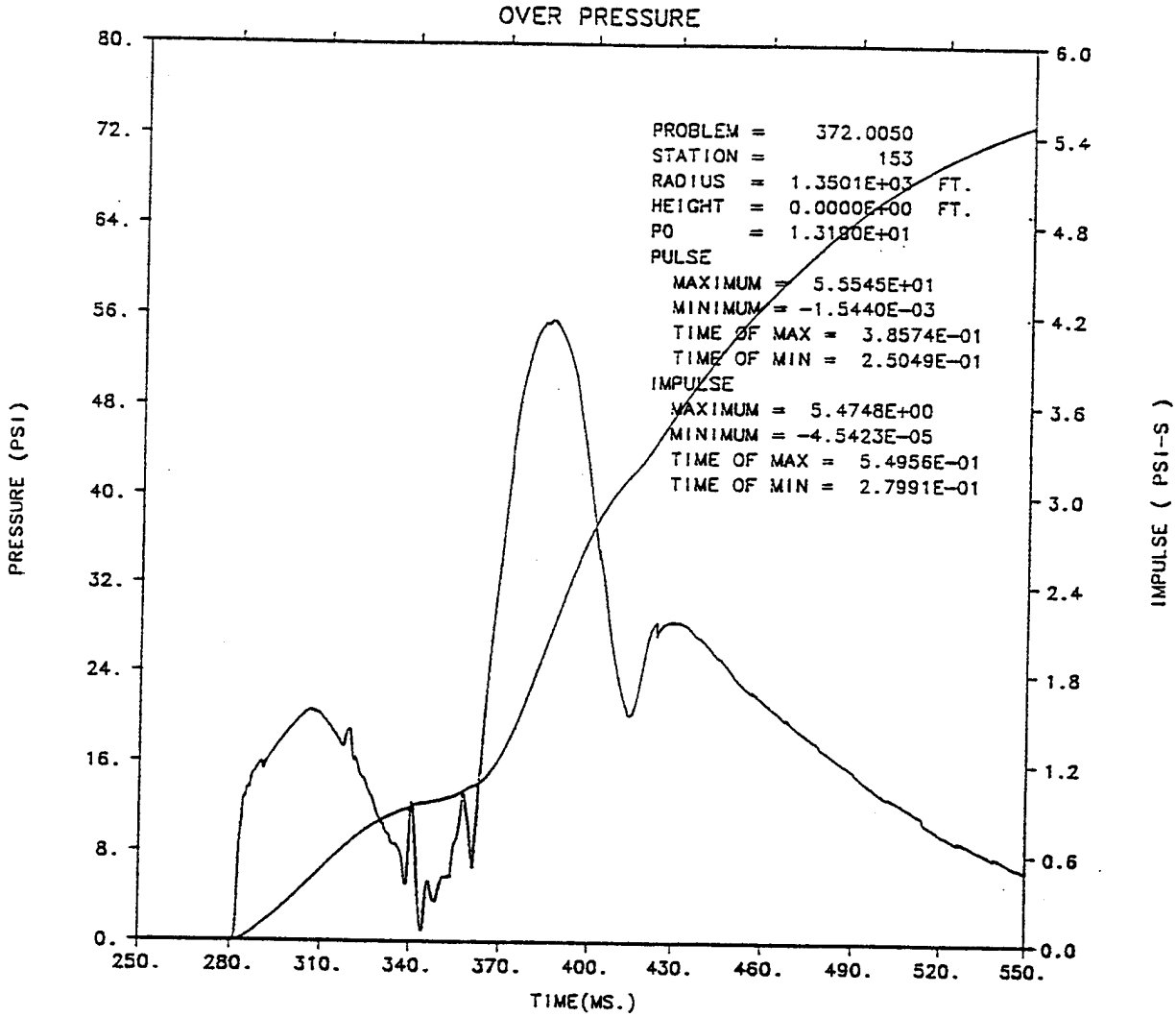

S-CUBED PRISCILLA - DESERT 30X30 CM THERMAL-KE- JEC 7/93

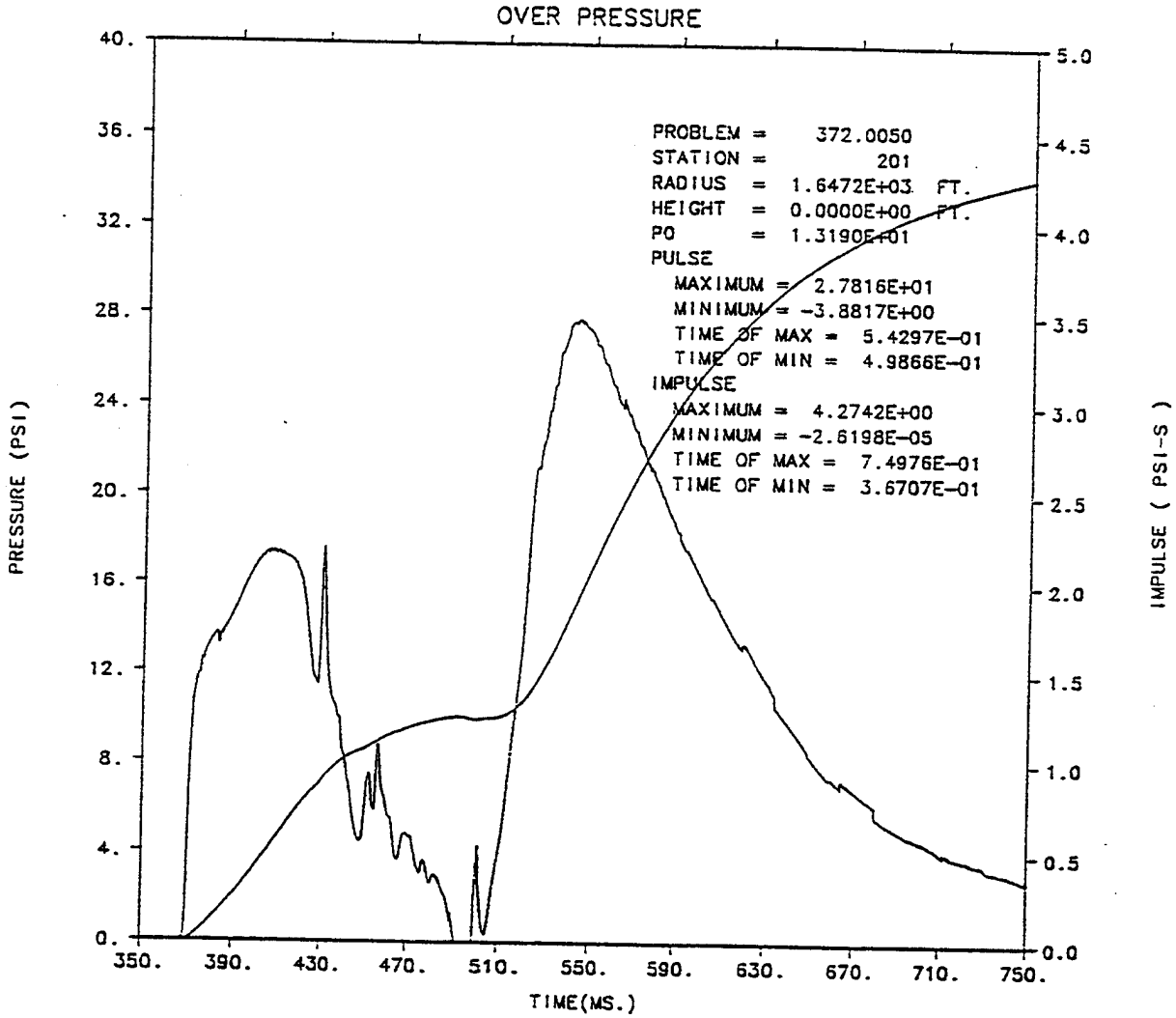

S-CUBED PRISCILLA - DESERT 30X30 CM THERMAL-KE- JEC 7/93

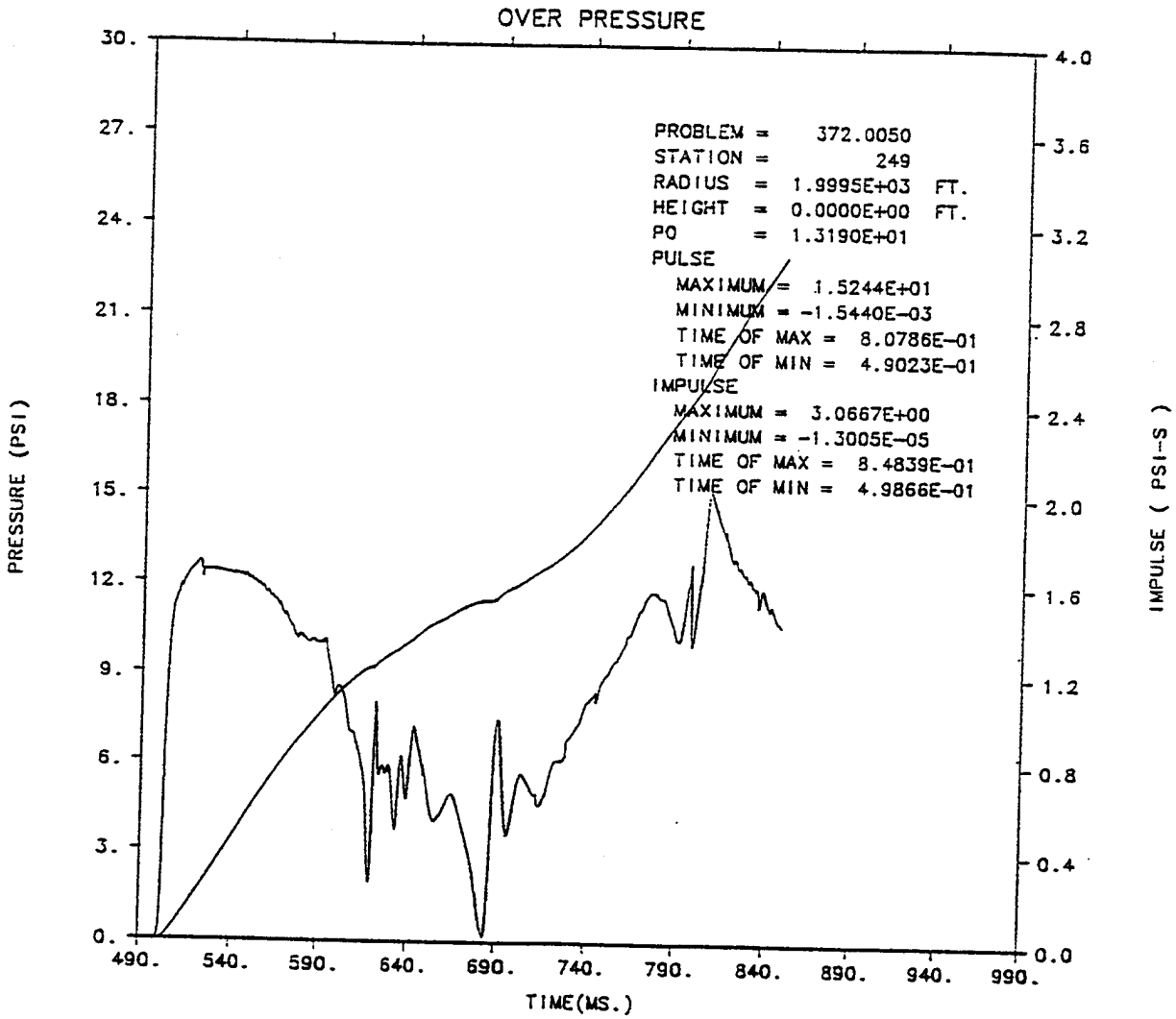

S-CUBED PRISCILLA - DESERT 30X30 CM THERMAL-KE- JEC 7/93

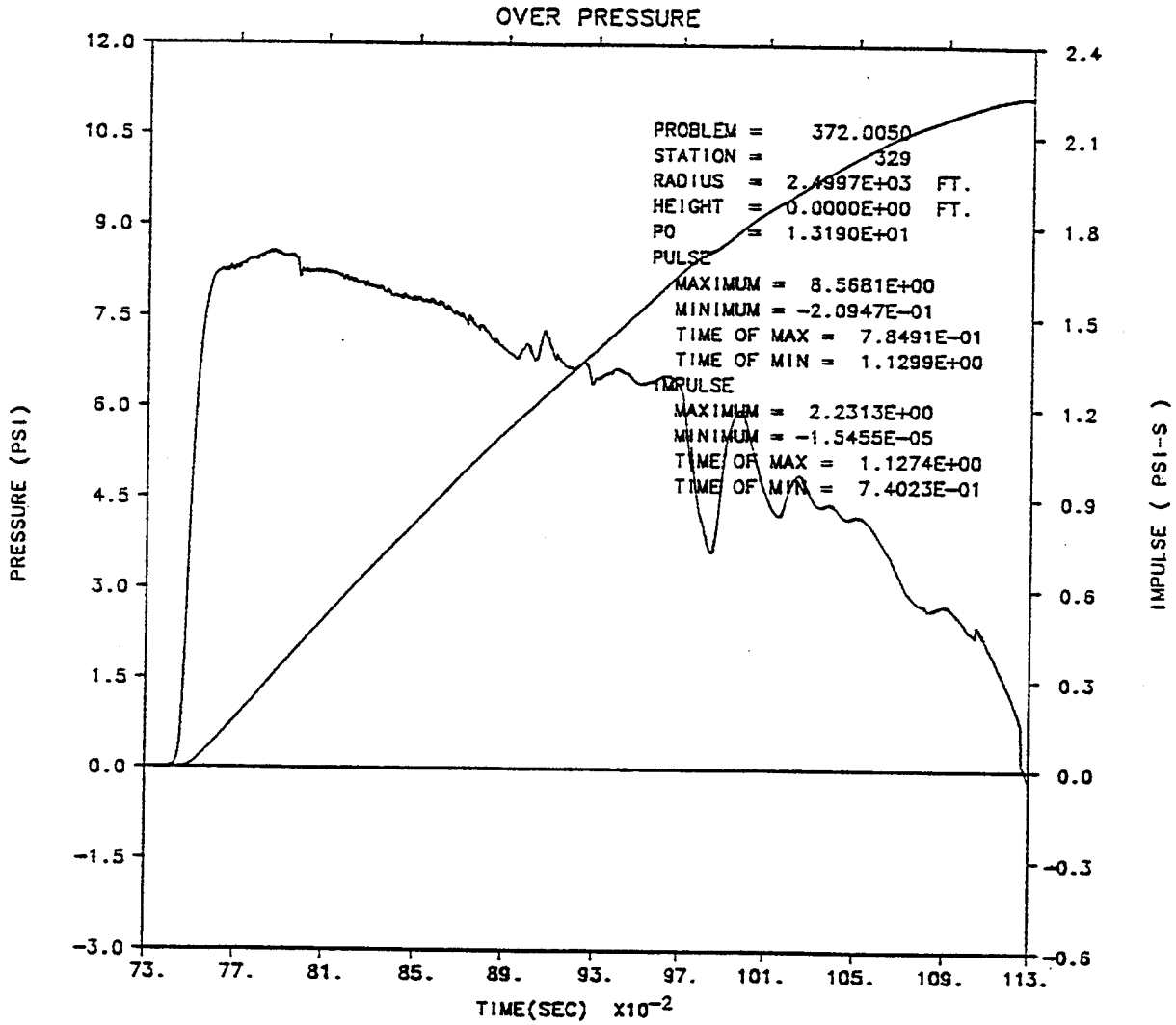

S-CUBED PRISCILLA - DESERT 30X30 CM THERMAL-KE- JEC 7/93

INTENTIONALLY LEFT BLANK.

APPENDIX H
SUMMARY OF CALCULATIONAL RESULTS AND COMPARISONS WITH EXPERIMENTAL DATA

PRISCILLA
ARRIVAL TIME AT GROUND LEVEL

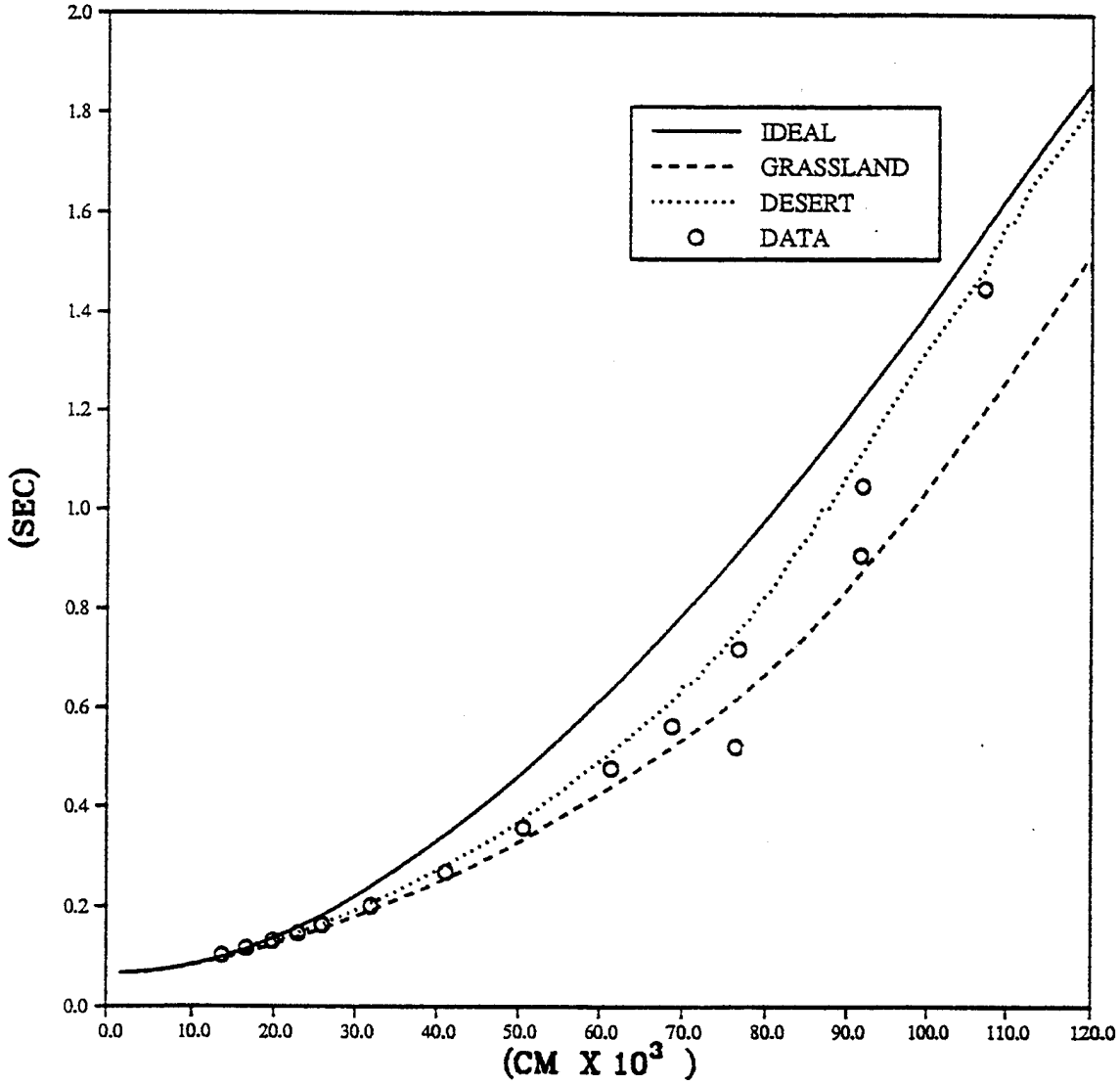

PRISCILLA COMPARISONS
OVERPRESSURE AT GROUND LEVEL

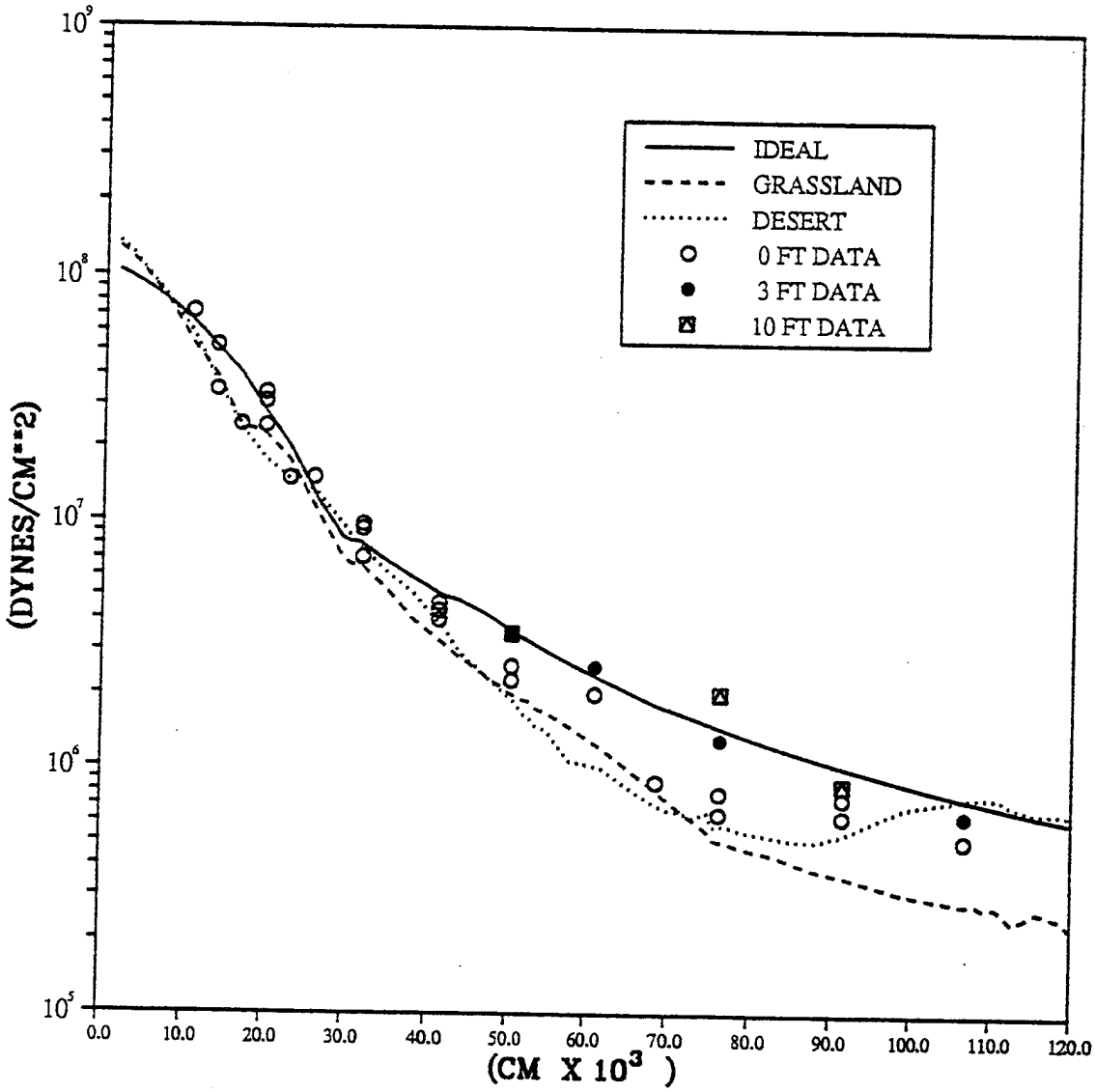

PRISCILLA COMPARISONS
OVERPRESSURE AT 91.44 CM LEVEL (3 FEET)

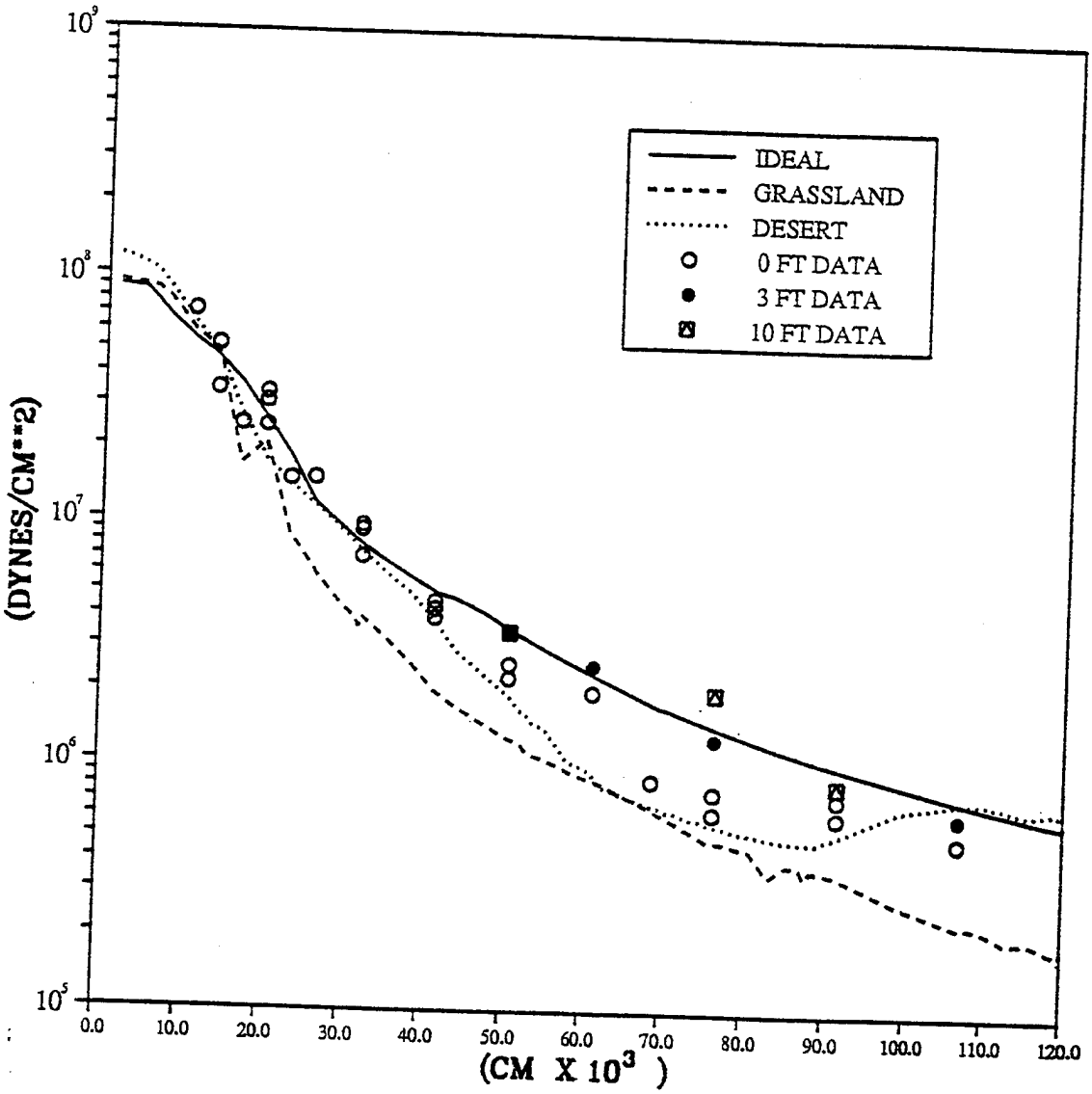

PRISCILLA COMPARISONS
OVERPRESSURE IMPULSE AT GROUND LEVEL

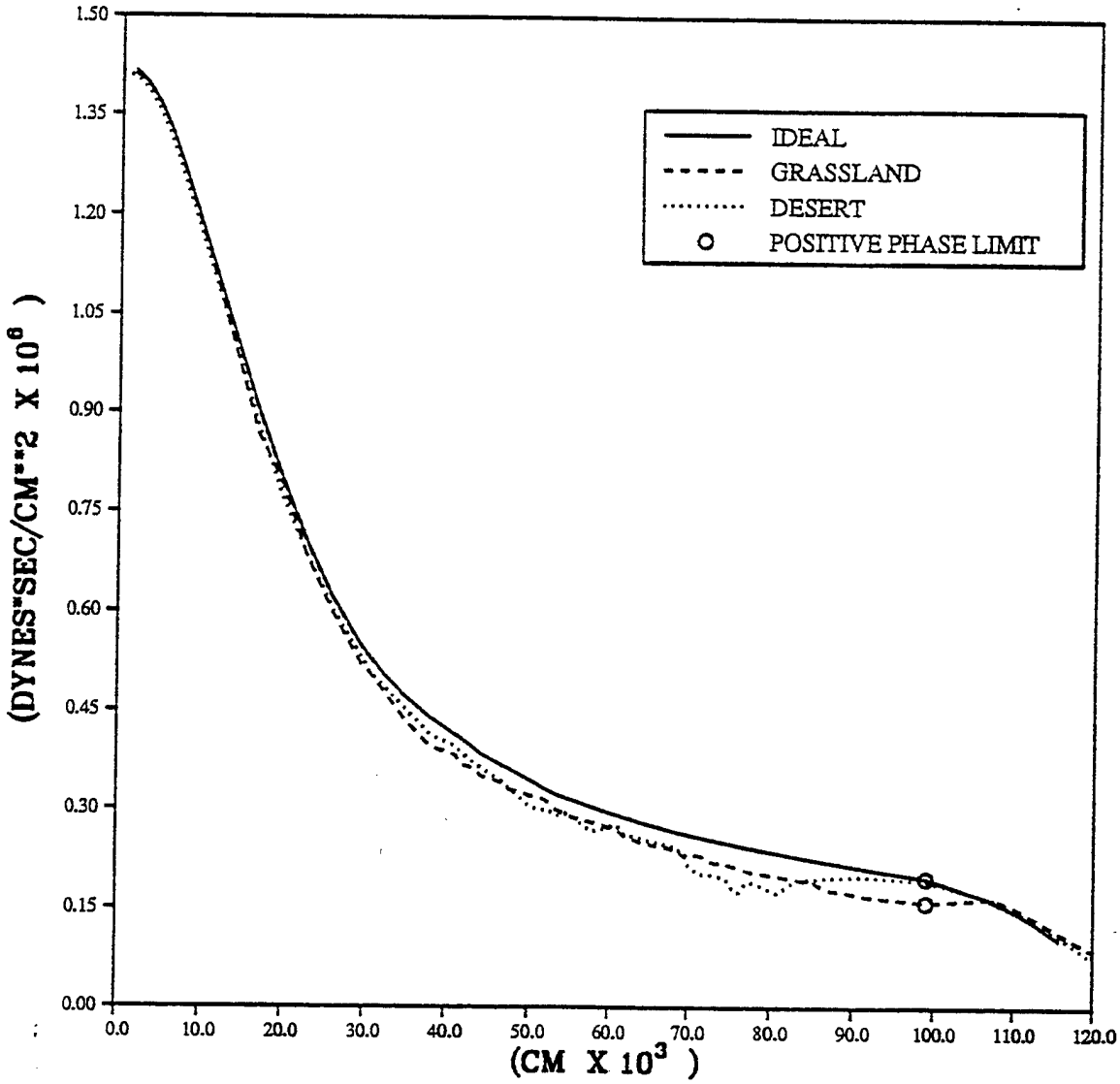

POSITIVE PHASE NOT COMPLETE BEYOND 99060 CM

PRISCILLA COMPARISONS
OVERPRESSURE IMPULSE AT 91.44 CM LEVEL (3 FEET)

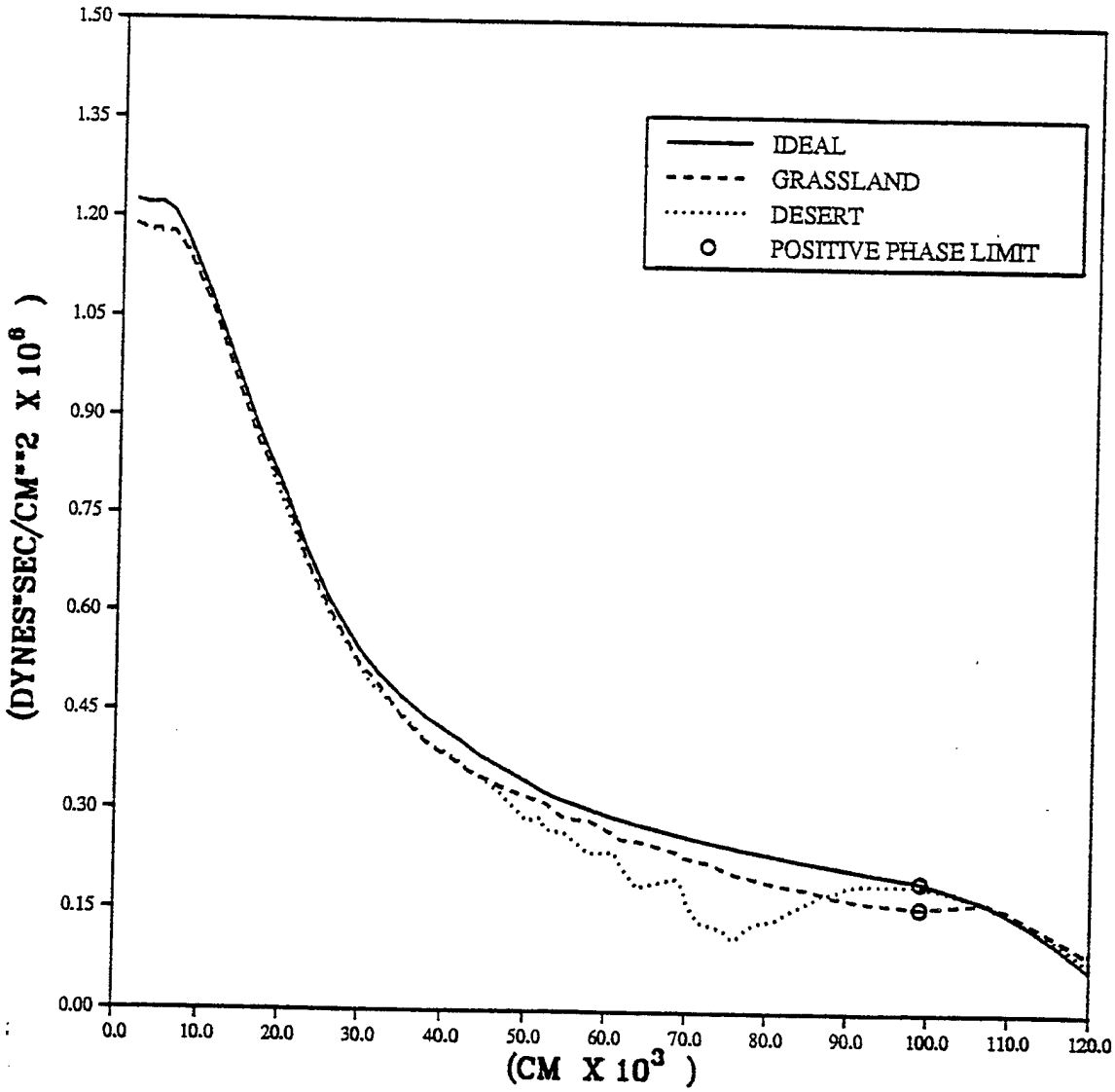

POSITIVE PHASE NOT COMPLETE BEYOND 99060 CM

PRISCILLA COMPARISONS
HORIZONTAL DYNAMIC PRESSURE PEAKS AT GROUND LEVEL

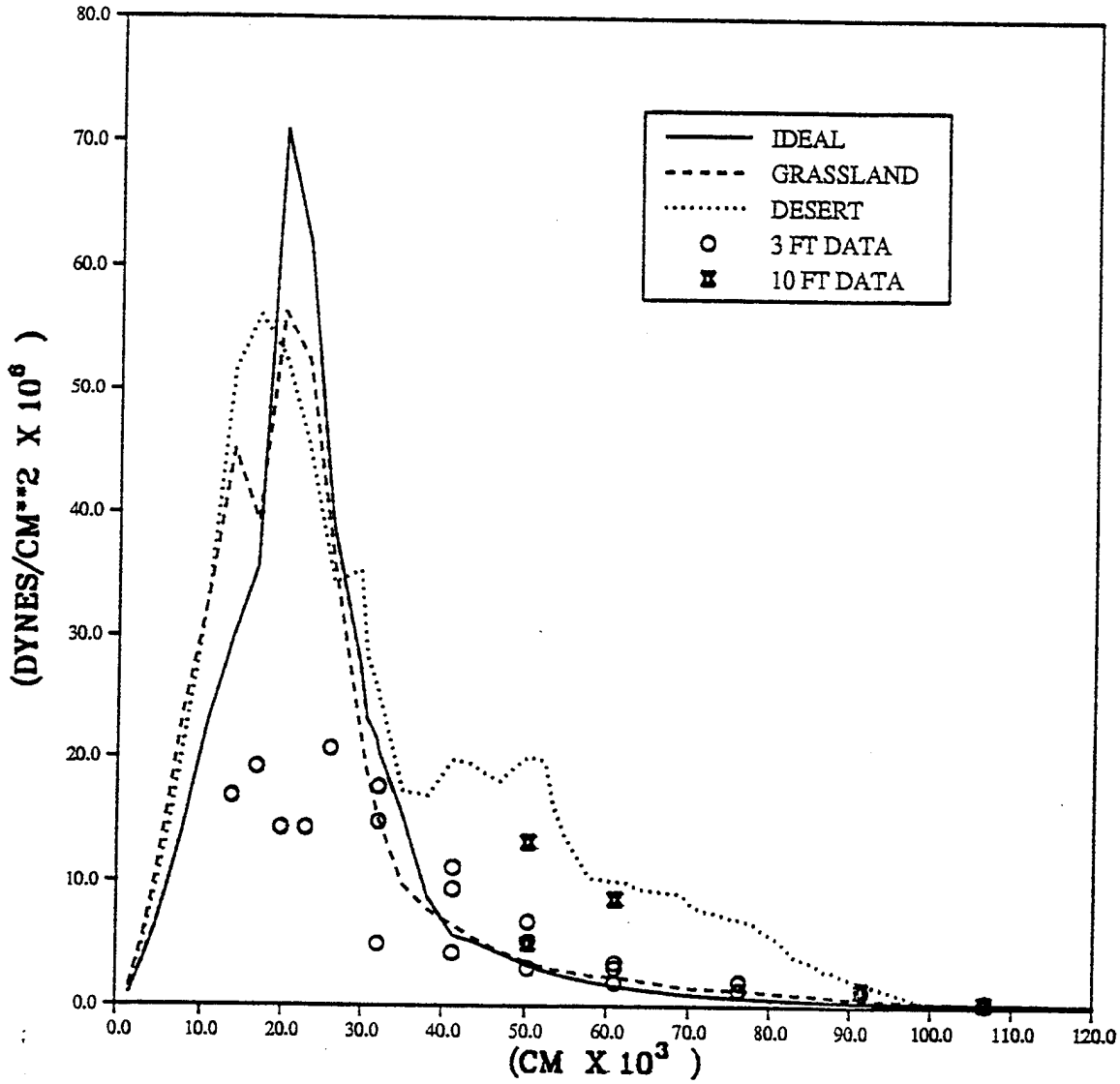

PRISCILLA COMPARISONS
HORIZONTAL DYNAMIC PRESSURE PEAKS AT 91.44 CM LEVEL (3 FEET)

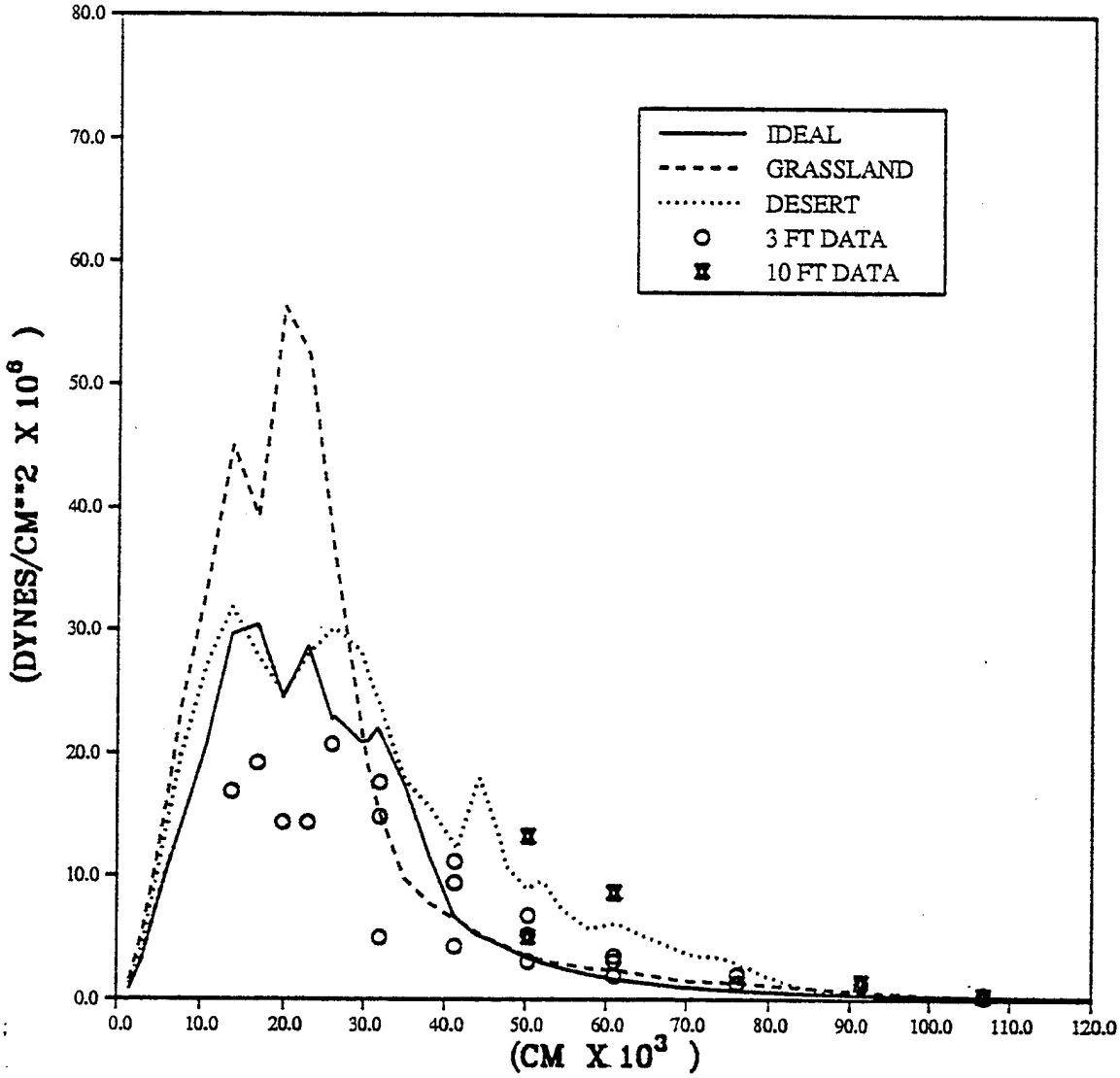

PRISCILLA COMPARISONS
HORIZONTAL DYNAMIC PRESSURE IMPULSE AT GROUND LEVEL

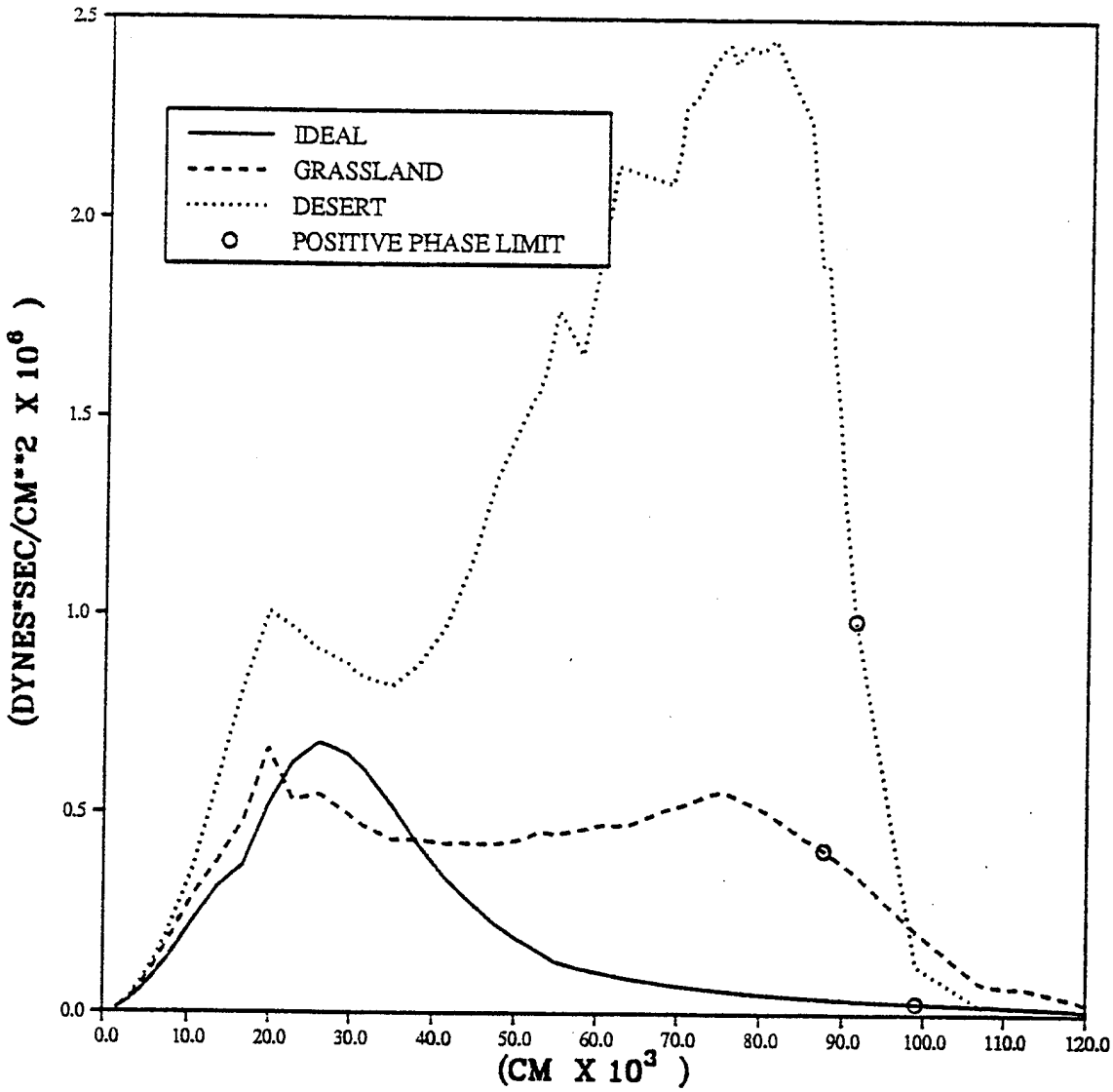

POSITIVE PHASE NOT COMPLETE BEYOND 99060 CM

PRISCILLA COMPARISONS
HORIZONTAL DYNAMIC PRESSURE IMPULSE
AT 91.44 CM LEVEL (3 FEET)

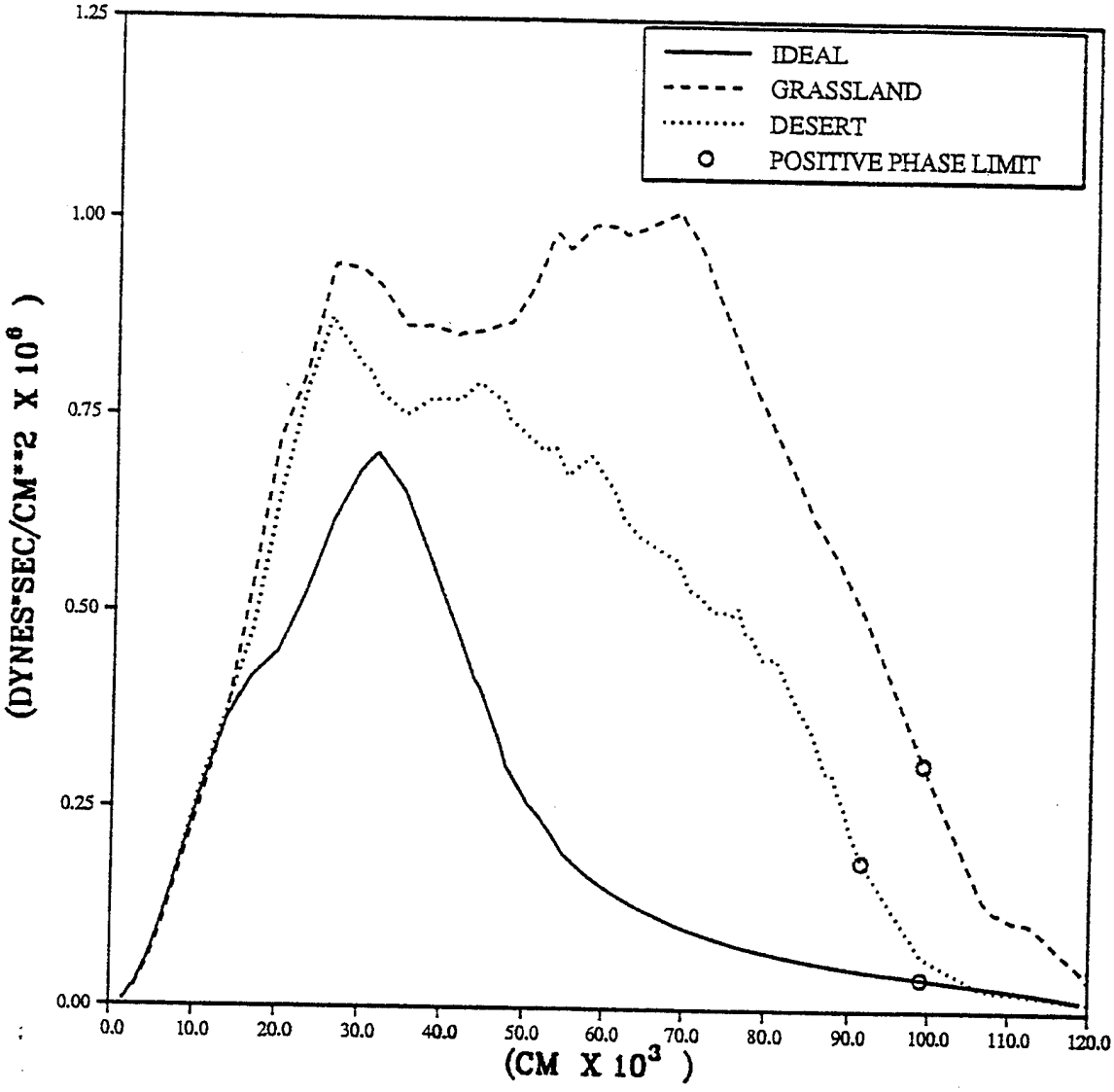

POSITIVE PHASE NOT COMPLETE BEYOND 99060 CM

INTENTIONALLY LEFT BLANK.

APPENDIX I
COMPARISON OF PRISCILLA EXPERIMENTAL WAVEFORMS WITH DESERT CALCULATION: OVERPRESSURE, DYNAMIC PRESSURES, AND IMPULSE

PRISCILLA
CALCULATION - DATA COMPARISONS
OVERPRESSURE AT 350 FEET (107 M)

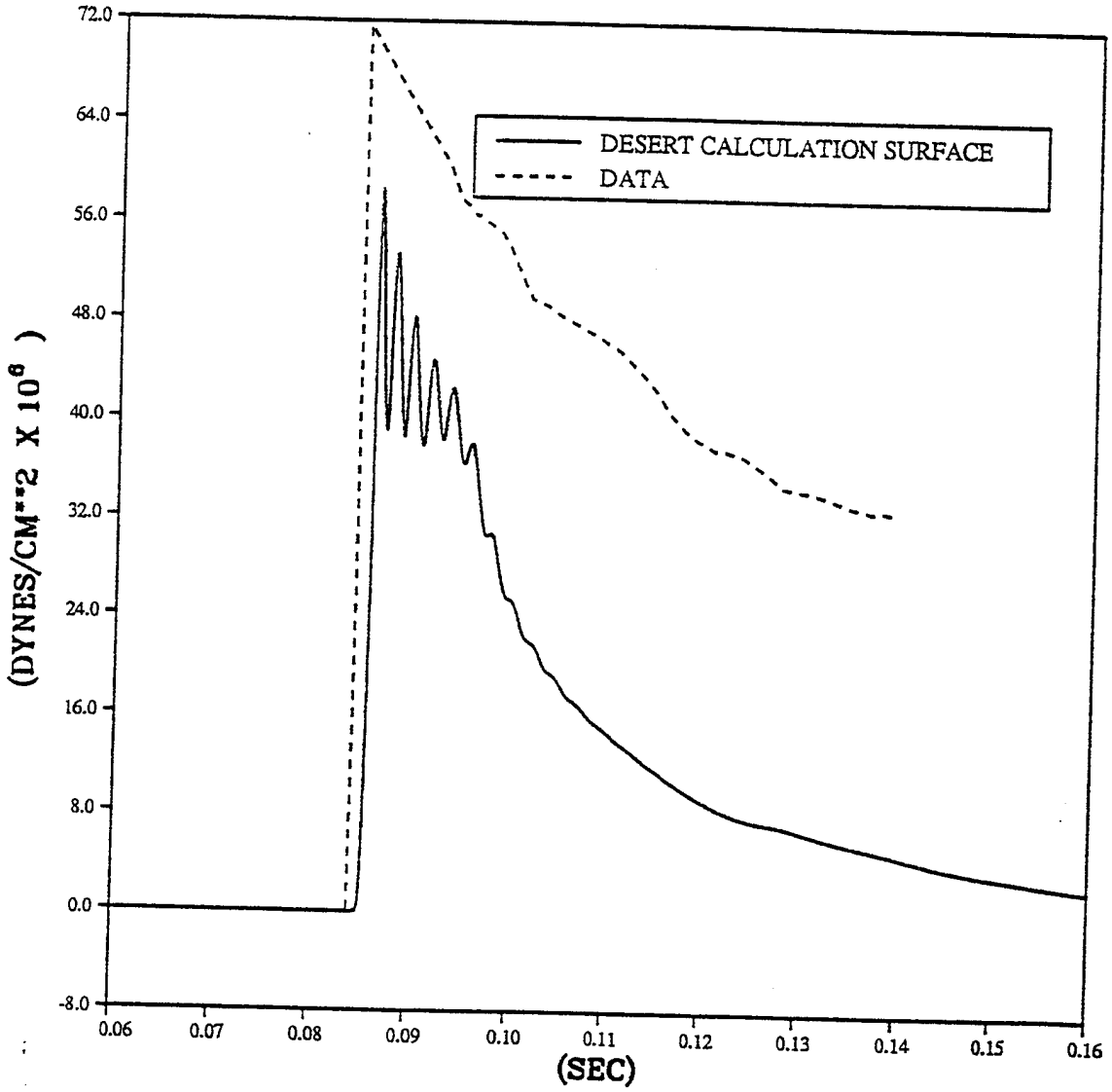

DATA TIME SHIFTED TO MATCH CALCULATION

PRISCILLA
CALCULATION - DATA COMPARISONS
OVERPRESSURE AT 850 FEET (260 M)

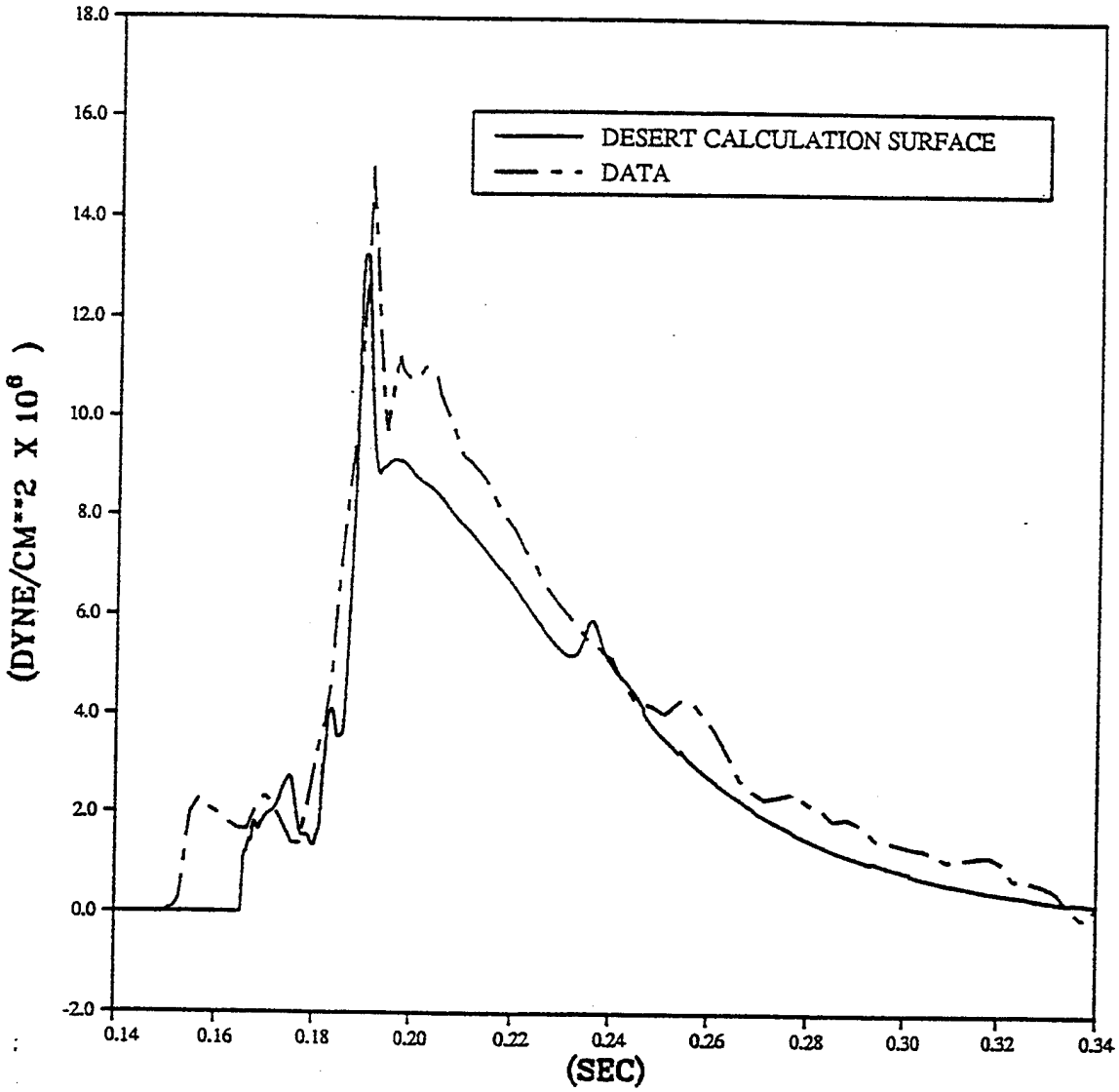

DATA TIME SHIFTED TO MATCH CALCULATION

PRISCILLA
CALCULATION - DATA COMPARISONS
OVERPRESSURE AT 1050 FEET (320 M)

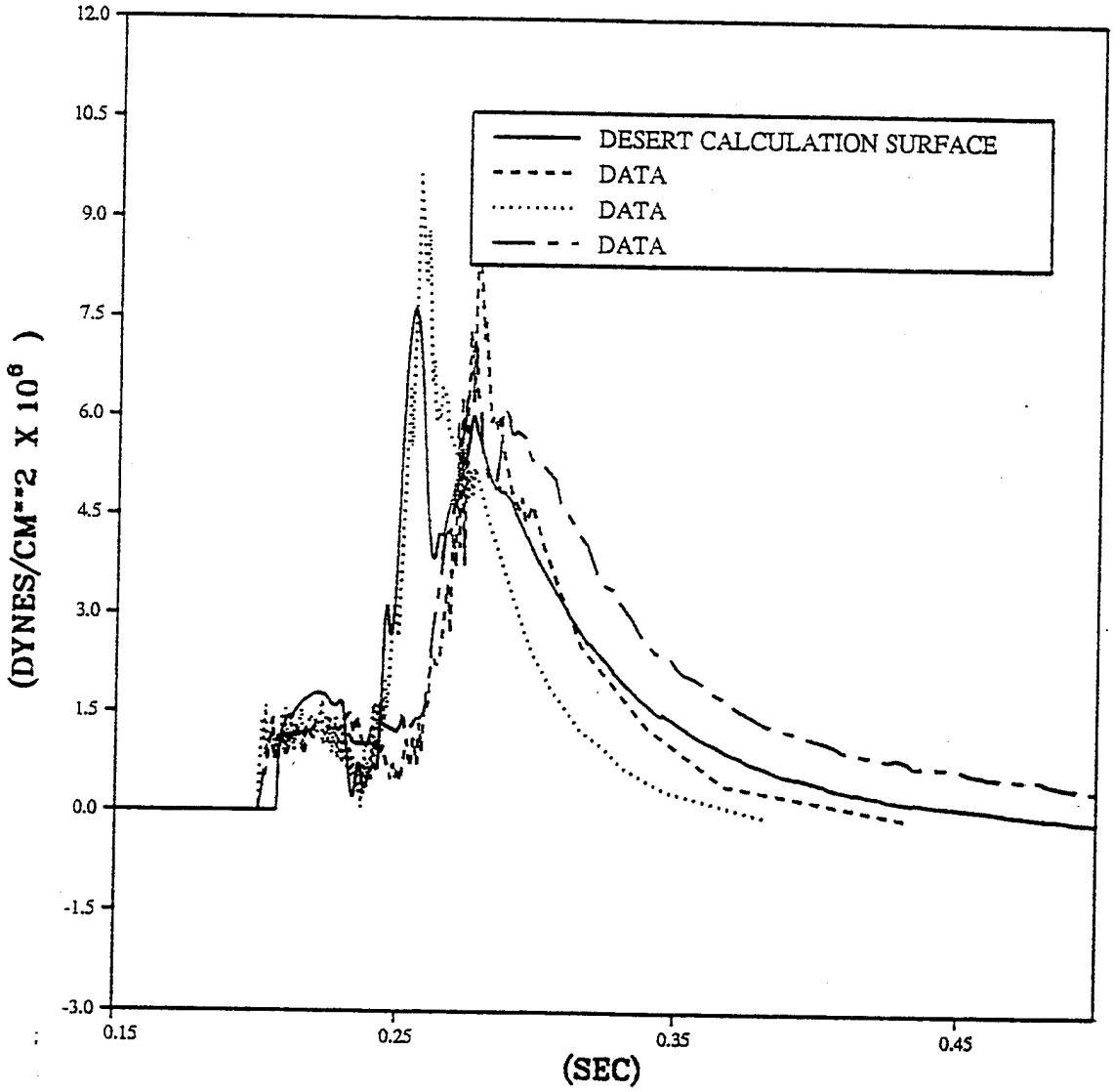

DATA TIME SHIFTED TO MATCH CALCULATION

PRISCILLA
CALCULATION - DATA COMPARISONS
OVERPRESSURE AT 1350 FEET (410 M)

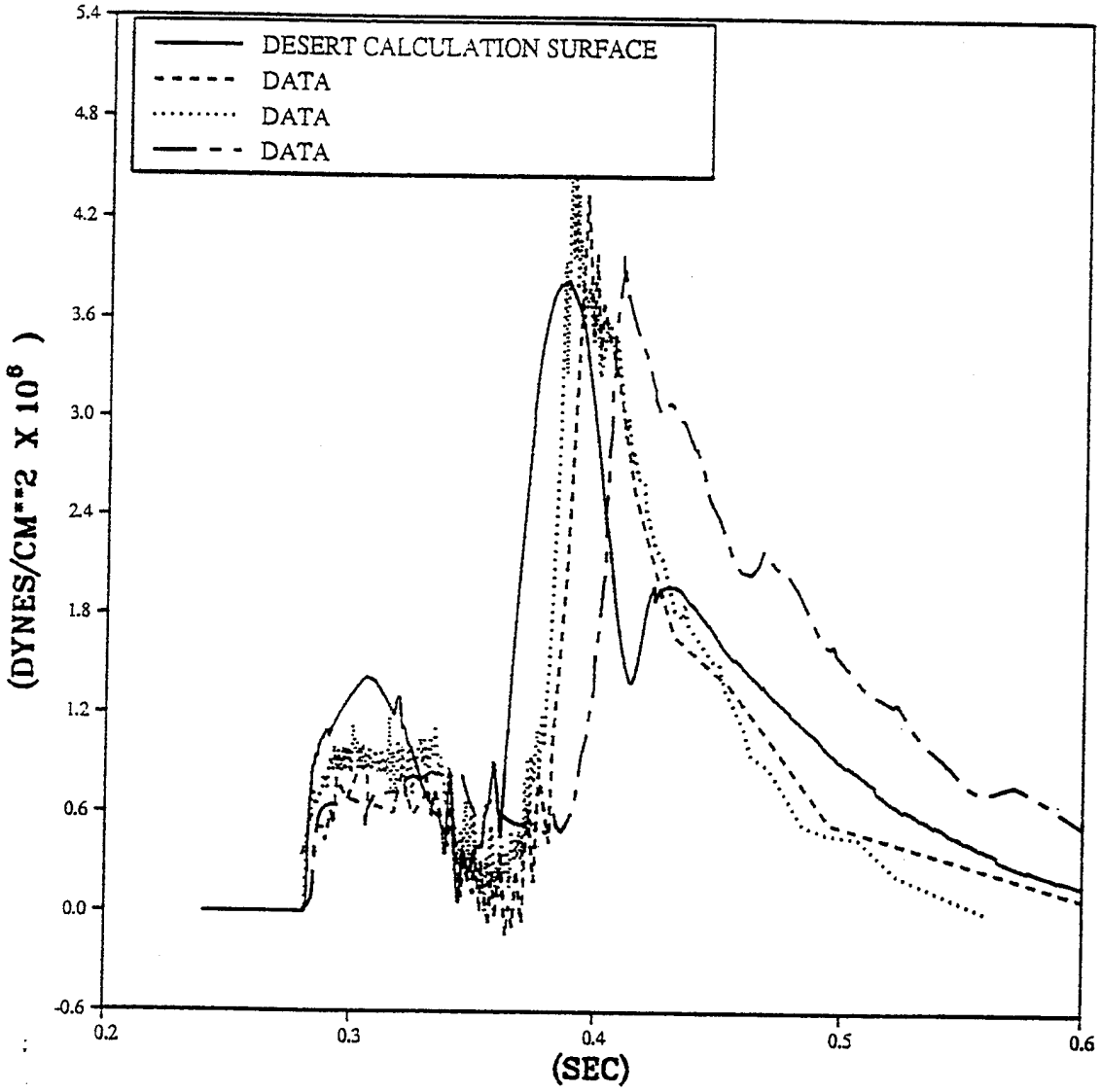

DATA TIME SHIFTED TO MATCH CALCULATION

PRISCILLA
CALCULATION - DATA COMPARISONS
OVERPRESSURE AT 1650 FEET (503 M)

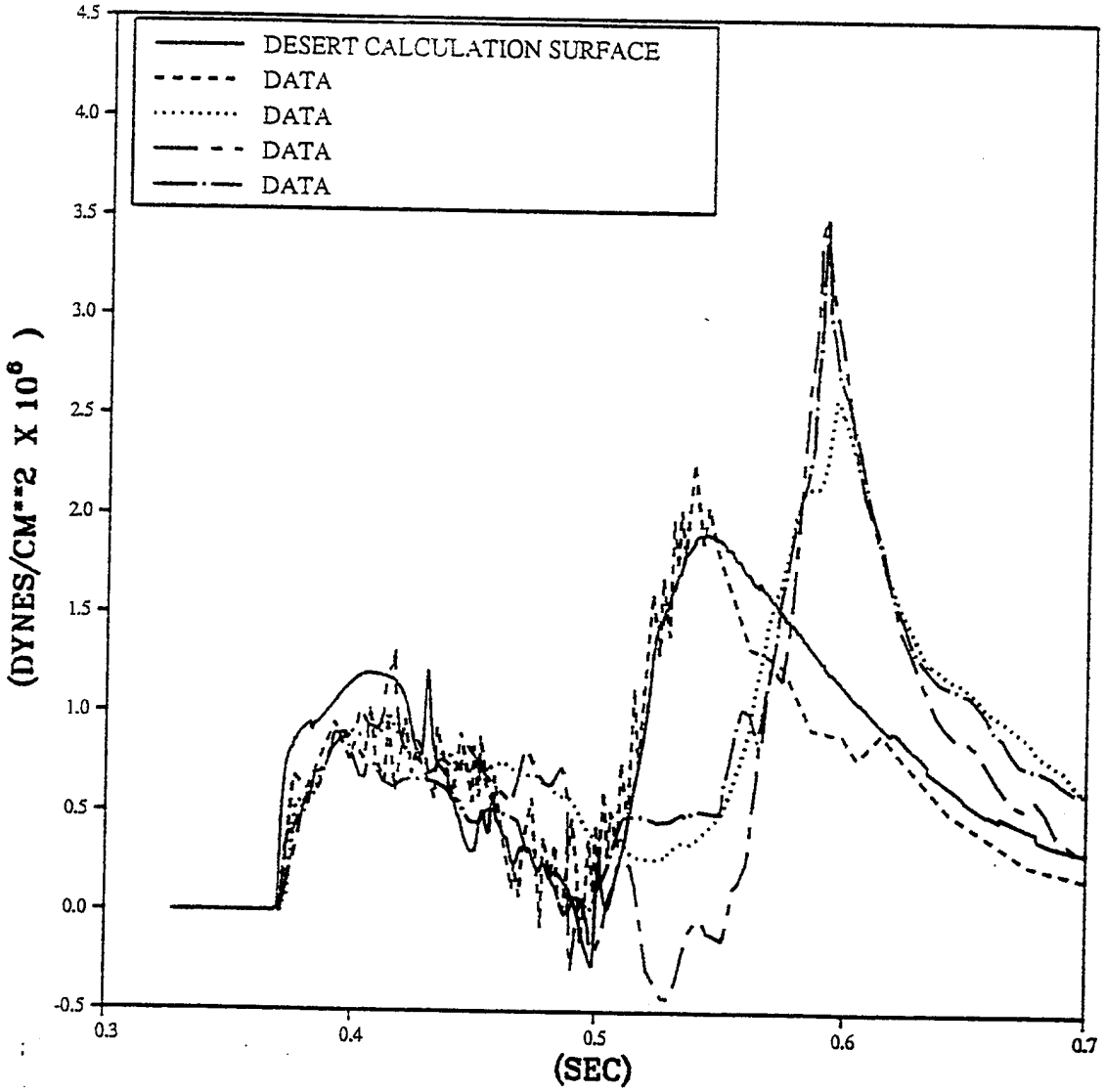

DATA TIME SHIFTED TO MATCH CALCULATION

PRISCILLA
CALCULATION - DATA COMPARISONS
OVERPRESSURE AT 2000 FEET (607 M)

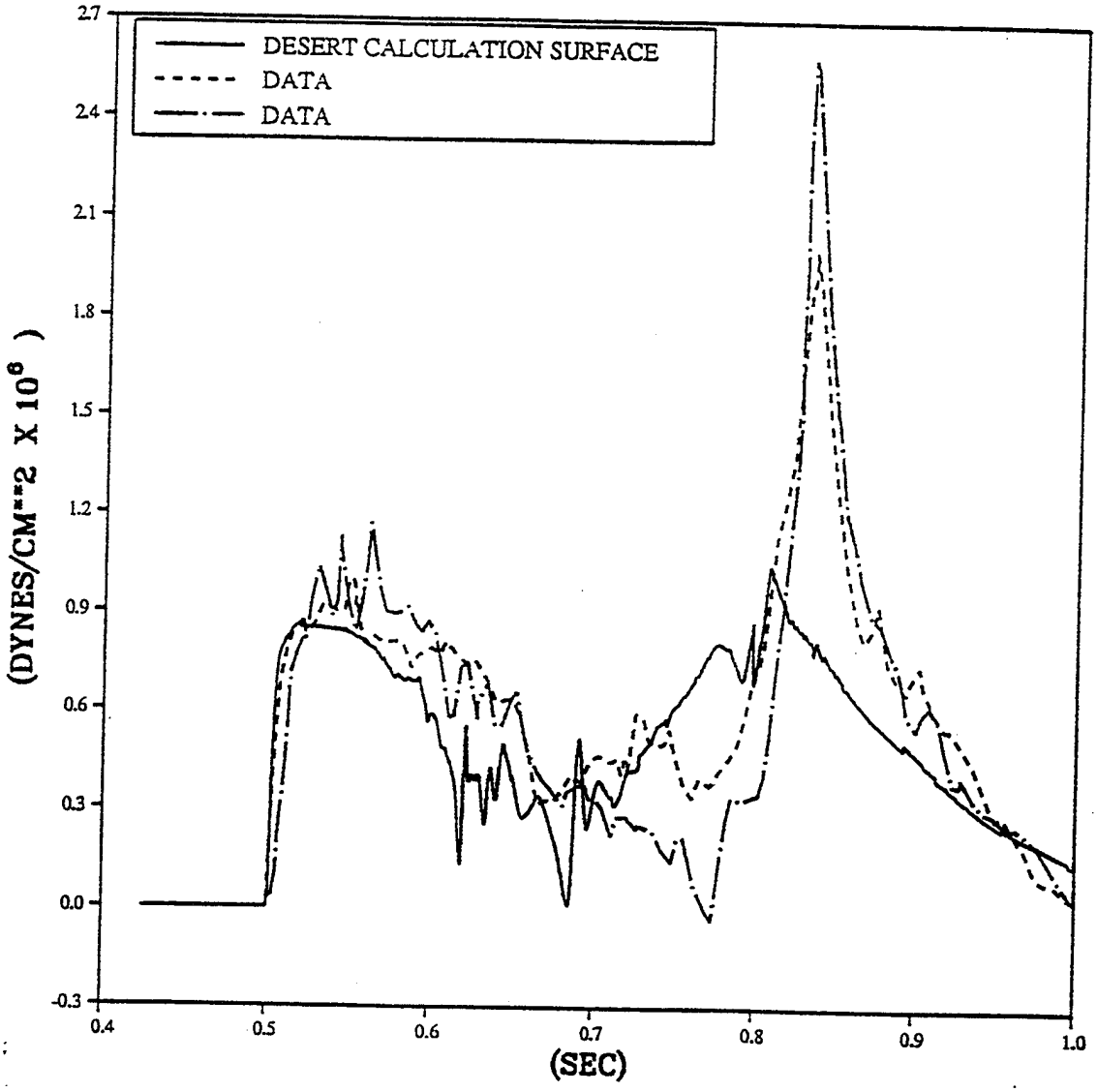

DATA TIME SHIFTED TO MATCH CALCULATION

PRISCILLA
CALCULATION - DATA COMPARISONS
OVERPRESSURE AT 2500 FEET (762 M)

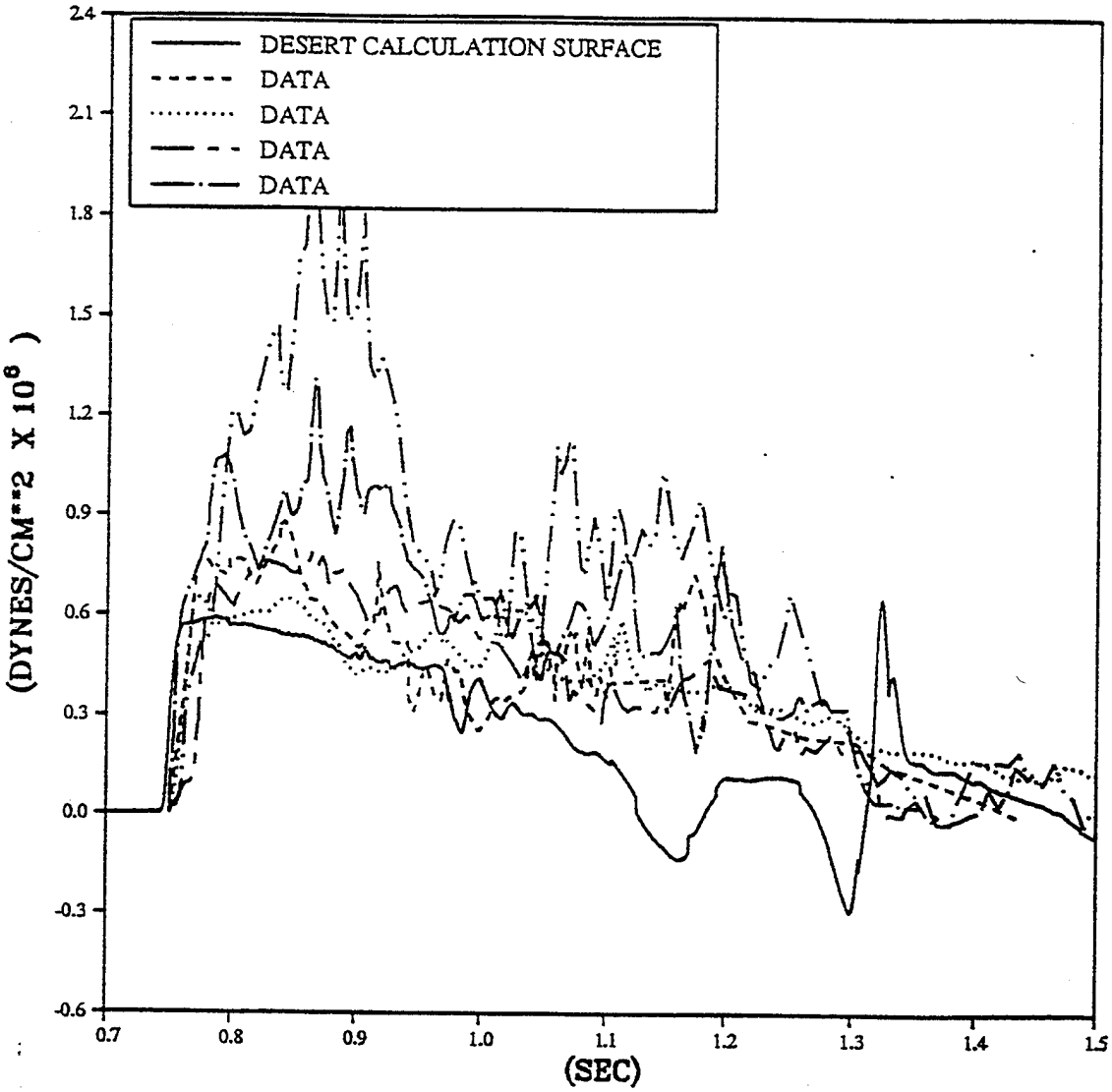

DATA TIME SHIFTED TO MATCH CALCULATION

INTENTIONALLY LEFT BLANK.

APPENDIX J:
CONVERSION TABLE

Conversion factors for U.S. Customary to metric (SI) units of measurement

MULTIPLY →	BY →	TO GET
TO GET ←	BY ←	DIVIDE

angstrom	1.000 000 X E -10	meters (m)
atmosphere (normal)	1.013 25 X E +2	kilo pascal (kPa)
bar	1.000 000 X E +2	kilo pascal (kPa)
barn	1.000 000 X E -28	meter ^{2} (m^2)
British thermal unit (thermochemical)	1.054 350 X E +3	joule (J)
calorie (thermochemical)	4.184 000	joule (J)
cal (thermochemical)/cm^2	4.184 000 X E -2	mega joule/m^2 (MJ/m^2)
curie	3.700 000 X E +1	* giga becquerel (GBq)
degree (angle)	1.745 329 X E -2	radian (rad)
degree Fahrenheit	$t_K = (t \cdot f + 459.67)/1.8$	degree kelvin (K)
electron volt	1.602 19 X E -19	joule (J)
erg	1.000 000 X E -7	joule (J)
erg/second	1.000 000 X E -7	watt (W)
foot	3.048 000 X E -1	meter (m)
foot-pound-force	1.355 818	joule (J)
gallon (U.S. liquid)	3.785 412 X E -3	meter ^{3} (m^3)
inch	2.540 000 X E -2	meter (m)
jerk	1.000 000 X E +9	joule (J)
joule/kilogram (J/kg) (radiation dose absorbed)	1.000 000	Gray (Gy)
kilotons	4.183	terajoules
kip (1000 lbf)	4.448 222 X E +3	newton (N)
kip/inch^2 (ksi)	6.894 757 X E +3	kilo pascal (kPa)
ktap	1.000 000 X E +2	newton-second/m^2 (N-s/m^2)
micron	1.000 000 X E -6	meter (m)
mil	2.540 000 X E -5	meter (m)
mile (international)	1.609 344 X E +3	meter (m)
ounce	2.834 952 X E -2	kilogram (kg)
pound-force (lbs avoirdupois)	4.448 222	newton (N)
pound-force inch	1.129 848 X E -1	newton-meter (N•m)
pound-force/inch	1.751 268 X E +2	newton/meter (N/m)
pound-force/foot^2	4.788 026 X E -2	kilo pascal (kPa)
pound-force/inch^2 (psi)	6.894 757	kilo pascal (kPa)
pound-mass (lbm avoirdupois)	4.535 924 X E -1	kilogram (kg)
pound-mass-foot^2 (moment of intertia)	4.214 011 X E -2	kilogram-meter ^{2} (kg•m^2)
pound-mass/foot^3	1.601 846 X E +1	kilogram/meter ^{3} (kg/m^3)
rad (radiation dose absorbed)	1.000 000 X E -2	** Gray (Gy)
roentgen	2.579 760 X E -4	coulomb/kilogram (C/kg)
shake	1.000 000 X E -8	second (s)
slug	1.459 390 X E +1	kilogram (kg)
torr (mm HG, O°C)	1.333 22 X E -1	kilo pascal (kPa)

* The becquerel (Bq) is the SI unit of radioactivity; 1 Bq = 1 event/s.
** The Gray (GY) is the SI unit of absorbed radiation.

A more complete listing of conversions may be found in "Metric Practice Guide E 380-74," American Society for Testing and Materials.

INTENTIONALLY LEFT BLANK.

NO. OF COPIES	ORGANIZATION
2	ADMINISTRATOR DEFENSE TECHNICAL INFO CTR ATTN DTIC DDA CAMERON STATION ALEXANDRIA VA 22304-6145
1	DIRECTOR US ARMY RESEARCH LAB ATTN AMSRL OP SD TA 2800 POWDER MILL RD ADELPHI MD 20783-1145
3	DIRECTOR US ARMY RESEARCH LAB ATTN AMSRL OP SD TL 2800 POWDER MILL RD ADELPHI MD 20783-1145
1	DIRECTOR US ARMY RESEARCH LAB ATTN AMSRL OP SD TP 2800 POWDER MILL RD ADELPHI MD 20783-1145
	ABERDEEN PROVING GROUND
5	DIR USARL ATTN AMSRL OP AP L (305)

NO. OF COPIES	ORGANIZATION
2	HQDA ATTN SARD TR MS K KOMINOS DR R CHAIT PENTAGON WASHINGTON DC 20310-0103
1	HQDA ATTN SARD TT DR F MILTON PENTAGON WASHINGTON DC 20310-0103
2	DIRECTOR FEDERAL EMERGENCY MNGMNT AGENCY ATTN PUBLIC RELATIONS OFFICE TECHNICAL LIBRARY WASHINGTON DC 20472
1	CHAIRMAN DOD EXPLOSIVES SAFETY BOARD ROOM 856 C HOFFMAN BLDG 1 2461 EISENHOWER AVENUE ALEXANDRIA VA 22331-0600
1	DIRECTOR OF DEFENSE RESEARCH AND ENGINEERING ATTN DD TWP WASHINGTON DC 20301
1	DIRECTOR DEFENSE INTELLIGENCY AGENCY ATTN DT 2 WPNS & SYS DIVISION WASHINGTON DC 20301
1	ASSISTANT SECRETARY OF DEFENSE ATOMIC ENERGY ATTN DOCUMENT CONTROL WASHINGTON DC 20301
9	DIRECTOR DEFENSE NUCLEAR AGENCY ATTN CSTI TECHNICAL LIBRARY DDIR DFSP NANS OPNA SPSD SPTD DFTD TDTR WASHINGTON DC 20305

NO. OF COPIES	ORGANIZATION
1	CHAIRMAN JOINT CHIEFS OF STAFF ATTN J5 R&D DIVISION WASHINGTON DC 20301
2	DA DCSOPS ATTN TECHNICAL LIBRARY DIR OF CHEM & NUC OPS WASHINGTON DC 20310
3	COMMANDER FIELD COMMAND DNA ATTN FCPR FCTMOF NMHE KIRTLAND AFB NM 87115
1	U S ARMY RESEARCH DEVELOPMENT AND STANDARDIZATION GROUP UK ATTN DR ROY E REICHENBACH PSC 802 BOX 15 FPO AE 09499-1500
10	CENTRAL INTELLIGENCE AGENCY DIR DB STANDARD ATTN GE 47 HQ WASHINGTON DC 20505
1	DIRECTOR ADVANCED RESEARCH PROJECTS AGENCY ATTN TECHNICAL LIBRARY 3701 NORTH FAIRFAX DRIVE ARLINGTON VA 22203-1714
2	COMMANDER US ARMY NRDEC ATTN AMSNA D DR D SIELING STRNC UE J CALLIGEROS NATICK MA 01762
2	COMMANDER US ARMY CECOM ATTN AMSEL RD AMSEL RO TPPO P FT MONMOUTH NJ 07703-5301
1	COMMANDER US ARMY CECOM R&D TECHNICAL LIBRARY ATTN ASQNC ELC IS L R MYER CTR FT MONMOUTH NJ 07703-5000

NO. OF COPIES	ORGANIZATION
1	MIT ATTN TECHNICAL LIBRARY CAMBRIDGE MA 02139
1	COMMANDER US ARMY NGIC ATTN RESEARCH & DATA BRANCH 220 7TH STREET NE CHARLOTTESVILLE VA 22901-5396
1	DIRECTOR US ARMY TRAC FT LEE ATTN ATRC L MR CAMERON FT LEE VA 23801-6140
1	US ARMY MISSILE & SPACE INTELLIGENCE CENTER ATTN AIAMS YDL REDSTONE ARSENAL AL 35898-5500
1	COMMANDING OFFICER CODE L51 NAVAL CIVIL ENGINEERING LABORATORY ATTN J TANCRETO PORT HUENEME CA 93043-5003
2	COMMANDER US ARMY STRATEGIC DEFENSE COMMAND ATTN CSSD H MPL TECH LIB CSSD H XM DR DAVIES PO BOX 1500 HUNTSVILLE AL 35807
3	COMMANDER US ARMY CORPS OF ENGINEERS WATERWAYS EXPERIMENT STATION ATTN CEWES SS R J WATT CEWES SE R J INGRAM CEWES TL TECH LIBRARY PO BOX 631 VICKSBURG MS 39180-0631
1	COMMANDER US ARMY ENGINEER DIVISION ATTN HNDED FD PO BOX 1500 HUNTSVILLE AL 35807
3	COMMANDER US ARMY NUCLEAR & CHEMICAL AGENCY 7150 HELLER LOOP SUITE 101 SPRINGFIELD VA 22150-3198

NO. OF COPIES	ORGANIZATION
1	COMMANDER US ARMY CORPS OF ENGINEERS FT WORTH DISTRICT ATTN CESWF PM J PO BOX 17300 FT WORTH TEXAS 76102-0300
1	DIRECTOR TRAC FLVN ATTN ATRC FT LEAVENWORTH KS 66027-5200
1	COMMANDER US ARMY RESEARCH OFFICE ATTN SLCRO D PO BOX 12211 RESEARCH TRIANGLE PARK NC 27709-2211
1	COMMANDER NAVAL ELECTRONIC SYSTEMS COMMAND ATTN PME 117 21A WASHINGTON DC 20360
1	DIRECTOR HQ TRAC RPD ATTN ATRC RPR RADDA FT MONROE VA 23651-5143
2	OFFICE OF NAVAL RESEARCH ATTN DR A FAULSTICK CODE 23 800 N QUINCY STREET ARLINGTON VA 22217
1	DIRECTOR TRAC WSMR ATTN ATRC WC KIRBY WSMR NM 88002-5502
1	COMMANDER NAVAL SEA SYSTEMS COMMAND ATTN CODE SEA 62R DEPARTMENT OF THE NAVY WASHINGTON DC 20362-5101
1	COMMANDER US ARMY WSMR ATTN STEWS NED DR MEASON WSMR NM 88002-5158

NO. OF COPIES	ORGANIZATION
2	CHIEF OF NAVAL OPERATIONS DEPARTMENT OF THE NAVY ATTN OP 03EG OP 985F WASHINGTON DC 20350
1	COMMANDER DAVID TAYLOR RESEARCH CENTER ATTN CODE 522 TECH INFO CTR BETHESDA MD 20084-5000
1	OFFICER IN CHARGE CODE L31 CIVIL ENGINEERING LABORATORY NAVAL CONSTRUCTION BATTALION CTR ATTN TECHNICAL LIBRARY PORT HUENEME CA 93041
1	COMMANDING OFFICER WHITE OAK WARFARE CENTER ATTN CODE WA501 NNPO SILVER SPRING MD 20902-5000
1	COMMANDER CODE 533 NAVAL WEAPONS CENTER ATTN TECHNICAL LIBRARY CHINA LAKE CA 93555-6001
1	COMMANDER DAHLGREN DIVISION NAVAL SURFACE WARFARE CENTER ATTN CODE E23 LIBRARY DAHLGREN VA 22448-5000
1	COMMANDER NAVAL RESEARCH LABORATORY ATTN CODE 2027 TECHNICAL LIBRARY WASHINGTON DC 20375
1	OFFICER IN CHARGE WHITE OAK WARFARE CTR DETACHMENT ATTN CODE E232 TECHNICAL LIBRARY 10901 NEW HAMPSHIRE AVENUE SILVER SPRING MD 20903-5000
1	AL LSCF ATTN J LEVINE EDWARDS AFB CA 93523-5000
1	COMMANDER NAVAL WEAPONS EVALUATION FAC ATTN DOCUMENT CONTROL KIRTLAND AFB NM 87117

NO. OF COPIES	ORGANIZATION
1	RADC EMTLD DOCUMENT LIBRARY GRIFFISS AFB NY 13441
1	AEDC ATTN R MCAMIS MAIL STOP 980 ARNOLD AFB TN 37389
1	AFESC RDCS ATTN PAUL ROSENGREN TYNDALL AFB FL 32403
1	OLAC PL TSTL ATTN D SHIPLETT EDWARDS AFB CA 93523-5000
1	AFIT ENY ATTN LTC HASEN PHD WRIGHT PATTERSON AFB OH 45433-6583
2	AIR FORCE ARMAMENT LABORATORY ATTN AFATL DOIL AFATL DLYV EGLIN AFB FL 32542-5000
1	DIRECTOR IDAHO NATIONAL ENGINEERING LAB ATTN SPEC PROGRAMS J PATTON 2151 NORTH BLVD MS 2802 IDAHO FALLS ID 83415
3	PHILLIPS LABORATORY AFWL ATTN NTE NTED NTES KIRTLAND AFB NM 87117-6008
1	DIRECTOR LAWRENCE LIVERMORE NATIONAL LAB ATTN TECH INFO DEPT L 3 PO BOX 808 LIVERMORE CA 94550
1	AFIT ATTN TECHNICAL LIBRARY BLDG 640 B WRIGHT PATTERSON AFB OH 45433

NO. OF COPIES	ORGANIZATION
1	DIRECTOR NATIONAL AERONAUTICS & SPACE ADMIN ATTN SCIENTIFIC & TECH INFO FAC PO BOX 8757 BWI AIRPORT BALTIMORE MD 21240
1	FTD NIIS WRIGHT PATTERSON AFB OH 45433
3	KAMAN SCIENCES CORPORATION ATTN LIBRARY PA ELLIS FH SHELTON PO BOX 7463 COLORADO SPRINGS CO 80933-7463
4	DIRECTOR IDAHO NATIONAL ENGINEERING LAB EG&G IDAHO INC ATTN R GUENZLER MS 3505 R HOLMAN MS 3510 R A BERRY W C REED PO BOX 1625 IDAHO FALLS ID 83415
5	DIRECTOR SANDIA NATIONAL LABS ATTN DOC CONTROL 3141 C CAMERON DIV 6215 A CHABAI DIV 7112 D GARDNER DIV 1421 J MCGLAUN DIV 1541 PO BOX 5800 ALBUQUERQUE NM 87185-5800
2	DIRECTOR LOS ALAMOS NATIONAL LABORATORY ATTN TH DOWLER MS F602 DOC CONTROL FOR REPORTS LIBRARY PO BOX 1663 LOS ALAMOS NM 87545
1	BLACK & VEATCH ENGINEERS ARCHITECTS ATTN HD LAVERENTZ 1500 MEADOW LAKE PARKWAY KANSAS CITY MO 64114

NO. OF COPIES	ORGANIZATION
1	DIRECTOR SANDIA NATIONAL LABORATORIES LIVERMORE LABORATORY ATTN DOC CONTROL FOR TECH LIB PO BOX 969 LIVERMORE CA 94550
1	DIRECTOR NASA AMES RESEARCH CENTER APPLIED COMPUTATIONAL AERO BRANCH ATTN DR T HOLTZ MS 202 14 MOFFETT FIELD CA 94035
1	DIRECTOR NASA LANGLEY RESEARCH CENTER ATTN TECHNICAL LIBRARY HAMPTON VA 23665
2	APPLIED RESEARCH ASSOCIATES INC ATTN J KEEFER NH ETHRIDGE PO BOX 548 ABERDEEN MD 21001
1	ADA TECHNOLOGIES INC ATTN JAMES R BUTZ HONEYWELL CENTER SUITE 110 304 INVERNESS WAY SOUTH ENGLEWOOD CO 80112
1	ALLIANT TECHSYSTEMS INC ATTN ROGER A RAUSCH 600 2ND STREET NE HOPKINS MN 55343-8367
1	CARPENTER RESEARCH CORPORATION ATTN H JERRY CARPENTER 27520 HAWTHORNE BLVD SUITE 263 PO BOX 2490 ROLLING HILLS ESTATES CA 90274
1	AEROSPACE CORPORATION ATTN TECH INFO SERVICES PO BOX 92957 LOS ANGELES CA 90009
1	THE BOEING COMPANY ATTN AEROSPACE LIBRARY PO BOX 3707 SEATTLE WA 98124

NO. OF COPIES	ORGANIZATION
2	FMC CORPORATION ADVANCED SYSTEMS CENTER ATTN J DROTLEFF C KREBS MDP 95 BOX 58123 2890 DE LA CRUZ BLVD SANTA CLARA CA 95052
1	CALIFORNIA RES & TECH INC ATTN M ROSENBLATT 20943 DEVONSHIRE STREET CHATSWORTH CA 91311
1	SVERDRUP TECHNOLOGY INC SVERDRUP CORPORATION AEDC ATTN BD HEIKKINEN MS 900 ARNOLD AFB TN 37389-9998
2	DYNAMICS TECHNOLOGY INC ATTN D T HOVE G P MASON 21311 HAWTHORNE BLVD SUITE 300 TORRANCE CA 90503
1	KTECH CORPORATION ATTN DR E GAFFNEY 901 PENNSYLVANIA AVE NE ALBUQUERQUE NM 87111
1	EATON CORPORATION DEFENSE VALVE & ACTUATOR DIV ATTN J WADA 2338 ALASKA AVE EL SEGUNDO CA 90245-4896
2	MCDONNELL DOUGLAS ASTRONAUTICS CORP ATTN ROBERT W HALPRIN KA HEINLY 5301 BOLSA AVENUE HUNTINGTON BEACH CA 92647
4	KAMAN AVIDYNE ATTN R RUETENIK 2 CP S CRISCIONE R MILLIGAN 83 SECOND AVENUE NORTHWEST INDUSTRIAL PARK BURLINGTON MA 01830

NO. OF COPIES	ORGANIZATION
1	MDA ENGINEERING INC ATTN DR DALE ANDERSON 500 EAST BORDER STREET SUITE 401 ARLINGTON TX 07601
2	PHYSICS INTERNATIONAL CORPORATION PO BOX 5010 SAN LEANDRO CA 94577-0599
2	KAMAN SCIENCES CORPORATION ATTN DASIAC PO DRAWER 1479 816 STATE STREET SANTA BARBARA CA 93102-1479
1	R&D ASSOCIATES ATTN GP GANONG PO BOX 9377 ALBUQUERQUE NM 87119
1	LOCKHEED MISSILES & SPACE CO ATTN J J MURPHY DEPT 81 11 BLDG 154 PO BOX 504 SUNNYVALE CA 94086
2	SCIENCE CENTER ROCKWELL INTERNATIONAL CORP ATTN DR S CHAKRAVARTHY DR D OTA 1049 CAMINO DOS RIOS THOUSAND OAKS CA 91358
1	ORLANDO TECHNOLOGY INC ATTN D MATUSKA 60 SECOND STREET BLDG 5 SHALIMAR FL 32579
3	S CUBED A DIVISION OF MAXWELL LABS INC ATTN TECHNICAL LIBRARY R DUFF K PYATT PO BOX 1620 LA JOLLA CA 92037-1620
2	THE RALPH M PARSONS COMPANY ATTN T M JACKSON LB TS PROJECT MANAGER 100 WEST WALNUT STREET PASADENA CA 91124

NO. OF COPIES	ORGANIZATION
1	SAIC ATTN J GUEST 2301 YALE BLVD SE SUITE E ALBUQUERQUE NM 87106
1	SUNBURST RECOVERY INC ATTN DR C YOUNG PO BOX 2129 STEAMBOAT SPRINGS CO 80477
1	SAIC ATTN N SINHA 501 OFFICE CENTER DRIVE APT 420 FT WASHINGTON PA 19034-3211
1	SVERDRUP TECHNOLOGY INC ATTN RF STARR PO BOX 884 TULLAHOMA TN 37388
2	S CUBED A DIVISION OF MAXWELL LABS INC ATTN C E NEEDHAM L KENNEDY 2501 YALE BLVD SE ALBUQUERQUE NM 87106
3	SRI INTERNATIONAL ATTN DR GR ABRAHAMSON DR J GRAN DR B HOLMES 333 RAVENWOOD AVENUE MENLO PARK CA 94025
1	TRW BALLISTIC MISSILE DIVISION ATTN H KORMAN MAIL STATION 526 614 PO BOX 1310 SAN BERNADINO CA 92402
1	BATTELLE TWSTIAC 505 KING AVENUE COLUMBUS OH 43201-2693
1	THERMAL SCIENCE INC ATTN R FELDMAN 2200 CASSENS DRIVE ST LOUIS MO 63026

NO. OF COPIES	ORGANIZATION
2	DENVER RESEARCH INSTITUTE ATTN J WISOTSKI TECHNICAL LIBRARY PO BOX 10758 DENVER CO 80210
1	STATE UNIVERSITY OF NEW YORK MECHANICAL & AEROSPACE ENGINEERING ATTN DR PEYMAN GIVI BUFFALO NY 14260
2	UNIVERSITY OF MARYLAND INSTITUTE FOR ADV COMPUTER STUDIES ATTN L DAVIS G SOBIESKI COLLEGE PARK MD 20742
2	THINKING MACHINES CORPORATION ATTN G SABOT R FERREL 245 FIRST STREET CAMBRIDGE MA 02142-1264
1	NORTHROP UNIVERSITY ATTN DR FB SAFFORD 5800 W ARBOR VITAE STREET LOS ANGELES CA 90045
1	CALIFORNIA INSTITUTE OF TECHNOLOGY ATTN T J AHRENS 1201 E CALIFORNIA BLVD PASADENA CA 91109
1	STANFORD UNIVERSITY ATTN DR D BERSHADER DURAND LABORATORY STANFORD CA 94305
1	UNIVERSITY OF MINNESOTA ARMY HIGH PERF COMP RES CTR ATTN DR TAYFUN E TEZDUYAR 1100 WASHINGTON AVE SOUTH MINNEAPOLIS MN 55415
3	SOUTHWEST RESEARCH INSTITUTE ATTN DR C ANDERSON S MULLIN A B WENZEL PO DRAWER 28255 SAN ANTONIO TX 78228-0255

NO. OF COPIES	ORGANIZATION
2	COMMANDER US ARMY NRDEC ATTN SSCNC YSD J ROACH SSCNC WST A MURPHY KANSAS STREET NATICK MA 10760-5018

NO. OF COPIES	ORGANIZATION
	ABERDEEN PROVING GROUND
1	CDR USATECOM ATTN AMSTE TE F L TELETSKI
1	CDR USATHAMA ATTN AMSTH TE
1	CDR USATC ATTN STEC LI
26	DIR USARL ATTN AMSRL SC C H BREAUX AMSRL SC CC C NIETUBICZ C ELLIS D HISLEY N PATEL T KENDALL R SHEROKE AMSRL SC I W STUREK AMSRL SC AE M COLEMAN AMSRL SC S R PEARSON AMSRL SL CM E FIORVANTE AMSRL WT N J INGRAM AMSRL WT NA R KEHS AMSRL WT NC R LOTTERO B MCGUIRE A MIHALCIN P MULLER R LOUCKS S SCHRAML AMSRL WT ND J MILETTA AMSRL WT NF L JASPER AMSRL WT NG T OLDHAM AMSRL WT NH J CORRIGAN AMSRL WT PB P WEIHNACHT B GUIDOS AMSRL WT TC K KIMSEY

USER EVALUATION SHEET/CHANGE OF ADDRESS

This Laboratory undertakes a continuing effort to improve the quality of the reports it publishes. Your comments/answers to the items/questions below will aid us in our efforts.

1. ARL Report Number ARL-CR-277 Date of Report October 1995

2. Date Report Received _____

3. Does this report satisfy a need? (Comment on purpose, related project, or other area of interest for which the report will be used.) _____

4. Specifically, how is the report being used? (Information source, design data, procedure, source of ideas, etc.) _____

5. Has the information in this report led to any quantitative savings as far as man-hours or dollars saved, operating costs avoided, or efficiencies achieved, etc? If so, please elaborate. _____

6. General Comments. What do you think should be changed to improve future reports? (Indicate changes to organization, technical content, format, etc.) _____

CURRENT ADDRESS

Organization

Name

Street or P.O. Box No.

City, State, Zip Code

7. If indicating a Change of Address or Address Correction, please provide the Current or Correct address above and the Old or Incorrect address below.

OLD ADDRESS

Organization

Name

Street or P.O. Box No.

City, State, Zip Code

(Remove this sheet, fold as indicated, tape closed, and mail.)

(DO NOT STAPLE)